Version 2.0
June 1998

Space Telescope Imaging Spectrograph Instrument Handbook

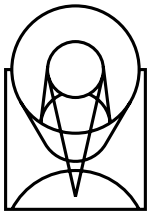

SPACE
TELESCOPE
SCIENCE
INSTITUTE

Science Support Division
3700 San Martin Drive
Baltimore, Maryland 21218

Operated by the Association of Universities for Research in Astronomy, Inc., for the National Aeronautics and Space Administration

User Support

For prompt answers to any question, please contact the STscI Help Desk.

- **E-mail:** `help@stsci.edu`
- **Phone:** (410) 338-1082

World Wide Web

Information and other resources are available on the STIS World Wide Web page:

- **URL:** `http://www.stsci.edu/instruments/stis`

Revision History

Version	Date	Editor
1.0	June 1996	S. Baum
2.0	June 1998	N. Walborn and S. Baum

Send comments or corrections to:
Science Support Division
Space Telescope Science Institute
3700 San Martin Drive
Baltimore, Maryland 21218
E-mail: help@stsci.edu

Authorship

This document is written and maintained by the Spectrographs Group in the Science Support Division of STScI. At the time of the writing of this manual the Group includes the following members, all of whom contributed directly to the writing of this Handbook: S. Baum, R. Bohlin (honorary), J. Christensen, J. Debes, R. Downes, H. Ferguson, A. Gonnella, P. Goudfrooij, J. Hayes, P. Hodge (honorary), S. Hulbert, R. Katsanis, T. Keyes, H. Lanning, C. Leitherer, M. McGrath, K. Sahu, R. Shaw, E. Smith, N. Walborn, and J. Wilson. Chuck Bowers (GSFC) also contributed a section.

Acknowledgments

It is with pleasure that we thank the ST-ECF, in particular Michael Rosa, Eline Tolstoy, and Jeremy Walsh, for their numerous contributions, and the STIS Instrument Definition Team at GSFC, in particular Bruce Woodgate (PI), Randy Kimble, Chuck Bowers, Ted Gull, and Mary Beth Kaiser, for ongoing technical interaction, for material provided in support of this Handbook, and for a careful review of the Handbook. We also thank Don Lindler (ACC) for his technical contributions and many illuminating discussions, and Myron Smith for a careful review of this Handbook. Finally, we thank Mark Stevens for his dedicated efforts in the typesetting and formatting of this large document.

Table of Contents

PART 1

Introduction

The chapters in this part explain how to use this Handbook, where to go for help, and special considerations for using STIS in Cycle 8.

CHAPTER 1
Introduction

In This Chapter...

STIS is a versatile imaging spectrograph. The instrument provides spatially resolved spectroscopy from 1150 to 10,300 Å at low to medium spectral resolution, echelle spectroscopy in the ultraviolet, solar-blind imaging in the ultraviolet, time tagging of photons in the ultraviolet for high time resolution, and direct and coronographic imaging in the optical. This Handbook provides instrument-specific information you need to propose for STIS observations (Phase I), design accepted programs (Phase II), and understand STIS in detail.

This chapter explains the layout of the Handbook and describes how to use the Help Desk at STScI and the STScI STIS World Wide Web (WWW) site to get help and further information. Instrument and operating updates will be posted on the STIS web page.

Purpose

The *STIS Instrument Handbook* is the basic reference manual for the Space Telescope Imaging Spectrograph; it describes the instrument's properties, performance, operations, and calibration. The Handbook is maintained by scientists at STScI. Wherever possible, the most recent operational data have been incorporated into this revised edition.

We have designed the document to serve three purposes:

- To provide instrument-specific information for preparing Phase I STIS observing proposals.
- To provide instrument-specific information to support the design of Phase II proposals for accepted STIS programs.
- To provide technical information about the performance and operation of the instrument which can help in the understanding of problems and in the interpretation of data acquired with STIS.

This Handbook is not meant to serve as a manual for the reduction and analysis of data taken with STIS. The *HST Data Handbook* (available from the STScI Help Desk or the STIS World Wide Web page; see pages 8 and 9, respectively) describes how to work with STIS data.

Document Conventions

This document follows the usual STScI convention in which terms, words, and phrases which are to be entered by the user in a literal way on an HST proposal are shown in a typewriter font (e.g., `STIS/CCD,SHADOW`). Names of software packages or commands (e.g., **calstis**) are given in bold type.

Wavelength units in this Handbook are in Angstroms (Å).

Examples Used in this Handbook

The Handbook uses six observational examples throughout the text. These same examples form the basis of the Phase II templates posted on the STIS web page (see page 9). The examples are:

- Long-slit optical spectroscopy of the nearby galaxy NGC 4406 (M86).
- Long-slit optical and ultraviolet spectroscopy and optical imaging of NGC 6543, the Cat's Eye planetary nebula.
- First-order low-resolution spectroscopy covering STIS's full wavelength range from 1150 Å in the UV to 10,300 Å in the near-IR of the continuous viewing zone (CVZ) solar analog star P041-C.
- Echelle spectroscopy of the O-type star Sk-69˚215 in the Large Magellanic Cloud (LMC), a target in the CVZ.
- Deep optical imaging of a random field.
- Time-resolved ultraviolet spectroscopy of the flare star AU Mic.

In addition, we use stellar spectra throughout the Handbook to illustrate signal-to-noise ratio calculations and derive limiting magnitudes. Figure 1.1 below shows the normalized spectra of O, A, G, and M stars that we use.

Figure 1.1: Normalized Spectra of O5V, A0V, G0V, and M0V Stars Used Throughout the Handbook. Note the dramatic differences in the UV properties.

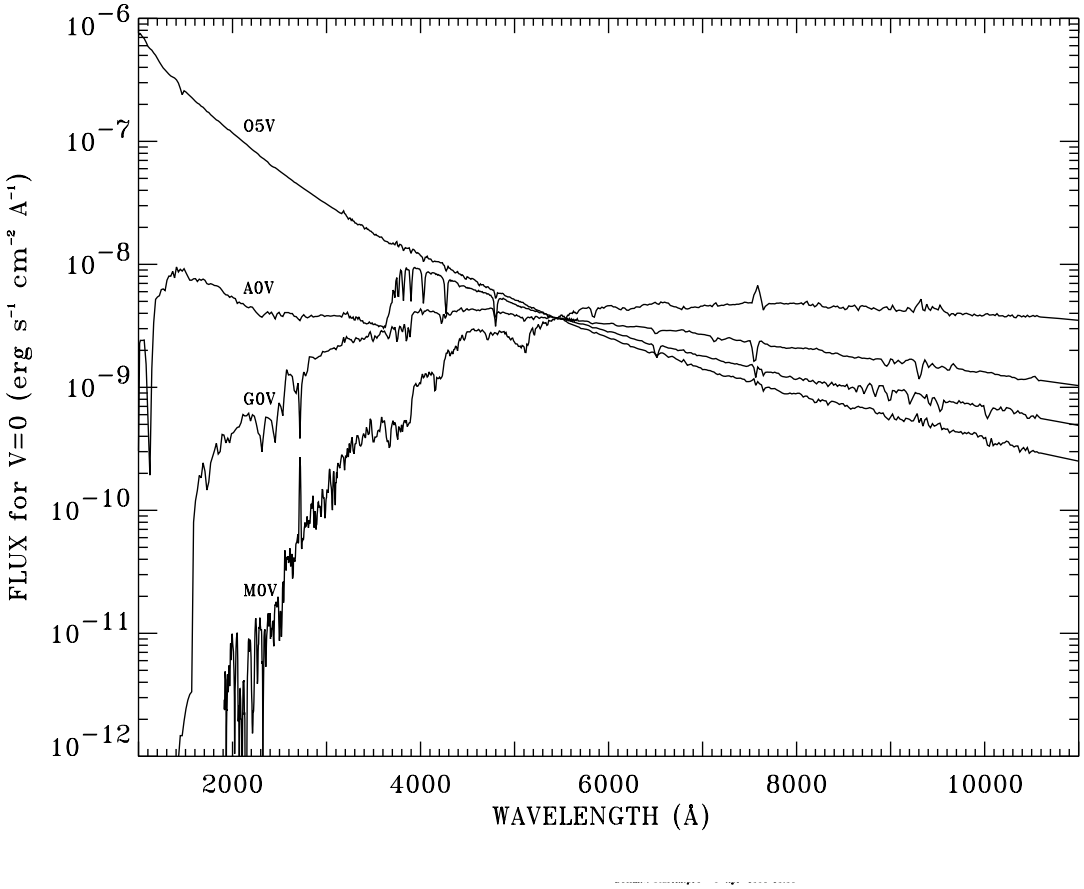

Handbook Layout

To guide you through STIS's capabilities and help optimize your scientific use of the instrument we have divided this Handbook into four parts:

- Part 1 - Introduction.
- Part 2 - User's Guide.
- Part 3 - Supporting Material.
- Part 4 - Calibration.

Figure 1.2 provides a roadmap to the use of this Handbook.

The Supporting Material and Calibration sections contain technical information which supports the material found in the User's Guide; readers are referred to the information at appropriate points in the User's Guide.

Figure 1.2: Handbook Roadmap

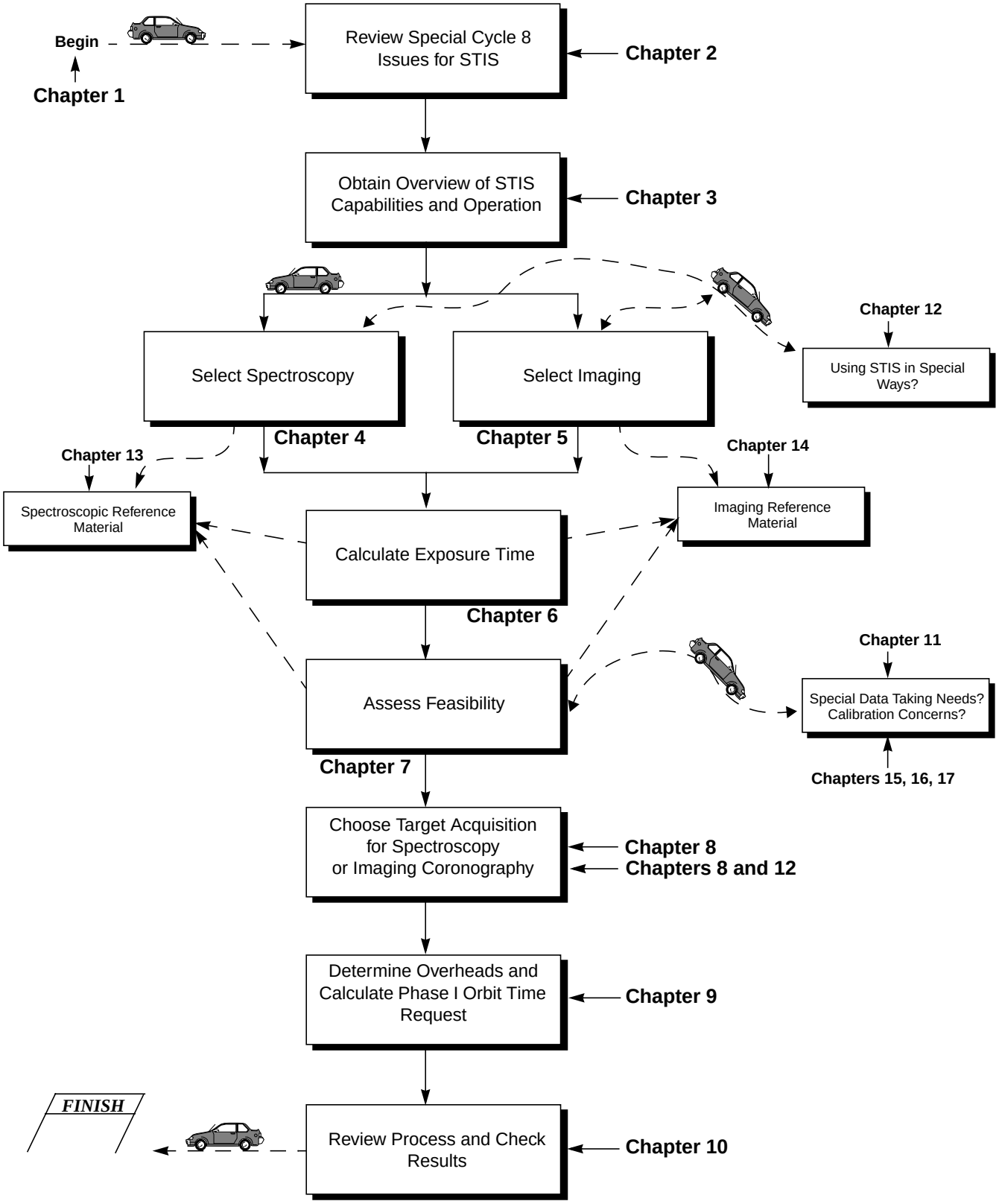

The chapters of this Handbook are as follows:

- Part 1 - Introduction
  - Chapter 1, *Introduction*, includes information about getting help and additional information about STIS.
  - Chapter 2, *Special Considerations for Cycle 8*, describes special policy considerations for using STIS during Cycle 8.
- Part 2 - User's Guide
  - Chapter 3, *Introduction to STIS*, provides an overview of STIS's full capabilities. A discussion is provided to help guide you through the technical details you need to consider in choosing the optimum STIS configuration and in determining the number of orbits to request.
  - Chapter 4, *Spectroscopy*, provides a detailed, grating-by-grating description of STIS's spectroscopic capabilities, including spectral resolutions, throughputs, and descriptions of the slits and apertures.
  - Chapter 5, *Imaging*, provides a detailed, filter-by-filter description of STIS's imaging capabilities.
  - Chapter 6, *Exposure-Time Calculations*, describes how to perform signal-to-noise calculations, either by using pencil and paper, or by using software tools that are provided on the World Wide Web.
  - Chapter 7, *Feasibility and Detector Performance*, provides a description of the three detectors and their physical characteristics, capabilities, and limitations, including saturation, linearity, and bright-object limits.
  - Chapter 8, *Target Acquisition*, helps you select the optimum target acquisition sequence needed to place the target in the desired science aperture.
  - Chapter 9, *Overheads and Orbit-Time Determination*, provides information to convert from a series of planned science exposures to an estimate of the number of orbits, including spacecraft and STIS overheads. This chapter applies principally to the planning of Phase I proposals.
  - Chapter 10, *Summary and Checklist*, presents a summary and a checklist that you should use to assure there are no major omissions in your Phase I and Phase II proposals.
- Part 3 - Supporting Material
  - Chapter 11, *Data Taking*, describes data taking with STIS, including the instrument operating modes (`ACCUM`, `TIME-TAG`), the use of subarrays and binning, and the various types of "associated" observations and contemporaneous calibrations (`WAVECALS`, `CCDFLATS`, `CR-SPLIT`, `PATTERNS`). This chapter also discusses how to orient the long slits and dithering.
  - Chapter 12, *Special Uses of STIS*, provides information on special science uses of STIS, covering slitless spectroscopy and long-slit echelle spectroscopy, time-resolved spectroscopy and imaging, observations of very bright targets, techniques for obtaining higher signal-to-noise and spectral sampling, observations of planetary objects, parallel observing, and coronographic spectroscopy and imaging.

- Chapter 13, *Spectroscopic Reference Material*, contains the detailed plots of sensitivity, line-spread functions, aperture throughputs, and tables of bright-object limits referred to in Chapter 4.
- Chapter 14, *Imaging Reference Material*, contains the detailed plots of sensitivities and tables of bright-object limits referred to in Chapter 5.

• Part 4 - Calibration

- Chapter 15, *Overview of Pipeline Calibration*, briefly describes the processing of STIS data by the STScI pipeline and the products that are sent to observers.
- Chapter 16, *Accuracies*, summarizes the accuracies for STIS data calibrated by the STScI pipeline.
- Chapter 17, *Calibration Status and Plans*, provides an overview of the current state of STIS calibration and development plans for the immediate future.

Preparing and Observing with STIS

Use the *STIS Instrument Handbook* together with the *Cycle 8 Call for Proposals and Phase I Proposal Instructions* (CP) when assembling your STIS Phase I Proposal. The CP provides policy and instructions for proposing; the *STIS Instrument Handbook* contains technical information about STIS, describing its expected performance, and presenting suggestions for use. The next chapter in the Handbook describes special considerations for Cycle 8.

If your Phase I proposal is accepted, you will be asked to submit a Phase II proposal in which you specify the exact configurations, exposures times, and sequences of observations that STIS and the telescope should perform. To assemble your Phase II proposal, you should use the *STIS Instrument Handbook* in conjunction with the *Phase II Proposal Instructions*. These instructions describe the exact rules and syntax that apply to the planning and scheduling of STIS observations and provide relevant observatory information.

The Help Desk at STScI

STScI maintains a Help Desk, the staff of which quickly provide answers on any HST-related topic, including questions regarding STIS and the proposal process. The Help Desk staff have access to all of the resources available at the Institute, and they maintain a database of answers so that frequently asked questions can be immediately answered. The Help Desk staff also provide STScI documentation, in either hardcopy or electronic form, including *Instrument Science Reports*, and *Instrument Handbooks*. Questions sent to the Help Desk are answered within two working days. Usually, the Help Desk staff will reply with the answer to a question, but occasionally they will need more time to investigate the answer. In these cases, they will reply with an estimate of the time needed to reply with the full answer.

We ask that you please send *all* initial inquiries to the Help Desk. If your question requires a STIS Instrument Scientist to answer it, the Help Desk staff will put one in contact with you. By sending your request to the Help Desk, you are guaranteed that someone will provide you a timely response.

To contact the Help Desk at STScI:

- **Send E-mail**: `help@stsci.edu`
- **Phone**: 1-410-338-1082
  Toll-free in the U.S.: 1-800-544-8125

The Space Telescope European Coordinating Facility (ST-ECF) also maintains a Help Desk. European users should generally contact the (ST-ECF) for help; all other users should contact STScI. To contact the ST-ECF Help Desk:

- **Send E-mail**: `stdesk@eso.org`

The STIS Instrument Team at STScI

STScI maintains a team of Instrument Scientists, Scientific Programmers, and Data Analysts who support the development, operation, and calibration of STIS. The team is also responsible for supporting STIS users. A full listing of the STScI Spectrographs Group is provided on the STIS WWW pages under “Help”; the Spectrographs Group is responsible for STIS as well as FOS and GHRS archival support.

The STIS Web Page and Supporting Information

The Spectrographs Group at STScI maintains a World Wide Web (WWW) page (Figure 1.3), as part of STScI’s web service. The address for the STScI STIS web page is:

`http://www.stsci.edu/instruments/stis`

The recently renovated STIS web page includes timely information about STIS operations and performance organized into the categories listed below. Additionally, you can now search for specific information as all STIS documentation is indexed on STIS-specific keywords.

The categories are:

- ***Analysis***: The *GO Primer* and things you need to know if you plan to visit STScI during the data-analysis phase of your program.
- ***Calibration***: A description of the current STIS calibration plan, the currently achievable calibration accuracies, and changes to the pipeline calibration software and reference files.
- ***Documentation***: Electronic versions of the Instrument and Data Handbooks; detailed technical information concerning the development, performance, testing, operation, and calibration of STIS contained in a series of

STIS Instrument Science Reports (ISRs) and STScI Analysis Newsletters (STANs). These reports can be downloaded from the WWW or paper copies can be requested from the Help Desk.

- ***Frequently Asked Questions***: A list of frequently asked questions about STIS and their answers, ranging from proposal preparation through data analysis.
- ***Performance***: On-orbit performance reports giving the latest information on STIS and "data foibles"—things to watch out for in your STIS data.
- ***Proposals***: Things you need to know to successfully complete a proposal to observe with STIS, both for Phase I and for Phase II.
- ***Special Topics***: Interesting things being done with STIS, such as the STIS parallel program.
- ***Tools***: Software tools that can be retrieved (e.g., an IRAF script for creating daily dark reference files) or run directly over the network (e.g., exposure-time calculators and a target-acquisition simulator).

As always, if you are stuck, just send E-mail to `help@stsci.edu`.

Figure 1.3: STIS Web Page

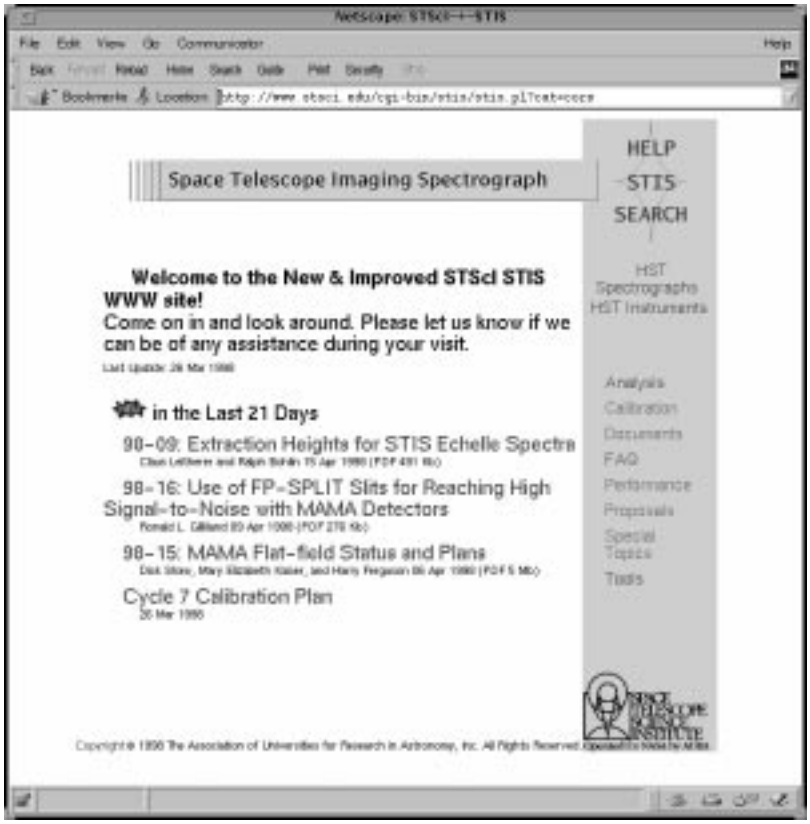

Nonproprietary STIS Data

There is a large amount of existing, nonproprietary STIS data available for retrieval from the HST Data Archive. They include observations obtained in the Second Servicing Mission Early Release programs (EROs—see *Ap.J. Letters*, Vol. 492, No. 2, 1998), the STIS Archival Pure Parallel Program (see page 213), the ongoing calibration programs (see Chapter 17), and data taken in connection with the Hubble Deep Field program (proposal ID 7410). For the immediate future in support of the Cycle 8 Call for Proposals, an updated high level list of these public data will be maintained on the STIS WWW page under “Special Topics,” and of course you can use the HST Archive interface to search for such data directly. Any such data may be freely acquired, as described in the *HST Data Handbook*, for technical or scientific use. Examples of nonproprietary STIS science data are shown as illustrative examples interspersed in this Handbook.

CHAPTER 2
Special Considerations for Cycle 8

In This Chapter...

STIS has been in orbit for over one year and has been operating superbly, returning a multitude of new and unique scientific results despite the fact that it is still early in its Cycle 7 use. We have learned a significant amount about the instrument and its operation in that time. Based on our current knowledge of the instrument, we list below the STIS-specific policy items needing consideration in proposals to use STIS in Cycle 8.

Support of STIS Capabilities for Cycle 8

We have established a set of core scientific capabilities of STIS which will be supported for Cycle 8 and which are described in this Handbook. They provide an enormous range of scientific applications and substantially enhance the power of HST.

STIS has additional capabilities that are not described in this Handbook, and which are not supported for Cycle 8. They include additional slits and data-taking formats. These capabilities are “available”, upon consultation with a STIS Instrument Scientist. If you find that your science *cannot* be performed with the parameters described in this Handbook, you may wish to consider use of an unsupported capability. A full list of STIS’s available and engineering-only capabilities are described in a separate appendix to this Handbook.

Use of unsupported modes comes at a price, and they should be used only if the technical requirement and scientific justification are particularly compelling. Proposers should be aware of the following caveats regarding unsupported modes:

- Calibrations for unsupported capabilities will not be provided by STScI. Either users must determine that they can create calibration files from data in the HST Archive or they must obtain calibrations as part of their observations. The STScI pipeline will not calibrate data taken in unsupported modes but will deliver uncalibrated FITS files (or in some cases partially calibrated FITS files) to the observer and the HST Archive.
- STScI adopts a policy of shared risk with the observer for the use of unsupported capabilities. Requests to repeat failed observations taken with unsupported capabilities will not be honored if the failure is related to the use of the unsupported capability.
- User support from STScI for observation planning, as well as data reduction and analysis, with unsupported capabilities will be limited and provided at a low priority. Users taking data with unsupported capabilities should be prepared to shoulder the increased burden of the planning, calibration, reduction, and analysis.

Cycle 8 Phase I proposals that include use of unsupported STIS capabilities must include a justification of why the science cannot be done with a supported configuration, must include a request for any observing time needed to perform calibrations, must justify the added risk of using an unsupported mode in terms of the scientific payback, and must include a demonstration that the observers are able to bear the increased burden of calibration, reduction, and analysis of their data.

MAMA Scheduling Policies

Since the MAMA (see “Detectors” on page 21) control electronics were found in orbit to be subject to resets due to cosmic-ray upsets, the MAMAs are operated only during the contiguous orbits of each day which are free of the South Atlantic Anomaly (SAA). We therefore limit the duration of any single MAMA visit (i.e., a single continuous observation series) to five orbits. Additionally, to facilitate scheduling and maximize the orbits available for MAMA observations, we require observers to split their CCD and MAMA exposures into separate visits. Specifically, for STIS programs containing both CCD and MAMA scientific (not target-acquisition) exposures, in which there are more than 30 minutes of observing time using the CCD at a single target position (inclusive of overheads), and for which that target is observed for more than a single orbit, you *must* split the exposures into visits which separate the CCD from the MAMA exposures. For programs which *require* CCD and MAMA scientific exposures in the same visit (e.g., variability monitoring programs), exceptions can be made, if you provide a well-justified explanation in the Special Requirements section of your Phase I proposal.

Prime and Parallel Observing with the STIS MAMA Detectors

As explained in greater detail in “MAMA Bright-Object Limits” on page 115, the MAMA detectors that STIS uses in the ultraviolet are subject to damage at high illumination rates. To protect the instrument, we have established limits on the maximum count rate at which the detectors may be illuminated. These count-rate limits translate into a set of configuration-dependent bright-object screening magnitudes. The spectroscopic bright-object screening magnitudes are summarized in Table 13.38 on page 312, and the imaging counterparts in Table 14.33 on page 369.

STScI will perform screening of all MAMA exposures prior to scheduling. Targets not established as safe for the configuration in which they are being observed will not be scheduled. Observations that pass screening but are lost in orbit due to a bright-object violation will not be rescheduled. Observers are responsible for assuring that their observations do not violate the MAMA count-rate limits. A detailed description of the MAMA bright-object limits and the observers’ responsibility is presented in “MAMA Bright-Object Limits” on page 115.

To assure that STScI can adequately screen observations, special constraints are imposed on parallel observing with the MAMAs:

- No pure parallels are allowed using the MAMA detectors.
- Coordinated parallels are allowed with the MAMA detectors only if an exact spacecraft orientation (`ORIENT`) is requested and the RA and Dec of the parallel field determined. Note that the specification of an exact orient limits the scheduling of observations to a ~4–8 week period each year. The observer is responsible for assuring that observations do not violate the MAMA count rate limits both for coordinated parallel MAMA observations and for primes.
- The number of MAMA *imaging snapshot* visits accepted in Cycle 8 will be limited to about 100 to facilitate screening for bright objects, and MAMA snapshot imaging targets observed will be only those unambiguously cleared of bright-object concerns.

Table 2.1 below summarizes the policy with respect to MAMA observing in Cycle 8.

Targets that are one magnitude or more fainter than the magnitude limits in the screening tables generally automatically pass screening. For a target that is within one magnitude of the screening limits after correction for extinction and slit losses, observers must provide a spectrogram of the source at the intended observing wavelength. If such a spectrogram is not available, the prospective GO must request an orbit in Phase I for a pre-qualification exposure, during which the target spectrum must be determined by observation in an allowed configuration (see “MAMA Bright-Object Limits” on page 115 for more details).

Table 2.1: Bright-Object Protection Policy for MAMA Observations

Type of Observing	Spectroscopy	Imaging
Prime	Allowed if target passes screening	Allowed if target passes screening
Snapshots	Unrestricted	Limited in total number to <~100
Coordinated parallel	Allowed only if ORIENT is exactly specified and field passes screening	Allowed only if ORIENT is exactly specified and field passes screening
Pure parallel	Not allowed	Not allowed

Please also note that if you are proposing MAMA target-of-opportunity observations, we ask you to provide an explanation in your Phase I proposal of how you will ensure that your target can be safely observed.

PART 2

User's Guide

The chapters in this part describe the basics of observing with STIS. Included are a description of the instrumental layout and basic operations; the spectroscopic and imaging capabilities of STIS, the performance and limitations of its detectors, exposure-time calculations, target acquisitions, and overhead and orbit-request determinations.

This part of the Handbook is all you need to read to plan your Phase I STIS Proposal.

CHAPTER 3
Introduction to STIS

In This Chapter...

In this chapter we provide an overview of the capabilities and scientific applications of STIS. We describe the opto-mechanical layout and basic operation of the instrument, and we provide a flow chart and discussion to help you design a technically feasible and scientifically optimized STIS observing proposal.

Instrument Capabilities

STIS uses two-dimensional detectors operating from the ultraviolet to the near infrared. STIS has first-order gratings covering this spectral range, which are designed for spatially resolved spectroscopy using a long slit, and echelle gratings, available only in the ultraviolet, which are designed to maximize the spectral coverage in single observations of point sources. The STIS Flight Software supports onboard target acquisitions and peakups to place targets on slits and coronographic bars. The optics and detectors have been designed to exploit HST's high spatial resolution.

STIS can be used to obtain:

- Spatially resolved, long-slit (or slitless) spectroscopy from the ultraviolet to the near infrared (1150–10,300 Å) at low to medium spectral resolution (R ~ 500–17,000) in first order.
- Echelle spectroscopy at medium to high spectral resolution (R ~ 30,000–110,000), covering a broad simultaneous spectral range ($\Delta\lambda$ ~ 800 or 200 Å, respectively) in the ultraviolet (1150–3100 Å).

In addition to the these two prime capabilities, STIS also provides:

- An imaging capability using the solar-blind far-ultraviolet MAMA detector (1150–1700 Å), the solar-insensitive near-ultraviolet MAMA detector (1150–3100 Å), and the optical CCD (2000–10,300 Å), through a small complement of narrowband and broadband filters.
- Objective-prism spectroscopy (R ~500–10) in the vacuum ultraviolet (1150–3100 Å).
- High-time-resolution ($\Delta\tau$ = 125 microseconds) imaging and spectroscopy in the ultraviolet (1150–3100 Å) and moderate-time-resolution ($\Delta\tau$ ~20 seconds) CCD imaging and spectroscopy in the near UV, optical, and near IR (2000–10,300 Å).
- Coronographic imaging in the near UV, optical, and near IR (2000–10,300 Å) and bar-occulted spectroscopy over the entire spectral range (1150–10,300 Å).

Table 4.1 on page 34 and Table 5.1 on page 50 provide full lists of gratings for spectroscopy and filters for imaging, respectively.

STIS is a versatile instrument that can be applied to a broad range of scientific programs. For instance, the combination of high spectral resolution covering a large simultaneous wavelength range and low per-pixel background improves the efficiency of programs such as quasi-stellar object (QSO) and interstellar absorption-line studies; STIS's wavelength coverage in a single exposure is 15 to 35 times that of GHRS for such applications. Studies of the dynamics of galactic nuclei and the kinematics of active galaxies and diffuse galactic nebulae benefit from the ability to obtain spatially resolved spectroscopy over a 50 arcsecond slit and from the high quantum efficiency in the optical provided by the charge-coupled device (CCD). The wide wavelength coverage of STIS facilitates line-ratio studies; for instance, the low-resolution, first-order gratings span the range 1150–10,000 Å in just four exposures. Slitless spectroscopy provides emission-line images of astronomical objects, and coronographic imaging and spectroscopy can reveal the nature of extended gaseous regions surrounding bright continuum sources.

Instrument Design

In this section, we provide a high-level summary of the basic design and operation of STIS, concentrating on the information most relevant to the design of your HST observing proposal. Subsequent chapters provide more detailed information.

Detectors

STIS uses three large-format (1024 x 1024 pixel) detectors (see Chapter 7 for more detail), as follows:

- A Scientific Image Technologies (SITe) CCD, called the `STIS/CCD`, with ~0.05 arcsecond square pixels, covering a nominal 52 x 52 arcsecond square field of view (FOV), operating from ~2000 to 11,000 Å.
- A Cs_2Te Multi-Anode Microchannel Array (MAMA) detector, called the `STIS/NUV-MAMA`, with ~0.024 arcsecond square pixels, and a nominal 25 x 25 arcsecond square field of view (FOV), operating in the near ultraviolet from 1600 to 3100 Å.
- A solar-blind CsI MAMA, the `STIS/FUV-MAMA`, with ~0.024 arcsec pixels, and a nominal 25 x 25 arcsecond square FOV, operating in the far ultraviolet from 1150–1700 Å.

The CCD

The CCD provides high quantum efficiency and good dynamic range in the near ultraviolet through near infrared. The CCD produces a time-integrated image in the so-called `ACCUM` data-taking mode. As with all CCDs, there is noise (*read noise*) and time (*read time*) associated with reading out the detector. Time-resolved work with this detector is done by taking a series of multiple short exposures. The minimum exposure time is 0.1 sec, and the minimum time between successive identical exposures is 45 sec for full-frame and can be reduced to 20 sec for subarray readouts. CCD detectors are capable of high-dynamic-range observations. The dynamic range, for a single exposure, ultimately is limited by the depth of the CCD full well (which in this case is 144,000 e^-), which determines the total amount of charge (or counts) that can accumulate in any one pixel during any one exposure, without saturation. Cosmic rays will affect all CCD exposures: CCD observations should be broken into multiple exposures whenever possible, to allow removal of cosmic rays in post-observation data processing; during Phase II you can use the `CR-SPLIT` optional parameter to do this (see Chapter 11).

The MAMAs

The two MAMAs are *photon-counting* detectors which provide a two-dimensional ultraviolet capability. They can be operated either in `ACCUM` mode, to produce a time-integrated image, or in `TIME-TAG` mode to produce an event stream with high (125 μsec) time resolution. Doppler correction for the spacecraft motion is applied automatically onboard for data taken in `ACCUM` high-spectral-resolution modes.

The STIS MAMA detectors are subject to both *scientific* and *absolute* brightness limits. At high local (≥50 counts sec^{-1} $pixel^{-1}$) and global (>285,000 counts sec^{-1}) illumination rates, counting becomes nonlinear in a way that is not correctable. At only slightly higher illumination rates, the MAMA detectors are subject to damage. We have therefore defined absolute local and global count-rate limits, which translate to a set of configuration-dependent bright-object screening limits. Sources which violate the absolute count rate limits in a given

configuration *cannot be observed in those configurations*, as discussed under “MAMA Bright-Object Limits” on page 115.

Early concerns about the signal-to-noise attainable with the MAMAs have been alleviated by experience in orbit. Values of 50:1 per spectral resolution element in extracted spectra are routinely obtained for point sources with sufficient counting statistics, integrated over the extraction aperture. Higher values of 100–300 can be obtained by stepping the target along the slit in the first-order modes, or by use of special multiple slits with the echelles (see Chapter 12). Current information indicates that the flat fields are stable to ±1–2%, but the UV flat-field lamps have been used sparingly due to their limited lifetimes, so the long-term stability of the flats is not yet certain. See also “Summary of Accuracies” on page 379.

STIS Physical Configuration

The STIS optical design includes corrective optics to compensate for HST’s spherical aberration, a telescope focal-plane slit-wheel assembly, collimating optics, a grating-selection mechanism, fixed optics, and camera focal-plane detectors. An independent calibration-lamp assembly can illuminate the focal plane with a range of continuum and emission-line lamps. A simplified schematic showing major mechanisms and detectors, and a medium-resolution echelle-mode light path, is shown in Figure 3.1. More complete diagrams can be found on the STIS WWW page under “Calibration.”

Figure 3.1: Simplified STIS Optical Design

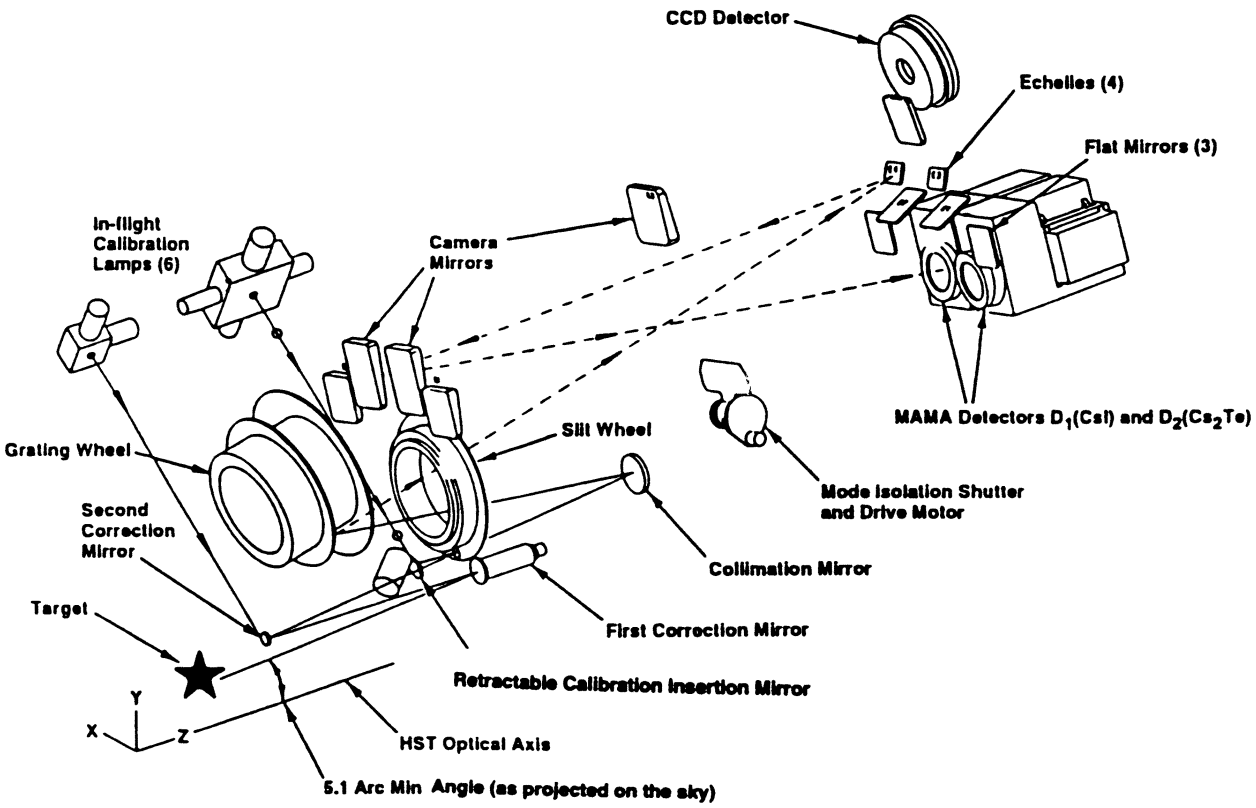

Slit and Grating Wheels

The *slit wheel* contains apertures and slits for spectroscopic use and the clear, filtered, and coronographic apertures for imaging. The slit-wheel positioning is repeatable to very high precision: ± 7.5 and 2.5 milli-arcseconds in the spatial and spectral directions, respectively.

The *grating wheel*, or so-called Mode-Selection Mechanism (MSM), contains the first-order gratings, the cross-disperser gratings used with the echelles, the prism, and the mirrors used for imaging. The MSM is a nutating wheel which can orient optical elements in three dimensions. It permits the selection of one of its 21 optics as well as adjustment of the tip and tilt angles of the selected grating or mirror. As described in “Routine Wavecals” below, the grating wheel exhibits non-repeatability which is corrected for in post-observation data processing using contemporaneously obtained comparison-lamp exposures.

For some gratings, only a portion of the spectral range of the grating falls on the detector in any one exposure. These gratings can be scanned (tilted by the MSM) so that different segments of the spectral format are moved onto the detector for different exposures. For these gratings a set of pre-specified central wavelengths, corresponding to specific MSM positions, i.e., grating tilts, has been defined (see Chapter 4).

Calibration-Lamp Systems

STIS has two independent calibration subsystems, the so-called HITM (Hole in the Mirror) system and the IM (Insert Mechanism) system. The HITM system contains two Pt-Cr/Ne line lamps, used to obtain wavelength comparison exposures and to illuminate the slit during target acquisitions. Light from the HITM lamps is projected through a hole in the second correction mirror (CM2); thus, when the HITM lamps are used light from the external sky still falls on the detector, unless the STIS external shutter (not shown in Figure 3.1) is closed. The IM system contains flat-fielding lamps (a tungsten lamp for CCD flats, a deuterium lamp for NUV-MAMA flats, and a krypton lamp for FUV-MAMA flats) and a single Pt-Cr/Ne line comparison lamp. When the IM lamps are used, the Calibration Insert Mechanism (CIM) is inserted into the light path and all external light is blocked. Observers will be relieved to know that the ground system will *automatically* choose the right subsystem (see next section) and provide the necessary wavelength calibration exposures.

Basic Instrument Operations

Target Acquisitions and Peakups

Once the telescope acquires its guide stars, your target will be within ~1–2 arcseconds of the aperture center. For science observations taken through slits which are smaller than 3 arcseconds in either dimension, and for use of the coronographic bars, you will need to specify a target-acquisition exposure to center the target in the science aperture. The nominal accuracy of STIS point source (V<21) target acquisitions is 0.01 arcsecond. If either dimension of the aperture is less than or equal to 0.1 arcsecond, the acquisition exposure should be followed by one or more peakup exposures to refine the centering of point or point-like sources. Peakup accuracy is 5% of the slit width used. Acquisition exposures always use the CCD, one of the filtered or unfiltered apertures for CCD imaging, and a mirror as the optical element in the grating wheel. Peakup exposures use a science slit or coronographic aperture and also use the CCD, with either a mirror or a spectroscopic element in the grating wheel. Target acquisitions and acquisition peakups are described in detail in Chapter 8.

Routine Wavecals

Each time the MSM is moved to select a new optical element or to tilt a grating, the resulting spectrum is projected onto the detector with an error (lack of repeatability) of ≤±3 pixels. Additionally, thermal effects can cause small drifts over multi-orbit observations. An internal calibration-lamp observation (`WAVECAL`) will automatically be taken following each use of a new grating element or new tilt position and after ~1 orbit in any one setting in order to allow calibration of the zero point of the wavelength (dispersion) and spatial (perpendicular to dispersion) axes in the spectroscopic science data during post-observation data processing. These routine, automatically-occurring, wavecal observations are expected to provide sufficient wavelength zeropoint accuracy for the vast majority of GO science. Only if your science requires

particularly accurate tracking of the wavelength zeropoints do you need to insert additional wavecal observations in your exposure sequence (see also “GO Wavecals” on page 188).

Data Storage and Transfer

At the conclusion of each ACCUMULATE exposure, the science data is read out from the detector in use and placed in STIS’s internal buffer memory, where it is stored until it can be transferred to the HST data recorder (and thereafter to the ground). This design makes for more efficient use of the instrument, as up to eight CCD or 1024 x 1024 MAMA, or two 2048 x 2048 MAMA (see “Highres” on page 183) full-frame images can be stored in the internal buffer at any time. A frame can be transferred out of the internal buffer to the data recorder during subsequent exposures, so long as those exposures are longer than 3 minutes in duration.

STIS’s internal buffer stores the data in a 16 bit-per-pixel format. This structure imposes a maximum of 65,536 data numbers per pixel. For the MAMA detectors this maximum is equivalent to a limit on the total number of *photons* per pixel which can be accumulated in a single exposure. For the CCD, the full well (and not the 16 bit buffer format) limits the photons per pixel which can be accumulated without saturating in a single exposure. See Chapters 7 and 11 for a detailed description of detectors and data taking with STIS.

Parallel Operations

STIS’s three detectors do *not* operate in parallel with one another—only one detector can be used at any one time. Exposures with different STIS detectors can, however, be freely interleaved in an observing sequence, and there is no extra setup time or overhead in moving from one detector to another. The three detectors, sharing the bulk of their optical paths, also share a common field of view of the sky.

STIS *can* be used in parallel with any of the other science instruments on HST. Figure 3.2 shows the HST field of view following the second servicing mission, with STIS and NICMOS installed. Dimensions in this figure are approximate; accurate aperture positions can be found on STScI’s Observatory web page under “Pointing.”[1] The STIS dispersion is along AXIS1 and the slits are parallel to AXIS2. Policy for applying for parallel observing is described in the Call for Proposals. We provide suggestions for designing parallel observations with STIS in “Parallel Observing with STIS” on page 212. While the STIS CCD can always be used in parallel with another instrument, there are some restrictions on the use of the MAMA detectors in parallel, as described in “Support of STIS Capabilities for Cycle 8” on page 13.

---

1. Pointing web page: http://www.stsci.edu/ftp/instrument_news/Observatory/taps.html

Figure 3.2: HST Field of View Following the Second Servicing Mission (Only STIS, WFPC2, and FGS are available in Cycle 8)—Approximate Dimensions

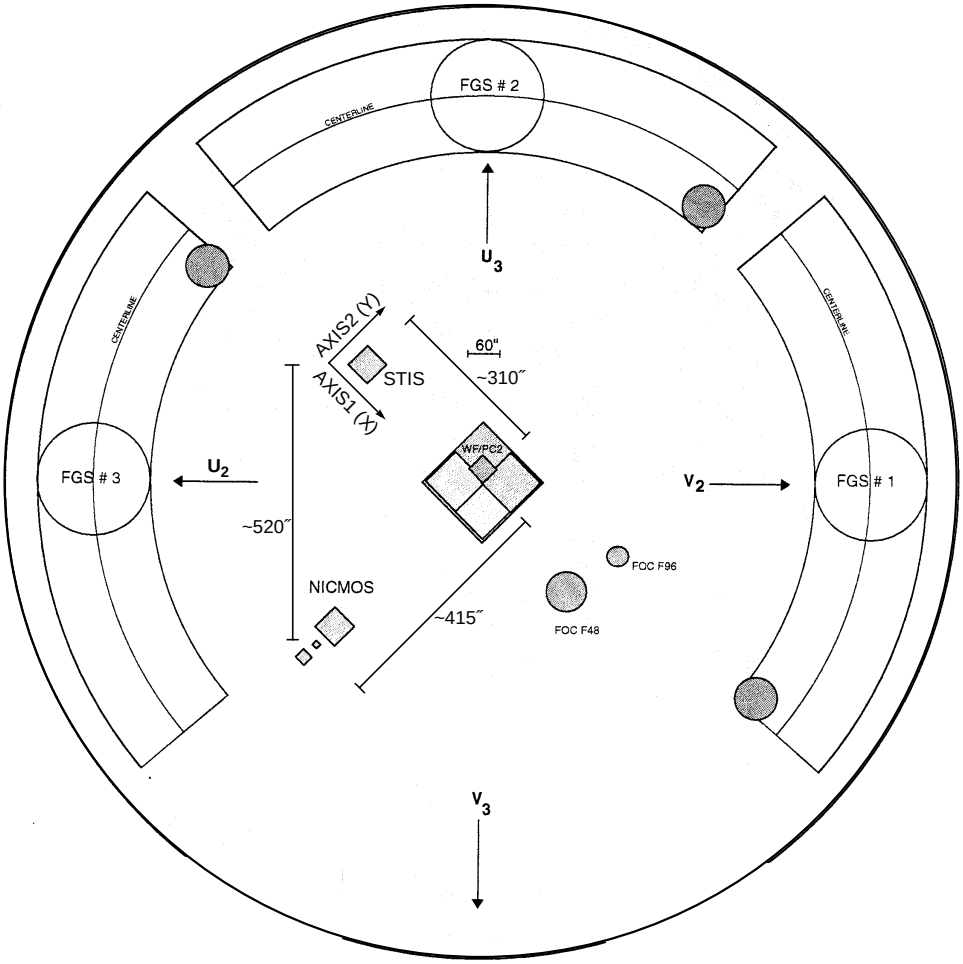

Typical STIS Observing Sequence

In the optical, STIS is expected to be used principally to observe extended objects, so long observations are expected to be the norm. The combination of high spatial resolution, spectral resolution, and low read noise from the CCD will encourage the taking of multiple (~20 minute) exposures, to allow cosmic ray rejection. Observations with the MAMA detectors do not suffer from cosmic rays or read noise, but long integration times will often be needed to obtain sufficient signal-to-noise in the photon-starved ultraviolet.

A typical STIS observing sequence is expected to consist of an initial target acquisition and possibly an acquisition peakup to center the target in a long or echelle slit, followed by a series of long (~10–40 minute) exposures with a single optical element at a given wavelength setting. It may also include a series of multiple long exposures taken with different gratings or with a single grating at a number of tilts. Observers will generally not take their own wavecal exposures;

routine automatic wavecals will allow wavelength and spatial zero-points to be determined in post-observation data processing, requiring no input from the user. Observations at ≥7500 Å should be accompanied by fringe-flat exposures as discussed in Chapter 11.

Designing STIS Observations

In this section, we describe the sequence of steps you will need to take when designing your STIS observing proposal. The process is an iterative one, as you trade off between maximum spatial and spectral resolution, signal-to-noise, and the limitations of the instrument itself. The basic sequence of steps in defining a STIS observation (see Figure 3.3, below) is:

- Identify science requirements and select basic STIS configuration to support those requirements.
- Estimate exposure time to achieve required signal-to-noise ratio and check feasibility, including saturation and bright-object limits.
- Identify any additional non-science (target acquisition, peakup, and calibration) exposures needed.
- Calculate total number of orbits required, taking into account the overhead.

Identify Science Requirements and Define STIS Configuration

First and foremost, of course, you must identify the science you wish to achieve with STIS. Basic decisions you will need to make are:

- Spectroscopy or Imaging?
- Wavelength region(s) of interest?
- Spectral resolution and spectral coverage required?
- Nature of target—extended source (long slit or full aperture) or point source?

In addition you will need to establish whether you require:

- High signal-to-noise ratio.
- Time resolution.
- Coronography.
- High photometric accuracy.

As you choose your science requirements and work to match them to the instrument's capabilities, keep in mind that those capabilities differ greatly depending on whether you are observing in the optical with the CCD, or in the ultraviolet, using the MAMA detectors. Tradeoffs are described in Table 3.1.

Figure 3.3: Defining a STIS Observation

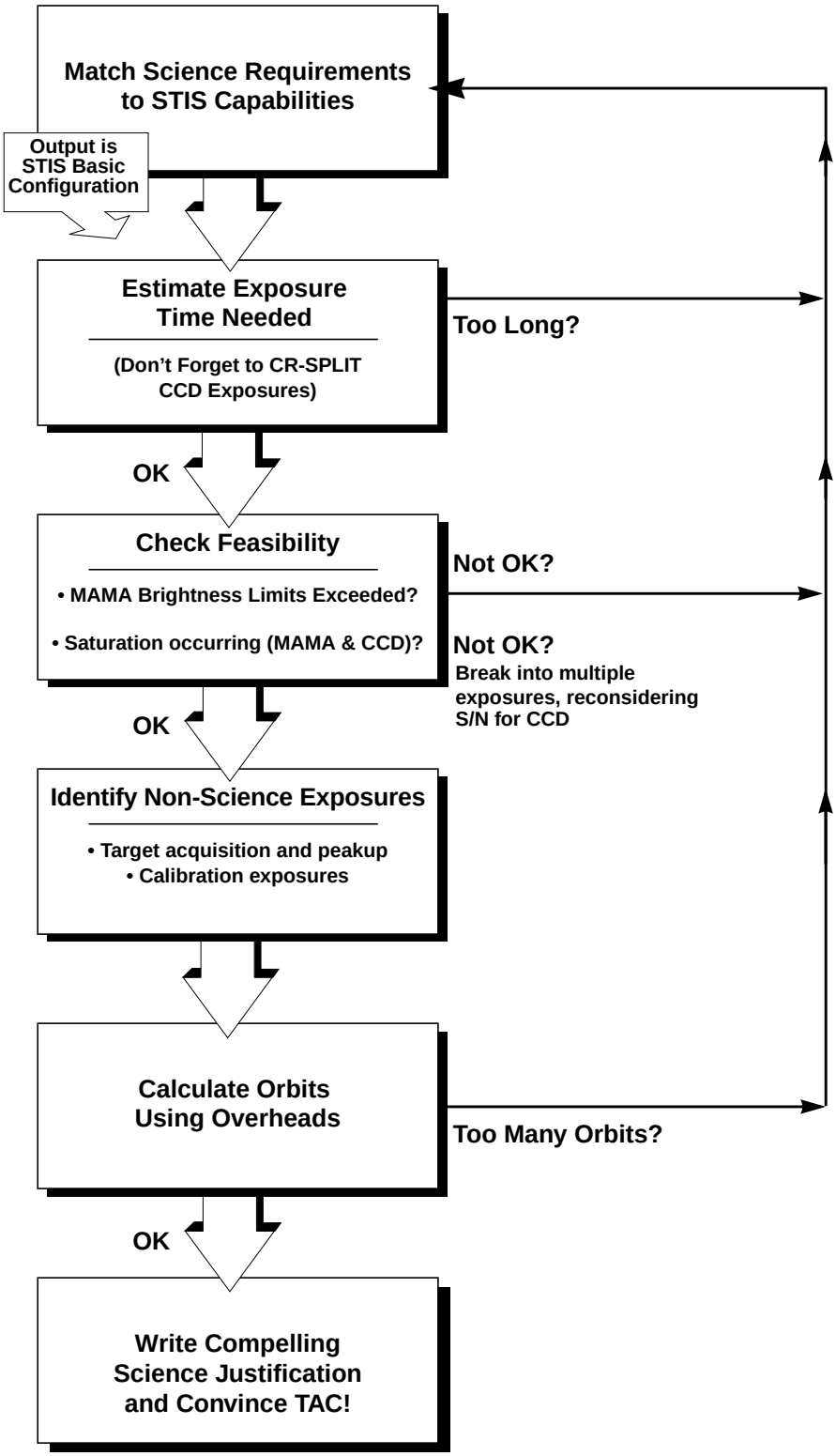

Table 3.1: Science Decision Guide

Decision	Affects	Tradeoffs
Wavelength regime	Detector and gratings	2000–10,300 Å—CCD 1600–3100 Å—NUV-MAMA 1150–1700 Å—FUV-MAMA
Spectral resolution	Gratings and detector	R < 20,000 (first order) with CCD, NUV- or FUV-MAMA, or R ≥ 30,000 (echelle) with NUV- or FUV-MAMA only.
Spectral range	Gratings	Spectral range covered in a single exposure differs radically for different gratings.
Extended or point source	Gratings	First-order gratings designed for spatially resolved and point-source observations. Echelle gratings designed for point-source observations (long-slit echelle spectroscopy will suffer order overlap for extended sources, but can be done for sources with weak continua).
Time resolution	Detector	If time resolution <20 seconds required must use NUV- or FUV-MAMA.
Coronography	Detector and aperture	*Bright-object*[a] coronography available with CCD only. Coronographic imaging available with CCD only. Barred coronographic spectroscopy available with all detectors.

a. The bright-object limits for MAMA observations apply to coronographic observations as well, i.e., coronographic observations of targets which are too bright for the MAMA detectors are not allowed.

Spectroscopy

For spectroscopic observations, the base configuration you need is: detector (Configuration), operating mode (Mode=ACCUM or TIME-TAG), slit (Aperture), grating (Spectral Element), and central wavelength. In Chapter 4, we provide detailed information about each of the spectroscopic grating modes of STIS.

Imaging

For imaging observations, the base configuration is detector (Configuration), operating mode (Mode=ACCUM or TIME-TAG), and filter (Aperture).[2] Chapter 5 presents detailed information about each of STIS's imaging modes.

Special Uses

We refer you to Chapter 12 if you are interested in any of the following special uses of STIS: slitless spectroscopy or extended-source echelle observations, time-resolved work, bright-object or high signal-to-noise ratio observations, planetary studies, parallel observations, and coronography.

Determine Exposure Time and Check Feasibility

Once you have selected your basic STIS configuration, the next steps are to:

- Estimate the exposure time needed to achieve your required signal-to-noise ratio, given your source brightness. (You can use the STIS Exposure-Time Calculator for this, see Chapter 6 and the plots in Chapters 13 and 14).

2. The mirror will be used as the spectral element for imaging observations.

- For observations using the MAMA detectors, assure that your observations do not exceed brightness (count-rate) limits.
- For observations using the MAMA detectors, assure that for pixels of interest, your observations do not exceed the limit of 65,536 accumulated counts per pixel per exposure imposed by the STIS 16 bit buffer.
- For observations using the CCD detector, assure that for pixels of interest, you do not exceed the per pixel saturation count limit of the CCD full well (the full-well limit supersedes the STIS buffer limit on counts per pixel).
- For MAMA `TIME-TAG` exposures check that your observations are feasible and do not violate any `TIME-TAG` specific count rate or data volume constraints (see Chapter 11).

To determine your exposure-time requirements consult Chapter 6 where an explanation of how to calculate signal-to-noise and a description of the sky backgrounds are provided. To assess whether you are close to the brightness, signal-to-noise, and dynamic-range limitations of the detectors, refer to Chapter 7. For a consideration of data-taking strategies and calibration exposures, consult Chapter 11.

If you find that the exposure time needed to meet your signal-to-noise requirements is too great, or that you are constrained by the detector's brightness or dynamic-range limitations, you will need to adjust your base STIS configuration. Table 3.2 summarizes the options available to you and steps you may wish to take as you iterate to select a STIS configuration which is both suited to your science and technically feasible.

Table 3.2: Feasibility Guide

Action	Outcome	Recourse
Estimate exposure time	If too long -> re-evaluate instrument configuration.	Reduce resolving power, or use wider slit, or change detectors and wavelength regime.
Check full-well limit for CCD observations	If full well exceeded and you wish to avoid saturation-> reduce time per exposure.	Divide total exposure time into multiple, short exposures.[a,b]
Check bright-object limits for MAMA observations	If source is too bright -> re-evaluate instrument configuration.	Increase spectral resolution, or choose narrower slit, or use neutral-density filter, or change detectors and wavelength regime.
Check 65,536 counts-per-pixel limit for MAMA observations	If limit exceeded -> reduce time per exposure.	Divide total exposure time into multiple, short exposures.[a,b]

a. Splitting CCD exposures affects the exposure time needed to achieve a given signal-to-noise ratio because of the read noise. Splitting MAMA exposures has no effect since there is no read noise with the MAMAs.
b. Splitting an exposure into multiple exposures increases the overheads, slightly reducing on-source time.

Identify Need for Non-Science Exposures and Constraints

Having identified your desired sequence of *science* exposures, you need to determine what *non-science* exposures you may require to achieve your scientific goals. Specifically, you need to:

- Determine which (if any) target-acquisition and acquisition-peakup exposures will be needed to center your target in your aperture to the accuracy required for your scientific aims (e.g., you may wish to center the nucleus of a galaxy in the 52 x 0.1 arcsecond slit and orient the long axis of the slit along the major axis of the galaxy to some accuracy). To assess your acquisition needs, refer to Chapter 8. To determine a specific orientation for the STIS long slit, refer to Chapter 11.
- If you require more accurate wavelength zeropoints than the routine calibrations provide, you can insert additional comparison-lamp exposures (`TARGET_NAME=WAVE`) at shorter intervals or of longer duration than the routine, automatic `WAVECAL` observations. To determine your wavelength-calibration exposure needs, refer to Chapter 11.
- CCD observations longward of 7500 Å are subject to severe fringing, which can be well corrected only by flat-field exposures obtained contemporaneously with the science exposures. Hence, you should include such flat-field exposures if observing near 7500 Å or longward. Fringing is discussed on in Chapter 7 and the specification of corrective flat fields (`CCDFLAT`s) is discussed in Chapter 11.

Determine Total Orbit Request

In this, the final step, you place all your exposures (science and non-science, alike) into orbits, including tabulated overheads, and determine the total number of orbits you require. Refer to Chapter 9 when performing this step. If you are observing a point source and find your total time request is significantly affected by data-transfer overheads (which will be the case *only* if you are taking many separate exposures under 3 minutes), you can consider the use of CCD subarrays to lessen the data volume. Subarrays are described on page 179.

There are some special constraints on the duration and structure of MAMA visits, due to the sensitivity of certain STIS electronic components to charged particles, which precludes operating the MAMAs at all during orbits which cross the South Atlantic Anomaly (SAA). Since there are a limited number of SAA-free orbits per day, MAMA visits are limited to a maximum of five orbits. Longer programs must be broken into shorter visits. Moreover, in order to conserve orbits available for MAMA observations, programs which combine CCD and MAMA observations must be divided into separate visits with each detector type, unless the CCD portion consumes less than 30 minutes including overheads (see Chapter 2).

At this point, if you are happy with the total number of orbits required, you're done! If you are unhappy with the total number of orbits required, you can, of

course, iterate, adjusting your instrument configuration, lessening your acquisition requirements, changing your signal-to-noise or wavelength requirements, until you find a scenario which allows you to achieve (and convince the Telescope Allocation Committee (TAC) of the merits of) your science goals with STIS.

CHAPTER 4
Spectroscopy

In This Chapter...

In this chapter, we provide information to help you choose the most appropriate spectroscopic configuration for your scientific application. We briefly describe the properties of each grating mode and its associated slits, and provide an overview of their scientific uses. Curves of sensitivity, the central wavelengths and wavelength ranges for the grating settings, and the detailed aperture throughputs and line-spread functions referenced in this chapter are presented in Chapter 13.

For MAMA spectroscopy there are bright-object limits. We mention these limits here, and describe them in detail in Chapter 7. Tables of the MAMA spectroscopic bright-object screening magnitudes by spectral type and mode are presented in Chapter 13.

Overview

There are 15 spectroscopic modes, summarized in Table 4.1. They comprise low- and intermediate-resolution, first-order modes designed to be used with a complement of long slits over the entire wavelength range; and intermediate- and high-resolution echelle modes which have been optimized for point-source observations through short echelle slits, and are available only in the ultraviolet (see Figure 4.1).

Table 4.1: STIS Spectroscopic Capabilities

Grating	Spectral Range (Å)		Spectral Resolution		# Prime Tilts[a]	Detector	reference material page	Slits (apertures)[b, c, d, e]
	Complete	Per Tilt	Scale Δλ (Å per pixel)	Resolving Power (λ/2Δλ)				
CCD First-Order Spectroscopy								
G750L	5240–10,270	5030	4.92	530–1040	1	CCD	228	52X0.05 52X0.1 52X0.2 52X0.5 52X2 52X0.2F1
G750M	5450–10,140	570	0.56	4870–9050	9	CCD	231	
G430L	2900–5700	2800	2.73	530–1040	1	CCD	234	
G430M	3020–5610	286	0.28	5390–10,020	10	CCD	237	
G230LB	1680–3060	1380	1.35	620–1130	1	CCD	240	
G230MB	1640–3190	155	0.15	5470–10,630	11	CCD	245	
MAMA First-Order Spectroscopy								
G230L	1570–3180	1610	1.58	500–1010	1	NUV-MAMA	250	
G230M	1640–3100	90	0.09	9110–17,220	18	NUV-MAMA	253	
G140L	1150–1730	610	0.60	960–1440	1	FUV-MAMA	256	
G140M	1140–1740	55	0.05	11,400–17,400	12	FUV-MAMA	259	
MAMA Echelle Spectroscopy								
E230M	1570–3110	800	λ/60,000	30,000	2	NUV-MAMA	262	0.2X0.2, 0.2X0.06
E230H	1620–3150	267	λ/228,000	114,000	6	NUV-MAMA	265	0.2X0.2, 0.2X0.09
E140M	1150–1710	620	λ/91,700	45,800	1	FUV-MAMA	268	0.2X0.2, 0.2X0.06
E140H	1150–1700	210	λ/228,000	114,000	3	FUV-MAMA	271	0.2X0.2, 0.2X0.09
MAMA Prism Spectroscopy								
PRISM	1150–3100	1950	1.2–120	480–10	2	NUV-MAMA	274	52X0.05,52X0.2

a. Number of exposures at distinct tilts needed to cover spectral range of grating, with 10% wavelength overlap between adjacent settings.
b. Naming convention gives dimensions of slit in arcseconds. For example `52X0.1` indicates the slit is 52 arcsec long perpendicular to the dispersion direction and 0.1 arcsec wide in the dispersion direction. The `F` (e.g., in `52X0.2F1`) indicates that it is the fiducial bar which is specified for coronographic spectroscopy.
c. For the MAMA first-order modes, only ~ 25 arcseconds of the long slit projects on the detector. (See also “Slits for First-Order Spectroscopy” on page 42.)
d. Full-aperture clear (`50CCD` or `25MAMA`), longpass-filtered (`F25QTZ` or `F25SRF2` in UV), and neutral-density-filtered slitless spectroscopy are also supported with the appropriate first-order and echelle gratings, as well as the prism. `F25MGII` is supported with `E230H` and `E230M`.
e. A 6 arcsec-long slit (`6X0.2`) is also supported for use with the echelle gratings, but with order overlap; and the high-S/N multislits `0.2X0.2FP(A-E)` and `0.2X0.06FP(A-E)` (see Chapter 12) as well as the very narrow `0.1X0.03` for maximum spectral resolution are likewise supported with the echelles.

Figure 4.1: Sample Uncalibrated Spectral Images (distortion is exaggerated)

a.) Uncalibrated Long-Slit Spectrogram of Point Source

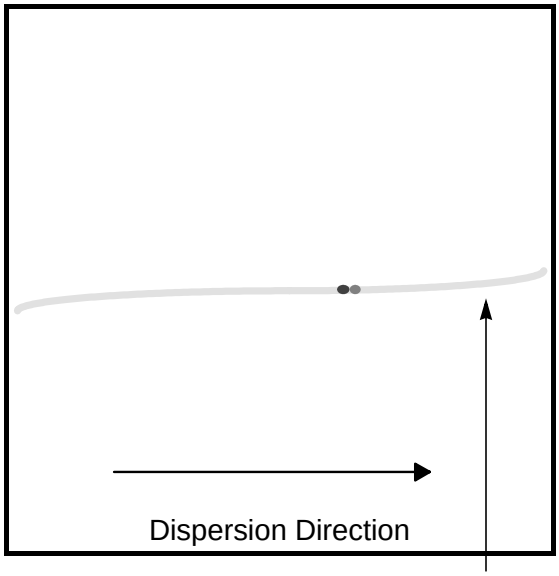

Point source showing continuum and two strong emission lines

b.) Uncalibrated Long-Slit Spectrogram of Diffuse Source

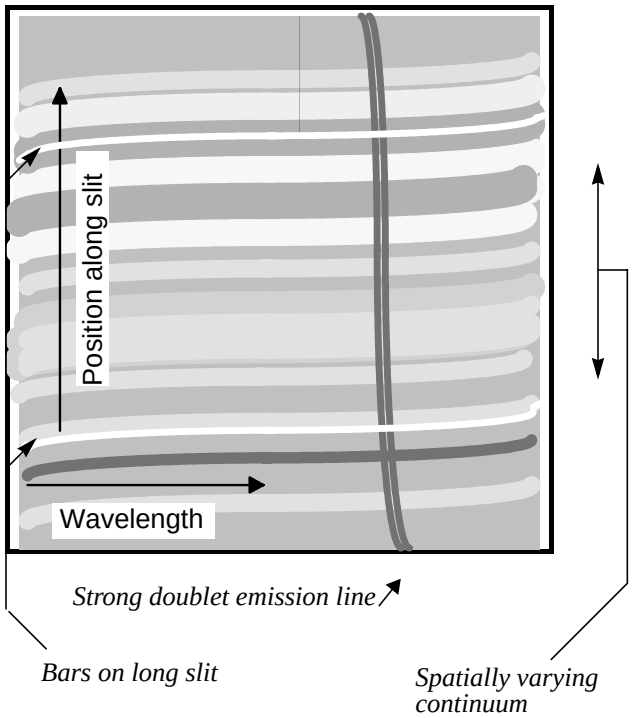

Strong doublet emission line

Bars on long slit

Spatially varying continuum

c.) Echelle Spectrogram of Point Source Showing Multiple Orders on One Image

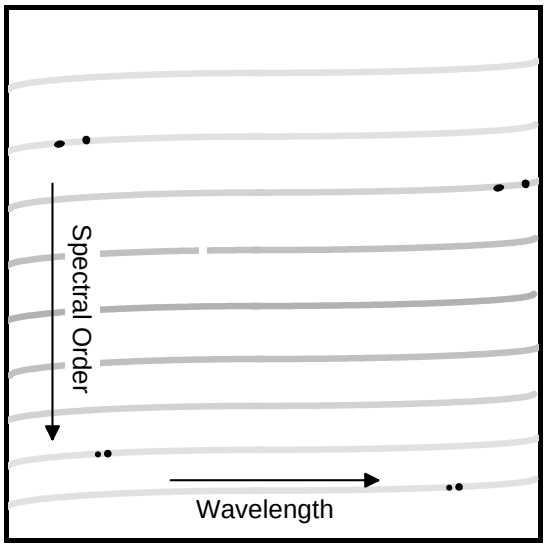

Two strong emission lines. Adjacent orders have ~10% overlap in wavelength so lines appearing at the start of one order will also appear at the end of the next.

d.) Echelle Spectrogram of Diffuse Source

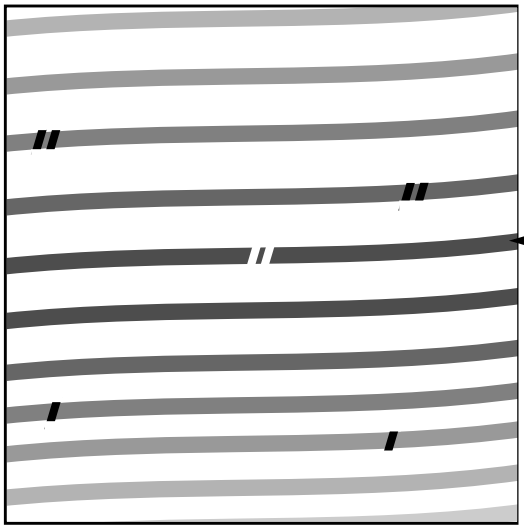

Absorption lines at wavelength near center of order. Continuum from extended object fills short slit.

Throughputs

To illustrate the broad wavelength coverage provided by STIS, and the relative throughputs achievable across STIS's wavelength regime, we show, in Figure 4.2, the system throughput of the four low-resolution, first-order modes on a single plot (where the throughput is defined as the end-to-end effective area divided by the geometric area of a filled, unobstructed, 2.4 meter aperture). To allow you to judge the relative throughputs of different spectroscopic configurations, we plot, in Figure 4.3, the efficiency of all grating modes for each of the four primary wavelength regimes on a common plot. These plots allow you to gauge the relative efficiencies of STIS in different configurations.

Figure 4.2: System Throughput of STIS's Low-Resolution, First-Order Grating Modes

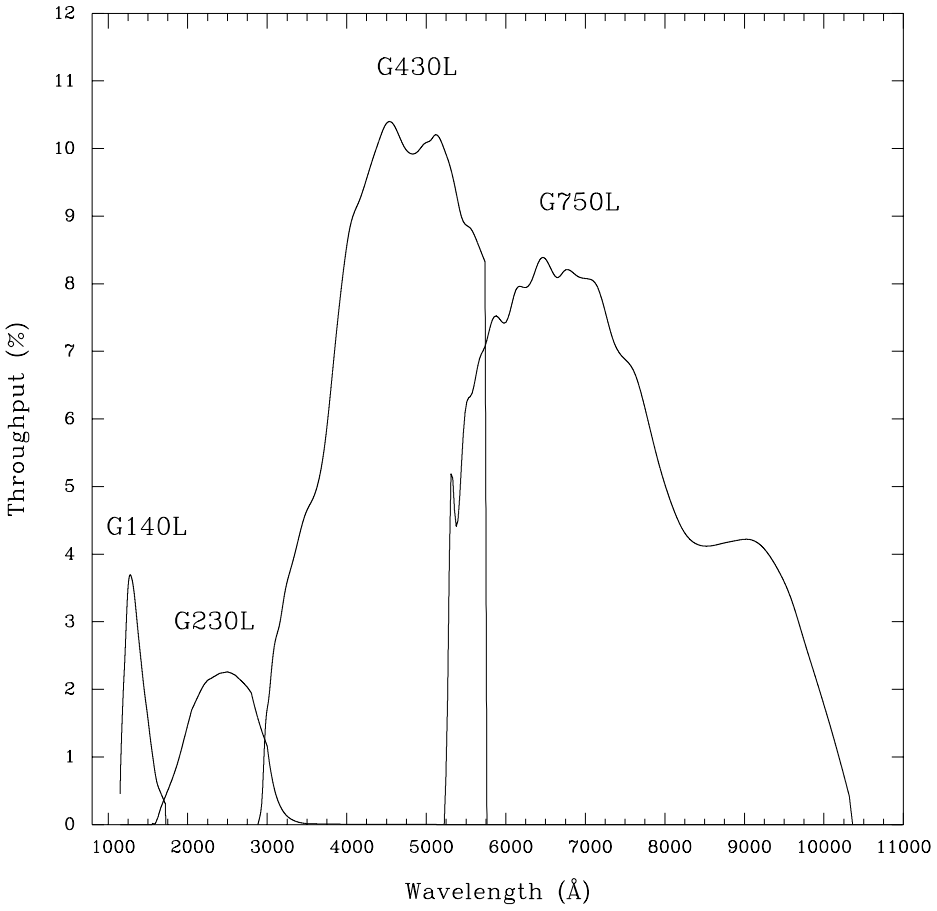

Figure 4.3: System Throughput of STIS's Grating Modes

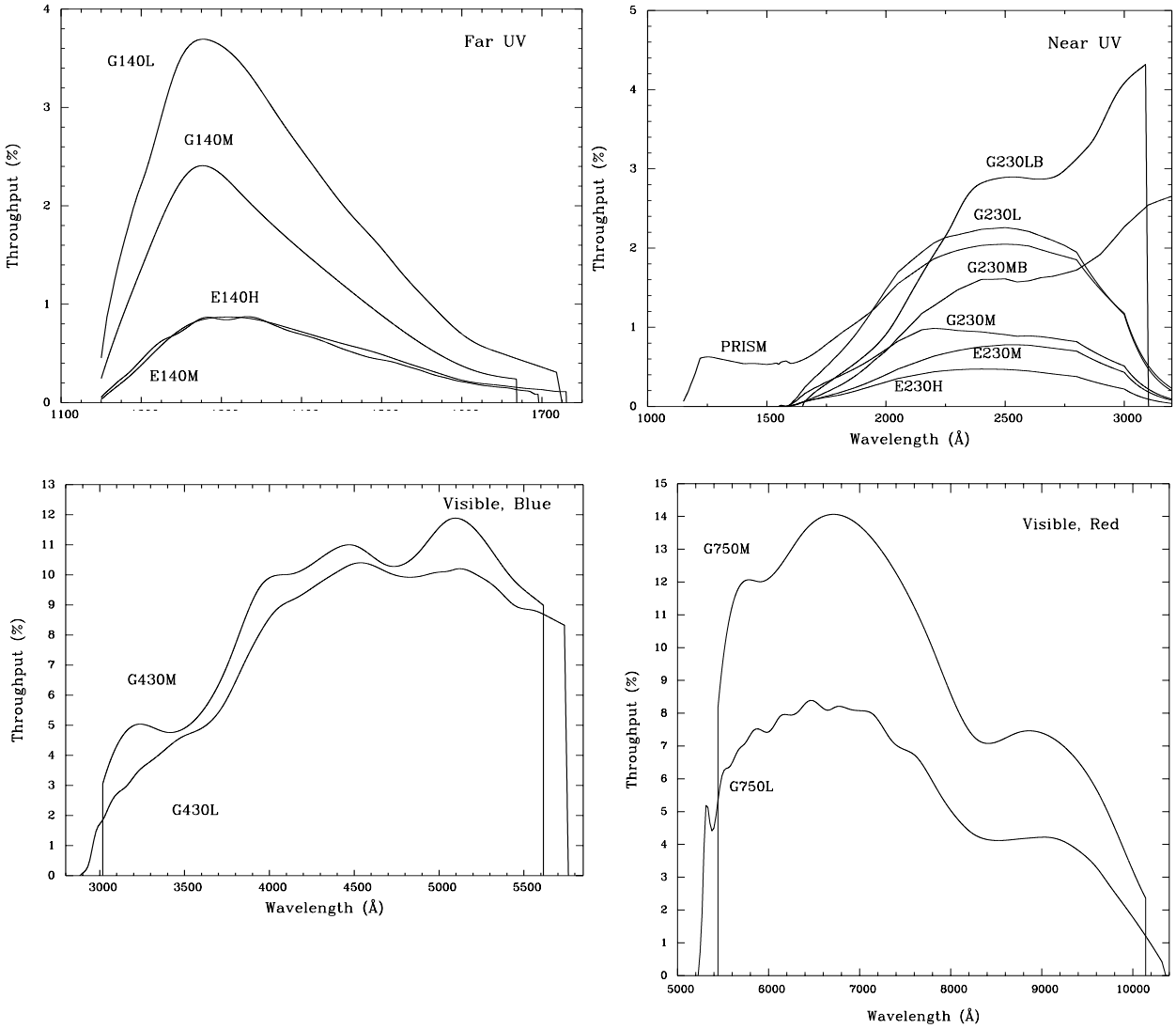

Limiting Magnitudes

In Table 4.2 below, we give the A0 V type star V magnitude reached during a 1 hour integration which produces a signal-to-noise ratio of 10 in the continuum per spectral resolution element around the peak of the grating response, where we have integrated over the PSF in the direction perpendicular to the dispersion, and assumed the `52X0.2` slit for the first-order gratings and the `0.2X0.2` slit for the echelles.

Table 4.2: Limiting A Star V Magnitudes

Grating	Wavelength (Å)	Magnitude	Grating	Wavelength (Å)	Magnitude
G750L	7000	20.9	G140L	1350	17.1
G750M	7000	19.1	G140M	1350	13.8
G430L	5500	20.9	E230M	2700	13.5
G430M	5500	18.5	E230H	2600	11.4
G230LB	3000	18.4	E140M	1400	11.4
G230MB	3000	15.4	E140H	1350	10.5
G230L	2600	18.6	PRISM		20.3 @ λ = 2300 (slitless)
G230M	2600	14.5			

Saturation

Both CCD and MAMA observations are subject to saturation at high total accumulated counts per pixel, the CCD due to the depth of the full well, and the MAMA due to the 16-bit format of the MAMA buffer memory. The nature of the saturation for CCD and MAMA spectroscopic observations is described in Chapter 7 under “CCD Saturation: the CCD Full Well” on page 102 and “MAMA Saturation—Overflowing the 16 Bit Buffer” on page 110, respectively.

MAMA Bright-Object Limits

The MAMA detectors are subject to:

- Absolute bright-object limits, above which targets cannot be observed.
- Science limits, above which the MAMA response becomes non-linear and photometric information is lost.

We direct MAMA observers to the discussion presented in “MAMA Bright-Object Limits” on page 115. For summary tables of bright-object screening magnitudes for all spectroscopic modes, see “MAMA Spectroscopic Bright-Object Limits” on page 311. It is the observers’ responsibility to be sure they do not exceed the MAMA bright-object limits.

Scanned Gratings: Prime and Secondary Positions

For the intermediate-resolution gratings and echelles (except E140M), only a portion of the full spectral range of the grating falls on the detector in any one exposure, and the gratings must be scanned (tilted), with a separate exposure taken at each tilt, in order to cover the full spectral range (see Figures 4.4 and 4.5 below). Accordingly, for these scanned gratings, a single exposure at a given

wavelength, or a series of exposures at different wavelengths to cover a larger wavelength range, can be selected by the user. You must choose either prime or secondary settings. The prime settings cover the full spectral range with 10% wavelength overlap between observations taken at adjacent settings. The secondary settings cover selected absorption or emission lines and may be more convenient to use in some applications. We expect the photometric and wavelength calibration accuracies to be higher for the prime settings than for most of the intermediate settings, as calibrations for the latter will be inferred from those taken at prime settings. A few frequently used intermediate settings are being calibrated directly as noted in Chapter 13. The central wavelengths, and corresponding minimum and maximum wavelengths, are presented in the individual grating sections in Chapter 13.

Figure 4.4: Scanned First-Order Gratings

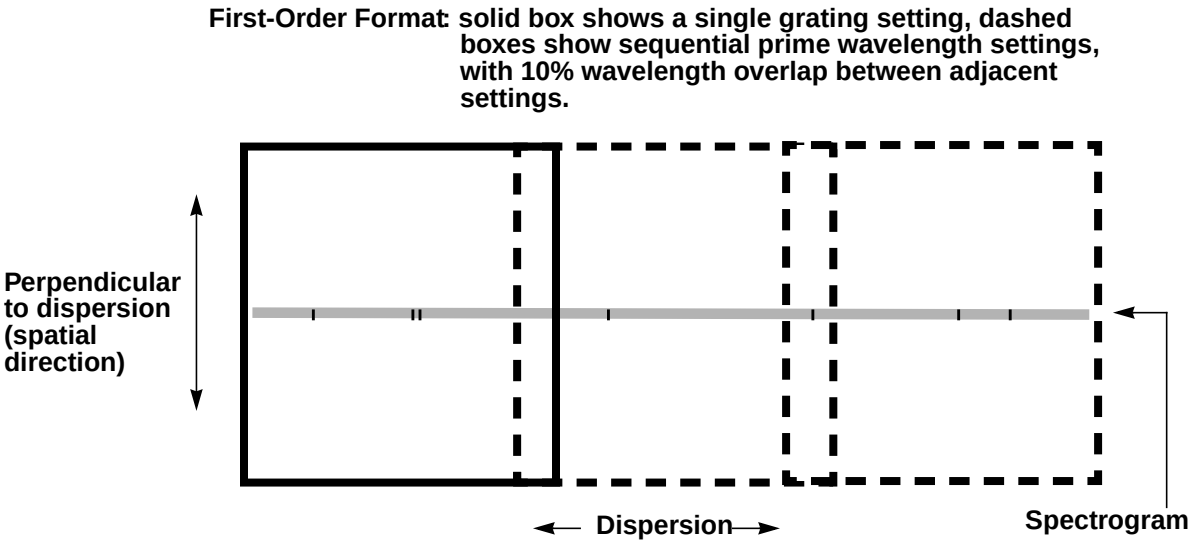

Figure 4.5: Scanned Echelle Gratings

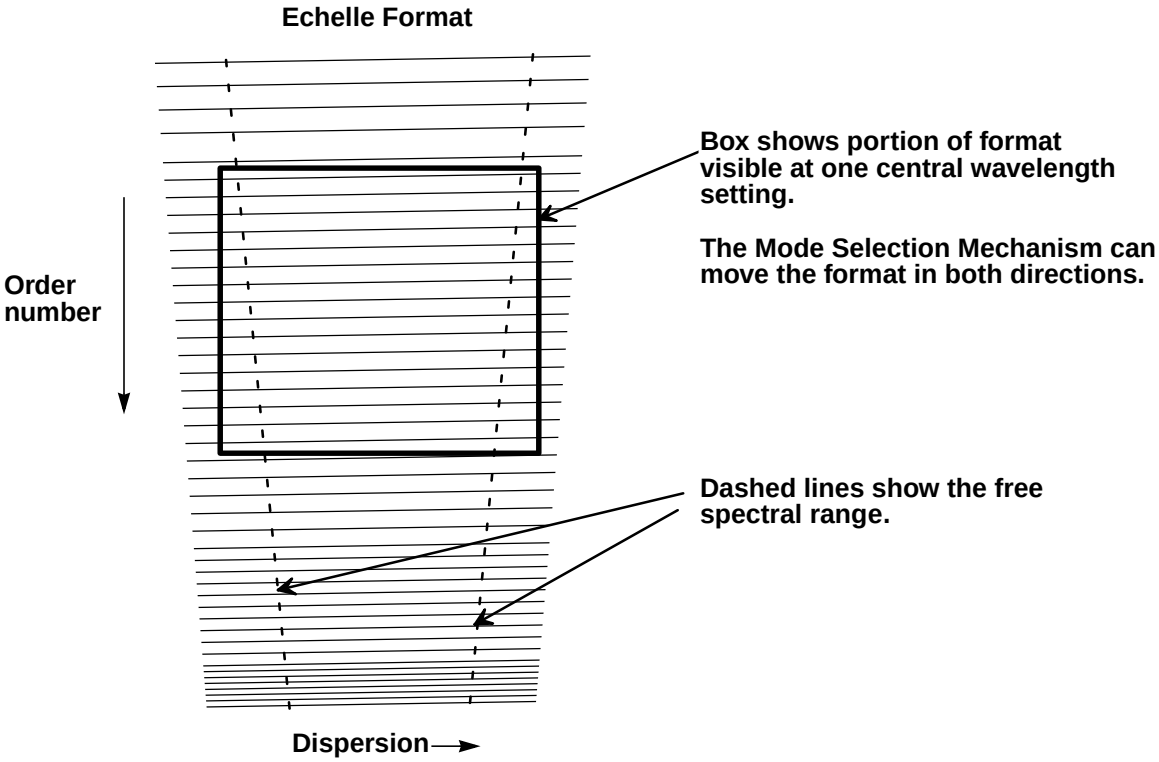

Cross-Over Regions

In the near UV, where the CCD has comparable sensitivity to the NUV-MAMA, you may want to consider using the G230LB or G230MB gratings with the CCD instead of the more standard G230L and G230M gratings with the MAMA. You will get improved throughput down to at least 2500 Å, a larger slit length, and use of the CCD rather than the MAMA (see Figure 4.3 and Chapter 13). On the other hand, the CCD has read noise, cosmic-ray sensitivity, and hot pixels. Also, for *red* objects scattered light can be more of a problem with the red-sensitive CCD than with the solar-insensitive NUV-MAMA.

First-Order Long-Slit Spectroscopy

STIS first-order mode long-slit spectroscopy has a wide range of applications from the near IR through the optical and into the ultraviolet. Figure 4.6 shows a recent result measuring the black hole mass in the nucleus of a nearby galaxy.

Figure 4.6: Greyscale Representation of STIS G750M 52X0.2 Long-Slit Spectrum of the nuclear region of M84, showing the velocity structure of the H alpha, [NII], and [SII] emission lines in the inner gaseous disk. The continuum has been subtracted from the data and they have been renormalized. (Figure courtesy of Gary Bower and Richard Green, see also Bower et al. 1997, in The 1997 HST Calibration Workshop Proceedings).

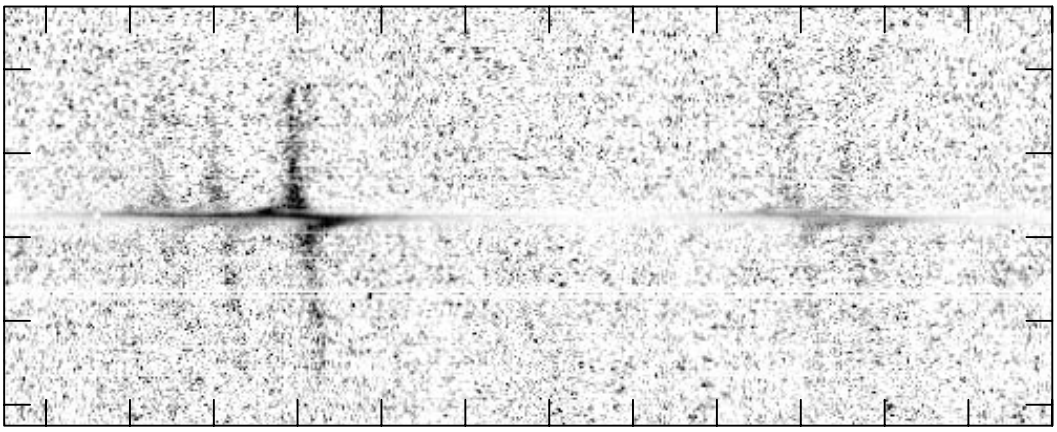

Gratings for First-Order Spectroscopy

There are 10 first-order gratings available for long-slit spectroscopy, providing resolving powers of ~500–17,000 from the UV at 1150 Å through the near IR at ~ 10,000 Å. The wavelength coverage and kinematic resolution of the first-order gratings are summarized in Figure 4.7. Briefly:

- For resolutions of ~500 km sec^{-1} use:
  - G140L at 1150–1700 Å.
  - G230L (MAMA) or G230LB (CCD) at 1600–3100 Å.
  - G430L at 2900–5700 Å.
  - G750L at 5250–10,300 Å.
- For resolutions of ~50 km sec^{-1} use:
  - G140M at 1150–1700 Å.
  - G230M (MAMA) or G230MB (CCD) at 1650–3100 Å.
  - G430M at 3050–5600 Å.
  - G750M at 5450–10,100 Å.

Figure 4.7: Wavelength Coverage Versus Kinematic Resolution of First-Order Modes. The hatches indicate the wavelength coverage at a single scan setting.

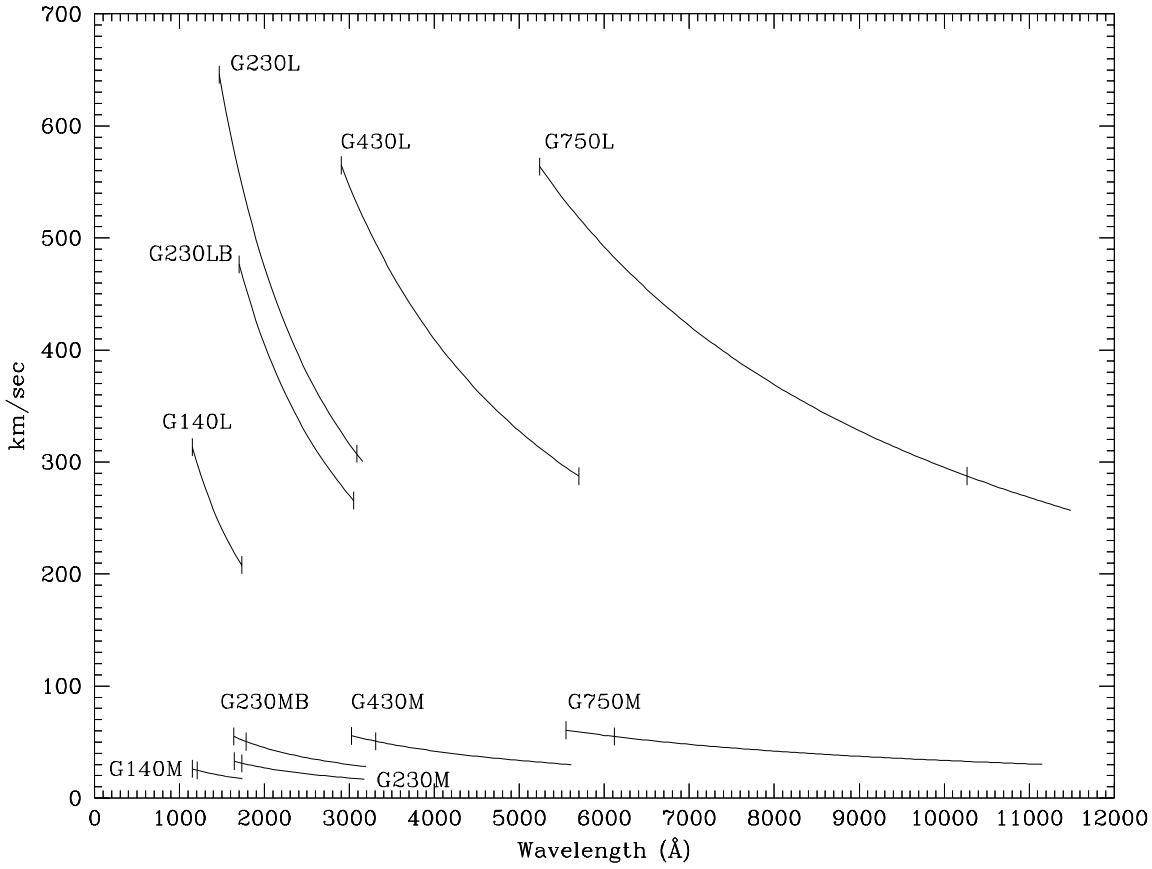

Slits for First-Order Spectroscopy

Supported for use with the first-order gratings are long slits of widths 0.05, 0.1, 0.2, 0.5, and 2.0 arcseconds (in the dispersion direction), and 52 arcsecond length (as projected on the CCD detector), or 25 arcsecond length (projected on the MAMA detectors) for the MAMA low-resolution, first-order gratings (G230L and G140L) and 28 arcsecond length for the MAMA intermediate-resolution, first-order gratings (G230M and G140M).[1] Note that the 0.1 arcsecond width matches the 2 pixel resolution of the CCD, while the 0.05 arcsecond width does so for the MAMAs providing maximum spectral resolution. The narrow 0.05 arcsecond-wide slit provides the maximum spectral and spatial resolution. The 0.2 arcsecond-wide slit is the general utility slit used most often; it provides a good compromise between resolution and throughput. Programs requiring accurate absorption-line measurements in continuum sources should always use slits of widths ≤0.2 arcsecond, since for larger apertures the spectral purity is significantly degraded by the telescope plus instrumental PSF; see “Spectral Purity, Order

1. The MAMA first-order modes have varying spatial plate scales; see Chapter 13.

Confusion, and Peculiarities” on page 304. Finally, we expect the wider 0.5 and 2.0 arcsecond-wide slits to be used predominantly in photon-starved ultraviolet observations of extended sources, but provide them for use in the optical as well to assure that line-ratio studies with coverage from the ultraviolet to the optical can sample the same physical region on the sky. Additionally, they are the most photometric slits as their throughput is least affected by centering and telescope breathing. Of course, observations of *extended* sources with wide slits will have correspondingly degraded spectral resolutions.

The first-order gratings can also be used “slitless” to obtain two-dimensional objective grating spectra of targets, or pseudo “images.” Slitless spectroscopic data will not be fully calibrated by the STScI pipeline, and it will require directed post-observation data processing by the user, as ambiguous overlap of wavelengths from different parts of sources can occur in the image (see “Slitless First-Order Spectroscopy” on page 199). Figure 4.8 shows an example of the use of the `52X2` slit with the `G750M` to obtain such a series of emission line images of SN1987A.

Figure 4.8: STIS G750M 6581 Å 52X2 Spectral Image of SN1987A. This shows the images of the inner circumstellar ring in H alpha, and NII Diffuse H alpha emission from the LMC fills the 52X2 arcsecond slit. The image shown is a 950 x 450 subsection of the 1024 x 1024 image. Figure courtesy of (Jason Pun and George Sonnenborn, see also Sonneborn et al. 1998, ApJ, 492, L139).

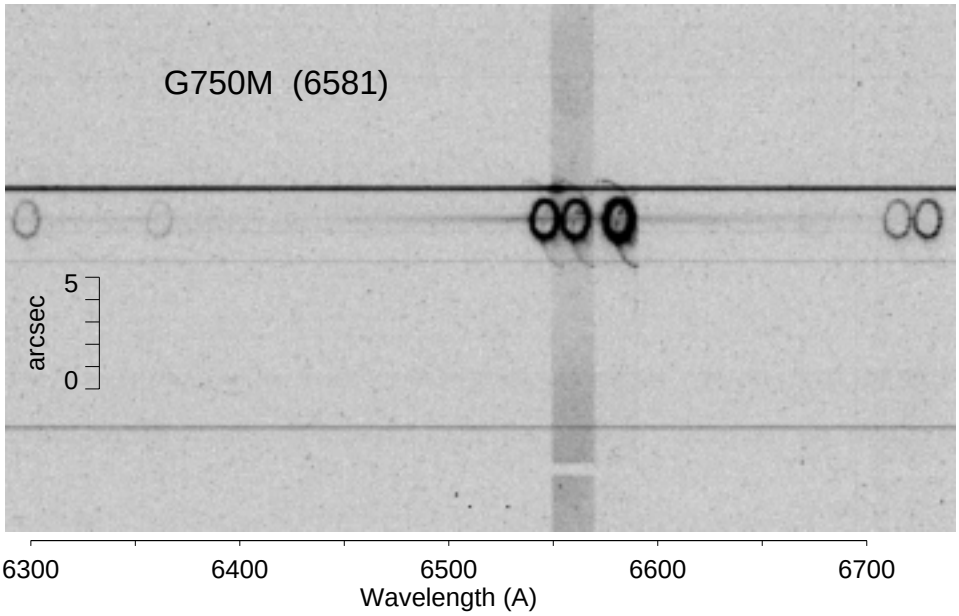

Note that for the FUV-MAMA first-order modes, the projection of the spectrum on the detector has deliberately been shifted 120 pixels or 3 arcseconds off of center to avoid having the spectrum fall on the shadow of the repeller wire (see also “MAMA Spectral Offsetting” on page 115 and “MAMA ACCUM Mode” on page 181). This shift applies to all data taken with the G140L and G140M grating, regardless of the aperture used.

Note also the MAMA monthly charge offsetting which can additionally shift the projection of the spectrum on the detector by ~ ±80 in `AXIS2` pixels in a given month. This latter shifting applies to all MAMA modes (see “MAMA ACCUM Mode” on page 181).

Detailed First-Order Spectroscopic Information

The properties of each of the first-order gratings are described in detail, grating by grating, in Chapter 13; see the second-to-last column of Table 4.1 on page 34 for easy reference to the appropriate page for each grating.

The detailed properties of the long slits (e.g., throughputs and line-spread functions as functions of wavelength), plate scales, and encircled energies for the first-order gratings are presented under “Apertures” on page 277, cross dispersion profiles on page 293, and line-spread functions on page 299.

Echelle Spectroscopy in the Ultraviolet

An example of STIS E230H echelle spectroscopy (both the echellogram and a few sample extracted orders) of star CPD-59D2603 showing the interstellar absorption from the Carina Nebula is shown in Figure 15.3 on page 377.

Echelle Gratings

There are four echelle grating modes, providing spectroscopic coverage from 1150 Å to 3100 Å at resolutions from R~30,000 to R~110,000. Through simultaneous observation of multiple orders, they are designed to maximize the spectral coverage achieved in a single exposure of a point source. Figure 4.9 summarizes the wavelength coverage and kinematic resolutions of the echelle gratings. In short:

- For ~10 km sec^{-1} resolution use:
  - E140M at 1150–1700 Å.
  - E230M at 1600–3100 Å.
- For ~2.5 km sec^{-1} resolution use:
  - E140H at 1150–1700 Å.
  - E230H at 1600–3100 Å.

Figure 4.9: Echelle Wavelength Coverage Versus Kinematic Resolution. Hatches indicate wavelength coverage at a single scan setting.

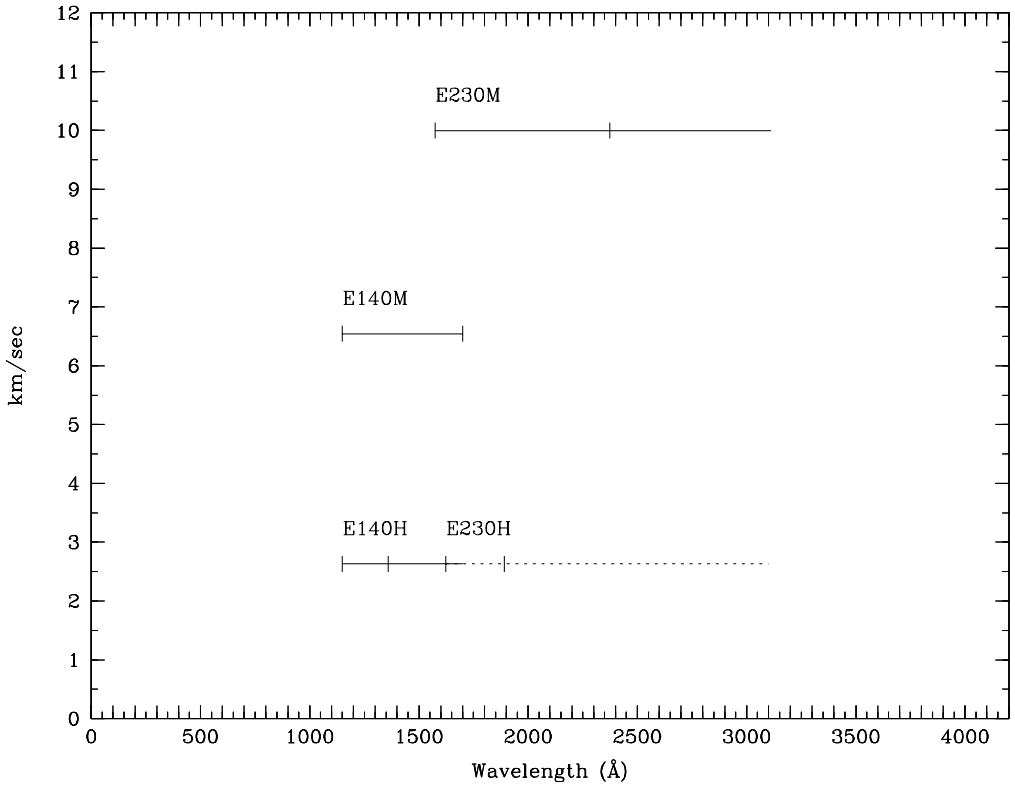

Slits for Echelle Spectroscopy

Short echelle slits, which ensure order separation, are available for use with the echelle gratings. For each mode a short slit of width 0.2 arcsecond is provided, along with a slit whose width matches two pixels in the dispersion direction, either 0.09 arcsecond for the H modes, or 0.06 arcsecond for the M modes. In addition, an ultra-narrow slit of width 0.025 arcsecond (`0.1X0.03` in the Proposal Instructions) is supported with all of the echelles, for the highest spectral resolution of bright objects. Also, two multislits with different widths (called the `FP-SPLIT` slits) are supported with the echelles for optimally placed multiple exposures to maximize S/N; their use is discussed in Chapter 12.

Although we don't recommend routine use, the echelle gratings can be used with a long slit (6 x 0.2 arcseconds) to obtain echelle spectroscopy of extended objects with weak continua. Long-slit echelle spectroscopy is more complicated, as order overlap will occur. Long-slit echelle data will not be calibrated by the STScI pipeline, and they will require more extensive post-observation processing by the user since ambiguous overlap of wavelengths from different parts of sources will occur in the image (see "Long-Slit Echelle Spectroscopy" on page 201 if you are considering such observations). In addition to the

spectral-purity considerations in the dispersion direction mentioned above for the first-order gratings, echelle observations are subject to contamination across the dispersion by the PSFs of adjacent orders. This effect is aggravated toward shorter wavelengths as the orders become more crowded. Continuum sources should never be observed with slit lengths greater than 0.2 arcsecond, and even then special data analysis may be required to optimize the accuracy of the results. See “Spectral Purity, Order Confusion, and Peculiarities” on page 304.

Detailed Echelle Information

The properties of each of the echelle gratings are described in detail, grating by grating, in Chapter 13; see the second-to-last column of Table 4.1 on page 34 for easy reference to the appropriate page for each grating.

The detailed properties of the echelle slits (e.g., throughputs and line-spread functions as functions of wavelength), the plate scales, and the encircled energies for the echelle modes are presented under “Apertures” on page 277, “Spatial Profiles” on page 293, and “Line-Spread Functions” on page 299.

Objective-Prism Spectroscopy

The STIS `PRISM` is used with the `STIS/NUV-MAMA` and provides spectrograms from 1150 to 3100 Å at resolving powers of ~500 in the ultraviolet declining to ~10 in the optical. A highly idealized schematic of a STIS objective-prism observation of a star cluster is shown in Figure 4.10. This example illustrates the power of the prism mode to simultaneously provide spectrograms covering a wide wavelength range of many objects in a single field of view.

Figure 4.10: Schematic Example of a PRISM Image of a Star Cluster

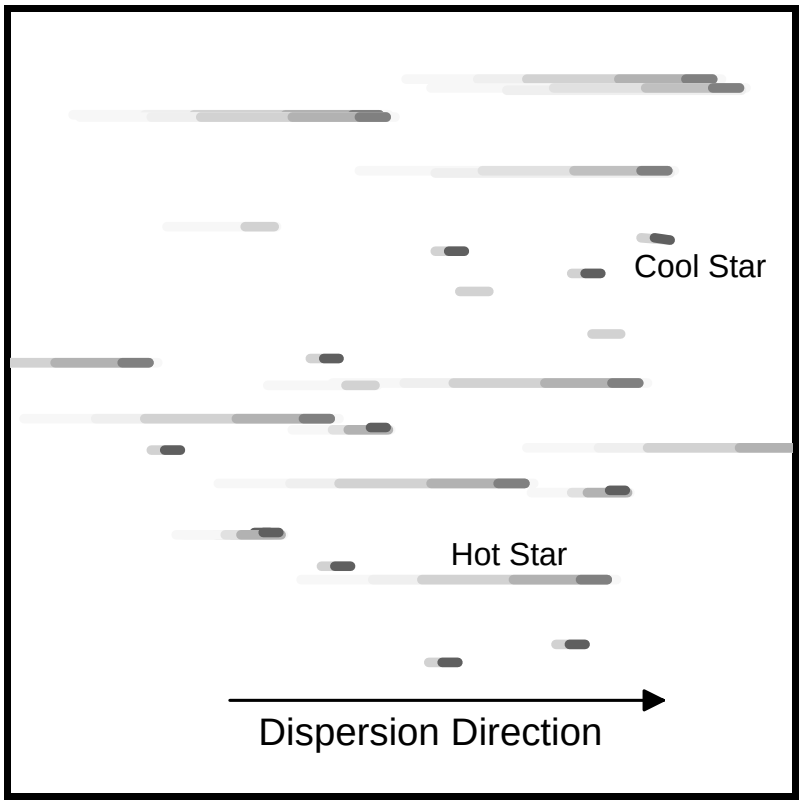

The PRISM can be used with the clear MAMA aperture (25MAMA) or with either longpass ultraviolet filtered aperture (F25SRF2 or F25QTZ) to provide a 25 x 25 arcsecond field of view (see also “F25SRF2—NUV-MAMA, Longpass” on page 338 and “F25QTZ—NUV-MAMA, Longpass” on page 335). The longpass filter F25SRF2 blocks geocoronal Lyman-α 1216 Å and the F25QTZ longpass filter blocks both geocoronal Lyman-α and geocoronal O I 1302 Å, significantly reducing the background from these lines (which is otherwise spread throughout the image), at the price of losing the short-wavelength range of the spectrum. In addition, the neutral-density filters (Table 5.1) are supported for PRISM spectroscopy, as are the 52X0.05 and 52X0.2 long slits.

Observers will generally want to obtain a *direct image* of the field they are taking a prism image of, so they can later determine the centering of the objects in their prism data. Because the PRISM and the mirrors used for imaging are both in the Mode Selection Mechanism, zero-point shifts will occur between the PRISM and direct data (see “Slit and Grating Wheels” on page 23). These shifts can be corrected for by means of a wavecal image of a short slit with the mirror in place. For Phase I planning purposes, prospective GOs should allot the additional time for the direct image plus an additional 5 minutes’ overhead for this extra zero-point wavecal image. Phase II examples providing information about how to assure that the proper calibration is obtained for this mode will be provided during Phase II.

Note that PRISM spectroscopy produces images in which, a priori, the wavelength at a given pixel is not known, and in which source-dependent overlap of spectrograms can occur. For these reasons, PRISM spectroscopic data will not be calibrated automatically by the STScI pipeline. Instead, users will have to reduce and analyze their data off-line.

CHAPTER 5
Imaging

In This Chapter...

In this chapter we describe the imaging capabilities of STIS. Each imaging mode is described, and plots of throughput and comparisons to the capabilities of WFPC2 are provided. (Signal-to-noise comparisons to WFPC2 ensure the use of the WF chips.) Curves of sensitivity and exposure time as a function of source brightness to achieve a given signal-to-noise ratio are referenced in this chapter, but presented in Chapter 14. We note the existence of bright-object observing limits for MAMA imaging modes; these are described in detail in Chapter 7, and tables of the MAMA imaging bright-object screening magnitudes as a function of mode and spectral type are presented in Chapter 14.

Imaging Overview

STIS can be used to obtain images in undispersed light in the optical and ultraviolet. When STIS is used in imaging mode, the appropriate clear or filtered aperture on the slit wheel is rotated into position, and a mirror on the Mode-Selection Mechanism is moved into position (see Figure 3.1 on page 23).

Table 5.1 below provides a complete summary of the clear and filtered apertures available for imaging with each detector. In Figures 5.1 through 5.4 we show the integrated system throughputs.

Table 5.1: STIS Imaging Capabilities

Aperture Name	Filter	Central Wavelength (λ_c in Å)	FWHM ($\Delta\lambda$ in Å)	Field of View (arcsec)	Detector	reference material page
		Visible - plate scale ~0.05 arcseconds per pixel				
50CCD	Clear	5850	4410	52 x 52	STIS/CCD	319
F28X50LP	Optical longpass	7230	2720	28 x 52[a]	STIS/CCD	322
F28X50OIII	[O III]	5007	5	28 x 52[a]	STIS/CCD	325
F28X50OII	[O II]	3740	80	28 x 52[a]	STIS/CCD	328
50CORON	Clear + coronographic fingers	5850	4410	52 x 52	STIS/CCD	331
		Ultraviolet - plate scale ~0.024 arcseconds per pixel				
25MAMA	Clear	2220	1200	25 x 25	STIS/NUV-MAMA	332
		1370	320		STIS/FUV-MAMA	352
F25QTZ	UV near longpass	2320	1010	25 x 25	STIS/NUV-MAMA	335
		1590	220		STIS/FUV-MAMA	354
F25SRF2	UV far longpass	2270	1110	25 x 25	STIS/NUV-MAMA	338
		1480	280		STIS/FUV-MAMA	358
F25MGII	Mg II	2800	70	25 x 25	STIS/NUV-MAMA	340
F25CN270	Continuum near 2700 Å	2700	350	25 x 25	STIS/NUV-MAMA	343
F25CIII	C III]	1909	70	25 x 25	STIS/NUV-MAMA	346
F25CN182	Continuum near 1800 Å	1820	350	25 x 25	STIS/NUV-MAMA	349
F25LYA	Lyman-α	1216	85	25 x 25	STIS/FUV-MAMA	361
		Neutral-Density-Filtered Imaging				
F25NDQ1	Neutral-density filter, ND=10^{-1}	1150–10,300 Å		12 x 12	CCD, NUV-MAMA, FUV-MAMA	67
F25NDQ2	Neutral-density filter, ND=10^{-2}			12 x 12		
F25NDQ3	Neutral-density filter, ND=10^{-3}			12 x 12		
F25NDQ4	Neutral-density filter, ND=10^{-4}			12 x 12		
F25ND3	Neutral-density filter, ND=10^{-3}	1150–10,300 Å		25 x 25		
F25ND5	Neutral-density filter, ND=10^{-6}	1150–10,300 Å		25 x 25		

a. The dimensions are 28 arcsec on AXIS2=Y and 52 arcsec on AXIS1=X. See Figure 3.2 and Figure 11.1.

Why Image With STIS?

Despite its limited complement of filters, STIS brings four valuable imaging capabilities to HST:

- The STIS CCD detector, although it covers a much smaller field of view (51 x 51 arcsec) than the WFPC2, has higher throughput over a much wider range of the spectrum (2000–11,000 Å) than does WFPC2. The STIS CCD also has a low read noise and dark current; thus STIS CCD observations with the clear aperture have significantly higher sensitivity to faint sources than WFPC2 (see Figure 5.5 on page 57). The STIS CCD clear imaging mode is scientifically useful when no color information is needed, for example, for finding faint variable sources, or imaging the faintest possible sources in a given integration time.
- The wings of the point-spread function in the STIS CCD imaging modes are suppressed by an internal Lyot stop. This feature provides a significant advantage over WFPC2 for detecting faint sources near much brighter sources.
- The STIS MAMA detectors enable true solar-blind imaging from 1150 to 1700 Å using the FUV-MAMA with a considerably higher throughput than WFPC2. The NUV-MAMA is also relatively insensitive to red light and has high relative throughput. Both provide near critical sampling of the PSF (0.024 arcsecond per pixel). See “Unfiltered (Clear) MAMA Imaging—25MAMA” on page 62.
- The STIS MAMA detectors enable very high time resolution (τ ~125 microseconds) imaging in the ultraviolet, by means of `TIME-TAG` mode.

Caveats For STIS Imaging

There are several important points about imaging with STIS which should be kept in mind:

- The filters are housed in the slit wheel, and while they are displaced from the focal plane, they are not far out of focus. This location means that imperfections (e.g., scratches, pinholes, etc.) in the filters cause artifacts in the images. These features do not directly flat-field out because the projection of the focal plane on the detector shifts from image to image due to the nonrepeatability of the Mode Selection Mechanism’s placement of the mirror (careful post-processing may be able to account for registration errors).
- Accurate across-the-detector photometric calibration of the imaging modes requires mapping of the two-dimensional illumination pattern of the sky; for the MAMAs this is a time-intensive process, which will limit the photometric accuracy obtained (see “Summary of Accuracies” on page 379).
- The focus varies across the field of view for imaging modes, with the optical performance degrading by ~30% at the edges of the field of view for MAMA imaging and less so for the CCD (see “Spatial Dependence of the STIS PSF” on page 365).

- Two of the STIS narrowband filters (F28X50OIII and F25MGII) have substantial red leaks (see Figure 5.7 and Figure 5.12, respectively).
- Relative to WFPC2, a STIS CCD image will have a slightly larger proportion of the pixels affected by cosmic rays and "hot" dark current.
- Programs requiring high photometric precision with the CCD should use GAIN=1. At GAIN=4 the CCD exhibits a read-noise pattern that is correlated on scales of tens of pixels. (See "Analog-To-Digital Conversion" on page 101.)
- At wavelengths longward of ~900 nm, internal scattering in the STIS CCD produces an extended PSF halo (see "Optical Performance" on page 99).
- The dark current in the MAMA detectors varies with time, and in the FUV-MAMA, it also varies strongly with position, although it is far lower overall than in the NUV-MAMA (see the discussion of MAMA darks in Chapter 7).
- The repeller wire in the FUV-MAMA detector (see page 107 in Chapter 7) leaves a 5 pixel wide shadow that runs from pixel 0,543 to 1024,563 in a slightly curved line.

These caveats are not intended to discourage observers from using STIS for imaging; indeed, for many imaging projects, particularly those not requiring a large field of view or the range of filters provided by WFPC2, STIS may be the best choice.

Dithering strategies to cope with flat-field variations and other detector nonuniformities are discussed in Chapter 11 (page 177).

Throughputs and Limiting Magnitudes

In Figure 5.1 below, we show the throughput (where the throughput is defined as the end-to-end effective area divided by the geometric area of a filled (unobstructed) 2.4 meter aperture) of the three STIS clear imaging modes, with the CCD, the NUV-MAMA, and the FUV-MAMA. Superposed on this plot, we show the broadband WFPC2 throughputs. In Figures 5.2, 5.3, and 5.4 below, we show the throughputs of the full set of available filters for the CCD, the NUV-MAMA, and the FUV-MAMA, respectively.

Figure 5.1: STIS's Clear Imaging Throughputs Versus WFPC2

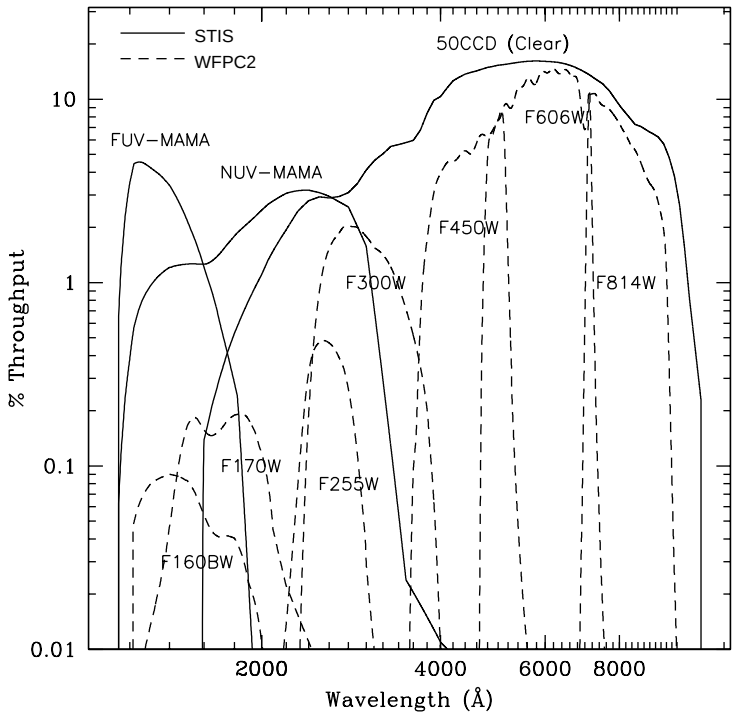

Figure 5.2: STIS's CCD Clear and Filtered Imaging Mode Throughputs

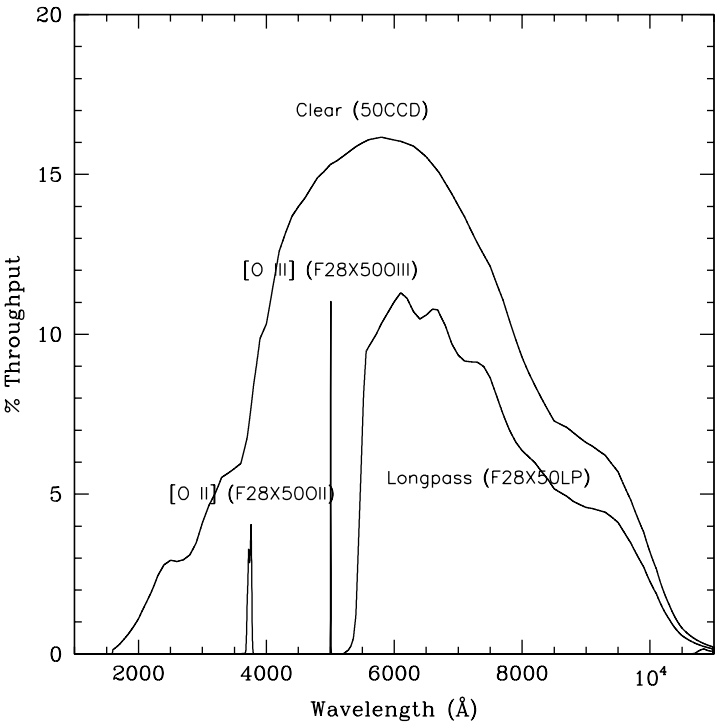

Figure 5.3: STIS's NUV-MAMA Clear and Filtered Imaging Mode Throughputs

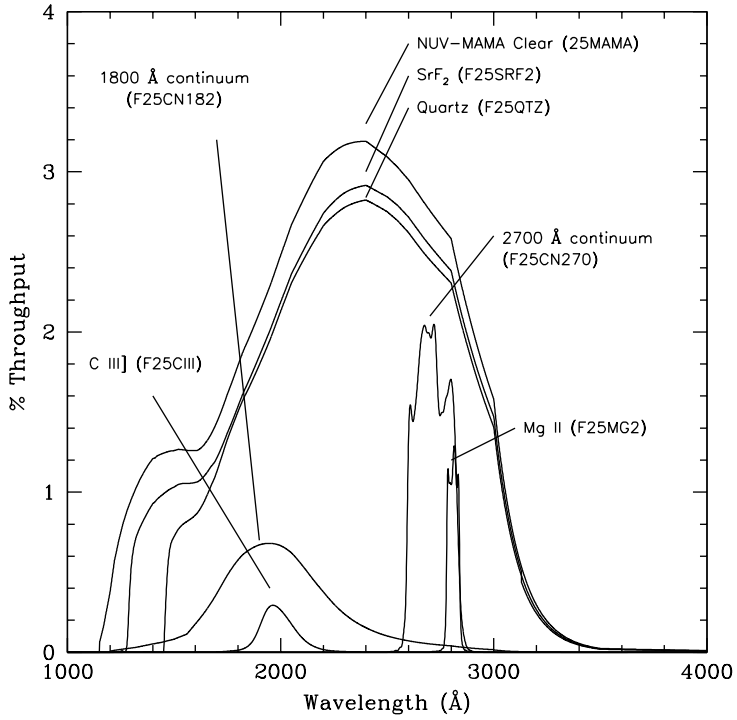

Figure 5.4: STIS's FUV-MAMA Clear and Filtered Imaging Mode Throughputs

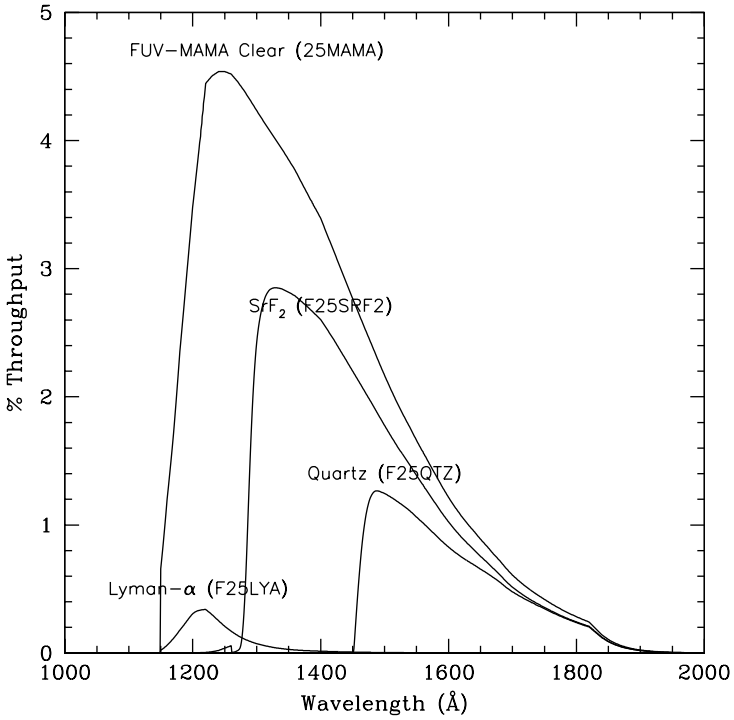

Limiting Magnitudes

In Table 5.2 below, we give the A0 V star V magnitude reached during a one-hour integration which produces a signal-to-noise ratio of 10 integrated over the number of pixels needed to encircle 80% of the PSF flux. The observations are assumed to take place in SHADOW, with average zodiacal background.

Table 5.2: Limiting A Star V Magnitudes

Detector	Filter	Magnitude	Filter	Magnitude
CCD	Clear	27.7	[O II]	21.9
CCD	Longpass	26.7	[O III]	21.2
NUV-MAMA	Clear	24.3		
NUV-MAMA	Longpass quartz	24.3	Longpass SrF_2	24.3
NUV-MAMA	C III]	20.1	1800 Å continuum	22.2
NUV-MAMA	Mg II	20.3	2700 Å continuum	22.2
FUV-MAMA	Clear	21.4	Lyman-α	16.8
FUV-MAMA	Longpass quartz	22.7	Longpass SrF_2	23.3

Signal-To-Noise Ratios

In Chapter 14 we present, for each imaging mode, plots of exposure time versus magnitude to achieve a desired signal-to-noise ratio. These plots, which are referenced in the individual imaging-mode sections below, are useful for getting an idea of the exposure time you need to accomplish your scientific objectives.

Saturation

Both CCD and MAMA imaging observations are subject to saturation at high total accumulated counts per pixel: the CCD due to the depth of the full well, and the MAMA, due to the 16-bit format of the buffer memory (see “CCD Saturation: the CCD Full Well” on page 102 and“MAMA Saturation—Overflowing the 16 Bit Buffer” on page 110). In Chapter 14, saturation levels as functions of source magnitude and exposure time are presented in the S/N plots for each imaging mode.

Optical CCD Imaging

The CCD imaging capability of STIS was designed primarily for target acquisitions, and therefore, only a small number of filters are available. Nevertheless, STIS CCD imaging has scientific utility of its own, due to the high throughput and relatively low read noise of the CCD detector. STIS CCD imaging

can be obtained as prime pointings or in parallel with other instruments. In each filter section below, we include comparisons to the existing WFPC2 imaging capabilities (you should keep in mind, of course, that the WFPC2 field of view covers roughly eight times more sky area than the STIS CCD).

The optical performance of the CCD in image mode is good and the plate scale of the CCD is ~0.05 arcsecond per pixel, providing a good compromise between sampling of the PSF and field of view. There is some degradation of the image quality towards the edge of the field. Observers can assume that 15 to 20% of the light from a point source falls in a single STIS CCD pixel and that ~80% of the light from a point source is contained within a 5 x 5 pixel region. See Chapter 14 for encircled energies at the field center for the different imaging modes and information on the field dependence of the PSF.

The throughputs used for the CCD imaging modes are for the most part based on pre-flight measurements. Preliminary analysis of Cycle 7 calibration data indicates that the throughputs are accurate to within 5% for the `50CCD` mode, and to within 10% for the narrowband filters. The throughput of the `F28X50LP` mode measured in orbit was 0.77 times the ground-test measurement. The throughputs in this Handbook have been updated to reflect this change, and are accurate to within 10% uncertainty.

Unfiltered (Clear) CCD Imaging—50CCD

The `50CCD` aperture is a clear, unvignetted aperture which provides maximum sensitivity over the full 52 x 52 arcsecond field of view. The shape of the bandpass is governed by the detector, which has sensitivity from ~2000 to 11,000 Å. Figure 5.1 on page 53 shows the throughput as a function of wavelength for this imaging mode (see also page 319 for sensitivities, and signal-to-noise and saturation plots).

Figure 5.5 shows a plot of time to achieve a signal-to-noise ratio of 5 for this aperture, with results for the WFPC2 broadband filter modes superposed, assuming an A0 V star spectrum for the source. If color information and a wide field of view are not required, then there is a clear advantage of this imaging mode over the WFPC2.

Figure 12.5 on page 214 shows an example of a deep CCD image of a random field taken as part of the Archival Pure Parallel Program.

Figure 5.5: Comparison of STIS 50CCD Imaging with WFPC2. The plot shows the limiting V magnitude for an A0 V star at a signal-to-noise ratio of 5 versus exposure time. STIS F28X50LP is nearly identical to WFPC2 F814W in this plot.

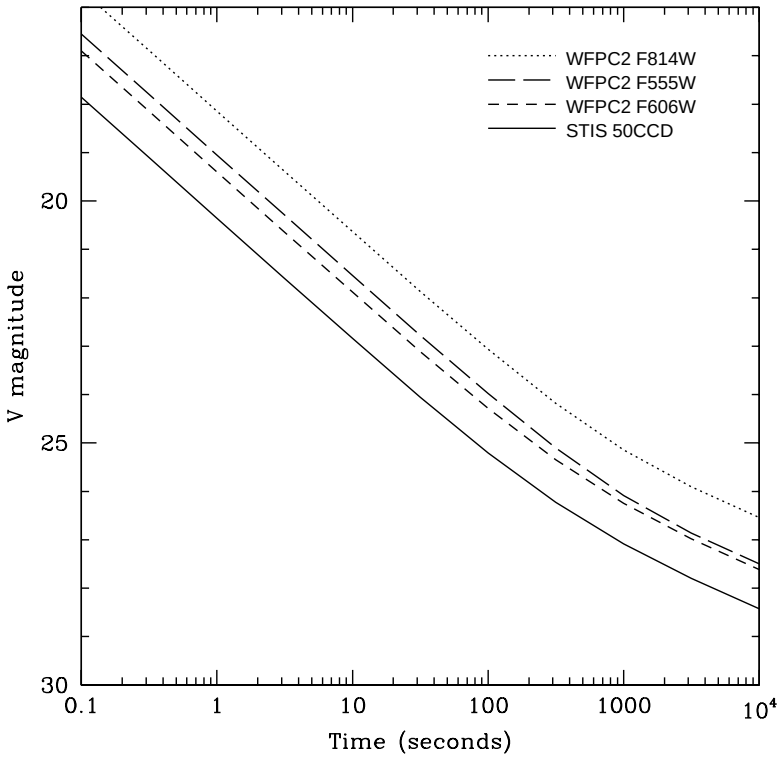

Optical Longpass—F28X50LP

STIS's longpass filter cuts off at $\lambda < 5500$ Å. It images a 28 x 52 arcsecond field of view. The `F28X50LP` filter is the principal target-acquisition aperture (see "Selecting the Imaging Aperture" on page 134). The integrated system throughput for this filter is given in Figure 5.2 on page 53 (see also page 322 for sensitivities, and signal-to-noise and saturation plots).

The combination of `50CCD` and `F28X50LP` can provide deep imaging with sufficient color information for some types of color-magnitude diagrams.

[O III]—F28X50OIII

This filter images a 28 x 50 arcsecond field of view and can be used in target acquisitions or for direct imaging in the light of [O III]. The [O III] filter integrated system throughput and a signal-to-noise comparison with the WFPC2 [O III] filter are shown in Figure 5.6 (see also page 325 for sensitivities, and signal-to-noise and saturation plots). The STIS [O III] filter is very narrow: only 5 Å wide, compared to the WFPC2 [O III] filter which is roughly 30 Å wide. The STIS filter has a substantial red leak that begins at 10,600 Å and continues to at least 12,000 Å. In the case of a very red star (K0 spectral type), the red leak will

contribute approximately one third of the detected counts. The red leak for this filter is included in the passbands used by the STIS Exposure Time Calculator (ETC) and **synphot**. Observers are encouraged to use these tools to predict source and background count rates carefully.

Figure 5.6: F28X50OIII: (a) Integrated System Throughput and (b) Flux vs. Exposure Time to achieve a signal-to-noise=5 compared to WFPC2 for a FWHM=1 Å line, integrated over an area of one square arcsecond.

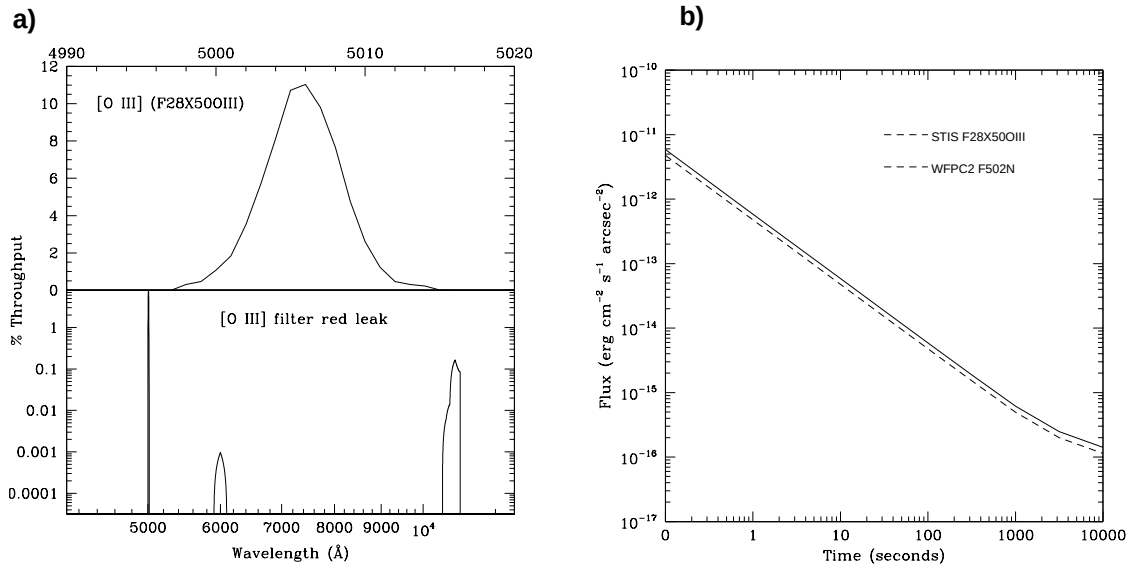

Figure 5.7: F28X50OII: (a) Integrated System Throughput and (b) Flux vs. Exposure Time to achieve a signal-to-noise=5 compared to WFPC2 for a FWHM=1 Å line, integrated over an area of one square arcsecond.

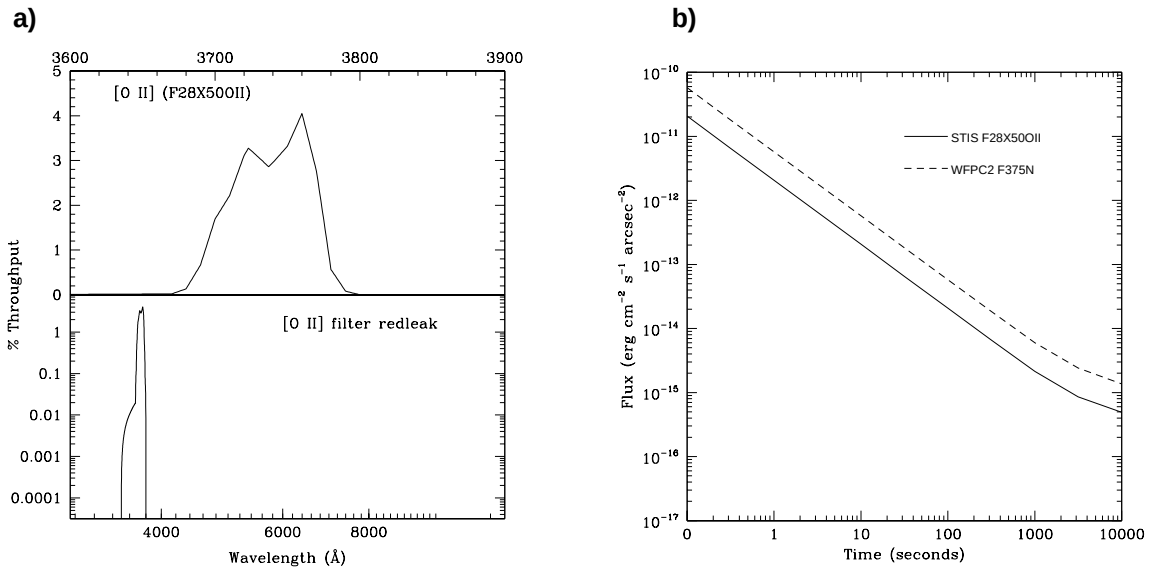

[O II]—F28X50OII

The [O II] filter images a 28 x 52 arcsecond field of view and can be used in target acquisitions or for direct imaging in the light of [O II]. The [O II] filter integrated system throughput and a signal-to-noise ratio comparison with WFPC2's [O II] filter are shown in Figure 5.7 (see also page 328 for sensitivities, and signal-to-noise and saturation plots).

Coronographic Imaging—50CORON

The coronographic mask (see Figure 12.7 on page 216) comprises a pair of crossed wedges and one finger at the edge of the field of view. The mask resides in the slit wheel and provides a clear (unfiltered) coronographic imaging capability. See "Unfiltered (Clear) CCD Imaging—50CCD" on page 56 for the spectral properties of the images obtained. A number of locations on the occulting masks have been specified, to correspond to widths of 2.75, 2.5, 2.0, 1.75 and 1.0 arseconds on each wedge. See "Coronographic Imaging and Spectroscopy" on page 215 for more information about the use of the coronographic aperture.

Below in Figure 5.8 we provide a comparison of the PSF suppression provided by STIS coronographic imaging relative to WFPC2 imaging and the Optical Telescope Assembly scatter. We do not have comparable PSF data for the direct (e.g., `50CCD`) imaging but we expect it to be similar to that shown for the coronograph. The optical only performance of STIS clear without the coronograph will be comparable to that with the coronograph, however without the coronograph, the CCD long wavelength halo from the central source and the window reflection ghosts will be present. We expect to update this plot to include comparison with the direct STIS PSF as well in the future and results will be posted to the WWW page. The inner limit to which the PSF is displayed was dictated by the particular data used.

Figure 5.8: Comparison of PSF Suppression: STIS Coronograph, WFPC2, and the Diffraction of the OTA

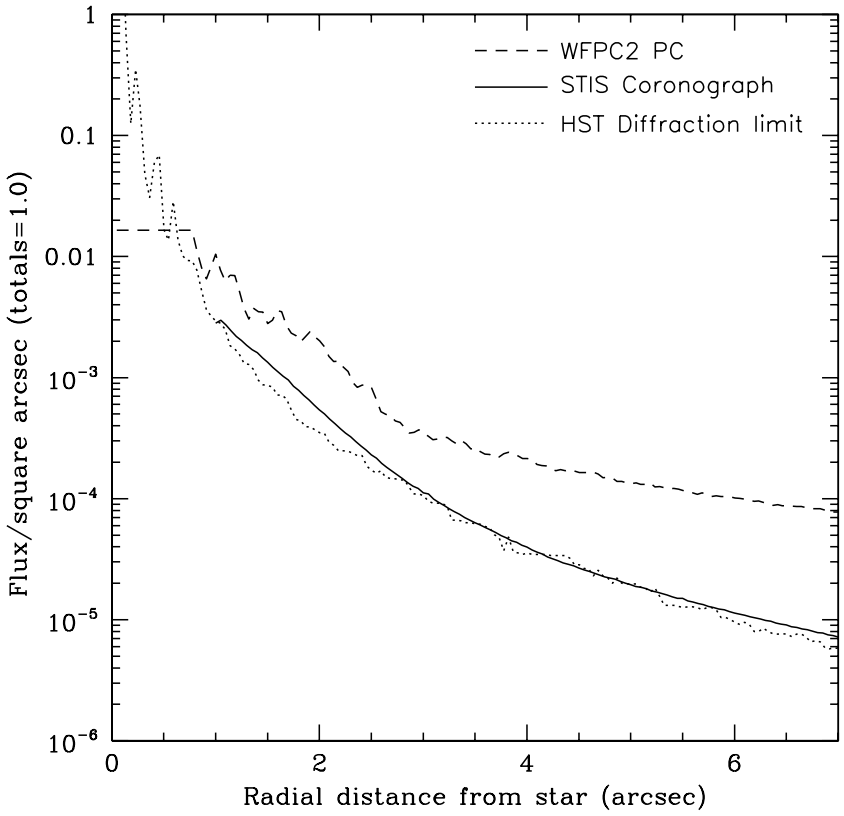

Ultraviolet Imaging with the MAMA Detectors

The filtered and clear apertures available for ultraviolet imaging are summarized in Table 5.1 on page 50. Although there are only a small number of filters available, the solar-blind and solar-insensitive properties of the FUV-MAMA and NUV-MAMA detectors, respectively, coupled with their 25 x 25 arcsecond field of view, good spatial sampling, and ability to detect rapid variability, make the STIS ultraviolet imaging capability unique to HST.

The throughputs of the STIS MAMA imaging modes in this Handbook are a hybrid of ground-test measurements and in orbit measurements. The transmission vs. wavelength of the filters was measured in the UV while in orbit and the curves in this Handbook use those measurements. The total system throughput depends as well on the detector quantum efficiency and the reflectivity of the imaging mode mirrors. These have not yet been updated. Preliminary analysis of Cycle 7 observations of spectrophotometric standards indicates that throughputs are good to within 5% in the FUV and 15% in the NUV. The throughputs in the ETC, the calibration reference files, and in the STSDAS **synphot** package will be updated when the analysis is complete.

Figure 5.9 shows an example of MAMA imaging data of cluster taken as part of the Cycle 7 calibration of STIS using the quartz filter and the NUV-MAMA.

Figure 5.9: 320 Second NUV-MAMA Image of NGC6681 Taken with the F25QTZ Filter as Part of the Cycle 7 Calibration Monitoring Program 7720. All the points are stars.

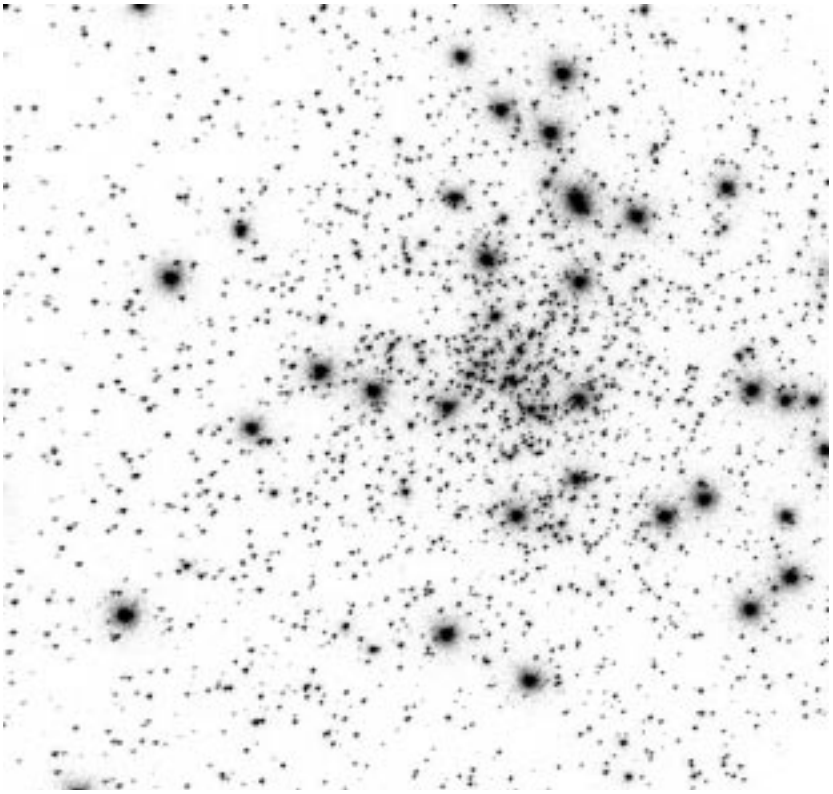

Bright-Object Limits

The MAMA detectors are subject to absolute bright-object limits, above which targets cannot be observed. They are particularly stringent for the MAMA imaging modes (being as faint as V=20.5 for the clear modes), and apply to all sources illuminating the field of view.

We direct MAMA observers to “MAMA Bright-Object Limits” on page 115. For summary tables of absolute bright-object screening magnitudes for the imaging modes, see “MAMA Imaging Bright Object Limits” on page 368.

It is the observers’ responsibility to ensure that their observations do not exceed the MAMA bright-object limits.

Optical Performance

The MAMA plate scale is ~0.024 arcsecond pixel^{-1} in image mode, providing a good compromise between sampling of the PSF in the ultraviolet and field of

view. Chapter 14 shows encircled energies as a function of wavelength for MAMA imaging. The MAMA detector PSFs exhibit broad wings, which are substantially higher in the NUV-MAMA than the FUV-MAMA. Figure 7.6 on page 110 shows sample detector PSFs for the MAMAs.

Unfiltered (Clear) MAMA Imaging—25MAMA

Each MAMA can be used with the 25MAMA clear aperture to image a 25 x 25 arcsecond field of view of the sky, providing the maximum throughput and wavelength coverage in the NUV and FUV as shown in Figure 5.1 on page 53. The FUV-MAMA quantum efficiency drops dramatically longward of ~3000 Å making it effectively solar blind, while the NUV-MAMA also has a reduced response toward the red, longward of ~3500 Å (see Figure 5.10 on page 63 below). Tables 5.3 and 5.4 give the percentages of detected photons arising in the UV versus optical for observations of different stellar types with the clear MAMA imaging modes. The red rejection of the MAMA detectors makes them well suited to UV imaging of red objects.

However, NUV-MAMA clear direct images will be slightly out of focus, because the corresponding mirror on the MSM optimally focuses for use of a filter. It is recommended that the F25SRF2 longpass filter (see next section) be used instead of 25MAMA (clear) for direct imaging with the NUV-MAMA. The same does not apply to the FUV-MAMA, which has separate MSM mirrors for clear and filtered imaging.

The sky background can be significant for unfiltered FUV-MAMA observations. The strongest contributor is the geocoronal Lyman-α line. Global count rates of several 10^4 counts per second over the whole detector are not unusual during daytime observations. The same applies to slitless far-UV spectroscopy. For observations of large, UV-faint targets, where background subtraction becomes critical, unfiltered imaging may introduce significant noise. In addition, the background may be variable during long exposures. Longpass filtered imaging may be profitable in this case.

Table 5.3: Visible-Light Rejection of the FUV-MAMA Clear Imaging Mode

Stellar Type	Percentage of all Detected Photons which have λ<1800 Å	Percentage of all Detected Photons which have λ<3000 Å
O5	99.5	100
B1 V	99.4	100
A0 V	98.1	100
G0 V	72.7	99.8
K0 V	35.1	94.4

Table 5.4: Visible-Light Rejection of the NUV-MAMA Clear Imaging Mode

Stellar Type	Percentage of all Detected Photons which have λ<3000 Å	Percentage of all Detected Photons which have λ<5000 Å
O5	98.1	100
B1 V	97.6	100
A0 V	94.3	99.9
G0 V	68.1	99.0
K0 V	56.4	97.6

Figure 5.10: Out-of-Band Spectral Responses of FUV- and NUV-MAMA Clear Imaging Modes.

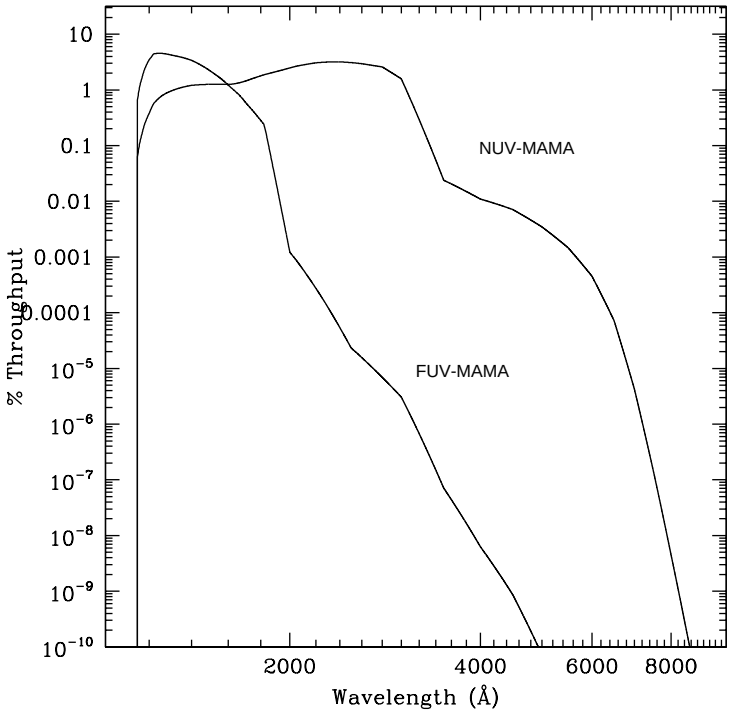

Longpass-Filtered MAMA Imaging—F25SRF2 and F25QTZ

The integrated system throughputs of the two UV longpass filters when used with the NUV-MAMA and FUV-MAMA are shown in Figure 5.4 on page 54 (see also Chapter 14 for sensitivities, and signal-to-noise and saturation plots). The filter (only) throughputs of these two filters are shown in Figure 5.11. These filters image a 25 x 25 arcsecond field of view. Their cutoff wavelengths were chosen to exclude geocoronal Lyman-α 1216 Å and O I 1302 + 1356 Å, respectively; use of

these filters significantly reduces the total sky background in the ultraviolet. These filters can be used by themselves in imaging mode, or with the prism or any first-order UV grating in slitless spectroscopic observations, to reduce the background due to geocoronal emission (see “Objective-Prism Spectroscopy” on page 46 and “Slitless First-Order Spectroscopy” on page 199). F25SRF2 images, combined with images taken in series with the FUV-MAMA/25MAMA clear, can also be used to obtain Lyman-α images (see “Lyman Alpha—F25LYA and Clear-minus-SRF2” on page 66).

Figure 5.11: F25SRF2 and F25QTZ Filter-Only Transmissions

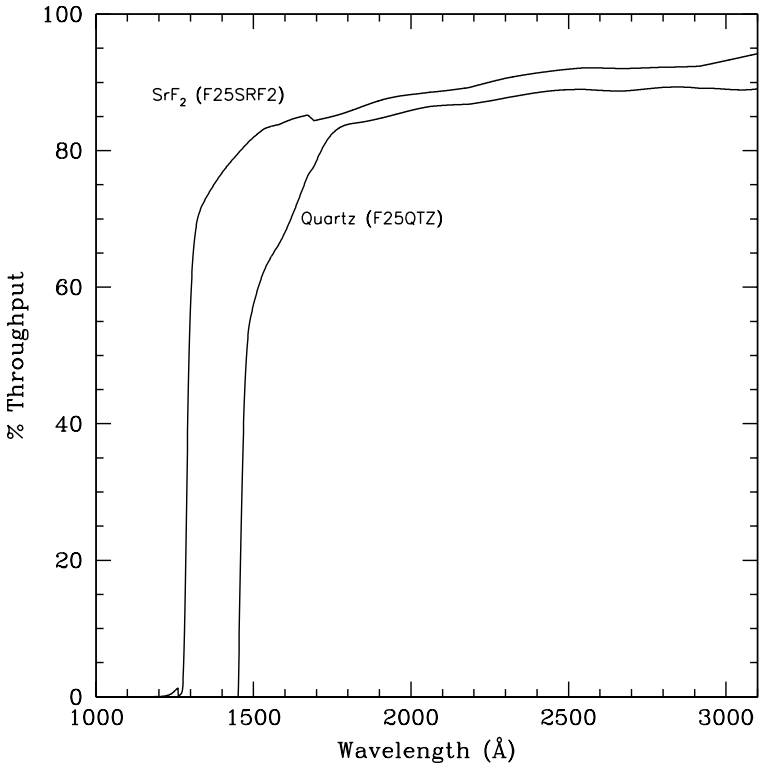

MAMA Narrowband-Filtered Imaging

The filters for MAMA imaging include:

- A narrowband filter (F25MGII) which images the magnesium doublet at 2796–2803 Å, and a matched mediumband continuum filter (F25CN270) centered at 2700 Å.
- A narrowband filter (F25CIII) which images the semi-forbidden C III] lines at 1906–1909 Å, among the strongest nebular (low-density) lines in the UV, and a matched mediumband continuum filter (F25CN182) centered at 1800 Å.

- A narrowband filter which images Lyman-α; this filter has an unusually poor throughput, and we recommend that you consider, instead, obtaining two FUV-MAMA images, one through the 25MAMA unfiltered aperture and a second with the SRF2 longpass filter. The difference of these two images will isolate Lyman-α with much higher throughput than the F25LYA filter.

Mg II—F25MGII

The F25MGII filter images a 25 x 25 arcsecond field of view in the light of the doublet lines of Mg II (2796 and 2803 Å). Figure 5.12 shows the integrated system throughput (see also page 340 for sensitivities, and signal-to-noise and saturation plots). There is a substantial red leak in this filter starting at approximately 4200 Å and extending to at least 13,000 Å. For stellar spectral types O and B less than 2% of the detected counts will be due to red leak. This percentage rises to 7% for an A0 star. For a K0 star, 75% of the counts will be due to red leak. The red leak for this filter is included in the passbands used by the STIS Exposure Time Calculator and **synphot**. Observers are encouraged to use these tools to predict source and background count rates carefully.

Figure 5.12: F25MGII and F25CN270 Integrated System Throughputs

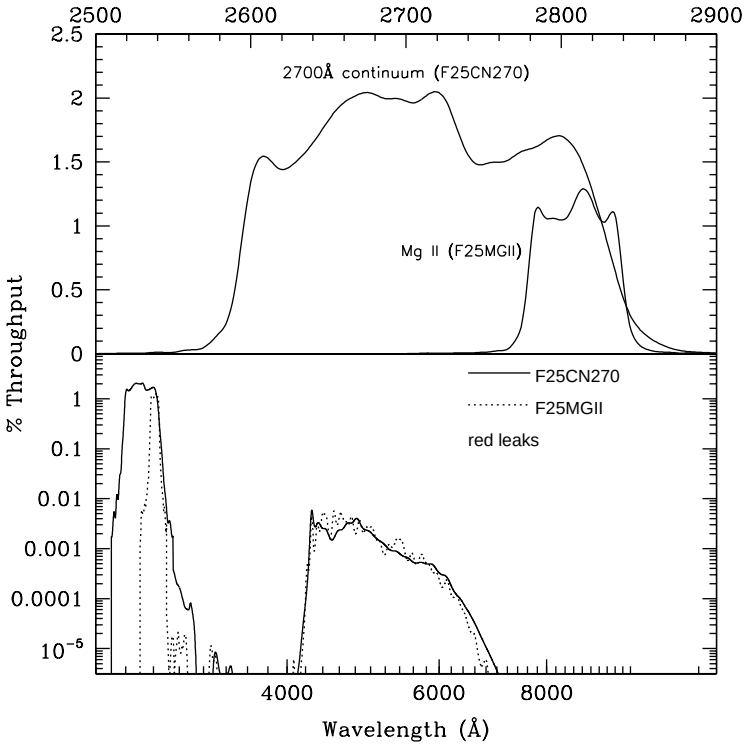

2700 Å Continuum—F25CN270

The 2700 Å continuum filter images a 25 x 25 arcsecond field of view and can be used to measure the continuum for Mg II emission-line images. The F25CN270 filter integrated system throughput is shown in Figure 5.12 above (see also page 343 for sensitivities, and signal-to-noise and saturation plots). There is a substantial red leak in this filter starting at approximately 4200 Å and extending to

at least 12,000 Å. For a K0 star, roughly 40% of the detected counts will be due to red leak. The red leak for this filter is included in the passbands used by the STIS Exposure Time Calculator and **synphot**. Observers are encouraged to use these tools to predict source and background count rates carefully.

C III]—F25CIII

The F25CIII filter images a 25 x 25 arcsecond field of view in the light of C III] at 1906–1909 Å. The F25CIII integrated system throughput is shown in Figure 5.13 (see also page 346 for sensitivities, and signal-to-noise and saturation plots). The out-of-band suppression for this filter is fairly good. The discontinuity in the C III] filter throughput in Figure 5.13 reflects the fact that the UV throughput comes from in orbit measurements and the optical throughput comes from ground testing. The optical throughputs of the UV filters will be measured during the course of Cycle 7 calibration.

Figure 5.13: F25CIII and F25CN182 Integrated System Throughputs

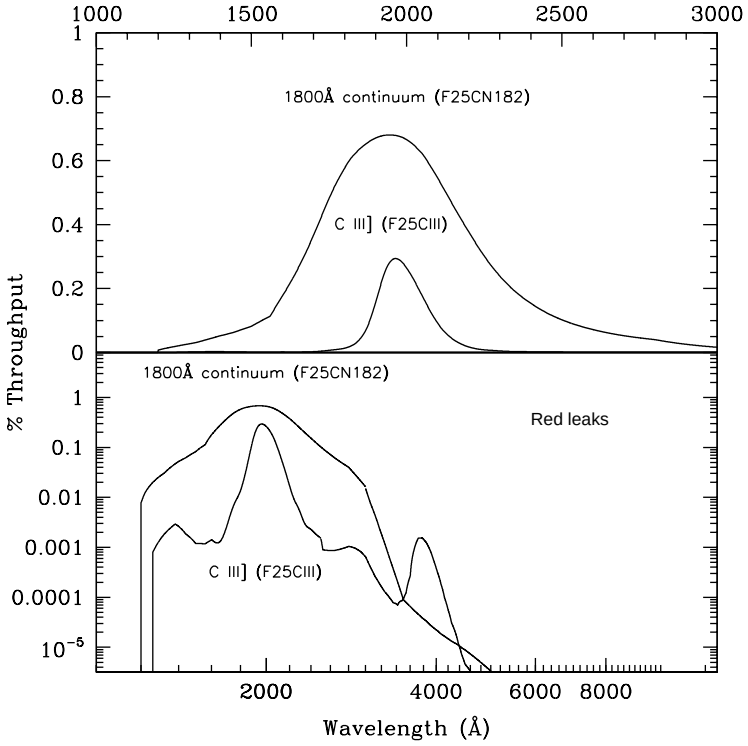

1800 Å Continuum—F25CN182

The 1800 Å continuum filter images a 25 x 25 arcsecond field of view, and can be used to measure the continuum for C III] emission-line images. The F25CN182 filter integrated system throughput is shown in Figure 5.13 above (see also page 349 for sensitivities, and signal-to-noise and saturation plots).

Lyman Alpha—F25LYA and Clear-minus-SRF2

The F25LYA filter images a 25 x 25 arcsecond field of view and can be used to obtain emission-line images in the light of Lyman-α. The F25LYA filter

integrated system throughput is shown in Figure 5.14 (see also page 361 for sensitivities, and signal-to-noise and saturation plots). The throughput longward of 1850 Å comes from ground test measurements and will be updated as part of Cycle 7 calibration.

At the price of a slightly wider bandpass, and the need to take two exposures, Lyman-α can be isolated by taking one image with the clear (25MAMA) aperture and a second with the longpass (F25SRF2) filter and differencing the two. The integrated system throughput for this imaging sequence is appreciably higher than for the narrowband F25LYA filter, as shown Figure 5.14.

Figure 5.14: Lyman-α Imaging Integrated System Throughputs

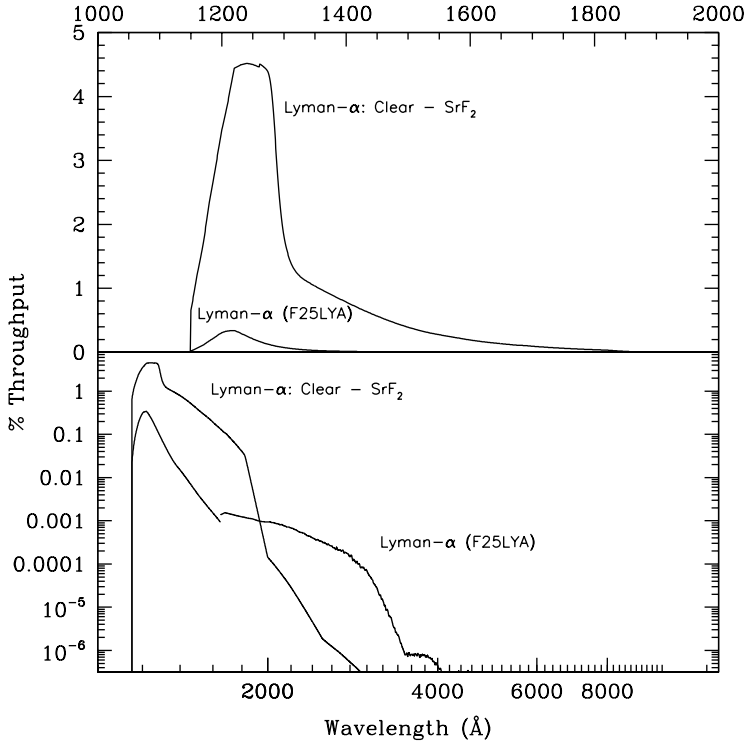

Neutral-Density Filters

STIS has a complement of neutral-density (ND) filters, spanning from ND1 (attenuation of 10^{-1}) to ND5 (attenuation of 10^{-5}, or 12.5 magnitudes), which can be used with the CCD, the NUV-MAMA, and the FUV-MAMA.

F25NDQ1, F25NDQ2, F25NDQ3, and F25NDQ4 are physically four separate quadrants of a single 25 x 25 arcsecond filter occupying a single position on the slit wheel. The target is centered in the appropriate quadrant when one of these apertures is requested. However, it should be noted that all four quadrants project onto the detector, and the full detector domain must be considered for bright-object limits.

F25ND3 and F25ND5 are each individual 25 x 25 arcsecond filtered apertures, occupying unique locations on the slit wheel.

CHAPTER 6
Exposure-Time Calculations

In This Chapter...

Overview

In this chapter we explain how to use sensitivities and throughputs provided in Chapters 13 and 14 to determine the expected count rate from your source and how to calculate exposure times to achieve a given signal-to-noise ratio for your STIS observations taking various background contributions into account. At the end of the chapter, in “Exposure-Time Examples” on page 85, you will find examples to guide you through specific cases.

The STIS Exposure Time Calculators

Three STIS Exposure-Time Calculators (ETCs) are available to help you with your proposal preparation. The three ETCs—available via the STIS web page—are: the imaging ETC, the spectroscopic ETC, and the target-acquisition ETC. These calculators provide count rates for given source and background parameters and calculate signal-to-noise ratios for a given exposure time, or count rates and exposure time for a given signal-to-noise ratio. If you have a calibrated spectrogram of your source, you can pass it as input directly to the Exposure-Time Calculator. The ETC also determines peak per-pixel count rates and total (integrated over the detector) count rates to aid you in your feasibility assessment and warns you if your observations exceed the local or global brightness limits for MAMA observations (see Chapter 7). Lastly, in the case of the spectroscopic

ETC, the task produces one-dimensional spectrograms for a given STIS configuration and source. A graphical interface allows WWW browsers to plot the output spectrograms or write them out as ASCII text files to your local disk. The spectroscopic ETC will have an emission-line tool by August 1998 which can be used to specify emission lines in addition to any underlying continuum spectrum. This is particularly useful for extended sources with narrow emission lines where the ETC will take the effect of the slit and the consequent degradation in the resolution into account. The input and output parameters in the target-acquisition ETC are specifically designed to facilitate exposure-time estimates for target-acquisition purposes (see Chapter 8 for more details on acquisitions). The ETCs have extensive online help which explains how to use them and the details of the performed calculations.

Determining Count Rates from Sensitivities

In the simplest terms, the instrumental sensitivity (*S*) times the flux from your object of interest gives the counts sec^{-1} (*C*) expected from your source, times the GAIN (i.e., it gives counts for the MAMA and electrons for the CCD):

$$C \times G = S \times Flux$$

Later in this chapter we provide specific formulae appropriate for imaging and spectroscopic modes, which can be used to calculate the expected count rates from your source and the signal-to-noise ratio. The formulae are given in terms of sensitivities, but we also provide transformation equations between the throughput (*T*) and sensitivity (*S*) for imaging and spectroscopic modes.

Sensitivities and throughputs are presented in graphical and tabular form as a function of wavelength for the spectroscopic modes in Chapter 13, “Spectroscopic Reference Material” on page 219, and for the imaging modes in Chapter 14, “Imaging Reference Material” on page 313. Given your source characteristics and the sensitivity of your STIS configuration, calculating the expected count rate over a given number of pixels is straightforward. The additional information you will need for spectroscopic observations is the aperture transmission (T_A), the encircled energy fraction (ε_f) in the direction perpendicular to the dispersion, the number of pixels per spectral resolution element (or line-spread function FWHMs) and the plate scale. For imaging observations you need only the encircled energies and plate scales. The location of this information is summarized in Table 6.1 below.

Below, we describe how to determine two quantities:

1. The counts sec^{-1} (*C*) from your source over some selected area of N_{pix} pixels.
2. The peak counts sec^{-1} $pixel^{-1}$ (P_{cr}) from your source—useful for avoiding saturated exposures and for assuring that MAMA observations do not exceed the bright-object limits.

Table 6.1: Location of Information Needed to Compute Expected Counts

Mode	Sensitivities	Slit Transmission	Line-Spread Function FWHM	Plate Scales	Encircled Energies
CCD first order	page 228	page 277	page 300	page 228	page 293
MAMA first order	page 250	page 277	page 300	page 250	page 293
MAMA echelle	page 262	page 277	page 302	page 262	page 293
PRISM	page 274	N/A	N/A	page 274	page 293[a]
CCD imaging	page 319	N/A	N/A	page 319	page 319
MAMA imaging	page 332	N/A	N/A	page 332	page 332

a. Numbers for G230M and G140M can be used for PRISM.

We consider the cases of point sources and diffuse sources separately.

Spectroscopy

Sensitivity Units and Conversions

The spectroscopic *point-source sensitivity,* S_λ^p, has the unit:

electrons sec^{-1} pix_λ^{-1} per incident erg cm^{-2} sec^{-1} $Å^{-1}$ for the CCD and

counts sec^{-1} pix_λ^{-1} per incident erg cm^{-2} sec^{-1} $Å^{-1}$ for the MAMA.

Where:

- pix_λ = a pixel in the dispersion direction.
- counts and electrons refer to the total received from the point source integrated over the PSF in the direction perpendicular to the dispersion (along the slit).

The spectroscopic *diffuse source sensitivity,* S_λ^d, has the unit:

electrons sec^{-1} pix_λ^{-1} pix_s^{-1} per incident erg sec^{-1} cm^{-2} $Å^{-1}$ $arcsec^{-2}$ for the CCD
counts sec^{-1} pix_λ^{-1} pix_s^{-1} per incident erg sec^{-1} cm^{-2} $Å^{-1}$ $arcsec^{-2}$ for the MAMA

Where:

- pix_λ= a pixel in the dispersion direction.
- pix_s= a pixel in the spatial direction.

S_λ^p and S_λ^d are related through the relation:

$$S_\lambda^d \cong (S_\lambda^p \times m_s \times W)$$

Where:

- m_s is the plate scale in arcsec per pixel in the spatial direction (i.e. in the direction perpendicular to the dispersion).

- W is the slit width in arcseconds.

Here, we have assumed that the diffuse source has a uniform brightness over the area of interest and the spectrum can be approximated as a continuum source (i.e., any emission or absorption lines are broader than the resolution after taking the effect of the slit into account).

Point Source

For a point source, the count rate, C, from the source integrated over an area of $N_{pix} = N_{\lambda pix}$ x N_{spix} pixels can be expressed as:

$$C = \frac{F_\lambda \times S_\lambda^p \times T_A \times \varepsilon_f \times N_{\lambda pix}}{G}$$

Where:

- G is the gain (always 1 for the MAMA, and 1 or 4 depending on the choice of `CCDGAIN` for the CCD).
- F_λ = the continuum flux from the astronomical source, in erg sec^{-1} cm^{-2} $Å^{-1}$.
- T_A = the aperture transmission (a fractional number less than 1).
- ε_f = the fraction of the point-source energy contained within N_{spix} pixels in the spatial direction.
- $N_{\lambda pix}$ = the number of wavelength pixels integrated over. For an unresolved emission line, $N_{\lambda pix}$ is just the number of pixels per spectral resolution element and F_λ is simply the total flux in the line in erg sec^{-1} cm^{-2} divided by the product of the dispersion in Å per pixel and $N_{\lambda pix}$ (i.e., divided by the FWHM of a resolution element in Å).

The peak counts sec^{-1} $pixel^{-1}$ from the point source, is given by:

$$P_{CR} = \frac{\varepsilon_f(1) \times F_\lambda \times S_\lambda^p \times T_A}{G}$$

Where:

- $\varepsilon_f(1)$ is the fraction of energy contained within the peak pixel.
- F_λ, S_λ^p ,and T_A are as above.

Diffuse Source

For a diffuse continuum source, the count rate C, due to the astronomical source integrated over $N_{pix} = N_{\lambda pix}$ x N_{spix} can be expressed as:

$$C = \frac{I_\lambda \times S_\lambda^d \times N_{\lambda pix} \times N_{spix}}{G}$$

Where:

- I_λ = the surface brightness of the astronomical source, in erg sec^{-1} cm^{-2} $Å^{-1}$ $arcsec^{-2}$.
- $N_{\lambda pix}$ = the number of wavelength pixels integrated over in dispersion. For an unresolved emission line, $N_{\lambda pix}$ is just the number of pixels per spectral resolution element and I_λ is simply the total flux in the line in ergs sec^{-1} cm^{-2} $arcsec^{-2}$ divided by the product of the dispersion in Å per pixel and $N_{\lambda pix}$, (i.e., divided by the FWHM of the resolution element in Angstroms).
- N_{spix} = the number of pixels integrated over in the spatial direction.

For a diffuse continuum source the peak counts sec^{-1} $pixel^{-1}$, P_{cr}, is given by:

$$P_{cr} = \frac{I_\lambda \times S_\lambda^d}{G}$$

For a diffuse, *spectrally unresolved emission line* source the peak counts sec^{-1} $pixel^{-1}$, P_{cr}, is essentially independent of slit size and is given by:

$$P_{cr} = \frac{I_{line} \times S_\lambda^d \times w}{G \cdot W \cdot FWHM}$$

Where:

- I_{line} is the intensity in erg sec^{-1} cm^{-2} $arcsec^{-2}$ in the line.
- *FWHM* is the full width half max of the instrumental profile in Angstroms, which for STIS is nearly always 2 x *d*, where *d* is the disperion in Å / pixel.
- *w* is the slit width in arcseconds which projects to *n* pixels in the detector plane where *n* is the width of the resolution element in pixels. Note that *w* is equal or close to twice the plate scale in the dispersion direction for all modes.
- *W* is the actual slit width in arcseconds.

Thus, for STIS in particular, this expression reduces to:

$$P_{cr} \sim \frac{I_{line} \times S_\lambda^d \times m_\lambda}{W \cdot d \cdot G}$$

Where:

- *d* is the dispersion in Angstroms per pixel.
- m_λ is the plate scale in the dispersion direction and all else is as above.

The counts from the emission line will be spread over $N_{\lambda pix}$ pixels where $N_{\lambda pix}$ is the slit width / plate scale in the dispersion direction ($N_{\lambda pix} = W / m_\lambda$).

Imaging

Sensitivity Units and Conversions

The *imaging point-source sensitivity,* S_λ^p, has the units:

electrons sec^{-1} $Å^{-1}$ per incident erg sec^{-1} cm^{-2} $Å^{-1}$

Where:

- electrons refer to the total electrons from the point source integrated over the PSF.

The *imaging diffuse-source sensitivity,* S_λ^d, has the unit:

electrons sec^{-1} $Å^{-1}$ $pixel^{-1}$ per incident erg sec^{-1} cm^{-2} $Å^{-1}$ $arcsec^{-2}$.

Thus S_λ^p and S_λ^d are related through the relation:

$$S_\lambda^d \cong (S_\lambda^p \times {m_s}^2)$$

where m_s is the plate scale in arcsec per pixel.

Point Source

For a point source, the count rate, *C*, over an area of N_{pix} pixels due to the astronomical source can be expressed as:

$$C = \frac{\int F_\lambda \times S_\lambda^p \times \varepsilon_f d\lambda}{G}$$

Where:

- F_λ = the flux from the astronomical source, in ergs sec^{-1} cm^{-2} $Å^{-1}$.
- ε_f = the fraction of the point source energy encircled within N_{pix} pixels.
- the integral is over the bandpass.

The peak counts sec^{-1} $pixel^{-1}$ from the point source, is given by:

$$Pcr = \frac{\int F_\lambda \times S_\lambda^p \times \varepsilon_f(1) d\lambda}{G}$$

Where:

- $\varepsilon_f(1)$ is the fraction of energy encircled within the peak pixel.
- $F_{\lambda,}$ and S_λ^p are as above.
- the integral is over the bandpass.

If the flux from your source can be approximated by a flat continuum, then:

$$C = \frac{F_\lambda \varepsilon_f \int S_\lambda^p d\lambda}{G}$$

We can now define an equivalent bandpass of the filter (B_λ) such that:

$$\int S_\lambda^p d\lambda = S_{peak}^p B_\lambda$$

Where:

- S_{peak}^p is the peak sensitivity.
- B_λ is the effective bandpass of the filter.

The count rate from the source can now be written as:

$$C = \frac{F_\lambda \varepsilon_f S_{peak}^p B_\lambda}{G}$$

In Chapter 14, we give the value of B_λ and S_{peak}^p for various filters.

Diffuse Source

For a diffuse source, the count rate, *C*, due to the astronomical source can be expressed as:

$$C = \frac{\int I_\lambda \times S_\lambda^d \times N_{pix} d\lambda}{G} = \frac{\int I_\lambda \times S_\lambda^p \times m_s^2 \times N_{pix} d\lambda}{G}$$

Where:

- I_λ = the surface brightness of the astronomical source, in erg sec^{-1} cm^{-2} $Å^{-1}$ $arcsec^{-2}$.
- N_{pix} = the number of pixels integrated over.
- the integral is over the bandpass.

For a diffuse source the peak counts sec^{-1} $pixel^{-1}$, P_{cr}, is given trivially by:

$$P_{cr} = \frac{\int I_\lambda \times S_\lambda^d d\lambda}{G}$$

where we have assumed the source to be uniformly bright.

Throughput and Sensitivity

So far, we have given the formulae for count rates in terms of the sensitivity (*S*). If you would like to use the throughput (*T*) rather than the sensitivity, you can use the following conversion equations.

In the case of *imaging modes*, the transformation between *T* and *S* is given by:

$$S_\lambda = \frac{T_\lambda A \lambda}{hc} = \frac{A_{eff} \lambda}{hc}$$

Where:

- S_λ is the sensitivity at wavelength λ.
- T_λ is the system throughput at λ.
- A is the area of an unobstructed 2.4 meter telescope (i.e., 45,239 cm^2).
- h is Planck's constant.
- c is the velocity of light.
- The effective area A_{eff} is given by $A_{eff} = T_\lambda A$

In the case of *spectroscopic modes*, the transformation equation can be written as:

$$S_\lambda = \frac{T_\lambda A \lambda d}{hc} = \frac{A_{eff} \lambda d}{hc}$$

Where d is the dispersion in Å / pixel.

In the first two examples given at the end of this chapter, we specifically show how the calculations can be done both in terms of the sensitivity and the throughput.

Computing Exposure Times

To derive the exposure time to achieve a given signal-to-noise ratio, or to derive the signal-to-noise ratio you will achieve in a given exposure time for your source, there are four principal ingredients:

- Expected counts from your source over some area (C).
- The area (in pixels) over which those counts are received (N_{pix}).
- Sky background (B_{sky}) in counts $pixel^{-1}$ sec^{-1}.
- The detector background, or dark, (B_{det}) in counts sec^{-1} $pixel^{-1}$ and the read noise (RN) in counts for the CCD.

"Detector and Sky Backgrounds" on page 78 provides the information you need to determine the sky-plus-detector background for your observation.

Calculating Exposure Times for a Given Signal-to-Noise

The signal-to-noise ratio, *StoN* is given by:

$$StoN = \frac{CtG}{\sqrt{CtG + N_{pix}(B_{sky} + B_{det})Gt + (N_{pix}/N_{bin})(N_{read}RN^2)}}$$

Where:

- C = the signal from the astronomical source in counts sec^{-1}.
- N_{pix} = the total number of detector pixels integrated over to achieve C.
- B_{sky} = the sky background in counts sec^{-1} $pixel^{-1}$.
- B_{det} = the detector dark current in counts sec^{-1} $pixel^{-1}$.
- N_{bin} = the total number of on-chip binned pixels for the CCD (N_{bin} = `BINAXIS1` x `BINAXIS2` (see “Binning” on page 179).
- RN = the read noise in electrons; = 0 for MAMA observations.
- N_{read} = the number of CCD readouts.
- t = the integration time in seconds.
- G = the gain (is always 1 for the MAMAs and 1 or 4 for the CCD, depending on your choice of `CCDGAIN`).

Observers using the CCD normally take sufficiently long integrations that the CCD read noise is not important. This condition is met when:

$$CGt + N_{pix}(B_{sky} + B_{det})Gt > 2(N_{pix}/N_{bin})N_{read}RN^2$$

If you are observing with the CCD and are in the regime where read noise is not important, and for all MAMA observations, the integration time to reach a signal-to-noise ratio *StoN*, is given by:

$$t = \frac{(StoN)^2(CG + N_{pix}G[B_{sky} + B_{det}])}{C^2G^2}$$

If your source count rate is much brighter than the sky plus detector backgrounds, then this expression reduces further to:

$$t = \frac{(StoN)^2}{CG}$$

More generally, the required integration time to reach a signal to noise ratio *StoN*, is given by:

$$t = \frac{(StoN)^2(CG + N_{pix}G[B_{sky} + B_{det}]) + \sqrt{(StoN)^4(CG + N_{pix}G[B_{sky} + B_{det}])^2 + 4(StoN)^2C^2G^2((N_{pix}/N_{bin})N_{read}RN^2)}}{2C^2G^2}$$

Special Case—Spectroscopic CCD Observations at λ<2500 Å

In the optical, each photon generates a single electron (i.e., counts times the gain correspond to the total number of electrons). However, in the near UV, shortward of ~3200 Å there is a finite probability of creating more than one electron per UV photon (see Christensen, O., 1976, *J. App. Phys.* **47**, 689). Theoretically, the quantum yield (*Q*, or the mean number of electrons generated per photon) is given by the energy of the photon divided by 3.65 eV, and ranges from *Q*=1.06 electrons for every UV photon at 3200 Å, to *Q*=1.89 electrons for every photon at 1800 Å. The actual electron yield of the STIS CCD has not been measured in the near UV.

The sensitivity plots correctly predict the number of electrons generated per UV photon. However, since multiple electrons are generated from a single photon, the signal-to-noise achieved in a given integration time is affected. The explicit expression is given by:

$$StoN = \frac{Q^{-1}CtG}{\sqrt{Q^{-1}(C + N_{pix}B_{sky})Gt + N_{pix}B_{det}Gt + (N_{pix}/N_{bin})N_{read}RN^2}}$$

For observations which are not in the read-noise or dark-current limited regime, the effective signal-to-noise you should expect to achieve is then ~1/sqrt(*Q*) times the signal-to-noise ratio calculated directly from the sensitivities given in Chapter 13 ignoring this effect. This effect is negligible at 3000 Å but amounts to 40% at 1800 Å.

Detector and Sky Backgrounds

When calculating expected signal-to-noise ratios or exposure times, the background from the sky and the background from the detector must be taken into account.

Detector Backgrounds

Table 6.2 shows the read-noise and dark-current characteristics of the detectors, taken from Chapter 7.

Table 6.2: Detector Backgrounds

	CCD	NUV-MAMA	FUV-MAMA
Read noise (electrons pix^{-1})	4.0 (for `CCDGAIN`=1) 6.8 (for `CCDGAIN`=4)	0	0
Dark current (electrons sec^{-1} pix^{-1})	2.5×10^{-3}	~1.0×10^{-3}	~7.0×10^{-6}

Sky Background

The sources of sky background which will affect STIS observations include:

- Earth shine (ES).
- Zodiacal light (ZL).
- Geocoronal emission (GC).

The continuum background in counts sec^{-1} $pixel^{-1}$ for spectroscopic observations can be computed as:

$$B_{sky} = \frac{I_\lambda \times S_\lambda^d}{G}$$

Where:

- I_λ is the surface brightness of the sky background, in erg sec^{-1} cm^{-2}Å^{-1} $arcsec^{-2}$.
- S_λ^d is the diffuse-source sensitivity for the grating mode.

The background in counts sec^{-1} $pixel^{-1}$ for imaging observations can be computed as:

$$B_{sky} = \frac{\int I_\lambda \times S_\lambda^d d\lambda}{G}$$

Where:

- I_λ is the surface brightness of the sky background, in erg sec^{-1} cm^{-2} Å^{-1} $arcsec^{-2}$.
- S_λ^d is the diffuse-source sensitivity for the imaging mode.
- The integral is over the bandpass.

In Figure 6.1 we plot high sky background intensity as a function of wavelength, identifying the separate components which contribute to the background. The information in this figure is presented in tabular form in Table 6.6 on page 92. The “average” values of the Earth shine and zodiacal contributions that you can use (and that the STIS Exposure Time Calculator uses) correspond to 50% of the “high” values presented here.

Figure 6.1: High Sky Background Intensity as a Function of Wavelength. The zodiacal contribution corresponds to a helio-ecliptic latitude and longitude of 30 and 180 degrees, respectively, which corresponds to m_V = 22.7 per square arc-sec. The Earthshine is for a target which is roughly 25 degrees from the limb of the sunlit Earth. Use Figure 6.2 to estimate background contributions at other angles. The geo-coronal line intensities are in erg cm^{-2} s^{-1} $arcsec^{-2}$.

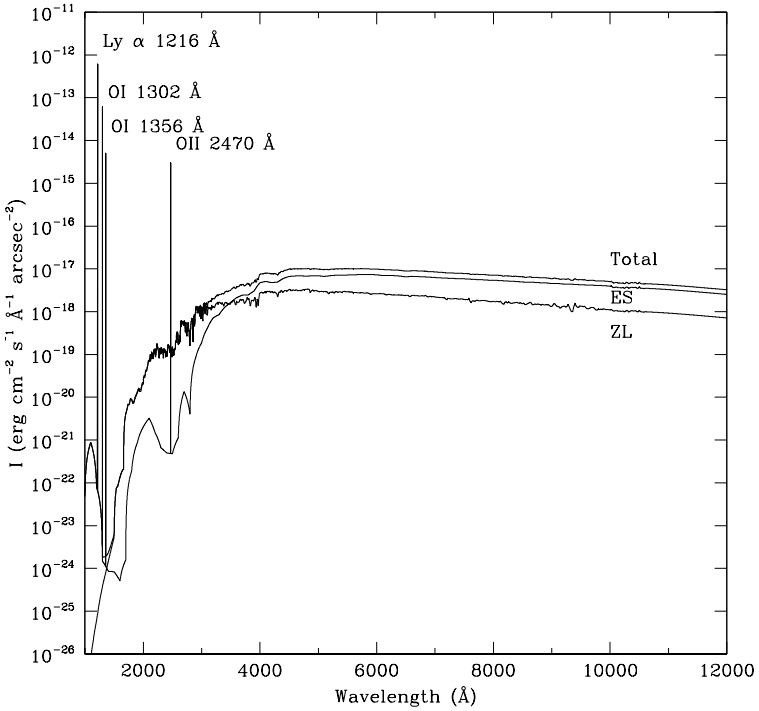

Background Variations and LOW-SKY

In the ultraviolet, the background contains important contributions from airglow lines. These vary from day to night and as a function of HST orbital position. The airglow lines are an important consideration for imaging-mode observations and can be for spectroscopic observations as well. Away from the airglow lines, at wavelengths shortward of ~3000 A, the background is dominated by zodiacal light, and is generally much lower than the intrinsic detector background. The contribution of zodiacal light does not vary dramatically with time, and is constant within a factor of about three throughout most of the sky. Table 6.3 gives the variation of the zodiacal background as a function of helio-ecliptic latitude and longitude.

Earthshine, on the other hand, varies strongly depending on the angle between the target and the bright Earth limb. The variation of the Earthshine as a function of limb angle from the sunlit Earth is shown in Figure 6.2. The figure also shows

the contribution of the moon which is typically much smaller, and the full range of the zodiacal contribution. In Figure 6.2, limits on the zodiacal light contribution are also given. For reference, the limb angle is approximately 24˚ when the HST is aligned toward its orbit pole (i.e., the center of the CVZ). The Earthshine contribution given in Table 6.3 and Figure 6.2 corresponds to this position.

Figure 6.2: Background Contributions in V Magnitude per arcsec^2 due to the Moon and the Sunlit Earth as a Function of Angle Between the Target and the Limb of the Earth or Moon

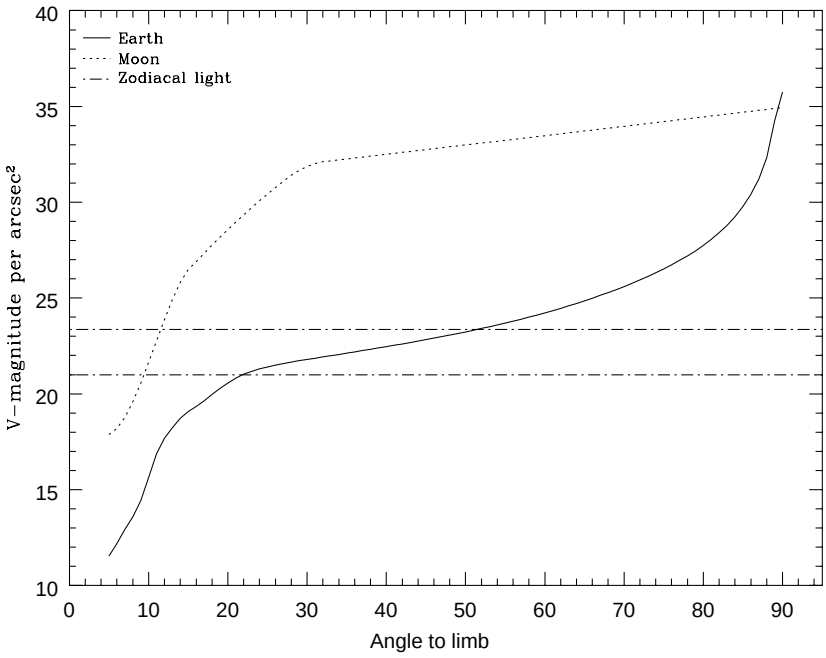

Note that for observations taken longward of 3500 Å the Earthshine dominates the background at small (<25˚) limb angles. In fact, the background increases exponentially for limb angles <25 ˚.The background near the bright limb can also vary by a factor of ~2 on timescales as short as two minutes, which suggests that the background from Earthshine also depends upon the reflectivity of the terrain over which HST passes during the course of an exposure. The background at limb angles greater than the bright-Earth avoidance angle of 20˚ appears to show no significant field dependence. Details of the sky background as it affects STIS are discussed by Shaw et al. (STIS ISR 98-21).

Table 6.3: Approximate Zodiacal Sky Background at V as a Function of Helio-ecliptic Latitude and Helio-ecliptic Longitude (in V magnitudes per square arcsecond)

Helioecliptic Longitude (deg)	Helioecliptic Latitude (deg)			
	0	30	60	90
180	22.1	22.7	23.2	23.3
145	22.4	22.9	23.3	23.3
110	22.3	22.9	23.3	23.3
50	20.9	22.2	22.9	23.3

In Table 6.4, we provide the expected count rates from different sky backgrounds in various STIS modes, which you can use to determine whether your observations would be background limited.

Table 6.4: Count Rates by Sky Background and STIS Mode

Mode	counts sec^{-1} pix^{-1}			
	Zodiacal[a]	Earthshine		
		High (day)[b]	Typical[c]	Dark (shadow)
CCD Clear	0.06	0.16	0.08	0
Longpass CCD	0.03	0.08	0.04	0.
NUV-MAMA Clear	4×10^{-5}	7×10^{-3}	3.45×10^{-3}	5.7×10^{-4}
FUV-MAMA Clear	1.2×10^{-8}	0.05	0.025	4.5×10^{-3}
SrF_2 (NUV-MAMA)	3.75×10^{-5}	1.2×10^{-3}	5×10^{-4}	6.25×10^{-6}
SrF_2 (FUV-MAMA)	1×10^{-8}	3.8×10^{-3}	1.6×10^{-3}	2.4×10^{-5}
Lyman-α	0	3.7×10^{-3}	1.85×10^{-3}	3.6×10^{-4}
QTZ (NUV-MAMA)	3.6×10^{-5}	3×10^{-4}	1.5×10^{-4}	1.4×10^{-6}

a. Zodiacal contribution is same as in Figure 6.1 and Table 6.6 (m_V=22.7 per square arcsec).
b. Corresponds to HST pointing 24˚ from the limb of the sunlit Earth.
c. Corresponds to HST pointing 40˚ from the limb of the sunlit Earth, when the Earth shine is ~50% of the “high” value.

If your observations are background limited, you may wish to consider requesting that the special requirement `LOW-SKY`. `LOW-SKY` observations are obtained when the total background light is no more than 30% greater than the yearly minimum value of the zodiacal background for the target. The exposures are also taken when the target is at least 40˚ from the bright Earth to minimize Earthshine, though in fact the zodiacal light can dominate Earthshine at limb angles as close as 25˚ .The `LOW-SKY` special requirement limits visibility time to

about 48 minutes per orbit. The values of the background when LOW-SKY is requested can be assumed to be ~15% of the typical high values in Figure 6.1 on page 67 and Table 6.3 on page 69. See “Imaging a Faint Stellar Source” on page 83 for an example of a background-limited observation which is greatly helped by requesting LOW-SKY.

Geocoronal Emission and Shadow

Background due to geocoronal emission originates mainly from hydrogen and oxygen atoms in the exosphere of the Earth. The emission is concentrated in a very few lines. The brightest line is Lyman–α at 1216 Å. The strength of the Lyman-α line varies between about 2 and 30 kilo-Rayleighs (i.e., between 6.1×10^{-14} and 9.2×10^{-13} erg sec^{-1} cm^{-2} $arcsec^{-2}$ where 1 Rayleigh = 10^6 photons sec^{-1} cm^{-2} per 4π steradians) depending on the time of the observation and the position of the target relative to the Sun. The next strongest line is the OI line at 1302 Å, which rarely exceeds 10% of Lyman-α. The typical strength of the O I 1302 Å line is about 2 kilo-Rayleighs (which corresponds to about 5.7×10^{-14} erg sec^{-1} cm^{-2} sec^{-1} $arcsec^{-2}$) at the daylight side and about 150 times fainter on the night side of the HST orbit. O I 1356 Å and O I 2470 Å lines may appear in observations on the daylight side of the orbit, but these lines are at least 3 times weaker than the O I 1302 Å line. The width of the lines also vary, the line widths given in Table 6.7 are representative values assuming a temperature of 2000 K.

The geocoronal emission lines are essentially unresolved at the resolution of STIS but the emission fills the slit in the spatial dimension. Using a wider slit or observing slitless does not increase the background counts per pixel from geocoronal emission, but does increase the area (range of wavelengths or pixels in the dispersion direction) over which that background is received. Observations with a slit which is *n* pixels wide in dispersion will be affected by geocoronal emission in a roughly *n* pixel region centered on the relevant geocoronal-emission line wavelength. For slitless spectroscopy in the UV, the effects of geocoronal emission must be taken into account at all pixels, unless a longpass filter is employed to block off the short wavelength emission (see also “Longpass-Filtered MAMA Imaging— F25SRF2 and F25QTZ” on page 63 and “Slitless First-Order Spectroscopy” on page 199).

It is possible to request that exposures be taken when HST is in the umbral shadow of the earth to minimize geocoronal emission (e.g., if you are observing weak lines at 1216 or 1304 Å) using the special requirement SHADOW. Exposures using this special requirement are limited to roughly 32 minutes per orbit, exclusive of the guide-star acquisition (or reacquisition) and can be scheduled only during a small percentage of the year. SHADOW reduces the contribution from the geocoronal emission lines by roughly a factor of ten. If you require SHADOW, you should request it in your Phase I proposal (see the Call for Proposals).

Extinction Correction

Extinction can dramatically alter the counts expected from your source, particularly in the ultraviolet. Figure 6.3 shows A_v / E (B – V) values applicable to our galaxy, taken from Seaton (*MNRAS*, **187**, 73P, 1979).

Extinction curves, however, have a strong metallicity dependence, particularly in the UV wavelengths. Sample extinction curves can be seen in Koornneef and Code, *ApJ*, **247**, 860 1981 (LMC); Bouchet et al., *A&A*, **149**, 330 1985 (SMC); and Calzetti, Kinney and Storchi-Bergmann, *ApJ*, **429**, 582, 1994, and references therein. At lower metallicities, the 2200 Å bump which is so prominent in the galactic extinction curve disappears, and A_v / E (B – V) increases at UV wavelengths.

The easiest way to understand how to determine the extinction correction for your source is to work through an example; see “Echelle Spectroscopy of a Bright Star with Large Extinction (Sk –69˚ 215)” on page 89.

Figure 6.3: Extinction versus Wavelength

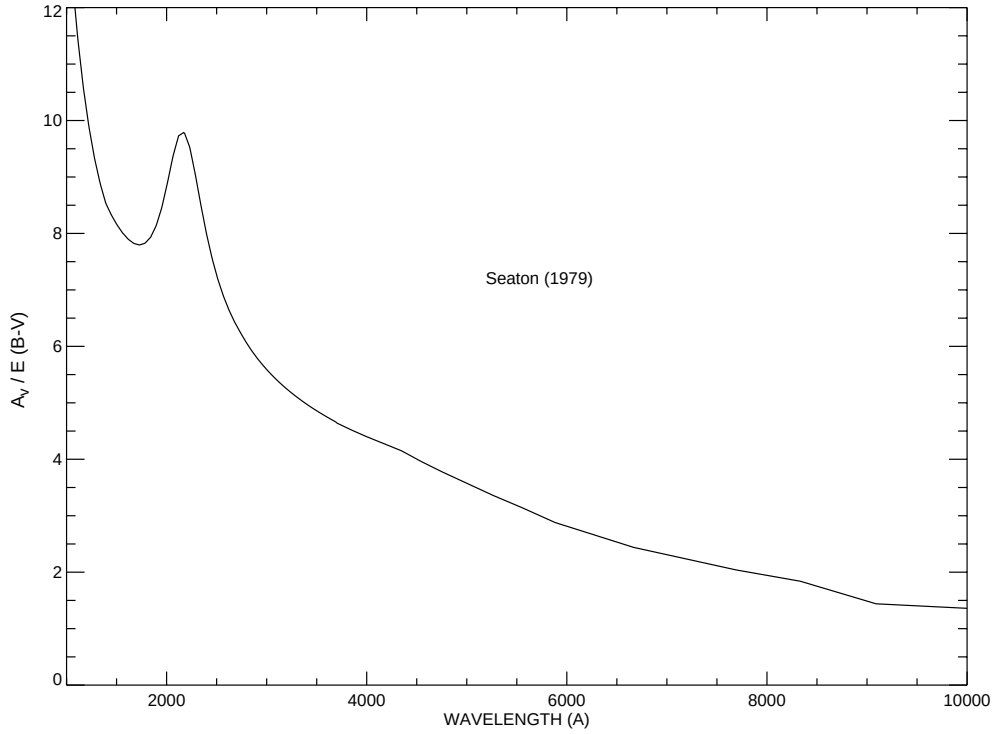

Exposure-Time Examples

Here are a few simple examples to illustrate how an integration time may be computed for point sources and diffuse sources. The flux values given here are for illustrative purposes only; you would need to check the flux values if you are planning your own observations of one of these targets.

Spectroscopy of Diffuse Source (M86)

We want to observe M86, an elliptical galaxy in Virgo, using the `G750M` grating at a central wavelength setting of λ_c=6768 Å, the CCD detector and the 52 x 0.2 arcsec slit. Our aim is to calculate the count rate in the central region of M86 and the expected signal-to-noise ratio per resolution element in an exposure time of 1 hour. M86 has an inhomogeneous surface brightness distribution in Hα and the line is well resolved with this grating. Let us consider a region with a Hα surface brightness of I_λ = 1.16 x 10^{-15} erg sec^{-1} cm^{-2} $Å^{-1}$ $arcsec^{-2}$ (note the unit - it is not the entire Hα flux but the flux per unit wavelength interval). To derive the count rate from the source we use from Chapter 13:

- S_λ^d = 1.1 x 10^{13} counts sec^{-1} pix_λ^{-1} pix_s^{-1} per incident erg sec^{-1} cm^{-2} $Å^{-1}$.
- $N_{\lambda pix}$ = 4 and N_{spix} = 2 (1 resolution element).

Using the equation given in the previous section, we get the count rate C = 0.0936 counts sec^{-1} at Hα.

The sky background is negligible in comparison, but the dark current (2.5 x 10^{-3} count sec^{-1} $pixel^{-1}$ * 8 pixels = 0.02 count sec^{-1}) and the read noise squared (16 electrons * 8 pixels * 3 reads = 384 counts, for `CR-SPLIT=3`) are important here. Substituting the numbers into the equation for signal-to-noise on page 77, we get:

$$StoN = 12 = \frac{0.0936 \times 3600}{\sqrt{0.0936 \times 3600 + 8 \times 0.0025 \times 3600 + 8 \times 3 \times 16}}$$

To increase our signal-to-noise or decrease our exposure time, we can consider using on-chip binning. We bin 2 pixels in the spatial direction so that N_{bin} = 2. To allow adequate sampling of our new binned pixels, we leave $N_{\lambda pix}$ = 4, but set N_{spix} = 4, so N_{pix} = 16 and C = 0.1872. To compute the time to achieve a signal-to-noise of 12 using this configuration, we use the full expression for

exposure time given on page 78 and determine that roughly 30 minutes are needed in this configuration:

$$t = 1806 = \frac{144 \times (0.1872 + 16 \times 0.0025) + \sqrt{20736 \times (0.1872 + 16 \times 0.0025)^2 + 4 \times 144 \times 0.1872^2 \times 8 \times 3 \times 16}}{2 \times 0.1872^2}$$

Spectroscopy of Solar-Analog Star P041-C

We wish to study the shape of the continuum spectrum of the solar-analog star P041-C from the near IR to the near UV. P041-C has $V = 12.0$. We wish to obtain spectroscopy with the CCD detector covering the entire useful spectral range from 2000 Å to 10,300 Å with gratings `G230LB`, `G430L`, and `G750L`. Since we require accurate photometry, we use the wide `52X0.5` slit. The goal is to reach a signal-to-noise ratio of 20 in the near UV (at 2300 Å), 100 in the blue, and 280 in the red.

The fluxes of P041-C at the desired wavelengths obtained from a spectrogram of the Sun scaled from $V = -26.75$ to $V = 12.0$, are available via the web at:

`http://www.stsci.edu/ftp/cdbs/cdbs2/calspec`

G230LB

We illustrate the calculation of the exposure time calculation for the `G230LB` grating. P041-C is found to have a flux of 1.7×10^{-15} erg sec^{-1} cm^{-2} Å^{-1} at 2300 Å.

We take for `G230LB` from Chapter 13:

- S^{p}_{2300} = 1.6 x 10^{14} counts sec^{-1} pix$_{\lambda}^{-1}$per incident erg sec^{-1} cm^{-2} Å^{-1}.
- T_A = 0.8 for the aperture throughput, taken from Chapter 13
- ε_f = 0.8.
- N_{spix}=3, since 80% of the point-source light is encircled with 3 pixels.
- $N_{\lambda pix}$= 2, since two pixels resolve the LSF .

Using the equation on page 72, we calculate a point-source count rate of C = 0.34 counts sec^{-1} over N_{pix} = 6 pixels.

The source count rates can be compared with the background and detector dark current rates. Both background and detector rates are negligibly small for this setting. Therefore we can neglect their contributions. Since we are aiming for a signal-to-noise ratio of 25, we can estimate that we must obtain 625 counts minimum, and setting CR-SPLIT=2 each exposure will have ~300 counts. The read noise squared (~192 over 6 pixels for 2 readouts) must be taken into account. We therefore scale the derived required exposure time by Q, where Q is ~1.5 at 2300 Å. Using the STIS Exposure Time Calculator, we estimate the required time

for S/N=20 is ~2600 seconds. To check that we indeed get S/N=20, we use the formula on page 77 as follows.

$$S/N \approx 20 \;=\; \frac{(0.34/1.5)\cdot 2600}{\sqrt{(0.34/1.5)\cdot 2600 + 192 + 40}}$$

Finally, since we are observing with the CCD in the near-UV, we must correct for the effect on the signal-to-noise calculation of the multiple-electron process (see page 78).

G750L and G430L

Exposure times for the two remaining wavelength settings can be calculated directly as *time* = signal-to-noise^2 / *C*. The results are summarized in Table 6.5.

Table 6.5: Low Resolution Spectroscopy of Solar Analog Star

Grating	G230LB	G430L	G750L λ_c=7751
Wavelength (Angstroms)	2300	5000	7800
Flux (ergs sec^{-1} cm^{-2} Å^{-1})	1.7x10^{-15}	6.0x10^{-14}	3.8x10^{-14}
Point Source Sensitivity (counts sec^{-1} pix$_\lambda^{-1}$ per ergs sec^{-1} cm^{-2} Å^{-1})	1.6x10^{14}	4.3x10^{15}	8.9x10^{15}
Aperture throughput (T_A)	80%	85%	85%
$N_{\lambda pix}$	2	2	2
N_{spix} to encircle 80% of PSF	3	3	3
C (counts sec^{-1} from source over N_{pix}=6)	0.34	200	277
Signal-to-noise ratio desired	25	100	280
Total exposure time	2431 seconds	50 seconds	300 seconds

Extended Source, with Flux in cgs units (NGC 6543): Imaging and Spectroscopy

Let us consider NGC 6543, the Cat's Eye planetary nebula, where the aim is to use the CCD to image using the [O II] filter, and to do spectroscopy both in the visible and in the UV.

Imaging

The aim is to get a signal-to-noise ratio of 30 using the [O II] filter. We know that NGC 6543 is about 6 times fainter in [O II] than in Hβ, and its total flux at [O II] 3727 Å is ~4.4 x 10^{-11} erg sec^{-1} cm^{-2} contained within 1 Å. Since the radius of the object is about 10 arcsec, the average [O II] surface brightness is about 1.4 x 10^{-13} erg sec^{-1} cm^{-2} arcsec^{-2} Å^{-1}.

We take:

- S_{λ}^{d} = 9.5 x 10^{11} counts sec^{-1} pix^{-1} $Å^{-1}$per incident erg sec^{-1} cm^{-2} $Å^{-1}$ $arcsec^{-2}$ as given in Chapter 14.
- We take N_{pix} = 4 x 4 = 16, since two pixels are a resolution element (see Chapter 13).

To calculate the count rate we use the equation on page 75 for diffuse sources and determine a per-pixel count rate of 0.13 counts sec^{-1} $pixel^{-1}$ or a count rate C = 2.1 counts sec^{-1}over four pixels. The background and the dark current can be neglected. To get a signal-to-noise of 30 we need 10^3 counts, so the read noise can also be neglected and we can use the simplified expression to calculate exposure time (see page 77). We obtain 10^4 counts in ~476 seconds. To allow post-observation removal of cosmic rays we use `CR-SPLIT=2`. We note that in each ~240 second exposure we predict a mean of ~120 counts $pixel^{-1}$, and thus we are safely within the limits of the CCD full well.

Diffuse-Source Spectroscopy in the Visible and UV Regions

In the visible, the aim is to get a signal-to-noise of about 100 at λ = 4861 Å, with the `G430M` grating at a central wavelength setting of λ_c = 4961 Å, the CCD detector, and the `52X0.1` arcsec slit. In the UV, the aim is to get a signal-to-noise ratio of about 10 at the C IV ~1550 Å line with the `G140M` grating at a central wavelength setting of λ_c = 1550 and the FUV-MAMA detector. To increase our signal-to-noise ratio in the UV, we use the `52X0.2` arcsec slit for the G140M spectroscopic observations.

Visible Region

NGC 6543 has an average Hβ surface brightness of S(Hβ) ~ 8.37 x 10^{-13} erg sec^{-1} cm^{-2} $Å^{-1}$ $arcsec^{-2}$ at 4861 Å and has a radius of about 10 arcsec.

We take from Chapter 13:

- S_{λ}^{d} = 1.65 x 10^{12} counts sec^{-1} pix_{λ}^{-1} pix_{s}^{-1} per incident erg sec^{-1} cm^{-2} $Å^{-1}$ $arcsec^{-2}$ for `G430M`.
- $N_{\lambda pix}$ = N_{spix} =2 since 2 pixels resolves the LSF and PSF.

Using the equation for diffuse sources on page 72, we derive a per-pixel count rate of 1.4 counts sec^{-1} $pixel^{-1}$ and a count rate integrated over the four pixels of C = 5.6 counts sec^{-1} at 4861 Å from the astronomical source. The sky background and the detector background are much lower. To allow cosmic-ray removal in post-observation data processing, we use `CR-SPLIT=3`. To achieve a signal-to-noise of 100, we require a total of roughly 10,000 counts, so read noise should be negligible, even over 4 pixels and with `NREAD` = 3. We calculate the time required to achieve signal-to-noise of 100, using the simplified equation on page 77, and determine that we require roughly 130 minutes.

$$t = 1785 = \frac{10000}{5.6}$$

At a count rate of ~1 count sec^{-1} $pixel^{-1}$ for 700 seconds per `CR-SPLIT` exposure, we are in no danger of hitting the CCD full-well limit.

UV Region

The C IV flux of NGC 6543 is ~ 2.5 x 10^{-12} erg sec^{-1} cm^{-2} $arcsec^{-2}$ spread over ~1 Å. The line, with a FWHM ~ 0.4 Å, will be well resolved in the `G140M` configuration using the `52X0.2` slit.

We take from Chapter 13:

- S_{λ}^{d} = 5.5 x10^{9} counts sec^{-1} pix_{λ}^{-1} pix_{s}^{-1} per incident erg sec^{-1} cm^{-2} $Å^{-1}$ $arcsec^{-2}$ for G140M at λ=1550Å using the 0.2 arcsecond wide slit.
- We take $N_{\lambda pix} = N_{spix} = 8$, since the line emission is spread over the ~8 pixels of the slit width in dispersion, and we are willing to integrate flux along the slit to improve the signal-to-noise ratio.

Using the equation for diffuse sources on page 72, we determine a per-pixel peak count rate of ~0.014 counts sec^{-1} $pixel^{-1}$ and a count-rate over the 64 pixels of C = 0.91 counts sec^{-1} at 1550 Å from the astronomical source. The sky and detector backgrounds are still negligible, and the read noise is zero for the MAMA detector so we can use the simplified equation for exposure time on page 77 directly. We determine that we require ~7 minutes.

$$t = 440 = \frac{400}{0.91}$$

We are well below the MAMA local linearity limit of 50 counts sec^{-1} $pixel^{-1}$. Even assuming the nebula evenly illuminates the full 28 arcseconds of the long slit, we are well below the global absolute and linearity limits, since the flux from the nebula is concentrated in the C IV emission line. Then the global count rate, if the source fully fills the slit in the spatial direction, is given roughly by 0.015 * 8 * 1024 << 200,000 counts sec^{-1}. Finally, we are well below the MAMA 16 bit buffer limit of a maximum of 65,536 counts $pixel^{-1}$ integrated over the exposure duration.

Echelle Spectroscopy of a Bright Star with Large Extinction (Sk –69˚ 215)

The aim here is to do high-resolution echelle spectroscopy of an O5 star in the LMC (such as Sk –69˚ 215) at 2500 Å, using the `E230H` grating at a central wavelength of λ_{c} = 2513 Å and using the `0.2X0.09` arcsec slit. The aim is to get a signal-to-noise ratio of about 50 from photon statistics. We will assume that the exact UV flux of the star is unknown and we need to estimate it from the optical data. This calculation of the stellar flux at 2500 Å involves 2 steps:

1. Calculation of the dereddened flux at 5500 Å.
2. Calculation of predicted flux at 2500 Å taking reddening with standard extinction and stellar models into account.

Dereddened Magnitude and Prediction of 2500 Å Flux

We assume that it is an O5 star with $V = 11.6$ (its exact spectral type is slightly uncertain). The expected $B - V$ value from such a star is –0.35, whereas the observed $B - V$ is –0.09; we thus get $E(B - V) = 0.26$ mag.

We assume all the extinction to be due to LMC, and use the appropriate extinction law (Koornneef and Code, *ApJ*, **247**, 860, 1981). The total visual extinction is then R x $E(B - V)$ = 3.1 x 0.26 = 0.82, leading to an unreddened magnitude of $V_0 = 10.78$. The corresponding flux at 5500 Å (using the standard zero point where $V = 0$ corresponds to F(5500 Å) = 3.55 x 10^{-9} erg sec^{-1} cm^{-2} $Å^{-1}$) is F(5500 Å) = 1.73 x 10^{-13} erg sec^{-1} cm^{-2} $Å^{-1}$.

The model atmosphere of Kurucz predicts F(2500 Å) / F(5500 Å) = 17.2 for an O5 star, which leads to a flux of F2500 Å = 2.98 x 10^{-12} erg sec^{-1} cm^{-2} $Å^{-1}$ at 2500 Å for the unreddened star. Reddening will diminish this flux by a factor of $10^{-0.4xA(2500\ Å)}$, where the absorption at 2500 Å can be determined from the extinction curve; the result in this case is A (2500 Å) = 1.3. Thus the predicted flux of this star at 2500 A is 9.0 x 10^{-13} erg sec^{-1} cm^{-2} $Å^{-1}$.

Exposure-Time Calculation

We take from Chapter 13:

- $S^{p}_{2500\ Å}$ = 3.2 x 10^{11} counts sec^{-1} pix_{λ}^{-1}per incident erg sec^{-1} cm^{-2} $Å^{-1}$ for `E230H`.
- $T_A = 0.6$ for the aperture throughput.
- $\varepsilon_f = 0.8$ for the encircled energy.
- $N_{\lambda pix} = 3$, since two pixels resolve the LSF.
- $N_{spix} = 3$, since 80% of the point source light is encircled with 3 pixels.

Using the equation for point sources on page 72, we determine a total count rate from the star of $C = 0.3$ counts sec^{-1} over 8 pixels. From Chapter 13 we see that ~22 percent of the point-source flux will be contained within the peak pixel. Thus the peak per pixel count rate will be approximately 0.3 x 0.22 / (0.8 x 2) = 0.045 counts sec^{-1} $pixel^{-1}$ and well within the local linear counting regime. We can use the information that we register ~0.3 counts sec^{-1} for every two pixels in the dispersion direction to estimate the global count rate (over the entire detector) as follows. Each order contains ~1024 pixels, and the `E230H` grating at the central wavelength setting of 2513 Å covers 33 orders (see Chapter 13). A rough estimate of the global count rate is thus ~33 x 512 x 0.3/ 0.8 ~6400 count sec^{-1} and we are well within the linear range.

To calculate the integration time, we can ignore both the sky background and the detector dark current which are several orders of magnitude fainter than the source. To achieve a signal-to-noise ratio of 50 we then require ~2500 counts which would take a total of ~2.3 hours. Fortunately, this is a CVZ target!

Imaging a Faint Stellar Source

Consider a case where the aim is to image a faint (V = 28), A-type star with the clear filter and the CCD detector. We want to calculate the integration time required to achieve a signal-to-noise ratio of 5. The count rate from the source is 0.14 counts sec^{-1} distributed over about 25 pixels using the information in Chapter 14. If we assume the background to be “typical high” (Table 6.6 on page 92), the count rate due to the background integrated over the bandpass is ~ 0.22 counts sec^{-1} $pixel^{-1}$ or 5.6 counts sec^{-1} in 25 pixels (and the detector dark rate is 50 times lower). We will need to be able to robustly distinguish cosmic rays if we are looking for faint sources, so we will use `CR-SPLIT=4`. We use the STIS Exposure Time Calculator to estimate the required exposure time to be 7333 seconds. To reproduce the numbers given by the ETC, we use the equation on page 77:

$$S/N = 5 = \frac{0.14 \cdot 2431}{\sqrt{0.14 \cdot 7333 + 0.23 \times 25 \times 7333 + 0.0025 \times 25 \times 7333 + 25 \times 16 \times 4}}$$

Alternately, we could have requested `LOW-SKY` (see “Sky Background” on page 79), since these observations are sky-background limited. In that case the sky background integrated over the bandpass produces ~0.018 counts sec^{-1} $pixel^{-1}$ to which we add the detector dark current to get a total background of 0.020 counts sec^{-1} $pixel^{-1}$. Using the full equation for exposure time again, we then determine that we require only ~30 minutes. This option is preferable to perform this experiment. To check the S/N, we use the equation on page 77:

$$S/N = 5 = \frac{0.14 \times 1860}{\sqrt{0.14 \times 1860 \quad + 0.02 \times 25 \times 1860 + 0.0025 \times 25 \times 1860 + 25 \times 16 \times 4}}$$

Time-Tag Observations of a Flare Star (AU Mic)

Suppose the aim is to do `TIME-TAG` observations of a flare star such as AU Mic, in the hydrogen Lyman-α 1216 Å line (see “MAMA TIME-TAG Mode” on page 184. We wish to observe it with the `G140M` grating, the MAMA detector and a 0.2 arcsec slit. AU Mic has V = 8.75, the intensity of its the Ly α line is about 6 (± 3) x 10^{-12} erg sec^{-1} cm^{-2} $Å^{-1}$, and the width (FWHM) of the line is about 0.7 (± 0.2) Å. We will assume that during bursts, the flux might vary by a factor of 10, so that the line flux may be up to 60 x 10^{-12} erg cm^{-2} sec^{-1} $Å^{-1}$. AU Mic is an M star and its ultraviolet continuum is weak and can be neglected.

We use from Chapter 13:

- S_λ^p = 1.97 x 10^{12} counts sec^{-1} $pix_\lambda{}^{-1}$per incident erg sec^{-1} cm^{-2} $Å^{-1}$.
- Aperture throughput T_A = 0.6.
- Encircled energy ε_f = 0.8.

- N_{spix} = 8.
- Derive $N_{\lambda pix}$= 14 since the line FWHM is ~ 0.7 Å and the dispersive plate scale for G140M is 0.05 Å pixel^{-1}.

Plugging these values into the point-source equation on page 72, we get C = 795 counts sec^{-1} over 8 x 14 pixels, or ~1000 counts sec^{-1} from the source (taking ε_f = 1.0). This is well below the MAMA `TIME-TAG` global linearity limit of 30,000 count sec^{-1} and the continuous observing limit of 26,000 count sec^{-1}. The line is spread over 14 pixels in dispersion and roughly only 10% of the flux in the dispersion direction falls in the peak pixel; thus the peak per-pixel count rate, P_{cr}, is roughly 795 / (14 x 8) = 8 counts sec^{-1} pixel^{-1}, and we are not near the MAMA local linearity limit.

For a `TIME-TAG` exposure, we need to determine our maximum allowed total observation time, which is given by 6.0 x 10^7/ C seconds or roughly 1258 minutes = 21 hours. For Phase II only, we will also need to compute the value of the `BUFFER-TIME` parameter, which is the time in seconds to reach 2 x 10^6 counts, in this case 2515 seconds (=2x10^6/795).

Tabular Sky Backgrounds

We provide a table of the *high* sky background numbers as plotted in Figure 6.1, for easy reference. See the text for more details.

Table 6.6: High Sky Backgrounds

Wavelength	Earthshine	Zodiacal Light	Total Background
Å	erg sec^{-1} cm^{-2} Å^{-1} arcsec^{-2}	erg sec^{-1} cm^{-2} Å^{-1} arcsec^{-2}	erg sec^{-1} cm^{-2} Å^{-1} arcsec^{-2}
1000.	4.8E-23	7.3E-29	4.8E-23
1100.	8.8E-22	6.0E-27	8.8E-22
1200.	8.0E-23	6.1E-26	8.0E-23
1400.	8.6E-25	1.5E-24	2.3E-24
1500.	8.3E-25	5.3E-24	6.1E-24
1600.	5.1E-25	1.3E-22	1.3E-22
1700.	1.6E-24	4.1E-21	4.1E-21
1800.	1.9E-22	8.8E-21	8.9E-21
1900.	8.8E-22	1.3E-20	1.4E-20
2000.	2.0E-21	2.0E-20	2.2E-20
2100.	3.2E-21	7.0E-20	7.4E-20
2200.	1.5E-21	1.3E-19	1.3E-19
2300.	6.6E-22	1.0E-19	1.0E-19
2400.	5.0E-22	1.0E-19	1.0E-19
2500.	4.8E-22	1.4E-19	1.4E-19
2600.	1.1E-21	1.7E-19	1.7E-19

Table 6.6: High Sky Backgrounds (Continued)

Wavelength	Earthshine	Zodiacal Light	Total Background
Å	erg sec^{-1} cm^{-2} Å^{-1} arcsec^{-2}	erg sec^{-1} cm^{-2} Å^{-1} arcsec^{-2}	erg sec^{-1} cm^{-2} Å^{-1} arcsec^{-2}
2700.	1.4E-20	5.8E-19	5.9E-19
2800.	4.1E-21	1.6E-19	1.7E-19
2900.	8.6E-20	1.2E-18	1.3E-18
3000.	1.9E-19	7.0E-19	8.8E-19
3100.	4.1E-19	8.5E-19	1.3E-18
3200.	7.2E-19	1.3E-18	2.0E-18
3400.	1.3E-18	1.6E-18	2.9E-18
3500.	1.6E-18	1.6E-18	3.2E-18
3600.	2.1E-18	1.8E-18	3.9E-18
3700.	2.4E-18	1.9E-18	4.3E-18
3800.	2.5E-18	1.9E-18	4.3E-18
3900.	3.0E-18	1.9E-18	5.0E-18
4000.	4.8E-18	2.8E-18	7.5E-18
4200.	4.8E-18	2.9E-18	7.7E-18
4400.	6.0E-18	2.9E-18	8.9E-18
4600.	6.8E-18	3.1E-18	1.0E-17
4800.	6.7E-18	3.4E-18	1.0E-17
5000.	6.9E-18	3.0E-18	9.9E-18
5200.	6.9E-18	2.8E-18	9.7E-18
5400.	7.1E-18	2.8E-18	9.9E-18
5600.	7.4E-18	2.7E-18	1.0E-17
5800	7.4E--18	2.7E-18	1.0E-17
6000.	7.3E-18	2.6E-18	9.9E-18
6200.	7.0E-18	2.5E-18	9.5E-18
6400.	6.8E-18	2.5E-18	9.3E-18
6600.	6.7E-18	2.4E-18	9.1E-18
6800.	6.5E-18	2.3E-18	8.8E-18
7000.	6.3E-18	2.2E-18	8.5E-18
7200.	6.2E-18	2.2E-18	8.3E-18
7400.	5.9E-18	2.0E-18	7.9E-18
7600.	5.8E-18	1.7E-18	7.5E-18
7800.	5.6E-18	1.8E-18	7.4E-18
8000.	5.4E-18	1.7E-18	7.2E-18
8200.	5.2E-18	1.7E-18	6.9E-18
8400.	5.1E-18	1.6E-18	6.7E-18
8600.	4.9E-18	1.6E-18	6.4E-18
8800.	4.7E-18	1.5E-18	6.2E-18
9000.	4.5E-18	1.3E-18	5.9E-18

Table 6.6: High Sky Backgrounds (Continued)

Wavelength	Earthshine	Zodiacal Light	Total Background
Å	erg sec^{-1} cm^{-2} Å^{-1} arcsec^{-2}	erg sec^{-1} cm^{-2} Å^{-1} arcsec^{-2}	erg sec^{-1} cm^{-2} Å^{-1} arcsec^{-2}
9200.	4.4E-18	1.3E-18	5.8E-18
9400.	4.3E-18	1.6E-18	5.9E-18
9600.	4.2E-18	1.3E-18	5.6E-18
9800.	4.1E-18	1.2E-18	5.3E-18
10000.	3.9E-18	1.1E-18	5.0E-18
10200.	3.8E-18	1.1E-18	4.8E-18
10400.	3.6E-18	1.0E-18	4.7E-18
10700.	3.5E-18	9.8E-19	4.4E-18
10800.	3.4E-18	9.6E-19	4.4E-18
11000.	3.3E-18	9.3E-19	4.2E-18

Table 6.7: Geocoronal Emission Lines

Wavelength (Å)	ID	Line Width (Å)	Intensity			
			Day		Night	
			kilo-Rayleighs	erg s^{-1} cm^{-2} arcsec^{-2}	kilo-Rayleighs	erg s^{-1} cm^{-2} arcsec^{-2}
1216	Ly-α	0.04	~20	6.1 x 10^{-13}	2	6.1 x 10^{-14}
1302	O I	0.013	~2	5.7 x 10^{-14}	0.013	3.8 x 10^{-16}
1356	O I	0.013	~0.2	~5 x 10^{-15}	~ 0.001	~3 x 10^{-17}
2470	O I	0.023	< 0.2	<3 x 10^{-15}	< 0.001	<1.5 x 10^{-17}

CHAPTER 7
Feasibility and Detector Performance

In This Chapter...

STIS employs two fundamentally different types of detectors: a UV-optimized CCD for use from the near UV to the near IR, and Multi-Anode Microchannel Array detectors, known as MAMAs, for use in the ultraviolet. The CCD and the MAMA detectors are used in different ways and impose their own unique limitations on the feasibility of observations performed with them. In this chapter we present the properties of the STIS detectors, describe how to use them to optimize scientific programs, and list the steps you should take to ensure the feasibility of your observations.

The CCD

Detector Properties

The `STIS/CCD` is a low-noise device capable of high sensitivity in the visible and the near UV. It is a thinned, backside-illuminated device manufactured by Scientific Imaging Technologies (SITe). In order to provide a near-UV imaging performance, the CCD was backside-treated and coated with a wide-band anti-reflectance coating. The process produces acceptable near-UV quantum efficiency (QE) without compromising the high QE of the visible bandpass. The

CCD camera design incorporates a warm dewar window, designed to prevent buildup of contaminants on the window, which were found to cause a loss of UV throughput for the WFPC2 CCDs. A summary of the STIS/CCD's performance is given in Table 7.1. The performance values on read noise and dark current are those valid as of April 1998.

Table 7.1: CCD Detector Performance Characteristics

Characteristic	CCD Performance
Architecture	Thinned, backside illuminated
Wavelength range	2000–11,000 Å
Pixel format	1024 x 1024 illuminated pixels
Field of view	52 x 52 arcseconds
Pixel size	21 x 21 μm
Pixel plate scale	0.05071 arcseconds
Quantum efficiency	~20% @ 3000 Å ~67% @ 6000 Å ~29% @ 9000 Å
Dark count at –83˚ C	0.0025 e^{-} sec^{-1} pix^{-1}
Read noise	4.0 e^{-} rms at GAIN=1 6.8 e^{-} rms at GAIN=4
Full well	144,000 e^{-} over the inner portion of the detector 120,000 e^{-} over the outer portion of the detector
Saturation limit	33,000 e^{-} at GAIN=1 144,000 e^{-} at GAIN=4

CCD Spectral Response

The spectral response of the unfiltered CCD is shown in Figure 5.1 on page 53 (labeled as 50CCD). This figure illustrates the extremely wide bandpass over which this CCD can operate. The wide wavelength coverage is an advantage for deep optical imaging. The near-UV sensitivity of the CCD makes it a good alternative to the NUV-MAMA for low- and intermediate-resolution spectroscopy from ~2500 to 3100 Å using the G230LB and G230MB grating modes (see Table 4.1, "STIS Spectroscopic Capabilities," on page 34).

Based on data to date, the STIS CCD does not suffer from Quantum Efficiency Hysteresis (QEH)—that is, the CCD responds in the same way to light levels over its whole dynamic range, irrespective of the previous illumination level.

CCD Long-Wavelength Fringing

Like most CCDs, the STIS CCD exhibits fringing in the red, longward of ~7500 Å. This fringing limits the signal-to-noise routinely achievable in the red and near IR unless contemporaneous flats are obtained (see below). In principle, fringing can also affect imaging observations if the source's emission over the `50CCD` or `F28X50LP` bandpass is dominated by emission lines redward of 7500 Å. However, if the bulk of the emission comes from blueward of 7500 Å, then emission from multiple wavelengths will smooth over the fringe pattern so that imaging will not be affected by fringing.

The amplitude of the fringes is a strong function of wavelength and spectral resolution. Table 7.2 lists the observed percentile peak-to-peak and rms amplitudes of the fringes as a function of central wavelength for the `G750M` and `G750L` gratings. The listed "peak-to-peak" amplitudes are the best measure of the impact of the fringing on your data. The rms values at wavelengths < 7000 Å give a good indication of the counting statistics in the flat-field images used for this analysis.

Table 7.2: Fringing Amplitude in Percent as a Function of Wavelength

Wavelength (Å)	G750M peak-to-peak	G750M rms	G750L peak-to-peak	G750L rms
6100		1.21		
6250		1.23		
6600		1.23		
6750		1.29		
7250	4.62	1.52	3.18	2.13
7750	9.61	3.10	8.58	3.08
8250	10.53	3.26	6.76	2.80
8750	14.83	3.85	10.81	3.98
9250	27.16	9.00	23.42	7.92
9750	32.09	10.78	25.35	8.96
10250	18.23	6.04	17.30	5.89

The fringe pattern can be corrected for by rectification with an appropriate flat field. The fringe pattern is a convolution of the contours of constant distance between the front and back surfaces of the CCD and the wavelength of the light on a particular part of the CCD. The fringe pattern has been shown to be very stable, as long as the wavelength of light on a particular part of the CCD stays constant. However, due to the grating wheel positioning uncertainty (see page 23) and the effect of temperature drifts in orbit, the wavelength on a particular part of the CCD will vary from observation to observation. Thus, the best de-fringing results are obtained by using a contemporaneous flat ("fringe flat"), i.e., a tungsten flat

taken at the same grating wheel setting, during the same orbit as your scientific exposures.

Table 7.3 compares the estimated peak-to-peak fringe amplitudes *after* flat-fielding by the library flat and by those after flat fielding with an appropriately processed contemporaneous flat. These estimates are based upon actual measurements of spectrograms of both point sources and extended sources, made during Cycle 7 (the results for point sources and extended sources were essentially the same). Figure 7.1 shows such a comparison for a `G750L` spectrogram of a white dwarf; in this figure, the top panel shows white dwarf GD153 (central wavelength 7751 Å) with no flat field correction, the second spectrogram shows the result of de-fringing with the standard pipeline flat field, and the third spectrogram shows the result of de-fringing with a contemporaneous flat (all spectrograms were divided by a smooth spline fit to the stellar continuum). It is clear that a contemporaneous flat provides a great improvement over the use of a library flat. Therefore, if you are observing in the far red (> 7500 Å) and using grating `G750L` or `G750M`, you should take a contemporaneous flat field along with your scientific observations. More detailed information and analysis on fringe correction for STIS long-wavelength spectra can be found STIS ISR 98-19 and the references therein.

Table 7.3: Residual Fringe Amplitude (rms, in percent) After Flat-Fielding with Library Pipeline Flat and a Contemporaneous Flat

Wavelength (Å)	G750M, library flat: residual	G750M, contemp. flat: residual[a]	G750L, library flat: residual	G750L, contemp. flat: residual
7500	3.0	1.2	4.0	0.9
7750	2.5	1.3	5.3	0.8
8000	4.2	1.3	7.5	1.0
8250	4	1.0	5.3	0.9
8500	5	0.9	8.3	1.0
8750	6	0.9	6.5	0.9
9000	8	—	8.3	1.0
9250	10	—	17.5	1.4
9500	11	—	18.7	2.0
9750	12	—	19.7	2.4
10000	10	—	11.7	2.4

a. Measurements of the fringe amplitude had not been made yet for `G750M` wavelength settings redward of 8561 Å when this Handbook was issued. However, from our experience with fringe corrections we expect the residual fringe amplitudes to be of order 1% when contemporaneous fringe flats are used.

Figure 7.1: Comparison of De-fringing Capabilities of Pipeline Flats and Those of Contemporaneous Flats

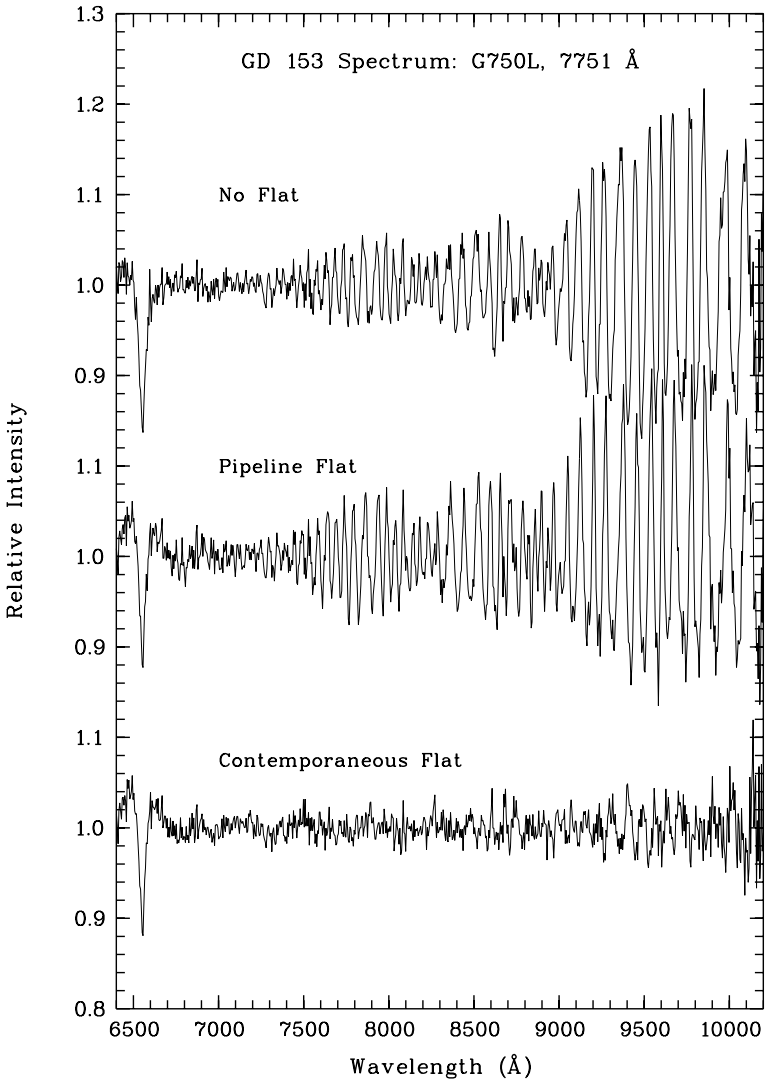

Optical Performance

Verification testing has shown that STIS meets its image-quality specifications. While the optics provide fine images at the focal plane, the detected point-spread functions (PSFs) are degraded somewhat more than expected by the CCD at wavelengths longward of about 7500 Å, where a broad halo appears, surrounding the PSF core. This halo is believed to be due to scatter within the CCD mounting substrate, which becomes more pronounced as the silicon transparency increases at long wavelengths. The effects of the red halo, which extend to radii greater than 100 pixels (5 arcsec), are not included in the encircled energies as a function of observing wavelength which are described for the CCD spectroscopic modes and the CCD imaging modes in Chapters 13 and 14, respectively. The integrated energy in the halo amounts to approximately 20% of the total at 8050 Å and 30%

at 9050 Å (see also STIS ISR 97-13 for the implication for long-slit spectroscopic observations at long wavelengths).

The CCD plate scale is 0.05071 arcseconds per pixel, for imaging observations and in the spatial (across the dispersion) direction for spectroscopic observations. Due to the effect of anamorphic magnification, the plate scale in the dispersion direction is slightly different and dependent on the grating used and its tilt. The plate scale in the dispersion direction ranges from 0.05121 to 0.05727 arcseconds per pixel (see STIS ISR 98-20).

The CCD detector produces a relatively faint, out-of-focus, ring-shaped "ghost" image, due to specular reflection from the CCD surface and window. The ring contains about 1% of the total energy in the image and is very stable. Additional rings of similar size can be seen at other locations in the field in grossly saturated images, but these contain only of order 10^{-5} of the total energy and are thus not likely to be detected in normal scientific images. Lines drawn from stars in images through their respective ghosts are found to converge at a "radiant point" located to the lower right of the image center. This effect is illustrated in Figure 7.2 where the line segments are drawn from pixel coordinates 528,342 (in 1024 x 1024 user coordinates) through the centroids of the brightest stars in the image. Note that these line segments intercept the centers of the ring-like ghosts very well. Observers who wish to avoid placing very faint objects within the range of the ghosts may want to take this geometry into account when writing Phase II proposals.

Figure 7.2: Ring-Shaped Ghost Images Near Bright Point Sources (50CCD Image)

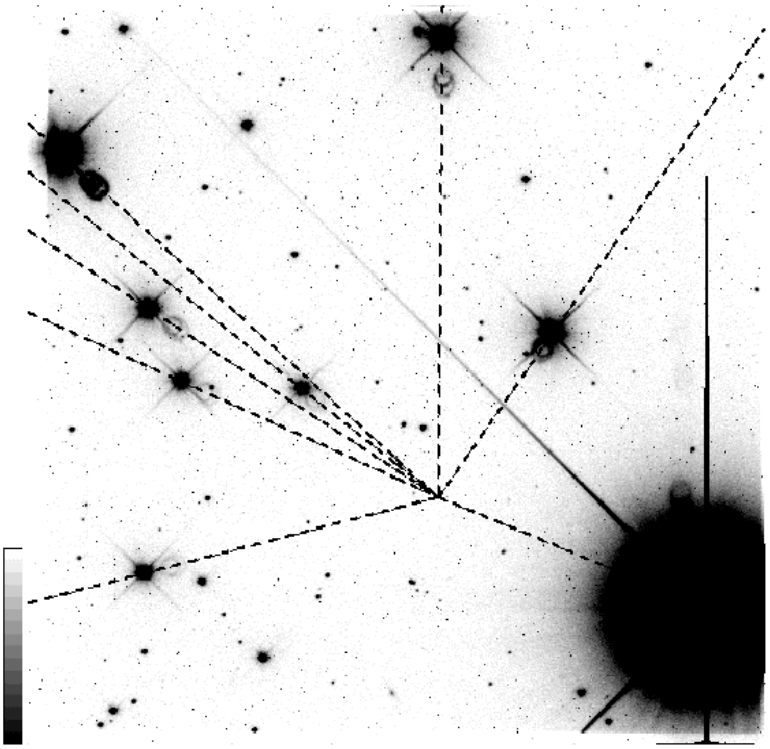

Readout Format

A full detector readout is 1062 x 1044 pixels including physical and virtual overscans. Scientific data are obtained on 1024 x 1024 pixels, each projecting to ~0.05 x 0.05 arcseconds on the sky. For spectroscopic observations, the dispersion axis runs along `AXIS1` (image X or along a row of the CCD), and the spatial axis of the slits runs along `AXIS2` (image Y or along a column of the CCD). The CCD supports the use of subarrays to read out only a portion of the detector, and on-chip binning. For more details see “CCD ACCUM Mode” on page 177.

Analog-To-Digital Conversion

Electrons which accumulate in the CCD wells are read out and converted to data numbers (DN, the format of the output image) by the analog-to-digital converter at a default `CCDGAIN` of 1 e^-/DN (i.e., every electron registers 1 DN). The CCD is also capable of operating at a gain of 4 e^-/DN. The analog-to-digital converter operates at 16 bits, producing a maximum of 65,536 DN $pixel^{-1}$. The readout noise and saturation limits of the CCD are rather strong functions of `CCDGAIN` setting, and are listed in Table 7.1. The `CCDGAIN=1` setting has the lowest readout noise and digitization noise, and is thus the most appropriate setting for observations of faint sources. Unfortunately however, saturation is already occurring at about 33,000 e^- at the `CCDGAIN=1` setting, so that the maximum 144,000 e^- of the CCD full well (see “CCD Saturation: the CCD Full Well” on page 102 below) *cannot* be reached.

While the `CCDGAIN=4` setting does allow one to reach the CCD full well, short exposures taken in `CCDGAIN=4` show large-scale pattern noise (“ripple”) that is not removed by the standard bias images. Figure 7.3 (a 0.2 second exposure of a lamp-illuminated small slit) shows an example of this effect. The peak-to-peak intensities of the ripples vary from near zero to about 1 DN, and there is a large amount of coherence in the noise pattern. This coherence makes background determination difficult and limits the precision of photometry in short exposures taken in `CCDGAIN=4`. Observers needing precise imaging photometry are therefore advised to use the default `CCDGAIN=1` setting, unless the brightest sources of interest will reach the saturation limit in a very short exposure time (< 0.2 seconds, see “CCD Shutter Effects” on page 103). Use of the `CCDGAIN=4` setting for imaging photometry is only recommended in the latter case.

Figure 7.3: Ripple Effect in Short Exposures with CCDGAIN=4

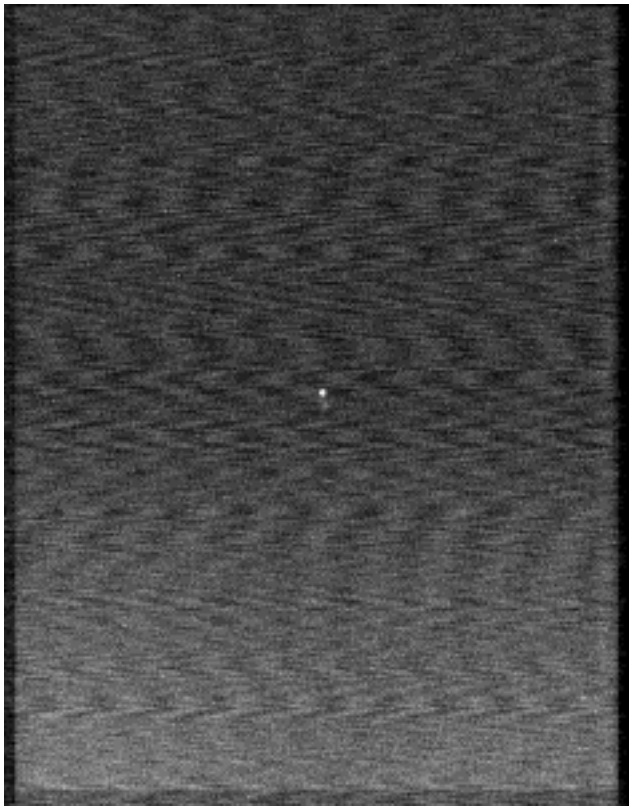

CCD Operation and Feasibility Considerations

CCD Saturation: the CCD Full Well

There are no hard bright-object limits to worry about for CCD observations, since the CCD cannot be damaged by observations of bright sources. However, the CCD pixels do saturate at high accumulated count levels, due to the finite depth of the CCD full well. The CCD saturates at ~144,000 electrons pixel^{-1} in most of the effective area of the chip; however, over the outermost (serial) portion the CCD saturates at 120,000 electrons pixel^{-1}. The variation of the CCD full well over the chip occurs because of nonuniformity in the process of boron implantation, which creates the potential wells in this type of CCD.

Saturation imposes a limit on the product of the count rate and the integration time. Keep the total counts *in the pixels of interest* below the saturation level, either by keeping the exposure time short enough that the limit is not violated in any single integration or by choosing a more appropriate configuration. You can allow saturation to occur in regions of the image over which you do not wish to extract information (e.g., you can allow a star or single emission line to saturate if you are interested in other features). Remember, however, that once the CCD full

well is over full, charge will bleed along the columns of the CCD so that neighboring pixels (along the slit for spectroscopic observations) will also be affected. Saturation *cannot* be corrected for in post observation data processing.

In “Determining Count Rates from Sensitivities” on page 70, we explained how to determine the peak counts sec^{-1} $pixel^{-1}$ expected for your observation. In Chapter 13 for each grating mode and in Chapter 14 for each imaging mode, we provide, for spectroscopy and imaging, respectively, plots of exposure time to fill the CCD full well versus source flux for each STIS configuration. Lastly, an exposure-time calculator is available on the STScI STIS web page. Use one of these sources to ensure that your observations will not saturate sources of interest.

The minimum CCD exposure time is 0.1 seconds, providing a true limit to the brightest source that can be observed *without saturating*.

Keep the accumulated electrons $pixel^{-1}$ per exposure below 120,000 at `CCD-GAIN=4`, and below 30,000 at `CCDGAIN=1`.

CCD Shutter Effects

The STIS CCD camera features a high-speed shutter which eliminates the need for a shutter illumination correction, even at the shortest commandable exposure time of 0.1 seconds. The only two minor drawbacks of using this shortest exposure time are the following: (i) a non-reproducible large-scale variation in intensity of a very low amplitude (~0.2%) which is due to a slight non-uniformity of the shutter speed, and (ii) a mean count rate which is ~3% lower than those of longer exposures, which is due to an inaccuracy of the shutter timing at this setting. These minor effects *only* occur for the shortest exposure times, and disappear completely for exposure times of 0.3 seconds and longer.

Cosmic Rays

All CCD exposures are affected by cosmic rays. The rate of on-orbit cosmic ray hits in orbit is very high compared to ground-based observations. The current rate at which pixels are affected by cosmic-ray hits is 30.0 (± 3.7) pixels per second for the STIS CCD. To allow removal of cosmic rays in post-observation data processing we recommend that whenever possible, given signal-to-noise constraints, you take two or more exposures in any given CCD configuration (see also “CR-SPLIT” on page 188). The greater the number of independent exposures, the more robust is the removal of cosmic rays and for very long integrations it is convenient to split the exposure into more than two separate images to avoid coincident cosmic-ray hits. As an example, for two 1200 sec exposures, about 1250 CCD pixels will be hit in both images and will therefore be unrecoverable. Moreover, since cosmic ray hits typically affect ~5 pixels per event, these pixels will not be independently placed, but rather will frequently be adjacent to other unrecoverable pixels. However, observers must balance the

decrease in signal-to-noise which results from the splitting of exposures when in the read noise limited regime with the desire to remove cosmic rays.

In observations of faint sources, particularly for dispersed light exposures, the intrinsic count rates can be very low. The exposure time needed to reach a break-even between the read-out noise and the Poisson noise per pixel associated with the minimal sky background is ~15 minutes for imaging in `50CCD` mode, and ~36 minutes for slitless spectroscopy with G750L. With a dark current of ~0.003 e^- sec^{-1} it takes ~90 minutes of integration for the Poisson statistics on the detector background to equal the read noise. Therefore, repeated short exposures of faint sources, can significantly increase the total noise from added readouts. Selecting the correct number, and length of repeated integrations requires a consideration of the trade-off between increased readnoise and more robust cosmic-ray elimination. The STIS Exposure-Time Calculator, or the S/N plots in Chapters 13 and 14, can help you determine whether your observations are in the read-noise dominated regime.

Be sure to take at least two identical CCD exposures in each configuration to allow removal of cosmic rays in post-observation data processing.

Hot Pixels

Hot pixels, caused by radiation damage, occur in the STIS CCD. Dark frames are currently obtained twice a day in order to maintain a master list of hot pixels and to update the pipeline superdark reference files on a weekly basis. On a monthly time scale, the CCD is raised to ambient temperature, from its normal operating temperature of ~ –83˚ C, in order to permit annealing of hot pixels.

Analysis of data from orbit has shown that the annealing process is successful in that 80% of transient hot pixels (hotter than 0.1 electron sec^{-1} pix^{-1}) are annealed away each month. Apart from the transient hot pixels, there is a substantial number of hot pixels that stay persistently hot after anneals. At present, ~0.4% of the pixels of the STIS CCD are persistently hot. The total number of hot (>0.1 electron sec^{-1} pix^{-1}) pixels is currently ~6000 after an anneal (April 1998). A more detailed analysis of the hot-pixel growth rate, also a function of hot pixel intensity, can be found in STIS ISR 98-06.

While post-pipeline calibration using appropriate STIS reference superdarks allows one to subtract most hot pixels correctly (to within the Poisson uncertainty), the best way to eliminate all hot pixels is by *dithering* (making pixel-scale positional offsets between individual exposures). Dithering as a method of data-taking is described in detail in Chapter 11.

CCD Bias Subtraction and Low-Level Non-Linearity

Analysis of CCD images taken during ground calibration and in Cycle 7 has revealed the existence of low-level changes in the bias pattern (at the tenths of a DN level) and a low-level amplifier nonlinearity. The amplifier non-linearity was uncovered during the analysis of the overscan region on flat-field images. The bias value of a given row in the serial overscan region of flat-field images is *depressed* with respect to the nominal bias value by an amount proportional to the mean signal in that row. However, the small proportionality factors and low DN levels at which the nonlinearity occurs render the problem negligible for most STIS scientific applications. Instances of data that may be slightly affected by this problem (at the <1% level) are aperture photometry of faint sources (in imaging mode), especially in the case of a crowded region with nearby bright sources which would cause a local depression of the bias value, and photometry of diffuse extended objects which cover a large number of pixels. The brightest hot pixels (see “Hot Pixels” on page 104) also cause a measurable local depression in the bias value, but their effect is corrected for by using the appropriate superdark reference file during CCD calibration.

Observers obtaining full-frame CCD images obtain both physical serial overscan and virtual parallel overscan on their frames; the virtual overscan does not appear to be subject to the amplifier nonlinearity problem and can be used to estimate the importance of this effect in your images. Observers using subarrays (e.g., to reduce the time interval between reads and limit the data volume when performing variability observations in the optical; see also Chapter 11) will obtain only the serial overscan.

UV Light and the STIS CCD

In the optical, each photon generates a single electron. However, in the near UV, shortward of ~3200 Å there is a finite probability of creating more than one electron per UV photon (see Christensen, O., *J. App. Phys*. **47**, 689, 1976). Users will need to take this into account when calculating signal-to-noise ratios and exposure times for the `G230LB` and `G230MB` gratings, as described in “Special Case—Spectroscopic CCD Observations at l<2500 Å” on page 78.

Initial laboratory testing of STIS CCDs showed that excessive illumination by UV light can cause an elevation in residual dark current, due to a surface chemistry effect. However, the actual STIS flight CCD was tested for this effect during ground calibration by the STIS IDT and the effect was found to be much less than previously suspected; this effect is now a concern *only* for clear (`50CCD`) imaging of *extremely UV-bright targets*. Observations of fields with UV-bright objects should be dithered (i.e., positional offsets applied between readouts) to ensure that the UV tail from bright sources does not cause a residual elevation of the dark current for subsequent science observations. It is also recommended to use the longpass-filtered aperture, `F28X50LP`, rather than the `50CCD` clear aperture, during target acquisitions (see also “Selecting Target-Acquisition Parameters” on page 132) when possible. The specific results of the ground testing on the effect of UV overillumination are summarized in Table 7.4.

Table 7.4: Effect of CCD UV Overillumination on Elevation of Dark Current

Overillumination Rate (e^- $pixel^{-1}$)	Initial Dark Current Elevation (%)	Time to Return to Nominal
500,000	500	30 min
5,000,000	1500	40 min

The MAMA Detectors

MAMA Properties

There are two MAMA detectors: the `STIS/FUV-MAMA` provides coverage from 1150 to 1700 Å and the `STIS/NUV-MAMA` provides coverage from 1650 to 3100 Å (with lower response to below 1200 Å). The STIS MAMA detectors are photon-counting devices which process events serially. They can be used to take data in either an accumulate (`ACCUM`) mode in which a time-integrated image is produced, or in a time series (`TIME-TAG` mode) in which the detector location and time of arrival of each photon are recorded as an event stream (see “MAMA ACCUM Mode” on page 181 and “MAMA TIME-TAG Mode” on page 184, respectively). The primary benefits afforded by the STIS MAMAs, in comparison with previous HST UV spectroscopic detectors such as those of the GHRS and FOS, are high spatial resolution, two-dimensional imaging over a relatively large field of view, and low background for point sources. The MAMA detector was developed by J. Timothy and R. Bybee for X-ray and UV imaging applications. The properties of the STIS MAMA detectors are summarized in Table 7.5.

Table 7.5: STIS MAMA Detector Performance Characteristics

Characteristic	FUV-MAMA Performance	NUV-MAMA Performance
Photocathode	CsI	Cs_2Te
Wavelength range	1150–1700 Å	1600–3100 Å
Pixel format	1024 x 1024	1024 x 1024
Pixel size	25 x 25 μm	25 x 25 μm
Image mode pixel plate scale	0.0245 x 0.0247 arcseconds	0.0245 x 0.0247 arcseconds
Field of view	25.1 x 25.3 arcseconds	25.1 x 25.4 arcseconds
Quantum efficiency	25% @ 1216 Å	10% @ 2537 Å
Dark count	5×10^{-6} to 1×10^{-5} counts sec^{-1} pix^{-1}	8×10^{-4} to 1.7×10^{-3} counts sec^{-1} pix^{-1}
Global count-rate linearity limit[a]	285,000 counts sec^{-1}	285,000 counts sec^{-1}
Local count-rate linearity limit[a]	~220 counts sec^{-1} pix^{-1}	~340 counts sec^{-1} pix^{-1}

a. Rate at which counting shows 10% deviation from linearity. These count rates are well above the bright-object screening limits.

Figures 7.4 and 7.5 illustrate the design of the FUV- and NUV-MAMA, respectively. A photocathode material is deposited on the front surface. The FUV-MAMA has an opaque CsI photocathode deposited directly on the face of the curved microchannel plate (MCP); the NUV-MAMA has a semi-transparent Cs_2Te photocathode deposited on the back side of the detector's entrance window.

Target photons strike the photocathode, liberating single photoelectrons which pass into the microchannel plate (MCP). There they are multiplied to a pulse of $\sim 4 \times 10^5$ electrons. The pulse is recorded by an anode array behind the photocathode and detected by the MAMA electronics which process it, rejecting false pulses and determining the origin of the photon event on the detector.

The FUV-MAMA has a field electrode (or *repeller wire*, as it is affectionately called) which is used to repel electrons emitted away from the microchannel plate back into the channels. This provides an increase in quantum efficiency of the detector at the price of a small increase in the detector PSF halo. The repeller wire is always on for FUV-MAMA observations.

Figure 7.4: Design of the FUV-MAMA

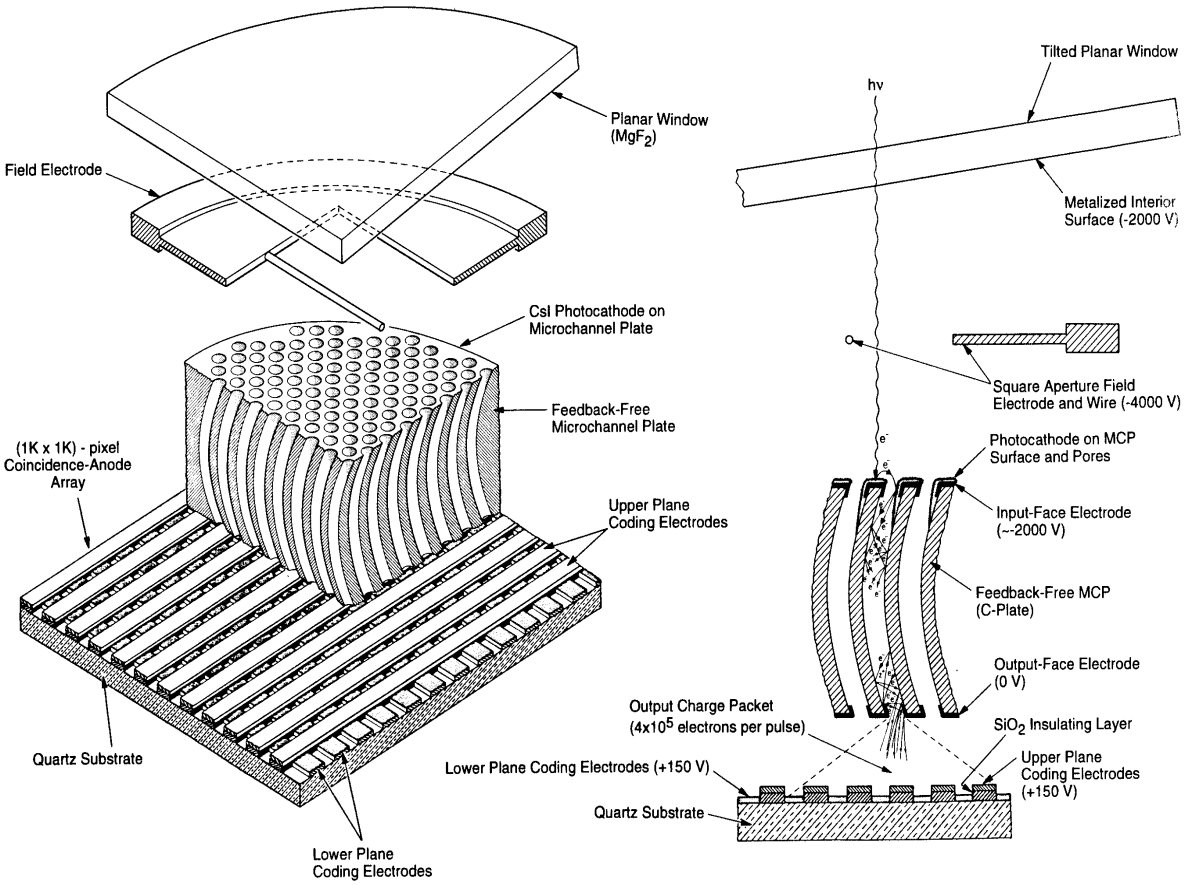

Figure 7.5: Design of the NUV-MAMA

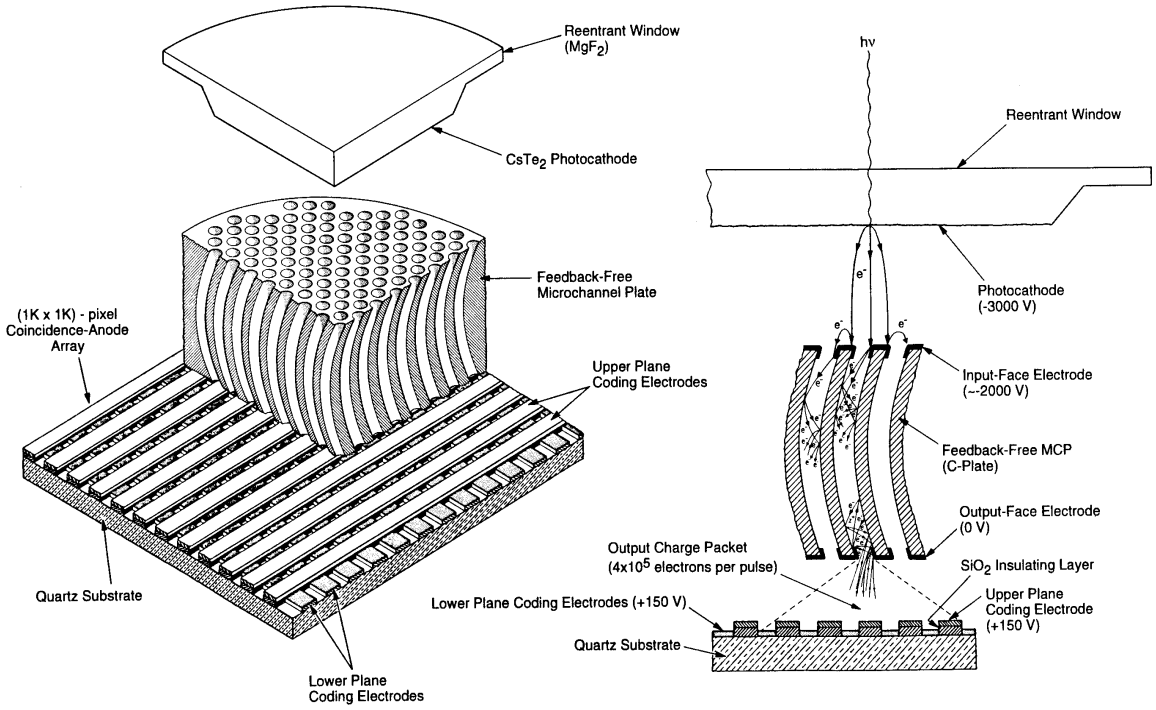

MAMA Spectral Response

The spectral responses of the unfiltered FUV- and NUV-MAMAs are illustrated in Figure 5.10 on page 63. The peak photocathode response of the FUV-MAMA occurs at Lyman-α. Its spectral response is defined by the cutoff of the MgF_2 window at 1150 Å at short wavelengths, and by the relatively steep decline of the CsI photocathode at long wavelengths. Out-of-band QE at longer wavelengths (>2000 Å) is $<10^{-6}$ yielding excellent solar-blind performance. The NUV-MAMA spectral response has a relatively flat maximum (~10%) which encompasses 1800–2600 Å. The photocathode QE declines to ~4% at 3150 Å, while at longer wavelengths the out-of-band QE is $\sim10^{-4}$. (See also “Unfiltered (Clear) MAMA Imaging—25MAMA” on page 62.)

Optical Performance

Both MAMAs exhibit low-level extended wings in their detector point-spread functions (PSFs), with the NUV-MAMA PSF being considerably worse. Sample MAMA detector PSFs are shown in Figure 7.6. For those wishing to model their effect on absorption- or emission-line equivalent-width measurements or coronographic observations, the LSFs and detector PSFs are maintained on the STScI STIS World Wide Web page.

Figure 7.6: MAMA Detector PSFs

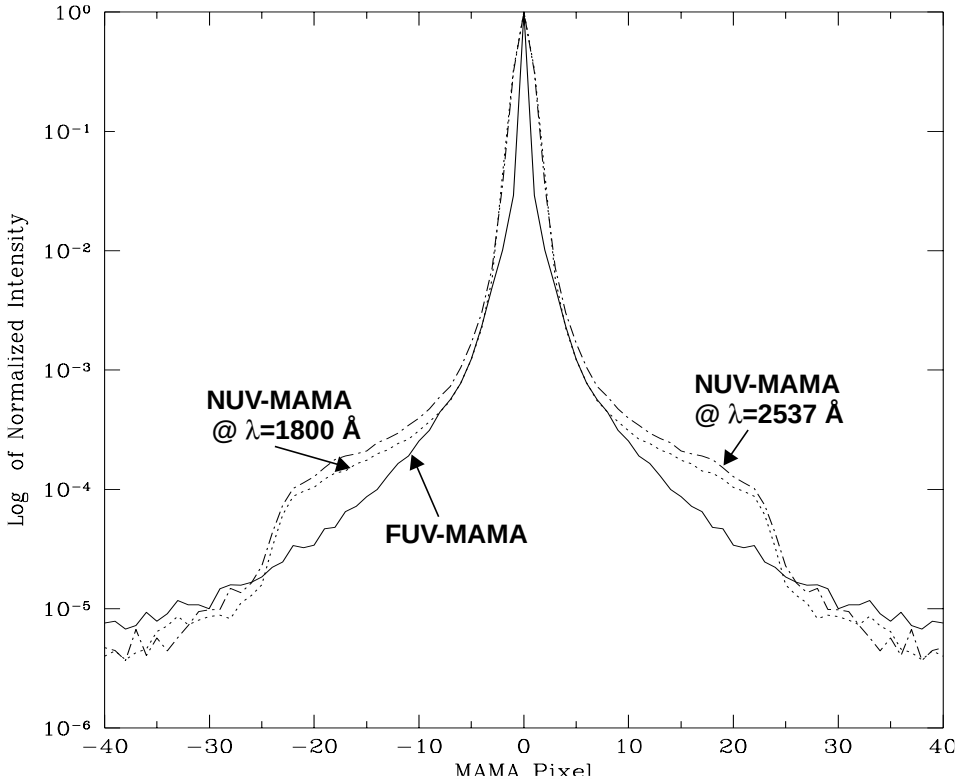

MAMA Operation and Feasibility Considerations

MAMA Saturation—Overflowing the 16 Bit Buffer

The MAMAs are photon-counting detectors: as each photon is recorded, it is placed into buffer memory. The STIS buffer memory stores values as 16-bit integers; hence the maximum number it can accommodate is 65,536 counts per pixel in a given ACCUM mode observation. When accumulated counts per pixel exceed this number, the values will wrap. As an example, if you are counting at 25 counts sec^{-1} $pixel^{-1}$, you will reach the MAMA saturation limit in ~24 minutes.

Keep accumulated counts per $pixel^{-1}$ below this value, by breaking individual exposures into multiple identical exposures (see also “Repeat Exposures” on page 191), each of which is short enough that fewer than 65,536 counts are accumulated per pixel. There is no read noise for MAMA observations, so no penalty is paid in lost signal-to-noise ratio when exposures are split. There is only a small overhead for each MAMA exposure (see Chapter 9 on page 159).

▽ Keep the accumulated counts per pixel below 65,536, by breaking single exposures into multiple exposures, as needed.

MAMA Darks

The STIS MAMA detectors have intrinsically very low dark currents. Dark currents measured during ground testing were less than 10 counts/sec for the FUV-MAMA and less than 30 counts/sec for the NUV over the whole detector. For the FUV-MAMA, this exceptionally low dark current was achieved on orbit. For the NUV-MAMA, charged particle impacts on the MgF_2 faceplate cause a faint glow that results in a dark current of 800–2000 counts per second, varying both with temperature and the past thermal history of the detector. This glow is not present for the FUV-MAMA, but the dark current nevertheless varies with time and with position on the detector. The different dark-current behaviors of the detectors are discussed in more detail below.

NUV-MAMA Dark Current

Most of the dark-current in the NUV-MAMA comes from phosphorescence of impurities in the MgF_2 detector faceplate. A simple model of the phenomenon has been developed by Jenkins and Kimble that envisions a population of impurity sites each having three levels: (1) a ground state, (2) an excited energy which can decay immediately to the ground state, and (3) a metastable level that is at an energy slightly below the one that can emit radiation. The metastable state can be thermally excited to the upper level, and this excitation rate is proportional to $e^{-\Delta E/kT}$, where ΔE is the energy difference between the levels. The behavior of the count rate vs. temperature leads to an estimate of 1.1 eV for Δ. At a fixed detector temperature of 30˚ C, the time-constant for the dark current to reach an equilibrium value is about 8 days. In practice because the MAMA high-voltage power supplies have to be shut down during SAA impacted orbits, the detector temperature varies from about 27˚ C to 35˚ C, and the dark current never reaches equilibrium.

However, the dark current can be predicted with about 20% accuracy using the contemporaneous temperature of the NUV-MAMA charge amplifier recorded in the `OM2CAT` parameter in the support file (`_spt`) that is part of the standard data products. Figure 7.7 shows the dark current vs. temperature measured from dark images taken from October 1997 to April 1998. The curve is: $dark = 9.012e10^{20} * \exp(-12710 / T)$.

Figure 7.7: Dark Current vs. Temperature

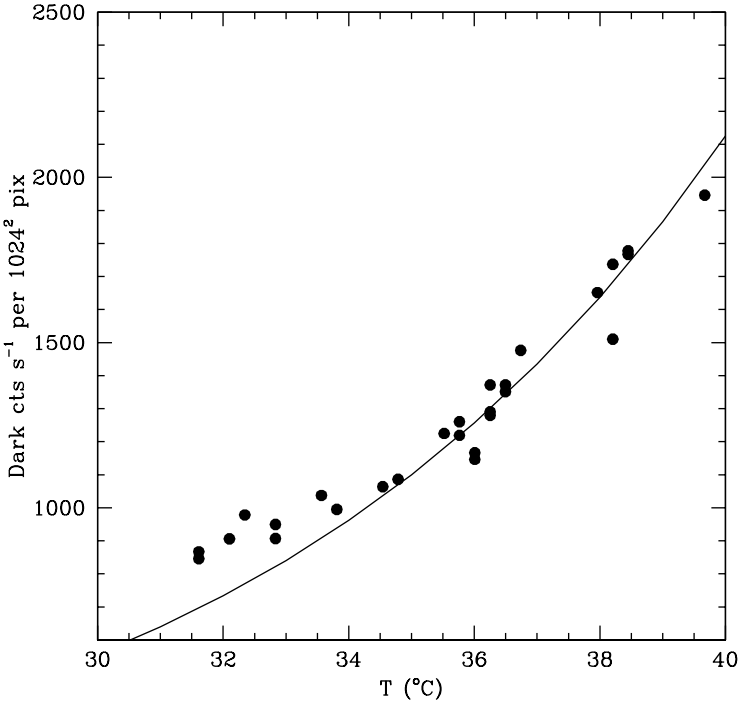

Because 99% of the NUV-MAMA dark current is due to photons hitting the detector, it is appropriate to apply the flat-field prior to subtracting the dark current. The dark current varies slowly across the face of the detector, being about 1.25 times higher near the lower left corner (`AXIS1`, `AXIS2` < 300) than at the center. This shape appears to be independent of temperature.

FUV-MAMA Dark Current

The FUV-MAMA dark current is typically about 7 counts/s across the face of the detector (7 x 10^{-6} counts s^{-1} pix^{-1}), but varies with time, particularly in one region of the detector. The reason for this time-dependence is not currently understood. It does not show the same dependence on temperature as the NUV-MAMA, and it was seen in ground testing. Thus it is probably not due to phosphorescence in the detector faceplate.

An example of the dark current variation across the detector can be seen in Figure 7.8, which is the sum of 20 1380 second dark frames taken during periods of high dark current. The dark current in the lower right quadrant (pixels [200:400,600:800]) appears to be stable to within 10% over time. The dark current in the upper left quadrant (pixels [900:1000,10:110]) varies with time. The total dark current is well approximated by the sum of a constant dark current plus a “glow” image, scaled to the net rate in the upper left quadrant. The behavior of the dark current vs. time in the “high” and “low” regions is shown in Figure 7.9 based the on-orbit darks. Dark current for the FUV-MAMA is not currently subtracted by the pipeline. However, the “glow” image is available from the STIS world-wide web pages, and can be used for off-line reduction.

Figure 7.8: Dark Current Variation Across Detector. The dark area has the higher dark current.

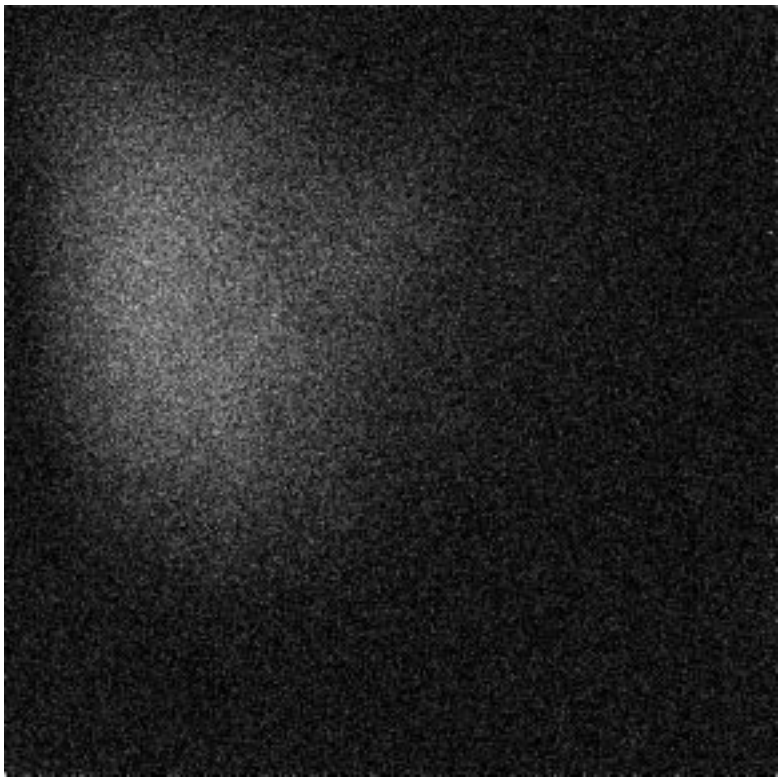

Figure 7.9: Dark Current vs. Time in High and Low Regions

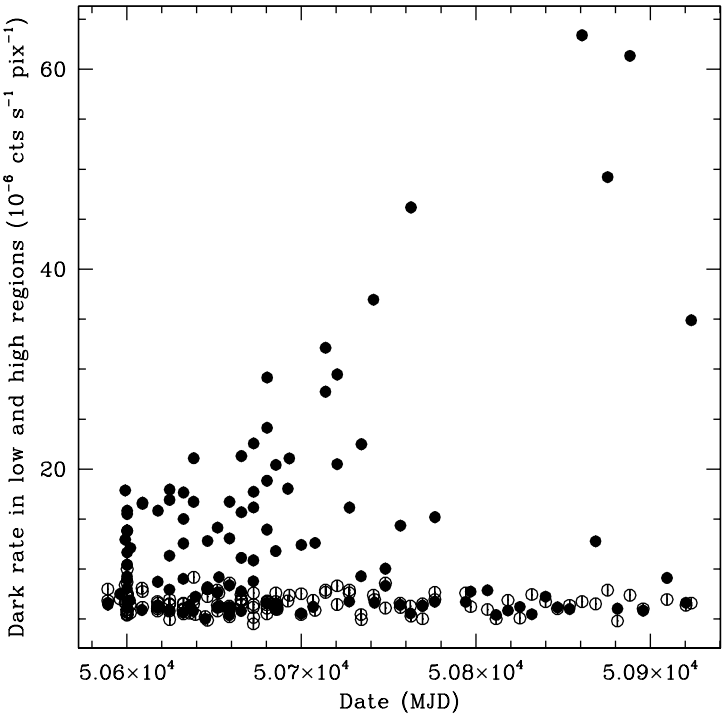

Because the dark current is so low in the MAMA detectors, a typical STIS FUV-MAMA observation will have less than one count per pixel from the dark. It is good to keep this in mind when reducing the data, as various standard measures of background (the median for example) are not good estimates when the data are quantized into just a few values. The best way to estimate the background is to identify hot pixels using the standard reference files, then use an unclipped mean for the remaining pixels in a source-free region of the image.

MAMA Signal-to-Noise Ratio Limitations

MAMA detectors are capable of delivering signal-to-noise ratios of the order of 100:1 per spectral resolution element (2 x 2 pixels) or even higher. Tests in orbit have demonstrated that such high S/N is possible with STIS (Kaiser et al.; Gilliland, STIS ISR 98-16.)

High S/N observations of several standard stars were obtained during STIS commissioning, and they were reduced with flats obtained during preflight testing of the detectors. Signal-to-noise ratios of 125 and 150 per spectral resolution element (for an 11 pixel extraction height in the across the dispersion) were achieved for the FUV- and NUV-MAMA observations, respectively; see Chapter 12 for a more detailed discussion.

For targets observed at a fixed position on the detector, the signal-to-noise ratio is limited by systematic uncertainties in the small-scale spatial and spectral response of the detector. The MAMA flats show a fixed pattern that is a combination of several effects including beating between the MCP array and the anode pixel array, variations in the charge-cloud structure at the anode, and low-level capacitive cross-coupling between the fine anode elements. Intrinsic pixel-to-pixel variations are 3.9% and 2.8% rms for the FUV- and NUV-MAMA, respectively, in 1024 x 1024 pixel format. (In the highres 2048 x 2048 format, see Chapter 11, the intrinsic variations are much larger.) This fixed pattern appears to be stable at the 1–2% level. The structure of the flat may vary slightly for different modes due to different incidence angles of the incoming photons on the microchannel-plate pores.

Observing strategies for achieving spectral S/N higher than ~50:1 are discussed in Chapter 12. For echelle-mode spectra, observers may want to consider the use of the FP-SPLIT slits, for first-order mode observations, they may wish to dither the target along the slit.

MAMA Nonlinearity

Global

The MAMA detectors begin to experience nonlinearity (photon impact rate not equal to photon count rate) at global (across the entire detector) count rates of 200,000 counts sec^{-1}. The non-linearity reaches 10% at 300,000 counts sec^{-1} and can be corrected for in post-observation data processing at the price of a loss of photometric reliability. Additionally, the MAMA detectors plus processing

software are not able to count reliably at rates exceeding 285,000 count sec^{-1}. For this reason and to protect the detectors, observations beyond this rate are not allowed (see “MAMA Bright-Object Limits” on page 115, below).

Local

The MAMA detectors remain linear to better than 1% in their counting up to ~22 counts sec^{-1} $pixel^{-1}$ for the FUV-MAMA and 34 counts sec^{-1} $pixel^{-1}$ for the NUV-MAMA. At higher rates, they experience local (at a given pixel) non-linearity. The nonlinearity effect is image dependent—that is, the non-linearity observed at a given pixel depends on the photon rate affecting neighboring pixels. This property makes it impossible to correct reliably for the local nonlinearity in post-observation data processing. In addition, the MAMA detectors are subject to damage at high local count rates (see the discussion of MAMA bright-object limits below).

MAMA Spectral Offsetting

For the FUV-MAMA, the repeller wire produces a small shadow on the detector with a depth of ~10% which is apparent on FUV-MAMA flat field images (see “MAMA Properties” on page 106). To avoid first-order mode spectra falling on the repeller wire shadow, all data taken with the `G140L` and `G140M` gratings are projected to fall 3 arcseconds or ~120 pixels (to `AXIS2` = 632) from the detector center (see also “MAMA ACCUM Mode” on page 181). This offsetting is done using the Mode Select Mechanism to tilt the grating.

For both the FUV- and the NUV-MAMA, the projection of the spectra on the detector for *all* spectroscopic modes are shifted slightly each month. This procedure is performed in order to minimize uneven charge depletion in the microchannel plates which would increase the non-uniformity of the flat fields. These monthly charge-offsetting shifts can shift the spectrum roughly ±30 pixels in `AXIS1` (dispersion) and ±80 pixels in `AXIS2` (cross-dispersion). Hence observers are advised to select settings that keep wavelength ranges of interest away from the extremes of wavelength settings and targets of interest away from the extreme ends of the long slits.

MAMA Bright-Object Limits

STScI has responsibility to ensure that the MAMA detectors are not damaged through over-illumination. Consequently, we have developed procedures and rules to protect the MAMAs. We ask all potential users to share in this responsibility by reading and taking note of the information in this section and designing observing programs which operate in the safe regime for these detectors.

Overview

The MAMA detectors are subject to catastrophic damage at high global and local count rates and cannot be used to observe sources which exceed the defined safety limits. The potential detector damage mechanisms include over-extraction of charge from the microchannel plates causing permanent reduction of response, and ion feedback from the microchannel plates causing damage to the photocathode and release of gas which can overpressure the tube.

To safeguard the detectors, checks of the global (over the whole detector) and local (per pixel) illumination rates are automatically performed in flight for all MAMA exposures. The *global illumination rate* is monitored continuously; if the global rate approaches the level where the detector can be damaged, the high voltage on the detector is automatically turned off. This event can result in the loss of all observations scheduled to be taken with that detector for the remainder of the calendar (~1 week). The *peak local illumination rate* is measured over the MAMA field at the start of each new exposure; if the local rate approaches the damage level, STIS will shutter, and the exposure will be lost.

Sources that would over-illuminate the MAMA detectors cannot be observed. It is the responsibility of the observer to avoid specifying observations that exceed the limits described below.

Observational Limits

To ensure the safety of the MAMA detectors and the robustness of the observing timeline, we have established observational limits on the incident count rates. Observations which exceed the allowed limits will not be scheduled. The allowed limits are given in Table 7.6, which includes separate limits for nonvariable and irregularly-variable sources. The global limits for irregular variable sources are a factor 2.5 more conservative than for sources with predictable fluxes. Predictable variables are treated as nonvariable for this purpose. Examples of sources whose variability is predictable are Cepheids or eclipsing binaries. Irregularly variable sources are, for instance, catacylsmic variables or AGN. Here and in general, “pixel” refers to the 1024 x 1024 format.

Table 7.6: Absolute MAMA Count-Rate Limits for Nonvariable and Variable Objects

Target	Limit Type	Mode	Channel	Screening Limit
Nonvariable	Global	All modes	FUV and NUV	200,000 c/s[a]
Nonvariable	Global	1st-order spectroscopy	FUV and NUV	30,000 c/s
Nonvariable	Local	Imaging	FUV and NUV	100 c/s/p[b]
Nonvariable	Local	Spectroscopy	FUV and NUV	75 c/s/p
Irregularly Variable	Global	All modes	FUV and NUV	80,000 c/s[c]
Irregularly Variable	Global	1st-order spectroscopy	FUV and NUV	12,000 c/s[c]
Irregularly Variable	Local	Imaging	FUV and NUV	100 c/s/p[c]
Irregularly Variable	Local	Spectroscopy	FUV and NUV	75 c/s/p[a]

a. c/s is counts sec^{-1}.
b. c/s/p is counts sec^{-1} pix^{-1}.
c. Applies to the phase when the target is brightest.

How Do You Determine if You Violate a Bright Object Limit?

As a first step, you can check your source V magnitude and peak flux against the bright-object screening magnitudes in Table 13.38 on page 312 or Table 14.33 on page 369 for your chosen observing configuration. In many cases, your source properties will be much fainter than these limits, and you need not worry further.

However, if you are near these limits (within 1 magnitude or a factor of 2.5 of the flux limits), then you need to carefully consider whether your source will be observable in that configuration. Remember the limits in these tables assume zero extinction and for spectroscopic observations do not include slit losses. Thus you will want to correct the limits appropriately for your source's reddening and the aperture throughput.

You can use the information presented in "Determining Count Rates from Sensitivities" on page 70 to calculate your peak and global count rates. Perhaps better, you can use the STIS Exposure-Time Calculator available through the STScI STIS World Wide Web page to calculate the expected count rate from your source. It has available to it a host of template stellar spectrograms. If you have a spectrum of your source (e.g., from IUE, FOS, or GHRS) you can also input it directly to the calculator. The calculator will evaluate the global and per pixel count rates and will warn you if your exposure exceeds the absolute bright-object limits. We recommend you use the STIS exposure time calculator if you are in *any doubt* that your exposure may exceed the bright-object MAMA limits.

Policy and Observers' Responsibility in Phase I and Phase II

It is the observers' responsibility to ensure that their observations do not exceed the bright-object count limits stated in Table 7.6.

It is your responsibility to ensure that you have checked your planned observations against the brightness limits prior to proposing for Phase I. If your proposal is accepted and we, or you, subsequently determine (in Phase II), that your source violates the absolute limits, then you will either have to change the target, if allowed, or lose the granted observing time. We encourage you to include a justification in your Phase I proposal if your target is within 1 magnitude of the bright-object limits for your observing configuration. For MAMA target-of-opportunity proposals, please provide an explanation of how you will ensure your target can be safely observed in your Phase I proposal.

STScI will screen all STIS observations that use the MAMA detectors to ensure that they do not exceed the bright-object limits. In Phase II, you will be required to provide sufficient information to allow screening to be performed.

Here we describe the required information you must provide.

Spectroscopy

To allow screening of your target in Phase II for spectroscopic MAMA observations you must provide the following for your target (i.e., for all sources which will illuminate the detector during your observations):

- V magnitude.
- Expected source flux at observing wavelength.
- Spectral type (one of the types in the screening tables).
- E_{B-V}.
- B-V color.

If you wish to observe a target which comes within one magnitude (or a factor of 2.5 in flux) of the limits in the spectroscopic bright-object screening table (Table 13.38 on page 312) for your configuration, after correction for aperture throughput and reddening, but which you believe will not exceed the absolute limits in Table 7.6 and so should be observable, you must provide auxiliary information to justify your request. Specifically:

- You must provide an existing UV spectrogram (e.g., obtained with IUE, FOS, or GHRS) of the star which proves that neither the global nor the local absolute limits will be exceeded.

- If you do not have such data, then you must obtain them, by taking a "pre-exposure" in a MAMA-safe configuration (e.g., with a ND filter in place or in a higher resolution mode) before we will schedule your observations. *Be sure to include the time (1 orbit in a separate visit) for such an observation in your Phase I Orbit Time Request, as needed.*

Imaging

The MAMA imaging bright-object screening magnitudes (see Table 14.33 on page 369) are very stringent, ranging from V = 15 to V = 20.5 for the different imaging apertures, and apply to all sources imaged onto the MAMA detector (i.e., not just the intended target of interest). Table 14.33 can be used to determine if the target of interest is above the bright-object limit. Starting in Cycle 8, STScI will use the second-generation Guide-Star Catalog (GSC II) to perform imaging screening for objects in the field of view other than the target itself. The GSC II contains measurements from photometrically calibrated photographic plates with color information for magnitudes down to at least V = 22 mag. This information will be used to support bright-object checking for fixed and for moving targets (major planets). STScI will make a best effort to perform the imaging screening using GSC II. However, observers should be prepared for the possibility that under exceptional circumstances GSC II may be insufficient. For instance, fields close to the Galactic plane may be too crowded to obtain reliable photometry. If for any reason the screening cannot be done with GSC II, the observer is responsible for providing the required photometry. In the case of moving targets, STScI will identify "safe" fields, and the observations will be scheduled accordingly. Observers will be updated on the status of their observations by their Contact Scientists. We anticipate that bright-object considerations will not have a significant effect on the scheduling of such observations.

Policy on Observations Which Fail Because they Exceed Bright-Object Limits

If your source passes screening, but causes the automatic flight checking to shutter your exposures or shut down the detector voltage causing the loss of your observing time, *then that lost time will not be returned to you*; it is the observer's responsibility to ensure that observations do not exceed the bright-object limits.

What To Do If Your Source is Too Bright for Your Chosen Configuration?

If your source is too bright for one configuration, it may be observable in another configuration (e.g., in a higher-dispersion configuration). The options open to you if your source count rate is too high in a given configuration include:

- Select a narrower slit which passes only a fraction of the source flux, for spectroscopic observations.
- Select a higher dispersion grating.
- For near-UV low-resolution and medium-resolution spectroscopy, consider using the CCD G230LB and G230MB modes (see "Cross-Over Regions" on page 40).

- Employ a neutral-density filter.
- Change configurations totally to observe a different portion of the spectrum of your target (e.g., switching to the CCD).

For further advice, see “Observing Too-Bright Objects with STIS” on page 205.

Bright-Object Protection for Solar System Observations

Observations of planets with STIS require particularly careful planning due to the very stringent overlight limits of the MAMAs. In principle Table 13.38 and Table 14.33 can be used to determine if a particular observation of a solar-system target exceeds the safety limit. In practice the simplest and most straightforward method of checking the bright object limits for a particular observation is to use the STIS Exposure-Time Calculator. With a user-supplied input spectrum, or assumptions about the spectral energy distribution of the target, the ETC will determine whether a specified observation violates any bright object limits.

Generally speaking, for small (<~0.5–1 arcsec) solar-system objects the local count rate limit is the more restrictive constraint, while for large objects (>~1–2 arcsec) the global limit is much more restrictive.

As a first approximation, small solar system targets can be regarded as point sources with a solar (G2 V) spectrum, and if the V magnitude is known, Table 13.38 and Table 14.33 can be used to estimate whether an observation with a particular STIS grating or filter is near the bright-object limits. V magnitudes for the most common solar-system targets (all planets and satellites, and the principal minor planets) can be found in the *Astronomical Almanac*. This approximation should provide a conservative estimate, particularly for the local limit, because it is equivalent to assuming that all the flux from the target falls on a single pixel, which is an overestimate, and because the albedos of solar-system objects are almost always < 1 (meaning that the flux of the object will be less than that of the assumed solar spectrum at UV wavelengths where the bright-object limits apply). A very conservative estimate of the global count rate can be obtained by estimating the peak (local) count rate assuming all the flux falls on one pixel, and then multiplying by the number of pixels subtended by the target. If these simple estimates produce numbers near the bright-object limits, more sophisticated estimates may be required to provide assurance that the object is not too bright to observe in a particular configuration.

For large solar-system targets, checking of the bright-object limits is most conveniently done by converting the integrated V magnitude (V_o, which can be found in the *Astronomical Almanac*) to V magnitude/arcsec^2 as follows:

$$V / \text{arcsec}^2 = V_o - 2.5 \log(1/area)$$

where *area* is the area of the target in arcsec^2. This V / arcsec^2 and the diameter of the target in arcsec can then be input into the ETC (choose the Kurucz model G2 V spectrum for the spectral energy distribution) to test whether the bright-object limits can be satisfied.

Alternatively, an observed spectrum obtained with a known slit size can be used as input to the ETC. Most calibration techniques produce units of flux (e.g., ergs sec^{-1} cm^{-2} $Å^{-1}$), even for extended targets. Such a calibration implicitly assumes a flux per solid angle (i.e., the angle subtended by the observing slit or object, whichever is smaller), and it is more appropriate to convert to units of surface brightness (ergs sec^{-1} cm^{-2} $Å^{-1}$ $arcsec^{-2}$) by dividing the calibrated flux by the appropriate area (slit size or object size, whichever is *smaller*). If such a spectrogram is available, it can be immediately examined and compared with the local limit in units of surface brightness given in Table 13.38 and Table 14.33, or passed to the ETC as a user-supplied spectrum. It can also be easily converted to counts sec^{-1} pix^{-1} by using the diffuse-source sensitivities for the appropriate grating or filter provided in this Handbook. Note that the sensitivities in this Handbook assume a specific slit *width*, so they need to be scaled by the desired slit width. The ETC provides another check of the local limit: if the peak count rate per pixel exceeds the local limit of 75 (for spectroscopic observations) or 100 (for imaging observations) counts sec^{-1} pix^{-1}, such an observation would not be allowed. The global limit can be checked by summing the count rate per pixel over wavelength, and multiplying by the desired slit length (in arcsec) divided by the pixel size (0.0247 arcsec) to produce total counts per second for the observation. If this number is larger than the appropriate global limit, the observation should not be performed because it will cause the instrument to enter safe mode. For such cases, a smaller slit size or higher-resolution grating could then be considered.

Jupiter and Saturn

To further aid the observer, we provide results of test simulations with Jupiter and Saturn; the input spectrograms are observed surface fluxes of Jupiter and Saturn from 1200 Å to 7000 Å. Jupiter and Saturn have corresponding visual magnitudes of V = 4.9 and 6.5 mag $arcsec^{-2}$, respectively. No variation of the surface brightness over the disk is taken into account. We assume that both planets have diameters >25 arcsec, i.e., exceeding the field size of the MAMA detectors. This assumption is appropriate for Jupiter and conservative for Saturn.

MAMA Spectroscopy

We adopt slit lengths of 6 and 25 arcsec for echelle and first-order grating observations, respectively. Slit widths are 1 arcsec in both cases. The slits are centered on the planets so that the planets overfill the apertures. The results for the local limits are in Table 7.7. The table gives the observed V magnitudes $arcsec^{-2}$ of the two planets and the limiting magnitudes for all echelle and first-order gratings. If the planet were as bright as the limiting magnitude, it would reach the limiting local count rates (75 counts sec^{-1} pix^{-1} for the FUV and NUV). No safety margin was added to the magnitudes listed in this and the subsequent tables. Table 7.7 suggests that only Jupiter observed with `G230L` would come close to the local brightness limit.

Table 7.7: Local Brightness Limits (V mag arcsec^{-2}) for Spectroscopy

	Observed	G140L	G140M	E140M	E140H	G230L	G230M	E230M	E230H
Jupiter	4.9	–5.2	–8.7	–10.2	–11.7	4.6	0.5	–0.5	–2.9
Saturn	6.5	-–.8	–9.2	–11.8	–12.8	4.4	0.3	–0.7	–3.1

Next we discuss the global limits. The global limits for echelle spectroscopy are in Table 7.8. As for point sources, they are determined by the screening limit count rate of 200,000 counts sec^{-1}. Both Jupiter and Saturn are fainter than the limit for the FUV echelles and brighter for the NUV echelles. Recall that a slit length of 6 arcsec was adopted, with the planets filling the aperture. This assumption makes the brightness limits 1.9 mag (2.5 x log 6) more stringent than for a point source having the same spectrum.

Table 7.8: Global Brightness Limits (V mag arcsec^{-2}) for Echelle Spectroscopy

	Observed	E140M	E140H	E230M	E230H
Jupiter	4.9	–0.6	–1.2	10.1	8.9
Saturn	6.5	–1.8	–2.7	9.9	8.7

The results for first-order spectroscopy are in Table 7.9. Since we assumed that both Jupiter and Saturn completely fill the 25 arcsec long slit, the limiting magnitude is determined by the global screening limit value of 200,000 counts/sec. This situation differs from that of point-source observations where the limiting magnitude is usually determined by the count rate per pixel or by the total number of counts along the dispersion direction. For extended objects, the total number of counts accumulated over the whole detector sets the limit. Note that the limits for the two planets are always set by the global, and not by the local rates. As was the case for echelle spectroscopy, both Jupiter and Saturn are fainter than the limit for the FUV and brighter for the NUV gratings.

Table 7.9: Global Brightness Limits (V mag arcsec^{-2}) for First-Order Spectroscopy

	Observed	G140L	G140M	G230L	G230M
Jupiter	4.9	1.4	0.0	12.9	10.1
Saturn	6.5	1.3	–1.0	12.8	9.9

The examples demonstrate that careful choices of slit sizes and neutral-density filters are required to prevent instrument damage.

MAMA Imaging

As is the case with spectroscopy, the global limit is much more restrictive than the local limit, and careful simulations are required to determine which filters can be safely used for imaging.

CHAPTER 8
Target Acquisition

In This Chapter...

Introduction

All STIS spectroscopy using slits (<3 arcseconds in size) and all coronographic observations will require an onboard STIS target-acquisition (ACQ) and possibly an acquisition/peakup exposure (ACQ/PEAK) to center the target in the scientific aperture. In this Chapter, we provide the basic information you need to choose an acquisition strategy for your program.

STIS target-acquisitions employ the CCD camera to image the target's field directly and onboard flight software processes the image to locate the position of the target. STIS acquisitions are very reliable, accurate (typically ±0.01 arcsecond for V < 21 point-sources), and quick (~6 minutes). For the narrow slits (≤0.1 arcsecond), an ACQ/PEAK is required, which is accurate to ~5% of the slit width used in the peakup, and takes typically ~6 minutes. For particularly faint targets (V<21) or complex diffuse sources, overheads will be somewhat more and accuracies somewhat reduced (see details below).

For Phase I proposals, you do not need to determine the details of your acquisition, but need only to determine if an ACQ, and possibly an ACQ/PEAK, is required, include the necessary orbital time (which is normally dominated by the associated overheads) and assure yourself that your program can be accomplished.

For Phase II, you will need to work out the details of your acquisition procedure, and we provide two tools to assist in this task, as well as examples of different TA scenarios (see "Examples" on page 148). To determine the correct exposure time, we provide (via the STIS web page) a Target-Acquisition Exposure-Time Calculator (TA ETC). The input and output parameters in the TA

ETC (as compared with the Imaging ETC) are specifically designed to facilitate exposure-time estimates for target-acquisition purposes. For example, the TA ETC input and output parameters take into account the following:

- The target-acquisition can be done only with the CCD detector.
- The `CHECKBOX` (see below) size is always 3 x 3 pixels for a point-source, and *n* x *n* where *n* is an odd number between 3 and 101 for a diffuse source.
- The `CCDGAIN` is always 4.
- The default S/N is 40 for the calculation of exposure time.

To determine the correct `CHECKBOX` size for `DIFFUSE` targets, we provide a Target-Acquisition Simulator (TAS), which implements the same algorithms as the flight software, and so should give results in good agreement with what will happen in orbit. The TAS takes as input an image, extracts a subarray centered on the coordinates provided, and searches for the brightest location by passing a `CHECKBOX` over the subarray.

Below we describe acquisition and peakup exposures for spectroscopy. More details on acquisitions and centering of targets behind the coronographic bars and wedges aredescribed in “Coronographic Imaging and Spectroscopy” on page 215, but examples are provided at the end of this chapter.

Initial Pointing

Following the initial guide-star acquisition for your visit, the target location in the aperture plane will be known to an accuracy of ~1–2 arcseconds. For scientific observations taken through spectroscopic slits which are less than 3 arcseconds in either dimension and for imaging observations taken using one of the coronographic apertures, you will need to use an on board STIS target-acquisition and possibly an acquisition peakup exposure to center your target.

Figure 8.1 shows a decision flow for selecting whether you require an acquisition or an acquisition and peakup to center your target.

Acquisitions

STIS target-acquisition exposures (`MODE=ACQ`) always use the CCD, one of the filtered or unfiltered apertures for CCD imaging, and a mirror as the optical element in the grating wheel. Acquisition exposures center your target in the slit or behind a coronographic bar to an accuracy (2σ) of ~0.01 arcsecond for a point-source, and 0.01 to 0.1 arcsecond for a diffuse object (larger targets have larger errors). A typical STIS point-source target-acquisition exposure takes ~6 minutes.

Figure 8.1: Determining Acquisition Requirements

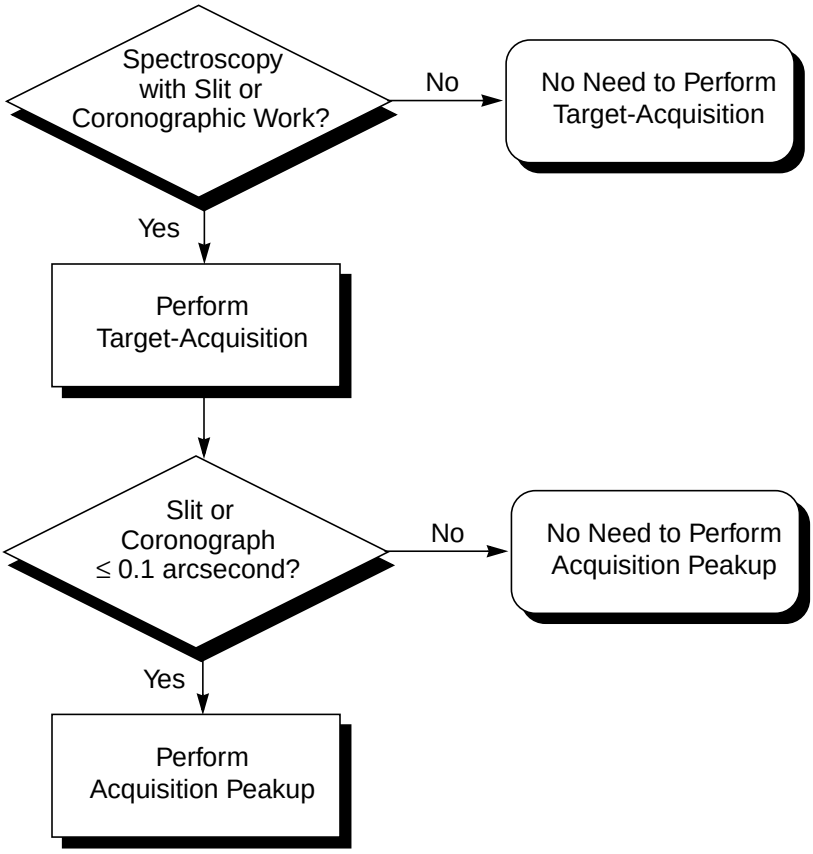

Peakups

Additionally, an acquisition peakup exposure (`MODE=ACQ/PEAKUP`) must be taken following the target-acquisition exposure to refine the target centering of point or point-like sources in slits less than or equal to 0.1 arcsecond wide (or tall). Peakup exposures use a slit or coronographic aperture and are taken with the CCD as the detector and with either a mirror or a spectroscopic element in position on the grating wheel. Typical centering accuracies following a peakup sequence are 0.05 times the dimension of the slit or bar. Typical STIS imaging point-source peakups take ~5–10 minutes; see Table 8.4 for the formulae needed to determine the duration of a peakup acquisition.

Figure 8.2 shows the complete decision tree for STIS target-acquisitions.

Figure 8.2: Process of Defining a Target-Acquisition Scheme

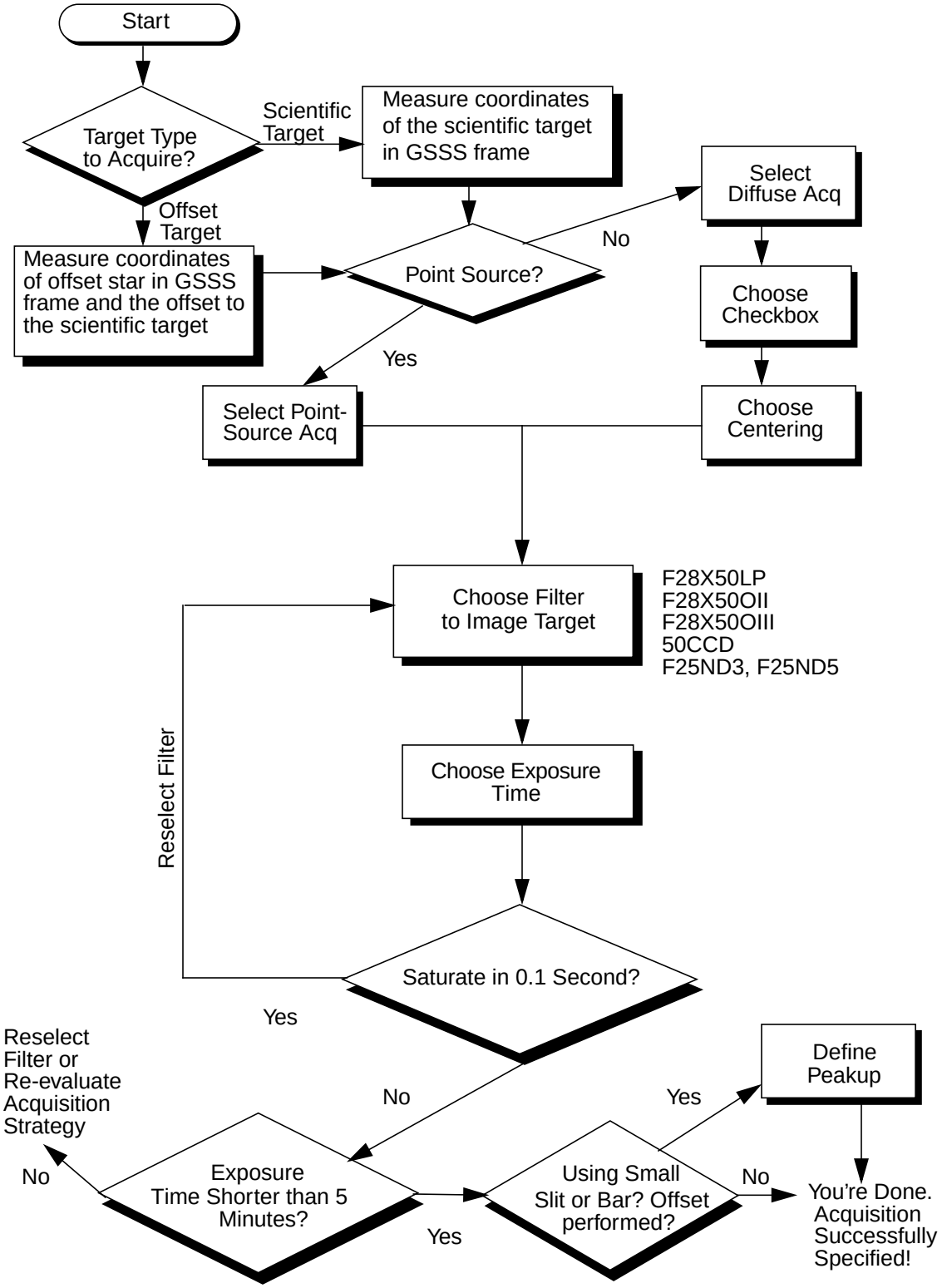

STIS Onboard CCD Target Acquisitions (ACQ)

How it Works

Acquisition exposures are controlled by the Flight Software (FSW). Figure 8.3 highlights the basic steps in the acquisition process. The sequence comprises two discrete stages: the coarse-locate phase (steps 1–2) and the fine-locate phase (steps 3–5); a sixth step centers the target in the program aperture. The coarse-locate phase is performed to place the target as close as possible to the aperture center prior to the final telescope move. This step ensures that the final slew needed to move the target into the aperture is a small one, and minimizes uncertainties in the calculation of the required slew caused by detector or optical distortions.

1. The target is located. A pair of 5 x 5 arcsecond (100 x 100 pixel) CCD images are taken of the sky using a user-selected filtered or unfiltered imaging aperture; for diffuse acquisitions, the field will be somewhat larger (see “Target-Location Algorithms” on page 129). The images are offset by 3 pixels in both X and Y to allow for removal of hot pixels via dithering. The flight software processes the images as needed (to realign the images, remove the bias level, flag bad pixels, and remove cosmic rays)[1] and applies one of two possible finding algorithms to determine the pixel coordinates of the target. The “bright” column on the edge is an artifact of the subarray readout, and is ignored by the flight software.
2. The spacecraft is then moved to place the target at the nominal center of the `0.2X0.2` slit.
3. The target is re-imaged and the target detector coordinates are redetermined. This second target location is performed to minimize the final slew in step 5, to reduce the error associated with that slew.
4. The location of the `0.2X0.2` slit is determined relative to the target. The external shutter is closed (to prevent a possible overlight condition), the `0.2X0.2` slit is rotated into position by the slit wheel, and an image is obtained with the slit illuminated by the HITM line lamps. The slit image is processed and a finding algorithm is then used to determine the pixel coordinates of the center of the slit.
5. The flight software calculates the offset between the target location and the `0.2X0.2` slit, and performs a small-angle maneuver of HST to place the target in the center of the aperture.
6. The object is placed in the program aperture (by a small-angle maneuver) just prior to the execution of the scientific exposure.

1. The processing done by the FSW is rudimentary; a single bias number is subtracted, bad pixels are set to the average of the 4 adjacent pixels, negative-valued pixels are set to zero, and each pixel is assigned the minimum from the two images (as a form of cosmic-ray and hot pixel rejection).

Figure 8.3: Target-Acquisition Schematic

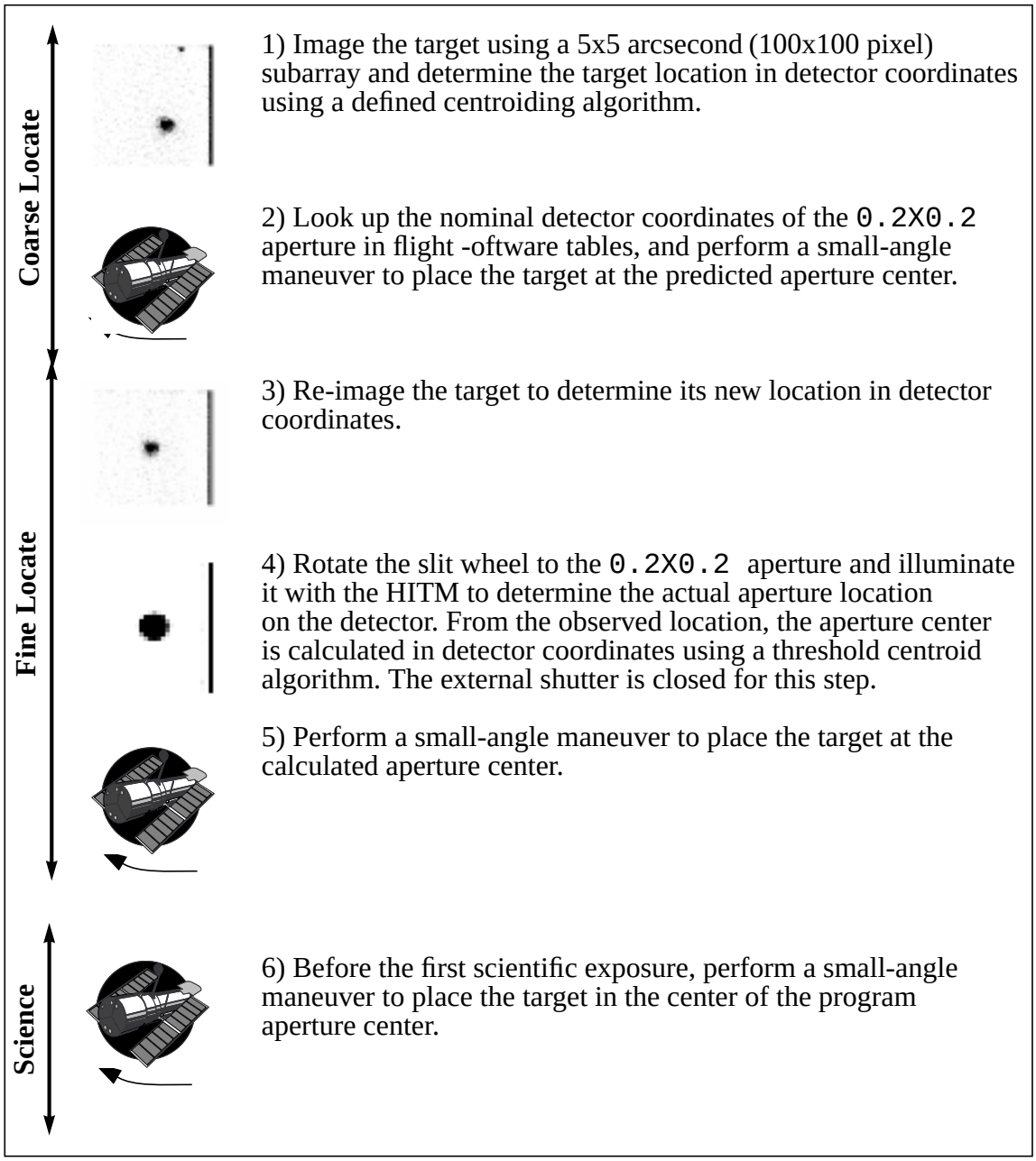

An acquisition exposure produces scientific data, which include the images of the target produced in steps 1 and 3, and the image of the `0.2X0.2` slit produced in step 4. These data will be returned to you with your scientific data as part of the pipeline products, and they can be analyzed with the **tastis** tool in STSDAS.

Target-Location Algorithms

STIS supports two basic types of acquisitions: point-source acquisitions (`ACQTYPE=POINT`) and diffuse-source acquisitions (`ACQTYPE=DIFFUSE`). Diffuse-source acquisitions are appropriate for sources that exhibit smooth or systematically peaking surface brightness *on some size scale*, such as centers of galaxies, some planets and planetary satellites (see “Solar-System Acquisitions” on page 138), or nebulae.

To locate the target, the flight software first passes a square *checkbox* over the image and determines the flux contained within the checkbox at each pixel in the subarray. The flight software then selects the checkbox with the maximum flux and determines the target center within that checkbox according to the type of acquisition specified.

Point-Source Acquisition

For point-source acquisitions (`ACQTYPE=POINT`), the checkbox size is fixed at 3 x 3 pixels (0.15x0.15 arcsecond) and the flight software determines the target location by finding the flux-weighted centroid of the pixels in the brightest checkbox (see Figure 8.4).

Diffuse Acquisition

For diffuse acquisitions (`ACQTYPE=DIFFUSE`), the flight software determines the target location either by finding the flux-weighted centroid of the pixels in the brightest checkbox or by determining the geometric center of the brightest checkbox (see Figure 8.5). For `DIFFUSE` acquisitions, the user must specify both the centering method (`DIFFUSE-CENTER=GEOMETRIC-CENTER` or `FLUX-CENTROID`) and the checkbox size. The user sets `CHECKBOX=`*n*, where *n* must be an odd number less than or equal to 105: the checkbox will then have dimension *n* x *n* pixels. `CHECKBOX` should be set to the minimum size which ensures that the brightest checkbox will be the one centered on the region of interest (i.e., if your object is peaked within a region of 1 arcsecond, set `CHECKBOX=21` (= 1 (+ 1 arcsecond/0.05 arcsecond pixel^{-1})). The maximum checkbox is 105 pixels on a side, or ~5 x 5 arcseconds. The subarray used for a diffuse-source acquisition target image is `CHECKBOX`+101 pixels on a side. The STIS Target-Acquisition Simulator can be used to determine the optimal `CHECKBOX` size.

Figure 8.6 shows a simulated example of a diffuse source, the nucleus of the galaxy M86, acquired using a diffuse-source acquisition.

Figure 8.4: How the Checkbox Works for Point-Source Acquisitions

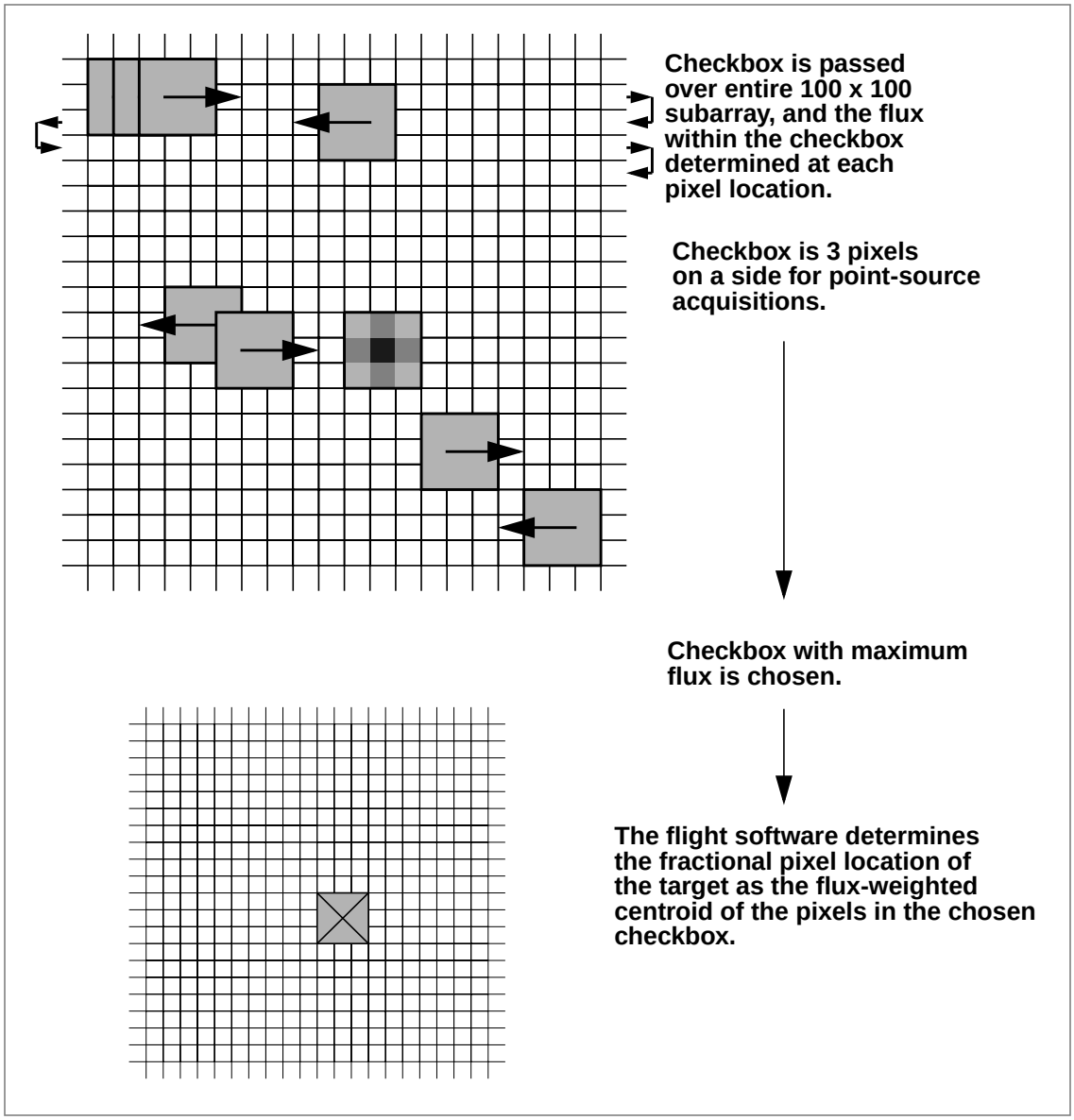

Figure 8.5: How the Checkbox Works for Diffuse Acquisitions

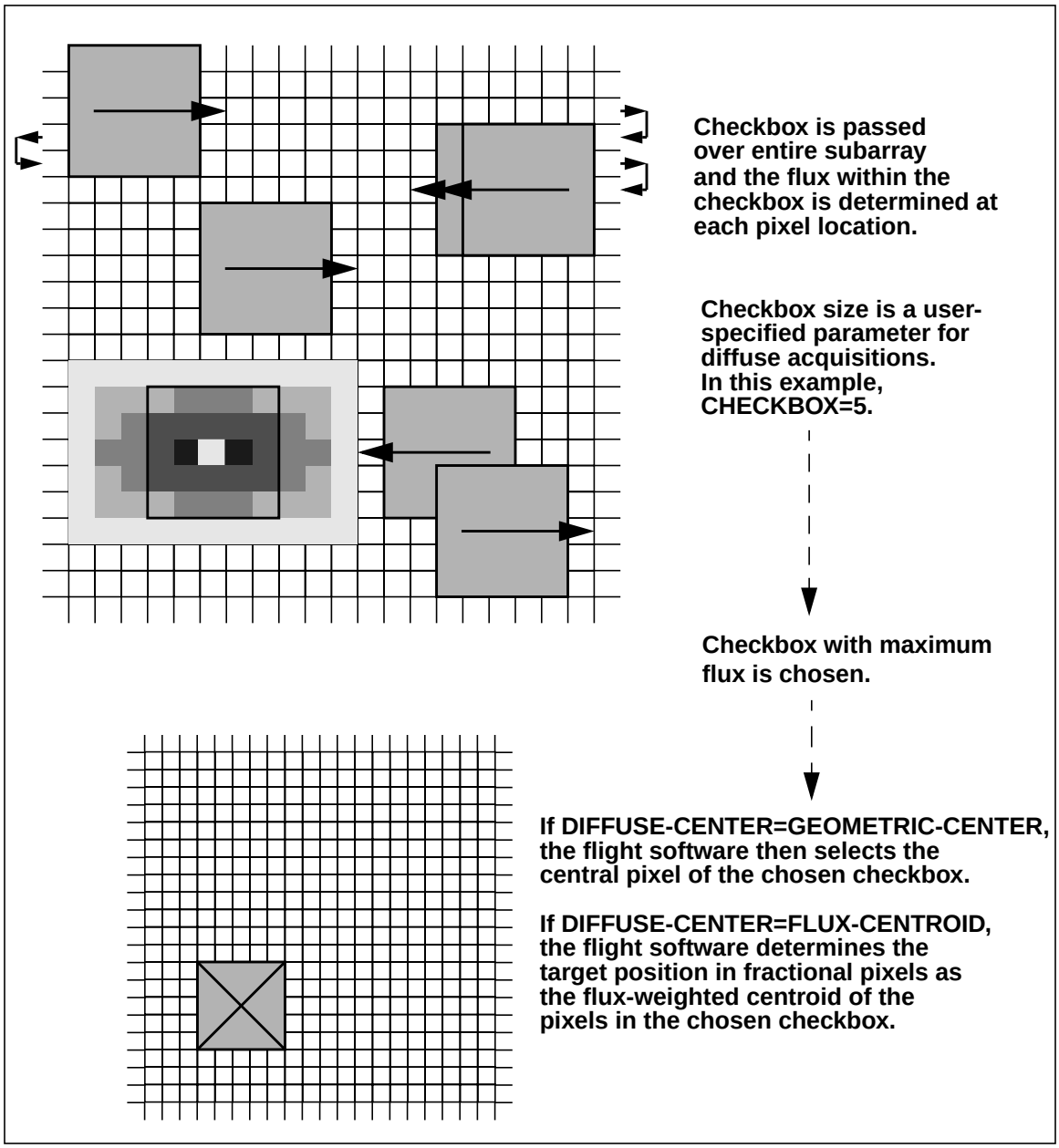

Figure 8.6: Simulated Diffuse Acquisition of Elliptical Galaxy M86. Created by running the flight-software algorithm on a STIS image. CHECKBOX=25 produced good centering. Smaller values caused checkbox to center on local brightness enhancements offset from galaxy center.

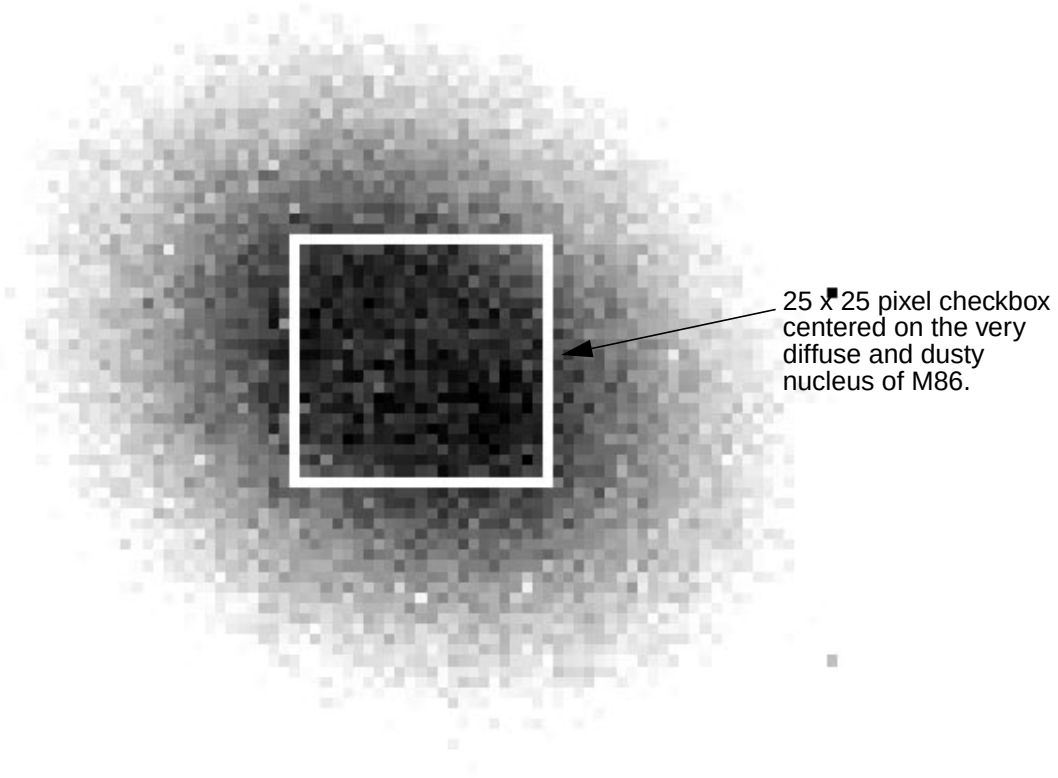

Selecting Target-Acquisition Parameters

To plan your acquisition, you must select:

- The target you are going to acquire (scientific target or offset object).
- The type of acquisition, point or diffuse, and if you are performing a diffuse acquisition, the centering algorithm and checkbox size.
- The filtered APERTURE to be used for target imaging during the acquisition.
- The exposure time for the image used to determine the location of the target.
- The program aperture, which determines if you need a peakup acquisition.

Figure 8.2 shows the flow of specifying a target-acquisition scheme.

Selecting the Acquisition Object

The first step is to determine what object you are going to use for your target-acquisition. Note that the STIS software will always acquire the brightest object in the 5x5 arcsecond search area. If your target is isolated, or if there are no brighter objects *in the STIS bandpass* you have selected (see below) within 5 arcseconds of your target, then you can acquire your target directly. If there are brighter targets nearby, then you will need to acquire an offset target (generally the brighter nearby star), and then perform a blind slew to the scientific target. The offset technique is also recommended for precise pointing to specific surface or atmospheric features for large (>~4 arcseconds) planetary targets such as Mars, Jupiter, and Saturn, with the offset target being a planetary satellite (see “Solar-System Acquisitions” on page 138 for further details). Note that HST performs small-angle maneuvers (SAMs) quite accurately, with a 3 arcsecond maneuver having an error of 0.003 arcsecond, while a 2 arcminute maneuver (the maximum to ensure that a single set of guide stars can be used for both targets) yields a 0.02 arcsecond error. The offset should not significantly affect target centering accuracy even in the smallest echelle slits, and your centering uncertainty will generally be dominated by your knowledge of the absolute offset between the acquisition star and your target. If you are uncertain whethera nearby object is brighter than your target in the STIS bandpass, it is safest to select an isolated object and perform your acquisition on it.

If you are observing a diffuse source, you should first check to see if there is a suitable star which you can use as an acquisition target; an offset can then be used to move to the desired position, as needed. If you wish to acquire a diffuse object directly, then it is important to know your source structure as seen at ~0.1 arcsecond resolution to properly plan your acquisition strategy if you need accurate (a few tenths of an arcsecond) centering. We recommend that you first check the HST archive to determine if your target has been observed by HST with WF/PC-1, WFPC2, FOC, or STIS. If it has, that exposure can be used to determine the optimal acquisition strategy using the Target-Acquisition Simulator. If it has not yet been observed with HST, we suggest you take an early acquisition image, either with the STIS or with WFPC2, which you can use to determine your optimal acquisition strategy. This is particularly important if your program requires placement of a narrow slit accurately on a diffuse object.

Once you have selected your acquisition object, you need to measure its coordinates in the Guide Star reference frame; information on measuring coordinates can be found on the following web page:

`http://www-gsss.stsci.edu/support/phase2.html`

You will need to include the `PLATE-ID` along with your coordinates so that we can be certain to select the guide stars for your observation from the same plate on which your measurement was based. If you are deriving coordinates from WFPC2 data (i.e., from the **metric** task) or STIS data (i.e., from the **xy2rd** task), you still need to provide a `PLATE-ID`; see “Determining the PLATE-ID of HST Observations” on page 147 for instructions on determining the `PLATE-ID` from HST data.

Note that the initial acquisition subarray is 5″ on a side; your target coordinates must be supplied accurately in the GSSS frame during Phase II to assure your target will be in the initial ACQ image, given that the initial guide star pointing accuracy is ~1–2″.

Selecting the Acquisition Type

If you are acquiring a point-like object, you should select the point-source acquisition (ACQTYPE=POINT). This selection will find the flux-weighted centroid of the object using a 3 x 3 checkbox. If you are acquiring a diffuse object, you should select the diffuse source acquisition (ACQTYPE=DIFFUSE). A diffuse acquisition will also require the selection of the centering algorithm (DIFFUSE-CENTER=FLUX-CENTROID or GEOMETRIC-CENTER) and a checkbox size (CHECKBOX=3-105). A Target-Acquisition Simulator is available to assist you in selecting the best checkbox size if you have an image at a similar resolution to STIS and in a similar bandpass.

Selecting the Imaging Aperture

The apertures available for target-acquisitions are the same set that can be used for CCD imaging and are listed in Table 8.1 below. They include the visible long pass filter, the clear unfiltered aperture, the [O III] narrowband filter, the [O II] narrowband filter, and the neutral-density filters which provide attenuations for bright sources of 10^{-3} and 10^{-5}. F28X50LP is the preferred target-acquisition aperture.

Table 8.1: Apertures for Target-Acquisitions

Aperture Name	Filter Type	Comment
F28X50LP	Optical longpass	Preferred target-acquisition aperture
F28X50OII	[O II]	Use for bright sources or to center on emission-line structure
F28X50OIII	[O III] (has severe red leak)	Use for bright sources or to center on emission -ine structure
F25ND3	Neutral density, ND=10^{-3}	Use only for targets too bright for other filters
F25ND5	Neutral density, ND=10^{-5}	Use only for targets too bright for other filters
50CCD	Clear	Use for acquisitions of faintest sources only

The longpass filter is the preferred target-acquisition aperture (compared to the clear 50CCD aperture) because it blocks the ultraviolet photons, which can otherwise elevate the detector dark count in the subsequent scientific exposures (see “UV Light and the STIS CCD” on page 105). For bright sources which saturate the CCD in 0.1 second with the longpass filter (see Table 8.1), you can use either the narrowband [O III] (F28X50OIII) or [O II] filters (F28X50OII) as the acquisition aperture, or one of the neutral density filters. The [O II] and [O

III] filters can also be used to locate the target in the light of an emission line. Note that the [O III] filter has a large red leak at $\lambda > 10{,}000$Å (see Chapter 14), so it should be used with caution; the [O II] filter has a smaller red leak.

We recommend the longpass `F28X50LP` filter for all target-acquisitions of sources with V magnitudes between 10 and 23.

Determining Exposure Time for the ACQ Exposure

To achieve robust target location:

- A signal-to-noise ratio of 40 (over the checkbox) or 1700 electrons (425 DN) must be obtained on each target image obtained during the `ACQ` exposure.
- For `DIFFUSE` acquisitions with large checkbox sizes (i.e., `CHECKBOX` > 9), 40 electrons pixel^{-1} (or equivalently 10 DN pixel^{-1}) must be obtained for the region of the source being “found”.
- The target image cannot be allowed to saturate the CCD full well (144,000 electrons).
- The exposure time must be less than 5 minutes for point-source acquisitions and less than the maximum allowed (see below) for diffuse acquisitions.
- A `CCDGAIN` of 4 must be used for all acquisition images.

The maximum possible exposure time for a point-source (`ACQTYPE=POINT`) acquisition exposure is 5 minutes; this limit restricts acquisitions to sources brighter than 24.5 magnitudes in V. This limit is imposed because, for longer exposure times, the target-acquisitions become compromised by coincident cosmic-ray impacts, which will lead to acquisition failures.

The maximum possible exposure time for a diffuse acquisition (`ACQTYPE=DIFFUSE`) depends on the checkbox and is given by:

$$t_{max} = 5 \times 100/(101 + CHECKBOX) \qquad minutes$$

The minimum exposure time allowed for an acquisition is 0.1 second. Table 8.1 gives the limiting magnitudes at which the CCD will saturate in a 0.1 second exposure; sources brighter than these limits cannot be acquired with the CCD using these filters. Remember that the ND filters can also be used to acquire targets; these filters provide attenuations of 10^{-3} (7.5 magnitudes) and 10^{-5} (12.5 magnitudes) relative to the clear (`50CCD`) filter. Note that the ND filters are contained in the slit wheel with other slits and apertures, and so cannot be used in conjunction with other filters. The table illustrates that it is possible to image any star using the suite of filters, including the neutral-density filters, available for STIS.

Figure 8.7 can help you estimate exposure times—it plots exposure time versus *V* magnitude to achieve a signal-to-noise ratio of 40 for stars having a

Table 8.2: V Magnitude Limits for 0.1 Second CCD Exposure Time as a Function of Aperture

Spectral Type	Limiting Magnitude			
	50CCD	F28X50LP	F28X50OII	F28X50OIII
O5 V	10.3	8.4	4.8	2.7
B1 V	10.2	8.4	4.6	2.7
B5 V	10.0	8.5	4.2	2.7
B8 V	9.9	8.5	3.8	2.7
A1 V	9.8	8.6	3.3	2.7
A3 V	9.8	8.6	3.2	2.7
A5 V	9.8	8.7	3.2	2.6
F0 V	9.8	8.8	3.2	2.6
F5 V	9.9	9.0	3.1	2.6
G2 V	9.9	9.1	2.8	2.6
G5 V	9.9	9.1	2.7	2.6
K0 V	9.9	9.2	2.2	2.6
K4 V	10.1	9.4	1.4	2.6
K7 V	10.2	9.7	0.9	2.8
M2 V	10.5	10.0	0.7	3.3
M6 V	10.5	10.0	0.6	3.3
PowerLaw	10.4	9.8	2.9	3.4

range of spectral types, for the clear, longpass, [O III], and [O II] filters. To determine the exact exposure time for your target, you should use the STIS Target-Acquisition Exposure Time Calculator (see “Examples” on page 148). Note that the overheads in target-acquisition are substantially longer than most exposure times, so as long as you do not saturate (i.e., come within 30% of the full well) you should increase your exposure time by a factor of 2–5 above the minimum required (e.g., if the exposure time to obtain a S/N of 40 is 0.3 second, then you should lengthen it to 1 second if no saturation occurs). The exposure time entered into your Phase II template is the time for each of the two exposures in the ACQ sequence, unlike the case of `CR-SPLIT` observations where it is the total time.

As part of your Phase II submission, you will need to specify the V magnitude of the object you are acquiring (the scientific target or the offset target). The RPS2 software will perform a check to make certain your target will not saturate the CCD (which would cause the acquisition to fail). Note that the test assumes the worst case (the `50CCD` aperture and an M6V spectral type), which may not be appropriate for your target and configuration. If RPS2 gives you a warning about

the acquisition exposure, please simply double check to make certain you will not saturate.

Figure 8.7: Time to Achieve a Signal-to-Noise ratio of 40 for CCD Acquisitions

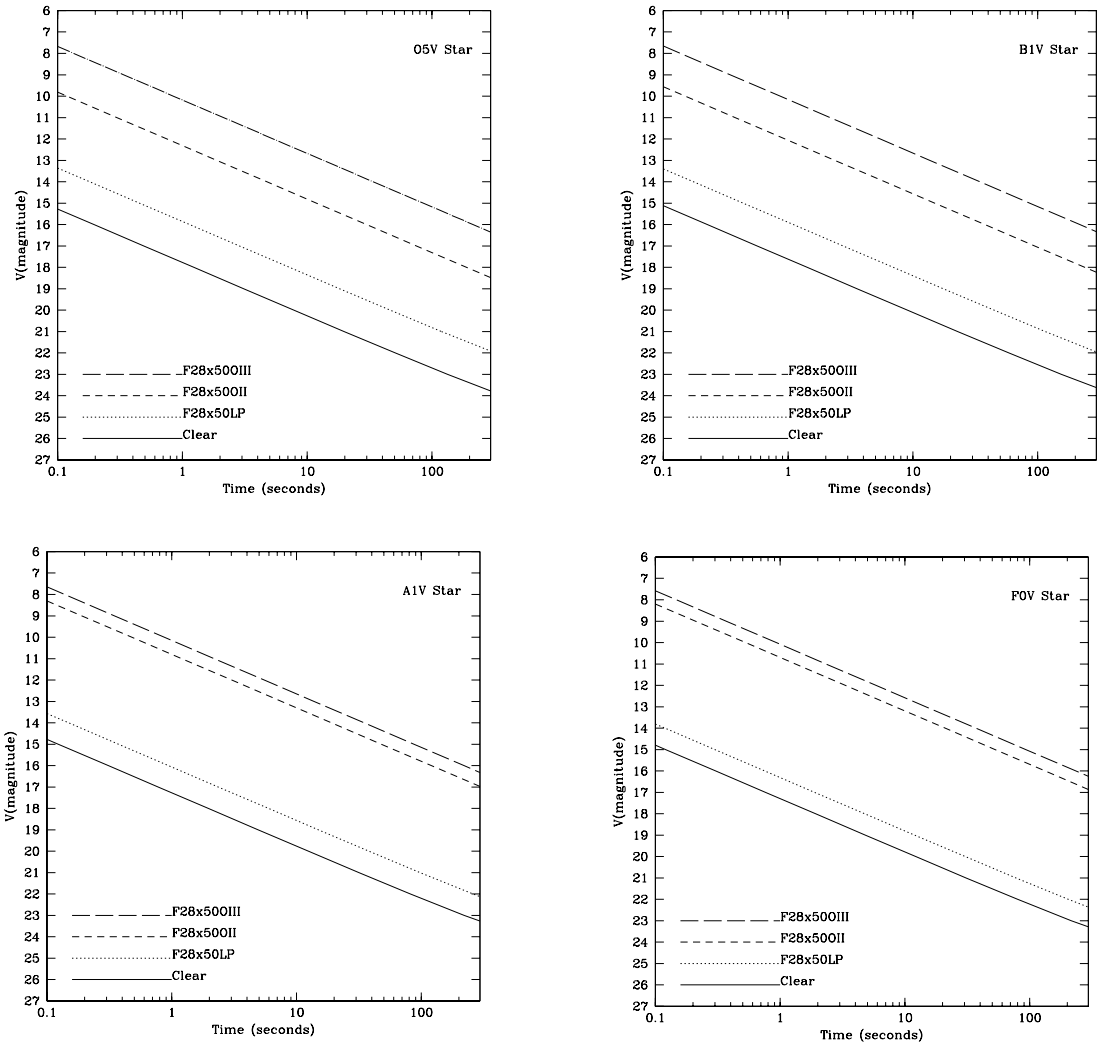

Figure 8.7 (Continued): Time to Achieve a Signal-to-Noise ratio of 40 for CCD Acquisitions

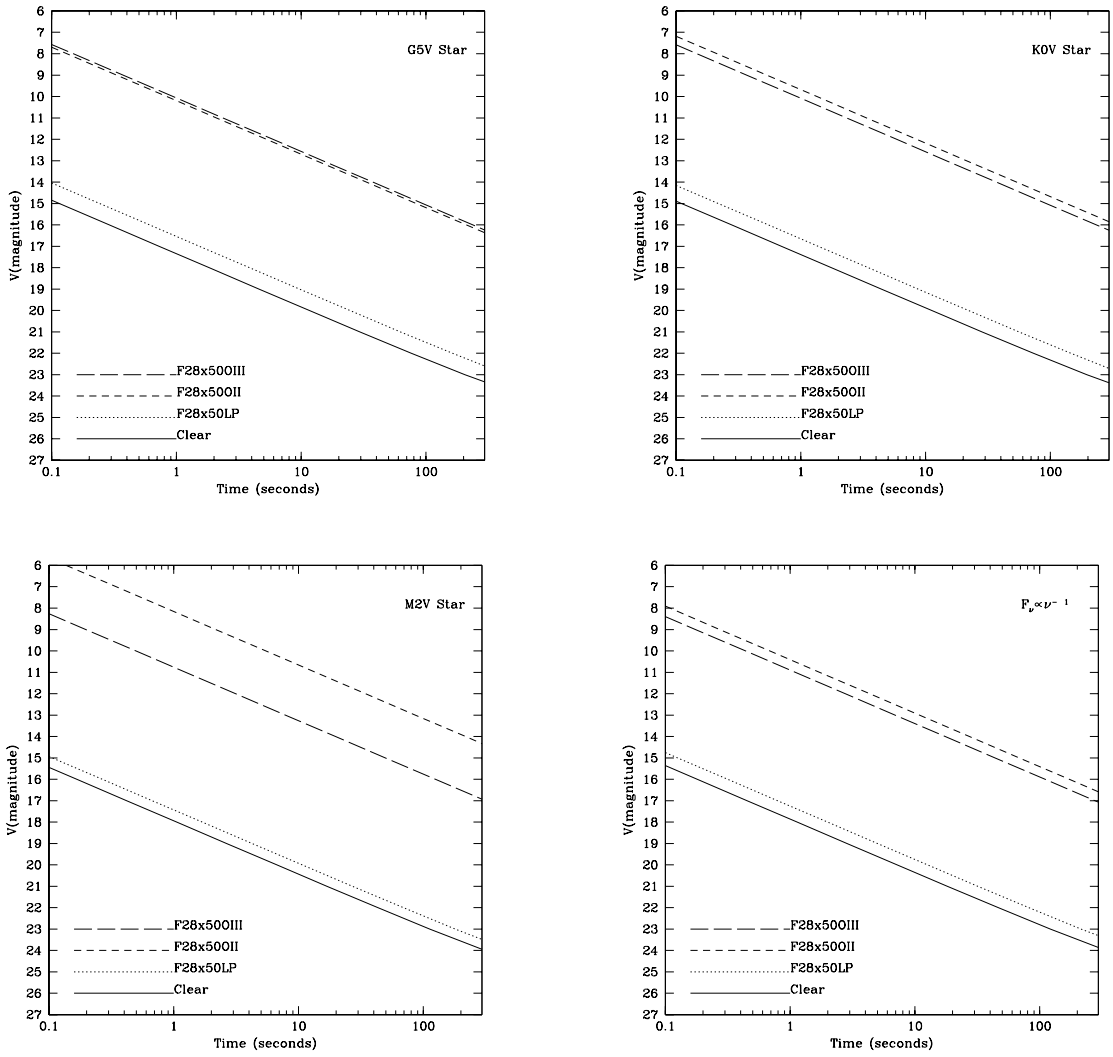

Solar-System Acquisitions

STIS acquisition techniques for solar-system targets are identical to those described in the preceding sections, and no special strategies are required. The one exception is that the offset target is almost always a satellite instead of a nearby star, and it is not necessary to measure the coordinates of satellites used as offset targets in the Guide Star reference frame.

Acquisition exposure times can be accurately estimated using the STIS Exposure-Time Calculator: use the Kurucz model G2 V (solar spectrum), and normalize it using the V magnitude for point-like objects or the V magnitude per arcsec^2 and the appropriate target size in arcseconds for more extended targets.

For convenience, we summarize the types of acquisitions recommended for the most common solar-system targets in Table 8.3 below. If precise pointing to a specific feature is not required, then blind pointing can be used for the larger targets such as Mars, Jupiter, and Saturn.

Table 8.3: Solar-System Acquisitions

Target	Type of Acquisition	Offset Target
Venus	Offset target	Star
Mars	Offset target	Deimos
Jupiter	Offset target	Galilean satellite
Saturn	Offset target	Satellite
Uranus	Diffuse source	
Neptune	Diffuse source	
Satellite or asteroid <~0.1 arcsec	Point source	
Satellite or asteroid >~0.1 arcsec	Diffuse source	
Comet	Diffuse source	

Specifying Acquisitions in Phase II

Acquisition exposures must be specified during Phase II as individual exposure-logsheet lines which precede the scientific exposures for which they are intended. The user requests a target-acquisition exposure by specifying `MODE=ACQ` on the proposal logsheet, and setting the optional parameter `ACQTYPE=POINT` or `ACQTYPE=DIFFUSE`. If `ACQTYPE=DIFFUSE` is selected, the observer must also specify `DIFFUSE-CENTER` and `CHECKBOX`. The special requirement "`ONBOARD ACQ FOR <exp IDs>`" must be supplied for acquisition exposures, where the <exp IDs> given identify the subsequent scientific exposures the acquisition is being taken for.

In addition, you are required to provide the V magnitude and spectral type of the acquisition target. This information will allow for checks of your target-acquisition exposure times, should they be needed.

Exposure-Time Calculator and RPS2 examples are provided in "Examples" on page 148.

Onboard Target-Acquisition Peakups (ACQ/PEAK)

When slits less than or equal to 0.1 arcsecond wide or the narrow coronographic bars are used, an acquisition-peakup exposure should be performed following the acquisition exposure to center the target in the slit or coronographic bar. You should also consider performing a peakup if you have acquired an offset star, rather than your target to compensate for any additional uncertainties in your knowledge of the offsets. The drift rate of HST is less than 10 milli-arcseconds per hour; thermal drifts internal to STIS at the slit plane are typically less. We recommend that for long series of exposures taken through slits which are less than or equal to 0.1 arcsecond in either dimension, a peakup be performed every 4–5 orbits. This will ensure that drifts do not cause the target to move out of the slit.

Figure 8.8 illustrates the basic peakup sequence. When a peakup exposure is performed, the telescope is moved to step the target across the slit or bar. At each step (or dwell point), an image[2] of the sky is taken and the total flux in a specified subarray is determined. To allow for a more accurate calculation, the minimum flux value in the peakup (the PEDESTAL) is subtracted from each step. The flight software (FSW) then selects the position of maximum flux, using a flux-weighted centroiding technique to determine the optimum position to a fraction of a dwell step. At the conclusion of the ACQ/PEAK exposure, the FSW moves the telescope to position the target at the derived optimal position within the aperture.

2. For CCD ACQ/PEAKs the same type of processing is applied as in acquisitions by the FSW to remove the bias and cosmic rays, with the only difference being that there is no offset performed between the two images taken at each pointing, for obvious reasons.

Figure 8.8: Schematic of Peakup Sequence

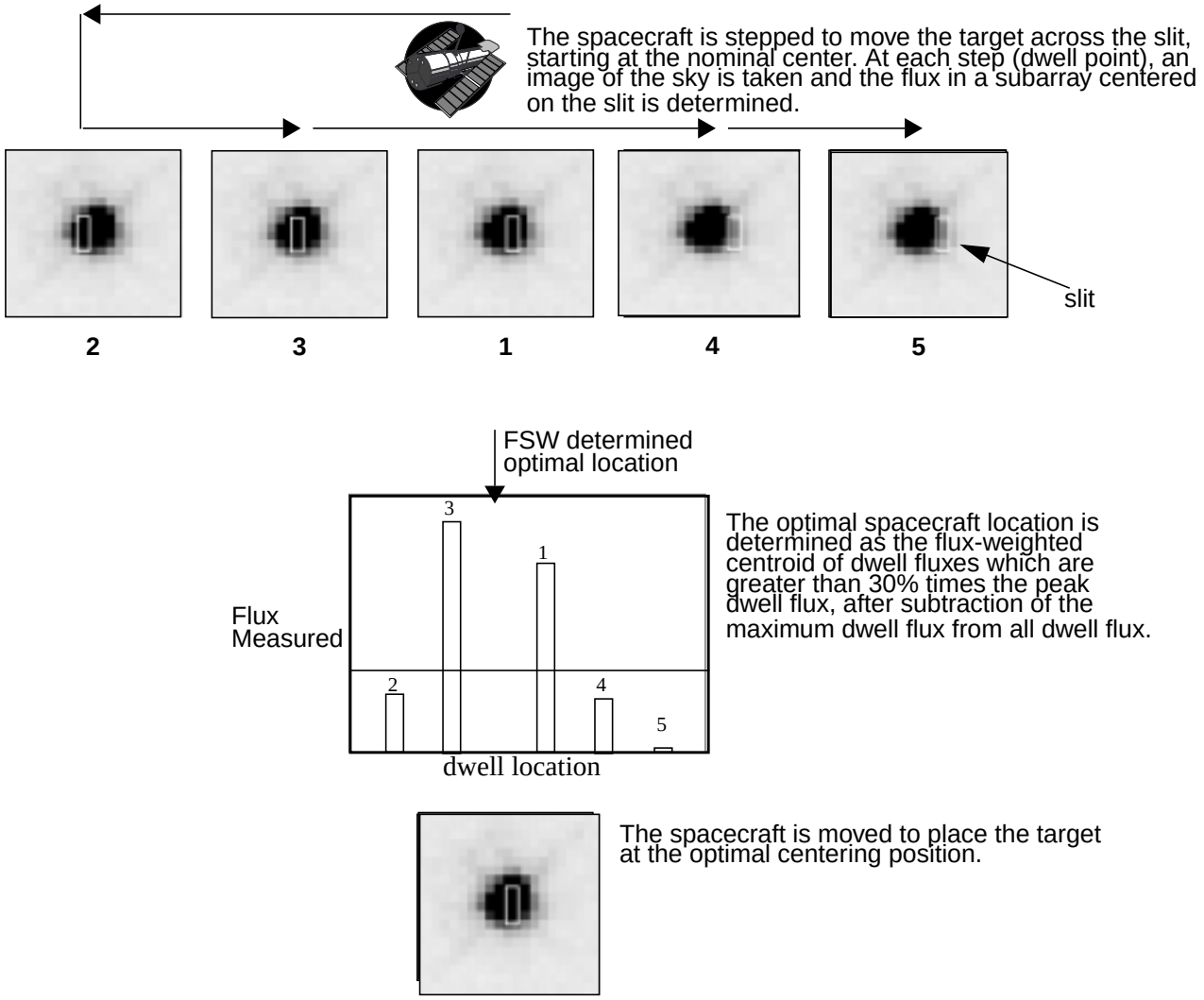

Peakup exposures can be taken with either a mirror (to peak up in undispersed white light) or a grating (to peak up in dispersed light) and with the CCD detector only. Subarrays can be specified to limit the region of the detector (sky) over which the flux is determined at each dwell point. The default subarray sizes, 32 by 32 for white-light (mirror) peakups and 32 across the dispersion by 1022 in dispersion for dispersed-light peakups, are appropriate for peakups on point-sources. They should be changed only if you are performing diffuse-source peakups or if you wish to isolate a single line in dispersed-light peakups, and only upon consultation with your Contact Scientist.

We recommend performing all CCD peakups using the mirror unless your target is too bright.

You do not specify the parameters of the stepping sequence employed during the peakup; it is predetermined, based on the aperture you have chosen. Table 8.4 below shows the scan sequence employed for all of the long and echelle slits. The scan sequence for a peakup may include a linear scan in the dispersion direction (`SEARCH=LINEARAXIS1`), a linear scan perpendicular to the dispersion axis (`SEARCH=LINEARAXIS2`), or a spiral search pattern (`SEARCH=SPIRAL`). Additional parameters are the number of steps (`NUMSTEPS`) and the step intervals between each dwell point (`STEPSIZE`).

Table 8.4: . Peakup Scan Sequences and Parameters for Supported Spectroscopic Slits

Slit (APERTURE)	AXIS2 spatial (arcsec)	AXIS1 dispersion (arcsec)	AXIS2 step size (arcsec)	AXIS1 step size (arcsec)	Scan Type	NSTEPS AXIS2	NSTEPS AXIS1	Total NSTEPS	CCD Duration (seconds)
All Long Slits									
52X0.05	52	0.05		0.036	LINEARAXIS1		7	7	$240+16*t_{exp}$
52X0.1	52	0.1		0.075	LINEARAXIS1		5	5	$180+12*t_{exp}$
52X0.2, 52X0.2F1-R	52	0.2		0.150	LINEARAXIS1		3	3	$120+8*t_{exp}$
6X0.2	6	0.2		0.150	LINEARAXIS1		3	3	$120+8*t_{exp}$
Echelle Slits for E230M and E140M									
0.2X0.06	0.2	0.063	0.048	0.048	1) LINEARAXIS1 2) LINEARAXIS2	3	7	10	$360+24*t_{exp}$
0.2X0.2	0.2	0.2	0.150	0.150	1) LINEARAXIS2 2) LINEARAXIS1	3	3	6	$240+16*t_{exp}$
Echelle Slits for E230H and E140H									
0.2X0.09	0.2	0.09	0.069	0.069	1) LINEARAXIS2 2) LINEARAXIS1	3	5	8	$300+20*t_{exp}$
0.2X0.2	0.2	0.2	0.150	0.150	1) LINEARAXIS2 2) LINEARAXIS1	3	3	6	$240+16*t_{exp}$
Speciality Slits									
0.2X0.05ND	0.2	0.05	0.150	0.039	1) LINEARAXIS1 2) LINEARAXIS2	3	7	10	$360+24*t_{exp}$
0.3X0.05ND	0.3	0.05	0.250	0.039	1) LINEARAXIS1 2) LINEARAXIS2	3	7	10	$360+24*t_{exp}$
0.2X0.06FP (A-E)	0.2	0.06	0.150	0.048	1) LINEARAXIS1 2) LINEARAXIS2	3	7	10	$360+24*t_{exp}$
0.2X0.2FP (A-E)	0.2	0.2	0.150	0.150	1) LINEARAXIS1 2) LINEARAXIS2	3	3	6	$240+16*t_{exp}$
0.1X0.03 (peakup in 0.2x0.2 followed by spiral in 0.1X0.03)	0.2 0.1	0.2 0.025	0.150 0.018	0.150 0.018	1) LINEARAXIS2 2) LINEARAXIS1 3) SPIRAL	3 3	3 3	6 9	$600+36*t_{exp}$

Selecting Peakup Parameters

To plan your acquisition peakup, you must specify:

- The optical element.
- The APERTURE (program slit) upon which to peak up.
- The exposure time for the peakup image.

Selecting the Optical Element

Peakups can be performed either with a dispersive element in a spectroscopic configuration with any of the allowed grating/detector combinations, or in undispersed white light in an imaging configuration. “Tips on Acquisition Peakups” on page 145 provides advice on when to use white light (mirror) and when to use a dispersive element (grating) for your peakup.

Selecting the Aperture

A peakup can be done using any of the long or echelle slits in Table 8.4 as the APERTURE. You will (typically) want to specify the peakup aperture as the aperture used for the subsequent scientific observations, although it is possible to specify a smaller aperture than your program aperture if you require higher centering accuracy. Instances in which you may wish to utilize a smaller aperture for the acquisition are coronographic observations, observations requiring accurate photometry (where you need to be properly centered in a large slit), and bright-source acquisitions.

For acquisitions under the narrow occulting fiducial (52X0.2F1), a peakup acquisition using a small slit should be used. The bar and wedge positions on the 50CORON aperture (imaging) are all large enough that a peakup is not required. However, if you require accurate centering (for example, to place a calibration star at the same position under the bar or wedge to measure the scattered-light profile), then a peakup is required. Note that a peakdown acquisition is no longer recommended. See “Coronographic Imaging and Spectroscopy” on page 215 and the examples on pages 154 and 156.

Determining the Peakup Exposure Time

The required exposure time for CCD imaging (mirror) peakups is the time to obtain a minimum of 5000 electrons (1250 DN) from a point-source, or equivalently, 5000 electrons from the peak of a diffuse source which is contained in a 4 x 4 pixel region. For CCD dispersive (grating) peakups, the exposure time is the time to obtain a minimum of 80,000 electrons (20,000 DN) integrated across the spectrum from a point-source (or equivalently, 80,000 electrons from the peak of a diffuse source integrated over 4 pixels perpendicular to the dispersion axis). For CCD dispersive peakups on a single emission line, the exposure time is the time to obtain a minimum of 5000 electrons in the chosen line; a small subarray is selected to isolate the line.

To determine the exact exposure time, you should use the STIS Target-Acquisition Exposure-Time Calculator (for imaging peakups) or the STIS Spectroscopic Exposure-Time Calculator (for dispersive peakups). Be sure to include the effect of your chosen slit throughput (see Chapter 13) in your

calculation (e.g., for imaging peakups, where the Exposure-Time Calculator does not currently account for slit loss). For CCD peakups you must be sure not to saturate the CCD during your exposure. Table 8.1 lists the brightest magnitude star for a range of spectral types on which a CCD peakup exposure can be performed in white light, assuming zero slit losses. Note that the overheads in target-acquisition are substantially longer than most exposure times, so as long as you do not saturate (within 30% of the full well) your target, you should increase your exposure time by a factor of 2–5 above the minimum required (e.g., if the exposure time to obtain the requisite number of electrons is 0.3 second, then you can lengthen it to 1 second if no saturation occurs).

There is a limit on the maximum exposure time allowed for CCD peakups, which is imposed to ensure that multiple coincident cosmic rays do not affect the centering accuracy. Table 8.5 lists the maximum CCD exposure time for point-source white-light and dispersed-light peakups for each aperture.[3]

Table 8.5: Maximum Allowed Exposure Times for CCD Peakups

Slit (APERTURE)	Imaging Maximum Exposure Time for Dwell (minutes)	Spectroscopic Maximum Exposure time for Dwell (minutes)
52X0.1	7.6	1.3
52X0.2, 52X0.2F1-R	9.8	1.7
6X0.2	9.8	1.7
0.2X0.06	7.6	1.3
0.2X0.2	9.8	1.7
0.2X0.09	7.6	1.3
0.2X0.05ND	6.4	1.1
0.3X0.05ND	6.4	1.1

Tips on Acquisition Peakups

When do you Need to do a Peakup?

We recommend that peakups be employed for all slits which are less than or equal to 0.1 arcsecond wide or tall. For the larger slits (`52X2`, `52X0.5`, `52X2`), there is no benefit in performing a peakup, and peakups are therefore not permitted with these slits.

3. More generally, the maximum allowed exposure time for CCD ACQ/PEAKs is: $t_{max} = 17 \times 1/\sqrt{numsteps \times SIZEAXIS1 \times SIZEAXIS2/(32 \times 32)}$ minutes.

White Light or Dispersed Light?

Most peakup exposures should be performed using the CCD in imaging mode (white light).

If your target is otherwise too bright to perform a CCD peakup with a camera mirror in place, you can use the echelle slits `0.2X0.05ND` (which has an ND filter with a factor of 100 attenuation or the `0.3X0.05ND`, with attenuation by a factor of 1000) or use a dispersed-light peakup. Also note that if you wish to peak up in a particular line for which there is no imaging filter, a dispersed-light peakup using a grating should be used. Observers should generally perform dispersed light peakups with the same gratings and apertures they intend to use for their scientific observations.

If extremely high centering accuracy is required, observers should consider peaking up in a smaller slit than the program slit; the slit-to-slit positioning accuracy is 0.005 arcsecond.

Specifying Acquisition Peakups in Phase II

The user requests a peakup acquisition exposure during Phase II by specifying `MODE=ACQ/PEAK` on the proposal logsheet. The default setting for the scan (`SEARCH`, `NUMSTEPS`, `STEPSIZE`) for your chosen `APERTURE` is then automatically selected from the lookup table. You specify a link to the scientific exposures following the target-acquisition, using the logsheet special requirement `ONBOARD ACQ FOR <exp IDs>`. Exposure-Time Calculator and RPS2 examples are provided in “Examples” on page 148.

STIS Post-Observation Target-Acquisition Analysis

Unlike with earlier HST spectrographs, it is now possible to determine what the instrument acquired during an observation. The methods described below can be used to make either a coarse (eyeball estimate) or a fine (exact pixel) determination.

Paper Products—Coarse Centering

After your observations are taken, you will receive, in addition to your data files, a set of paper products providing a high-level overview of your observations. Included in this package will be a summary page for the CCD acquisition, which contains an image of the initial HST pointing, as well as an image following the initial centering (step 3 in the acquisition sequence). The object in the center of this image is the target acquired by STIS; the remaining steps in the acquisition sequence just center that target in the aperture. This level of accuracy is sufficient to check your acquisition of point-sources. If you also performed an ACQ/PEAK, you will receive paper products which include a grid of the counts at each point in the peakup pattern and a confirmation image of the target after the final centering.

TAS—Fine Centering

Once you have your data, you can use the Target-Acquisition Simulator to determine the exact position of your source that was acquired. The TAS will take the STIS image of the initial pointing and, using the same algorithm as the flight software, tell you the location of the target, in pixel coordinates. This level of accuracy will be needed to check your acquisition on a diffuse source.

Did the Acquisition Succeed?

The *HST Data Handbook* describes in detail how to determine if your acquisition succeeded. To determine the accuracy of your acquisition, you must either have obtained a confirmation image immediately after your ACQ, or have performed a follow-on ACQ/PEAK (the amount of the ACQ/PEAK slew tells you the error in the ACQ). We recommend you use the **tastis** tool in STSDAS to determine how your acquisition worked.

Determining the PLATE-ID of HST Observations

All HST data have at least one guide-star ID in the Standard Header Packet (SHP). Data from the SHP will be recorded in the shh (WFPC2) or the spt (STIS) file that accompanies all HST observations. The guide stars that were used in any pointing will be recorded in the SHP as character strings associated with specific keywords in the header.

The *primary* or *dominant* guide star is associated with the keyword DGESTAR and the *secondary* or *subdominant* guide star is associated with the keyword SGESTAR. The guide-star ID is a concatenation of the star number, the region number from the Guide Star Catalogue, and the FGS used in the pointing, e.g. “0123406789F2”, as a quoted character string. The actual guide star in this example is 01234 06789 and FGS2 was used.

To find the PLATE-ID that was used for the coordinates, use the WWW Guide-Star Catalogue interface:

`http://www-gsss.stsci.edu/support/rgscid_form.html`

The form will prompt you for the guide-star ID (in two fields)—you should use the primary guide star only. This web page will provide the coordinates, estimated magnitude, associated errors, flags internal to the catalogue’s structure, and the PLATE-ID. Note that for most guide stars there will be multiple entries (corresponding to multiple PLATE-IDs), as the plates taken for the Guide-Star Catalogue overlap. The first line from your output will be for the primary plate—the preferred plate for the guide star in question, and, if two guide stars were used, the PLATE-ID you should specify in your Phase II program. If the observation used a single guide star, it is possible that a secondary plate was used. Please consult your Contact Scientist if this is the case.

Examples

Point-Source Acquisition of an Isolated Object

In this first example an isolated V = 19 mag QSO (z = 1.5) is to be acquired, with the scientific exposures to be obtained in the `52X0.5` slit.

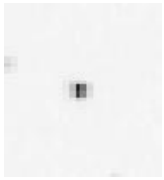

The target is isolated, so it will be acquired with a point-source acquisition. The object is faint, so we can use the preferred `F28X50LP` filter. The TA ETC is then used to determine an exposure time of 11.4 seconds. Note that the `GAIN=4` and `CR-SPLIT=1` *must be used* for the ETC to ensure that you have a S/N of at least 40 in each of the two images obtained during the `ACQ` process. The object does not saturate the CCD, and the exposure time is less than 5 minutes, so we have devised a valid target-acquisition. Given that the exposure time is so short, we can lengthen the time to 15.0 seconds (which yields a peak value of 1300 electrons, well below saturation) to make certain we have enough signal for a good acquisition. Since the data are being obtained in a wide slit, we do not need to perform an `ACQ/PEAKUP`, and our acquisition is complete.

Exposure-Time Calculator

```
Detector and filter:
     CCD, Longpass

Exposure Parameters
     Exposure time for S/N = 40

Spectral Distribution
     QSO, z=1.5

Flux
     V = 19, E(B-V) = 0

Background
     Zod. Light/Earth = Average

CCD Parameters
     Checkbox = 3
     Gain = 4 (REQUIRED)
     CR-SPLIT = 1 (REQUIRED)
```

RPS2

```
    Exposure_Number: 1
        Target_Name: QSO
             Config: STIS/CCD
             Opmode: ACQ
           Aperture: F28X50LP
         Sp_Element: MIRROR
       Wavelength:
Optional_Parameters: ACQTYPE=POINT
Number_of_Iterations: 1
   Time_Per_Exposure: 15.0 S
Special_Requirements: ONBOARD ACQ FOR 2
```

Point Source Acquisition of Bright, Isolated Object with CCD-dispersed Light Peakup

In this example—point-source acquisition of a bright, isolated object with a CCD dispersed light peakup—an isolated V = 3.5 mag M2 I star is to be acquired, with the scientific exposures to be obtained in the `0.2X0.06` echelle slit.

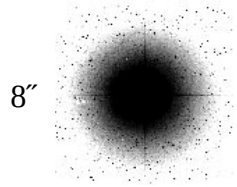

The scientific target will be acquired with a point-source acquisition, but because the object is so bright, we cannot use the preferred `F28X50LP` filter. Instead, we will use the `F28X50OII` filter, and the Target-Acquisition Exposure Time Calculator yields an exposure time of 0.06 seconds, which is less than the minimum allowed time of 0.1 seconds. Note that the `GAIN=4` and `CR-SPLIT=1` *must be used* for the ETC to assure that you have a S/N of at least 40 in each of the two images obtained during the `ACQ` process. We will therefore increase the exposure time to 1.0 seconds. The object does not saturate the CCD, and the exposure time is less than 5 minutes, so we have devised a valid target-acquisition.

The data are being obtained in a narrow slit, so we need to perform an `ACQ/PEAK` acquisition. The target is far too bright to perform the peakup with the `MIRROR`, so we will do a dispersed light peakup. Since we cannot perform a CCD peakup with an echelle grating, we will use the `G430M` grating with the CCD and the program slit (`0.2X0.06`); note that for an `ACQ/PEAK`, this combination is legal. A one second exposure (in the 50CCD) yields about 4000 electrons per pixel, while what is required is 80,000 electrons TOTAL in the spectrum. Since the spectrum is 1024 pixels long, our exposure time is valid, even after taking into account the slit loss. Given that the exposure time is so short, we can lengthen it to 3 seconds as an extra safety margin.

Exposure Time Calculator - ACQ

```
Detector and filter:
     CCD, F28X50OII

Exposure Parameters
     Exposure time for S/N = 40

Spectral Distribution
     Kurucz model M2 I

Flux
     V = 3.5, E(B-V) = 0

Background
      Zod. Light/Earth = Average

CCD Parameters
      Checkbox = 3
      Gain = 4 (REQUIRED)
      CR-SPLIT = 1 (REQUIRED)
```

Exposure Time Calculator - ACQ/PEAK

```
1st Order CCD
      G430M

Detector and filter
      CCD, 50CCD (Slitless)

Exposure Parameters
      S/N reached in Exp. time = 1s
      Central Wavelength = 4300

Spectral Distribution
      Kurucz model M2 I

Flux
       V = 3.5, E(B-V) = 0

Background
       Zod. Light/Earth = Average

CCD Parameters
       binning = 1X1
       Gain = 4 (REQUIRED)
       CR-SPLIT = 1 (REQUIRED)
```

RPS2 - ACQ

```
     Exposure_Number: 1
         Target_Name: BRIGHT-STAR
              Config: STIS/CCD
              Opmode: ACQ
           Aperture: F28X50OII
          Sp_Element: MIRROR
          Wavelength:
 Optional_Parameters: ACQTYPE=POINT
Number_of_Iterations: 1
   Time_Per_Exposure: 1.0 S
Special_Requirements: ONBOARD ACQ FOR 2
```

RPS2 - ACQ/PEAK

```
     Exposure_Number: 2
         Target_Name: BRIGHT-STAR
              Config: STIS/CCD
              Opmode: ACQ/PEAK
           Aperture: 0.2X0.06
          Sp_Element: G430M
          Wavelength: 4300
 Optional_Parameters:
Number_of_Iterations: 1
   Time_Per_Exposure: 3.0 S
Special_Requirements: ONBOARD ACQ FOR 3
```

Diffuse-Source Acquisition of a Spiral Galaxy

In this exampl an isolated galaxy with at flux of $1.5x10^{-14}$ erg cm^{-2} s^{-1} Å $^{-1}$ $arcsec^{-2}$ at 2000 Å is to be acquired, with the scientific exposures to be obtained in the `52X0.2` slit.

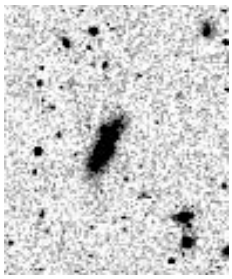

The target is isolated, so it will be acquired using a diffuse-source acquisition. After trying various checkbox sizes in the TAS (the image is from WFPC2), we determine that the appropriate `CHECKBOX` size is 9, and that we will use the `FLUX-CENTROID` algorithm. The object is faint, so we can use the preferred `F28X50LP` filter. The TA ETC is then used to determine an exposure time of 0.4 second. Note that the `GAIN=4` and `CR-SPLIT=1` *must be used* for the ETC to ensure that you have a S/N of at least 40 in each of the two images obtained during the `ACQ` process. The object does not saturate the CCD, and the exposure time is less than 5 minutes, so we have devised a valid target-acquisition. Given that the exposure time is so short, we can lengthen it to 2.0 seconds to make certain we have enough signal for a good acquisition. Since the data are being obtained in a wide slit, we do not need to perform an `ACQ/PEAKUP`, and our acquisition is complete.

Exposure Time Calculator

```
Detector and filter:
     CCD, Longpass

Exposure Parameters
     Exposure time for S/N = 40

Spectral Distribution
     Spiral Galaxy

Flux
      F(2000) = 1.5x10-14, E(B-V) = 0

      Extended source: 3 arcseconds

Background
        Zod. Light/Earth = Average

CCD Parameters
       Checkbox = 9
       Gain = 4 (REQUIRED)
       CR-SPLIT = 1 (REQUIRED)
```

RPS2

```
     Exposure_Number: 1
         Target_Name: GALAXY
              Config: STIS/CCD
              Opmode: ACQ
           Aperture: F28X50LP
          Sp_Element: MIRROR
          Wavelength:
 Optional_Parameters: ACQTYPE=DIFFUSE
          DIFFUSE-CENTER=FLUX-CENTROID
          CHECKBOX = 9
 Number_of_Iterations: 1
   Time_Per_Exposure: 2.0 S
Special_Requirements: ONBOARD ACQ FOR 2
```

Point-Source Acquisition in a Crowded Field

In this example a V = 19 mag nova in a field with a brighter companion is to be acquired, with the scientific exposures to be obtained in the `52X0.1` slit.

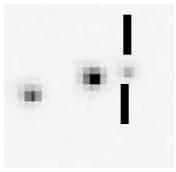

The target is in a crowded field, so we need to determine which object to acquire. If only a groundbased image were available, and the spectral types of the neighboring stars were unknown, then an isolated offset star outside of the immediate field of the nova would need to be acquired. However, the above image was obtained with WFPC2 and the `F555W` filter, which has a similar bandpass to the STIS `F28X50LP` filter. We therefore know that the object to the southeast of the nova is clearly the brightest object in the field (V = 16.5), and it will be our acquisition object. The object is faint enough that we can use the preferred `F28X50LP` filter. Since we do not know the spectral type of the acquisition star, we will make a worst-case (i.e., fewest counts) assumption that the star is of spectral type O5 and unreddened. The Target-Acquisition Exposure-Time Calculator is then used to determine an exposure time of 2.0 seconds. Note that the `GAIN=4` and `CR-SPLIT=1` *must be used* for the ETC to ensure that you have a S/N of at least 40 in each of the two images obtained during the `ACQ` process. The object does not saturate the CCD, and the exposure time is less than 5 minutes, so we have devised a valid target-acquisition. Note that since we do not know the spectral type of the object, we need to confirm that if the star had a spectral type of M6 V (which gives the most counts in the `F28X50LP` bandpass) it would still not saturate. Given that the exposure time is so short, we can lengthen it to 3.0 seconds to make certain we have enough signal for a good acquisition.

The data are being obtained in a narrow slit, so we need to perform an `ACQ/PEAK` acquisition. The peakup will be performed in program slit (`52X0.1`), and we will use the CCD and the `MIRROR`. A one-second exposure yields 655 electrons in the central 25pixels of the target, so an exposure time of 8 seconds yields 5240 electrons, which meets the minimum requirement of 5000 electrons. We need to lengthen the exposure time by a factor of 1.5 (see Chapter 13) to account for the slit throughput, for a final exposure time of 12.0 seconds. The object does not saturate the CCD, and the exposure time is less than 7.6 minutes (the maximum time for a peakup with the `52X0.1` slit), so we have devised a valid peakup target-acquisition.

Exposure-Time Calculator - ACQ

```
Detector and filter:
     CCD, Longpass

Exposure Parameters
     Exposure time for S/N = 40

Spectral Distribution
     Kurucz model O5

Flux
      V = 16.5, E(B-V) = 0

Background
       Zod. Light/Earth = Average

CCD Parameters
       Checkbox = 3
       Gain = 4 (REQUIRED)
       CR-SPLIT = 1 (REQUIRED)
```

Exposure Time Calculator - ACQ/PEAK

```
Detector and filter:
     CCD, CLEAR

Exposure Parameters
     S/N reached in Exp. time = 1s

Spectral Distribution
     User supplied spectrum = nova

Flux
      V = 19, E(B-V) = 0

Background
       Zod. Light/Earth = Average

CCD Parameters
       binning = 1X1
       Gain = 4 (REQUIRED)
       CR-SPLIT = 1 (REQUIRED)
```

RPS2 - ACQ

```
     Exposure_Number: 1
         Target_Name: OFFSET-STAR
              Config: STIS/CCD
              Opmode: ACQ
           Aperture: F28X50LP
          Sp_Element: MIRROR
          Wavelength:
  Optional_Parameters: ACQTYPE=POINT
 Number_of_Iterations: 1
   Time_Per_Exposure: 3.0 S
Special_Requirements: ONBOARD ACQ FOR 2
```

RPS2 - ACQ/PEAK

```
     Exposure_Number: 2
         Target_Name: NOVA
              Config: STIS/CCD
              Opmode: ACQ/PEAK
           Aperture: 52X0.1
          Sp_Element: MIRROR
          Wavelength:
  Optional_Parameters:
 Number_of_Iterations: 1
   Time_Per_Exposure: 12.0 S
Special_Requirements: ONBOARD ACQ FOR 3
```

Point-Source Acquisition of a QSO with Fuzz Behind the Fiduciary Bar

In this example an isolated V = 16.5 mag QSO (z = 0.2) is to be acquired, with the scientific exposures to be obtained with the QSO behind the `52X0.2F1` fiducial bar.

The target is isolated, so it will be acquired using a point-source acquisition. The object is faint, so we can use the preferred `F28X50LP` filter. The Target-Acquisition Exposure-Time Calculator is then used to determine an exposure time of 2.2 seconds. Note that the `GAIN=4` and `CR-SPLIT=1` *must be used* for the ETC to ensure that you have a S/N of at least 40 in each of the two images obtained during the `ACQ` process. The object does not saturate the CCD, and the exposure time is less than 5 minutes, so we have devised a valid target-acquisition. Given that the exposure time is so short, we can lengthen it to 3.0 seconds to make certain we have enough signal for a good acquisition.

The QSO is to be placed behind a fiducial bar, so to ensure an accurate centering we will perform an `ACQ/PEAK` acquisition. The peakup will be performed in the `52X0.2F1-R` slit. This peaks up the target at the offset reference position (see “Barred Spectroscopy” on page 215). Peakdown acquisitions are not recommended. We will use the CCD and the `MIRROR`. A one-second exposure yields 5400 electrons in the central 16 pixels of the target, and correcting for the aperture throughput (80%) yields 4320 electrons. We thus require slightly longer than 1 second to obtain the minimum requirement of 5000 electrons in the target, so we can expand our final exposure time to 5.0 seconds. The object does not saturate the CCD, and the exposure time is less than 9.8 minutes (the maximum time for a peakup with the `52X0.2` slit), so we have devised a valid peakup target-acquisition.

Exposure -Time Calculator - ACQ

```
Detector and filter:
     CCD, Longpass

Exposure Parameters
     Exposure time for S/N = 40

Spectral Distribution
     QSO, z=0.2

Flux
      V = 16.5, E(B-V) = 0

Background
       Zod. Light/Earth = Average

CCD Parameters
       Checkbox = 3
       Gain = 4 (REQUIRED)
       CR-SPLIT = 1 (REQUIRED)
```

Exposure-Time Calculator - ACQ/PEAK

```
Detector and filter:
     CCD, CLEAR

Exposure Parameters
     S/N reached in Exp. time = 1s

Spectral Distribution
     QSO, z=0.2

Flux
      V = 16.5, E(B-V) = 0

Background
       Zod. Light/Earth = Average

CCD Parameters
       binning = 1X1
       Gain = 4 (REQUIRED)
       CR-SPLIT = 1 (REQUIRED)
```

RPS2 - ACQ

```
     Exposure_Number: 1
         Target_Name: QSO-FUZZ
              Config: STIS/CCD
              Opmode: ACQ
           Aperture: F28X50LP
          Sp_Element: MIRROR
         Wavelength:
 Optional_Parameters: ACQTYPE=POINT
Number_of_Iterations: 1
   Time_Per_Exposure: 3.0 S
Special_Requirements: ONBOARD ACQ FOR 2
```

RPS2 - ACQ/PEAK

```
     Exposure_Number: 2
         Target_Name: QSO-FUZZ
              Config: STIS/CCD
              Opmode: ACQ/PEAK
           Aperture: 52X0.2F1-R
          Sp_Element: MIRROR
         Wavelength:
 Optional_Parameters:
Number_of_Iterations: 1
   Time_Per_Exposure: 5.0 S
Special_Requirements: ONBOARD ACQ FOR 3
```

Point-Source Acquisition of a Bright, Isolated Star Into the Wedge

In this example an isolated V = 6.0 mag G2 V star is to be acquired, with the scientific exposures to be obtained with the star behind the `WEDGEA1.8` mask.

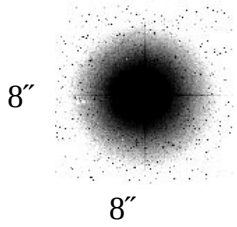

The target will be acquired with a point-source acquisition, but because the object is so bright, we cannot use the preferred `F28X50LP` filter. Instead, we will use the `F25ND3` neutral-density filter, and the Target-Acquisition Exposure-Time Calculator yields an exposure time of 0.01 second, which is less than the minimum allowed time of 0.1 second. Note that the `GAIN=4` and `CR-SPLIT=1` *must be used* for the ETC to assure that you have a S/N of at least 40 in each of the two images obtained during the `ACQ` process. We will therefore increase the exposure time to 0.5 second. The object does not saturate the CCD, and the exposure time is less than 5 minutes, so we have devised a valid target-acquisition.

The star is to be accurately placed behind the WEDGE which is 1.8″ in size, so we need to perform an `ACQ/PEAK` acquisition. The peakup will be performed in the `0.3X0.05ND` slit (peakdown acquisitions are not recommended), and we will use the CCD and the `MIRROR`. A one-second exposure yields 52,450 electrons in the target after correcting for the aperture throughput [both the neutral-density (10^{-3}) and the slit throughput (55%)], while the brightest pixel has 19,690 electrons. We have more than the minimum requirement of 5000 electrons in the target, the object does not saturate the CCD, and the exposure time is less than 6.4 minutes (the maximum time for a peakup with the `0.3X0.05ND` slit), so we have devised a valid peakup target-acquisition.

Exposure-Time Calculator - ACQ

```
Detector and filter:
     CCD, F25ND3

Exposure Parameters
     Exposure time for S/N = 40

Spectral Distribution
     Kurucz model G2 V

Flux
      V = 6.0, E(B-V) = 0

Background
       Zod. Light/Earth = Average

CCD Parameters
       Checkbox = 3
       Gain = 4 (REQUIRED)
       CR-SPLIT = 1 (REQUIRED)
```

Exposure-Time Calculator - ACQ/PEAK

```
Detector and filter:
     CCD, CLEAR

Exposure Parameters
     S/N reached in Exp. time = 1s

Spectral Distribution
     Kurucz model G2 V

Flux
      V = 6.0, E(B-V) = 0

Background
       Zod. Light/Earth = Average

CCD Parameters
       binning = 1X1
       Gain = 4 (REQUIRED)
       CR-SPLIT = 1 (REQUIRED)
```

RPS2 - ACQ

```
     Exposure_Number: 1
         Target_Name: G-STAR
              Config: STIS/CCD
              Opmode: ACQ
           Aperture: F25ND3
          Sp_Element: MIRROR
         Wavelength:
 Optional_Parameters: ACQTYPE=POINT
Number_of_Iterations: 1
   Time_Per_Exposure: 0.5 S
Special_Requirements: ONBOARD ACQ FOR 2
```

RPS2 - ACQ/PEAK

```
     Exposure_Number: 2
         Target_Name: G-STAR
              Config: STIS/CCD
              Opmode: ACQ/PEAK
           Aperture: 0.3X0.05ND
          Sp_Element: MIRROR
         Wavelength:
 Optional_Parameters:
Number_of_Iterations: 1
   Time_Per_Exposure: 1.0 S
Special_Requirements: ONBOARD ACQ FOR 3
```

CHAPTER 9
Overheads and Orbit-Time Determination

In This Chapter...

This chapter describes the overheads associated with STIS observations and it gives examples showing how to determine the number of orbits that your program will require.

Overview

After you establish the set of scientific exposures and any additional target-acquisition or calibration exposures that you require for your program, you are ready to determine the total number of orbits to request. Generally, this is a straightforward exercise involving compilation of the overheads on the individual exposures, packing the exposure plus overhead time into individual orbits, and tallying up the results to determine your total orbit request. In some cases, it may be an iterative process as you refine your exposure requests to more fully exploit the orbits.

The Phase I Proposal Instructions provide information on the Observatory policies and practices with respect to orbit-time requests and on the orbit-determination work sheets. Below, we provide a summary of the STIS-specific overheads and give several examples that illustrate how to calculate your orbit requirements for Phase I Proposals.

STIS Exposure Overheads

Our current estimates of the overheads on exposures are summarized in Table 9.1 and Table 9.2. All numbers given are approximate and rounded up to the nearest half minute; they do not differentiate in detail the overheads for different STIS modes and configurations. These overhead times are to be used (in conjunction with the actual exposure times and the Phase I Proposal Instructions) to estimate the total number of orbits for your proposal. After your HST proposal is accepted, you will be asked to submit a Phase II proposal to support scheduling of your approved observations. At that time you will be presented with actual, up-to-date overheads by the scheduling software. *Allowing sufficient time for overhead in your Phase I proposal is important; additional time to cover unplanned overhead will not be granted later.*

The following list presents important points for each type of overhead:

- ***Generic (Observatory Level) Overheads:***
  - The first time you acquire an object you must include the overhead for the guide-star acquisition (7 minutes).
  - In subsequent contiguous orbits you must include the overhead for the guide-star reacquisition (6 minutes); if you are observing in the Continuous Viewing Zone (see the Phase I Proposal Instructions), no guide-star *reacquisitions* are required.
  - Time needs to be allowed for each deliberate movement of the telescope; e.g., if you are performing a target-acquisition exposure on a nearby star and then offsetting to your target, or if you are taking a series of exposures in which you move the target relative to the slit, you must allow time for the moves (20 seconds to 60 seconds depending on length of slew, see Table 9.1 and Table 9.2).
  - Remember the policy with regard to MAMA and CCD observations in the same visit (see Chapter 2).
- ***Onboard STIS Target-Acquisition Overheads:***
  - All STIS spectroscopic exposures that use a slit (long slit or echelle slit) will need to include a target-acquisition exposure to place the target in the slit (see “STIS Onboard CCD Target Acquisitions (ACQ)” on page 127). As discussed in “Onboard Target-Acquisition Peakups (ACQ/PEAK)” on page 140, for the narrower slits you may also wish to perform a peakup exposure to center the target in the slit.
  - An on-board target-acquisition need be done only once in a series of continuous orbits (i.e., once per visit).
  - The drift rate induced by the Observatory is less than 10 milli-arcseconds per hour. Thermal drifts internal to STIS at the slit plane are less still. We recommend that for long series of exposures taken through slits which are less than or equal to 0.1 arcsecond in either dimension, a peakup be performed every 4-5 orbits. This procedure will ensure that drifts do not cause the target to move out of the slit. (See also “Exposure Sequences and Contemporaneous Calibrations” on page 186.)

- ***Scientific Exposures:***
  - The overhead times are dominated by the time to move the grating wheel (MSM), which is ~3.0 minutes per move, worst case, and the readout time (CCD). Again, we stress that in Phase II the overheads will frequently be less, but it is important to plan Phase I using the conservative overheads given in Table 9.2 to ensure you will have adequate time for your scientific goals.
- ***CCD and MAMA Spectroscopic Exposures and Wavecals:***
  - The quoted overheads on the first spectroscopic exposure in a visit, or a spectroscopic exposure within a visit containing a change of grating or grating tilt, allow for the taking of a single automatic wavecal exposure to permit post-observation determination of the zeropoint of the wavelength (and spatial) scales. If you plan a series of exposures at a given grating setting which extends over 40 minutes in exposure time, then you need to include time for an additional automatic wavecal for each 40 minute period.
- ***Moving Targets:***
  - Additional overheads will be incurred for observations of solar-system targets. Onboard tracking and commanding requirements do not allow an observation (exposure plus overhead) to exceed 33 minutes. Consequently, long exposures must be split into two or more shorter exposures, each carrying separate instrument overheads. The moving-target overheads (~1 minute in duration) are dependent upon current slew rates and are updated as necessary.

Table 9.1: Scientific Exposure Overheads: General, Acquisition, and Peakup

Action	Overhead
Generic (Observatory Level)	
Guide-star acquisition	Initial acquisition overhead = 7.0 minutes Reacquisitions on subsequent orbits = 6 minutes per orbit
Spacecraft pos-targ moves	For offsets less than 1 arcminute and more than 10 arcseconds = 1 min. For offsets between 10 arcseconds and 1 arcsecond = 0.5 minute For offsets less than 1 arcsecond in size = 20 seconds
Acquisitions and Peakups	
Target-acquisition (to place target in STIS aperture); see also Chapter 8, Target Acquisition.	For V ≤ 21 point-sources, 6 minutes Generally, $(500 + 4 * t_{exp} + 0.2 * \text{checkbox}^2)$ seconds
Acquisition peakups; (see also Chapter 8, Target Acquisition)	For V ≤ 21 , 6 minutes More generally, see Table 8.4

Table 9.2: STIS Scientific Exposure Overheads: Imaging and Spectroscopy

Action	Overhead			
	Imaging		Spectroscopy	
	CCD (minutes)	MAMA (minutes)	CCD (minutes)	MAMA (minutes)
First scientific exposure	4.5	5.0	5.0[a]	8.0[a]
Identical exposure in series (within an orbit)	1.0[b]	0.5	1.0	0.5
Exposure in series with grating move only	3.0	3.0	5.0[a]	8.0[a]
Move of aperture wheel (change of slit or aperture) (change of filter)	1.0	1.0	1.0	1.0
Additional automatic wavecal for series of identical exposures extending more than ~40 minutes	n/a	n/a	1.5	4.0
Overhead for data management for exposures > 3 minutes in duration	0	0	0	0
Overhead for data management, for a series of full-frame exposures, each SHORTER than 3 minutes in duration (see “Use of Subarrays to Reduce Data Volume” on page 149 for subarray rules)	3 minutes every 7 exposures	2 minutes every exposure	3 minutes every 7 exposures	2 minutes every exposure
Additional Calibration Exposures: Extra GO Wavecals[c] and fringe flats				
MAMA wavecal exposure	4.0 minutes			
CCD wavecal exposure	1.5 minutes			
CCD fringe flat exposure	2 minutes			

a. Includes auto wavecal. At Phase II, wavecals occurring at the beginning or end of an orbit will be pushed into occultation, providing increased time for scientific observing.
b. For `CR-SPLIT=`*n*, each exposure has a 1 minute overhead, so there will be (*n* – 1) minutes of *extra* overhead.
c. Use these only to add additional wavecal exposures beyond those taken automatically.

Orbit-Use-Determination Examples

The easiest way to learn to compute total orbit time requests is to work through a few examples. Below we provide five different examples:

- Example 1 is a pattern-stepped series of long-slit CCD spectroscopic exposures mapping out the Hα nebula in the center of the galaxy M86.
- Example 2 is a series of spectroscopic observations of the solar-analog, CVZ star P041-C, using all of the first-order, low-resolution CCD gratings.
- Example 3 is an imaging and spectroscopic program observing NGC 6543, the Cat's Eye Nebula.
- Example 4 is a set of long MAMA spectroscopic exposures of Sk -69˚ 215 using the E230H grating through a narrow echelle slit, taken in the CVZ.
- Example 5 is a faint CCD imaging program.

These examples represent fairly typical uses of STIS. The target-acquisitions used in each example differ slightly as well:

- Example 1 uses a diffuse-source acquisition and no peakup.
- Example 2 uses a point-source acquisition and peakup on the target.
- Example 3 uses a point-source acquisition.
- Example 4 uses a point-source acquisition and peakup on the target, and includes re-peakups during the course of the long observations.
- Example 5 uses no acquisition.

Sample Orbit Calculation 1: Long-Slit Spectroscopy of the Galaxy M86

This example is for an observation of the Hα nebula in the center of the Virgo elliptical M86, using the `52X0.2` slit and the `G750M` grating. A series of exposures is taken, each stepped relative to the next by 0.2 arcsecond, in the direction perpendicular to the slit, in order to cover the inner 0.6 arcseconds of the galaxy completely. Based on the signal-to-noise ratio calculation presented in "Spectroscopy of Diffuse Source (M86)" on page 85, we require an integration time of ~30 minutes per position to obtain a signal-to-noise ratio of ~10. The scientific exposures for this proposal, therefore, comprise *all* of the following:

- A `CR-SPLIT=2` ~30 minute spectroscopic exposure[1] with `G750M` at a central wavelength of λ=6768 Å at location 1.

1. Here and below, a `CR-SPLIT=`*n* *m* minute exposure implies there will be *n* exposures with a total of *m* minutes across the exposures. In this example there will be 2 exposures each of 15 minutes for a total of 30 minutes.

- A `CR-SPLIT=2` ~30 minute spectroscopic exposure with `G750M` at a central wavelength of λ=6768 Å at location 2.
- A `CR-SPLIT=2` ~30 minute spectroscopic exposure with `G750M` at a central wavelength of λ=6768 Å at location 3.

We need to include time for the guide-star acquisition at the start of the first orbit, followed by an acquisition exposure. No peakup will be done, since we are covering the nebula by stepping the slit. In this example, we assume that the acquisition is done using the diffuse acquisition, with a checkbox size of 25 pixels (roughly 1.25 arcseconds). The checkbox needs to be large as this galaxy has a very flat and dusty profile; see Figure 8.6.

The mean surface brightness of the galaxy within this region is ~2 x 10^{-15} ergs sec^{-1} cm^{-2} $Å^{-1}$ $arcsec^{-2}$, based on WFPC2 V band images in the HST archive. Using the information in “Computing Exposure Times” on page 76 or the STIS exposure time calculator we determine that, using the CCD LongPass filter, `F28X50LP`, for t_{exp}= 1 second, we more than achieve the required signal-to-noise ratio needed over the checkbox for the target-acquisition. We use the formula in Table 9.1, plug in CHECKBOX=25 and exptime=1.0, and determine that the acquisition will take roughly 10 minutes.

This is not a CVZ observation, so because more than 1 orbit is required we need to include time for the guide-star reacquisition at the beginning of each orbit. The individual exposures in this example are long enough that we do not need to include extra overhead for data management. We are satisfied with the automatic wavecal exposures which are taken for each spectroscopic observation at a new MSM position. We do not require fringe flats as we are observing at wavelengths shortward of 7500 Å.

We assume a visibility period of 52 minutes per orbit, appropriate for a target at M86’s declination (see the Call for Proposals). Based on the reasoning presented in Table 9.3, below, we conclude that the observations can be squeezed into ~2 orbits with some loss of sensitivity. Alternately, one could choose to increase the signal-to-noise, and ask for 3 orbits.

Sample Orbit Calculation 2; Low-Dispersion Spectroscopy of Solar-Analog Star P041-C

In this example the scientific objective is to observe the solar-analog CVZ star P041-C from the near IR to the near UV with STIS’s low-resolution, first-order gratings and the `52X0.5` arcsecond slit. The series includes:

- `CR-SPLIT=2,` ~4 minute spectroscopic exposure with`G750L` at a central wavelength of λ = 7751 Å.
- `CR-SPLIT=2`, ~4 minute spectroscopic exposure with `G430L` at the central wavelength of λ = 4300 Å.
- `CR-SPLIT=3`, ~45 minute spectroscopic exposure with`G230LB` at the central wavelength of λ = 2375 Å.

Table 9.3: Orbit Calculation for Example 1

Action	Time (minutes)	Explanation
	Orbit 1	
Initial guide-star acquisition	7.0	Needed at start of observation of new target
Target-acquisition	10.0	Diffuse acquisition with checkbox=25, t_{exp}=1.0 sec
Offset target 0.2″ to initial position	0.33	Position target to position 1 in pattern
Scientific exposure, `G750M`, λ_c = 6768 Å, position 1	33.0	27.0 minutes exposure time 5.0 minutes for first CCD spect. exposure in orbit 1.0 minutes for exposure overhead for `CR-SPLIT`
	Orbit 2	
Guide-Star Reacquisition	6.0	Start of new orbit
Offset target 0.2” to position 2	0.33	Move target to position 2 in pattern
Scientific exposure, `G750M`, λ_c = 6768 Å, position 2	23.0	22.0 minutes exposure time 1.0 minutes for exposure overhead for `CR-SPLIT`
Step target 0.2″ perp. to slit	0.33	Move to position 3 in pattern
Scientific exposure, `G750M`, λ_c = 6768 Å, position 3	23.0	22.0 minutes exposure time 1.0 minutes for exposure overhead for `CR-SPLIT`

We need to include time for the guide-star acquisition at the start of the first orbit, followed by an acquisition exposure. This target is a bright point-source; we will use the longpass filter `F28X50LP` for the target-acquisition and the default overhead of 6.0 minutes from Table 9.1 on page 161. No peakup is needed as we are using the 0.5 arcsecond-wide slit. This is a CVZ observation so each orbit is ~96 minutes. We need to include time for the CCD long-wavelength fringe flats, since this a CVZ observation, the fringe flat will not move into the occultation. As shown in Table 9.4, we can easily perform this observation in a single orbit.

Table 9.4: Orbit Calculation for Example 2

Action	Time (min)	Explanation
	Orbit 1	
Initial guide-star acquisition	7.0	Needed at start of observation of new target
Target-acquisition	6.0	Point-source acquisition on target
Scientific exposure, `G430L`, λ = 4300 Å	13.0	7.0 minutes exposure time 5.0 minutes - CCD spect. exp with grating-wheel move overhead 1.0 minutes for `CR-SPLIT=2` exposure overhead
Scientific exposure, `G230LB`, λ = 2375 Å	50.5	43.5 minutes exposure time 5.0 minutes - CCD spect. exp with grating-wheel move overhead 2.0 minutes for `CR-SPLIT=3` exposure overhead
Autowavecal	1.5	1.5 minutes for autowavecal after 40 minutes
Scientific exposure, `G750L`, λ = 7751 Å	11.0	5.0 minutes exposure time 5.0 minutes - CCD spect. exp with grating-wheel move overhead 1.0 minutes for `CR-SPLIT=2` exposure overhead
CCD fringe flat G750L	2.0	Fringe flat overhead

Sample Orbit Calculation 3: Imaging and Spectroscopy of the Cat's Eye Planetary Nebula, NGC6543

In this example the scientific objectives are to obtain an [O II] images of planetary nebula NGC 6543, as well as an optical spectrogram at Hβ and an ultraviolet spectrogram at C IV. The exposure-time calculations for these observations are presented on page 87. The specific exposures in this series include:

- A `CRSPLIT=2` ~5 minute exposure with the `F28X50OII` filter.
- A `CRSPLIT=2`, ~30 minute exposure with `G430M` at a central wavelength of λ_c = 4961 Å, using the `52X0.1` long slit and
- A ~30 minute exposure with `G140L` at C IV and the `52X0.1` long slit.

We need to include time for the guide-star acquisition at the start of the first orbit, followed by an acquisition exposure. The central star of the Cat's Eye Nebula is used as the acquisition target. It has a V magnitude ~11.5. Checking Table 8.2 on page 136, we conclude that the star is not so bright that it will saturate the CCD in imaging mode with the longpass aperture `F28X50LP` and we therefore use it for the target-acquisition. We use the overhead information in Table 9.1 and Table 9.2 directly and conclude that the target-acquisition will take 6 minutes. We wish to perform a peakup exposure as well, to center the star in the 0.1 arcsecond-wide slit. We consult Table 8.2 on page 136 and conclude that the source is not bright enough to saturate the CCD if we perform an undispersed (white-light) peakup with the mirror. Again using the information in Table 9.1 and Table 9.2, we conclude the peakup will take 6 minutes.

This is not a CVZ observation, so because more than 1 orbit is required we need to include time for the guide-star reacquisition at the beginning of each orbit. The individual exposures in this example are long enough that we do not need to include extra overhead for data management. We are satisfied with the automatic wavecal exposures which are taken for each spectroscopic observation at a new MSM position.

We assume a visibility period of 57 minutes per orbit, appropriate for a target at our source's declination of 66 degrees (see the Call for Proposals). Based on the reasoning presented in Table 9.5 below, we conclude that a total of 2 orbits is required to perform these observations. Note that the MAMA and CCD observations have been split into separate visits in accordance with the required policy.

Table 9.5: Orbit Calculation for Example 3

Action	Time (minutes)	Explanation
	Orbit 1	
Initial guide-star acquisition	7.0	Needed at start of observation of new target
Target-acquisition	6.0	Performed on central star
Peakup acquisition	6.0	White-light peakup performed on central star
`NUM-EXPOSURES=2` G140L scientific exposure	38.0	29.5 minutes scientific exposures time 8.0 minutes—first spectroscopic MAMA exposure 0.5 minutes—identical exposure in series
Orbit 2 (A whole new visit to keep MAMA and CCD exposures separate)		
Initial guide-star acquisition	7.0	Needed at start of observation of new target
Target-acquisition	6.0	Performed on central star
Peakup acquisition	6.0	White light peakup performed on nearby star
`CR-SPLIT=2` scientific exposure with G430M at λ_c = 4961 Å	28.0	22.0 minute total scientific exposure time 5.0 minutes first CCD spectroscopic exposure in visit 1.0 minutes for exposure overhead for `CR-SPLIT`
`CR-SPLIT=2` [O II] imaging using `F28X50OII`	10.0	5.0 minutes, total scientific exposure time 4.0 minutes overhead, imaging exposure 1.0 minutes for exposure overhead for `CR-SPLIT`

Sample Orbit Calculation 4: MAMA Echelle Spectroscopic Exposures in the CVZ

In this example we wish to obtain a long total integration (420 minutes) in the CVZ using `E230H` and the `0.2X0.09` slit. The exposure-time calculations for this example are presented in “Echelle Spectroscopy of a Bright Star with Large Extinction (Sk –69˚ 215)” on page 89.

We choose to break the observation up into roughly identical 60 minute exposures (though the actual scientific exposure time per orbit will be reduced to accommodate the required overheads and still remain within the MAMA 5orbit limit). We acquire the target using a CCD point-source acquisition and then peakup in dispersed light using the CCD and the same slit as intended for the scientific observations. The star is Sk –69˚ 215, an O5 star with a V magnitude of 11.6. Checking Table 8.2 on page 136, we conclude the source is not so bright that it will saturate the CCD if observed for 0.1 seconds in the longpass filter `F28X50LP`, and we choose to perform the acquisition then on Sk –69˚ 215 with this filter as the aperture. We take the acquisition time as 6 minutes, from the overheads in Table 9.1.

We then perform a dispersed-light peakup using the `G230LB` grating with the CCD detector. We can estimate the exposure time required by determining with the spectroscopic ETC the total counts over the detector in 1 second for the clear filter and scaling by 65% for the slit throughput (“0.2X0.09 Aperture” on

page 286) for `0.2X0.09`. Since we must attain 80,000 counts over the detector, we require roughly 9 seconds per dwell point of the peakup. The peakup overhead for this slit is 300 + 20*t_{exp}. We thus conclude that the peakup will require 300 + 20 x 9 = 480 seconds or ~8 minutes.

Since this is a CVZ observation, we do not need to include time for reacquisitions; however, since it is a long observation we decide we will re-perform a peakup midway through the observation.

Additionally, since this is a long observation taken at a given grating position, we need to include time for the automatic wavecals which will be taken every 40 minutes of elapsed pointed time.

Since this is CVZ time, an orbit is 96 minutes. We conclude we require a total of 5 orbits to perform this program, as summarized in Table 9.6.

Table 9.6: Orbit Calculation for Example 4

Action	Time (minutes)	Explanation
CVZ Observations - Total Time = 486 minutes or 486 / 96 = 5 orbits		
Initial guide-star acquisition	7.0	Needed at start of observation of new target
Target-acquisition	6.0	Point-source acquisition on target
Peakup exposure in `0.2X0.09` slit	8.0	Echelle slit dispersed-light peakup
First scientific exposure `E230H`	48.0	40.0 minutes exposure time 8.0 minutes for first MAMA spect. exposure in visit
Automatic wavecal after 40 minutes	4.0	4.0 minutes
Second scientific exposure `E230H`	41.0	40.0 minutes exposure time ~1 minute overhead on identical exposure
Automatic wavecal after 40 minutes	4.0	4.0 minutes
Third scientific exposure	41.0	40.0 minutes exposure time ~1 minute overhead on identical exposure
Automatic wavecal after 40 minutes	4.0	4.0 minutes
Fourth scientific exposure	41.0	40.0 minutes exposure time ~1 minute overhead on identical exposures
Automatic wavecal after 40 minutes	4.0	4.0 minutes
Fifth scientific exposure	41.0	40.0 minutes exposure time ~1 minute overhead on identical exposure
Automatic wavecal after 40 minutes	4.0	4.0 minutes
Peakup to recenter target	8.0	Echelle slit peakup
Sixth scientific exposure	41.0	40.0 minutes exposure time ~1 minute overhead on identical exposure
Automatic wavecal after 40 minutes	4.0	4.0 minutes
Seventh scientific exposure	41.0	40.0 minutes exposure time ~1 minute overhead on identical exposure
Automatic wavecal after 40 minutes	4.0	4.0 minutes
Eighth scientific exposure	41.0	40.0 minutes exposure time ~1 minute overhead on identical exposure
Automatic wavecal after 40 minutes	4.0	4.0 minutes
Ninth scientific exposure	41.0	40.0 minutes exposure time ~1 minute overhead on identical exposure
Automatic wavecal after 40 minutes	4.0	4.0 minutes
Tenth scientific exposure	41.0	40.0 minutes exposure time ~1 minute overhead on identical exposure
Automatic wavecal after 40 minutes	4.0	4.0 minutes

Sample Orbit Calculation 5: Faint CCD Imaging

In this program we wish to take deep images of a field to look for faint point-sources, as described in “Imaging a Faint Stellar Source” on page 91. We request `LOW-SKY` as this observation is background-limited. At our declination, we find from the CP/Phase I Proposal Instructions, that there are 45 minutes of visibility per orbit. The observations consist of:

- A single `CR-SPLIT=4` ~20 minute exposure using the `50CCD` clear aperture with the CCD.

We determine that we can execute this program in 1 orbit, as summarized in Table 9.7.

Table 9.7: Orbit Calculation for Example 5

Action	Time (minutes)	Explanation
	Orbit 1	
Initial guide-star acquisition	7.0	Needed at start of observation of new target
`CRSPLIT=4` exposure, using `50CCD` in imaging mode.	36.0	28.0 minutes exposure time 5.0 minutes for first imaging exposure in orbit 3.0 minute overhead for `CR-SPLIT` exposures

CHAPTER 10
Summary and Checklist

In This Chapter...

In this chapter we provide a summary and a checklist to help ensure that you have correctly planned your Phase I (proposing for HST time) and Phase II (scheduling your approved observations) submissions.

Phase I Proposing

At this point you should have assembled all the information you need to submit your Phase I HST observing-time proposal. During the course of this process you should review the items listed below.

For All Proposals:

- Check the catalog of previously executed and accepted programs to search for any duplications, and if present, justify them.
- Justify any special requirements (e.g., `SHADOW`, interactive acquisition, CVZ, target of opportunity, time-critical scheduling, or the re-use target capability).
- Consider any special calibrations (e.g., unusually accurate wavelength determination requiring additional (non-automatic) wavecal exposures or fringe flats), and account for their time in your request.
- Check your exposure times and configurations to ensure they are sufficient to provide the desired signal-to-noise ratios and accuracies, without saturation.

- Allocate time for a target acquisition with appropriate centering accuracy; if a pre-acquisition image is needed, include the necessary extra orbit in the total orbit-time request.
- Consider the need for, and benefit of, obtaining coordinated parallel exposures with WFPC2.
- Include all applicable overheads so that in Phase II you will have enough orbits available to successfully implement your observations.
- If applicable, justify the use of any available modes, and explain how you plan to deal with calibration issues.

For CCD Observations:

- Check that you are not exceeding the CCD full well counts pixel^{-1} limit for pixels (lines or objects) of interest.
- Allow time for `CR-SPLIT` observations and dithering, as needed.

For MAMA Observations:

- Check that your source does not exceed the absolute bright-object count-rate limits for MAMA exposures. For target-of-opportunity programs, explain how you plan to show the target does not exceed the bright object limits.
- Check that you are not exceeding the MAMA 65,536 counts pixel^{-1} buffer-imposed limit over pixels (lines or objects) of interest.
- Check that no MAMA visit is longer than 5 orbits.
- Justify the need for both MAMA and CCD scientific exposures in a single visit, or have allowed sufficient orbital time to allow separation of MAMA and CCD science exposures, if applicable.

Phase I Orbit-Allocation Examples

A sample Phase I orbit-allocation worksheet is presented in the Phase I Proposal Instructions. Examples of Phase I orbit estimations are worked through in this Handbook (see “Examples Used in this Handbook” on page 4, “Exposure-Time Examples” on page 85, and “Orbit-Use-Determination Examples” on page 163).

Phase II—Scheduling Approved Observations

Below, we provide a checklist for observers filling out Phase II proposals. You should do the following prior to submitting your program.

For All Proposals:

- Update the text in the Phase II template (“Observing Description” and “Special Requirements”—they were copied from your Phase I proposal and may need modification based on TAC comments and definition of the observation details).
- Specify your coordinates (especially for spectroscopic observations) in the “Guide Star Reference” frame. Specify proper motions if applicable.
- Specify accurate V magnitude, fluxes, spectral type, and colors for your target.
- Properly specify your exposures.
- Include target acquisitions and peakups as needed.
- Specify orientation requirements. Specify timing requirements. To facilitate scheduling, please provide the broadest possible ranges for your requirements. If multiple ORIENTs are possible, please include the alternatives.
- Specify any allocated coordinated parallel exposures.
- Include any additional wavecal exposures if needed.
- Verify the correct usage (i.e., direction) of your PATTERN optional requirement or `POS TARG`s (if used).
- For slitless spectroscopy or prism observations, remember to take an image and the proper calibration sequence.

For CCD Observations:

- `CR-SPLIT` CCD exposures, as appropriate.
- Add fringe-flat exposures for G750L and G750M observations at $\lambda > 7500$ Å.
- Consider the use of dithering for imaging observations, or stepping along the slit for spectroscopic observations.

For MAMA Observations:

- Re-verify that your target falls below the bright-object limits.
- For `TIME-TAG` observations, verify the value for `BUFFER-TIME`.
- Consider the use of dithering for imaging observations.
- Consider the use of stepping along the slit for first-order modes or the use of FP-SPLIT slits for echelle modes, when high signal-to-noise is required.

Phase II Templates

Phase II templates for the examples worked out in this Handbook will be made available on the World Wide Web in conjunction with the release of the Phase II Proposal Instructions.

PART 3

Supporting Material

The chapters in this Part present more detailed material in support of the User's Guide. Included are a description of the data-taking modes of STIS, special uses of the instrument, and spectroscopic and imaging reference material.

"Space is big, really big."
A. Douglas, HHG.

CHAPTER 11
Data Taking

In This Chapter...

In this chapter we describe the basic ways in which data can be taken with STIS. Included are descriptions of the operating modes of the STIS CCD and MAMAs, the use of subarrays, taking of time-resolved data, associated exposures in a series, automatic and extra wavecals, fringe flats, the use of patterns and dithering, and fixing the slit orientation on the sky.

Basic Operating Modes

STIS currently supports four basic operating modes:

- `ACCUM` operating modes for the CCD and MAMAs, which produce a time-integrated accumulated image. These are the most commonly used modes.
- `TIME-TAG` operating mode for the MAMA detectors, which outputs an event stream of high-time-resolution observations in the UV.
- `ACQ` (acquisition) and `ACQ/PEAKUP` operating modes for the CCD and MAMAs used to acquire targets in the spectroscopic slits and behind coronographic bars and masks. Target acquisitions are described further in Chapter 8, “Target Acquisition” on page 123.

CCD ACCUM Mode

The STIS CCD has only the single operating mode, `ACCUM`, for images and spectroscopy. The CCD pixels accumulate charge during the exposure in response to photons. The charge is read out at the end of the exposure and converted to 16

bit data numbers (DN) at a selectable gain (number of electrons per DN) by the A-to-D converter. The DN are stored as 16 bit words (with a range 0 to 65,535) in the STIS data-buffer memory array. At the default `CCDGAIN=1`, the CCD full well (33,000 e^-), and not the 16-bit format, limits the total counts that can be sustained in a single exposure without saturating (see also “Analog-To-Digital Conversion” on page 101 and “CCD Saturation: the CCD Full Well” on page 102). At the other supported gain, `CCDGAIN=4`, the CCD full well (144,000 e^- or 36,000 DN) still determines the saturation limit.

A full detector readout is actually 1062 x 1044 pixels with physical and virtual overscans. Scientific data are obtained on 1024 x 1024 pixels, each projecting to ~0.05 x 0.05 arcsecond on the sky. The dispersion axis runs along `AXIS1` (image x or along a row of the CCD), and the spatial dimension of the slit runs along `AXIS2` (image y or along a column of the CCD). Figure 11.1 illustrates the full CCD format and its orientation with respect to the spacecraft (U2 and U3 or V1 and V3) axes. The readout includes 19 columns of leading and 19 columns of trailing physical overscan in `AXIS1`, and 20 trailing rows of virtual overscan in `AXIS2`. The leading and trailing serial overscan as well as the parallel overscan pixels are used to determine the bias level in post-observation data processing. The parallel overscan can also be used in the diagnosis of charge-transfer problems.

Figure 11.1: CCD ACCUM Mode Format for a Long-Slit Spectrum

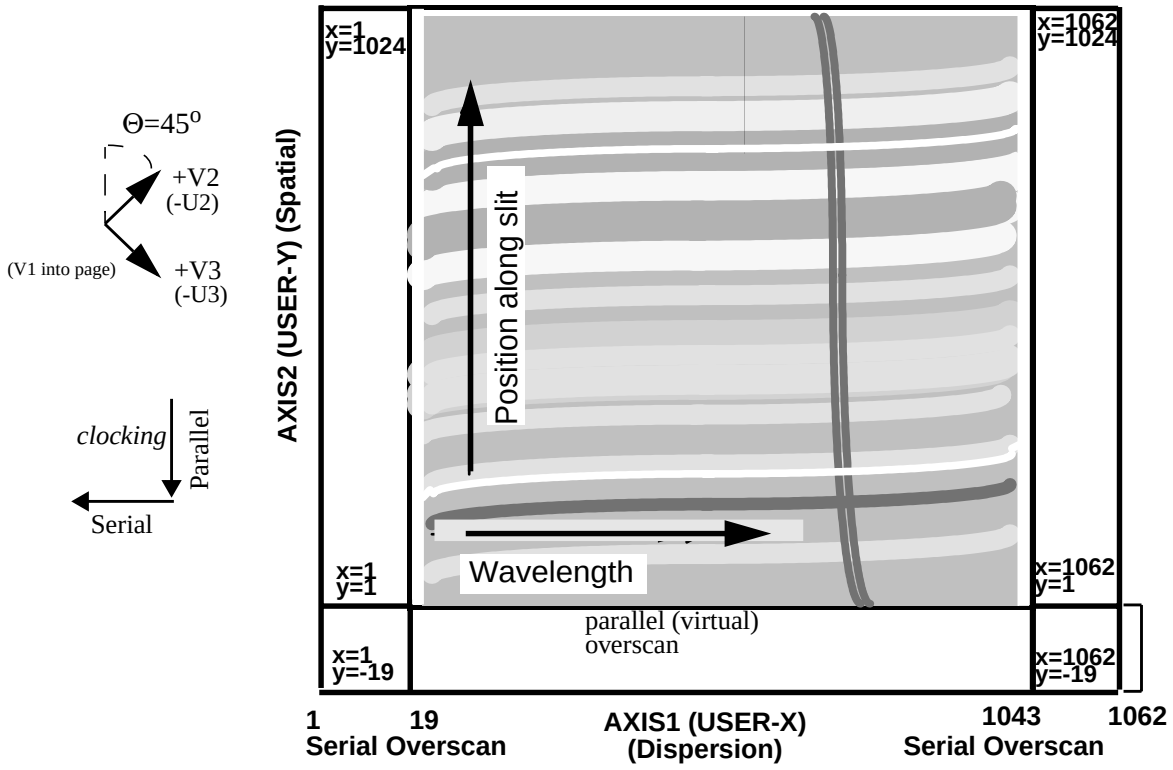

The minimum CCD exposure time is 0.1 second and the maximum possible exposure time is 4.7 hours (though we cannot imagine wanting a single exposure longer than 60 minutes). The minimum time between *identical* exposures for CCD full-frame (1062 x 1044) images is ~45 seconds.[1] This time is dominated by the time it takes to read out the CCD (28 seconds for the full frame) and can be reduced to ~20 seconds if you use a subarray (see “CCD Subarrays” on page 179).

Binning

The CCD supports on-chip binning. When on-chip binning is used the specified number of pixels in the serial and parallel directions is read out as a single pixel. The advantage of CCD binning is that the read noise per binned pixel is the same as the read noise per unbinned pixel. Thus if your signal-to-noise per pixel is dominated by read noise when no binning is used, you can increase the signal-to-noise by binning. The disadvantage of using on-chip binning is that it reduces the resolution of your spectrogram or image. On-chip binning of 1, 2, or 4 pixels in both the `AXIS1` and `AXIS2` directions is supported. Note that on-chip binning is not allowed when subarrays are used.

During Phase II, you specify the binning for your CCD observations using the `BINAXIS1` and `BINAXIS2` optional parameters. The default values are 1.

CCD Subarrays

Subarrays can be used when the CCD detector is read out. Generally, there is no need to use a subarray for STIS data. The primary scientific use of CCD subarrays is for time-resolved optical spectroscopy, where subarrays can be used to reduce the CCD read time and keep the data volume at a manageable level. CCD subarrays can also be specified for CCD `ACQ/PEAK` observations to limit the region in a diffuse object (e.g., a galaxy) over which the flux is summed for the peakup. When a subarray is used, only the portion of the detector which is within the specified subarray is read out and transmitted to the ground (see Figure 11.2—note that the spectrogram curvature is exaggerated in this figure).

---

1. This constraint implies there will be 45 seconds of overhead per full-frame `CR-SPLIT`, i.e., if `CR-SPLIT=3`, there will be 3 x 45 seconds of overhead on the set of 3 exposures due to CCD setup and readout.

Figure 11.2: Using Subarrays

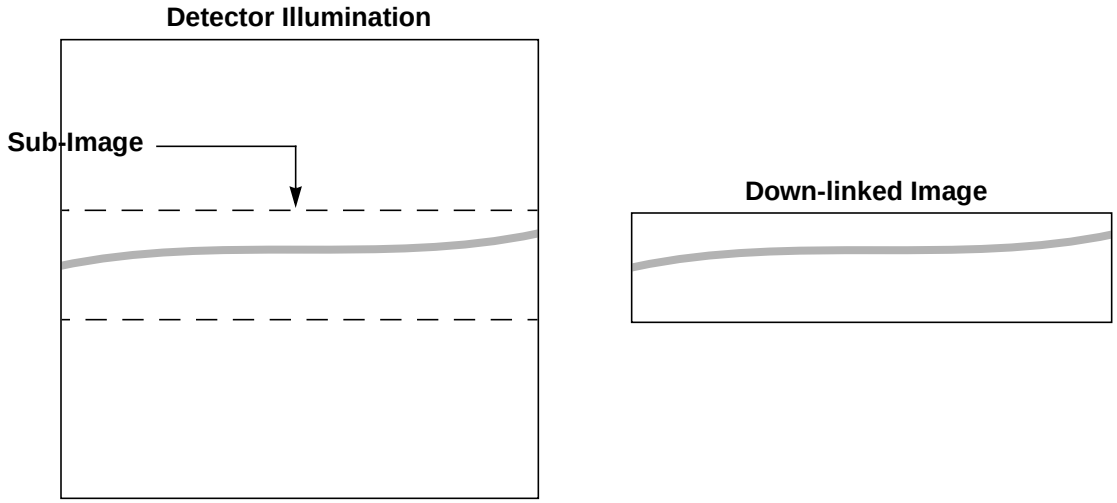

As described in “CCD ACCUM Mode” on page 177, full-frame CCD readouts are composed of 1062 x 1044 pixels; 1024 x 1024 data pixels, 19 leading and 19 trailing serial-overscan pixels, and 20 trailing parallel-overscan pixels. Dispersion runs along AXIS1 and the long dimension of the slit runs along AXIS2. Subarrays are required to span the full width of the CCD detector in the serial (dispersion) direction in order to ensure they contain the serial overscan needed to determine the bias level; however, you can control the height of the subarray in the parallel direction (i.e., along the slit for long-slit spectroscopic observations). Note that no parallel overscan is returned for subarrays (se also “CCD Bias Subtraction and Low-Level Non-Linearity” on page 105). Subarray sizes and centers, as specified in Phase II, are given by four parameters:

- SIZEAXIS1 – size in pixels of the subarray in the AXIS1 direction.
- SIZEAXIS2 – size in pixels of the subarray in the AXIS2 direction.
- CENTERAXIS1 – central pixel of the subarray in the AXIS1 direction.
- CENTERAXIS2 – central pixel of the subarray in the AXIS2 direction.

The minimum allowed value of SIZEAXIS2 for ACCUM mode observations is 32 pixels (corresponding to 1.6 arcsec), and SIZEAXIS2 must be an even number of pixels. The subarray is centered on the target position.

Use of Subarrays to Reduce the CCD Read Time

The minimum time between identical CCD exposures is the readtime + 16 seconds. The time to read out a CCD subarray is:

$$readtime = 2.0 + SIZEAXIS2 \times 0.026 \qquad \text{seconds}$$

Thus, using the smallest available subarray, which is 32 pixels high, you can reduce the minimum time between identical exposures to ~20 seconds (16 seconds overhead plus 3 seconds read time). The minimum time between full-frame CCD exposures is ~16 + 29~ 45 seconds.

Use of Subarrays to Reduce Data Volume

The format of the data you receive when you use a CCD subarray will have dimensions 1060 x SIZEAXIS2, will cover the full range in the dispersion direction, and will include the serial overscan. The STIS buffer can hold eight full-frame CCD exposures at one time, or 8 × (1024 / SIZEAXIS2) exposures at any one time. Full-frame CCD data acquired in one exposure can be transferred to the HST data recorder during the subsequent exposure(s) so long as the integration time of the subsequent exposure is longer than 3.0 minutes. If you are taking a series of exposures which are shorter than that, the buffer cannot be emptied during exposure, and once the STIS buffer fills up, there will be a pause in the exposures sequence of roughly 3 minutes as the buffer is emptied. This problem can sometimes be avoided with the judicious use of subarrays.

MAMA ACCUM Mode

In MAMA ACCUM mode exposures, photons are accumulated into a 2048 x 2048, 16 bit per element oversampled array in the STIS data buffer memory as they are received. At the end of the exposure, the data can be left in the oversampled (or highres) format, which is the default for scientific exposures, or they can be binned along AXIS1 and AXIS2 to produce a 1024 x 1024 native-format image. ACCUM is the mode of choice for all observations that do not require time resolution on minute or less scales. Dispersion runs along AXIS1 and the spatial dimension of the slit (and the orders for echelle observations) run along AXIS2. Figures 11.3 and 11.4 illustrate the format and coordinate system for MAMA images, showing how first-order and echelle ACCUM mode spectrograms appear. PRISM images have dispersion along AXIS1. Note that for FUV-MAMA G140L and G140M the spectrograms are shifted 120 pixels in AXIS 2 to AXIS2=632 to ensure that they will not fall on the shadow of the repeller wire (see “MAMA Spectral Offsetting” on page 115). Thus there will be ~3 arcseconds less spatial sky coverage to increasing AXIS2 and ~3 arcseconds more spatial sky coverage to decreasing AXIS2 along the slit. Said another way, slit center will project ~3 arcseconds from the detector center along AXIS2 for G140L and G140M observations. Note also the effects of the monthly offsetting which applies to all MAMA modes (see page 115).

Figure 11.3: MAMA ACCUM Mode Format for First-Order, Long-Slit Spectroscopy

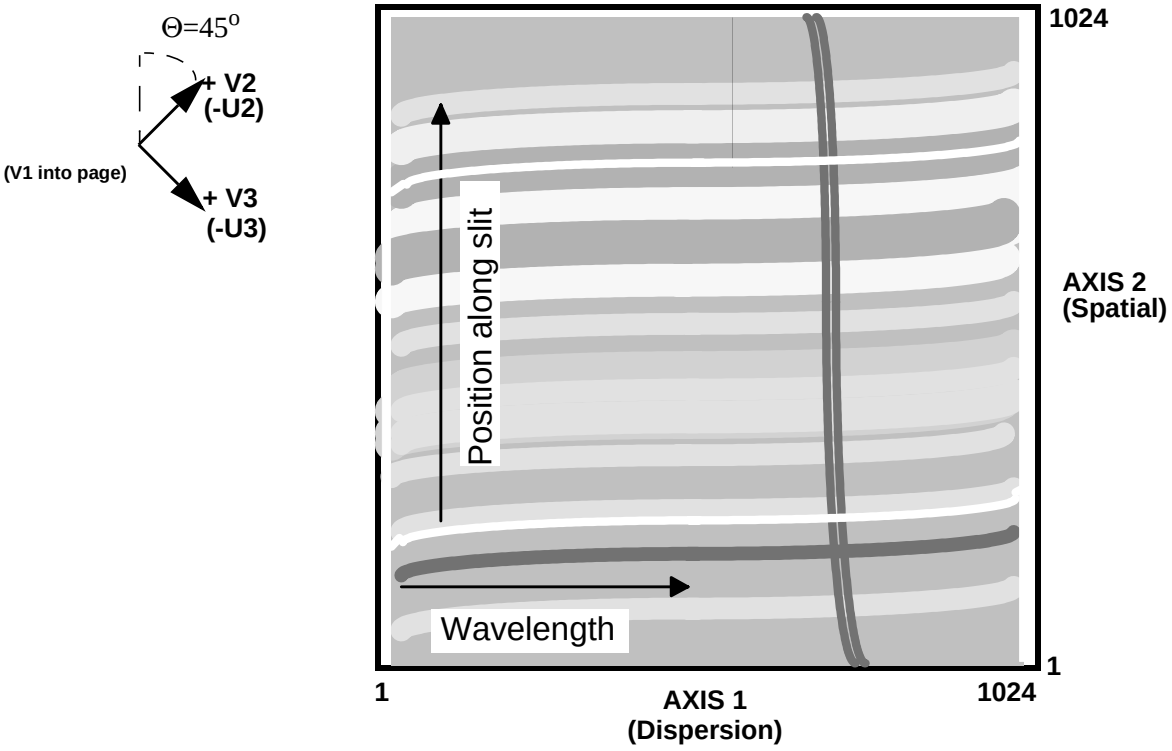

Figure 11.4: MAMA ACCUM Mode Format for Echelle Spectroscopy

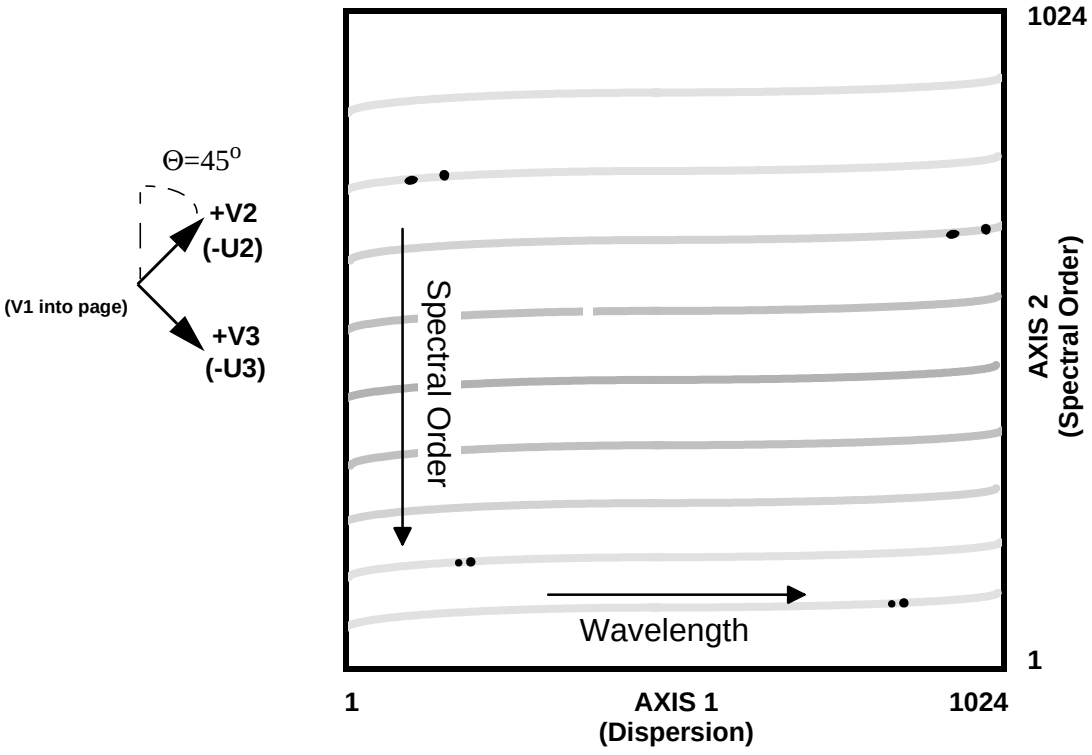

The minimum MAMA ACCUM mode exposure time is 0.1 second and the maximum exposure time is 1.8 hours. The minimum time between *identical* MAMA ACCUM exposures is ~30 seconds, for exposures which are longer than 3 minutes, and it is 2.5 minutes for exposures which are shorter than 3 minutes. This difference arises because in the former case the buffer can be dumped to the HST recorder during the subsequent exposure (i.e., in parallel), but in the latter case there is insufficient time to dump the buffer during the subsequent exposure and the buffer must be dumped serially (i.e, using observing time).

For the MAMA medium-resolution, first-order modes and medium and high-resolution echelle modes (i.e., gratings G140M, G230M, E230M, E230H, E140M, and E140H), a correction for Doppler shifting of the photon energies due to HST spacecraft motion is applied as the photons are counted, prior to their addressing in STIS data-buffer memory. The leading and trailing pixels in the dispersion direction (AXIS1) for Doppler-corrected exposures therefore receive less effective integration time, since source photons at the corresponding wavelengths have been Doppler-shifted off the edge of the detector for some fraction of the total exposure time. This effect is strongest in the high-resolution echelle modes, where for a maximum HST spacecraft velocity of 7.5 km sec^{-1}, the leading and trailing ~20 AXIS1 pixels will have reduced effective exposure times.

Highres

The MAMA detectors record scientific data in the so-called *highres* mode, producing 2048 x 2048 images of super resolution - one half the 1024 x1024 “native”-format pixel size defined by the microchannel plate itself. All scientific data are taken in this format by default. Below we explain in more detail the nature of highres data.

The MAMA detectors have 1024 x 1024 physical or so-called native-format pixels. However, each count is detected by multiple electrodes, so the charge distribution among the electrodes can be used to centroid the incident charge cloud to subpixel resolution. The gain of the highres 2048 x 2048 mode is a ~10–30% increase in resolution at the price of decreased signal-to-noise ratio per pixel arising from the increased fixed-pattern noise of the statistics of charge partition among the electrodes. The highres flat fields have much more structure than the 1024 x 1024 flats, with adjacent columns and rows differing by ~30% in an off/on pattern whose time variability is appreciably higher than for 1024 x 1024 format images. This effect and the inherently lower signal-to-noise ratio in the full-resolution flat-field images (nominally ~20 to 1 per highres pixel) suggest that it may be difficult to routinely realize the benefit in resolution. Highres is most likely to have application at low to intermediate signal-to-noise ratios (below 20:1) and low to intermediate incident count rates (exact range to be determined - expected to be applicable only at rates less than 5-10 counts sec^{-1} $pixel^{-1}$). However, we note that data taken in highres mode can always be binned to 1024 x 1024 on the ground in post-observation data processing, and since the extra overheads in highres mode are typically quite small, highres is the default data-taking mode for the MAMA. The pipeline bins the data to 1024 x 1024 format during calibration so that the pipeline-output calibrated images are native format (see the *HST Data Handbook* for more details).

MAMA TIME-TAG Mode

TIME-TAG mode is used for high-time-resolution spectroscopy and imaging in the ultraviolet. When used in TIME-TAG mode, the MAMA produces an event stream of AXIS1, AXIS2, and TIME data points, with a time resolution of 125 microseconds. The volume of data produced in TIME-TAG mode can be very large and the data therefore must be continuously transferred from the STIS internal buffer to the data recorders to sustain TIME-TAG exposures of any significant duration.

The axis orientation in TIME-TAG is the same as in ACCUM mode (see page 182). The spacecraft time (absolute zero point of the time) is routinely known to 10 millisecond accuracy. No Doppler correction is applied by the flight software for TIME-TAG mode, but the correction is applied in the calibration pipeline. The recorded times are the spacecraft times, which can be converted to heliocentric times using the ephemeris of the Earth and the spacecraft. TIME-TAG mode is illustrated in Figure 11.5. Processing of TIME-TAG data by the STScI pipeline is described in “Pipeline Processing Overview” on page 373.

Figure 11.5: TIME-TAG Mode

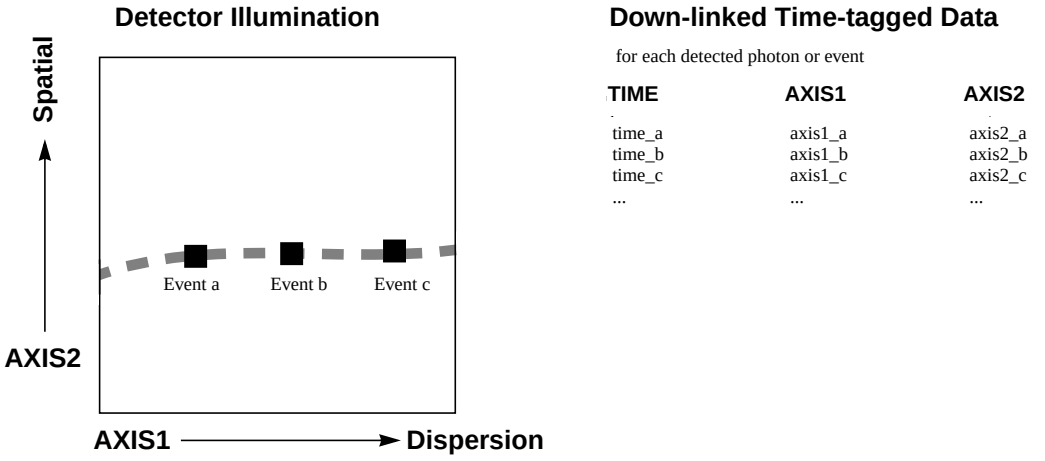

TIME-TAG Constraints

There are several limitations in TIME-TAG mode of which users should be aware:

- The maximum count rate from your source (within the full format or a specified subarray) must be less than 21,000 count sec^{-1} to sustain TIME-TAG exposures of any substantial duration (>3 minutes).
- At count rates larger than 21,000 count sec^{-1}, the maximum TIME-TAG exposure is $4 \times 10^6 / R$ seconds, where R is the count rate from the source. The MAMA detectors are not able to count reliably at rates greater than 30,000 count sec^{-1} in TIME-TAG mode (i.e., uncorrectable non-linearity and mis-time-tagging sets in).

- The maximum total *exposure duration* that can be sustained during any one visit (where a visit is a set of exposures at a single pointing which must be scheduled together) within TIME-TAG mode is 6.0 x 10^7 / *R* seconds. For example, at count rates of *R* = 21,000 count sec^{-1} the maximum exposure time in any one visit is ~48 minutes. In special cases, for special scientific needs, the HST data recorder can be devoted exclusively to a single observing program for a predetermined period of time, allowing longer total exposure durations. Requests for such special handling should be included in your Phase I proposal justification.

Specifying TIME-TAG Observations: BUFFER-TIME

The ground system must know the data rate to expect in order to schedule data transfers. Transfers are done in blocks of 8 megabytes (half the buffer capacity). The frequency of scheduled dumps depends on observer-specified information about the expected count rate. Specifically, during Phase II, TIME-TAG observers must specify a BUFFER-TIME parameter, where BUFFER-TIME is the time to fill half the STIS buffer, i.e., the time to accumulate 2 x 10^6 TIME-TAG events. Thus:

$$BUFFER-TIME = 2 \times 10^6 / R \qquad \text{sec}$$

where the parameter *R* is the maximum expected event rate in counts sec^{-1} from your source and any sky plus detector backgrounds.

Explicitly, for calculation of BUFFER-TIME (Phase II), *R* should be determined as the maximum total counts accumulated in any 99 second interval, divided by 99 seconds. This *R*, the maximum mean count rate sustained over any ~1.6 minute interval during your exposure, is equivalent to the maximum instantaneous count rate, so long as your source does not vary dramatically.

If you underestimate your count rate, you will overestimate the time it will take to fill the STIS buffer, and you will fill the STIS internal memory faster than it can be emptied to the HST data recorder. Once the STIS internal memory fills, events are not recorded until the buffer is emptied, at which point events are once more recorded, resulting in an exposure with periodic 99 second time gaps in it. You should also note that, at the end of each BUFFER-TIME, any unfilled part of the allocated STIS buffer (8 megabytes, equivalent to 2 x 10^6 counts) is filled with fill-data (zeros) before the buffer memory is dumped to the HST data recorder. If you overestimate your count rate and underestimate the time to fill the STIS buffer, your total exposure time will be restricted unnecessarily since the total integration time per visit should not be larger than 30 times the BUFFER-TIME. (As explained above, for special scientific needs, longer total exposure durations can be permitted but requests for such special handling should be included in your Phase I proposal justification.)

In summary, your BUFFER-TIME estimate should satisfy the following conditions:

- BUFFER-TIME > 99 seconds for continuous TIME-TAG observations longer than ~3 minutes.
- BUFFER-TIME < 2 x 10^6 / *R* sec (so that all the counts can be recorded).

- The total integration time in the visit must be < 30 x BUFFER-TIME (Under special circumstances this condition can be waived as explained in the text, if approved during Phase I).
- BUFFER-TIME < 0.5 x the total integration time (if your calculated BUFFER-TIME comes out to be larger than half the total integration time, just use half the integration time as your BUFFER-TIME. There is no reason to make the BUFFER-TIME any larger.)
- To assure linearity and reliable time-tagging, $R < 30{,}000$ counts sec^{-1}.

Remember to include the sky and detector backgrounds along with your source counts when computing *R*.

Exposure Sequences and Contemporaneous Calibrations

There are several instances when a series of associated STIS exposures (rather than a single exposure) will be taken. The data from these exposure sequences are generally processed as a single unit through the STScI calibration pipeline, with the scientific data from the multiple *associated* exposures appearing in a single file (for a high-level overview of the STIS calibration pipeline and the data-product format see Chapter 15, “Overview of Pipeline Calibration” on page 373). While you do not have to specify that you plan a series of associated exposures in your Phase I proposal, it is helpful to know about these sequences when planning your proposal. In Phase II, once your proposal has been accepted and you are working on scheduling your observations, you will be able to see and use these sequences. All are generated from a single exposure logsheet line in your Phase II proposal.

We discuss several types of associated exposures below:

- *Automatic* wavecal exposures taken with scientific data to allow calibration of the spectroscopic and spatial zeropoints.
- CCD CR-SPLIT exposures taken to allow removal of cosmic rays in the scientific data during post-observation data processing.
- Multiple identical *repeat* exposures, which can be taken to provide time resolutions of tens of seconds (CCD) or minutes (MAMA).
- *Pattern* sequences, in which the target is stepped, either along the slit or perpendicular to the slit (to map a two-dimensional region) for spectroscopic observations, or in a dither pattern for imaging observations.

In addition there are two types of contemporaneous calibration observations that observers may take with their scientific observations in special circumstances:

- *GO wavecals* which need only be taken if particular wavelength accuracy is required.
- *CCD fringe flats* (CCDFLAT) which need to be taken for near-IR (λ>7500 Å) observations in the grating modes if high signal-to-noise is required.

Auto-Wavecals

On STIS, the optical path from source to detector passes through the aperture (slit) wheel (where the filters for imaging also are housed) and then through the Mode Selection Mechanism (MSM) which houses the first-order gratings and prism, the cross-dispersers for use with the echelles, and the mirrors for imaging work (see Figure 3.1 on page 23). Lack of repeatability in the MSM causes the center of the spectrogram (as defined by the aperture and wavelength centers) to fall on a slightly different detector location each time there is a movement of the MSM (the MSM-induced offsets in dispersion and the spatial direction have been measured to be ±3 pixels or less). In addition, for MAMA observations, the aperture location on the detector is deliberately shifted each month to ensure equalization of extracted charge across the detector.

To allow calibration of the zero point of the aperture location and the zero point of the wavelength scale for spectroscopic observations, a line-lamp observation (so called wavecal) is taken *automatically* each time the MSM is moved. In addition, if a series of exposures or a single long exposure is taken at a single MSM setting, then an additional wavecal will automatically be taken when there is a pause in data taking *if* 40 minutes of exposure time has passed since the last wavecal. Here, 40 minutes is the time constant for thermal changes which might affect the wavelength accuracy. Testing in orbit has shown that in extreme conditions (when there is a swing from hot to cold), worst-case thermal shifts of roughly 0.3 pixels/hour can be seen; however, monitoring shows that under typical observing conditions thermal drifts are of the order of 0.1 pixels/hour (see also the monitoring information under “On Orbit Performance” on the STIS web page).

So to summarize, each set of spectroscopic scientific exposures taken at a given grating tilt (i.e., MSM position) will be accompanied by at least one automatically taken wavecal exposure, and if the exposures extend over a period of 40 minutes or more, multiple wavecals will be taken. These wavecal exposures will be processed along with the scientific data, and they will be used by the pipeline to automatically correct the zero-point offsets in the wavelength and spatial scales (see Chapter 15).

The automatic wavecals are designed to be of sufficient duration to produce spectrograms which contain at least 3 emission lines with 3 counts per pixel and 50 counts summed over the line. In those regions of the spectrum where 3 lines are not obtainable, there will be at least 1 emission line with 18 counts per pixel and 300 counts summed over the line. For the CCD where integration times are short, the automatic wavecals will typically be taken to ensure roughly 8 times this signal.

The combination of thermal changes between the wavecal and scientific exposures, coupled with the ability to measure the zero points in the wavecal exposures, limits the accuracy of the absolute zero points to ≤0.2 pixel (see “Summary of Accuracies” on page 379). In addition to the automatic wavecals, observers can also take their own wavecal exposures, using the WAVE target option (see “GO Wavecals”, below) if they desire more accurate wavelengths than will automatically be provided, or they are particularly concerned about the time variation of the zero point.

GO Wavecals

Only if you require particularly accurate wavelengths do you need to consider using the TARGET=WAVE option to insert additional wavecal exposures into your observing sequence.

The wavecals taken with TARGET=WAVE are identical to those taken automatically (i.e., the auto-wavecals) with two important exceptions. First, you can explicitly specify which aperture (slit) you wish to use for the TARGET=WAVE exposure (whereas for automatic wavecals the program slit or a pre-defined alternative for each grating is used). Second, you can take longer exposures, increasing the signal-to-noise of the lamp exposures or possibly saturating some lines to bring out weaker lines near astronomical lines of interest.

TARGET=WAVE exposures *cannot be taken with all slit-grating combinations* as the line lamps can be too bright for the MAMA detectors when used with wide slits. Therefore only certain aperture-grating combinations can be used for MAMA TARGET=WAVE observations (all are available for the CCD). Tables of lines and observed count rates from the line lamp for each grating mode for several different apertures and the list of allowed combinations are provided in the “calibration” area on the STIS web page. Although the slit-wheel repeatability is very high (see “Slit and Grating Wheels” on page 23), observers wishing particularly accurate wavelength calibrations are best off using a slit for their scientific exposures for which there is an allowed slit-grating wavecal; otherwise, the slit wheel will be moved each time they take a wavecal exposure, albeit producing an additional uncertainty.

TARGET=WAVE exposures are processed through the STScI pipeline as individual (unassociated) exposures and are not used to calibrate the scientific data in the pipeline itself.

CR-SPLIT

In order to allow rejection of cosmic rays in post-observation data processing, observers using the STIS CCD should always try (as much as possible given signal-to-noise ratio constraints when in the read-noise-limited regime) to obtain at least two—preferably three or more—identical CCD exposures (see “Cosmic Rays” on page 103). In Phase II, the CR-SPLIT optional parameter (default value 2) allows easy scheduling of such multiple associated exposures. You specify the total exposure time and set CR-SPLIT=*n*, where *n* is the number of exposures to break the total observing time into. For example, if the total exposure time is 12 minutes, and CR-SPLIT=3, then three 4 minute exposures will be

taken. Those three exposures will be associated with one another, passed through the STScI calibration pipeline as a unit, and a cosmic-ray free image will be produced during pipeline processing (see Chapter 21 of the *HST Data Handbook*). Allowed values of `CR-SPLIT` are integers from 1 to 8. Note that overheads are incurred for each `CR-SPLIT` subexposure.

Fringe Flat Fields

The STIS CCD exhibits fringing in the far red, limiting the signal-to-noise achievable at wavelengths longward of ~7500 Å in the `G750L` and `G750M` spectral modes. As discussed in Chapter 7 (“CCD Operation and Feasibility Considerations” on page 102) the best way of eliminating the fringes in the far red is by obtaining contemporaneous flat fields along with the scientific observations. These “fringe flats” must be taken at the same position of the Mode Selection Mechanism as the scientific data. STIS users can insert such contemporaneous fringe flat fields into the same visits as their scientific data, as described below.

Designing your Fringe-Flat-Field Observations

Observers of extended sources will typically want to take their fringe flat fields using the same slits as they use for their scientific targets, since the flat-field lamp will then illuminate the detector in the most similar way to the targets. However, observers of point sources will typically fare better if they use small slits (e.g., those which are otherwise used for echelle observations) for their fringe flat fields. The main reason for this difference is that the PSF of the STIS CCD features a substantial halo in the far red containing up to 20% of the total source flux, which causes the fringes in lamp flat fields to behave differently from those of external sources, especially in the case of point sources. (See also “Optical Performance” on page 99.) Fringe flat fields taken with short slits simulate the spatial structure of point sources significantly better than those taken with long slits.

The slits supported for scientific observations with the `G750L` and `G750M` gratings and the associated slits to use for fringe flat fields in the cases of both extended- and point-source observations in the far red are in Table 11.1 below.

Table 11.1: Slits for Extended-Source and Point-Source Fringe Flat Fields

Supported Scientific Slit	Fringe Flat Slit for Extended Source Observations	Fringe Flat Slit[a] for Point Source Observations
52X2	52X2	0.3X0.09
52X0.5	52X0.5	0.3X0.09
52X0.2	52X0.2	0.3X0.09
52X0.2F1	52X0.2F1	0.3X0.09
52X0.1	52X0.1	0.2X0.06

a. Short slits are chosen so as to be concentric with matched long slit.

A few notes are of importance on the use of short slits for obtaining fringe flat fields:

- Fringe removal for sources that are offset from the center of the (long) slit will not be possible with a short-slit fringe flat field; one has to use long-slit fringe flat fields for those cases.
- The limited length of the short slits used for obtaining contemporaneous flat fields of point sources (0.2–0.3 arcsec) does not allow one to sample the full PSF, so that absolute spectrophotometry cannot be performed with the short-slit fringe flat fields alone. However, a comparison with the pipeline-reduced point-source spectrograms will enable a proper flux calibration.
- The limited length of the short slits used for obtaining contemporaneous flat fields of point sources (0.2–0.3 arcsec) imposes a minimum requirement on the accuracy of the acquisition of target point sources in the slit. The final accuracy should be of the order of 1 pixel (i.e., ~0.05 arcsec). In case the observer has to use offset acquisition targets, it is therefore recommended that an `ACQ/PEAK` exposure in a short slit be performed to ensure centering in both directions (see Chapter 8).

Inserting Fringe Flat Field Exposures into RPS2

You specify a fringe flat field exposure in your RPS2 input (i.e., your Phase II proposal) as follows.

- Specify `Target_Name = CCDFLAT` to indicate the exposure as a fringe flat field. The flat-field exposure will automatically be taken at `CCDGAIN=4.`
- Specify `Number_Of_Iterations = 2` (to allow cosmic-ray rejection and to obtain adequate signal-to-noise)
- Specify `Config`, `Opmode`, `Aperture`, `Sp_Element`, and `Wavelength`.
  - `Config` must be `STIS/CCD`
  - `Opmode` must be `ACCUM`
  - `Aperture` must be one of `52X2`, `52X0.5`, `52X0.2`, `52X0.2F1`, `52X0.1`, `52X0.05`, `0.3X0.09`, or `0.2X0.06.`
  - `Sp_Element` and `Wavelength` must be one of the following combinations:

    `Sp_Element`: `G750L` and `Wavelength`: `7751`

    `Sp_Element`: `G750M` and `Wavelength:` one of `6768`, `7283`, `7795` `8311`, `8561`, `8825`, `9286`, `9336`, `9806`, or `9851`.
- Specify `Time_Per_Exposure` as `DEF` (Default). The default exposure time is determined from in-flight calibration data and ensures a signal-to-noise of 100 to 1 per pixel for all settings mentioned above and `Number_Of_Iterations = 2`.

- If the scientific data are taken in binned mode, specify Optional Parameters `BINAXIS1` and `BINAXIS2` in the same way as for scientific observations. Supported binning factors are 1, 2, and 4.

Two very important issues for fringe flat fields:

- Fringe-flat-field exposures are moved into the occulted period by RPS2 whenever they occur as the first or last exposure in an orbit. Thus you can fill the unocculted portion of your orbit with scientific observations and take the fringe flat during the occultation by placing it at the beginning or end of the orbit.
- Fringe flat fields are effective *only* if taken *without* a move of the Mode Selection Mechanism between the scientific exposure and the fringe flat field. *Observers must ensure that if the spectral element or wavelength setting is changed during an orbit in which they wish to obtain a fringe flat, then they place the fringe-flat-field exposure immediately before or after the scientific exposure(s) they wish to de-fringe.* In some cases (e.g., for a long series of exposures) the observer may choose to bracket the scientific exposures with fringe-flat-field exposures to be able to account for any thermal drifts.

Repeat Exposures

A series of multiple repeated identical exposures can be taken most easily using the `Number_Of_Iterations` optional parameter in Phase II. In this way, time-resolved observations at minimum time intervals of roughly 20 seconds for the CCD (if subarrays are used) and 30 seconds for the MAMA can be taken in `ACCUM` operating mode. The output of this mode is a series of identical exposures. If your exposure time is 60 seconds, and you set `Number_Of_Iterations=50`, you will obtain fifty 60 second exposures. These fifty exposures will be associated with one another and processed through the pipeline as a unit—the individual exposures will be fully calibrated and a summed image will also be produced for MAMA data and a cosmic-ray-rejected image for CCD data (see also Chapter 15).

Patterns and Dithering

A *pattern* refers to a series of exposures of a single target taken at slightly different telescope pointings, with the same set of guide stars. For STIS, patterns are commonly used to:

- *Dither* to decrease the effects of small-scale detector nonuniformity or increase the spatial resolution (the latter requires subpixel stepping) by offsetting the target along a long slit in the spatial direction for spectroscopic observations, or performing a small stepping pattern for imaging or slitless spectroscopic observations (see “Dither Strategies” on page 195).

- Spectroscopically map out a two-dimensional region of the sky, by stepping the slit across the object of interest.
- Spectroscopically subsample the line-spread function by stepping a fraction of a pixel along the dispersion direction—see “Improving the Sampling of the Line-Spread Function” on page 210.

Spectroscopic Patterns

Two standard pattern sequences for long-slit observations are available in Phase II. These are:

1. `PATTERN=ALONG-SLIT`, which allows stepping of the target along the slit (see Figure 11.6).
2. `PATTERN=PERP-TO-SLIT`, which allows stepping of the slit in a direction perpendicular to the slit length (see Figure 11.7).

Figure 11.6: Stepping Target Along Long Slit to Increase Dynamic Range

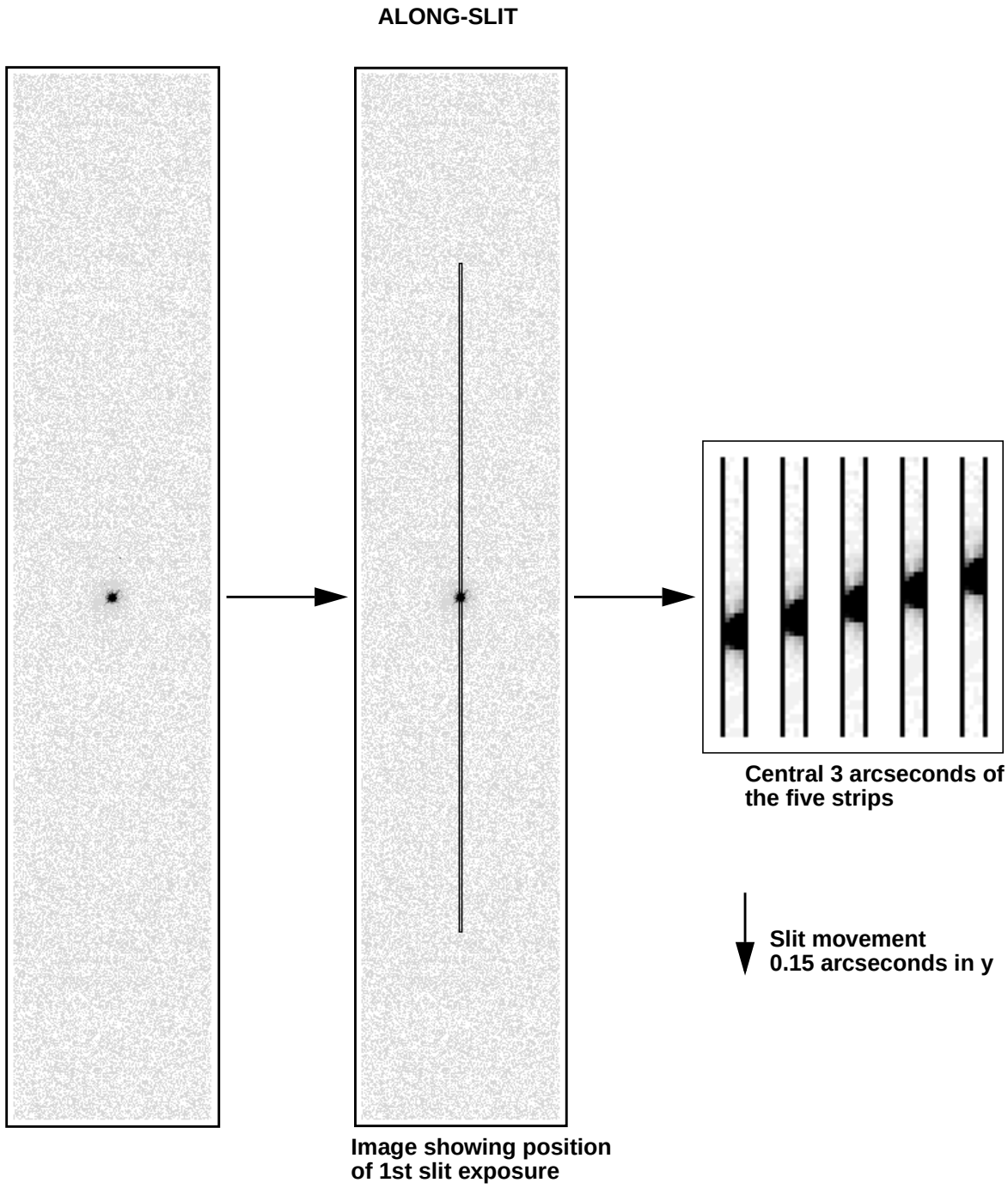

Figure 11.7: Stepping Target Perpendicular to Slit to Map 2-D Region of Sky

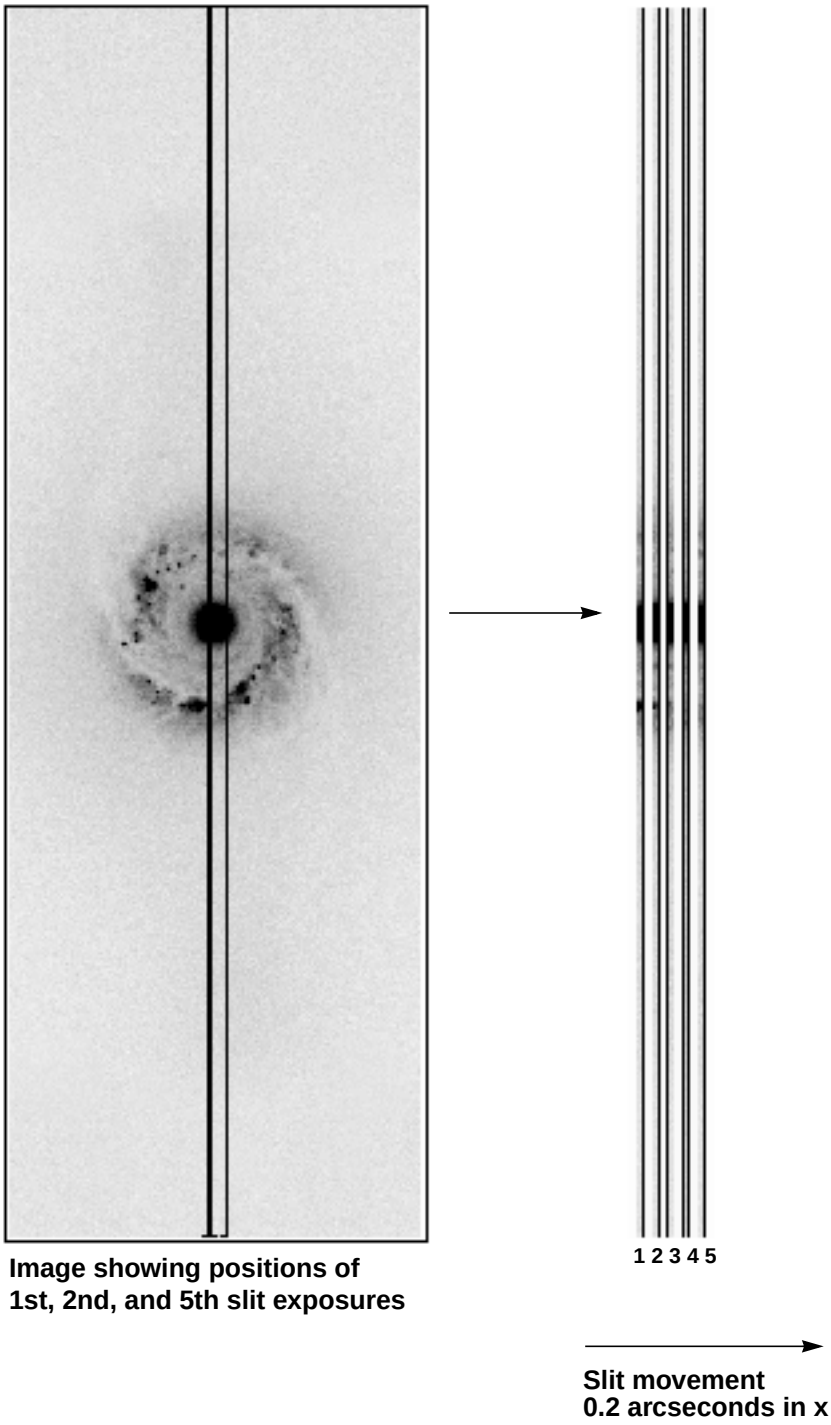

Dither Strategies

There is no single observing strategy that is entirely satisfactory in all circumstances for STIS. One must consider cosmic rays, hot pixels (pixels with high, time-variable dark current), and spatial undersampling of the image. One strategy that can be used to minimize the effects of undersampling and to reduce the effects of hot pixels is to *dither*, that is, to offset the telescope between exposures by either integer or subpixel steps. The best choice for the number and size of the dithers depends on the amount of time available and the goals of the project. In the following we will address a few issues related to dithering:

- ***Undersampling:*** Individual images taken with subpixel offsets can be combined to form an image with higher spatial resolution than that of the original images. A single dither from the original pixel position—call it (0,0)—to one offset by half a pixel in both x and y—(0.5,0.5)—will produce a gain in spatial information. On the other hand, very little extra information is gained from obtaining more than four positions. Therefore the recommended number of subpixel dither positions is between 2 and 4. Note that the STIS CCD only marginally undersamples the HST PSF at optical wavelengths, so that the overall gain will not be as substantial as in, e.g., the case of the WF CCDs of WFPC2.

- ***Hot Pixels:*** There are three ways to deal with hot pixels: correct using "superdark images" taken on the day of the observation, dither by an integer number of pixels, or use a task such as **warmpix** in STSDAS to filter out the known hot pixels. Note that the integer dither strategy would ideally consist of six images, i.e., two `CR-SPLIT` images at each of three different dither positions. The reason is that in addition to hot pixels, low or *cold* pixels can be present and simple strategies selecting the minimum of two pixel values can fail. However, even four images (two each at two dither positions) will greatly aid in eliminating hot-pixel artifacts.

  The MAMA detectors show few hot pixels and they appear to evolve slowly. Thus they are not usually an issue. Nevertheless, dithering is an easy way to avoid them, and there is no read noise or cosmic-ray removal penalty for doing so.

- ***Cosmic Rays:*** Although dithering naturally provides many images of the same field it is better to take several images at each individual pointing in order to remove cosmic rays. In principle, it should be possible to remove cosmic rays using only subpixel-dithered data. At present, however, no publicly released software is available for this task. Hence we recommend obtaining two or more images (i.e., `CR-SPLIT`) at each position in the dithered sequence (see also "Cosmic Rays" on page 103).

- ***Accuracy of Dithering:*** We do not yet have very good statistics on the accuracy of HST dither offsets. During the Hubble Deep Field campaign, nearly all dithers were placed to within 10 milli-arcsec (mas) (during ± 1.3 arcsec offsets and returns separated by multiple days), although in a few cases the dither was off by more than 25 mas, and on one occasion (out of 107 reacquisitions) the telescope locked on a secondary FGS peak causing the pointing to be off by approximately 1 arcsec, as well as a field rotation

of about 4 arcminutes. The software which was developed for the Hubble Deep Field is able to reconstruct images even for these nonoptimal dithers, still gaining in resolution over nondithered data. This software is presently available in STSDAS and is based on the variable-pixel linear-reconstruction technique developed by Fruchter and Hook (known as *drizzling*). It can be used successfully on STIS data.

- ***Flat-Field Accuracy:*** For the MAMAs, the accuracy of flat fielding has not been extensively tested, especially for the imaging modes. Dithering on scales of several pixels can help to smooth out pixel-to-pixel variations in detector sensitivity. For this purpose it is best to use dither steps that are not integral multiples of half a pixel (the intrinsic high-resolution format of the MAMAs), and integral pixel steps can be used instead.

The simplest way to schedule dithers with STIS in RPS2 is to use the option `PATTERN=BOX` (four-point parallelogram dithers, centering on half pixels to gain spatial resolution) or `PATTERN=ALONG-SLIT` (for linear dithers in the `AXIS2` direction, with user-specified offsets). An alternate approach is to use `POS TARG`.

Note that large dithers will incur small errors due to the camera geometric distortion which increases toward the CCD corners and alters the image scale by about 1% at the corners. For instance, a 20 pixel offset at the field center will suffer a 0.2 pixel error at the CCD corners. Large dithers may also occasionally require a different set of guide stars for each pointing, thus greatly reducing the expected pointing accuracy (accuracy of only ~1 arcsec due to limits to the accuracy of the Guide Star Catalogue).

For related articles on dither strategies, see the January 1995 issue of the WFPC2 Space Telescope Analysis Newsletter and the February 1995 issue of the ST-ECF Newsletter.

Fixing Orientation on the Sky

STIS users, particularly those using the long slit to observe extended sources, will commonly wish to specify the orientation of the slit on the sky. Observers planning coordinated parallel observations may also wish to specify the orientation of the HST focal plane, so as to place the appropriate instrument to cover a given patch of sky. When you set the orientation of the telescope, you effectively constrain the times when your observation can be scheduled, since HST must maintain a spacecraft orientation (sometimes called *roll angle*) which keeps its solar panels roughly perpendicular to the incoming sunlight.

The orientation of the spacecraft (and therefore of the STIS long slits which are fixed in relation to the HST focal plane) is controlled by the `ORIENT` special requirement, which is entered during Phase II. The Phase II Proposal Instructions will contain a detailed description of orientations and how to specify them. A specific orientation can be set, or a range of allowed orientations (e.g., 90–110 degrees) can be given. The tighter the constraints, the more difficult it will be to schedule the observation.

The ORIENT parameter gives the orientation of the HST focal plane projected onto the sky and is defined by U2 and U3 axes. Figure 3.2 on page 26 shows the HST focal plane containing all the HST instruments, with the U2 and U3 axes defined. Figure 11.1 on page 178 shows the relationship between these axes and the PA of the long slit on the sky. Note that to the accuracy of current knowledge the long slit is aligned with the detector's AXIS2, i.e., it is directly perpendicular to the dispersion axis (AXIS1). The important point to note is that if you fix the orientation of the long slit on the sky to be PA X, where X is measured in degrees east of north, then the ORIENT parameter (which determines where the other HST instruments lie for parallel observations) is given as X+45 or X+225 degrees. Likewise, for PRISM mode observations, if you wish to fix the orientation of the spatial direction (i.e., perpendicular to the dispersion) to be X, then the ORIENT parameter should be set to X+45 or X+225 degrees (note that it should be possible in RPS2 for Cycle 8 during Phase II to specify more than one permissible ORIENT range).

We show two examples below. Figure 11.8 on page 197 illustrates how to set the ORIENT parameter to place the long slit along the M87 jet. Figure 11.9 on page 198 illustrates how to set the ORIENT parameter to fix the dispersion axis for PRISM observations to be perpendicular to a double star system.

Figure 11.8: Placing the STIS Long Slit Along the Jet of M87

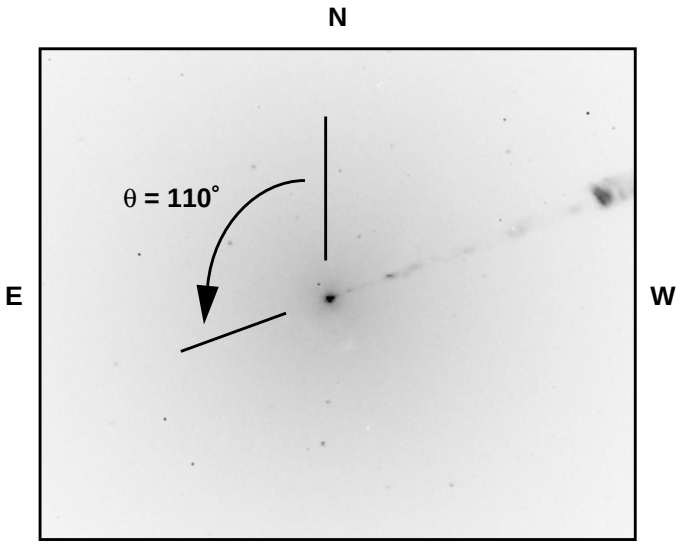

Radio galaxy with jet

θ = Angle of jet on sky = 110˚

To place long slit axis on jet:

Orient = θ + 45˚ or θ + 225˚

Orient = 110˚ + 45˚ or 110 ˚ + 225˚

Orient = 155˚ or 335˚

Figure 11.9: Placing Dispersion Direction Perpendicular to a Binary Star System

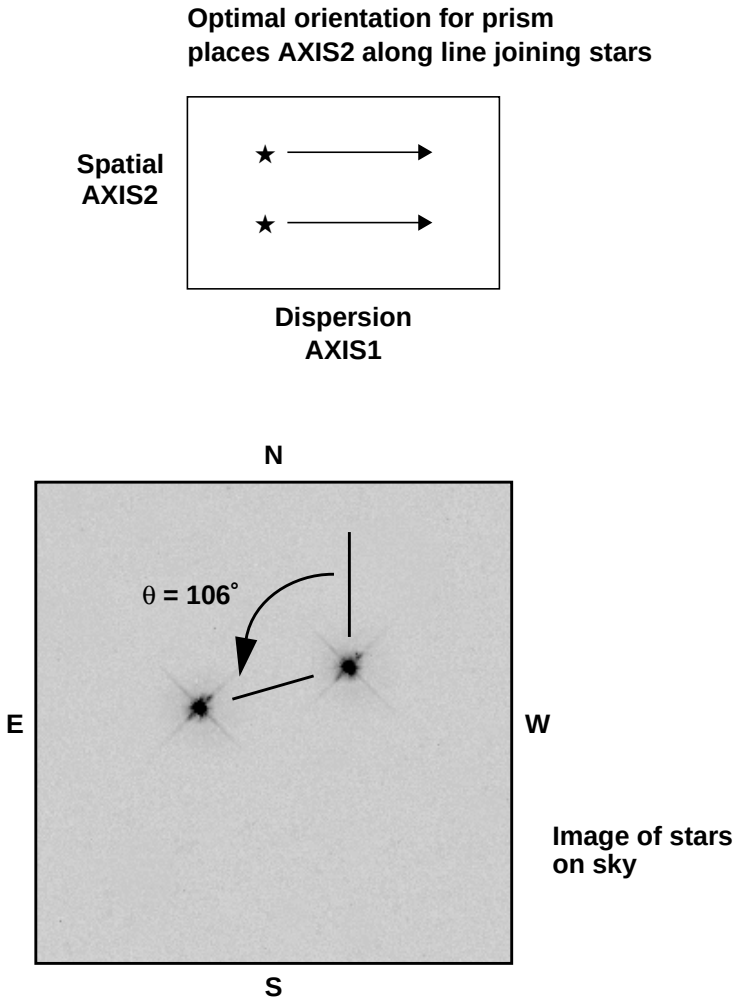

θ = Angle of line joining stars on sky = 106°

To place AXIS2 along θ:

Orient = θ + 45° or θ + 225°

Orient = 106° + 45° or 106° + 225°

Orient = 151° or 331°

CHAPTER 12
Special Uses of STIS

In This Chapter...

In this chapter we describe some of the nonstandard uses of STIS and provide guidance in the use of the standard capabilities for specific scientific purposes.

Slitless First-Order Spectroscopy

The vast majority of STIS first-order grating mode observations use a long slit. The use of a long slit ensures a clean separation of emission lines arising from different spatial features. However, all of STIS's first-order gratings (see Table 4.1 on page 34) can also be used slitless to obtain emission-line images. Figure 12.1 shows a simulated example of a slitless spectrogram, and see also Figure 4.8 on page 43.

Figure 12.1: Schematic Slitless Spectrogram of Planetary Nebula

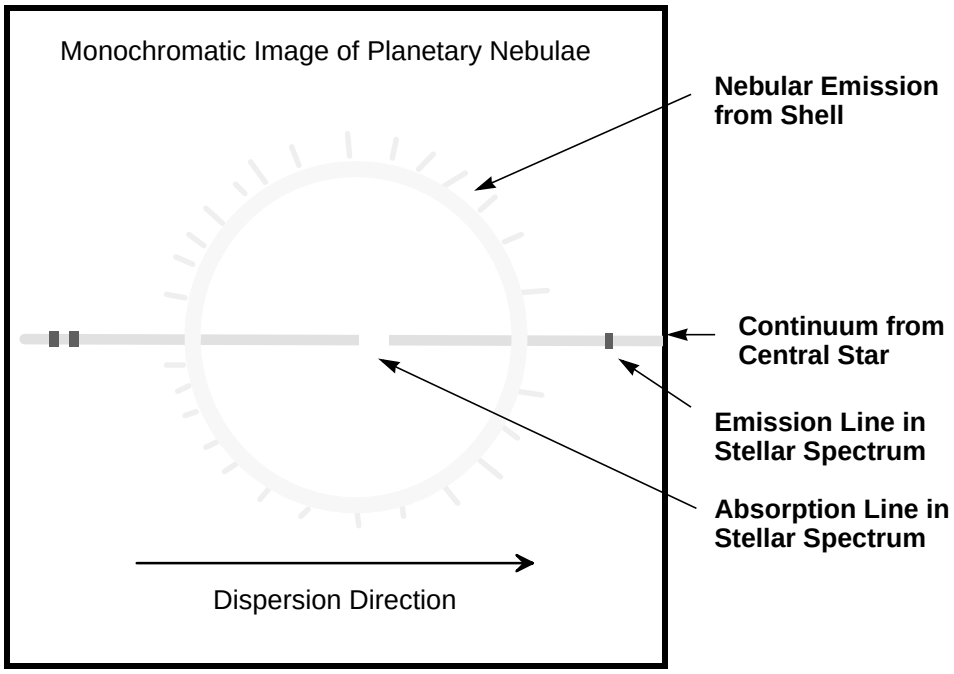

When STIS is used slitless (or with a wide slit), the image you obtain will be the sum of a series of monochromatic images of the field of view at a single wavelength, where prior to summing the monochromatic images are shifted relative to one another by the resolution (Å/pixel) of the grating. The range of wavelengths covered in the series of monochromatic images is dictated by the spectral range of the grating. The result is that there is *not* a one-to-one mapping of pixel location to wavelength in your image or of pixel location to spatial location on the sky. Depending on the structure of your source and the grating you use, it may be easy to deconvolve the spatial and spectral information, or it may be very difficult.

Slitless spectroscopy can be employed either for prime or parallel STIS observing. If you are designing a slitless spectroscopic observation there are a few important points to keep in mind:

- The more complex the emission-line, velocity, and spatial structure of your target field, the more difficult it will be to deconvolve the spatial and spectral information. It is important to match the grating you choose to the structure of your source. Gratings which produce images of multiple, kinematically resolved emission lines will be the most challenging to deconvolve. At the other extreme, a grating which covers only a single strong emission line at a resolution where the lines are kinematically unresolved will produce a clean image of the source in the single emission line (see Figure 12.1, above). You may also wish to specify the orientation for slitless spectroscopic observations to ensure that the most complex source structure is oriented perpendicular to the dispersion axis (see “Fixing Orientation on the Sky” on page 196).

- Since each point in the sky emits geocoronal light, the background due to the geocoronal emission lines (Lyman-α λ1216, O I λ1302 and occasionally on the day side O I λ1356 and O II λ2470; see “Geocoronal Emission and Shadow” on page 83) will be observed at all pixels in the image when a slitless spectrogram is obtained which covers these wavelengths. This background must be taken into account in your signal-to-noise calculations. Note that when a spectroscopic exposure is obtained with a slit, these sky emission lines are localized in the resulting image to the pixels at the corresponding wavelengths. For this reason, you may wish to consider using one of the two longpass ultraviolet blocking filters (see “Longpass-Filtered MAMA Imaging— F25SRF2 and F25QTZ” on page 63) instead of a clear aperture when performing ultraviolet slitless spectroscopy.
- An automatic wavecal (see “Auto-Wavecals” on page 187) will be taken for slitless spectroscopic observations with a narrow long slit, to allow post-observation determination of the wavelength zeropoints.
- Observers may want to obtain *images* of the fields they are taking slitless spectrograms of, to allow them to post-facto determine the centering of the objects in their data. Because the gratings and the mirrors used for imaging are both in the Mode Selection Mechanism, zero-point shifts will occur between the slitless spectrograms and image data (see “Slit and Grating Wheels” on page 23). These shifts can be taken out by means of a wavecal image of a short slit with the mirror in place. For Phase I planning purposes, GOs wishing to take such a target-finding image should allot the additional time for the image plus 5 minutes overhead for this extra zero-point wavecal image. In Phase II, an example containing information about how to ensure the proper calibration is taken in these cases will be provided.
- Slitless spectroscopic data will not be fully calibrated by the STScI STIS pipeline. Slitless spectroscopic data will be passed through the first phase of calibration and a flat-fielded calibrated image will be produced; however, the pipeline will not attempt to spectroscopically calibrate the data. This process must be interactively done by the observer since, as described above, ambiguous overlap of spatial and spectral information will occur. The **slitless** task in the **stsdas.contrib** package (originally contributed by ST-ECF) is available to aid in performing this post-pipeline processing.

Long-Slit Echelle Spectroscopy

The STIS echelle gratings (see “Echelle Gratings” on page 44) were designed to maximize the spectral range covered in a single echellogram. The orders are therefore closely spaced and to avoid overlap between orders, short echelle slits must be used. Indeed, the majority of STIS echelle observations are of point sources and use these customized echelle slits (see “Slits for Echelle Spectroscopy” on page 45). Nevertheless, at the price of confusion due to order overlap, the echelle gratings can be used with a long slit to obtain high-resolution spectroscopy of extended objects, or they can be used slitless with a full clear,

filtered, or ND aperture. An example of a scientific application that would benefit from long-slit echelle spectroscopy might be observations designed to map the kinematics of planetary nebulae and stellar outflows around young stars. Observers contemplating such observations should be aware that the problems of order overlap, scattered light, and the broad wings of the PSF from the OTA will make accurate calibration and line-profile work extremely complex for sources with a continuum (see “Spectral Purity, Order Confusion, and Peculiarities” on page 304).

The `6X0.2` slit (6 arcseconds in the spatial direction and 0.2 arcseconds wide in the dispersion direction) is supported for use with all four of the echelle gratings. However, because there will be ambiguous overlap of wavelengths in the resulting echellogram, the STIS STScI pipeline will not calibrate echelle data that use the long echelle slit. The pipeline will produce an uncalibrated FITS image and the user will be responsible for calibrating the data, since due to the ambiguous mapping of wavelength to pixel, the reduction of long-slit echelle data is an inherently source-dependent and interactive process.

Figure 12.2: Echelle Long-Slit Spectrogram of Extended Emission-Line Source Filling the Long Slit (partial image)

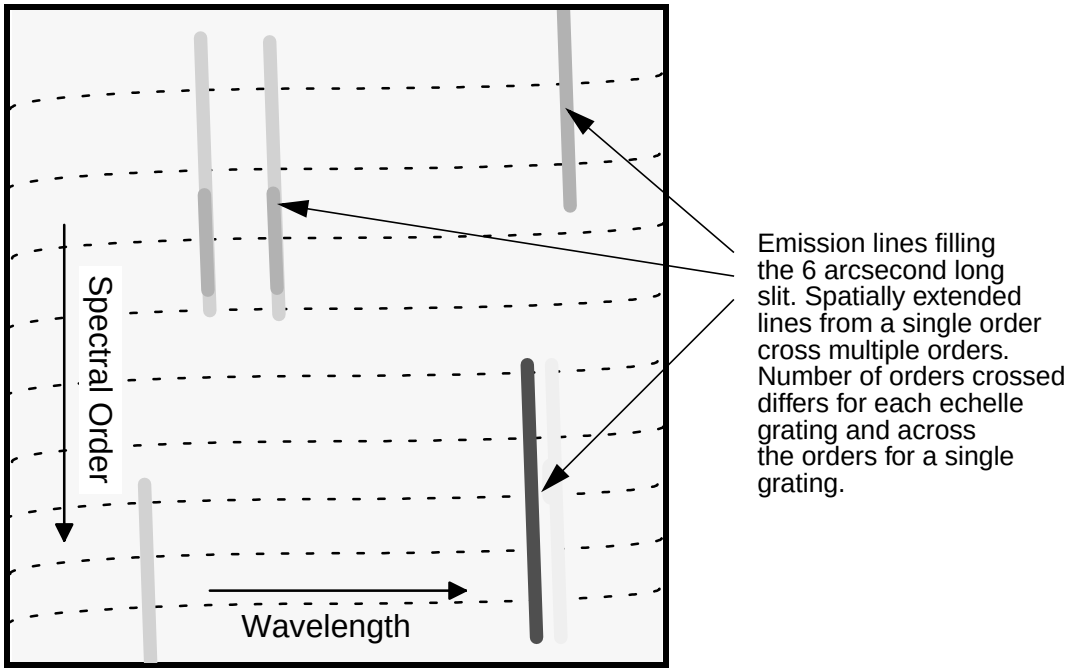

Time-Resolved Observations

There are two ways to obtain time-resolved spectroscopic and imaging observations with STIS:

- Use the MAMA TIME-TAG operating mode (described in “MAMA TIME-TAG Mode” on page 184) in the ultraviolet.
- Take a series of multiple, short, identical repeated observations (described in “Repeat Exposures” on page 191) of your target in ACCUM operating mode with either the CCD or the MAMAs.

Both the data products received (an event stream in the case of TIME-TAG and a series of individual images from each ACCUM-mode exposure in a repeated sequence) and the basic parameters of the time-resolved observations (e.g., sample time, interval between samples, total number of samples or equivalently duration) differ dramatically in these modes. In Table 12.1 we summarize and contrast the ranges of parameter space covered by the different methods of obtaining time-resolved observations.

The information presented in Table 12.1 can be summarized into the following set of guidelines for performing time-resolved observations with STIS:

- If you wish to observe variability on second or less timescales, observe in the ultraviolet using TIME-TAG mode. Figure 12.3 shows an example of a time profile of the Crab Pulsar obtained with STIS G140 in TIME-TAG mode overlaid on prior HSP observations.
- In the optical, variability can be observed on tens-of-seconds timescales using subarrays and multiple exposures with the CCD.
- In the ultraviolet variability on the several-minute or more timescale can be observed by multiple ACCUM-mode exposures with the MAMAs or using TIME-TAG.

- Remember that single MAMA visits are limited to five orbits (see Chapter 2), so continuous variability can be tracked for only that duration with the MAMAs.

Table 12.1: Summary of Time-Resolved Imaging and Spectroscopy

Observation Type	Detector	Spectral Range (Å)	Minimum Sample Time (τ)	Interval Between Samples ($\Delta\tau$)	Total Duration of Uninterrupted Time Series[a]
Repeat ACCUM	CCD	2000–10,300	0.1 sec	45 sec—full frame 20 sec—1060 x 32 subarray	For τ>3min, no limit For τ<3 min: dur=(τ+$\Delta\tau$)* 7, full frame (1062 x 1044) dur=(τ+$\Delta\tau$)* 256, 1060 x 32 subarray
Repeat ACCUM	MAMAs	1150–3100	0.1 sec	30 sec for τ > 3 min 2 min for τ < 3 min	No limit[b] No limit
TIME-TAG[c]	MAMAs	1150–3100	125 μsec	0	6.0×10^7 / *R* seconds if *R* < 21,000 counts/sec *or* 4.0×10^6 / *R* seconds if *R* > 21,000 counts/sec where *R* is rate in counts/sec,

a. τ = duration of an individual exposure.
b. Note, with BINAXIS1=BINAXIS2=2, 7 images separated by 1 minute and each of duration τ < 3 minutes can be obtained.
c. Linear for count rates less than 30,000 counts/sec.

Figure 12.3: Crab Pulsar Observed Using the STIS FUV-MAMA with G140L in TIME-TAG Mode. The resulting integrated time profile is shown superimposed on the early results from the HSP. (Figure courtesy of Don Lindler and Ted Gull, see also Lindler et al. 1997 in The 1997 HST Calibration Workshop Proceedings).

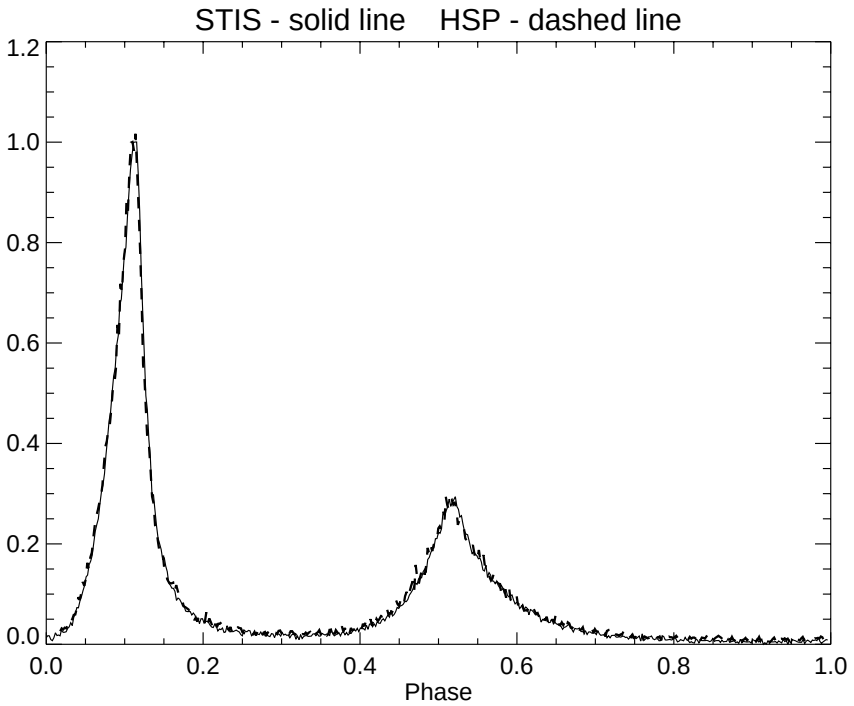

Observing Too-Bright Objects with STIS

As described in “MAMA Bright-Object Limits” on page 115, the STIS MAMA detectors can be damaged at high local and global count rates. The MAMA detectors also suffer uncorrectable non-linearity at similar count rates (see “MAMA Nonlinearity” on page 114). There are therefore configuration-specific count-rate limits for all observations that use the MAMA detectors; sources brighter than allowed by the limits *cannot be observed* in that configuration.

The STIS CCDs are not subject to the same bright-object constraints, as the CCD cannot be damaged by observations of bright sources. At high *accumulated* count/pixel levels, however, the CCD saturates and counting becomes nonlinear. As described previously (see “CCD Saturation: the CCD Full Well” on page 102), CCD saturation can be avoided by keeping exposure times short when observing bright targets. The minimum exposure time for CCD observations (0.1 sec) dictates the maximum source brightness which can be observed without saturating.

The only way to use STIS to observe a source that is too bright is to use a configuration which reduces the flux from the target, bringing it into the observable regime. The options available to achieve this reduction are:

- Use a smaller slit to reduce the transmitted light for spectroscopic observations (see “Apertures” on page 277—you will find there the percent flux transmitted through each slit as a function of wavelength).
- Select a more appropriate grating or filter configuration. The solution may be a configuration with higher resolving power if it is the local limit which is being violated, or a configuration that covers a smaller spectral range if the global limit is being violated. In more extreme cases, you may be forced to choose a grating (filter) that covers an entirely different region of the spectrum. Note that if you are observing in first order in the near-UV, you can consider using the CCD near-UV first-order spectroscopic modes `G230LB` and `G230MB` (see page “Cross-Over Regions” on page 40).
- Use a neutral-density filtered full aperture. The neutral-density filters are described in the section “Neutral-Density Filters” on page 67; they produce attenuations ranging by factors from 10^{-1} to 10^{-5}. Note, however, that the ND filters are located in the slit wheel. Thus, all supported ND full-filtered exposures will be slitless, i.e., you cannot use a slit and an ND full filter together. Similarly, you cannot use a ND full filter and a spectral filter in imaging mode. Also note that some ND filters come in quadrants, all of which are simultaneously imaged.
- Use one of the available-but-unsupported echelle or long calibration slits which contain neutral-density filters. The relevant slits are `31X0.05NDA` (with ND=0.4), `31X0.05NDB` (with ND=0.8), `31X0.05NDC` (with ND=1.2), and the `0.2X0.05ND` (with ND=2.0) and `0.3X0.05ND` (with

ND=3.0), where if ND=*x*, the flux is attenuated by 10^{-x}. For all the ND slits, the throughputs as a function of wavelength are posted on the STIS WWW orbital performance page.

High Signal-to-Noise Ratio Observations

The maximum achievable signal-to-noise (S/N) ratio of STIS observations for well exposed targets is, in general, limited by the S/N ratio and stability of the flatfields. CCD reference flats are obtained monthly and show excellent temporal stability. Ultimately, CCD flats in the pipeline should have an illumination of about 10,000 electrons/pixel. Thus, it should be routinely possible to achieve a S/N ratio in excess of 100:1 over larger spatial scales given sufficient source counts. Dithering techniques can and should be considered for high S/N CCD observations (see “Patterns and Dithering” on page 191). The realizable S/N ratio for spectroscopy will be less in the far red due to fringing, unless appropriate fringe flats are applied (see the caveats on long-wavelength spectroscopy in the red in “CCD Spectral Response” on page 96).

Observations of bright sources using the MAMA detectors may not match the S/N ratios achievable with the CCD, both because the S/N ratio of the MAMA flatfields is limited by the long integration times needed to acquire them (see “Summary of Accuracies” on page 379), and because the MAMA flats may be somewhat time variant (see “MAMA Signal-to-Noise Ratio Limitations” on page 114). S/N ratios of ~50:1 should routinely be achievable for spectroscopic observations of bright sources with the MAMAs if supported by counting statistics. It is possible to achieve even higher S/N ratios (>100:1 per wavelength bin), given sufficient counts from the source. If your program requires high S/N ratios, we recommend using some form of dithering (described below) and co-adding the spectrograms to ameliorate the structure in the flatfields.

Kaiser et al. (1998, *PASP*, submitted) and Gilliland (STIS ISR 98-16) reported quite high S/N ratios for spectrograms of bright standard stars obtained during a STIS commissioning program. The realizable S/N ratio depends on the technique used to correct for the flat-field variations, as shown in Table 12.2. The S/N ratios quoted are for wavelength bins from an extraction box of 2 x 11 lowres pixels (2 in AXIS1 or dispersion, 11 in AXIS2 or across the dispersion). In the table, the Poisson limit is just the S/N ratio that would be expected on the basis of counting statistics alone; “No Flat” means the realized S/N ratio without applying any flatfield at all to the data; “Reference Flat” means the realized S/N ratio after applying the best available reference flat, and the “Full FP-SPLIT Solution” is discussed under “FP-SPLIT Slits” below. Clearly, S/N ratios in excess of 100:1

per resolution element are well within the capabilities of the MAMAs for spectroscopy.

Table 12.2: Results of S/N Ratio Tests with STIS MAMAs in Orbit

Grating	Poisson Limit	No Flat	Reference Flat	Full FP-Split Solution[a]
E140M	470	200	360[b]	390
G140L	295	90	180	N/A
E230M	400	250	320[b]	380
G230M	200	100	150	N/A

a. Results obtainable in echelle modes using the FP-SPLIT slits and an iterative solution for the spectrogram and flatfield.
b. Results obtained using the FP-SPLIT slits and simply shifting, and co-adding the spectrograms after flat-fielding.

Dithering

In first-order spectroscopic modes, improved S/N ratios can be achieved by stepping the target along the slit, taking separate exposures at each location, which are subsequently shifted and added in post-observation data processing (PATTERN=ALONG-SLIT, see “Patterns and Dithering,” on page 191). This stepping, or dithering, in the spatial direction effectively smooths the detector response over the number of steps, achieving a reduction of pixel-to-pixel nonuniformity by the square root of the number of steps, assuming the pixel-to-pixel deviations are uncorrelated on the scale of the steps. In imaging modes, the same dithering can be done in two dimensions, i.e., the steps need not be along a straight line (see “Dither Strategies” on page 195). For echelle modes, stepping along the slit is possible only with the long echelle slit (6″x0.″2), but see long-slit echelle spectroscopy, above, and note the ameliorating effects of Doppler smearing as noted below.

In a slitless or wide-slit mode, stepping along the dispersion direction provides another method to achieve high S/N ratio data. Data so obtained permit, at least in principle, an independent solution for spectrogram and flat field, but at a cost of lower spectral resolution and line-profile confusion due to the wings of the LSFs transmitted through a wide slit (see “Spectral Purity, Order Confusion, and Peculiarities” on page 304). Such an approach for STIS data has not been attempted as of this writing.

FP-SPLIT Slits for Echelle Observations

A special kind of dithering in the spectral direction is possible for echelle-mode observations with one of two sets of fixed-pattern (or FP-SPLIT) slits. These slit sets, which are newly supported in Cycle 8, are each comprised of a mask with five apertures that are all either 0.″2 x 0.″2 or 0.″2 x 0.″06 in size. A

schematic of the configuration is shown in Figure 12.4. During a visit, the target is moved from one aperture to another, and the slit wheel is repositioned, so that the spectrogram is shifted (relative to the detector pixels) along the dispersion direction only. The slits are spaced to place the spectrogram at different detector locations, so that flat-field variations can be ameliorated by co-adding many such spectrograms. The FP-SPLIT slits can be a good choice for obtaining high S/N ratio echelle data, since it is usually not possible to dither in the spatial direction.

Figure 12.4: Schematic of the STIS Fixed-Pattern Slit Configuration. AXIS1 corresponds to the dispersion direction, and AXIS2 to the spatial direction. Dimensions are not to scale.

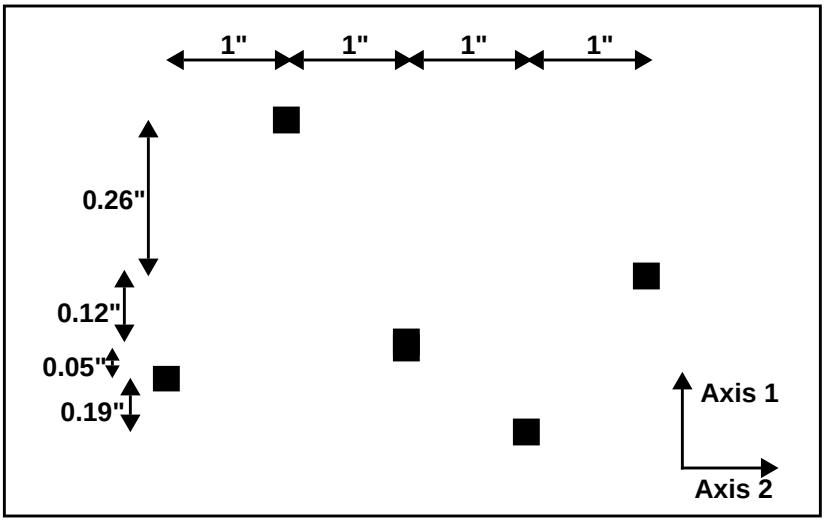

With echelle modes, Doppler-induced spectral shifts move the spectrogram on the detector. In reality, the STIS flight software automatically applies an onboard compensation for Doppler motion for echelle and medium-resolution, first-order data taken in ACCUM mode (see Chapter 11). The MAMA control electronics corrects (to the nearest highres pixel) the location of each event for the Doppler shift induced by the spacecraft motion prior to updating the counter in the image being collected. Thus, the flat-field correction for any image pixel would be an appropriately weighted average over a small range of nearby pixels and the effect of spacecraft-induced Doppler shifts is therefore to naturally provide some smoothing over the flat fields in the echelle modes.

The source of the Doppler-induced spectral shifts during an exposure is the variation of the projected HST spacecraft velocity along the line of sight to the target. Column 2 of Table 12.3 gives the maximum shift in highres pixels that would apply, based upon an HST orbital velocity of ~7.5 km/s during an orbit. The actual shift will of course depend upon the cosine of the target latitude, *i*, above or below the HST orbital plane, and upon the sine of the orbital phase at which the exposure is obtained. (Note that in general the observer can predict neither the latitude nor the orbit phase of the exposures in advance with any precision.) Column 3 gives, for a target lying in the HST orbit plane, the maximum duration of an exposure for which the Doppler shift will be one highres pixel or less; the actual duration will scale as sec(*i*), so that targets near the CVZ

are scarcely affected by Doppler motion. This information on T_{max} is relevant only if you are trying to derive the flatfield response simultaneously with the source spectrogram (see below) and not for the straightforward flat-field and shift-and-add methodology described above.

Table 12.3: Effect of Doppler Shift on Exposure Times

Grating	Maximum Doppler Shift (hi-res pixels)	T_{max}[a] (minutes)
E140H	11.41	2.7
E140M	4.59	7.0
E230H	11.41	2.7
E230M	3.00	11.3

a. For inclination $i = 0$; actual will scale as sec (i). See text for details.

Obtaining the Highest S/N Ratio with the FP-SPLIT Slits

As described above, the FP-SPLIT slits have been used with the echelles to provide signal-to-noise as high as ~350 with the direct *shift-and-add* method. Additionally, data obtained with the FP-SPLIT slits make it possible to solve independently for the fixed-pattern (i.e., the flat-field variation) and the source spectrogram. An iterative technique for combining FP-SPLIT data was applied successfully to data obtained with GHRS (see Lambert et al., *ApJ*, **420**, 756, 1994), based on a method described by Bagnuolo and Gies (*ApJ*, **376**, 266, 1991). This same technique was applied by Gilliland (STIS ISR 98-16) to STIS observations of a standard star. The S/N ratio that was achieved with these slits is summarized in the last column of Table 12.2, which shows that the FP-SPLIT slits can offer some advantage when one is attempting to achieve the highest possible S/N ratio. In general, though, it may be difficult to improve upon the S/N ratio that can be achieved by simply calibrating with the standard flatfield and co-adding the spectrograms.

There are a number of caveats to use of the FP-SPLIT slits to solve independently for the spectrogram and flatfield. The most notable is that the targets must be relatively bright point sources. The restriction to bright targets results both from the need to limit the duration of individual exposures to keep the Doppler-induced spectral shifts to less than one highres pixel, and from the need to have appreciable counts in the individual exposures—at least in the orders of interest. Very high counts in the sum of all exposures are essential for a good (and stable) solution to both the spectrogram and the underlying flatfield.

If you are using the FP-SPLIT slits to distinguish the signature of the flatfield from the target spectrogram, then Doppler smearing (and the discrete compensation) will defeat that solution. In this case, the exposures must be kept as short as if there were no Doppler compensation at all, if the goal is to solve for the pixel-to-pixel variation at a precision higher than that of the available flat-field reference files.

The utility of FP-SPLIT observations is also limited by the modest range of slit offsets in wavelength space, and by the distribution and character of the features in the target spectrum itself. That is, if the spectrum in the order(s) of interest is dominated by absorption over a width comparable to or larger than the largest offset range, the solution may not be stable or unique. A corollary is that some of the spectral orders must contain moderately prominent spectral features with good signal in order to distinguish the spectrum from flat-field variations. Table 12.4 gives the FP-SPLIT offsets for each grating, including offsets in Ångstroms for typical central-wavelength settings.

Table 12.4: Magnitude of Spectrogram Offset for the FP-SPLIT Slits

Grating	Minimum Offset (hires pix)	Maximum Offset (hires pix)	CENWAVE (Å)	Max. Offset @CENWAVE (Å)
E140H	2.128	26.383	1416	0.164
E140M	2.778	34.444	1425	0.535
E230H	2.128	26.383	2390	0.277
E230M	2.857	35.429	2340	1.382

A final complication concerns the ability of the MSM to move the slit wheel from one FP-SPLIT slit to the next such that the spectrogram is offset in the spectral direction only. Experience in orbit suggests that such a one-dimensional shift is typical, but that both the uncertainty in the MSM repeatability and thermal changes in the STIS optical bench can result in shifts of more than one lowres pixel in the spatial direction. In this case the solution for the underlying flatfield would have to be generalized to two dimensions to achieve the highest accuracy.

Improving the Sampling of the Line-Spread Function

In some configurations the point-source spectral-line FWHM is modeled to be less than two detector pixels (see “Line-Spread Functions” on page 299). The realized in-flight line-spread functions (LSFs) are still being evaluated as of the publication of this Handbook (see also STIS ISR 98-04) and updates will be posted on the STIS web page. Most observations should not be affected, but if you are observing lines which are near to being unresolved in the grating of interest and require accurate line profiles, you can consider the following technique:

- Stepping of the target in the dispersion direction in a wide slit or slitless aperture to subsample the line-spread function by displacing the spectrogram. This technique can also be used to increase the signal-to-noise (see above). Note that in employing this strategy one will have to trade off the

benefits of the sampling with the negative impact of increased wings in the line-spread function with a wide slit, particularly for MAMA observations (see “Spectral Purity, Order Confusion, and Peculiarities” on page 304).

- For MAMA observations, use of *highres* sampling may provide ~15–30% better sampling; however, flat-field variability and rate dependence may make it difficult to realize the benefit in resolution (see “Highres” on page 183). Note that all STIS data are taken by default in highres format, and then binned in calibration on the ground so all you need to do is recalibrate your data, changing the switch settings (see the *HST Data Handbook*) to fully exploit the highres data.
- Use of a higher resolution grating mode in which your LSF is fully sampled.

Considerations for Observing Planetary Targets

STIS’s FUV solar-blind and NUV solar-insensitive MAMA detectors make it particularly well suited to slitted spectroscopic and imaging planetary observations. In addition, the `52X2` long slit (2 arcseconds wide in the dispersion direction) is particularly well suited to the “slitless” ultraviolet spectroscopic study of small planetary bodies (using a slit limits the background continuum contribution; see “Sky Background” on page 79). STIS was used successfully in Cycle 7 to perform long-slit and echelle spectroscopy and UV imaging of several solar-system objects including comets, planetary satellites, and planets.

Planetary observers may wish to use the `PERP-TO-SLIT` pattern sequence (see “Patterns and Dithering” on page 191) to map out the surface of a planet by taking a series of long-slit observations, each one stepped by the slit width perpendicular to the slit’s long dimension, relative to the last. Advice on performing target acquisition for solar-system targets is provided in Chapter 8.

Long-Slit Spectroscopy

Planetary observers requiring specific long-slit orientations will want to be aware of the tight scheduling constraints of specific orientations for observations of targets in the ecliptic plane (see discussion of “Orient from Nominal” in the Phase II instructions).

For example, say an observer wanted to orient the STIS long (52 arcsecond) slit in the north-south direction on Jupiter. For a Jupiter north-pole position angle of ~20˚ from celestial north, this would require an `ORIENT` constraint of ~20–25˚ or ~200–205˚ would be required. The nominal roll angle (orientation) for Jupiter varies from ~250˚ before opposition to ~70˚ after opposition, and it goes through the intervening 180˚ range during a four-day period centered on opposition. Deviations from nominal roll are allowed as follows:

- 5˚ when the sun-target angle is 50–90˚.

- 30˚ when the sun-target angle is 90–178˚.
- Unlimited when the sun-target angle is 178–180˚.

Thus orientation of the long slit in a north-south direction on Jupiter is possible only during a single four-day period near Jovian opposition, since no allowable deviation from nominal roll is large enough at any other time to permit a north-south orientation of the slit on the planet. Although the situation for Saturn is not nearly as extreme, observers should be aware of the tight scheduling constraints on observations requiring specific slit orientations.

Parallel Observing with STIS

The second servicing mission installed solid-state data recorders on HST. The volume capacity of these recorders is roughly ten times that of the mechanical tape recorders in use for Cycles 1 through 6. Coupled with changes to the ground system and the flight software of the second-generation instruments designed to fully exploit this capability, this translates into a greatly increased capability for parallel observing.

In Cycle 8, STIS, WFPC2, and FGS can be used to observe simultaneously. Figure 3.2 on page 26 shows the HST field of view following the second servicing mission; the three infrared cameras of NICMOS (which themselves could be operated in parallel), STIS, WFPC2, and FOC are all shown, with their fields of view drawn to scale, in their relative focal-plane positions. Note that NICMOS and FOC are *not* operational in Cycle 8. The three STIS cameras share a common field of view, and only one can be used at a time.

The policy for proposing for parallel observations and technical advice on parallel observing are provided in the Call for Proposals/Phase I Proposal Instructions. We remind you that there are two types of parallel observations:

- Coordinated parallels, in which you explicitly link the taking of exposures in parallel to your own prime scientific exposures.
- Pure parallels, in which exposures are taken in parallel with other observers' prime exposures.

Both coordinated and pure parallels must be explicitly proposed in Phase I. Implementing parallels requires significant resources; only those recommended by the TAC process will be implemented. If you are considering coordinated parallels, you may wish to consider constraining the orientation of HST, to place an object of interest in the parallel instrument's field of view. `ORIENT` constraints do affect observation scheduling, however, and should not be entered lightly (see Chapter 11).

Using STIS in Parallel with Other Instruments

Observations for which STIS is the parallel instrument are likely to be most useful when the full STIS field of view is used. If you wish to use a small slit, the STIS should be used as prime, and the other imaging instruments used in parallel with it.

The MAMA detectors cannot be used for *pure* parallel observing. The MAMA detectors can be used in coordinated parallel observing if an explicit `ORIENT` is specified and precise RA and Dec coordinates for the parallel field are given (see “Prime and Parallel Observing with the STIS MAMA Detectors” on page 15).

Four types of STIS exposures which have particular scientific utility with STIS as the parallel instrument are:

- Optical imaging taking advantage of the ability to go deep very fast with the `50CCD` wide-open mode.
- Optical slitless spectroscopy.
- Ultraviolet slitless spectroscopy (available only for coordinated parallels with exact `ORIENT` specification).
- Prism and ultraviolet imaging observations (available only for coordinated parallels with exact `ORIENT` specification).

The STIS Archival Pure Parallel Program

Following on the recommendations of the Cycle 7 HST Time Allocation Committee, and following the advice of the Parallels Working Group, an HST Archival Pure Parallel Program was begun at the start of the Cycle 7 GO era. This program was designed to maximize the scientific return from HST to the community by taking parallel data with STIS, NICMOS, and WFPC2, whenever these instruments were not prime. The data immediately become nonproprietary and are available through the HST Archive. This program continues today.

The STIS Archival Pure Parallel observing program consists of:

- `G750L` slitless spectroscopy to search for star-forming galaxies and AGNs out of the plane, and brown dwarfs in the plane.
- `50CCD` and `F50X28LP` imaging in the outskirts of nearby galaxies and globular clusters for stellar-population studies.
- Short (≤1 orbit) `50CCD` images of extragalactic fields to study cosmic shear.
- Narrowband [O II] and [O III] CCD images of the outskirts of nebulae in the Galactic Plane.
- Deep CCD imaging of extragalactic fields.

Figure 12.5 shows an example of a deep 50CCD STIS Archival Pure Parallel image and Figure 12.6 shows an example of slitless spectroscopy from the Archival Pure Parallel Program. More information on the STIS Archival Pure Parallel Program is available on the STIS web page under “Special Projects.”

Figure 12.5: Deep 50CCD STIS Pure Parallel Image from the Archival Pure Parallel Program, with 3.72 hours of Integration Time. (Figure courtesy of Ed Smith.)

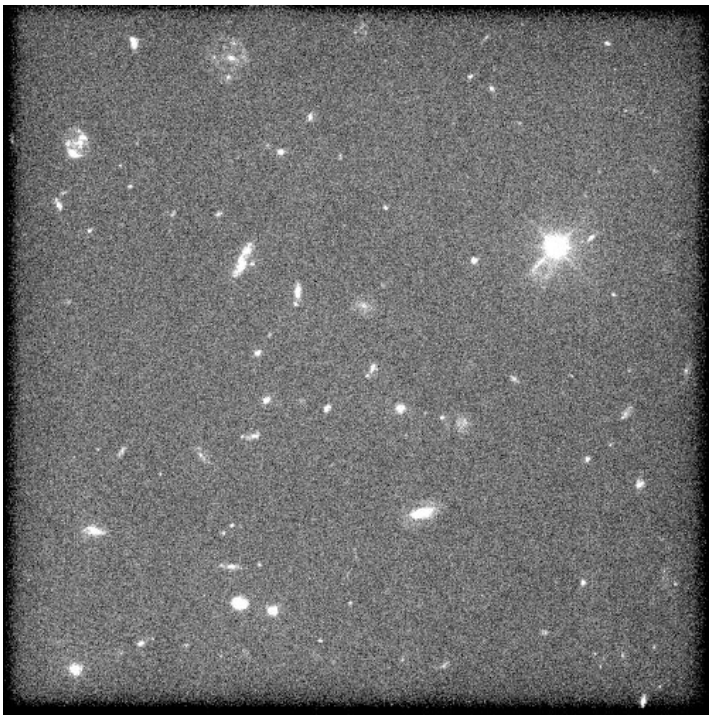

Figure 12.6: G750L Slitless Spectroscopy from the Archival Pure Parallel Program Showing the Detection of a High Redshift Emission Line in a Galaxy. (Figure courtesy of Jon Gardner, see also Gardner et al. 1987, in the 1997 HST Calibration Workshop Proceedings.) Left and below are the G750L slitless spectra. Top right is the image of the field.

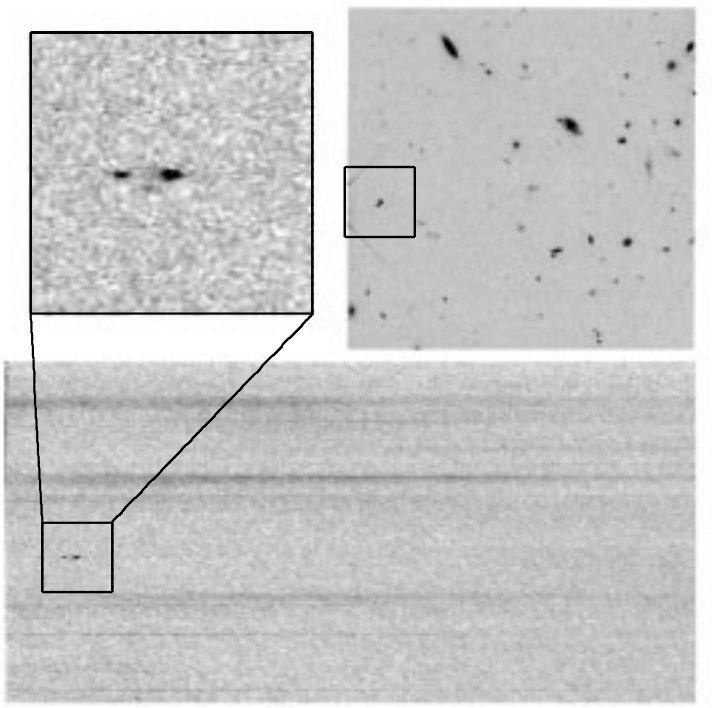

Coronographic Imaging and Spectroscopy

STIS offers the capability to perform spectroscopic observations with occulting bars located in the long slits, and imaging observations with occulting bars in the coronographic mask `50CORON`.

Barred Spectroscopy

The 0.5 arcsecond bar in the `52X0.2F1` long slit is available for occulted observations. This occulting bar is well suited to scientific programs conducting spectroscopy of faint extended material around a bright central source. Typical examples of such a program include QSO host galaxies, dynamics of jets in young stellar objects, and spectroscopy of resolved binaries. Observers performing barred spectroscopy should be sure to consult the section “Spectroscopic Mode Peculiarities” on page 306.

Spectroscopic observations with the 0.5 arcsecond occulting bar are limited to first-order spectroscopic modes. It should be noted that when the occulting bar is chosen the slit wheel places the occulting bar at the center of the field of view, so the full 52 arcseconds width of the longslit is not available, and the slit is slightly tilted.[1]

To simplify the use of the occulting bar, an aperture has been assigned for the occulting bar itself, as well as an aperture for the reference position located just off the bar. The reference aperture is used if the observer wishes to peakup the source in the slit, prior to offsetting to place the target behind the occulting bar. (Note that peakdowns behind the occulting bar, while possible in principle, are not recommended in practice).

The table below shows the complete set of aperture names and their application for the 0.5 arcsecond fiducial on the `52X0.2` slit. An example of an acquisition into the `52X0.2F1` aperture is provided in Chapter 8.

Table 12.5: Aperture Names and Applications on 52X0.2 Slit

Aperture Name	Description	Destination	Application
`52X0.2`	Slit (width=0.″2, length=52″)	Target centered in slit	Long-slit spectroscopy
`52X0.2F1-R`	Slit (width=0.″2, length=52″). Fiducial=0.″5 Reference point off-fiducial	Target centered in slit at reference position, offset from fiducial bar.	Locates target at reference position ready for peakup in slit.
`52X0.2F1`	Slit (width=0.″2, length=52″). Fiducial=0.″5	Target centered in slit and located under fiducial bar	Locates target under bar ready for occulted observation

1. This offsets the specification of `ORIENT` for this slit. Contact your Contact Scientist for details.

Coronographic Imaging

STIS has one coronographic mask aperture for direct imaging. The aperture contains one occulting bar and two intersecting wedges (see Figure 12.7 on page 216). The aperture cannot be combined with a filter and so, when used with the CCD, yields a bandpass of ~2000–10,300 Å. The mask is not available for use with the MAMA detectors due to concerns about bright-object protection of the MAMAs. In combination with the option of a coronographic mask, there is a limited amount of apodization via a Lyot stop which masks the outer perimeter of the re-imaged exit pupil. Consequently, diffraction from the secondary mirror assembly and the telescope spider is not apodized. The STIS coronographic imaging facility is well suited to imaging problems involving faint material surrounding a relatively bright source. Typical examples include circumstellar disks, such as β Pictoris, and the host galaxies of bright QSOs. (See also “Coronographic Imaging—50CORON” on page 59.)

Figure 12.7: Design of the STIS Coronographic Mask

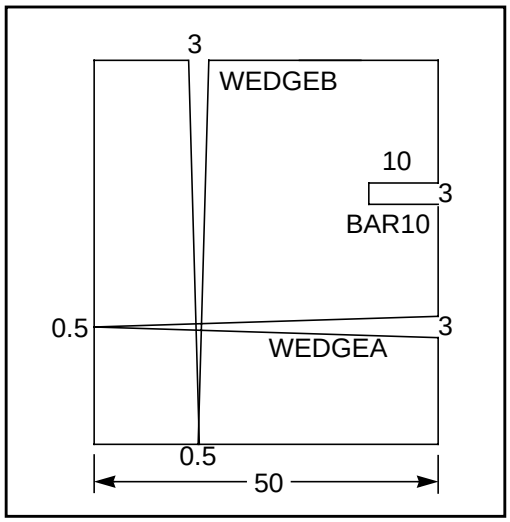

A series of apertures has been defined for the coronographic mask so that targets can be placed on the 3˝ wide bar and 5 locations on each of the two wedges. These apertures are summarized in Table 12.6 below.

Table 12.6: Apertures for Coronographic Mask

Proposal Instructions Aperture Name	Description
50CORON	Coronographic mask—clear aperture in center of the field of view
BAR10	Coronographic bar of width 3.″0
WEDGEA2.8	Coronographic Wedge A (vertical in AXIS1) Posn. 1: bar width = 2.″75
WEDGEA2.5	Coronographic Wedge A (vertical in AXIS1) Posn. 2: bar width = 2.″5
WEDGEA2.0	Coronographic Wedge A (vertical in AXIS1) Posn. 3: bar width = 2.″0
WEDGEA1.8	Coronographic Wedge A (vertical in AXIS1) Posn. 4: bar width = 1.″75
WEDGEA1.0	Coronographic Wedge A (vertical in AXIS1) Posn. 5: bar width = 1.″0
WEDGEB2.8	Coronographic Wedge B (vertical in AXIS2) Posn. 1: bar width = 2.″75
WEDGEB2.5	Coronographic Wedge B (vertical in AXIS2) Posn. 2: bar width = 2.″5
WEDGEB2.0	Coronographic Wedge B (vertical in AXIS2) Posn. 3: bar width = 2.″0
WEDGEB1.8	Coronographic Wedge B (vertical in AXIS2) Posn. 4: bar width = 1.″75
WEDGEB1.0	Coronographic Wedge B (vertical in AXIS2) Posn. 5: bar width = 1.″0

In planning an observing program with the 50CORON aperture, observers should carefully consider the required orientation of the target. The telescope's V2 and V3 axes are at 45˚ to the STIS AXIS1/AXIS2 coordinate system (see Figure 11.1 on page 178) and so diffraction spikes further reduce the unocculted field of view.

If an observer wishes to image the full 360˚ region around a target, two observations, one each on the vertical and horizontal wedges, are required. By combining two such images, the full 360˚ coverage is obtained, with the exception of the regions occupied by the diffraction spikes. Two options are available to address this problem: either roll the telescope by ~15˚ on the second exposure, or schedule a second visit when the nominal telescope roll has changed by ~45˚.

Coronographic Target Acquisitions

We defined a special coronographic acquisition technique for placing stars under the coronographic bars on the 50CORON aperture. The method involves performing a bright-target acquisition with a filtered aperture, then a peakup in a small slit, followed by a slew to a predefined aperture on the coronographic mask. An example of an acquisition into one of the bars on the 50CORON aperture is provided in Chapter 9.

CHAPTER 13
Spectroscopic Reference Material

In This Chapter...

In this chapter, we provide spectroscopic reference material, in support of the information presented in Chapter 4.

Introduction

The information in this chapter will help you select your grating configuration and observing slit and determine your observing plan (e.g., total required exposure time, and number of exposures). This chapter is basically organized by *grating and slit* (corresponding to `Spectral Element` and `Aperture` in the Phase II Proposal Instructions.)

For each grating mode the following are provided:

- A brief description of the grating mode's specifications, including recommended uses and special considerations.
- The central-wavelength settings and range of wavelength covered at each setting, together with the dispersions and plate scales.

- Plots and tables of sensitivities and throughputs as a function of wavelength.
- Plots of signal-to-noise as a function of V+STMAG$_\lambda$, F_λ, and exposure time.

For each slit the following are provided:

- A brief description of the slit's specifications, including recommended uses and special considerations.
- Plots and tables of relative throughputs as a function of wavelength.

For representative grating-slit combinations we provide:

- Tables of encircled energy for the flux in the default pipeline extraction aperture, and the percent flux contained in the peak pixel.
- Plots of representative spatial (perpendicular to the dispersion) profiles at selected wavelengths.
- Line-spread functions and FWHM as a function of wavelength.

In addition,

- "MAMA Spectroscopic Bright-Object Limits" on page 311 provides a summary of the screening brightness limits for the MAMA spectroscopic modes.

The next section explains the plots and tables found in the grating sections in this chapter.

Using the Information in this Chapter

Wavelength Ranges

The complete wavelength range, as well as the wavelength coverage per tilt for the scanned grating modes, is shown in a table and graphically. The exact wavelengths at the ends of the ranges for the MAMA detectors will depend on the MAMA monthly offsetting. This procedure shifts the spectrogram so that it falls on slightly different parts of the MAMA detectors from month to month in order to minimize charge depletion in the microchannel plates and can cause the loss of ±30 pixels from either end of the spectrogram in dispersion (`AXIS1`) and ±80 pixels in cross-dispersion (`AXIS2`). Spectral format plots of the STIS grating and central wavelength settings are available from the STIS web page under "Calibration." For the echelles, the monthly offsetting will project the extreme orders of formats off of the detector in some months. The wavelength ranges for the echelles given in the chapter therefore include only the orders which are guaranteed to project onto the detector. Whenever possible, choose a central wavelength that keeps your features of interest away from the extremes of the wavelength ranges.

Grating Sensitivities and Throughputs

This chapter contains plots and tables of sensitivities and throughputs for each grating mode. “Determining Count Rates from Sensitivities” on page 70 in the Exposure-Time Calculation chapter explains how to use these sensitivities to calculate expected count rates from your source.

The total system[1] *spectroscopic point-source sensitivity,* S_λ^p, has the unit:

counts sec^{-1} pix_λ^{-1} per incident erg cm^{-2} sec^{-1} $Å^{-1}$ for the MAMA and electrons sec^{-1} pix_λ^{-1} per incident erg cm^{-2} sec^{-1} $Å^{-1}$ for the CCD,

where:

- pix_λ = a pixel in the dispersion direction.
- counts refer to the total counts from the point source integrated over the PSF in the direction perpendicular to the dispersion (along the slit).

Note that the spectroscopic point-source sensitivity does not include slit losses.

The *spectroscopic diffuse source sensitivity,* S_λ^d, has the unit:

counts sec^{-1} pix_λ^{-1} pix_s^{-1} per incident dimensional erg sec^{-1} cm^{-2} $Å^{-1}$ $arcsec^{-2}$ for the MAMA and
electrons sec^{-1} pix_λ^{-1} pix_s^{-1} per incident erg sec^{-1} cm^{-2} $Å^{-1}$ $arcsec^{-2}$ for the CCD,

where:

- pix_λ= a pixel in the dispersion direction.
- pix_s= a pixel in the spatial direction.

S_λ^p and S_λ^d are related through the relation:

$$S_\lambda^d \cong S_\lambda^p \times m_s \times W$$

where:

- m_s is the platescale in arcsec per pixel in the direction perpendicular to the dispersion.
- W is the width of the slit used in arcsec.

Here, we have assumed that the diffuse source has a uniform brightness over the area of interest and that the spectrum can be approximated as a continuum source. The throughput is defined as the end-to-end effective area divided by the geometric area of a filled, unobstructed 2.4 meter aperture (see Chapter 6).

The tables of sensitivities and throughputs given are derived for a point source in the largest clear aperture for each detector. The sensitivity plots give values for point and diffuse sources. In the plots in this chapter we show the diffuse source

1. STIS plus HST Optical Telescope Assembly (OTA).

sensitivity for a 0.1 arcsec wide slit. For an extended continuum source, S_λ^d scales directly with slit width, as above.

For the echelles, the sensitivities given were derived from fits of a smooth curve as a function of wavelength to the measured sensitivities at the central wavelength of each order (i.e., they do not include the effect of the echelle ripple). The STIS Exposure-Time Calculator (see Chapter 6) will properly take the echelle ripple into account and should be used for more detailed S/N analysis.

Signal-To-Noise Plots

For each grating mode, a plot is provided to help you estimate the signal-to-noise (S/N) for a class of sources and a range of exposure times, corresponding to a fiducial taken at wavelengths near the peak of the responses. The fiducial wavelength is indicated in the ordinate label of each plot. To estimate signal-to-noise at alternate wavelengths, you can scale your source flux or magnitude by the relative sensitivities (or throughputs) at the wavelength of interest and at the fiducial. The point source plots show S/N as a function of F_λ and of V+STMAG(λ) for a range of exposure times; the diffuse source plots show I_λ and V+STMAG(λ) per arcsec^2 for a range of exposure times. Using STMAG units is natural in this plot given that a particular STMAG value corresponds to a flux distribution with a constant value of F_λ. In producing these plots we assumed an average sky background (as described in Chapter 6) and the appropriate values for read noise and dark current for each detector. Note the following:

- The point-source S/N has been calculated per two dispersion pixels, and has been integrated over the PSF to contain 80% of the flux in the spatial direction.
- The point-source S/N calculations assume the use of the `52X0.2` slit for the first-order modes and the use of the `0.2X0.2` slit for the echelle modes.
- The diffuse-source S/N is calculated with the 0.2 arcsecond wide slit and the assumption that the slit is fully filled by a diffuse continuum source. The S/N is given per 2 spatial pixels and 4 spectral pixels for the CCD and is given per 2 spatial pixels and 6 spectral pixels for the MAMA (these are the equivalent spectral resolution elements for these observations).
- For the CCD, the plots assume `CR-SPLIT=2` and `CCDGAIN=1`.
- The different line styles in the S/N figures delineate regions where different sources of noise dominate. A particular source of noise (readnoise for example) is presumed to dominate if it contributes more than half the total noise in the observations.
- The vertical line indicates the MAMA bright-object *observing* limits; if F_λ (or I_λ) exceeds the indicated value, the observation would exceed the observing limits (recall that the observing limits are at slightly higher count rates than the *screening* limits given in Table 13.38). For diffuse sources we

indicate only the local rate limit, since the global limit is dependent on the source extent. If no line is seen on plot, it indicates the limit is higher than the range of fluxes plotted.

In situations requiring more detailed calculations (non-stellar spectra, extended sources, other sky background levels, etc.), the STIS Exposure-Time Calculator, located at the STIS WWW site under "Tools," should be used instead.

Follow these steps to use the S/N plots:

1. Look up in Table 13.1 the spectral type and wavelength region of interest of your target observation (e.g., G0 V @ 4300 Å). Interpolate in the table to get $STMAG_\lambda$.
2. Add the V magnitude of the target to the interpolated value of $STMAG_\lambda$ derived from the table.
3. Find the appropriate plot for the desired grating, and locate $V+STMAG_\lambda$ on the horizontal axis. Read off the S/N for the desired exposure time, or vice-versa. Alternatively use F_λ directly on the horizontal axis.
4. To get accurate values for repeated or CR-SPLIT exposures, one should use the sub-exposure time when consulting the plot, and then multiply the resulting S/N by $\sqrt{N}$, where N is the number of sub-exposures to be averaged. Recall that these plots assume `CR-SPLIT=2` for CCD observations.

Dotted lines across the top of each plot indicate the onset of saturation, in the case of the CCD, and local count rate limit, in the case of the MAMA detectors.

We now give a sample S/N calculation using these plots. Consider a V=18 star of spectral class B0 V, for which we want to derive the S/N for a 100 sec `CR-SPLIT` exposure in `G430L` with the CCD. We look up the B0 V spectral class and interpolate in the table between 4000 Å ($STMAG_\lambda$ = –1.20) and 4500 Å ($STMAG_\lambda$ = –0.78) to obtain $STMAG_\lambda$ ~–1 at 4300 Å. We thus have $V+STMAG_\lambda$ = 17. We look at Figure 13.12 and find this value on the horizontal axis. We locate exposure time 100 and find S/N ~10. This exposure is well below the saturation lines in the plot, so saturation is not a concern.

Plate Scales

In each grating section, the plate scale, in arcseconds per pixel, is given in the table for that grating. For the first-order modes a single value is given for the spatial and dispersion directions, which has been approximated at 0.05 arcseconds for the CCD modes and 0.025 arcseconds for the MAMA modes. In reality, the plate scale in the spatial direction is reliably given by that determined from the CCD and MAMA imaging modes: 0.05071 arcseconds/pixel for the CCD and 0.025 for the MAMA (see "Image-Mode Geometric Distortion" on page 364). However, the gratings introduce anamorphic magnification which causes the plate scale in the dispersion direction to increase relative to that in the cross-dispersion direction, as a function of wavelength and grating tilt. Thus, for example, at the central wavelength of `G750L` the cross dispersion plate scale is calculated to be 0.05121 arcseconds/pixel and that of `G430L` 0.05269 arcseconds per pixel. As

another example for G750M at 6768 Å the cross dispersion plate scale is calculated as 0.05477 arcseconds/pixel while at 8825 Å it is calculated as 0.05616 arcseconds/pixel or a change of ~3%. A full description of the plate scale effects of anamorphic distortion is provided in STIS ISR 98-20.

Apertures

For each supported slit (aperture) we provide a table giving the name of the slit, length (in the spatial direction) and width (in the dispersion direction) of the slit as well as a table and plot of the relative throughput of the slit (with respect to a large clear aperture) as a function of wavelength. Recall, that the point source sensitivities that we have derived assume zero slit losses. Your calculations of exposure times must account for light losses for the desired slit. The aperture throughput information provided in the tables is based on models. Early SMOV and Cycle 7 observations show small deviations (~5–10%) from the predicted throughputs. We expect to update the aperture throughput values based on orbital measurements; information will be posted to the STIS web page and incorporated into the pipeline as it becomes available.

Fiducials on Bars

Each STIS long slit has two fiducial bars, located 11.2 arcseconds above and below the slit center (see Figure 13.1, below). They have several purposes. First, the bars provide structural integrity for the long slits. Second, the image of the bars obtained in wavecal (and target acquisition) images is used by the calibration software to locate the projection of the aperture on the detector in post-observation data processing. Lastly, the bars can be used to occult a source thereby providing a coronographic spectroscopic capability for STIS. For Cycle 8, we continue to support use of the 0.5 arcseconds long bar on the 52X0.2 arcseconds slit (the 52X0.2F1 aperture) for such observations. We refer you to “Coronographic Imaging and Spectroscopy” on page 215 for more information about performing coronographic spectroscopy, and “Spectroscopic Mode Peculiarities” on page 306 for some caveats.

Figure 13.1: 52” Long Slits and Location of Fiducial Bars

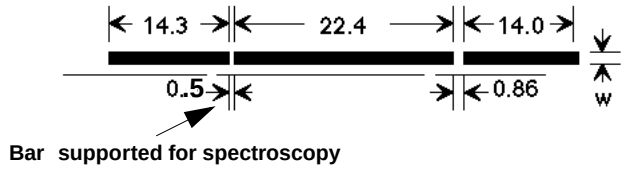

Spatial Profiles

For each grating mode information about the cross dispersion (spatial) profiles is provided as follows:

- Plots of model fits to on-orbit data of the spectral profile in the cross dispersion (spatial) direction) for a series of central wavelengths and gratings.
- A table of “encircled energies” containing two values: the percent of the total flux contained in the default calibration pipeline 1-D spectrum extraction aperture and the percent of the total flux contained in the central pixel.

Line-Spread Functions (Instrumental Profiles)

We show plots of predicted line spread functions (LSFs) for CCD and MAMA spectroscopic modes, as a function of wavelength and slit width. While these plots are based on prelaunch models of the PSFs at the aperture plane and detector PSFs from non-flight detectors, our preliminary comparison with on-orbit observations of internal lamps and external sources for the first-order modes indicates that the models are adequate for planning purposes. As part of the STIS calibration program, we will be making additional observations to characterize the LSF of the echelle modes and updates will be posted to the STIS web page in the “On-Orbit Performance” area as they become available.

Gratings

Below, for each grating mode of STIS, we provide the basic properties of the mode, wavelength ranges covered in each central wavelength setting, sensitivities and throughputs, dispersions and plate scales. Advice on use is provided where appropriate and comparisons of the `G230L`, `G230M` MAMA modes with their `G230LB`, `G230MB` CCD counterparts are shown.

Table 13.1: $STMAG_\lambda$ as a Function of Wavelength for Stellar Objects. $STMAG_\lambda$ is defined as the color-dependent correction from V magnitude to STMAG at wavelength λ.

Spectrum	Wavelength (Å)												
	1500	**2000**	**2500**	**3000**	**3500**	**4000**	**4500**	**5000**	**6000**	**7000**	**8000**	**9000**	**10000**
O5 V	-4.80	-3.84	-3.03	-2.35	-1.74	-1.24	-0.77	-0.34	0.41	1.05	1.61	2.10	2.54
B0 V	-4.56	-3.47	-2.77	-2.10	-1.65	-1.20	-0.78	-0.37	0.43	1.03	1.57	2.04	2.48
B5 V	-3.01	-2.02	-1.64	-1.29	-1.00	-1.02	-0.68	-0.30	0.34	0.91	1.38	1.80	2.19
Vega	-0.75	-0.48	-0.13	0.01	0.17	-0.85	-0.60	-0.26	0.33	0.82	1.28	1.81	2.08
A0 V	-0.83	-0.41	-0.02	0.09	0.19	-0.79	-0.59	-0.27	0.31	0.80	1.25	1.58	1.87
A5 V	3.69	0.46	0.82	0.44	0.38	-0.57	-0.50	-0.22	0.27	0.72	1.10	1.40	1.67
F2 V	8.86	2.00	1.66	0.62	0.42	-0.24	-0.28	-0.13	0.17	0.49	0.78	1.04	1.31
F5 V	10.86	3.35	2.03	0.78	0.43	-0.16	-0.23	-0.09	0.13	0.43	0.70	0.96	1.21
G0 V	13.82	5.63	3.32	1.25	0.62	0.13	-0.12	-0.05	0.10	0.29	0.52	0.76	0.98
Sun	10.80	6.02	3.73	1.52	0.69	0.10	-0.11	-0.01	0.07	0.32	0.55	0.82	1.03
K0 V	7.08	6.72	5.13	2.49	1.18	0.53	0.05	0.01	0.01	0.18	0.39	0.61	0.84
M0 V	8.58	8.22	6.64	3.99	2.69	1.80	0.57	0.46	-0.22	-0.39	-0.49	-0.45	-0.38
B0.5 III	-3.86	-2.90	-2.43	-1.88	-1.47	-1.14	-0.71	-0.32	0.39	0.99	1.52	1.98	2.41
A0 III	-1.33	-0.76	-0.24	-0.12	0.05	-0.92	-0.60	-0.28	0.33	0.85	1.32	1.57	1.96
F0 III	8.93	2.09	1.84	0.80	0.51	-0.31	-0.38	-0.18	0.21	0.58	0.92	1.15	1.43
O9.5 I	-4.09	-3.20	-2.59	-2.01	-1.61	-1.19	-0.74	-0.33	0.40	1.02	1.57	2.04	2.48
B0 I	-3.78	-2.91	-2.45	-1.88	-1.48	-1.10	-0.70	-0.31	0.37	0.94	1.43	1.87	2.27
B5 I	-1.86	-1.33	-1.26	-1.11	-0.87	-0.92	-0.58	-0.26	0.31	0.85	1.34	1.63	2.06

Table 13.2: $STMAG_\lambda$ as a Function of Wavelength for Non-Stellar Objects. $STMAG_\lambda$ is defined as the color-dependent correction from V magnitude to STMAG at wavelength λ.

Spectrum	Wavelength (Å)												
	1500	2000	2500	3000	3500	4000	4500	5000	6000	7000	8000	9000	10000
Elliptical	3.35	3.19	4.17	2.92	1.60	0.70	0.17	0.15	-0.04	-0.08	-0.07	-0.13	n/a
S0	4.63	3.95	3.27	2.23	1.61	0.71	0.18	0.13	-0.03	-0.13	-0.02	-0.08	n/a
Sa	2.64	2.27	2.39	1.78	1.31	0.36	0.12	0.07	-0.06	-0.05	-0.00	0.02	n/a
Sb	1.70	2.59	2.04	1.32	1.12	0.43	0.17	0.10	0.02	-0.05	-0.01	-0.04	n/a
Sc	-0.18	0.44	-0.17	-0.68	-0.67	-0.51	-0.44	-1.25	0.18	0.40	n/a	n/a	n/a
Starburst,E(B-V)<0.1	-1.71	-1.15	-0.68	-0.43	-0.13	-0.42	-0.23	-1.24	0.21	0.40	0.70	0.85	n/a
Starburst,0.25<E(B-V)<0.35	-0.95	-0.87	-0.33	-0.10	0.08	-0.19	-0.19	-0.28	0.15	0.44	0.41	0.47	n/a
Starburst,0.51<E(B-V)<0.60	-0.40	-0.18	0.01	0.23	0.03	-0.14	-0.12	-0.36	0.07	0.07	0.18	0.29	n/a
Starburst,0.61<E(B-V)<0.70	0.05	0.31	0.31	0.15	0.27	-0.17	-0.13	-0.11	0.06	0.17	0.26	0.24	n/a

How to Use The $STMAG_\lambda$ Tables

1. Interpolate in the table to get $STMAG_\lambda$ for the spectral type and wavelength region of your target observation (e.g. G0 V @ 4300Å).
2. Add the target V magnitude to the $STMAG_\lambda$ derived from Step 1.
3. Find the S/N plot for the grating you want to use.
4. Locate $V+STMAG_\lambda$ on the horizontal axis and read off the S/N for the desired exposure time (or read off the exposure time for the desired S/N).

First-Order Grating G750L

Description

The G750L grating is used with the CCD. It has high throughput but low resolving power (~500), and is designed for efficient, full spectral coverage. The grating has one prime tilt setting.

Recommended Uses

This grating is recommended for observations where high spectral resolution is not required, but efficient coverage in the red portion of the optical is desired.

Special Considerations

Fringing in the CCD compromises the realizable signal-to-noise longward of 7500 Å if contemporaneous fringe flats are not obtained (see “CCD Operation and Feasibility Considerations” on page 102).

Grating	Spectral Range		Average Dispersion (Å / Pixel)	Plate Scale (arcsec / pixel)	Tilts	Central Wavelengths
	Complete	Per Tilt				
G750L	5240–10270	5030	4.92	0.05	***Prime***	7751

Figure 13.2: Wavelength Range for the G750L Grating Setting

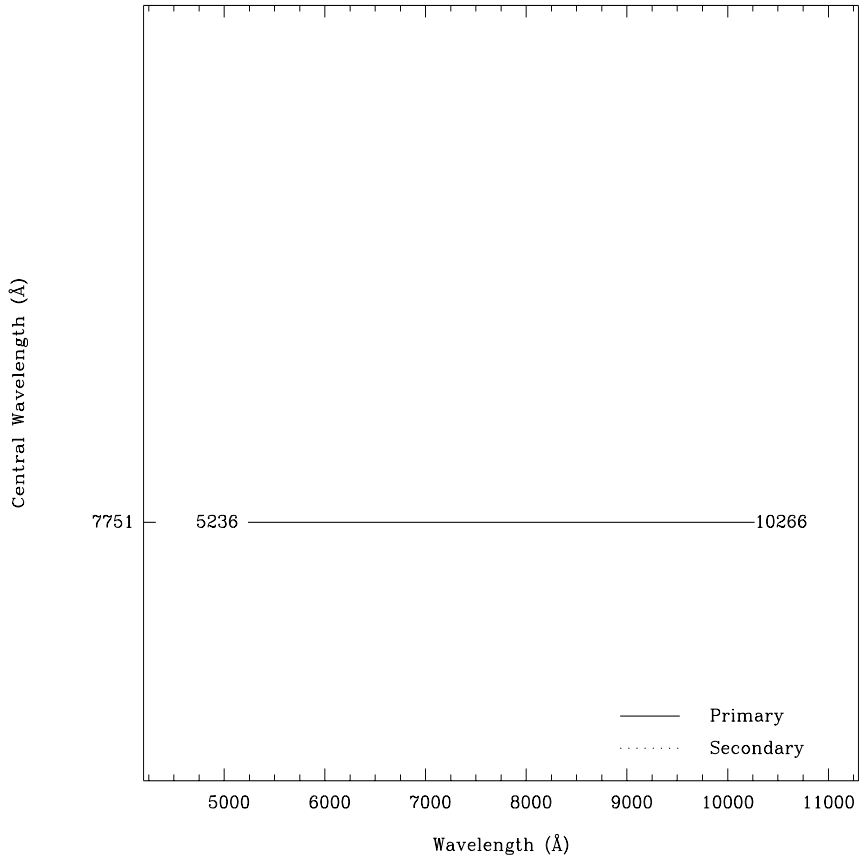

G750L Sensitivities

Table 13.3: G750L Sensitivities & Throughputs for a Point Source

λ	Sensitivity	Throughput
5500	3.8E15	6.2
6000	5.0E15	7.4
6500	6.1E15	8.4
7000	6.3E15	8.1
7500	5.8E15	6.9
8000	4.5E15	5.0
8500	3.9E15	4.1
9000	4.2E15	4.2
9500	3.8E15	3.6
10000	2.0E15	1.8

Figure 13.3: G750L Point Source (left axis), and Diffuse Source (right axis) Sensitivities

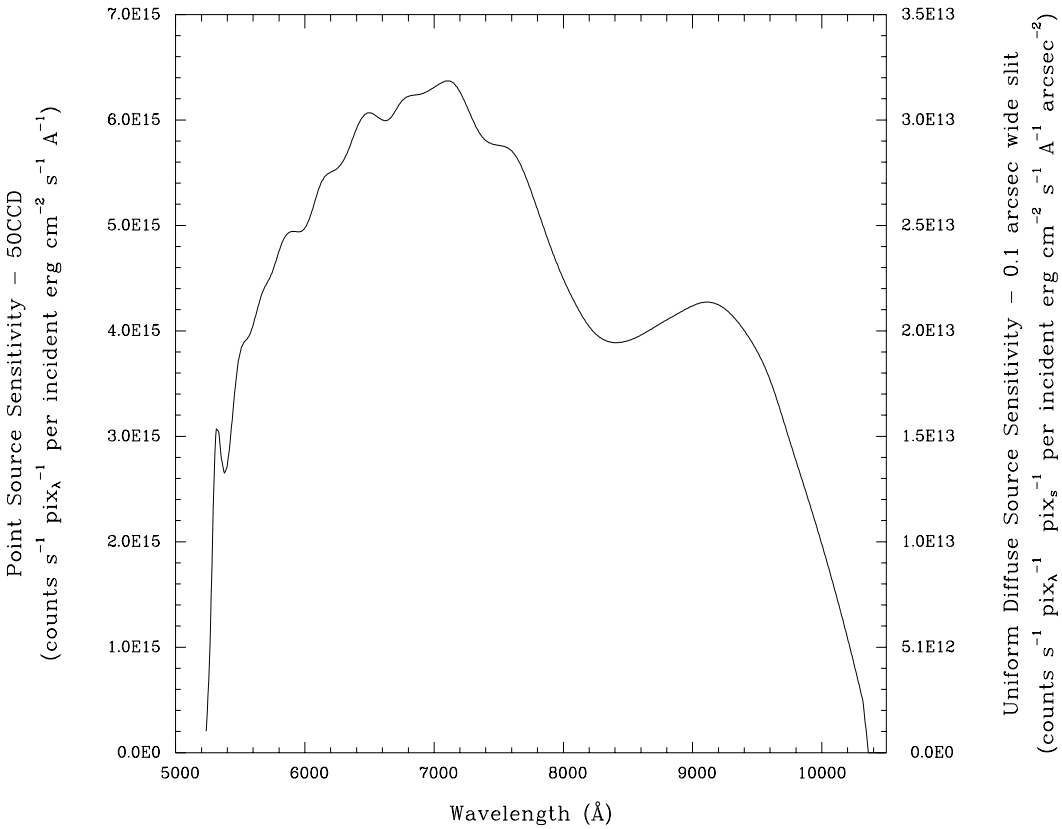

Note

Point source sensitivity assumes full transmission (zero slit losses). Diffuse source sensitivity assumes a 0.1” wide slit. To convert point source sensitivities to diffuse source sensitivities multiply the point source values by the grating spatial (cross dispersion) plate scale in units of arcseconds per pixel and by the width of the desired slit in units of arcseconds.

G750L Signal-to-Noise

Note:

The top axis displays constant F_λ values corresponding to the STMAG units (V+STMAG$_\lambda$) on the bottom axis. Recall that STMAG=0 is equivalent to F_λ = 3.63E-9 erg cm^{-2} s^{-1} Å^{-1}. The curves are labeled with exposure times in seconds

Figure 13.4: Diffuse SourceSignal-to-Noise as a Function of STMAG for G750L. λ Fiducial = 7500 Å.

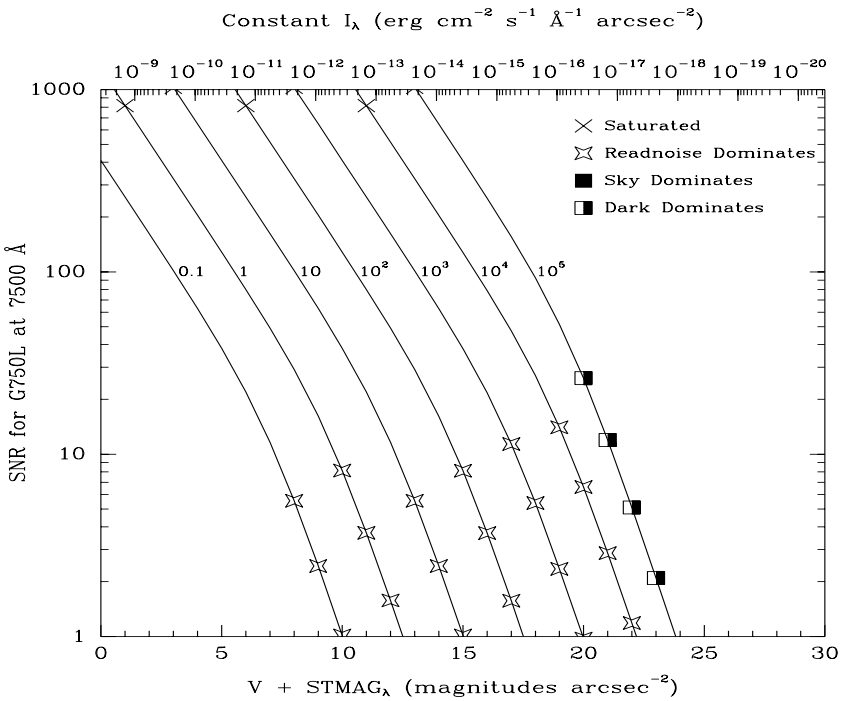

Figure 13.5: Point Source Signal-to-Noise as a Function of STMAG for G750L

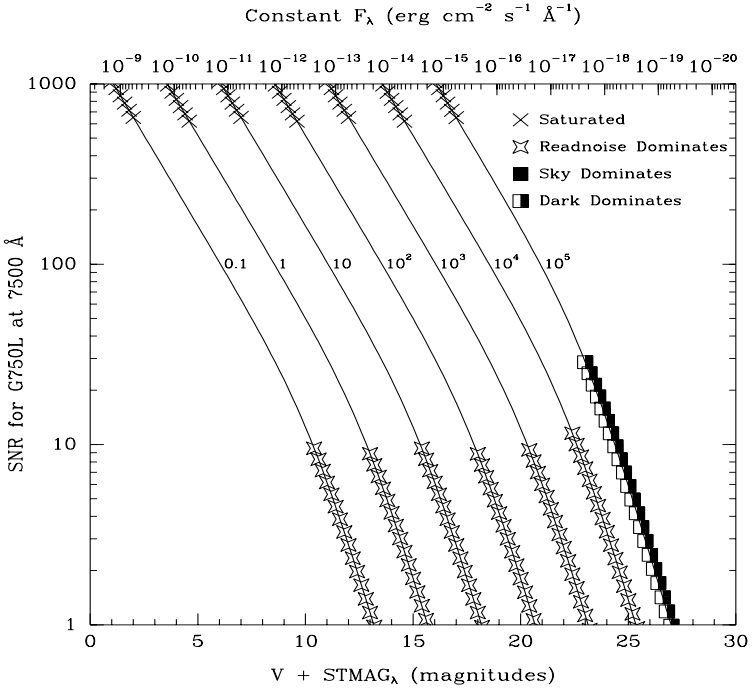

First-Order Grating G750M

Description

Like G750L, the G750M grating is used with the CCD and has a spectral range from 5500–10,000 Å. With a resolving power R~5000, a single exposure with this grating covers only 570 Å, and the grating must be scanned, with a series of exposures taken at 9 distinct settings to cover the full range of the grating.

Recommended Uses

This grating is designed for relatively high spectral resolution work centered on selected wavelength regions of the optical to near-IR.

Special Considerations

There is a partial ghost spectrum present in the λ_c=5734 setting which is ~1.2% of, is inverted with respect to, is offset by ~ 70 pixels from, the prime spectrum, arising from back reflections between the CCD and the order sorter.

Fringing in the CCD compromises the realizable signal-to-noise longward of 7500 Å if contemporaneous fringe flats are not obtained (see “CCD Operation and Feasibility Considerations” on page 102).

The secondary central wavelengths at 6581 & 8561 Å have had direct sensitivity and wavelength calibrations performed during Cycle 7 to support the large number of observations using these positions.

Grating	Spectral Range		Average Dispersion (Å per Pixel)	Plate Scale (arcsec / pixel)	Tilts	Central Wavelengths
	Complete	Per Tilt				
G750M	5450-10140	570	0.56	0.05	***Prime***	**5734**, **6252**, **6768**, **7283**, **7795**, **8311**, **8825**, **9336**, **9851**
					Secondary	6094, 6581, 8561, 9286, 9806

Figure 13.6: Wavelength Ranges for the G750M Grating Settings

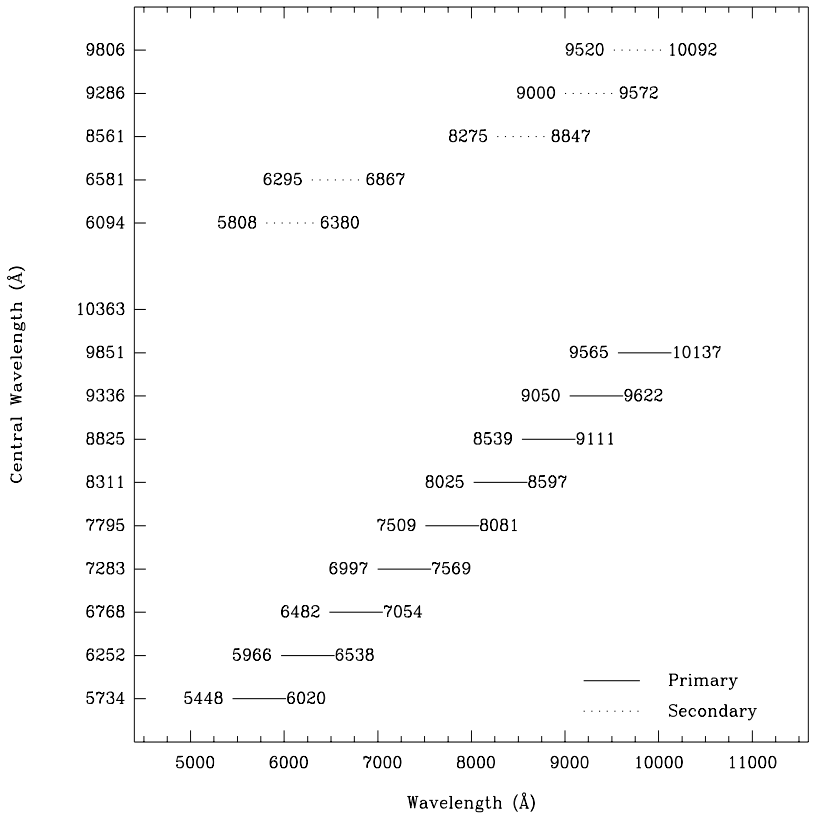

G750M Sensitivities

Table 13.4: G750M Sensitivities & Throughputs

λ	Sensitivity	Throughput
5550	7.4E14	10.6
5800	8.8E14	12.1
6050	9.3E14	12.2
6300	1.0E15	13.2
6550	1.1E15	13.9
6800	1.2E15	14.0
7050	1.2E15	13.6
7300	1.2E15	12.7
7550	1.1E15	11.5
7800	9.7E14	10.0
8050	8.3E14	8.3
8300	7.5E14	7.2
8550	7.7E14	7.2
8800	8.2E14	7.5
9050	8.3E14	7.3
9300	8.0E14	6.8
9550	7.1E14	5.9
9800	5.5E14	4.5
10050	3.6E14	2.9

Figure 13.7: G750M Point Source (left axis), and Diffuse Source (right axis) Sensitivities.

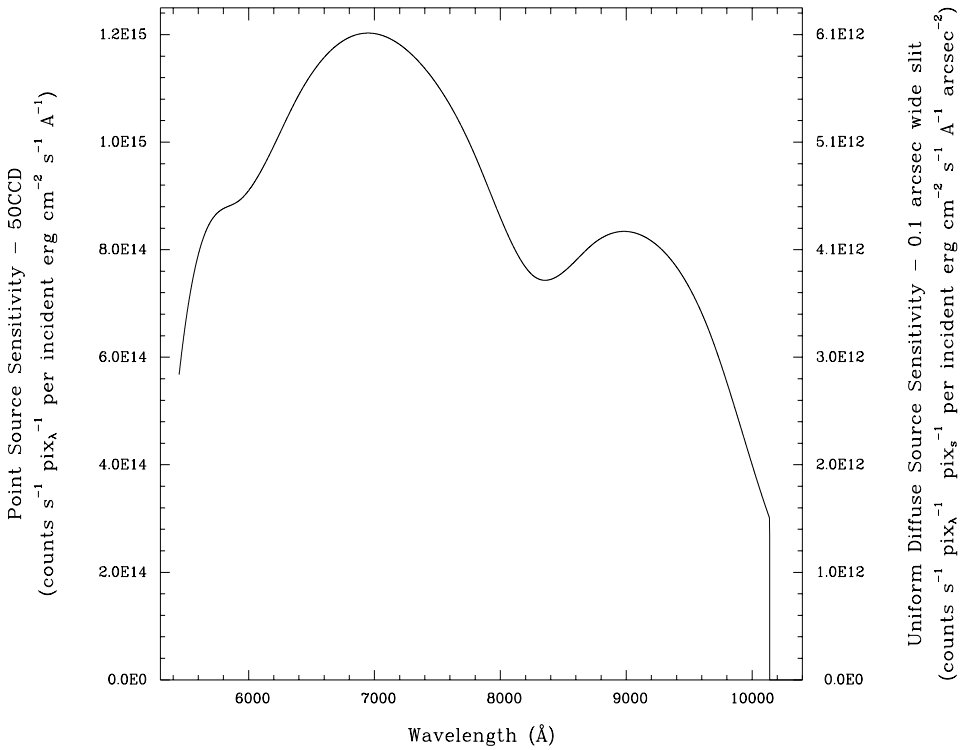

Note

Point source sensitivity assumes full transmission (zero slit losses). Diffuse source sensitivity assumes a 0.1” wide slit. To convert point source sensitivities to diffuse source sensitivities multiply the point source values by the grating spatial (cross dispersion) plate scale in units of arcseconds per pixel and by the width of the desired slit in units of arcseconds.

G750M Signal-to-Noise

Note:

The top axis displays constant F_λ values corresponding to the STMAG units (V+STMAG$_\lambda$) on the bottom axis. Recall that STMAG=0 is equivalent to F_λ = 3.63E-9 erg cm^{-2} s^{-1} Å^{-1}. The curves are labeled with exposure times in seconds

Figure 13.8: Diffuse Source Signal-to-Noise as a Function of STMAG for G750M

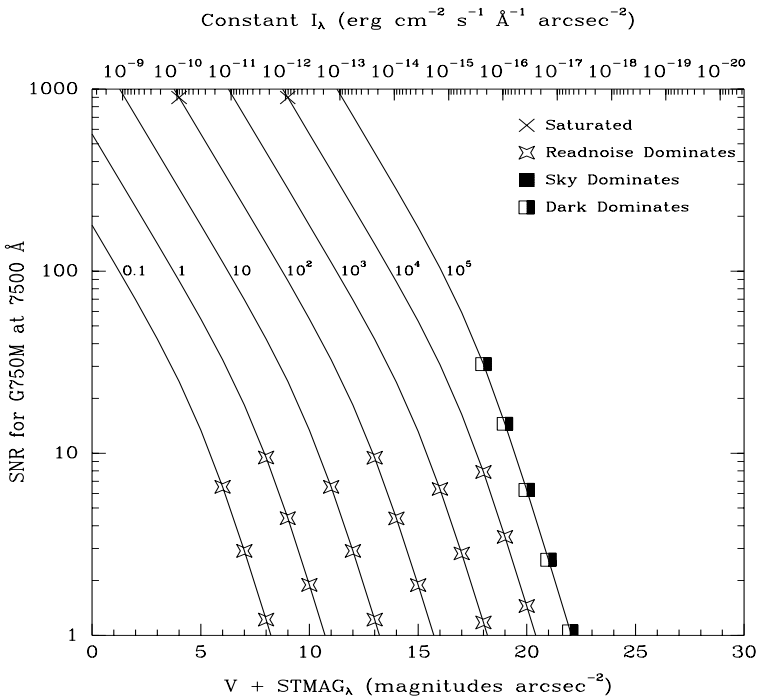

Figure 13.9: Point Source Signal-to-Noise as a Function of STMAG for G750M

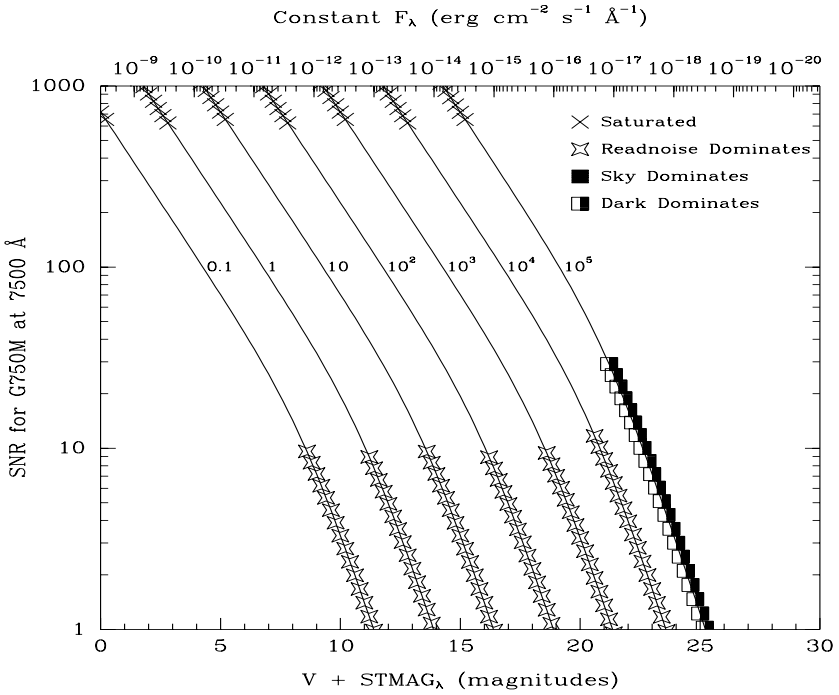

First-Order Grating G430L

Description

G430L, used with the CCD, is a low resolution grating (R~500) with a relatively high throughput. The grating has only a single setting.

Recommended Uses

This grating is designed for observations where high spectral resolution is not required, but efficient spectral coverage in the blue portion of the optical is desired.

Special Considerations

Notice, that by taking two observations, one with G750L and one with G430L, the full spectral region, from the near-IR at 10000 Å through the optical at 3000 Å can be efficiently observed at an R~500.

Grating	Spectral Range		Average Dispersion (Å per Pixel)	Plate Scale (arcsec / pixel)	Tilts	Central Wavelengths
	Complete	Per Tilt				
G430L	2900-5700	2800	2.73	0.05	***Prime***	**4300**

Figure 13.10: Wavelength Ranges for the G430L Grating Settings

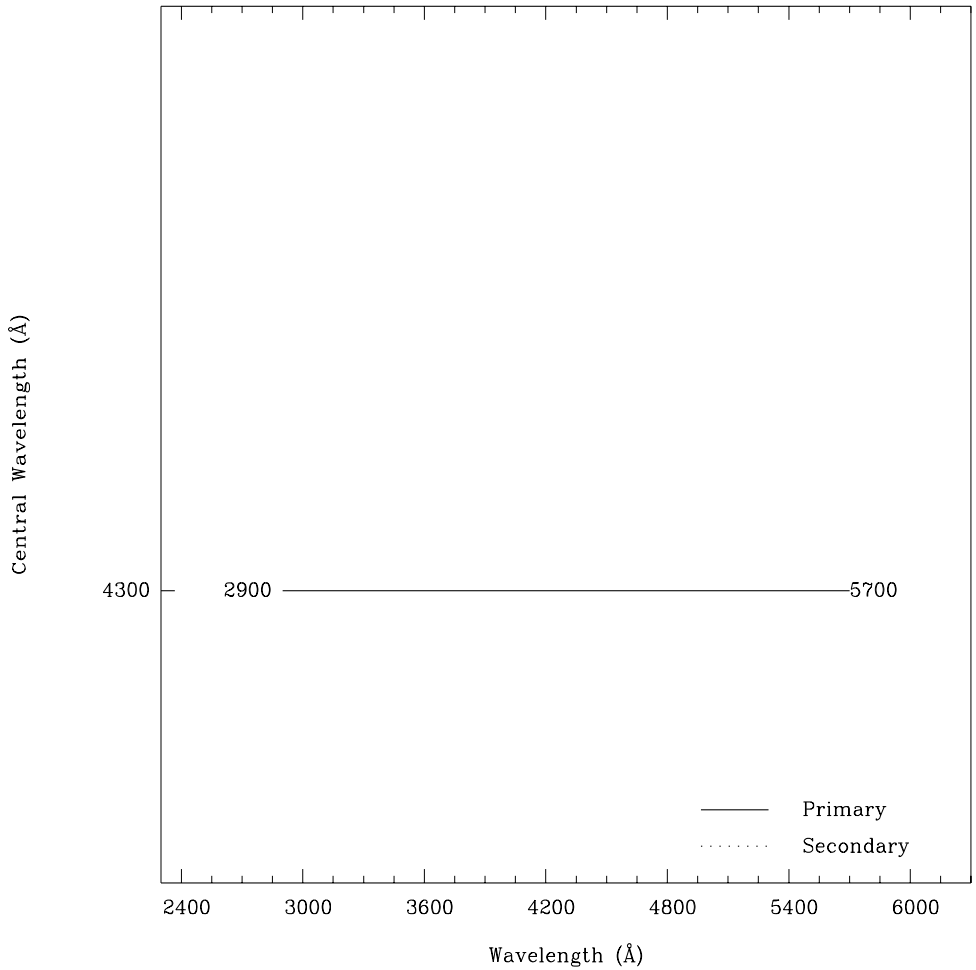

G430L Sensitivities

Table 13.5: G430L Sensitivities & Throughputs

λ	Sensitivity	Throughput
3000	3.2E14	1.7
3250	7.2E14	3.6
3500	1.0E15	4.6
3750	1.4E15	5.9
4000	2.1E15	8.6
4250	2.5E15	9.6
4500	2.9E15	10.4
4750	2.9E15	10.0
5000	3.1E15	10.1
5250	3.2E15	9.9
5500	3.0E15	8.9

Figure 13.11: G430L Point Source (left axis), and Diffuse Source (right axis) Sensitivities.

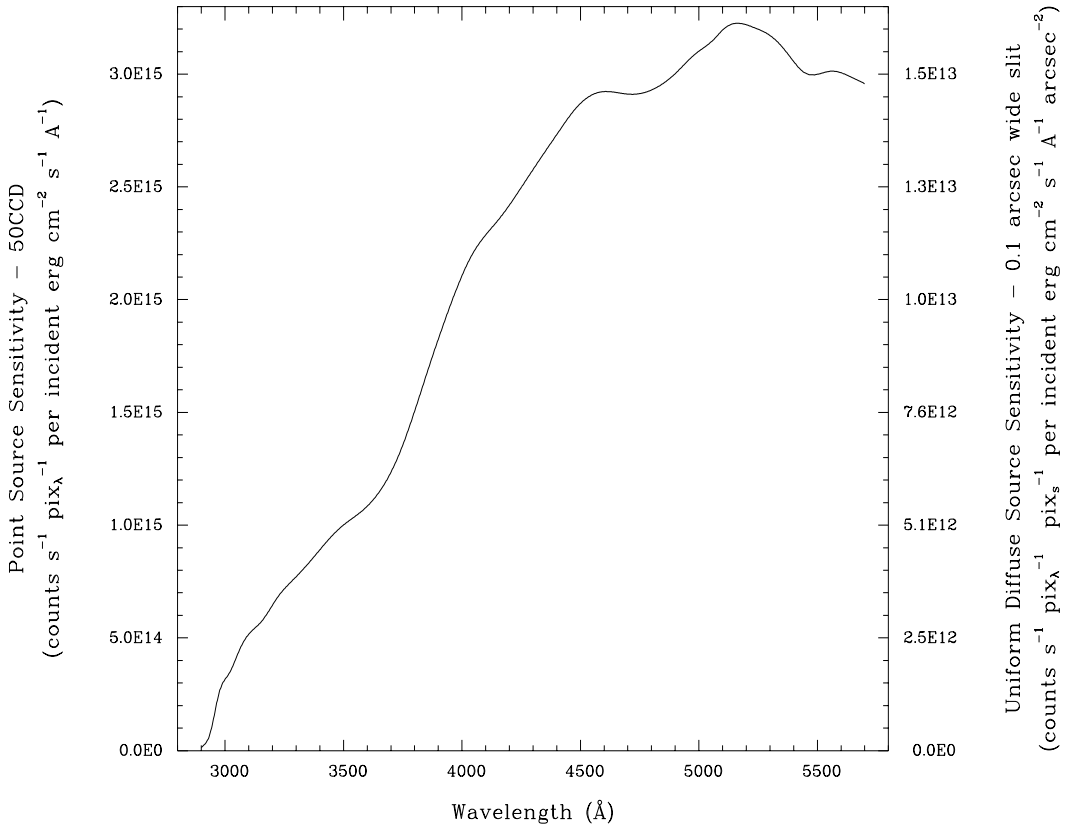

Note

Point source sensitivity assumes full transmission (zero slit losses). Diffuse source sensitivity assumes a 0.1” wide slit. To convert point source sensitivities to diffuse source sensitivities multiply the point source values by the grating spatial (cross dispersion) plate scale in units of arcseconds per pixel and by the width of the desired slit in units of arcseconds.

G430L Signal-to-Noise

Note:

The top axis displays constant F_λ values corresponding to the STMAG units (V+STMAG$_\lambda$) on the bottom axis. Recall that STMAG=0 is equivalent to F_λ = 3.63E-9 erg cm^{-2} s^{-1} Å^{-1}. The curves are labeled with exposure times in seconds

Figure 13.12: Diffuse Source Signal-to-Noise as a Function of STMAG for G430L

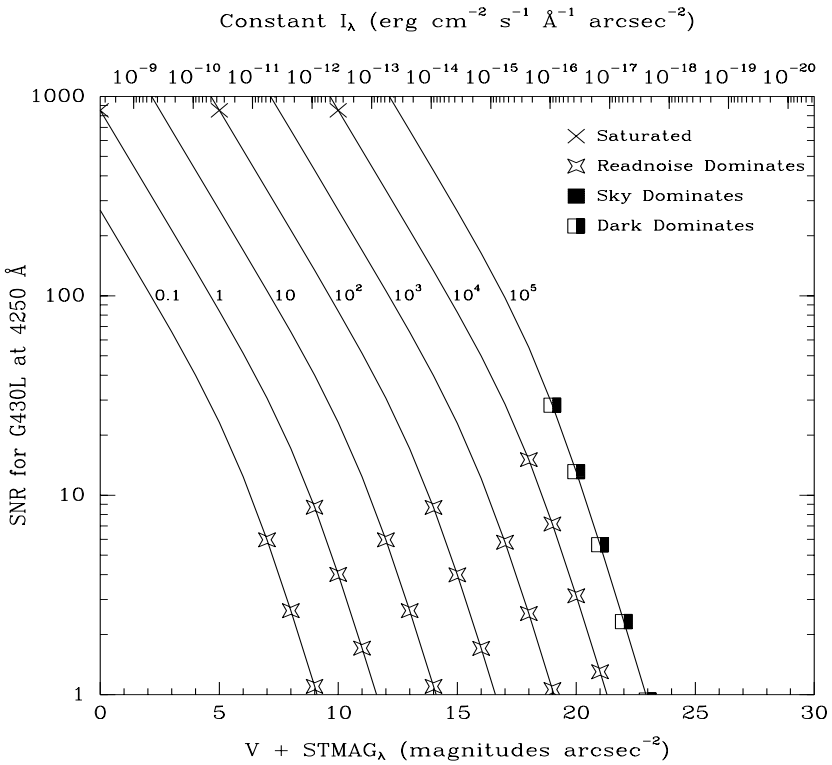

Figure 13.13: Point Source Signal-to-Noise as a Function of STMAG for G430L

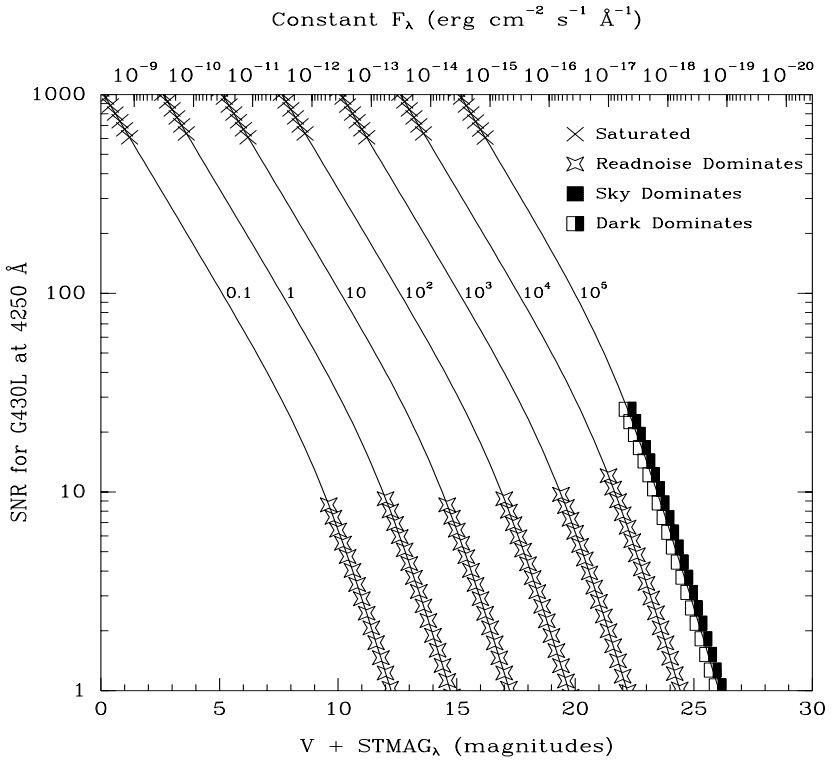

First-Order Grating G430M

Description

Like the G430L grating, the G430M grating is used with the CCD and has a spectral range from 3020–5600 Å.

Since a single exposure taken with this grating covers only 286 Å the grating must be scanned, with a series of exposures taken at 10 distinct settings, to cover the full spectral range of the grating.

Recommended Uses

The G430M grating mode is designed for observations where spatially resolved, long slit spectroscopy is desired at relatively high spectral resolution (R~6000) over a limited region of the near-ultraviolet or optical spectrum.

Grating	Spectral Range		Average Dispersion (Å per Pixel)	Plate Scale (arcsec / pixel)	Tilts	Central Wavelengths
	Complete	Per Tilt				
G430M	3020-5610	286	0.28	0.05	***Prime***	**3165, 3423, 3680, 3936, 4194, 4451, 4706, 4961, 5216, 5471**
					Secondary	3305, 3843, 4781, 5093

Figure 13.14: Wavelength Ranges for the G430M Grating Settings

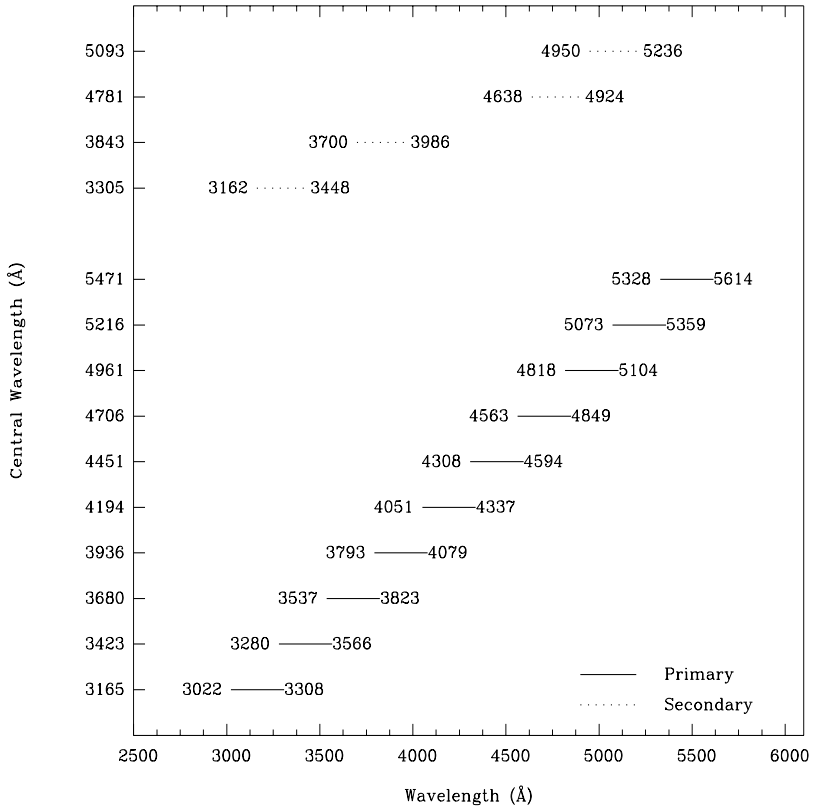

G430M Sensitivities

Table 13.6: G430M Sensitivities & Throughputs

λ	Sensitivity	Throughput
3100	8.5E13	4.3
3200	1.0E14	5.0
3300	1.0E14	5.0
3400	1.0E14	4.8
3500	1.1E14	4.9
3600	1.2E14	5.4
3700	1.5E14	6.3
3800	1.9E14	7.7
3900	2.3E14	9.1
4000	2.5E14	9.9
4100	2.6E14	10.0
4200	2.7E14	10.2
4300	2.9E14	10.5
4400	3.1E14	10.9
4500	3.1E14	11.0
4600	3.1E14	10.6
4700	3.1E14	10.3
4800	3.2E14	10.4
4900	3.4E14	10.9
5000	3.7E14	11.6
5100	3.9E14	11.9
5200	3.8E14	11.6
5300	3.7E14	10.9
5400	3.5E14	10.1
5500	3.3E14	9.5
5600	3.2E14	9.1

Figure 13.15: G430M Point Source (left axis), and Diffuse Source (right axis) Sensitivities.

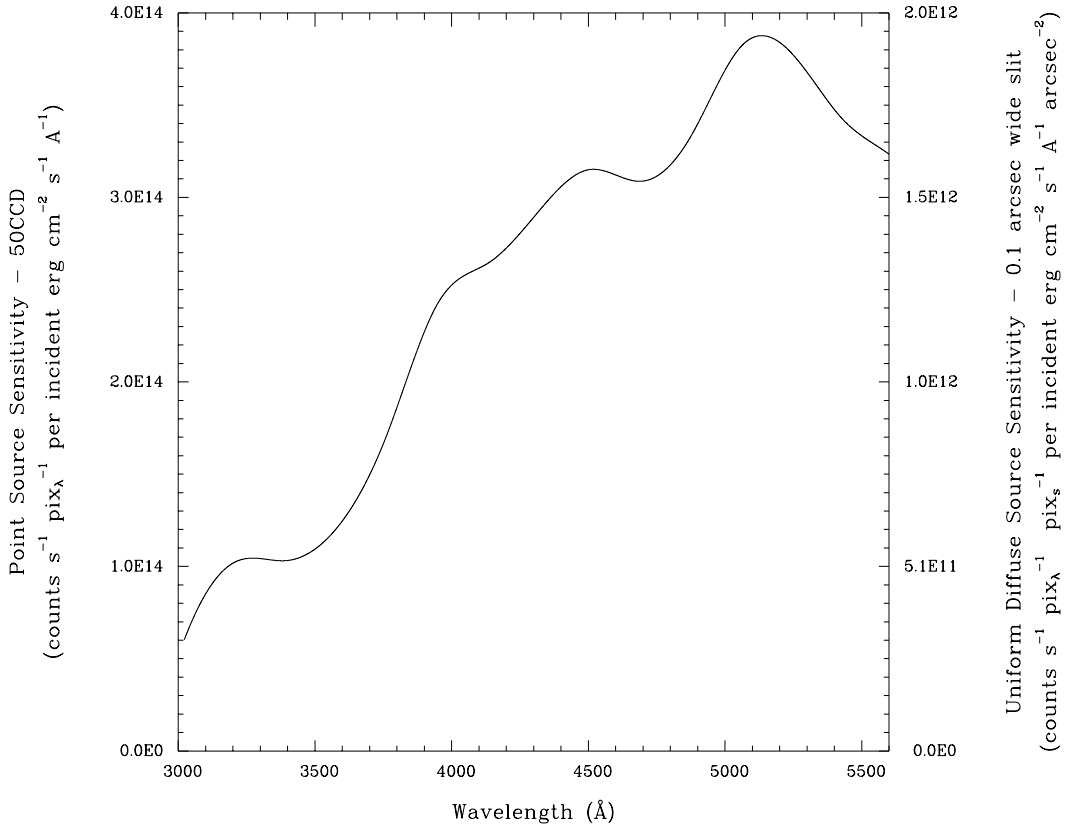

Note

Point source sensitivity assumes full transmission (zero slit losses). Diffuse source sensitivity assumes a 0.1” wide slit. To convert point source sensitivities to diffuse source sensitivities multiply the point source values by the grating spatial (cross dispersion) plate scale in units of arcseconds per pixel and by the width of the desired slit in units of arcseconds.

G430M Signal-to-Noise

Note:

The top axis displays constant F_λ values corresponding to the STMAG units (V+STMAG$_\lambda$) on the bottom axis. Recall that STMAG=0 is equivalent to F_λ = 3.63E-9 erg cm^{-2} s^{-1} Å^{-1}. The curves are labeled with exposure times in seconds.

Figure 13.16: Diffuse Source Signal-to-Noise as a Function of STMAG for G430M

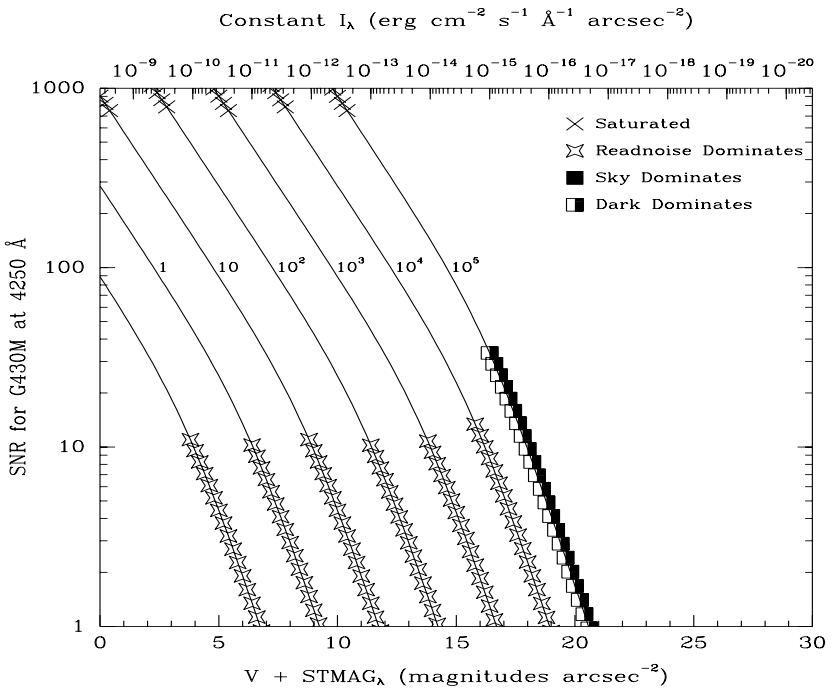

Figure 13.17: Point Source Signal-to-Noise as a Function of STMAG for G430M

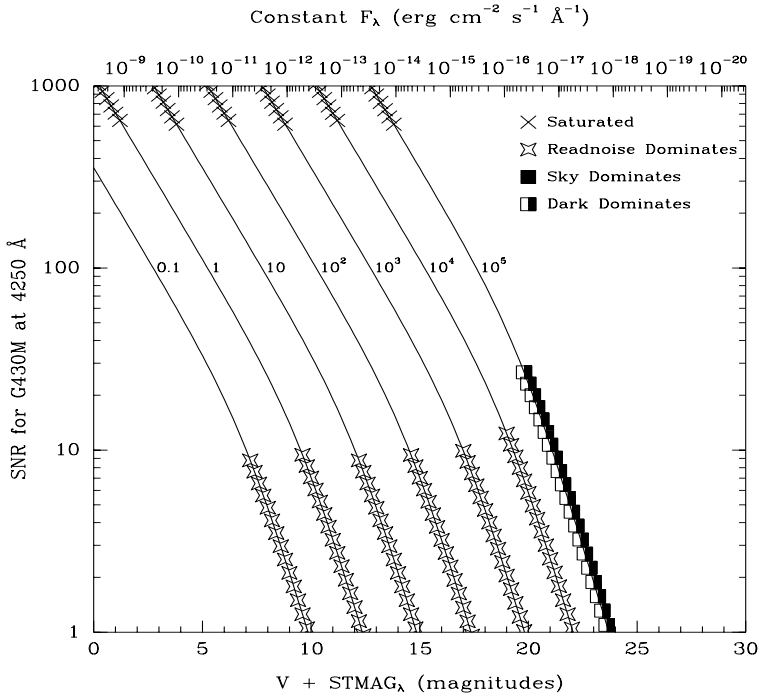

First-Order Grating G230LB

Description

The G230LB grating mode uses a low resolution grating originally designed for use with the STIS/NUV-MAMA which has been re-directed for use with the STIS/CCD to enable R~700 spectroscopy in the near-UV which takes advantage of the CCD's higher throughput and dynamic range longward of λ=2500 Å.

Recommended Uses

The G230LB grating mode is designed for programs needing the highest available sensitivity in the near-UV from ~2500 to 3100 Å or more generally to allow observation of sources too bright for the MAMA in the near UV.

Special Considerations

In making the plots for the G230LB grating mode, we assumed that the CCD is subject to a change in the effective quantum yield resulting in the creation of multiple electron-hole pairs per photon for λ<3400 Å .

Also be aware that because of the high sensitivity of the CCD to red light, observations of red stars with G230LB are more likely to be affected by scatter than observations of red stars using the MAMA G230L mode.

Grating	Spectral Range		Average Dispersion (Å per Pixel)	Plate Scale (arcsec / pixel)	Tilts	Central Wavelengths
	Complete	Per Tilt				
G230LB	1680-3060	1380	1.35	0.05	***Prime***	**2375**

Figure 13.18: Wavelength Range for the G230LB Grating Setting

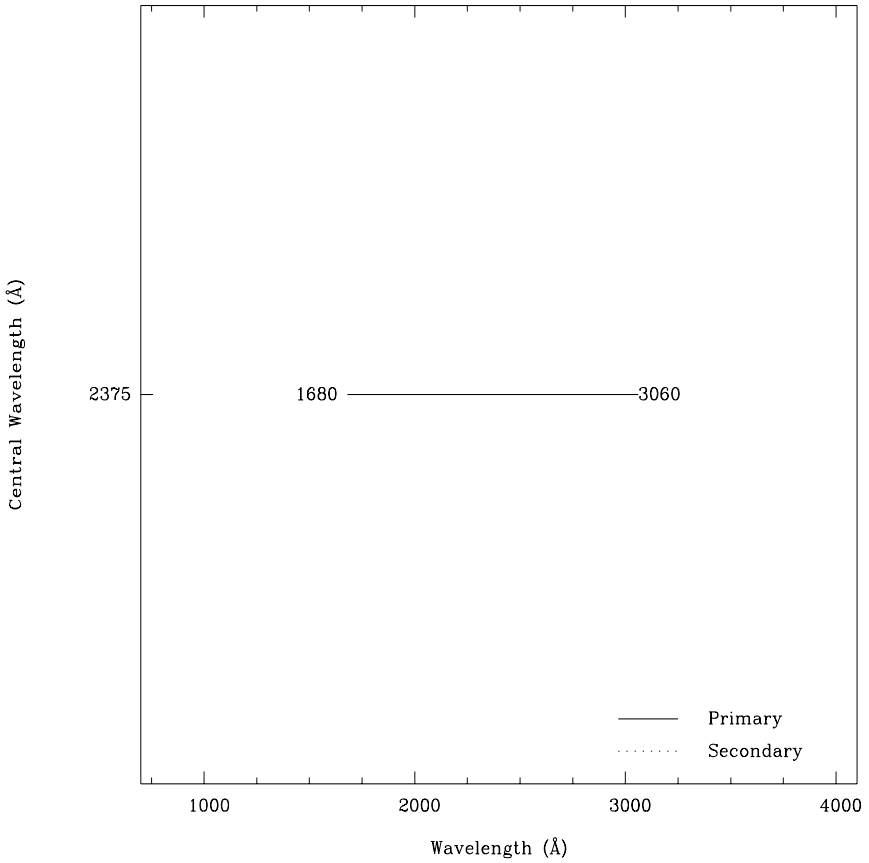

G230LB Sensitivities

Table 13.7: G230LB Sensitivities & Throughputs

λ	Sensitivity	Throughput
1750	1.5E13	0.3
1850	2.7E13	0.5
1950	4.3E13	0.7
2050	6.9E13	1.1
2150	1.1E14	1.7
2250	1.4E14	2.2
2350	1.9E14	2.7
2450	2.1E14	2.9
2550	2.2E14	2.9
2650	2.3E14	2.9
2750	2.4E14	3.0
2850	2.8E14	3.3
2950	3.4E14	3.8
3050	3.8E14	4.2

Figure 13.19: G230LB Point Source (left axis), and Diffuse Source (right axis) Sensitivities.

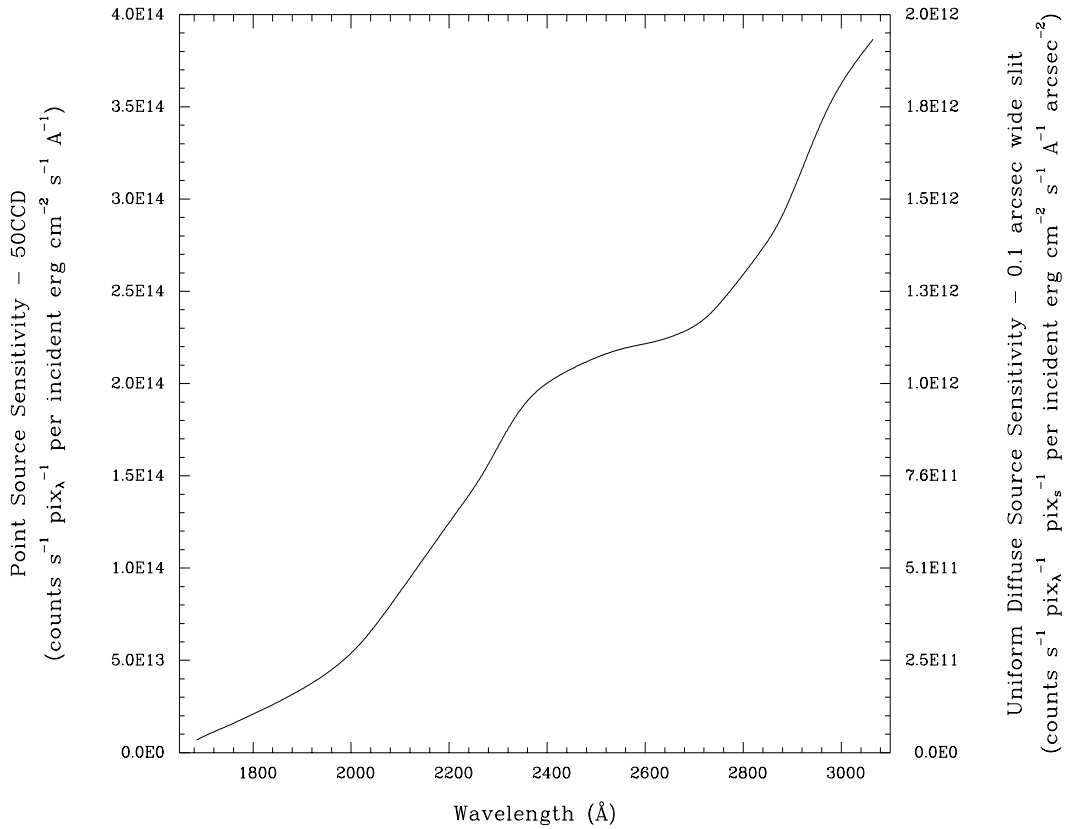

Note

Point source sensitivity assumes full transmission (zero slit losses). Diffuse source sensitivity assumes a 0.1” wide slit. To convert point source sensitivities to diffuse source sensitivities multiply the point source values by the grating spatial (cross dispersion) plate scale in units of arcseconds per pixel and by the width of the desired slit in units of arcseconds.

G230LB Signal-to-Noise

Note:

The top axis displays constant F_λ values corresponding to the STMAG units ($V+STMAG_\lambda$) on the bottom axis. Recall that STMAG=0 is equivalent to F_λ = 3.63E-9 erg cm^{-2} s^{-1} $Å^{-1}$. The curves are labeled with exposure times in seconds.

Figure 13.20: Diffuse Source Signal-to-Noise as a Function of STMAG for G230LB

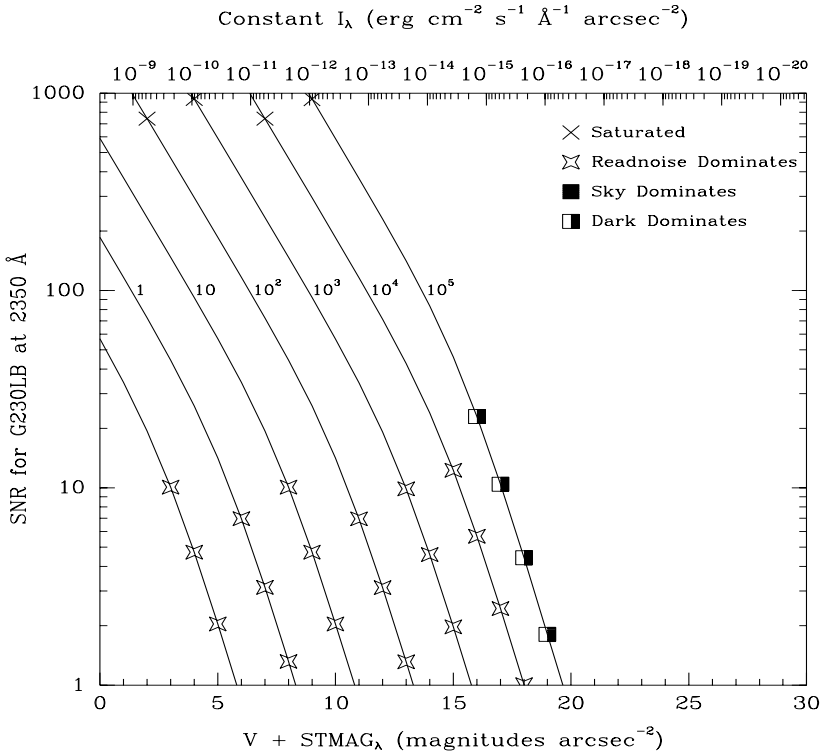

Figure 13.21: Point Source Signal-to-Noise as a Function of STMAG for G230LB

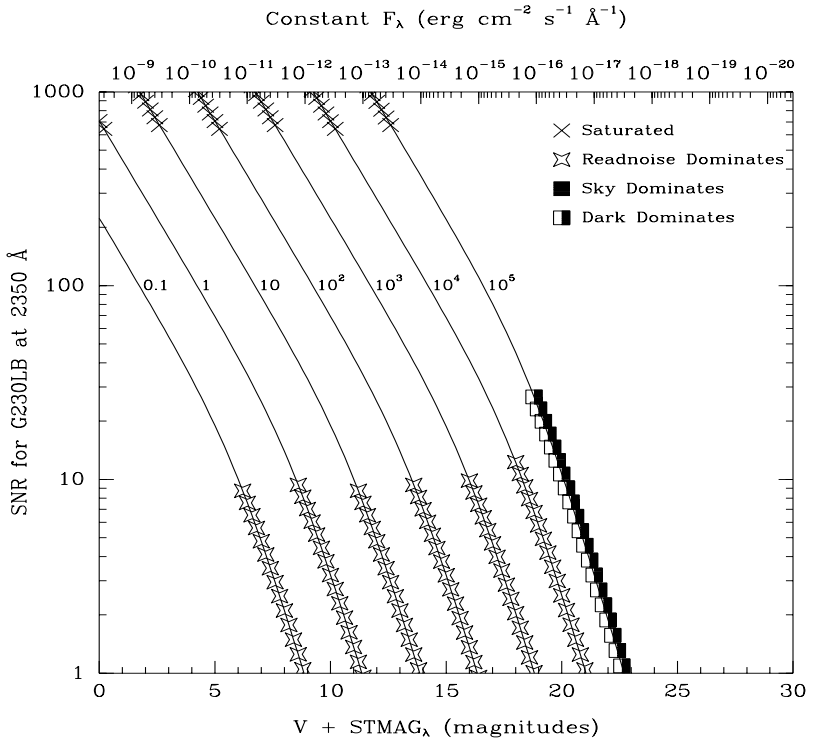

Comparison of G230LB and G230L

The trade-off between using the G230LB or the G230L (which uses the NUV-MAMA), depends sensitively on the science goals and your source properties, since the CCD has read noise, where the MAMA does not; the CCD does not have bright object limits, where the MAMA does; the detector PSF of the CCD is much cleaner than that of the NUV-MAMA; the spatial sampling of the MAMA is better than that of the CCD; the CCD does not enable high time resolution ($\Delta\tau$<10 seconds), where the MAMA does; and the NUV-MAMA is solar insensitive whereas the CCD is not.

Figure 13.22: Comparison of Limiting Magnitudes and Fluxes for G230LB and G230L. Plotted are the limiting source magnitudes and fluxes for G230LB and G230L to achieve a signal-to-noise ratio of 10 per 2-pixel spectral resolution element integrated across the PSF, in 1 hour.

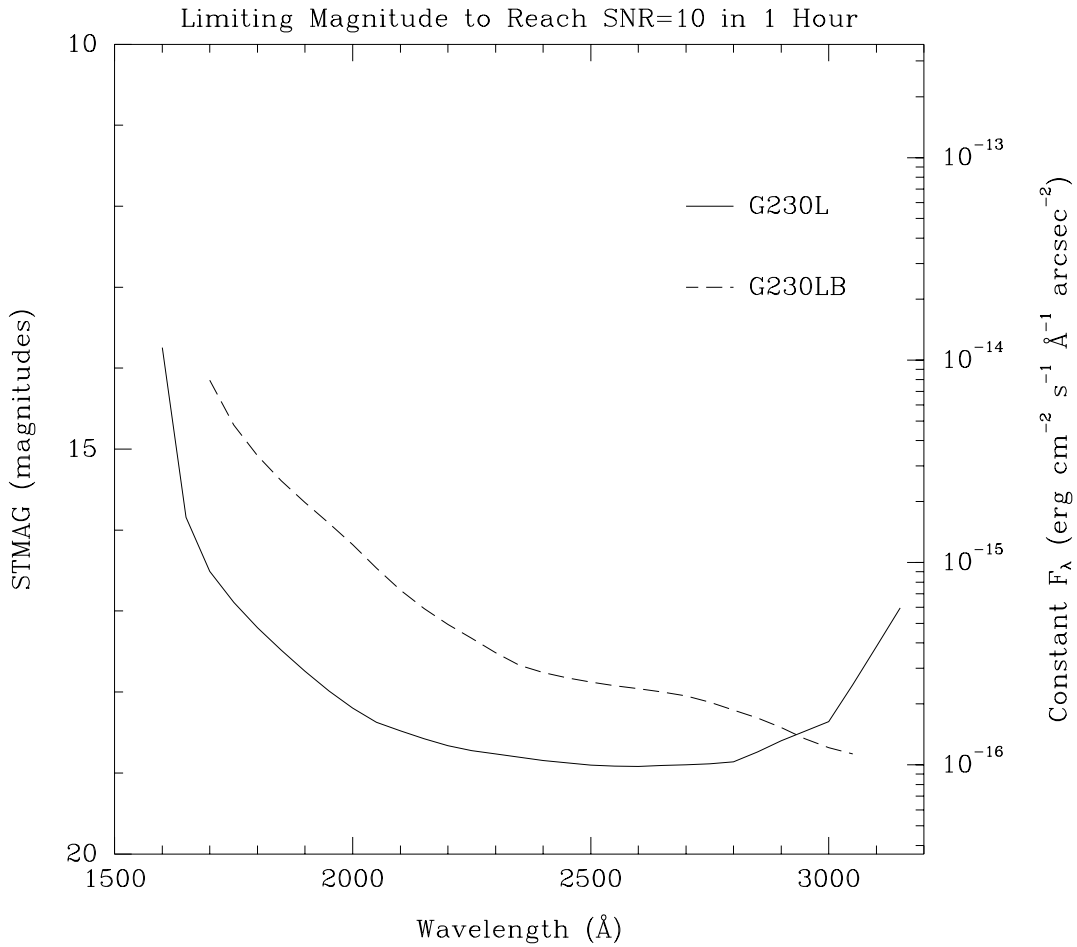

Figure 13.23: Comparison of LSFs for G230LB and G230L

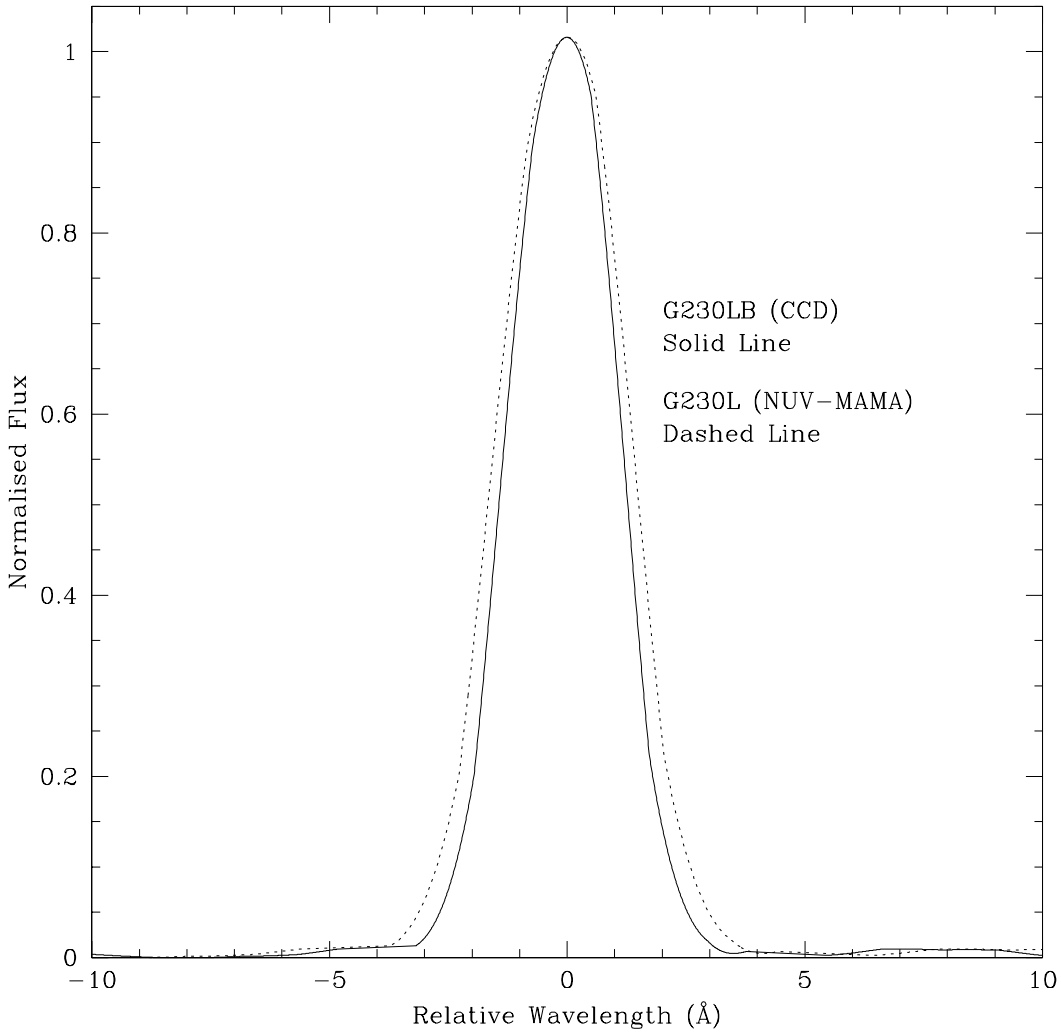

First-Order Grating G230MB

Description

The G230MB grating mode uses an intermediate resolution grating originally designed for use with the NUV-MAMA which has been redirected for use with the CCD to provide R~6000 spectroscopy in the near-UV which takes advantage of the CCD's higher throughput longward of λ=2500 Å. The G230MB grating mode has a spectral range from 1640-3190 Å.

As a single exposure with this grating covers only 150 Å, the grating must be scanned with a series of exposures taken at 11 distinct settings to cover the full spectral range of the grating.

Recommended Uses

The G230MB grating is designed for programs that require the highest available sensitivity in the near-UV from ~2500 to 3100Å or more generally to allow observations of sources too bright for the MAMAs in near-UV.

Special Considerations

In making the plots for the G230MB grating mode, we assumed that the CCD is subject to a change in the effective quantum yield resulting in the creation of multiple electron-hole pairs per photon for λ<3400 Å.

Also be aware that because of the high sensitivity of the CCD to red light, observations of red stars with G230MB are more likely be affected by scatter than observations of red stars using the MAMA G230M mode.

Grating	Spectral Range		Average Dispersion (Å per Pixel)	Plate Scale (arcsec / pixel)	Tilts	Central Wavelengths
	Complete	Per Tilt				
G230MB	1640-3190	155	0.15	0.05	***Prime***	**1713, 1854,1995, 2135, 2276, 2416, 2557, 2697, 2836, 2976, 3115**
					Secondary	2794

Figure 13.24: Wavelength Ranges for the G230MB Grating Settings

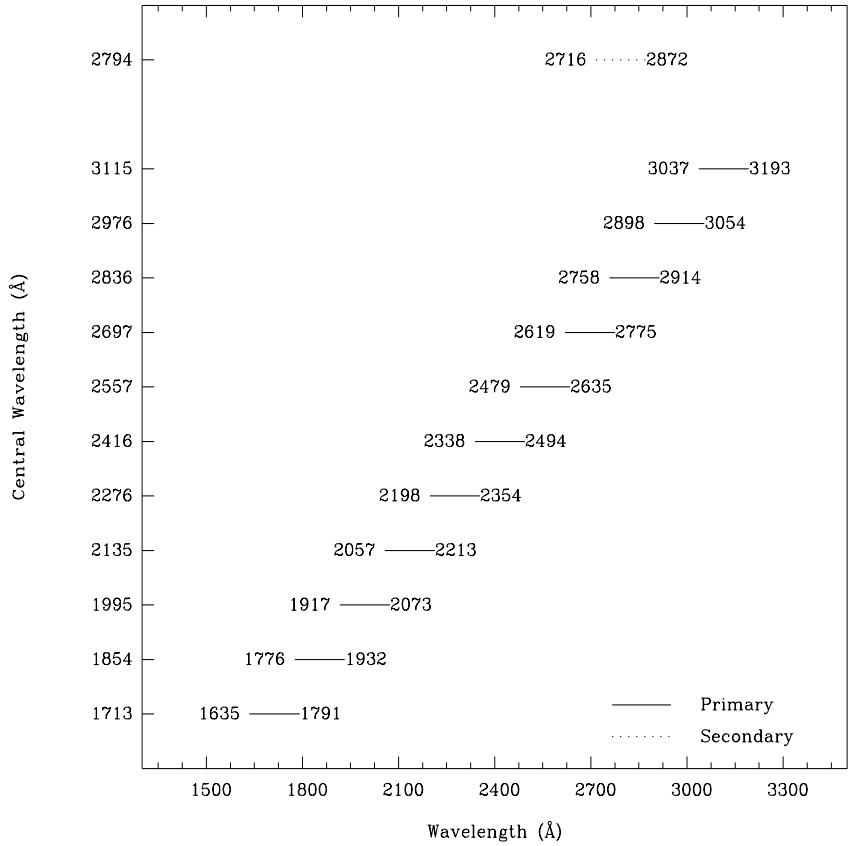

G230MB Sensitivities

Table 13.8: Throughputs & Sensitivities for G230MB

λ	Sensitivity	Throughput
1700	6.8E11	0.1
1800	1.6E12	0.3
1900	2.9E12	0.5
2000	4.8E12	0.7
2100	7.3E12	1.0
2200	9.5E12	1.3
2300	1.2E13	1.5
2400	1.3E13	1.6
2500	1.4E13	1.6
2600	1.4E13	1.6
2700	1.5E13	1.6
2800	1.6E13	1.7
2900	1.9E13	1.9
3000	2.3E13	2.3
3100	2.7E13	2.5

Figure 13.25: G230MB Point Source (left axis), and Diffuse Source (right axis) Sensitivities.

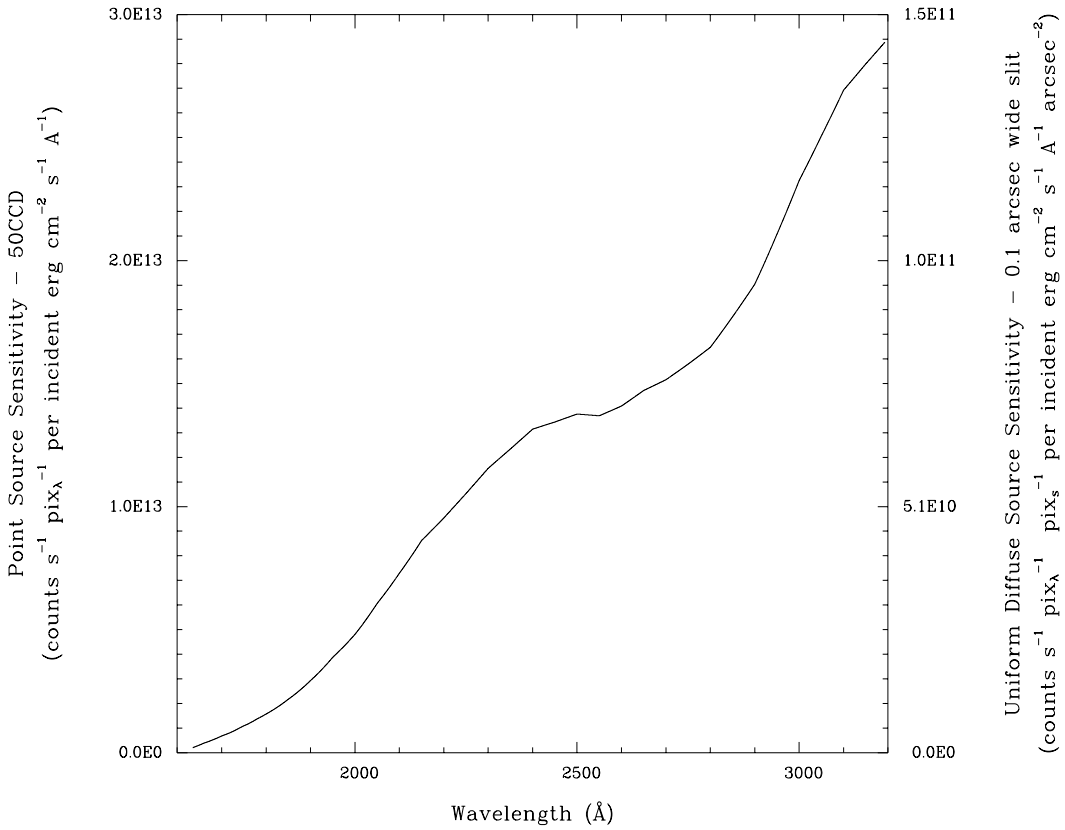

Note

Point source sensitivity assumes full transmission (zero slit losses). Diffuse source sensitivity assumes a 0.1” wide slit. To convert point source sensitivities to diffuse source sensitivities multiply the point source values by the grating spatial (cross dispersion) plate scale in units of arcseconds per pixel and by the width of the desired slit in units of arcseconds.

G230MB Signal-to-Noise

Note:

The top axis displays constant F_λ values corresponding to the STMAG units (V+STMAG$_\lambda$) on the bottom axis. Recall that STMAG=0 is equivalent to F_λ = 3.63E-9 erg cm^{-2} s^{-1} Å^{-1}. The curves are labeled with exposure times in seconds.

Figure 13.26: Diffuse Source Signal-to-Noise as a Function of STMAG for G230MB

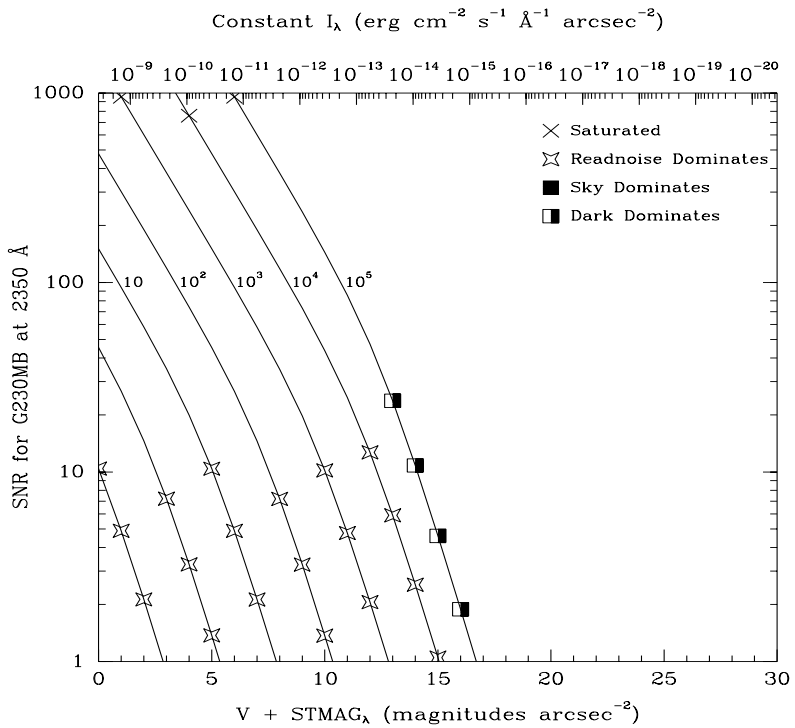

Figure 13.27: Point Source Signal-to-Noise as a Function of STMAG for G230MB

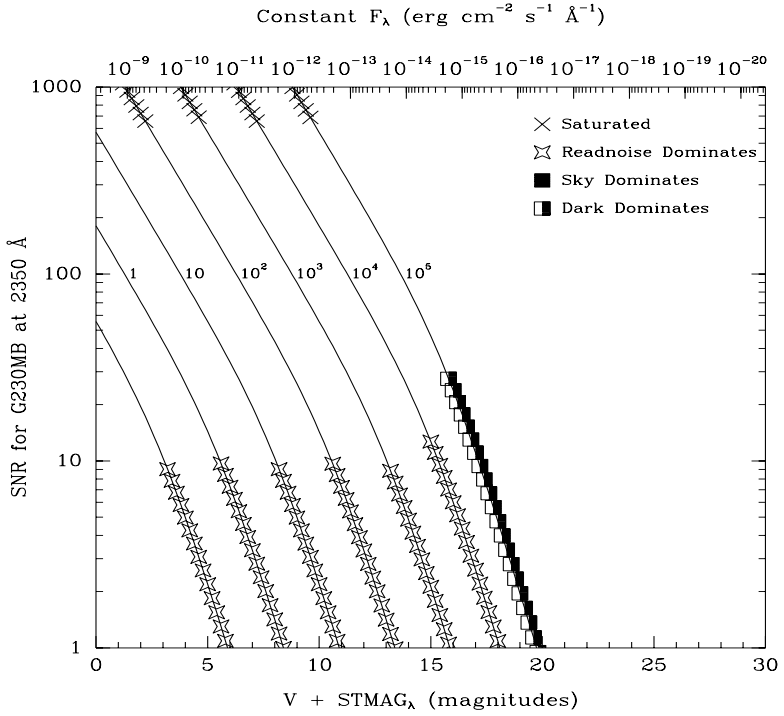

Comparison of G230MB and G230M

The trade-off between using the G230MB or the G230M (which uses the NUV-MAMA) grating modes, depends sensitively on the science goals and your source properties, as described above in “Comparison of G230LB and G230L” on page 243. Figures below show a direct comparison of some of the properties of the G230MB and G230M modes.

Figure 13.28: .Comparison of Limiting Magnitudes and Fluxes for G230MB and G230M. Plotted are the limiting source magnitudes and fluxes for G230MB and G230M to achieve a signal-to-noise ratio of 10 in 1 hour per 2 dispersion pixels and integrated over the PSF.

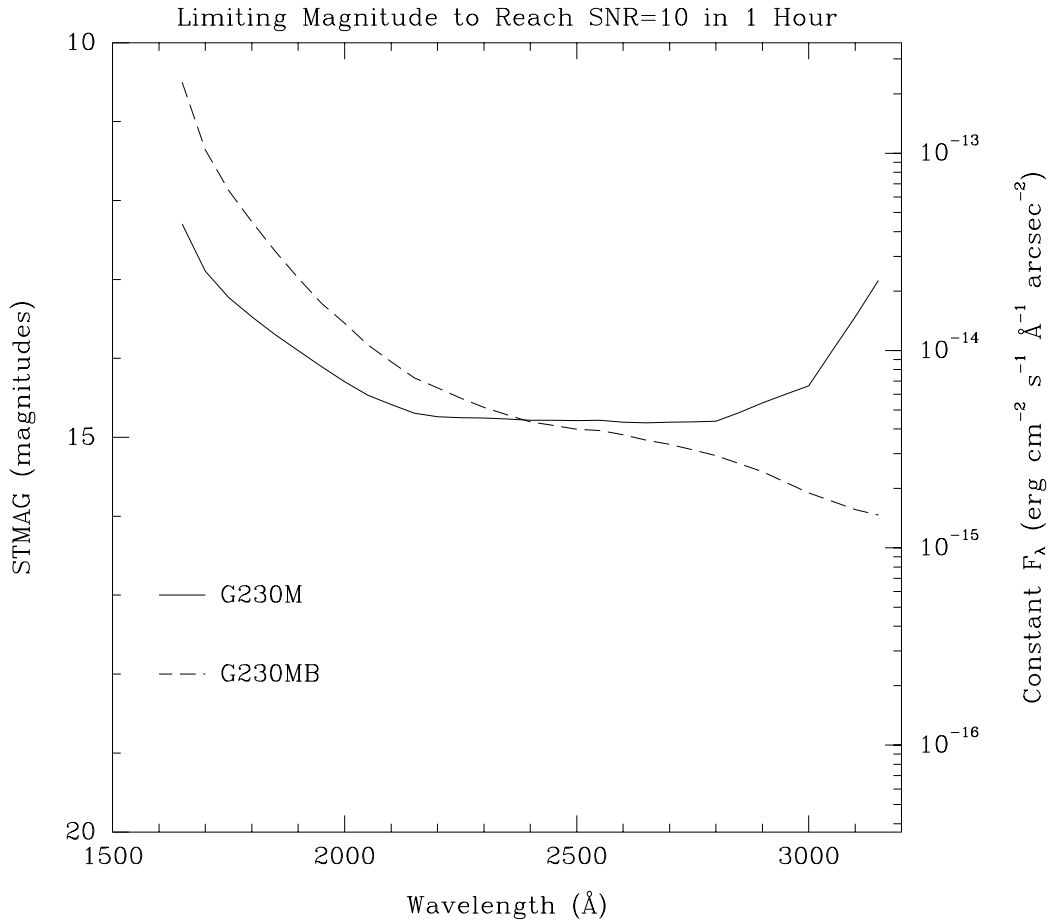

Figure 13.29: Comparison of LSFs for G230MB and G230M

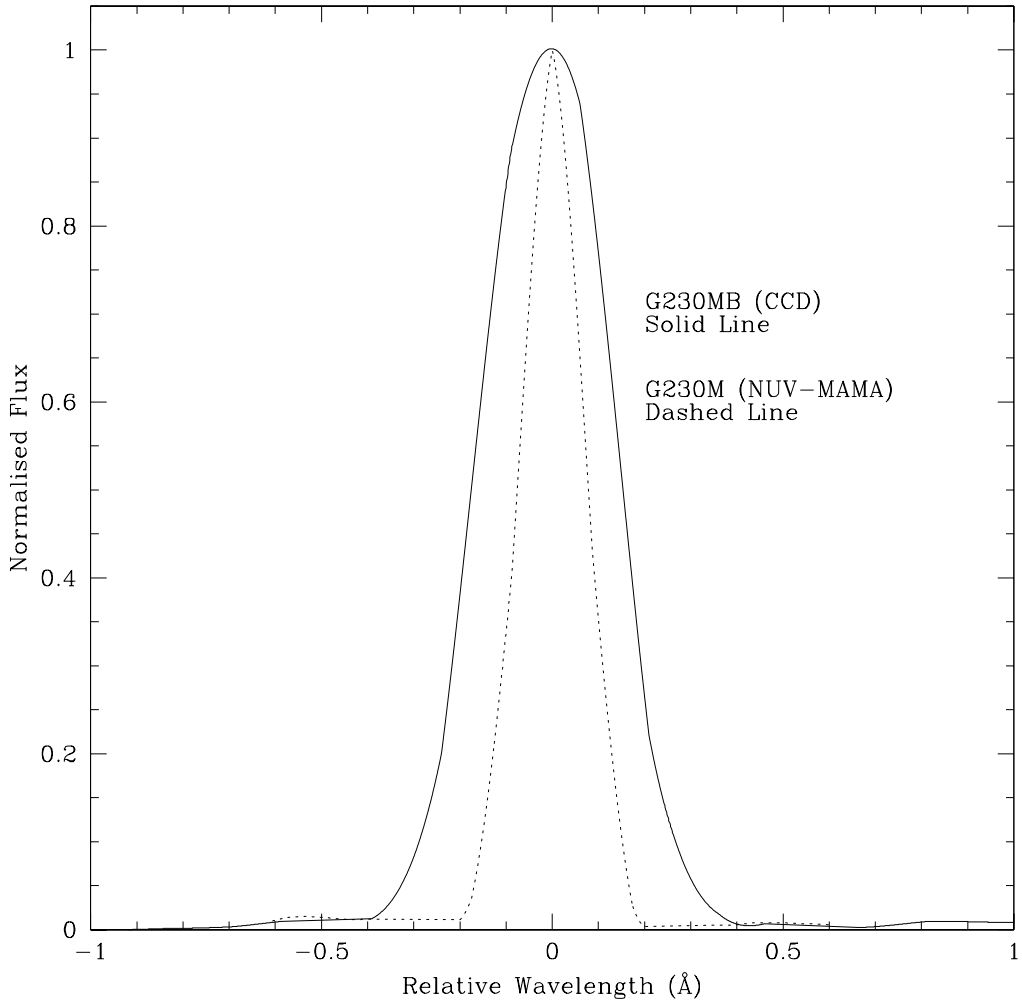

First-Order Grating G230L

Description

The G230L grating is used with the NUV-MAMA and has a relatively high throughput and a resolving power of ~500.

Recommended Uses

G230L is designed for observations where high spectral resolution is not required, but efficient, spatially resolved spectroscopy with full spectral coverage in the near-ultraviolet is desired.

Special Considerations

Notice that the CCD G230LB grating mode also covers the near-ultraviolet with comparable resolution; see “Comparison of G230LB and G230L” on page 243 for a detailed comparison of these two grating modes in that wavelength regime.

Grating	Spectral Range		Average Dispersion (Å per Pixel)	Plate Scale (arcsec / pixel)	Tilts	Central Wavelengths
	Complete	Per Tilt				
G230L	1570-3180	1610	1.58	0.024	***Prime***	**2376**

Figure 13.30: Wavelength Range for the G230L Grating Settings

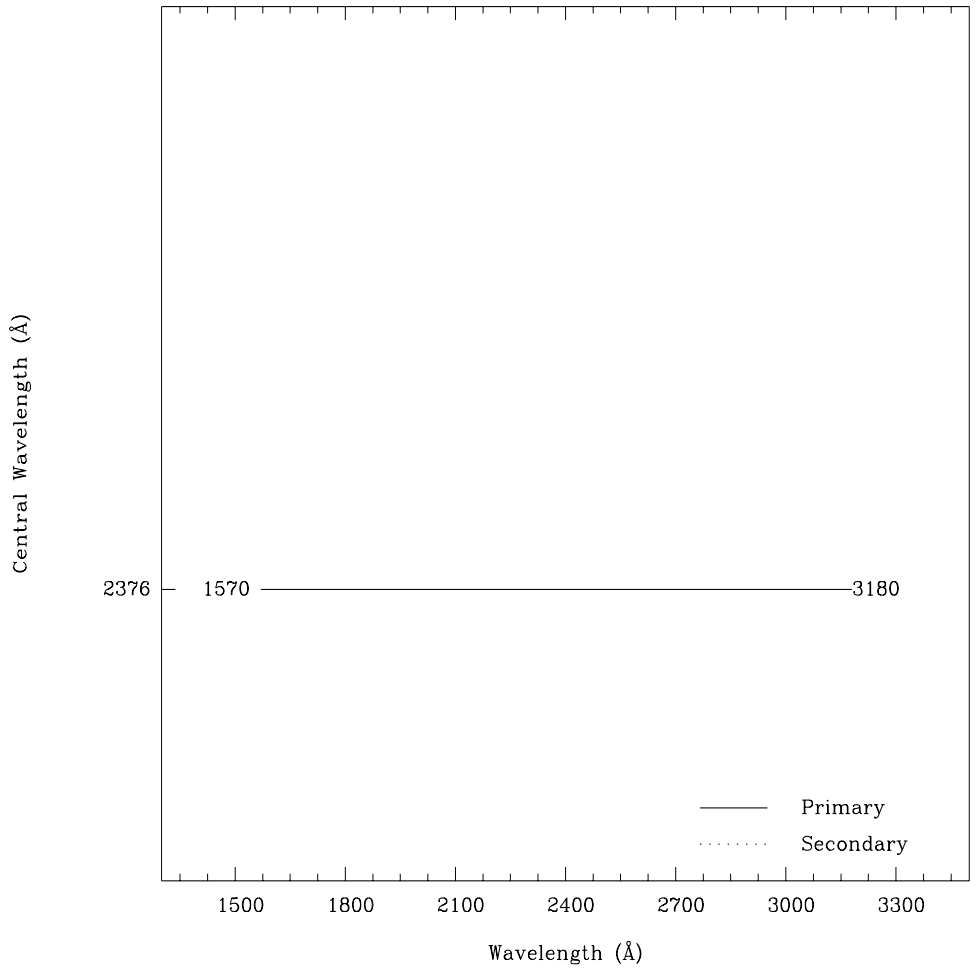

G230L Sensitivities

Table 13.9: Throughputs and Sensitivities for G230L

λ	Sensitivity	Throughput
1600	1.8E12	0.0
1700	2.3E13	0.4
1800	4.3E13	0.7
1900	7.1E13	1.0
2000	1.1E14	1.5
2100	1.4E14	1.8
2200	1.7E14	2.1
2300	1.8E14	2.2
2400	2.0E14	2.2
2500	2.1E14	2.3
2600	2.1E14	2.2
2700	2.1E14	2.1
2800	2.0E14	1.9
2900	1.6E14	1.5
3000	1.3E14	1.2
3100	5.4E13	0.5

Figure 13.31: G230L Point Source (left axis), and Diffuse Source (right axis) Sensitivities.

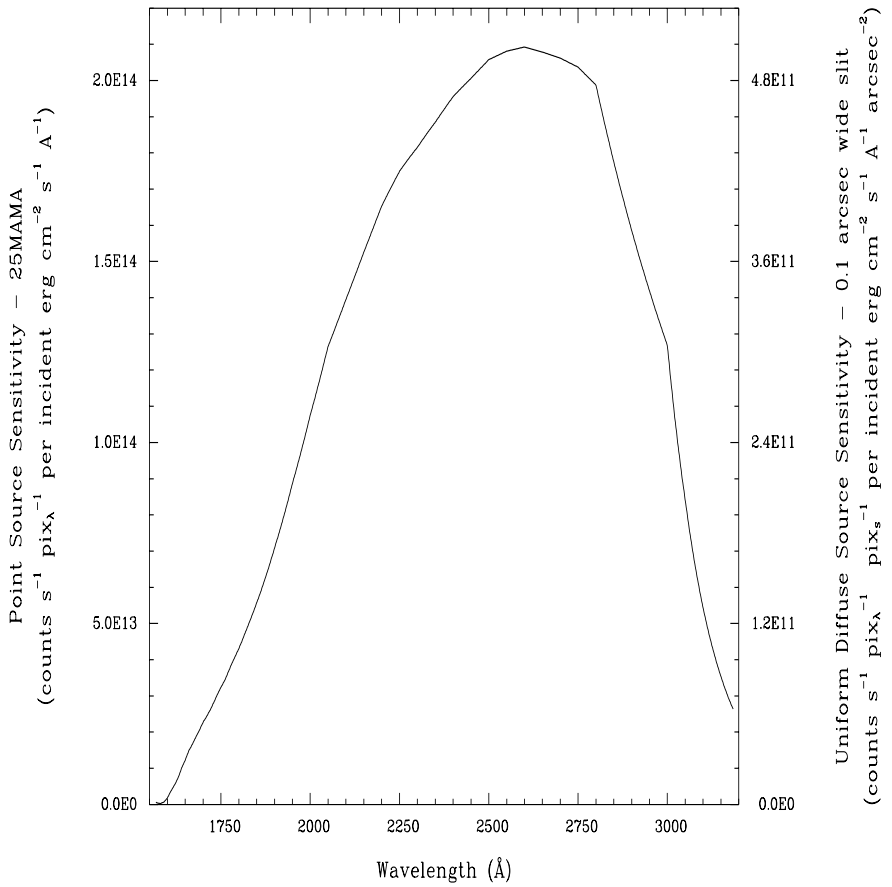

Note

Point source sensitivity assumes full transmission (zero slit losses). Diffuse source sensitivity assumes a 0.1” wide slit. To convert point source sensitivities to diffuse source sensitivities multiply the point source values by the grating spatial plate scale in units of arcseconds per pixel and by the width of the desired slit in units of arcseconds.

G230L Signal-to-Noise

Note:

The top axis displays constant F_λ values corresponding to the STMAG units (V+STMAG$_\lambda$) on the bottom axis. Recall that STMAG=0 is equivalent to F_λ = 3.63E-9 erg cm^{-2} s^{-1} Å^{-1}. The curves are labeled with exposure times in seconds.

Figure 13.32: Diffuse Source Signal-to-Noise as a function of STMAG for G230L

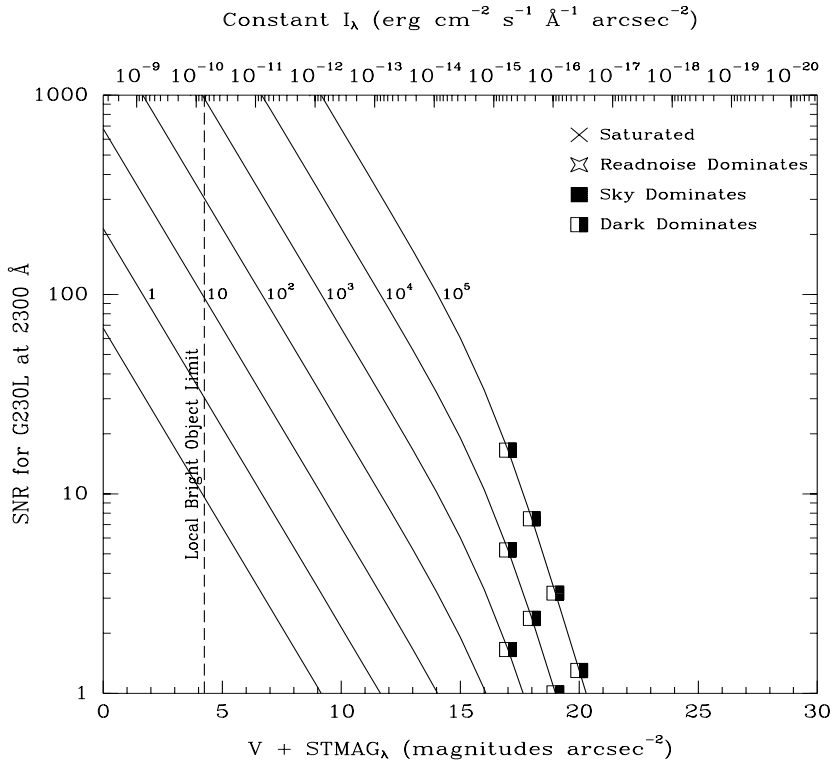

Figure 13.33: Point Source Signal-to-Noise as a Function of STMAG for G230L

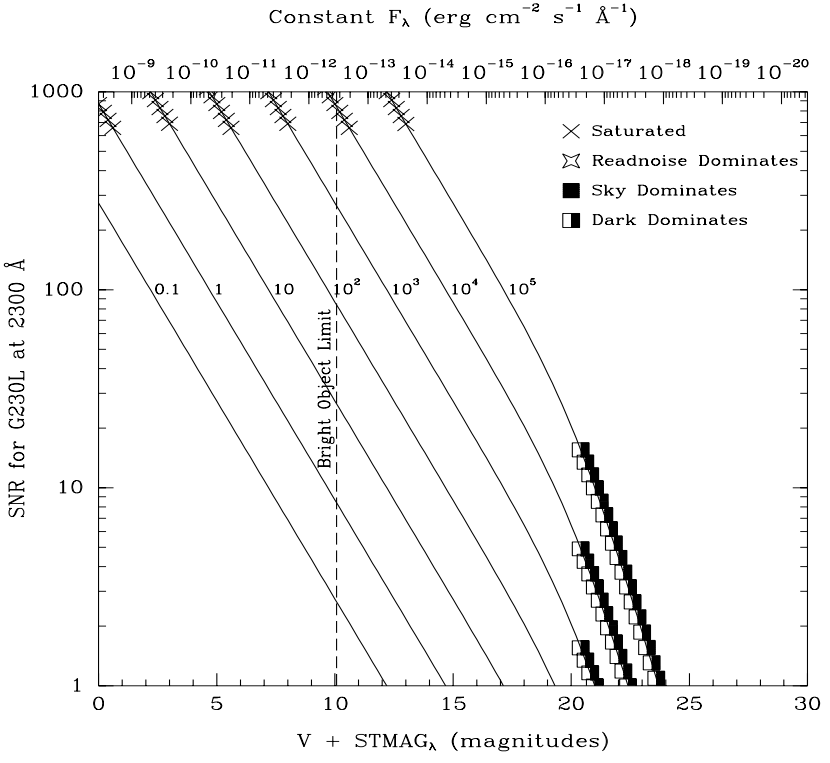

First-Order Grating G230M

Description

Like the G230L grating, the G230M grating is used with the NUV-MAMA; it has a spectral range from 1650-3100 Å, however, with a resolving power R~10,000 a single exposure with the G230M grating covers only 90 Å, and the grating must be scanned, with a series of exposures taken at 18 distinct settings to cover the full spectral range.

Recommended Uses

The G230M grating mode is designed for observations where spatially resolved, long slit, spectroscopy is desired at relatively high spectral resolution covering a limited region of the near-ultraviolet spectrum.

Special Considerations

Notice that the CCD G230MB grating mode also covers the near-ultraviolet with comparable resolution. See “Comparison of G230MB and G230M” on page 248 for a detailed comparison of these two grating modes in that wavelength regime.

Grating	Spectral Range		Average Dispersion (Å per Pixel)	Plate Scale (arcsec / pixel)	Tilts	Central Wavelengths
	Complete	Per Tilt				
G230M	1640-3100	90	0.09	0.029	***Prime***	**1687, 1769, 1851, 1933, 2014, 2095, 2176, 2257, 2338, 2419, 2499, 2579, 2659, 2739, 2818, 2898, 2977, 3055**
					Secondary	1884, 2600, 2800, 2828

Figure 13.34: Wavelength Ranges for the G230M Grating Settings

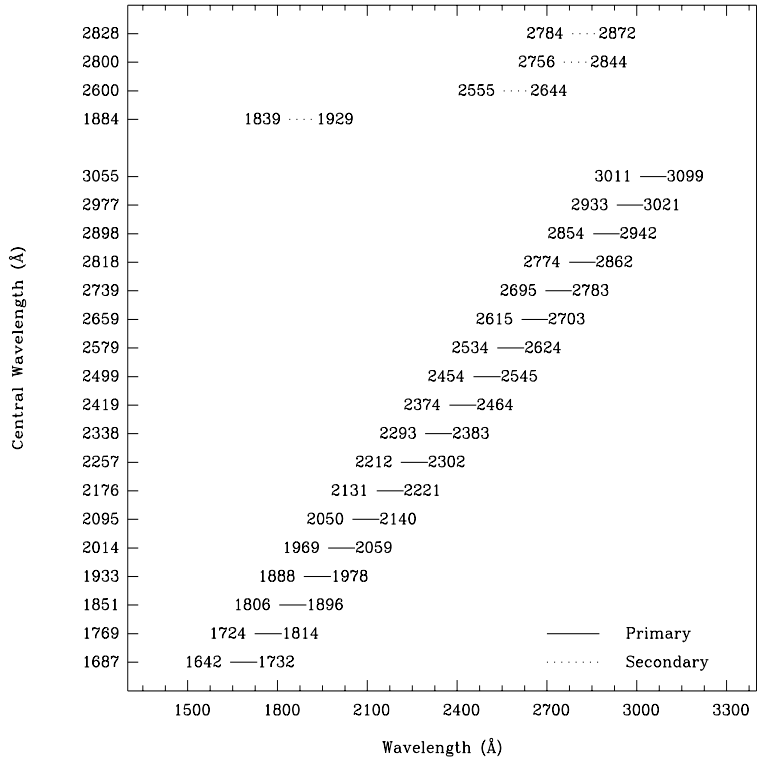

G230M Sensitivities

Table 13.10: G230M Throughput & Sensitivity

λ	Sensitivity	Throughput
1700	8.2E11	0.2
1800	1.4E12	0.4
1900	2.1E12	0.5
2000	3.0E12	0.7
2100	3.9E12	0.9
2200	4.4E12	1.0
2300	4.5E12	1.0
2400	4.6E12	0.9
2500	4.6E12	0.9
2600	4.8E12	0.9
2700	4.8E12	0.9
2800	4.7E12	0.8
2900	3.8E12	0.6
3000	3.1E12	0.5
3100	1.4E12	0.2

Figure 13.35: G230M Point Source (left axis), and Diffuse Source (right axis) Sensitivities.

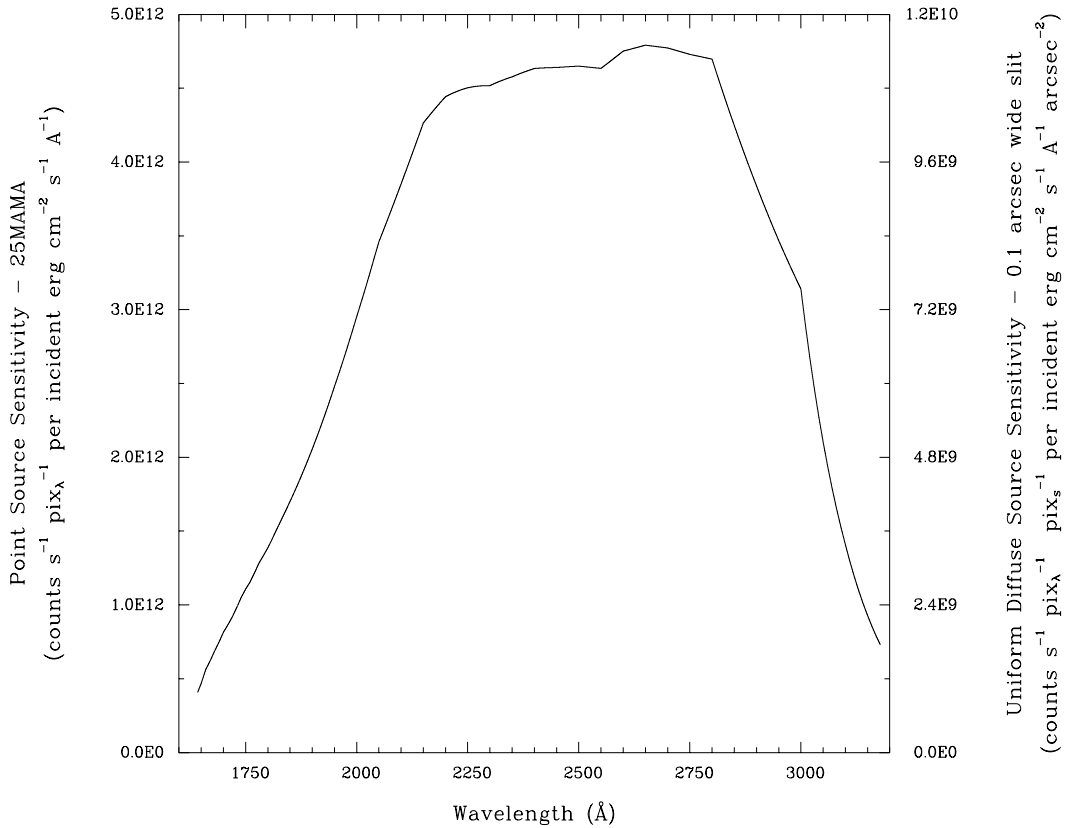

Note

Point source sensitivity assumes full transmission (zero slit losses). Diffuse source sensitivity assumes a 0.1” wide slit. To convert point source sensitivities to diffuse source sensitivities multiply the point source values by the grating spatial (cross dispersion) plate scale in units of arcseconds per pixel and by the width of the desired slit in units of arcseconds.

G230M Signal-to-Noise

Note:

The top axis displays constant F_λ values corresponding to the STMAG units (V+STMAG$_\lambda$) on the bottom axis. Recall that STMAG=0 is equivalent to F_λ = 3.63E-9 erg cm^{-2} s^{-1} Å^{-1}. The curves are labeled with exposure times in seconds.

Figure 13.36: Diffuse Source Signal-to-Noise as a Function of STMAG for G230M

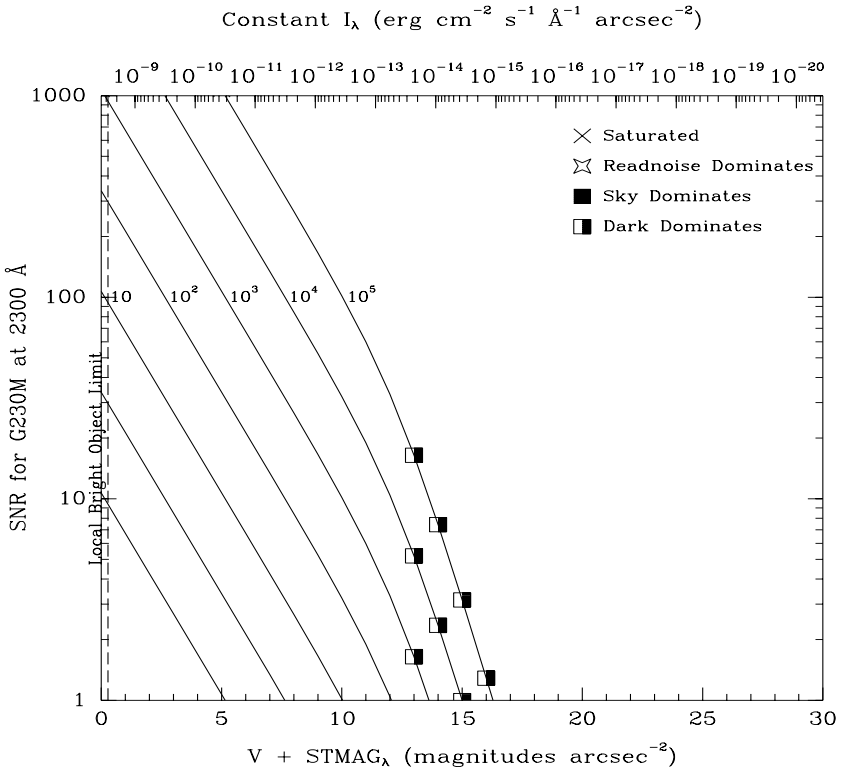

Figure 13.37: Point Source Signal-to-Noise as a Function of STMAG for G230M

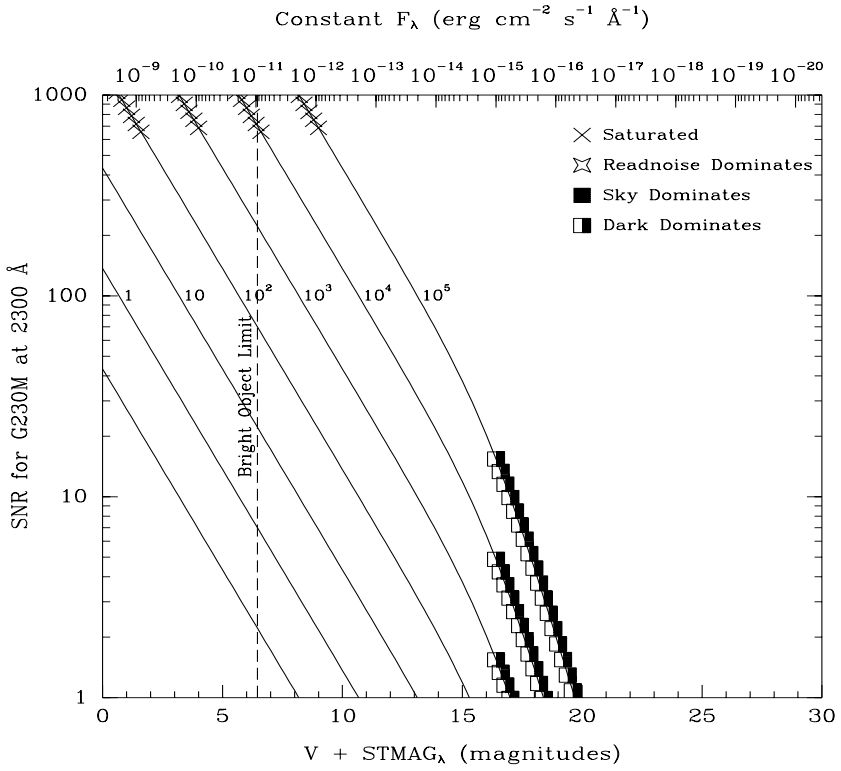

First-Order Grating G140L

Description

The G140L grating mode is used with the FUV-MAMA, has a resolving power R~1000, and covers a spectral range from 1150 to 1700 Å in a single exposure.

Notice, that with two observations, one with G140L and one with G230L, the full spectral region, from 1150 to 3100 Å can be efficiently observed at an R~1000.

Recommended Uses

The G140L grating mode is designed for observations where high spectral resolution is not required, but efficient, spatially resolved spectroscopy providing wide spectral coverage in the ultraviolet is desired.

Grating	Spectral Range		Average Dispersion (Å per Pixel)	Plate Scale (arcsec / pixel)	Tilts	Central Wavelengths
	Complete	Per Tilt				
G140L	1150-1730	610	0.6	0.024	***Prime***	**1425**

Figure 13.38: Wavelength Range for the G140L Grating Setting

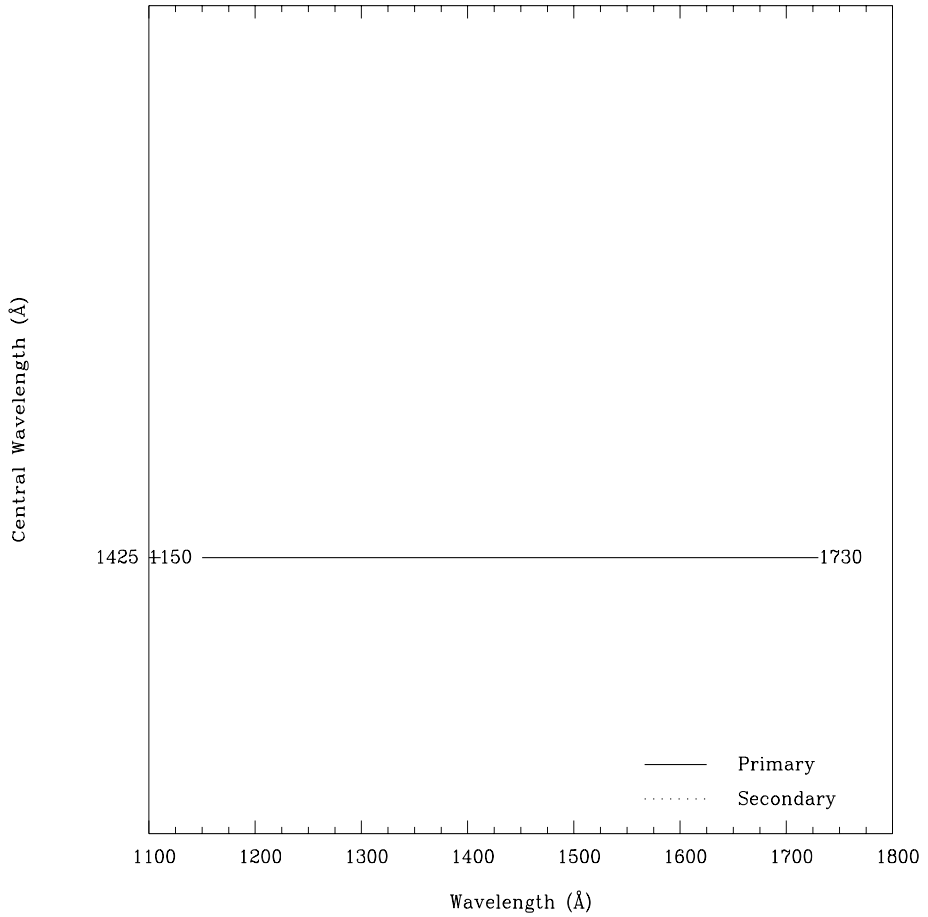

G140L Sensitivity

Table 13.11: Throughputs & Sensitivities for G140L

λ	Sensitivity	Throughput
1200	3.6E13	2.2
1250	6.0E13	3.5
1300	6.4E13	3.6
1350	5.8E13	3.2
1400	4.9E13	2.6
1450	4.0E13	2.0
1500	3.2E13	1.6
1550	2.3E13	1.1
1600	1.5E13	0.7
1650	1.1E13	0.5
1700	8.4E12	0.4

Figure 13.39: G140L Point Source (left axis), and Diffuse Source (right axis) Sensitivities.

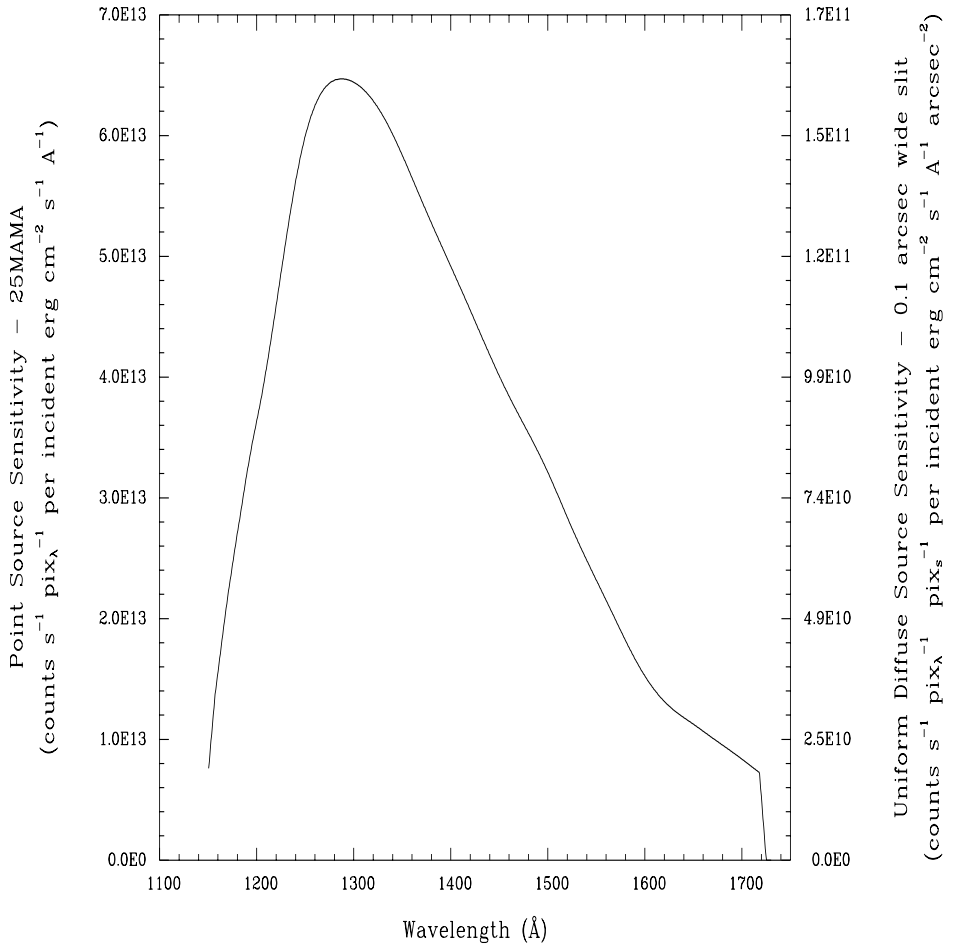

Note

Point source sensitivity assumes full transmission (zero slit losses). Diffuse source sensitivity assumes a 0.1” wide slit. To convert point source sensitivities to diffuse source sensitivities multiply the point source values by the grating spatial plate scale in units of arcseconds per pixel and by the width of the desired slit in units of arcseconds.

G140L Signal-to-Noise

Note:

The top axis displays constant F_λ values corresponding to the STMAG units (V+STMAG$_\lambda$) on the bottom axis. Recall that STMAG=0 is equivalent to F_λ = 3.63E-9 erg cm^{-2} s^{-1} Å^{-1}. The curves are labeled with exposure times in seconds.

Figure 13.40: Diffuse Signal-to-Noise as a Function of STMAG for G140L

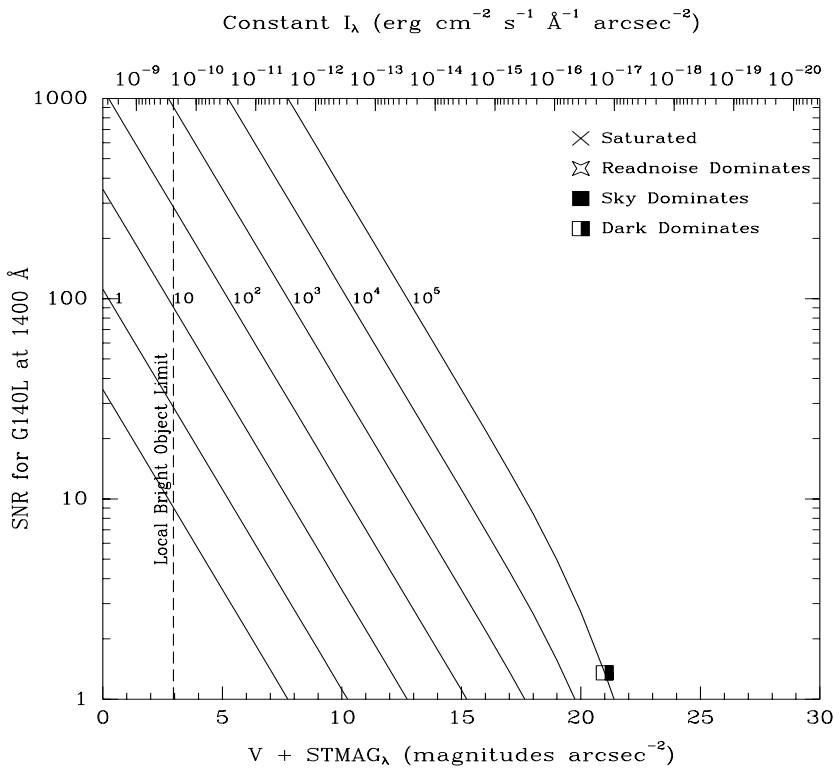

Figure 13.41: Point Source Signal-to-Noise as a Function of STMAG for G140L

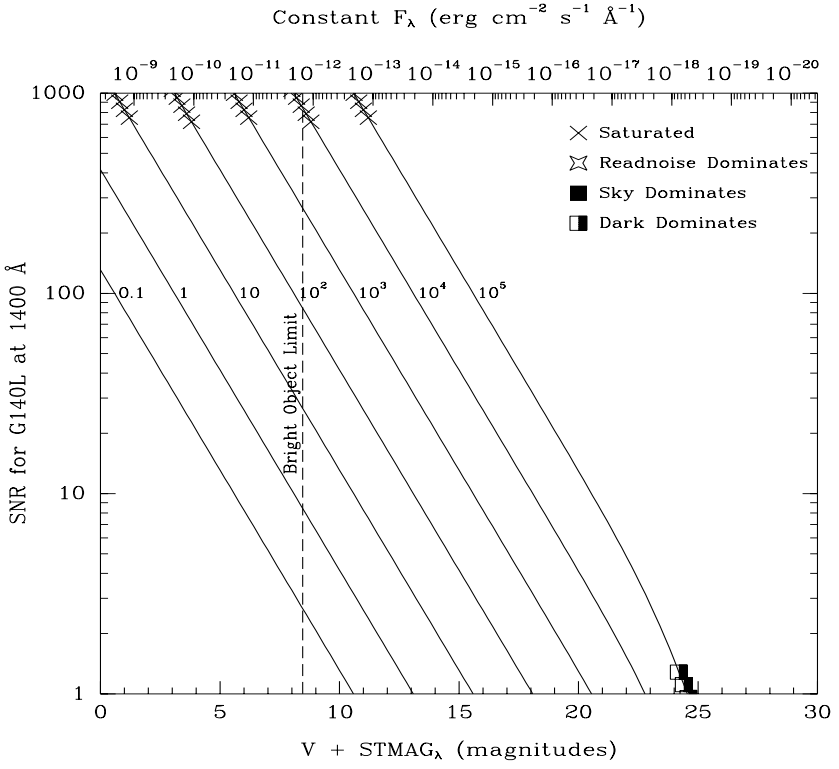

First-Order Grating G140M

Description

The G140M grating mode is used with the FUV-MAMA and has a spectral range from 1150 to 1700 Å.

With a resolving power R~10,000, a single exposure with this grating covers only 55 Å. The grating must be scanned, with a series of exposures taken at 12 distinct settings to cover the full spectral range.

Recommended Uses

The G140M grating mode is designed for observations where spatially resolved, long slit, spectroscopy is desired at relatively high spectral resolution over a limited region of the ultraviolet spectrum.

Grating	Spectral Range		Average Dispersion (Å per Pixel)	Plate Scale (arcsec / pixel)	Tilts	Central Wavelengths
	Complete	Per Tilt				
G140M	1140-1740	55	0.05	0.029	***Prime***	**1173, 1222, 1272, 1321, 1371, 1420, 1470, 1518, 1567, 1616, 1665, 1714**
					Secondary	1218, 1387, 1400, 1540, 1550, 1640

Figure 13.42: Wavelength Ranges for the G140M Grating Settings

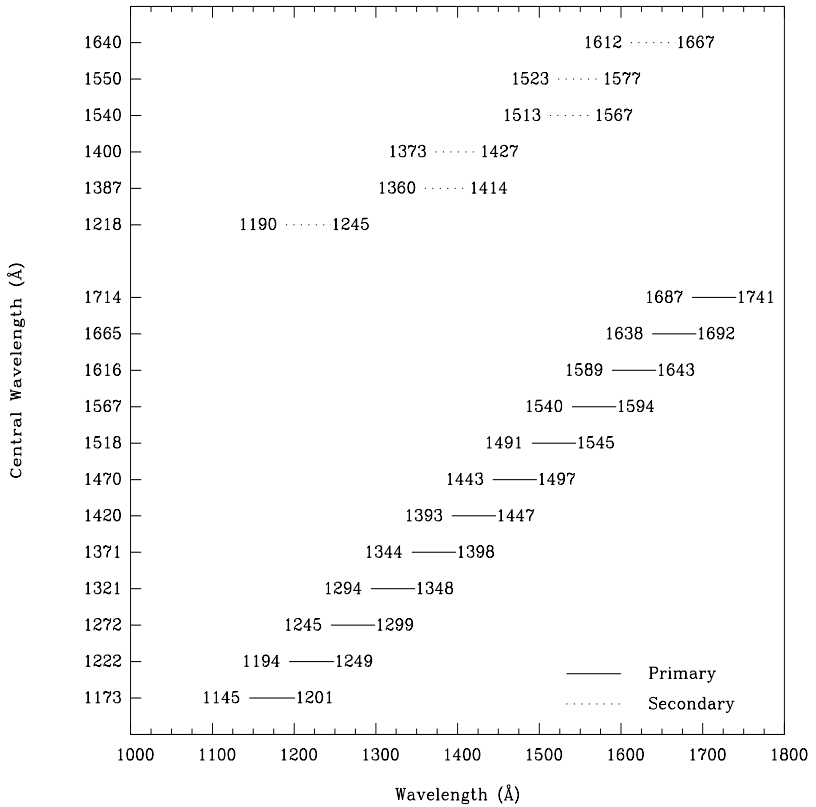

G140M Sensitivities

Table 13.12: Throughputs & Sensitivities for G140M

λ	Sensitivity	Throughput
1200	1.9E12	1.4
1250	3.2E12	2.3
1300	3.4E12	2.3
1350	2.9E12	1.9
1400	2.5E12	1.5
1450	2.0E12	1.2
1500	1.5E12	0.9
1550	1.1E12	0.6
1600	6.8E11	0.4
1650	4.9E11	0.3
1700	0.0E0	0.0

Figure 13.43: G140M Point Source (left axis), and Diffuse Source (right axis) Sensitivities.

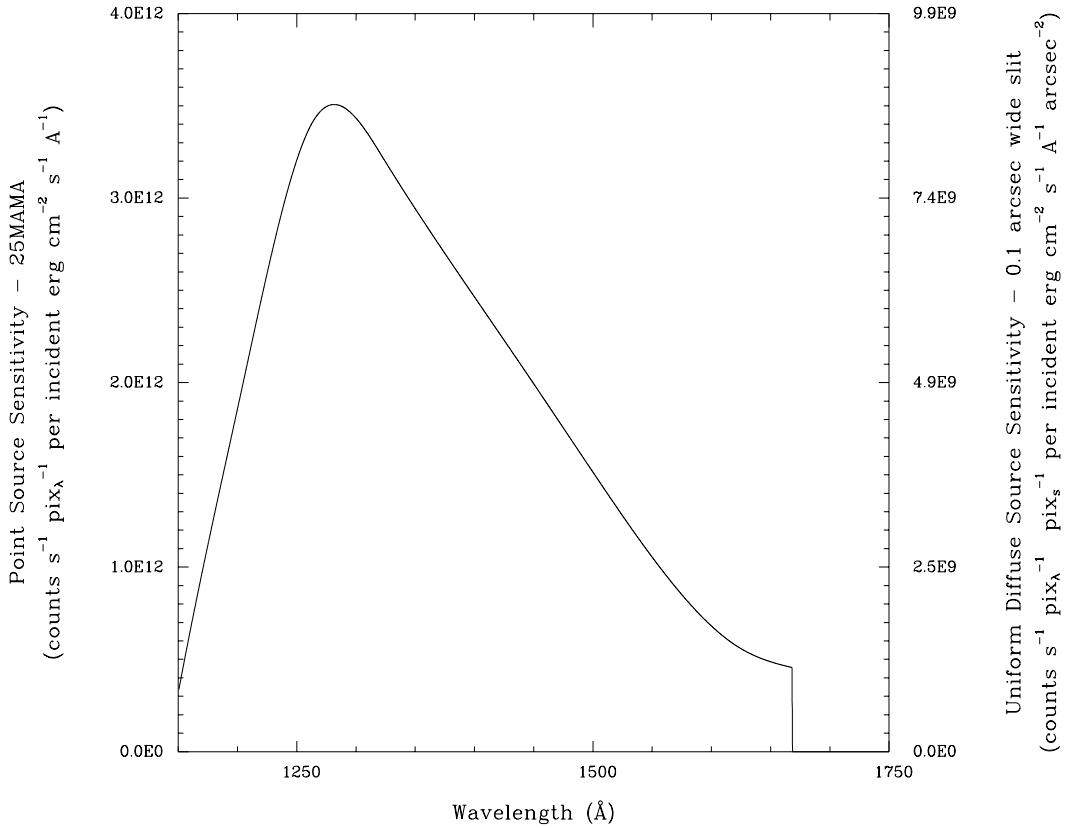

Note

Point source sensitivity assumes full transmission (zero slit losses). Diffuse source sensitivity assumes a 0.1” wide slit. To convert point source sensitivities to diffuse source sensitivities multiply the point source values by the grating spatial plate scale in units of arcseconds per pixel and by the width of the desired slit in units of arcseconds.

G140M Signal-to-Noise

Note:

The top axis displays constant F_λ values corresponding to the STMAG units (V+STMAG$_\lambda$) on the bottom axis. Recall that STMAG=0 is equivalent to F_λ = 3.63E-9 erg cm^{-2} s^{-1} Å^{-1}. The curves are labeled with exposure times in seconds.

Figure 13.44: Diffuse Source Signal-to-Noise as a Function of STMAG for G140M

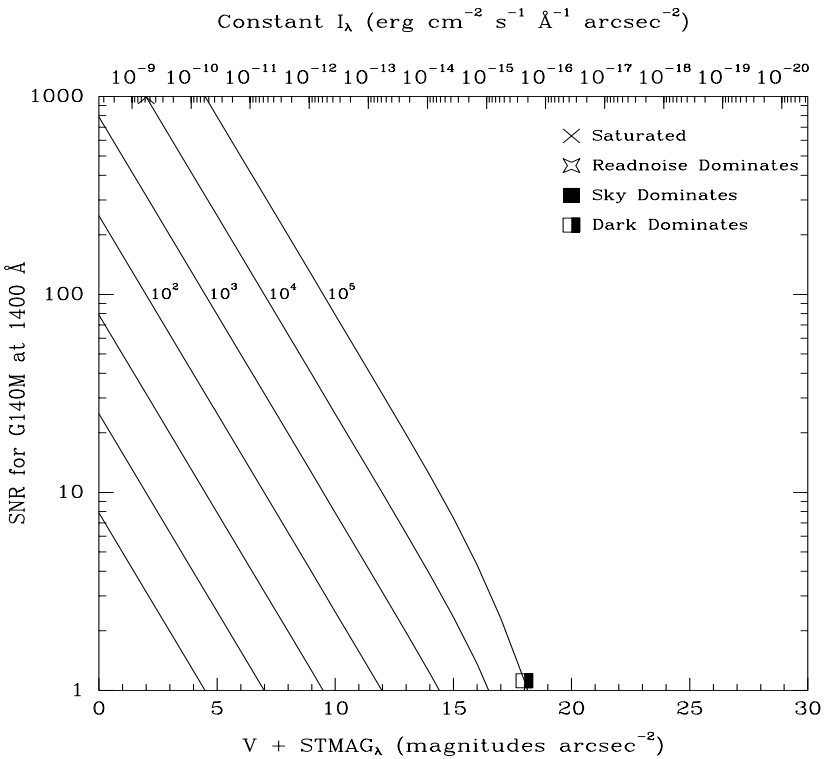

Figure 13.45: Point Source Signal-to-Noise as a Function of STMAG for G140M

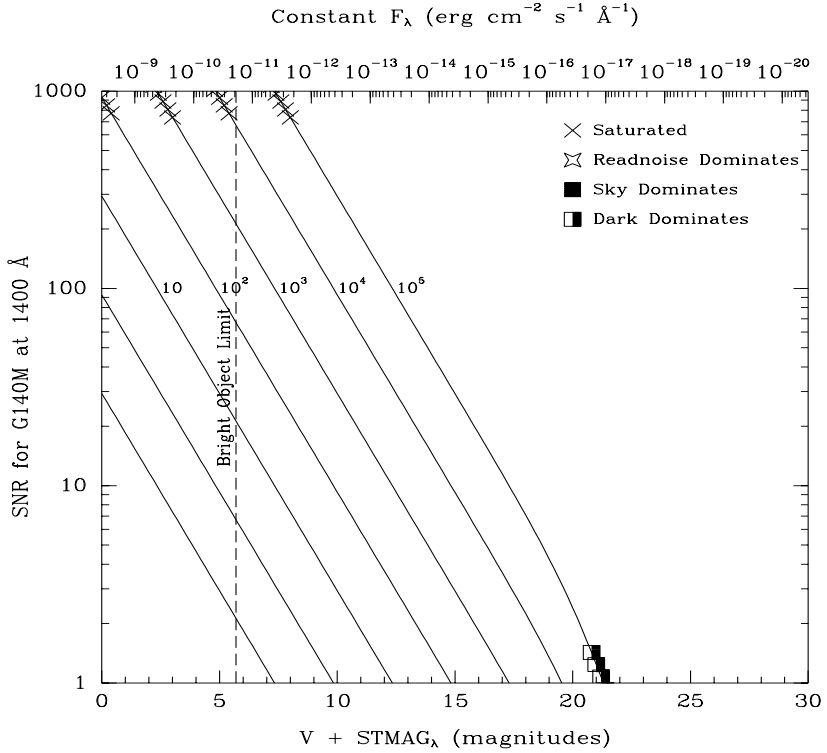

Echelle Grating E230M

Description

The E230M grating is used with the NUV-MAMA and provides echelle spectra at a resolving power of 30,000 from 1570 to 3100 Å.

Special Considerations

A single exposure with this grating covers 800 Å over ~20-40 orders. The interorder separation is ~18 pixels (0.52 arcseconds) at 1650 Å and 62.5 pixels (~1.8 arcseconds) at 3100 Å. The grating must be scanned, with exposures taken at two distinct settings to cover the full spectral range of the grating.

Grating	Spectral Range		Average Dispersion (Å per Pixel)	Dispersion, Cross Dispersion Plate Scales (arcsec / pixel)	Tilts	Central Wavelengths
	Complete	Per Tilt				
E230M	1570-3110	~800	λ/60,000	0.035,0.029	***Prime***	**1978, 2707**
					Secondary	2124, 2269, 2415, 2561

Figure 13.46: Wavelength Ranges for the E230M Grating Settings

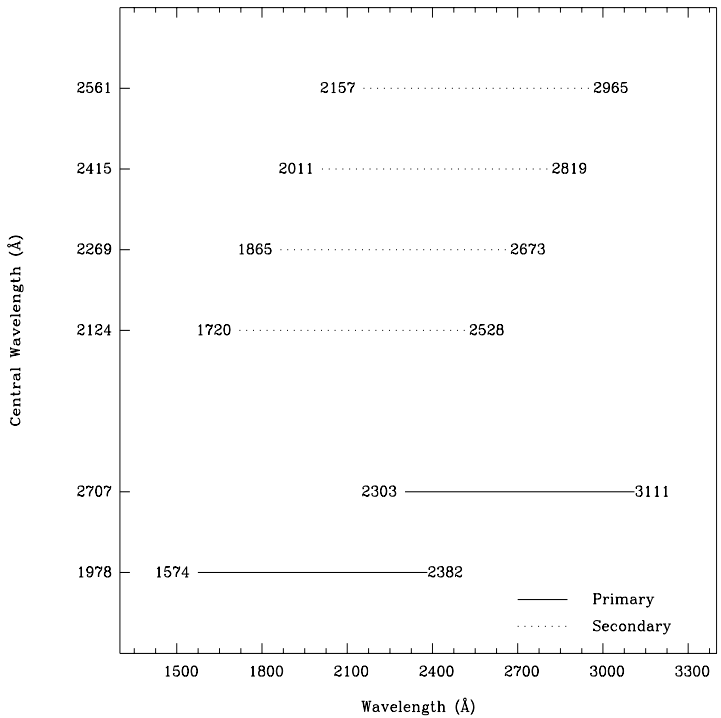

E230M Sensitivities

Table 13.13: Throughputs & Sensitivities for E230M

λ	Sensitivity	Throughput
1700	1.4E11	0.13
1800	2.9E11	0.24
1900	4.4E11	0.32
2000	6.4E11	0.42
2100	9.9E11	0.59
2200	1.4E12	0.76
2300	1.7E12	0.86
2400	2.0E12	0.93
2500	2.4E12	0.99
2600	2.6E12	1.01
2700	2.7E12	0.97
2800	2.6E12	0.88
2900	2.4E12	0.75
3000	1.9E12	0.54

Figure 13.47: E230M Point Source (left axis), and Diffuse Source (right axis) Sensitivities.

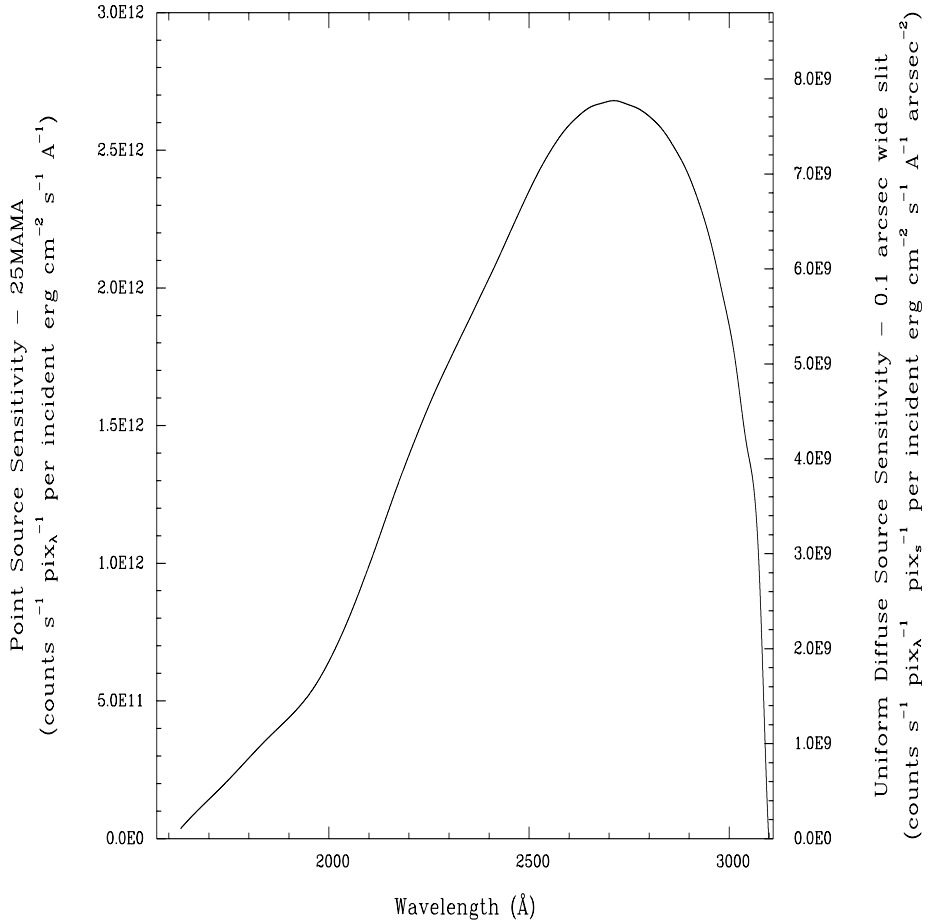

Note

Point source sensitivity assumes full transmission (zero slit losses). Diffuse source sensitivity assumes a 0.1” wide slit. To convert point source sensitivities to diffuse source sensitivities multiply the point source values by the grating spatial (cross dispersion) plate scale in units of arcseconds per pixel and by the width of the desired slit in units of arcseconds.

E230M Signal-to-Noise

Note:

The top axis displays constant F_λ values corresponding to the STMAG units (V+STMAG$_\lambda$) on the bottom axis. Recall that STMAG=0 is equivalent to F_λ = 3.63E-9 erg cm^{-2} s^{-1} Å^{-1}. The curves are labeled with exposure times in seconds.

Figure 13.48: Diffuse Source Signal-to-Noise as a function of STMAG for E230M

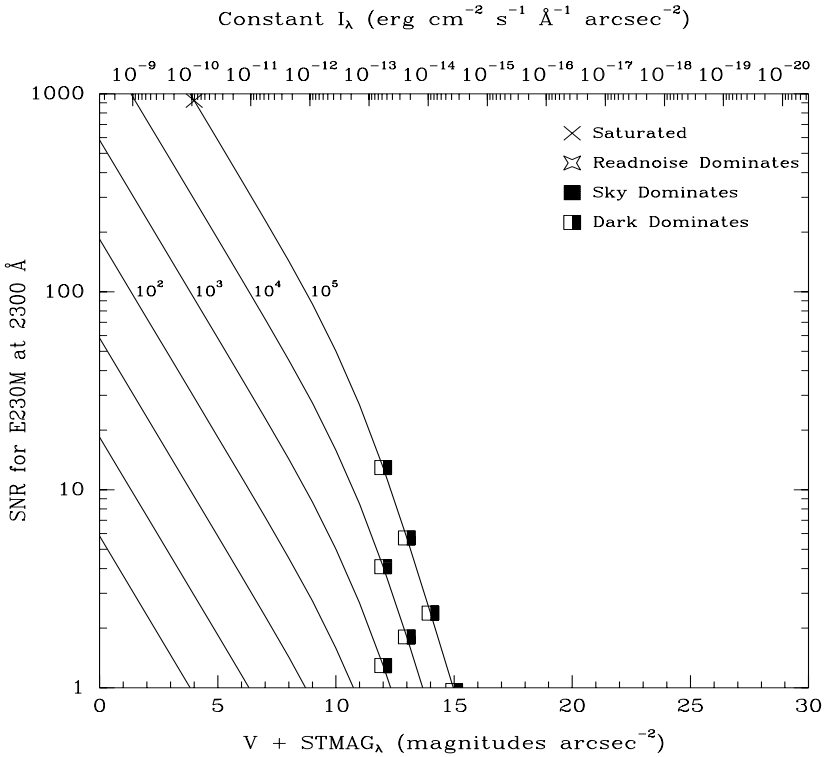

Figure 13.49: Point Source Signal-to-Noise as a Function of STMAG for E230M

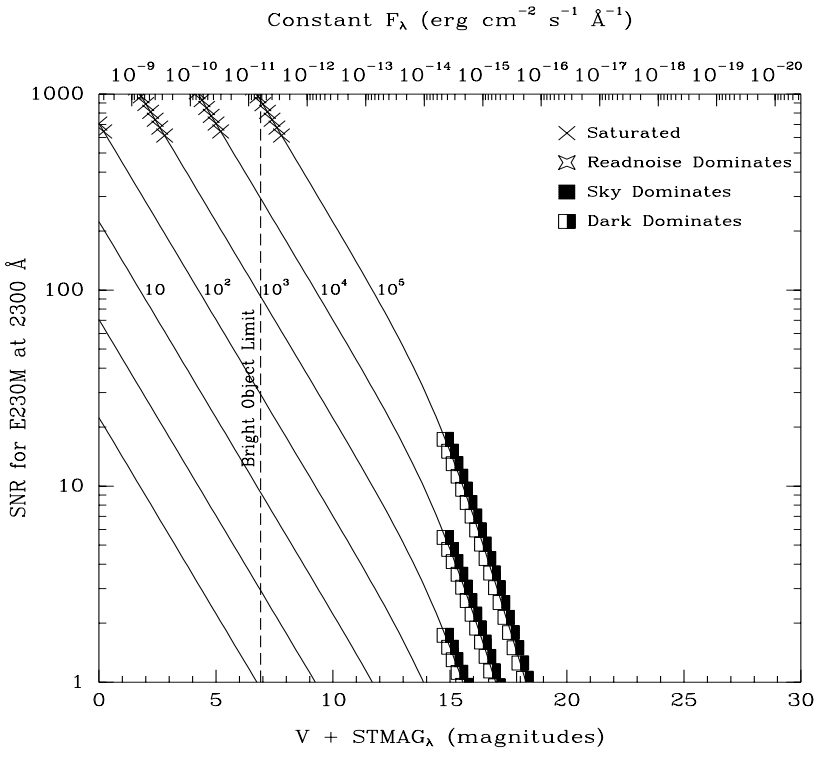

Echelle Grating E230H

Description

The E230H grating is used with the NUV-MAMA and provides echelle spectra at a resolving power of ~110,000 from 1620 to 3100 Å.

Special Considerations

A single E230H echellogram covers ~267 Å, over ~20-70 orders. The orders are spaced by only ~ 12.7 pixels (0.37 arcseconds) at 1650 Å and 47.2 pixels (~1.38 arcseconds) at 3100 Å. The grating must be scanned, with exposures taken at six distinct settings to cover the full spectral range of the grating.

The secondary central wavelength at 2812 Å has had direct sensitivity calibrations performed during Cycle 7 to support the large number of observations using that position.

Grating	Spectral Range		Average Dispersion (Å per Pixel)	Dispersion, Cross Dispersion Plate Scale (arcsec / pixel)	Tilts	Central Wavelengths
	Complete	Per Tilt				
E230H	1620-3150	~267	λ/228,000	0.047,0.029	***Prime***	**1763, 2013, 2263, 2513, 2762, 3012**
					Secondary	1813, 1863, 1913, 1963, 2063, 2113, 2163, 2213, 2313, 2363, 2413, 2463, 2563, 2613, 2663, 2713, 2812, 2862, 2912, 2962

Figure 13.50: Wavelength Ranges for the E230H Grating Settings

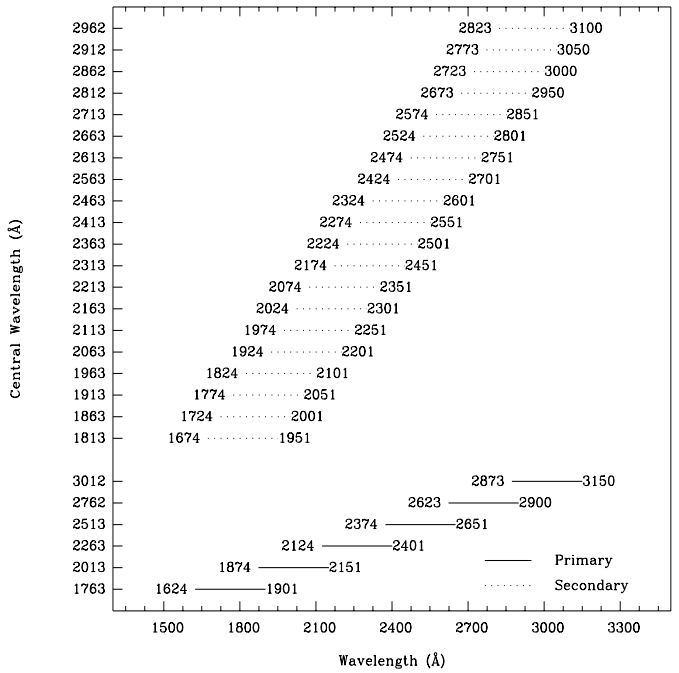

E230H Sensitivities

Table 13.14: Throughputs and Sensitivities for E230H

λ	Sensitivity	Throughput
1700	4.2E10	0.15
1800	7.4E10	0.23
1900	1.0E11	0.28
2000	1.4E11	0.34
2100	1.9E11	0.44
2200	2.6E11	0.53
2300	3.1E11	0.59
2400	3.4E11	0.59
2500	3.8E11	0.61
2600	4.1E11	0.60
2700	4.1E11	0.56
2800	4.0E11	0.51
2900	3.6E11	0.43
3000	2.8E11	0.31
3100	1.7E11	0.17

Figure 13.51: E230H Point Source (left axis), and Diffuse Source (right axis) Sensitivities.

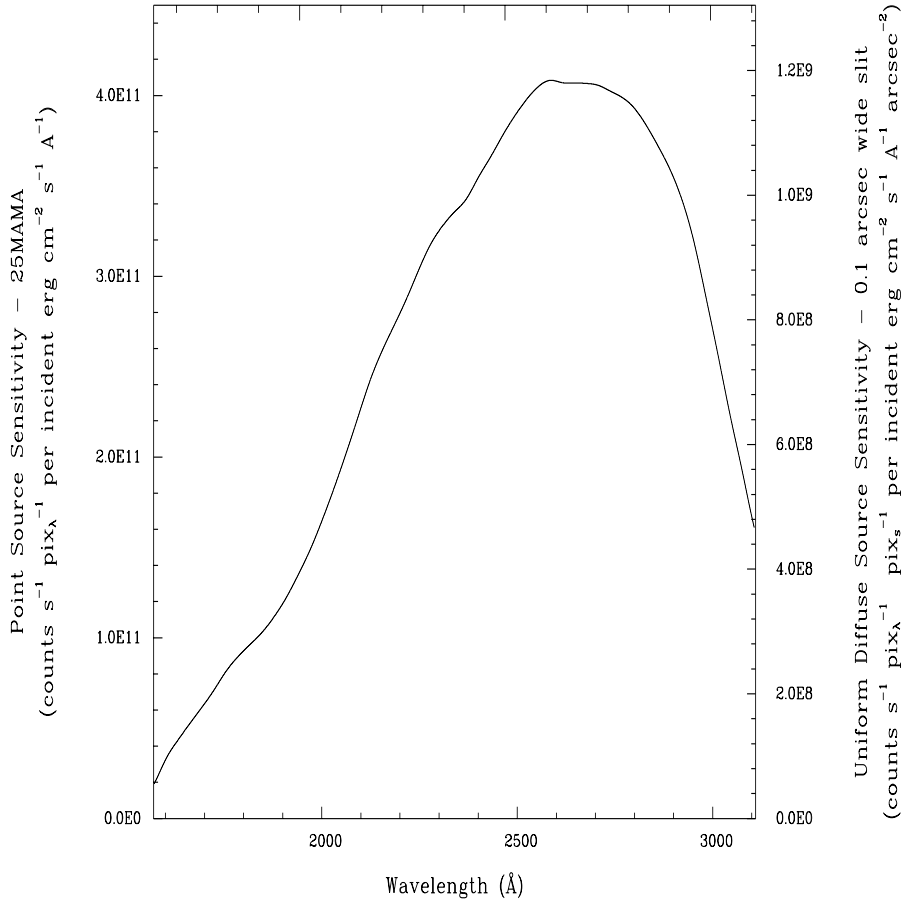

Note

Point source sensitivity assumes full transmission (zero slit losses). Diffuse source sensitivity assumes a 0.1” wide slit. To convert point source sensitivities to diffuse source sensitivities multiply the point source values by the grating spatial (cross dispersion) plate scale in units of arcseconds per pixel and by the width of the desired slit in units of arcseconds.

E230H Signal-to-Noise

Note:

The top axis displays constant F_λ values corresponding to the STMAG units (V+STMAG$_\lambda$) on the bottom axis. Recall that STMAG=0 is equivalent to F_λ = 3.63E-9 erg cm^{-2} s^{-1} Å^{-1}. The curves are labeled with exposure times in seconds.

Figure 13.52: Diffuse Source Signal-to-Noise as a Function of STMAG for E230H

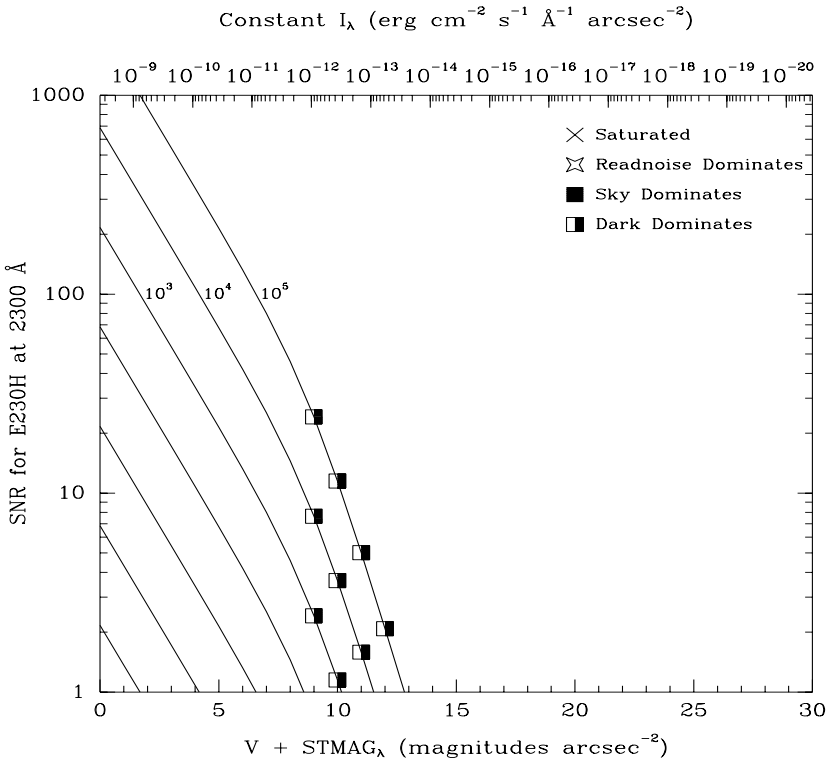

Figure 13.53: Point Source Signal-to-Noise as a Function of STMAG for E230H

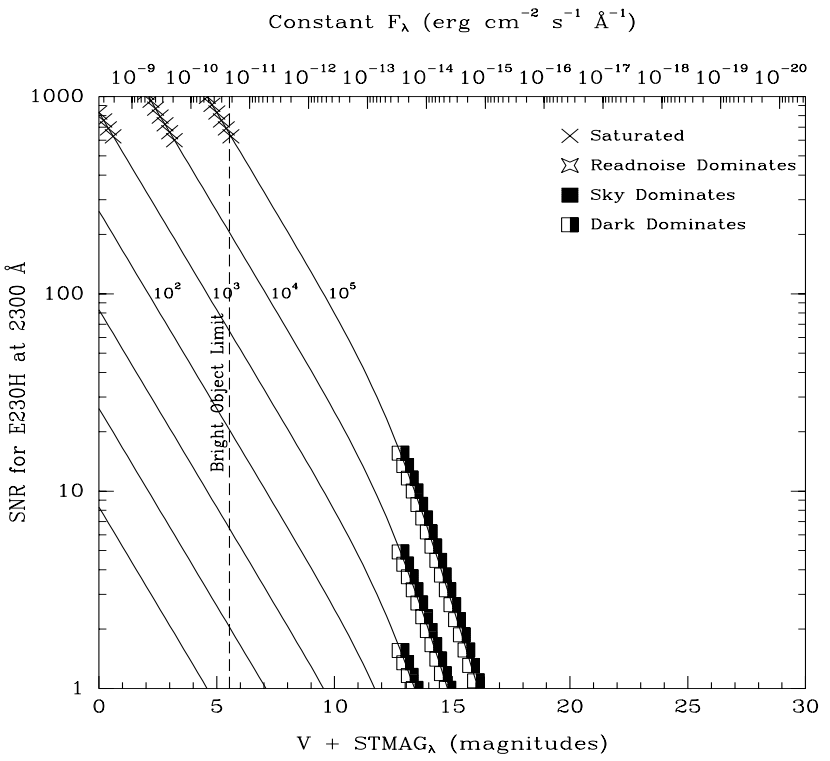

Echelle Grating E140M

Description

The E140M grating is used with the FUV-MAMA and provides echelle spectra at a resolving power of 45,800 from 1123–1710 Å.

Special Considerations

A single E140M echellogram covers ~600 Å, however at wavelengths longward of 1649 Å, the echelle orders overrun the width of the detector in the dispersion direction, so there will be three small gaps in the wavelength coverage. One gap of ~0.2 Å, one of ~0.4 Å, and one of ~0.7 Å occur between 1649 and 1700 Å.

The separation between orders is ~15 pixels (or 0.44 arcseconds) at 1150 Å and ~33 (0.96 arcseconds) at 1700 Å.

Grating	Spectral Range		Average Dispersion (Å per Pixel)	Dispersion, Cross Dispersion Plate Scale (arcsec / pixel)	Tilts	Central Wavelengths
	Complete	Per Tilt				
E140M	1123–1710	620	λ/91,700	0.036,0.029	***Prime***	**1425**

Figure 13.54: Wavelength Range for the E140M Grating Setting

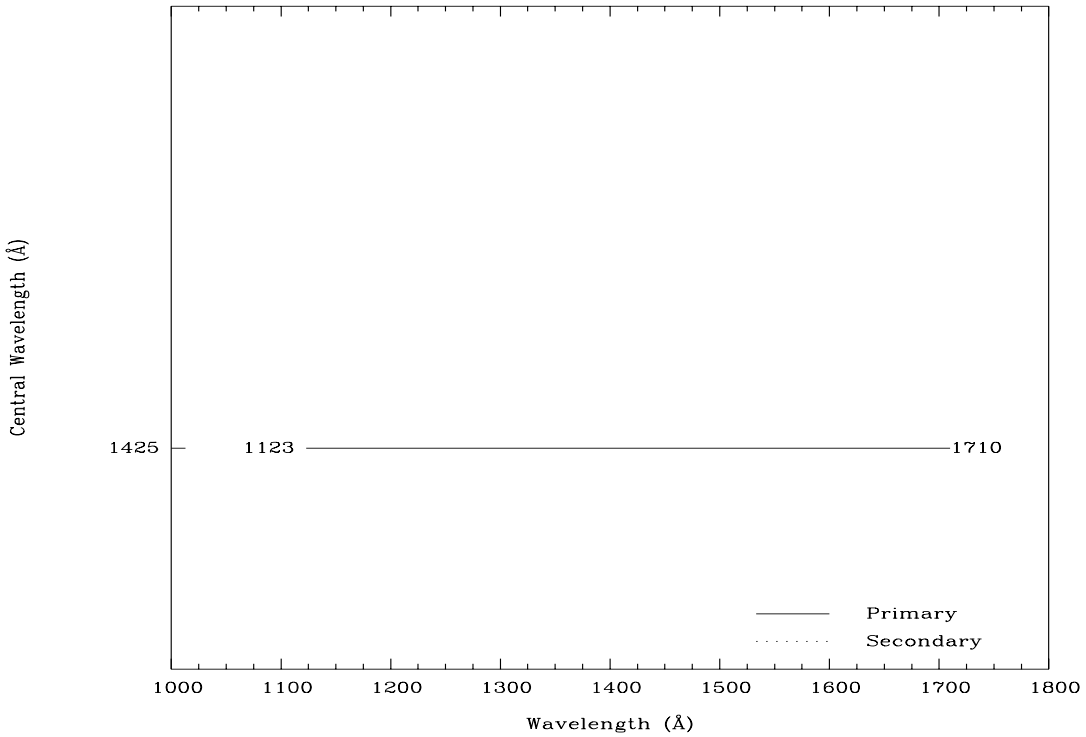

E140M Sensitivity

Table 13.15: Throughputs & Sensitivities for E140M

λ	Sensitivity	Throughput
1200	2.1E11	0.38
1250	4.4E11	0.75
1300	5.6E11	0.87
1350	5.8E11	0.83
1400	5.4E11	0.72
1450	4.8E11	0.60
1500	4.2E11	0.49
1550	3.2E11	0.35
1600	2.2E11	0.23
1650	1.8E11	0.17
1700	1.4E11	0.13

Figure 13.55: E140M Point Source (left axis), and Diffuse Source (right axis) Sensitivities.

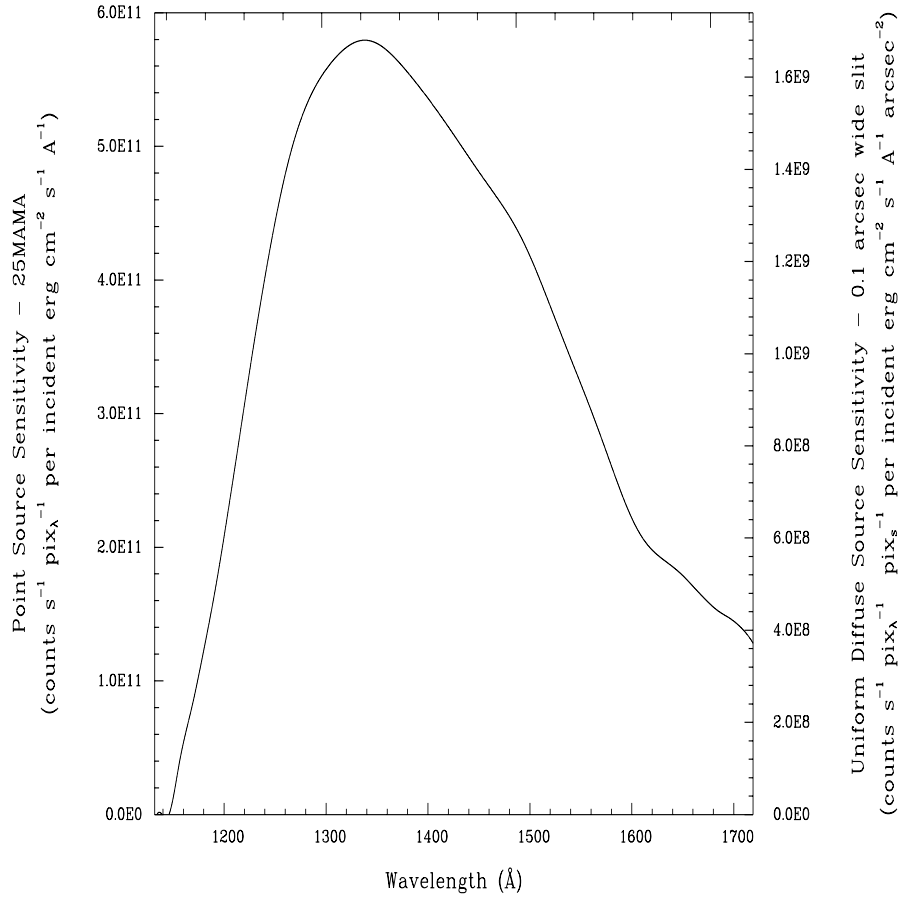

Note

Point source sensitivity assumes full transmission (zero slit losses). Diffuse source sensitivity assumes a 0.1” wide slit. To convert point source sensitivities to diffuse source sensitivities multiply the point source values by the grating spatial (cross dispersion) plate scale in units of arcseconds per pixel and by the width of the desired slit in units of arcseconds.

E140M Signal-to-Noise

Note:

The top axis displays constant F_λ values corresponding to the STMAG units (V+STMAG$_\lambda$) on the bottom axis. Recall that STMAG=0 is equivalent to F_λ = 3.63E-9 erg cm^{-2} s^{-1} Å^{-1}. The curves are labeled with exposure times in seconds.

Figure 13.56: Diffuse Source Signal-to-Noise as a Function of STMAG for E140M

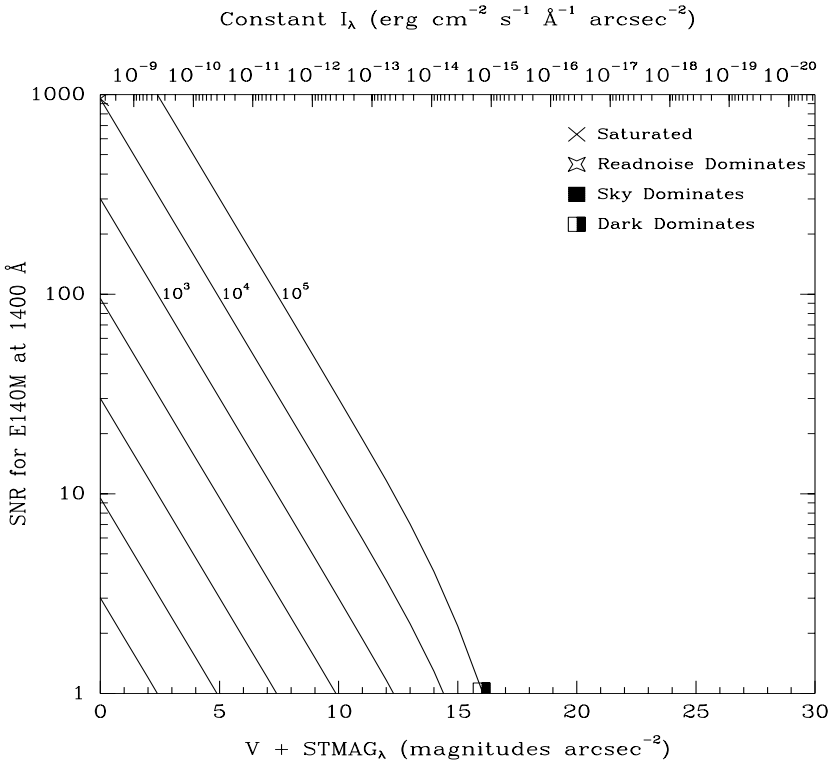

Figure 13.57: Point Source Signal-to-Noise as a Function of STMAG for E140M

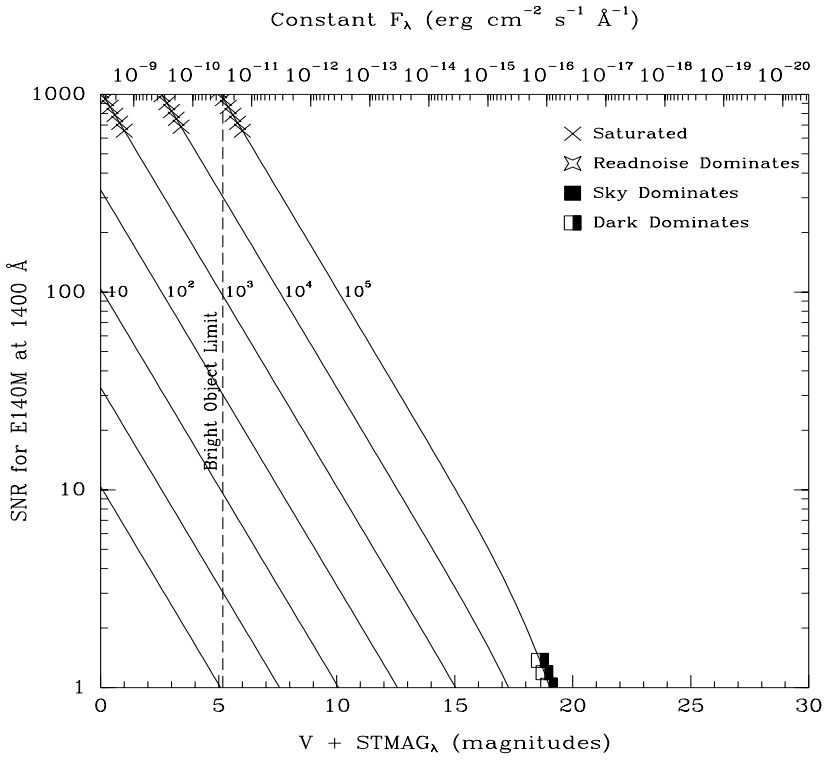

Echelle Grating E140H

Description

The E140H grating is used with the FUV-MAMA and provides echelle spectra at a resolving power of ~110,000 from 1140 to 1700 Å

Special Considerations

A single E140H echellogram covers 210 Å over ~50 orders. The order separation is ~16 pixels (0.47 arcseconds) at 1150 Å and ~36 pixels (1.05 arcseconds) at 1700 Å. The grating must be scanned, with exposures taken at three distinct settings to cover the full spectral range of the grating.

The secondary central wavelength at 1271 Å has had direct sensitivity and wavelength calibrations performed during Cycle 7 to support the large number of observations using these positions.

Grating	Spectral Range		Average Dispersion (Å per Pixel)	Dispersion, Cross Dispersion Plate Scale (arcsec / pixel)	Tilts	Central Wavelengths
	Complete	Per Tilt				
E140H	1140-1700	~210	λ/228,000	0.047,0.029	***Prime***	**1234, 1416, 1598**
					Secondary	1271, 1307, 1343, 1380, 1453, 1489, 1526, 1562

Figure 13.58: Wavelength Ranges for the E140H Grating Settings

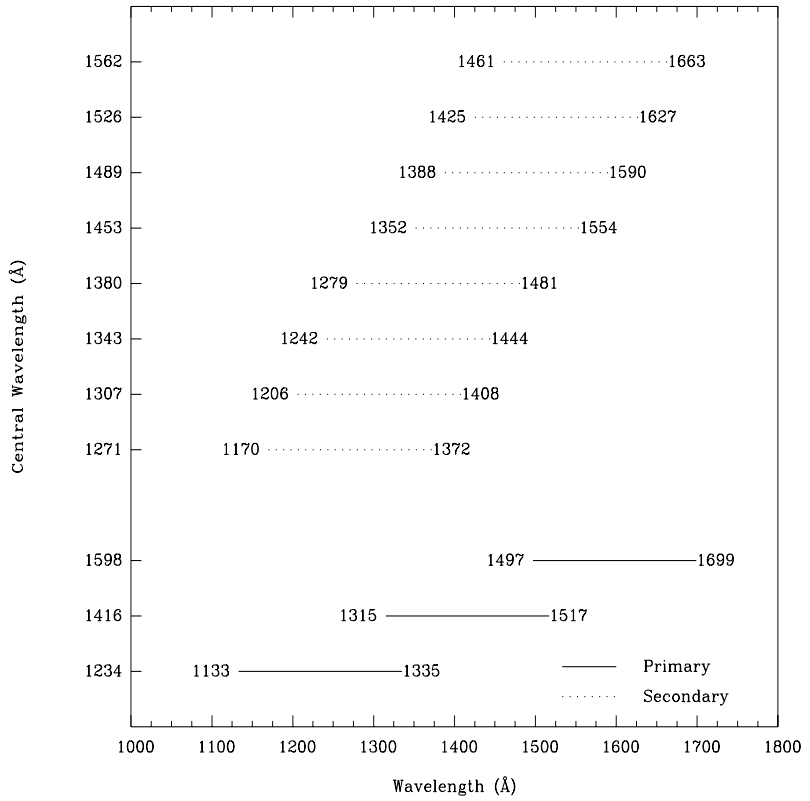

E140H Sensitivity

Table 13.16: Throughputs & Sensitivities for E140H

λ	Sensitivity	Throughput
1200	6.2E10	0.43
1250	1.1E11	0.72
1300	1.4E11	0.85
1350	1.5E11	0.84
1400	1.4E11	0.69
1450	1.2E11	0.55
1500	9.7E10	0.43
1550	7.7E10	0.32
1600	5.5E10	0.21
1650	4.2E10	0.15

Figure 13.59: E140H Point Source (left axis), and Diffuse Source (right axis) Sensitivities.

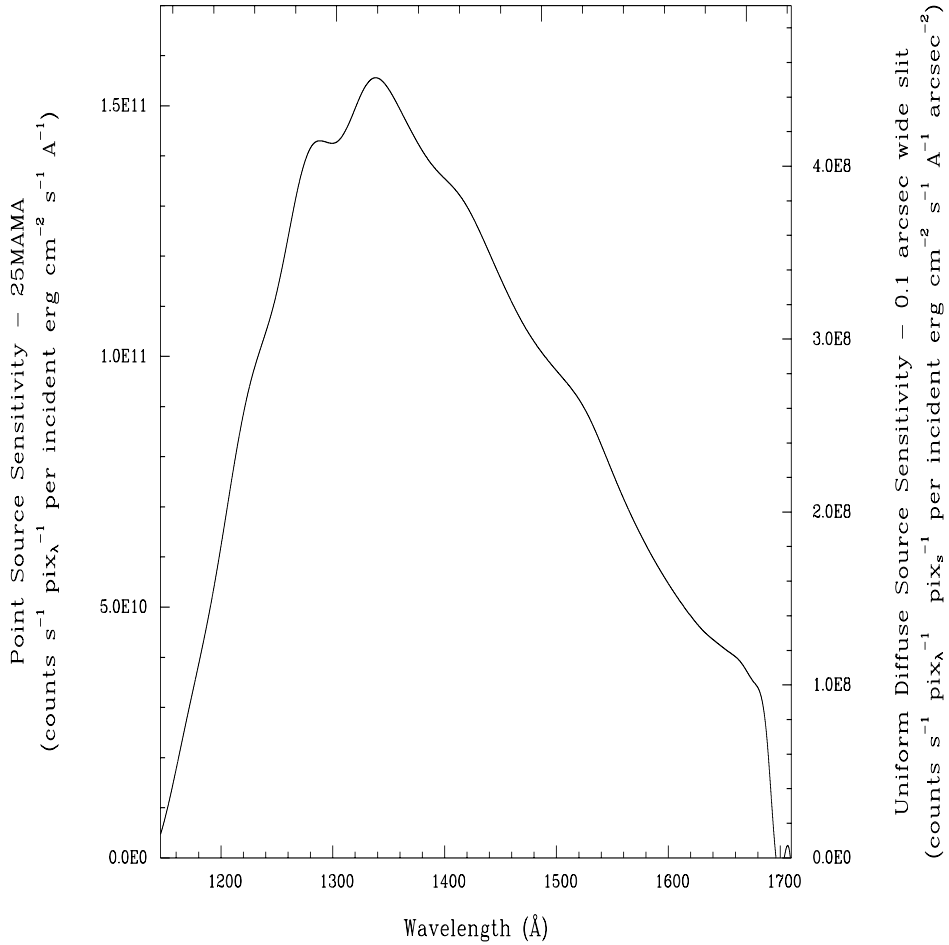

Note

Point source sensitivity assumes full transmission (zero slit losses). Diffuse source sensitivity assumes a 0.1” wide slit. To convert point source sensitivities to diffuse source sensitivities multiply the point source values by the grating spatial (cross dispersion) plate scale in units of arcseconds per pixel and by the width of the desired slit in units of arcseconds.

E140H Signal-to-Noise

Note:

The top axis displays constant F_λ values corresponding to the STMAG units (V+STMAG$_\lambda$) on the bottom axis. Recall that STMAG=0 is equivalent to F_λ = 3.63E-9 erg cm^{-2} s^{-1} Å^{-1}. The curves are labeled with exposure times in seconds.

Figure 13.60: Diffuse Source Signal-to-Noise as a Function of STMAG for E140H

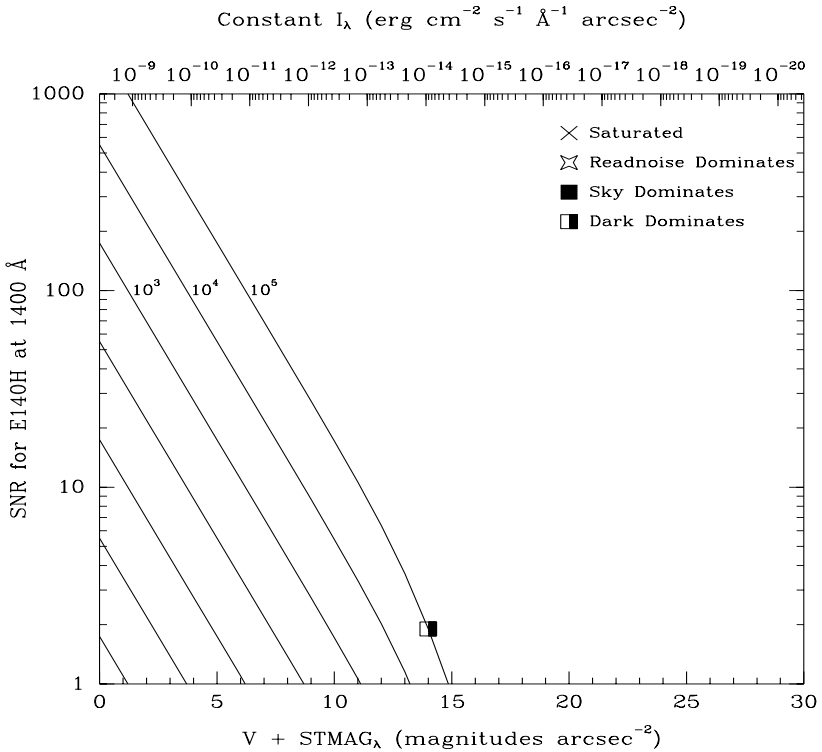

Figure 13.61: Point Source Signal-to-Noise as a Function of STMAG for E140H

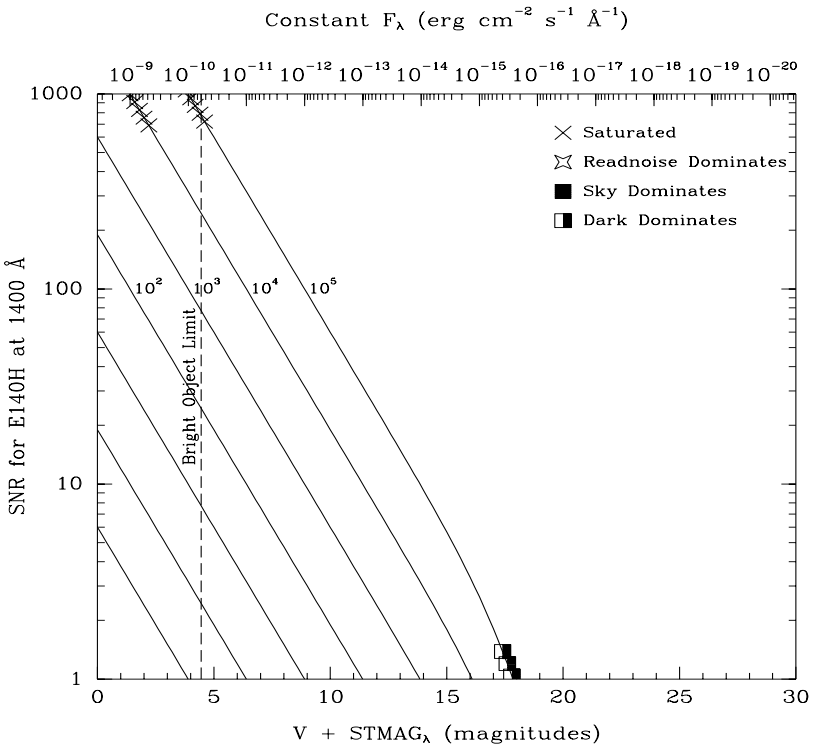

PRISM

Description

The PRISM has two central wavelength settings—one optimized to cover the optical through the near-UV, and the second selected to provide coverage of the far-UV tail down to 1150 Å.

The PRISM is used with the NUV-MAMA.

Special Considerations

The full dispersion spreads over ~450 pixels in dispersion as can be seen in Figure 13.64; thus if you have sources covering the field of view in the dispersion direction, the blue tail will be lost off the field of view if you use the 2125 Å setting, and likewise the red tail will be lost if you use the 1200 Å setting.

We note that the dispersion of the PRISM at wavelengths longer than ~2600 Å is very poorly known at this time.

Grating	Spectral Range		Average Dispersion (Å per Pixel)	Plate Scale (arcsec / pixel)	Tilts	Central Wavelengths
	Complete	Per Tilt				
PRISM	1150-3100	1950	1.2–120	0.029	***Prime***	**1200, 2125**

Figure 13.62: Wavelength Ranges for the Prism Settings

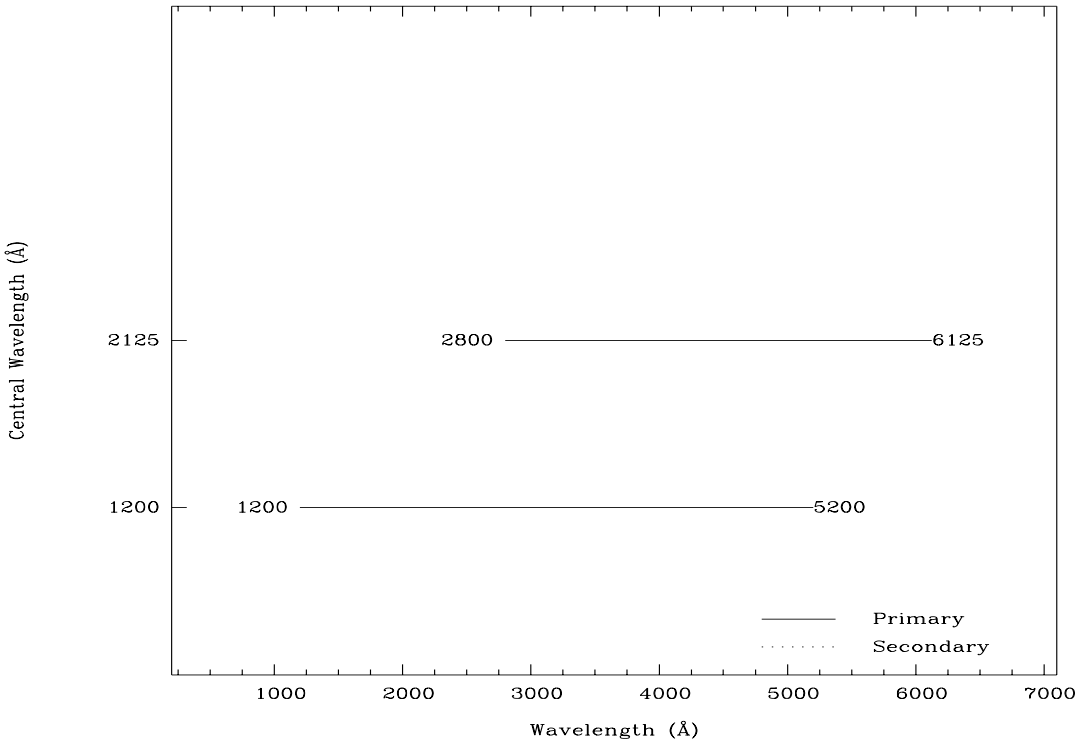

PRISM Sensitivities

Table 13.17: PRISM Throughputs & Sensitivities

λ	Sensitivity	Throughput
1200	5.4E12	0.4
1400	3.2E13	0.5
1600	7.8E13	0.5
1800	2.5E14	0.9
2000	6.6E14	1.4
2200	1.4E15	1.9
2400	2.3E15	2.0
2600	3.3E15	2.0
2800	4.2E15	1.8
3000	3.4E15	1.1
3200	9.0E14	0.2
3400	2.2E14	0.0
3600	1.0E14	0.0

Figure 13.63: Prism Point Source (left axis), and Diffuse Source (right axis) Sensitivities. .

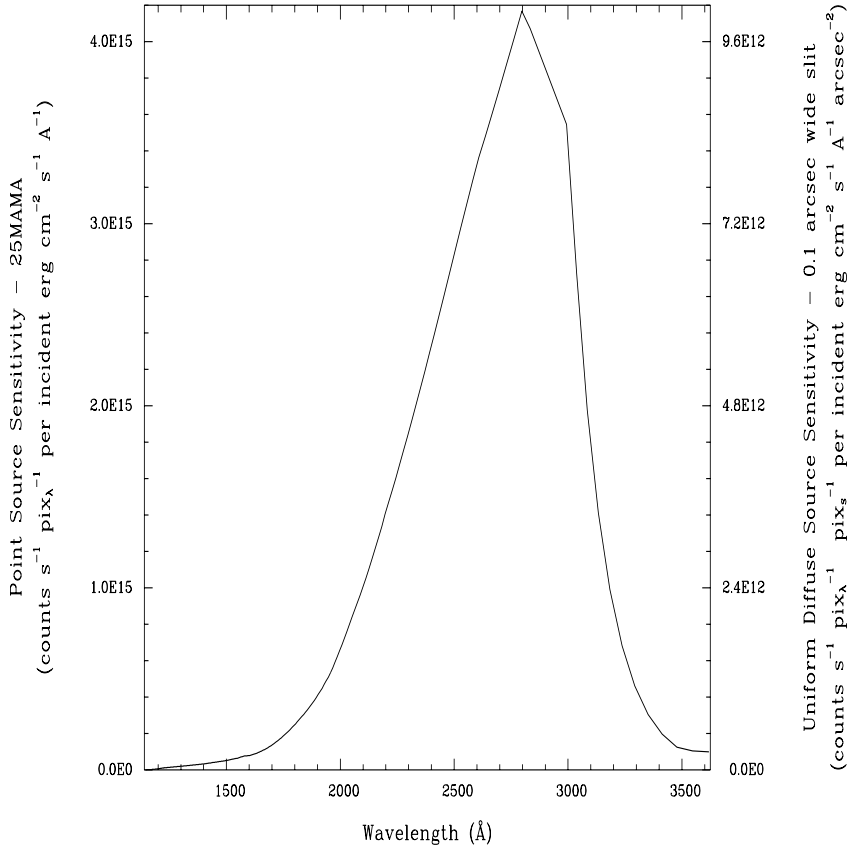

Note

Point source sensitivity assumes full transmission (zero slit losses). Diffuse source sensitivity assumes a 0.1” wide slit. To convert point source sensitivities to diffuse source sensitivities multiply the point source values by the grating spatial (cross dispersion) plate scale in units of arcseconds per pixel and by the width of the desired slit in units of arcseconds.

Prism Wavelength Relation

Relationship between pixel offset and wavelength for the PRISM.

Figure 13.64: PRISM Wavelengths

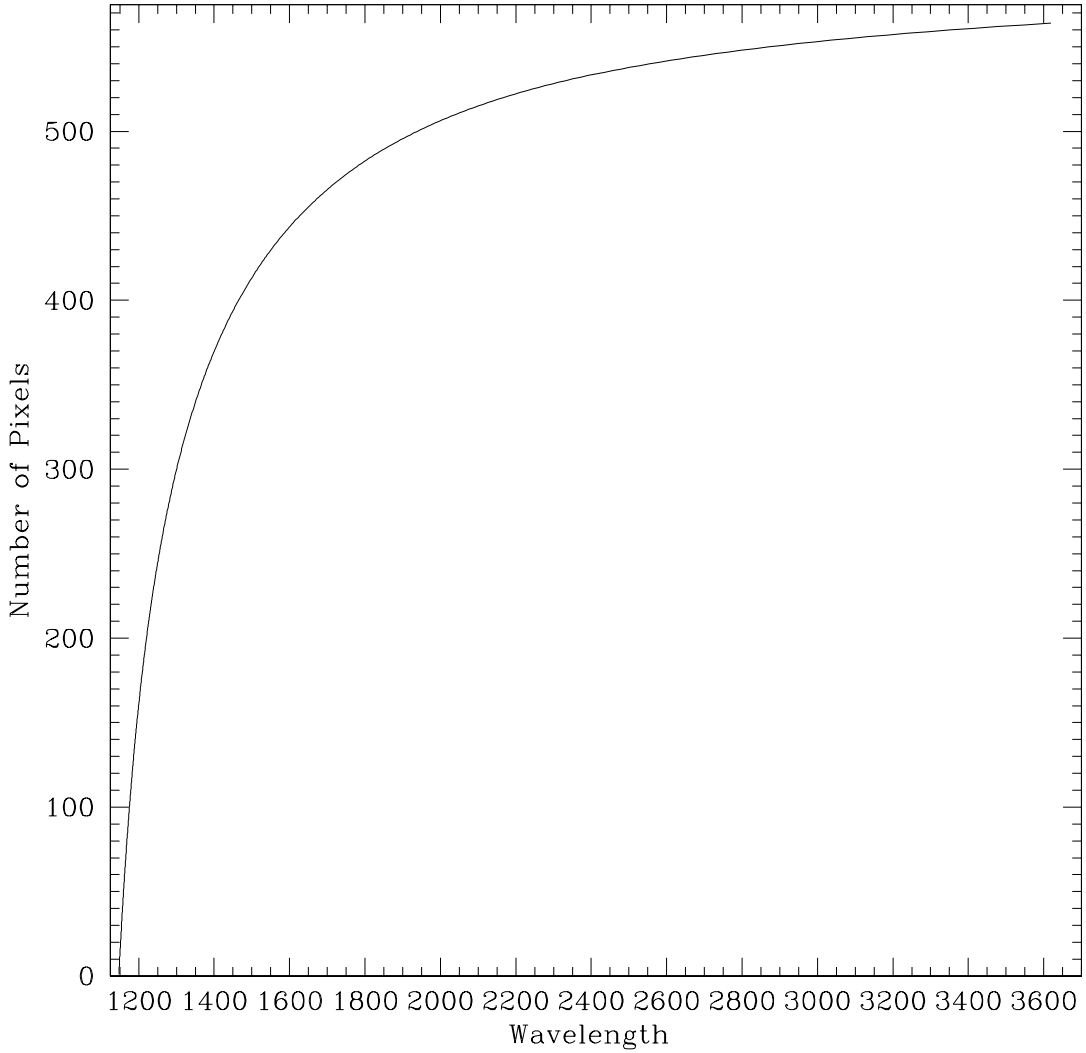

Apertures

On the following pages we provide, for each supported aperture, a description of the aperture, the wavelength dependent point source throughput of the aperture, and some advice on its use.

52X0.05 Aperture

Description

This slit is supported with use of the first-order gratings and provides the best spatial and spectral resolution of the long slits. This aperture is the 2 pixel wide slit in the dispersion direction for the MAMA first-order modes.

Special Considerations

Observations with this slit require a PEAKUP prior to science observations.

Table 13.18: 52X0.05 Throughputs

λ	% Throughput
1200	32.4
1600	43.7
2000	49.9
2400	53.3
2800	55.4
3200	56.4
3600	56.4
4000	55.8
4400	54.7
4800	53.3
5200	51.7
5600	50.0
6000	48.3
6400	46.6
6800	44.9
7200	43.3
7600	41.8
8000	40.3
8400	38.9

	Projected Length (arcsec)			
Aperture	CCD	MAMA (M-modes)	MAMA (L-modes)	Width (arcsec)
52X0.05	52.0	28.0	25.0	0.05

Figure 13.65: 52X0.05 Aperture Throughput as a Function of Wavelength.

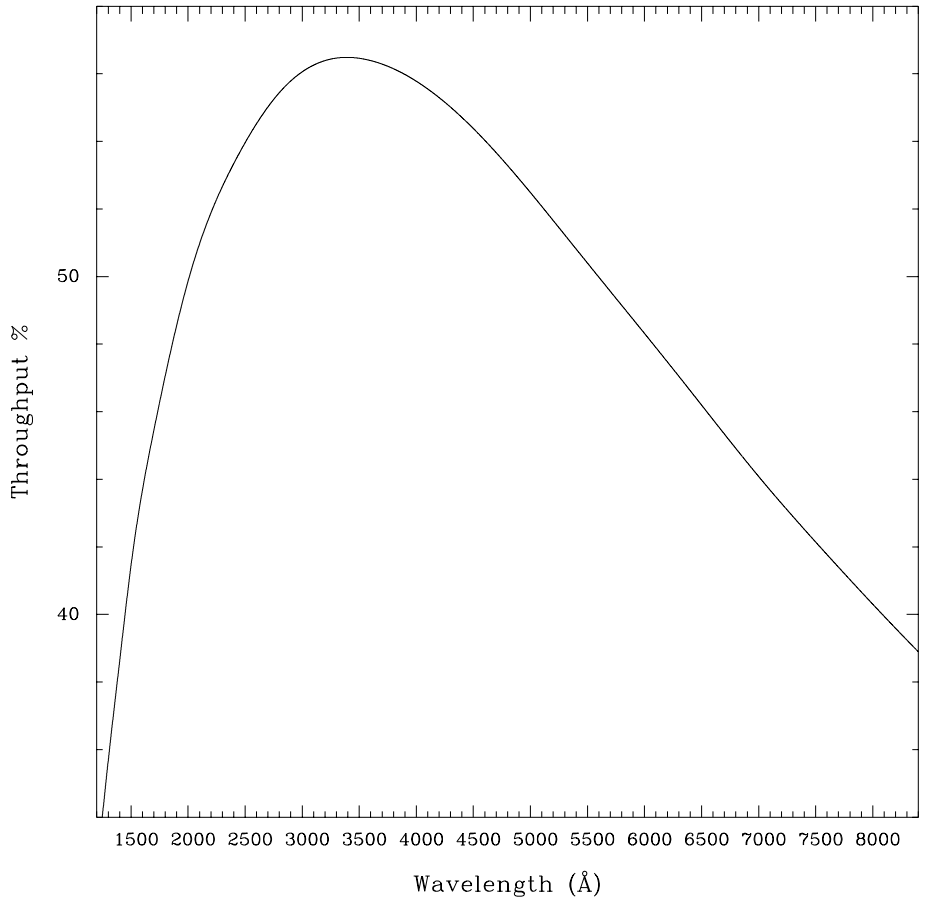

52X0.1 Aperture

Description

This slit is supported with the first-order gratings. This aperture is the 2 pixel wide slit in the dispersion direction for the CCD first-order modes.

Special Considerations

Observations with this slit require a PEAKUP prior to scientific observations.

Table 13.19: 52X0.1 Throughputs

λ	% Throughput
1200	45.5
1600	55.9
2000	63.5
2400	68.6
2800	71.5
3200	72.7
3600	72.5
4000	71.7
4400	70.9
4800	70.2
5200	69.7
5600	69.2
6000	68.7
6400	68.2
6800	67.5
7200	66.7
7600	65.9
8000	64.9
8400	64.0

	Projected Length (arcsec)			
Aperture	CCD	MAMA (M-modes)	MAMA (L-modes)	Width (arcsec)
52X0.1	52.0	28.0	25.0	0.1

Figure 13.66: 52X0.1 Aperture Throughput as a Function of Wavelength.

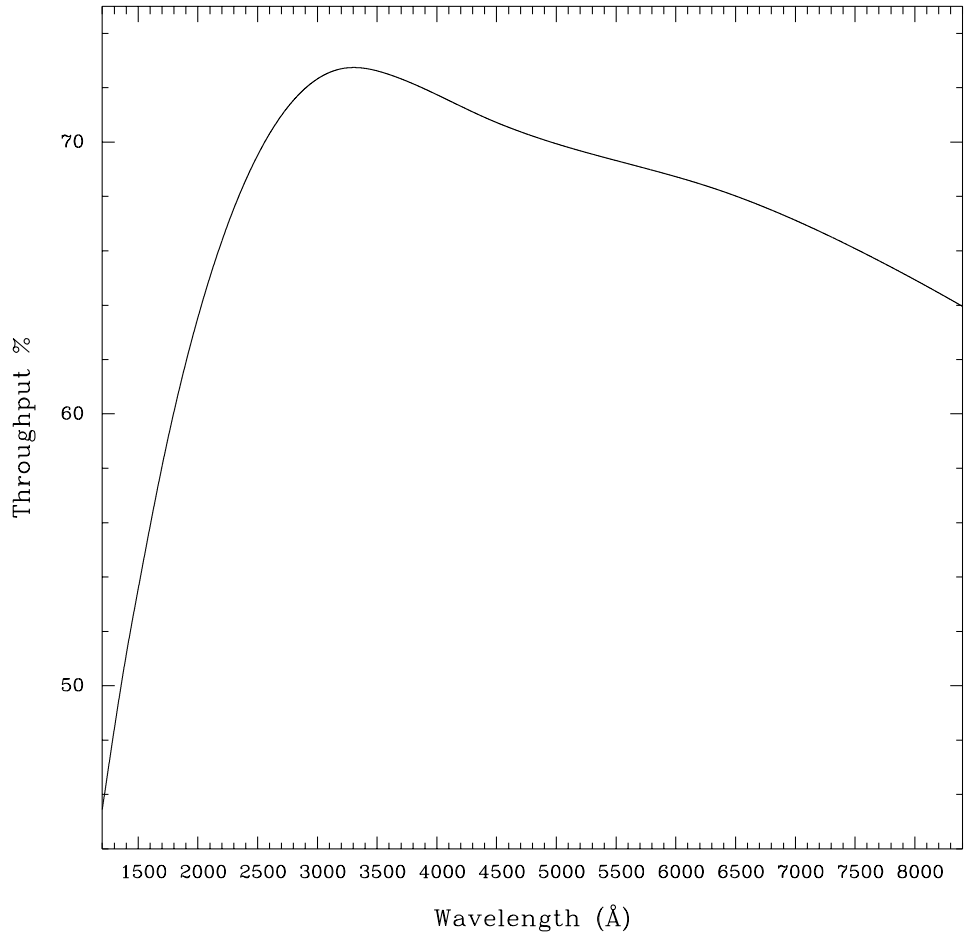

52X0.2 Aperture

Description

This is the “utility” slit used with first-order gratings. It provides a good compromise between spectral resolution and photometric throughput.

Special Considerations

Observations using this slit do not need to be preceded by a PEAKUP.

Table 13.20: 52X0.2 Throughputs

λ	% Throughput
1200	59.2
1700	67.3
2200	73.0
2700	76.3
3200	79.2
3700	81.4
4200	82.5
4700	83.3
5200	84.1
5700	84.3
6200	82.9
6700	80.8
7200	81.5
7700	81.1
8200	75.7

	Projected Length (arcsec)			
Aperture	**CCD**	**MAMA (M-modes)**	**MAMA (L-modes)**	**Width (arcsec)**
52X0.2	52.0	28.0	25.0	0.2

Figure 13.67: 52X0.2 Aperture Throughput as a Function of Wavelength

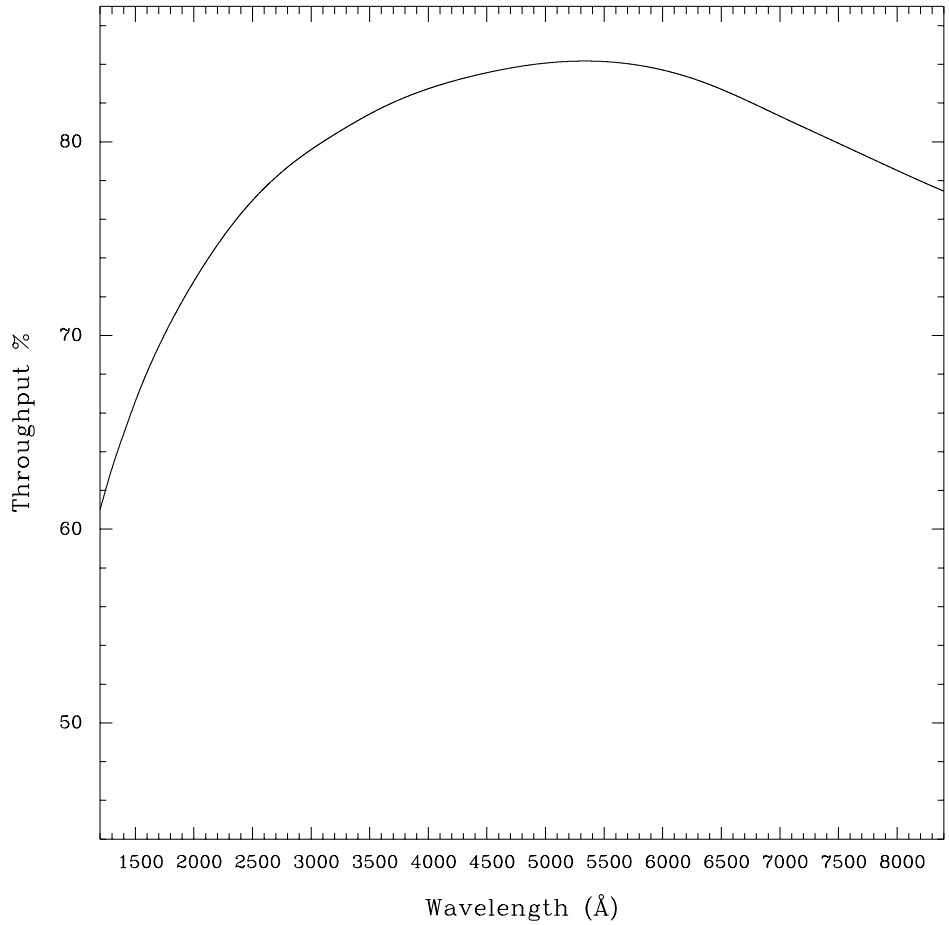

52X0.5 Aperture

Description

This slit is designated for use with the first-order gratings and is a good slit for spectrophotometric observations of point sources.

Special Considerations

Observations with this slit do not need to be preceded by a PEAKUP. Be aware of effects of OTA scatter on the line profiles when observing point sources in wide slits (see “Spectral Purity, Order Confusion, and Peculiarities” on page 304).

λ	% Throughput
1200	77.5
1700	82.1
2200	85.4
2700	87.0
3200	88.2
3700	89.3
4200	90.0
4700	90.2
5200	90.1
5700	90.3
6200	90.2
6700	89.8
7200	89.9
7700	89.5
8200	87.5

Aperture	Projected Length (arcsec)			Width (arcsec)
	CCD	MAMA (M-modes)	MAMA (L-modes)	
52X0.5	52.0	28.0	25.0	0.5

Figure 13.68: 52X0.5 Aperture Throughput as a Function of Wavelength

52X2 Aperture

Description

The last in the series of supported long slits used with the first-order gratings and is a good slit for spectrophotometric observations of point sources.

Special Consideration

Observations using this slit do not need to be preceded by a PEAKUP. Be aware of effects of OTA scatter on the line profiles when observing point sources in the wide slits (see “Spectral Purity, Order Confusion, and Peculiarities” on page 304).

λ	% Throughput
1200	94.6
1700	96.3
2200	97.2
2700	97.3
3200	97.3
3700	97.3
4200	97.3
4700	97.1
5200	97.0
5700	96.9
6200	96.7
6700	96.6
7200	96.8
7700	96.2
8200	94.2

	Projected Length (arcsec)			
Aperture	CCD	MAMA (M-modes)	MAMA (L-modes)	Width (arcsec)
52X2	52.0	28.0	25.0	2.0

Figure 13.69: 52X2 Aperture Throughput as a Function of Wavelength

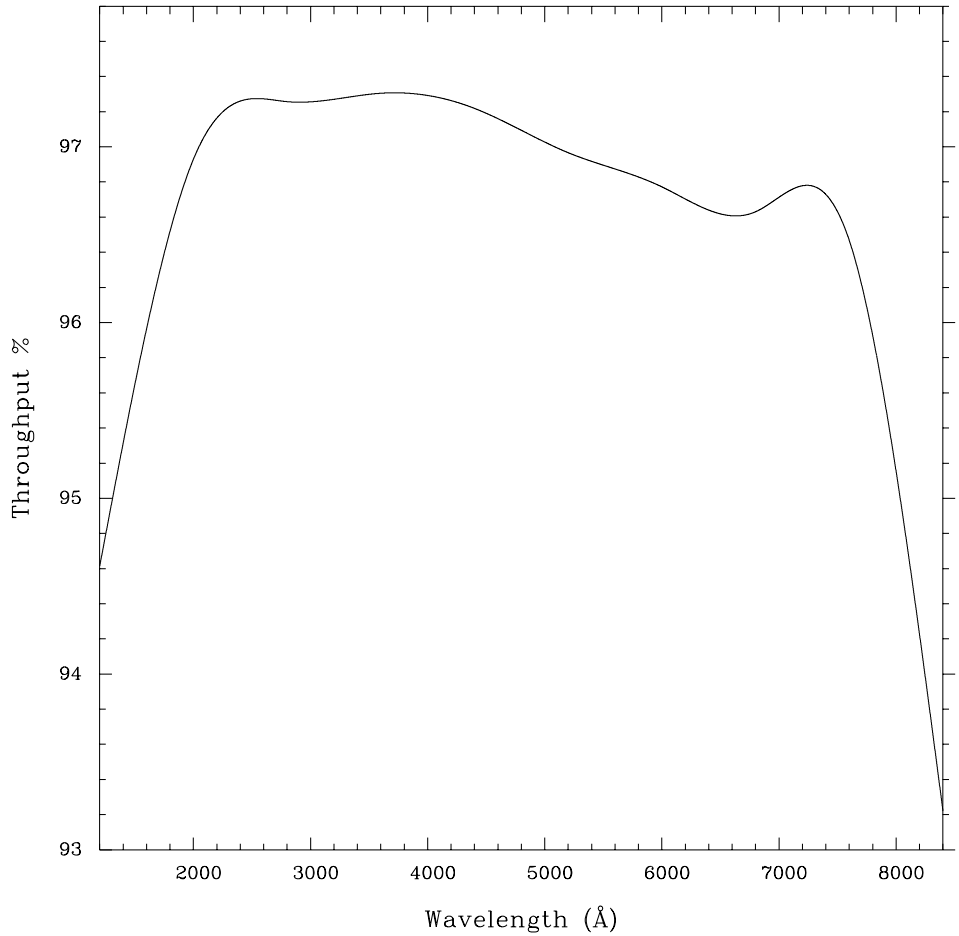

52X0.2F1 Aperture

Description

The same physical aperture as the 52X0.2 but used at the position of the smaller of the two fiducials. The fiducial bar can be used for spectroscopic coronographic observations.

Table 13.21: 52X0.2F1 Throughputs

λ	% Throughput
1200	61.0
1600	68.1
2000	72.8
2400	76.3
2800	78.7
3200	80.4
3600	81.7
4000	82.7
4400	83.4
4800	83.9
5200	84.2
5600	84.1
6000	83.7
6400	83.0
6800	81.9
7200	80.8
7600	79.6
8000	78.5
8400	77.4

	Projected Length (arcsec)			
Aperture	**CCD**	**MAMA (M-modes)**	**MAMA (L-modes)**	**Width (arcsec)**
52X0.2F1	52.0	28.0	25.0	0.2
Fiducial	0.5	0.5	0.5	0.2

Figure 13.70: 52X0.2F1 Aperture Throughput as a Function of Wavelength

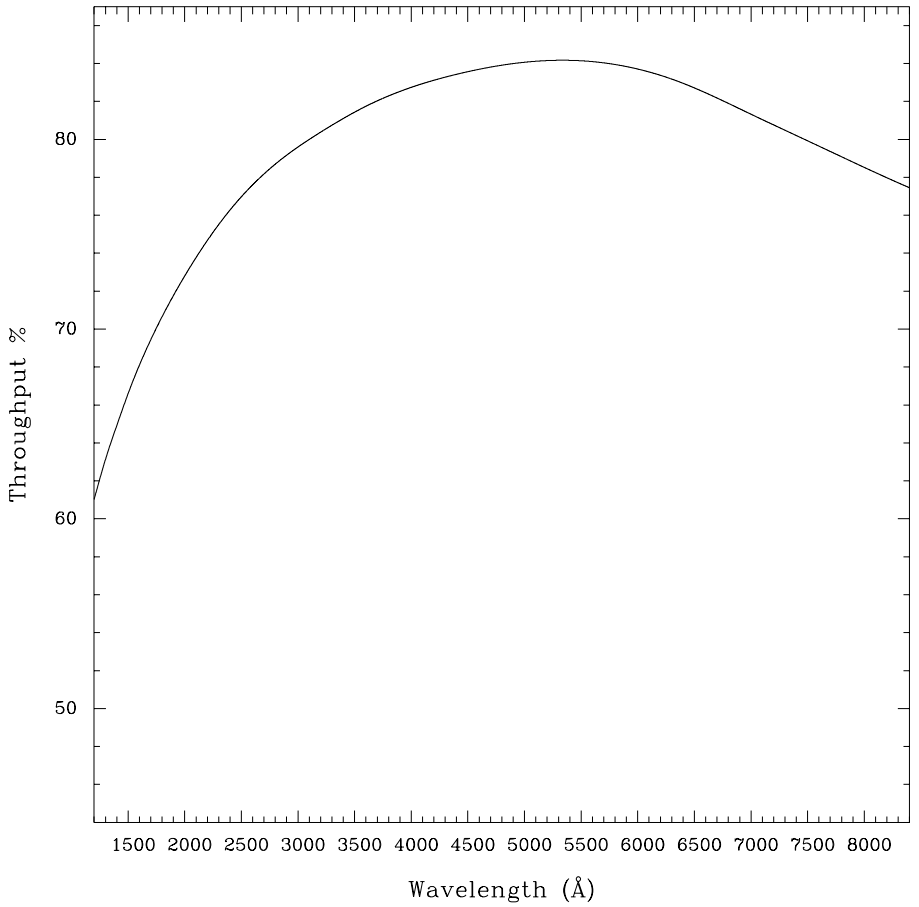

0.2X0.06 Aperture

Description

Supported slit for use with the medium resolution echelle gratings. This slit is two pixels wide in dispersion for these gratings, providing optimal spectral resolution and line profiles.

Special Considerations

Used with `E230M` and `E140M` gratings. Observations with this slit require a prior PEAKUP.

Table 13.22: 0.2X0.06 Throughputs

λ	% Throughput
1200	32.1
1700	45.6
2200	53.7
2700	56.3
3200	58.6

Aperture	Projected Length (arcsec) (MAMA E-modes)	Width (arcsec)
0.2X0.06	0.2	0.06

Figure 13.71: 0.2X0.06 Aperture Throughput as a Function of Wavelength

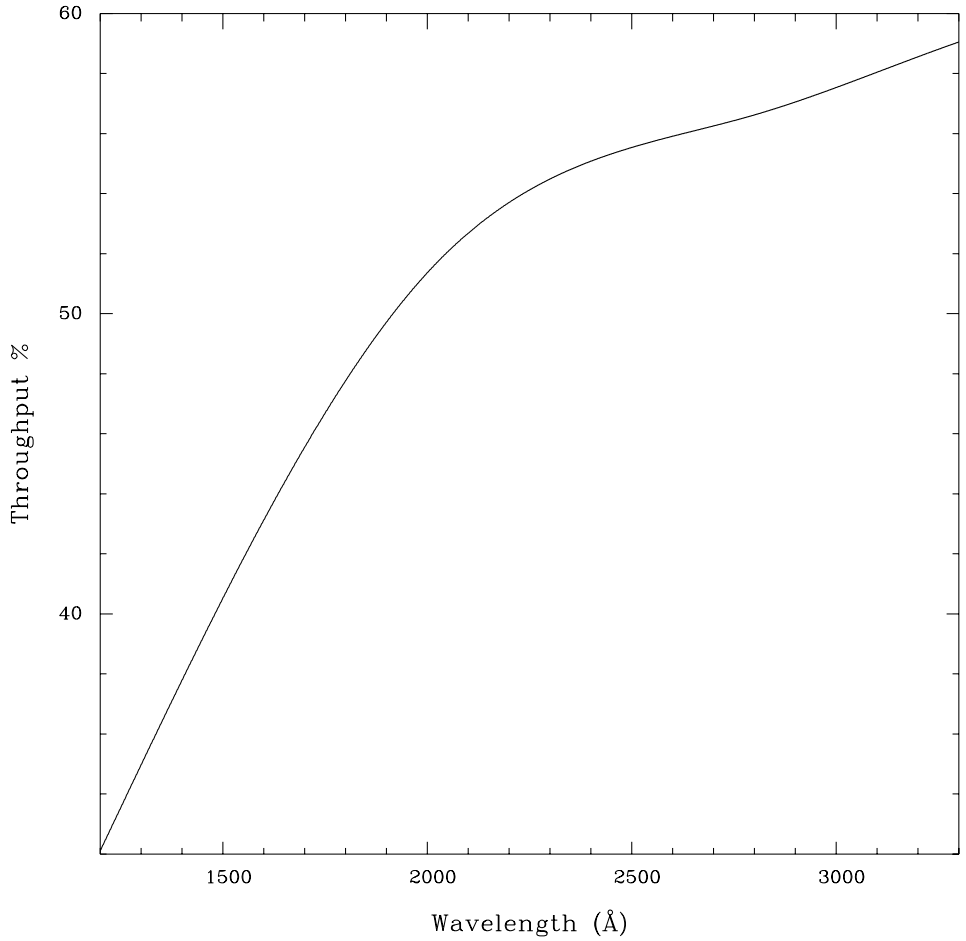

0.2X0.2 Aperture

Description

The “utility” slit for the echelle gratings. This slit is the most photometric of the echelle slits and has the highest throughput for photon statistics.

Aperture	Projected Length (arcsec) (MAMA E-modes)	Width (arcsec)
0.2X0.2	0.2	0.2

Table 13.23: 0.2X0.2 Throughputs

λ	% Throughput
1200	47.9
1700	59.5
2200	67.3
2700	70.8
3200	73.6

Figure 13.72: 0.2X0.2 Aperture Throughput as a Function of Wavelength

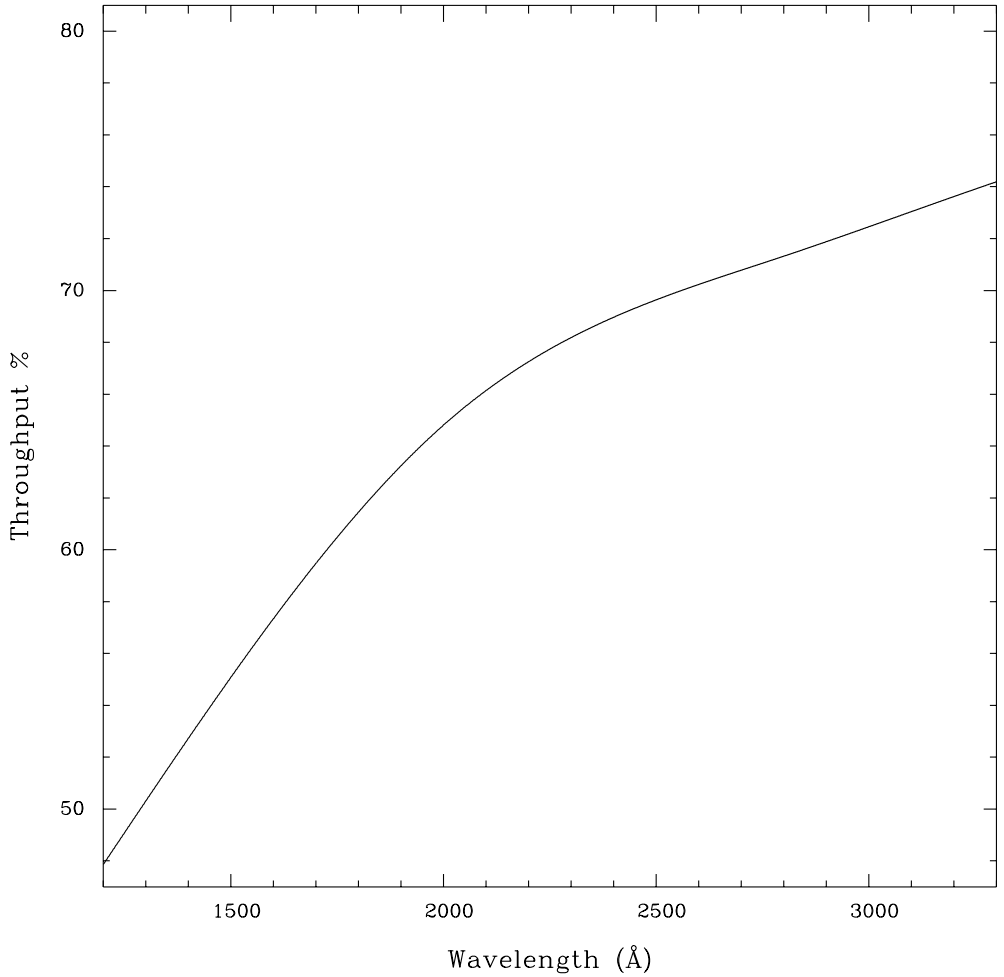

0.2X0.09 Aperture

Description

This slit is used with high resolution echelle gratings. This slit is two pixels wide in dispersion for these gratings, providing optimal spectral resolution and line profiles.

Special Considerations

Used with `E140H and E230H` grating only. Observations with this slit require a prior PEAKUP.

Table 13.24: 0.2X0.09 Throughputs

λ	% Throughput
1200	38.1
1700	51.0
2200	60.1
2700	64.5
3200	66.4

Aperture	Projected Length (arcsec) (MAMA E-modes)	Width (arcsec)
0.2X0.09	0.2	0.09

Figure 13.73: 0.2X0.09 Aperture Throughput as a Function of Wavelength

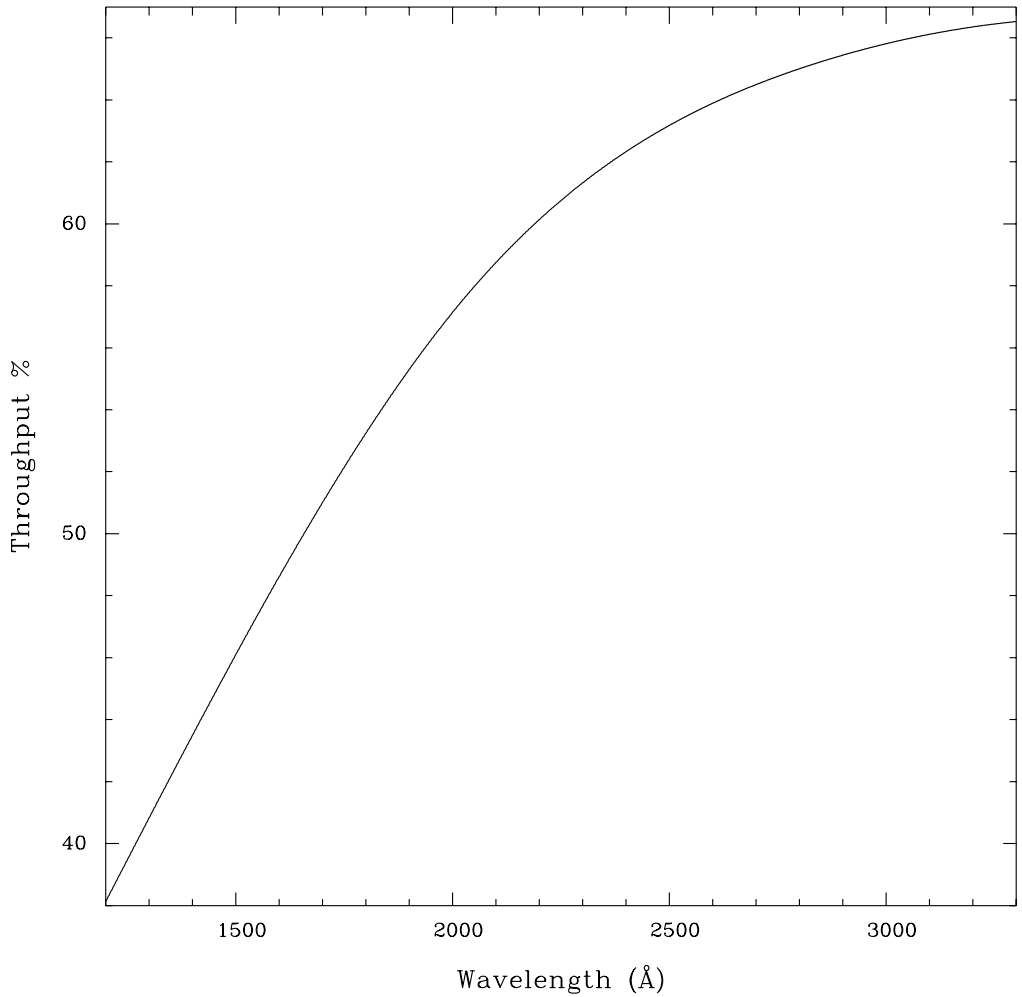

6X0.2 Aperture

Description

This slit is used with echelle gratings.

Recommended Uses

A good slit for echelle observations of extended sources with isolated emission lines.

Special Considerations

This slit can be used with all echelle gratings. Please note that use of this slit with an extended source will produce order overlap and may make analysis difficult (see also “Spectral Purity, Order Confusion, and Peculiarities” on page 304).

Table 13.25: 6X0.2 Aperture Throughputs

λ	% Throughput
1200	60.6
1400	63.9
1600	67.2
1800	70.1
2000	72.6
2200	74.6
2400	76.1
2600	77.3
2800	78.2
3000	79.0
3200	79.7
3400	80.4

Aperture	Projected Length (arcsec) (MAMA E-modes)	Width (arcsec)
6X0.2	6.0	0.2

Figure 13.74: 6X0.2 Aperture Throughput as a Function of Wavelength

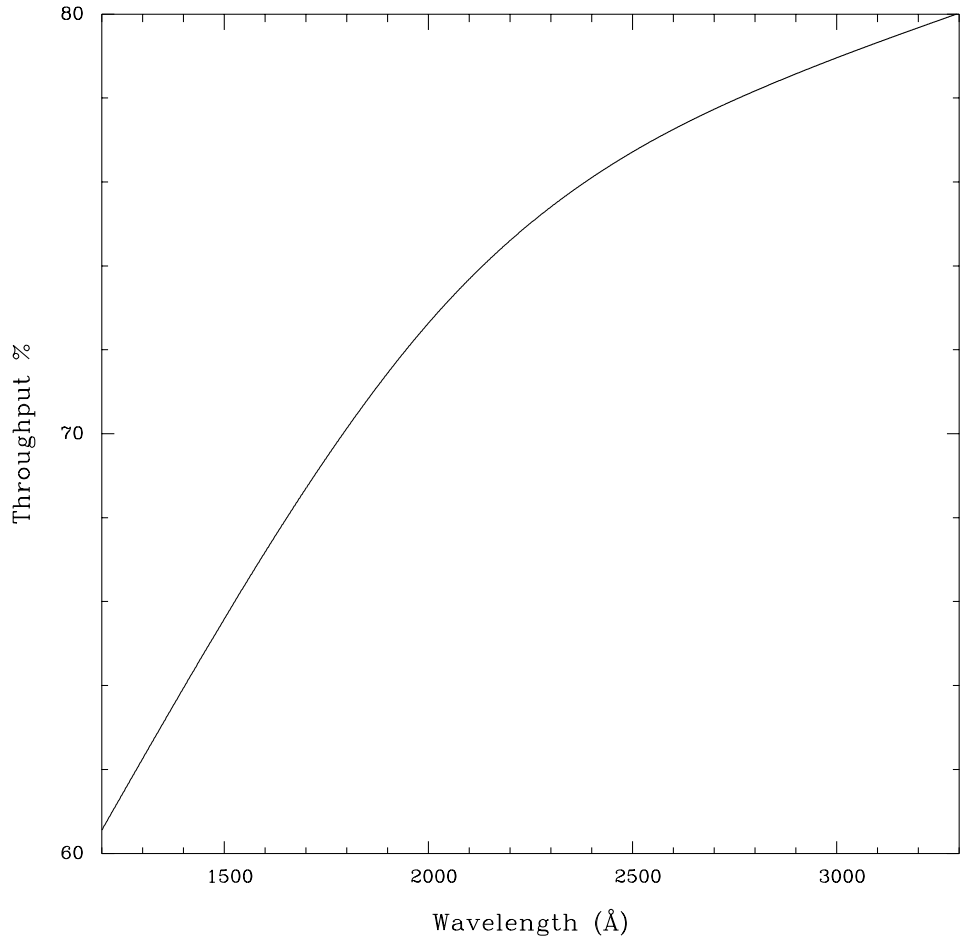

FPSPLIT Slits

0.2X0.06FP(A-E) Apertures

Description

The FPSPLIT slits consist of two sets of five slits; in each set the slits are all the same size. They are for use with the MAMA echelle gratings. It is possible to achieve high S/N data for bright targets, independently of the quality of the flat-field, by means of a special observing strategy wherein multiple spectrograms are obtained through these slits.

Special Considerations

See Chapter 12 for more details on obtaining high S/N spectral data. Observations with this slit require a prior PEAKUP.

Aperture	Projected Length (arcsec)	Width (arcsec)
0.2X0.06FPA	0.2	0.06
0.2X0.06FPB	0.2	0.06
0.2X0.06FPC	0.2	0.06
0.2X0.06FPD	0.2	0.06
0.2X0.06FPE	0.2	0.06

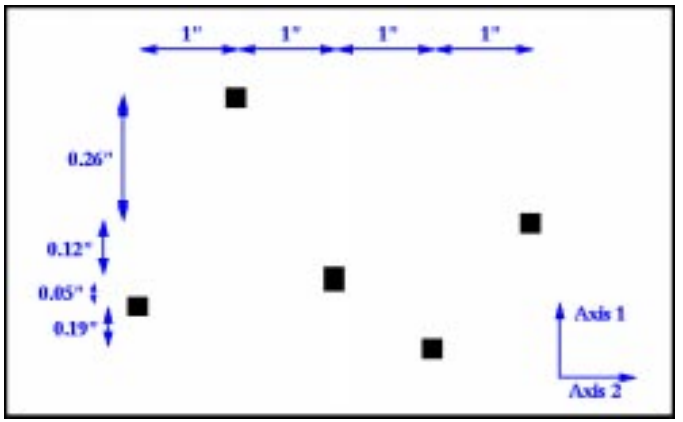

Table 13.26: Throughput for 0.2X0.06FP(A-E)

λ	% Throughput
1200	32.1
1400	37.8
1600	43.1
1800	47.8
2000	51.4
2200	53.7
2400	55.1
2600	55.9
2800	56.6
3000	57.5
3200	58.6
3400	59.5

Figure 13.75: 0.2X0.06FP(A-E) Aperture Throughput as a Function of Wavelength

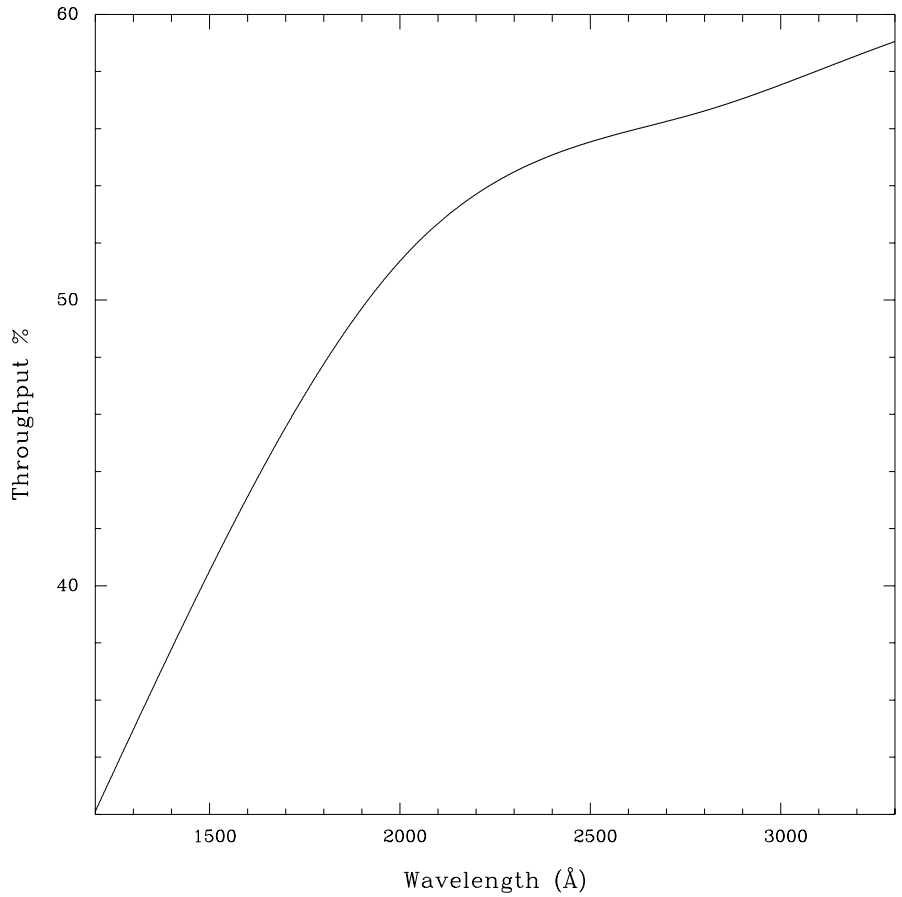

0.2X0.2FP(A-E) Apertures

Description

The FPSPLIT slits consist of two sets of five slits–in each set the slits are all the same size. They are for use with the MAMA echelle gratings. It is possible to achieve high S/N data for bright targets, independently of the quality of the flat-field, by means of a special observing strategy wherein multiple spectrograms are obtained through these slits.

Special Considerations

See Chapter 12 for more details on obtaining high S/N spectral data.

Aperture	Projected Length (arcsec)	Width (arcsec)
0.2X0.2FPA	0.2	0.2
0.2X0.2FPB	0.2	0.2
0.2X0.2FPC	0.2	0.2
0.2X0.2FPD	0.2	0.2
0.2X0.2FPE	0.2	0.2

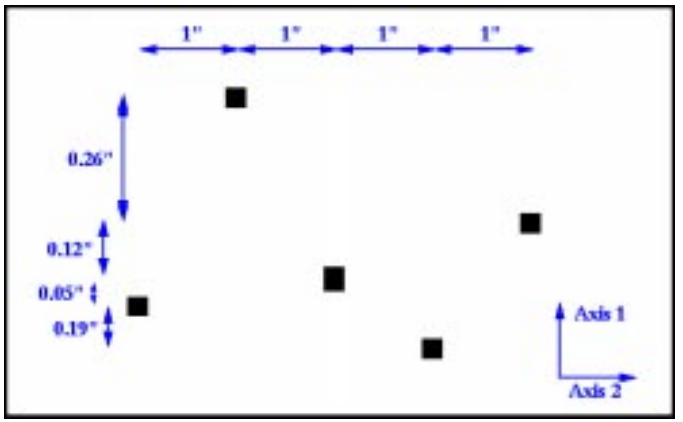

Table 13.27: 0.2X0.2FP(A-E) Slit Throughputs

λ	% Throughput
1200	47.9
1700	59.5
2200	67.3
2700	70.8
3200	73.6

Figure 13.76: 0.2X0.2FP(A-E) Aperture Throughput as a Function of Wavelength

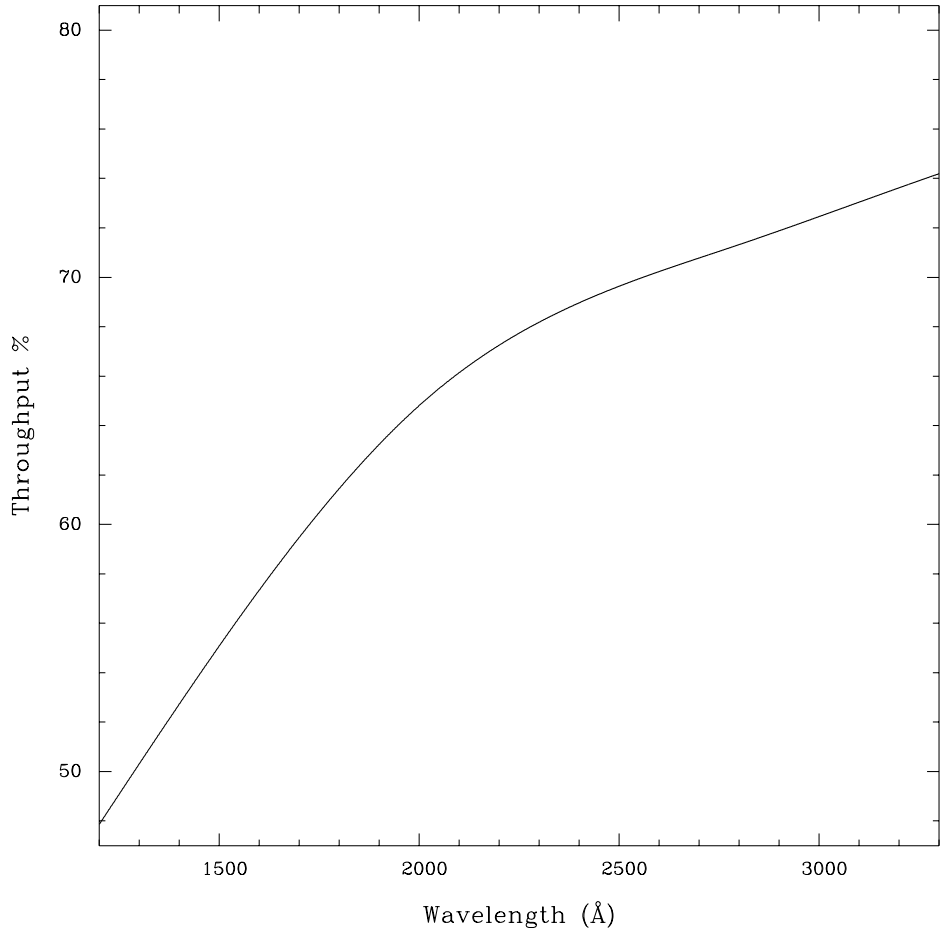

0.1X0.03 Aperture

Description

This slit provides the highest spectral resolution of any STIS slit and is restricted to use with the MAMA echelle gratings. Tests during ground calibration with this slit to obtain MAMA exposures of a mono-isotopic platinum lamp source produced resolving powers in excess of 200,000.

Special Considerations

Observations with this slit require a prior PEAKUP.

Table 13.28: 0.1X0.03 Throughputs

λ	% Throughput
1200	20.9
1700	33.3
2200	40.7
2700	42.1
3200	41.4

Aperture	Projected Length (arcsec)	Width (arcsec)
0.1X0.03	0.1	0.025

Figure 13.77: 0.1X0.03 Aperture Throughput as a Function of Wavelength

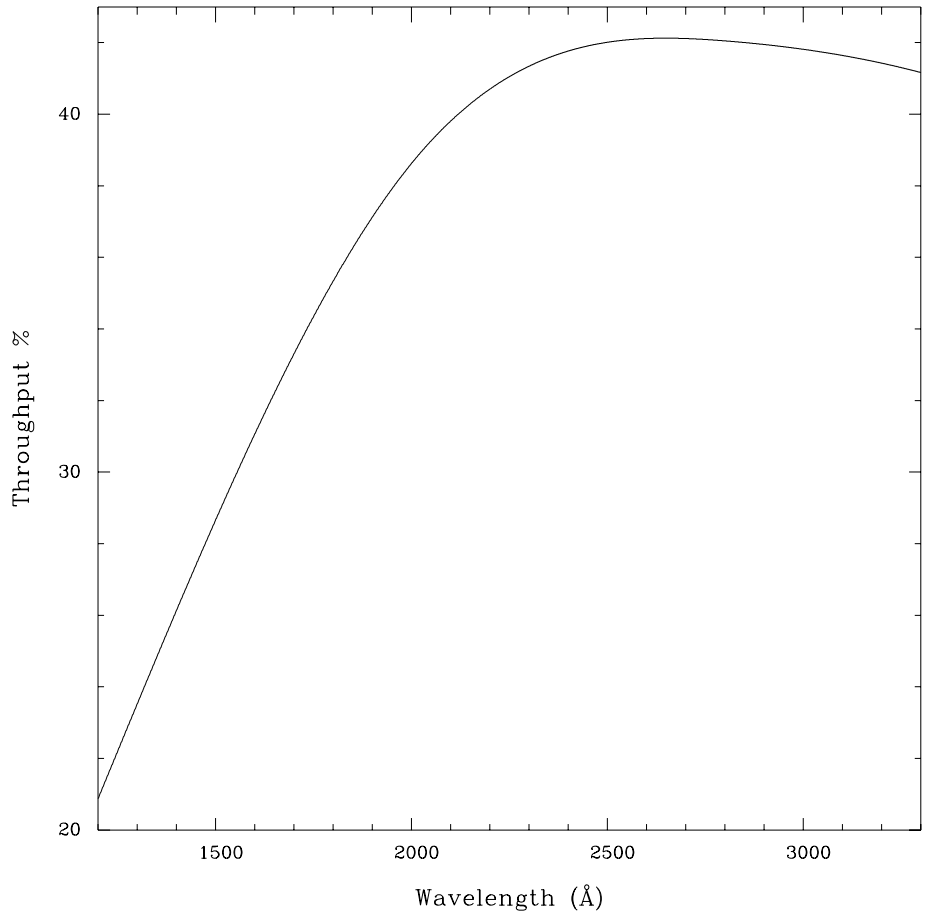

Spatial Profiles

Below we provide encircled energy tables for each grating mode. Included are the values for the percent of the total flux contained in the default point source extraction aperture (not the same as the physical aperture) during pipeline processing. **calstis**, the pipeline code, sums a number of pixels to obtain the spectral flux ; this number of pixels is given by the “Extraction Height.” These tables also give the percent flux in the peak pixels. Accompanying figures show sample spatial profiles (i.e., in the direction perpendicular to the dispersion).

First-Order Spatial Profiles

Table 13.29: Encircled Energies for G140L, G140M, G230L, G230M

Grating[a]	λ	Slit[b]	Extraction Height (pixels)	Flux (%) in Center Pixel	Flux in Extraction Aperture
G140L & G140M	1200	52X0.2	11	0.2049	0.8197
	1400			0.2655	0.8850
	1700			0.2703	0.9009
G230L & G230M	2000	52X0.2	11	0.2838	0.9009
	2500			0.3272	0.9091
	3000			0.3182	0.9091

a. M mode profiles are assumed to be identical to L mode profiles.
b. Values are only weakly dependent on observing slit.

Figure 13.78: G140L, G140M, G230L, G230M Spatial Profiles

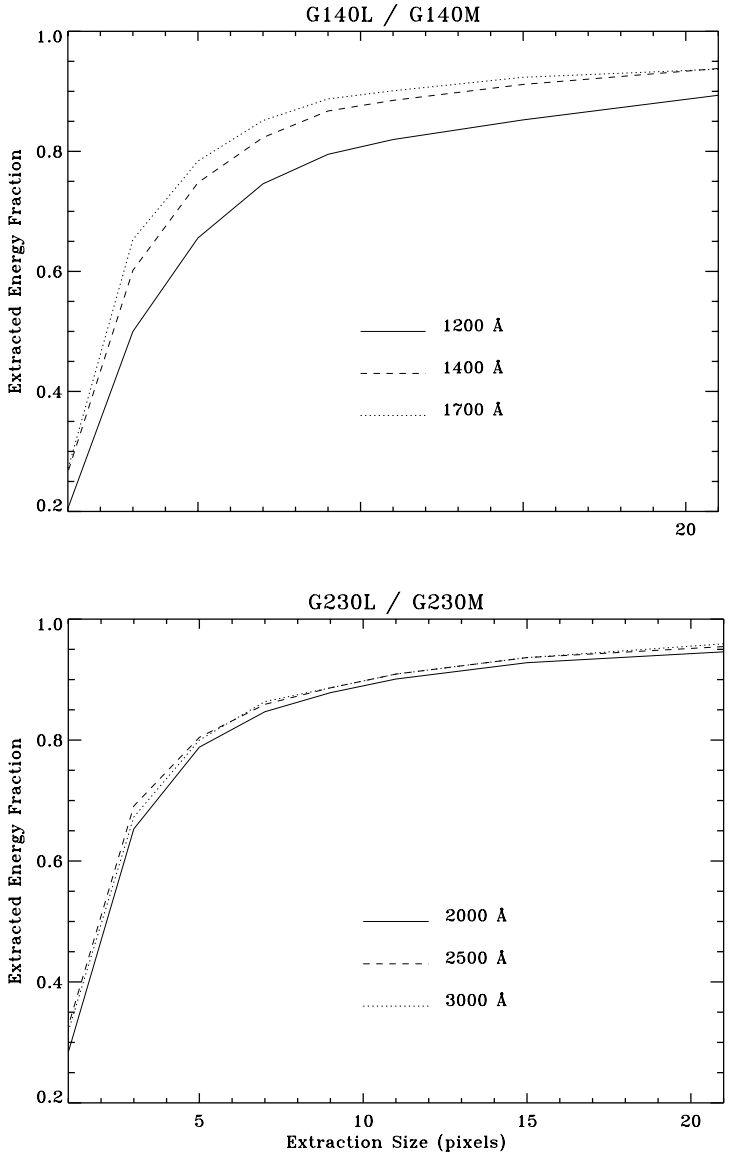

Table 13.30: Encircled Energies for G230LB and G230MB

Grating[a]	λ	Slit[b]	Extraction Height (pixels)	Flux (%) in Center Pixel	Flux in Extraction Aperture
G230LB & G230MB	2000	52X2	7	0.3008	0.8130
	2500			0.3390	0.8475
	3000			0.3017	0.8621

a. M mode profiles are assumed to be identical to L mode profiles.

b. Values are only weakly dependent on observing slit.

Figure 13.79: G230LB and G230MB Spatial Profiles

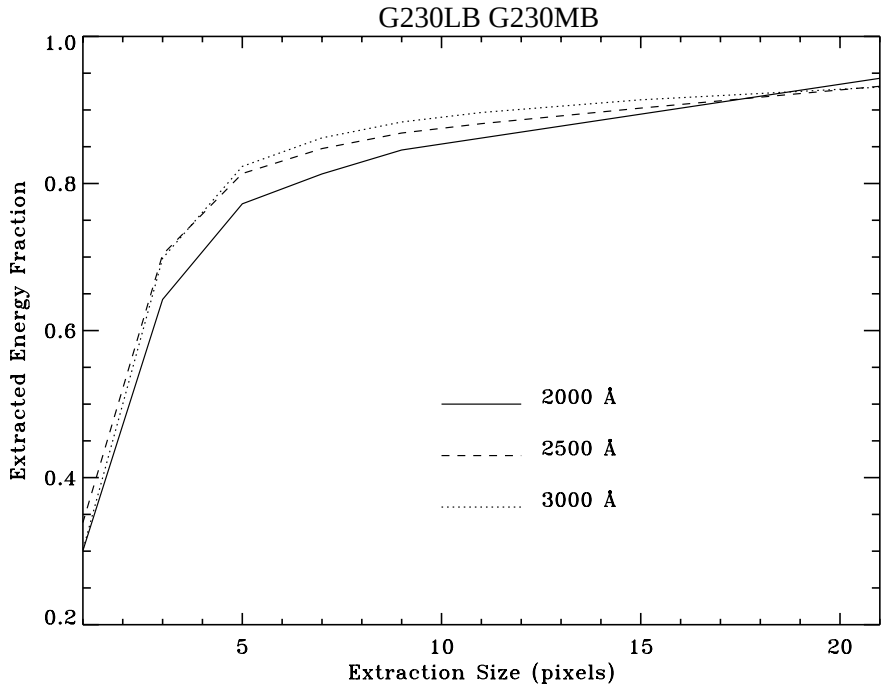

Table 13.31: Encircled Energies for G430L, G430M, G750L, G750M

Grating[a]	λ	Slit[b]	Extraction Height (pixels)	Flux (%) in Center Pixel	Flux in Extraction Aperture
G430L & G430M	3000	52X0.2	7	0.4299	0.9348
	4000			0.3551	0.9346
	5000			0.3879	0.9346
G750L & G750M	5500	52X0.2	7	0.3163	0.9302
	7000			0.3571	0.8929
	9000			0.1985	0.7353

a. M mode profiles are assumed to be identical to L mode profiles.

b. Values are only weakly dependent on observing slit.

Figure 13.80: G430L, G430M, G750L, and G750M Spatial Profiles

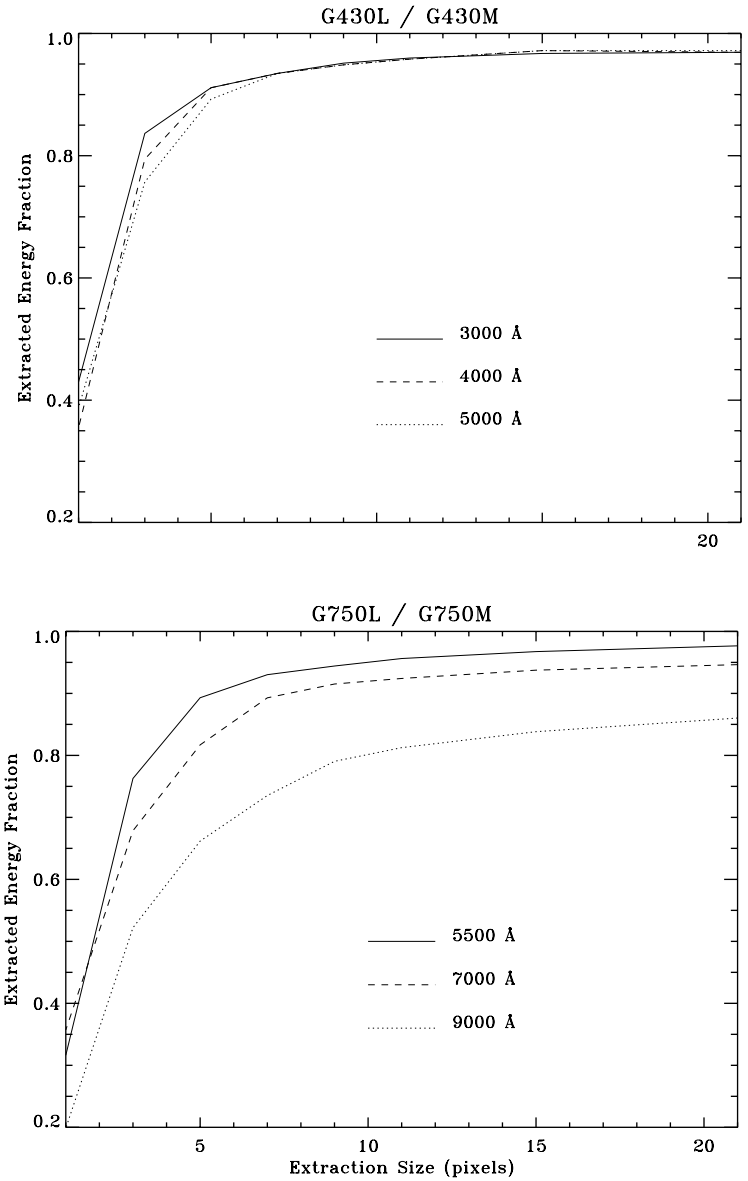

Echelle Spatial Profiles

Table 13.32: Encircled Energies for Echelle M Modes

Grating	λ	Slit	Extraction Height (pixels)	Flux (%) in Center Pixel	Flux in Extraction Aperture
E140M	1170	0.2X0.2[a]	7	0.274	0.944
	1400			0.308	0.959
	1600			0.331	0.961
E230M	1900	0.2X0.2	7	0.347	0.973
	2550			0.359	0.947
	3000			0.391	0.949

a. Values are only weakly dependent on observing slit.

Figure 13.81: Echelle M Modes Spatial Profiles

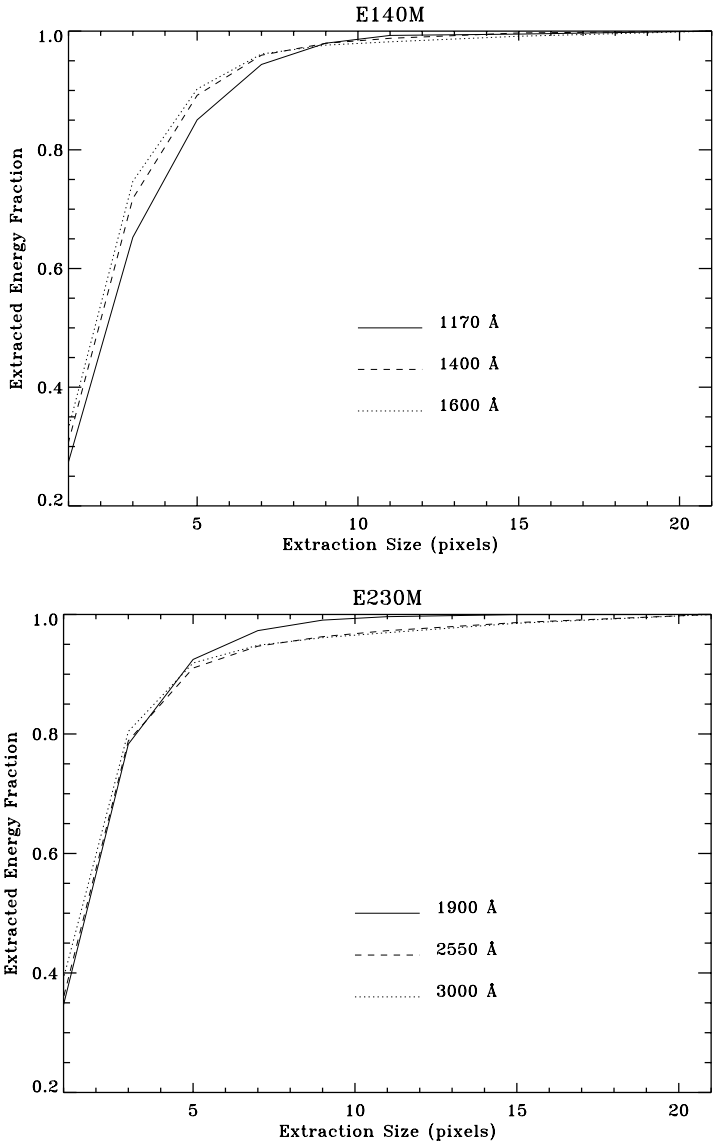

Table 13.33: Encircled Energies Echelle H Modes

Grating	λ	Slit	Extraction Height (pixels)	Flux (%) in Center Pixel	Flux in Extraction Aperture
E140H	1170	0.2X0.2[a]	7	0.276	0.948
	1400			0.300	0.983
	1600			0.335	0.981
E230H	1700	0.2X0.2	7	0.323	0.970
	2550			0.382	0.979
	2700			0.342	0.968

a. Values are only weakly dependent on observing slit.

Figure 13.82: Echelle H Mode Spatial Profiles

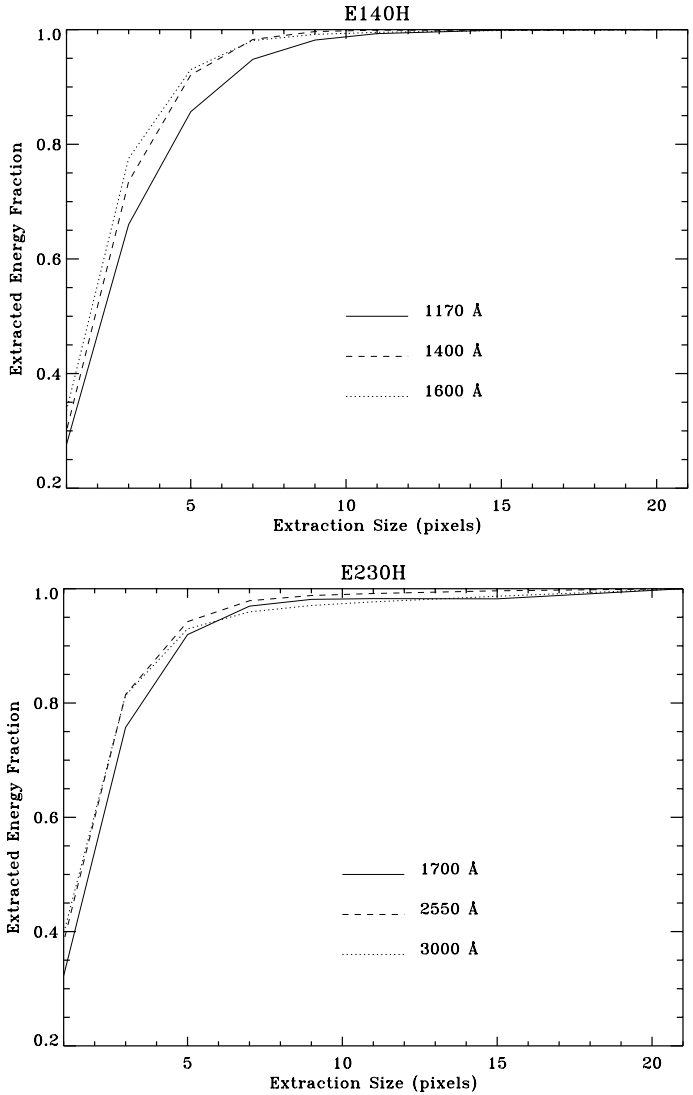

Line-Spread Functions

Below we provide model line spread functions (i.e., instrumental profiles) for point source observations through a sample of supported slits in first-order and echelle modes as a function of observing wavelength. Early on orbit internal lamp observations confirm the excellent optical performance of STIS (see e.g., STIS ISR 98-04). Data from external targets on the line spread functions is just becoming available through the Cycle 7 Calibration Program (see Chapter 17) so these models have not yet been confirmed in detail. Nevertheless they are ample for proposal planning.

These plots and the derived FWHM presented below in tabular form show that increasing the slit width for point source observations has very little effect on the FWHM of the observed lines but does broaden the wings of the LSFs. This occurs because a wider aperture allows more of the wings of the HST Optical Telescope Assembly PSF to enter but does not change the shape of the inner part of the PSF which is quite narrow. The implications of the LSF wings on line profile and equivalent width measures are discussed in more detail in “Spectral Purity, Order Confusion, and Peculiarities” on page 304. For diffuse source observations, don’t forget that widening the slit, while it allows more light to enter, also will degrade the spectral resolution obtained.

First-Order Line Spread Functions

Table 13.34: Spectral Resolution for CCD First-Order Modes

Slit	Spectral Resolution (FWHM in pixels)				
	Point Source				Extended Source
	3200 Å	5500 Å	7000 Å	10000 Å	
52X0.05	1.3	1.4	1.5	1.7	2
52X0.1	1.3	1.4	1.5	1.7	~2-3
52X0.2	1.3	1.5	1.6	2.0	~4
52X0.5	1.3	1.5	1.6	2.0	~10
52X2	1.3	1.5	1.6	2.0	~40

Figure 13.83: CCD First-Order L-Mode Line Spread Functions

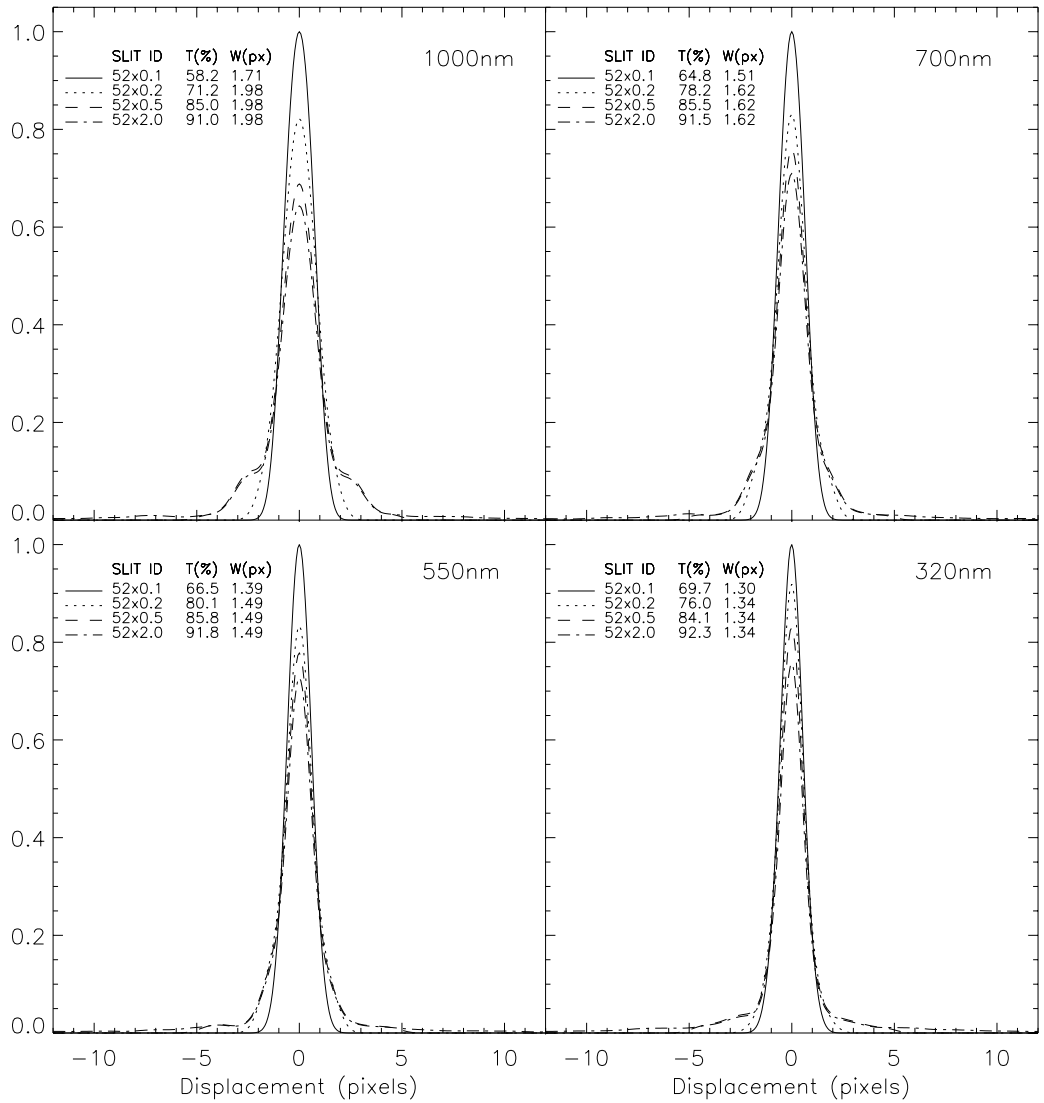

Table 13.35: Spectral Resolution for MAMA First Order Modes

Slit	Spectral Resolution (FWHM in pixels)				
	Point Source				Extended Source
	1200 Å	1500 Å	1700 Å	2400 Å	
52X0.05	1.6	1.5	1.4[a] 2.2[b]	2.1	-2
52X0.1	1.6	1.5	1.4[a] 2.2[b]	2.1	~4
52X0.2	1.7	1.5	1.4[a] 2.2[b]	2.1	~8
52X0.5	1.7	1.5	1.4[a] 2.2[b]	2.1	~20
52X2	1.7	1.5	1.4[a] 2.2[b]	2.1	~80

a. FWHM with FUV-MAMA (G140L, G140M).
b. FWHM with NUV-MAMA (G230L, G230M).

Figure 13.84: MAMA First-Order Line Spread Functions. Top G140L and G140M, bottom G230L and G230M

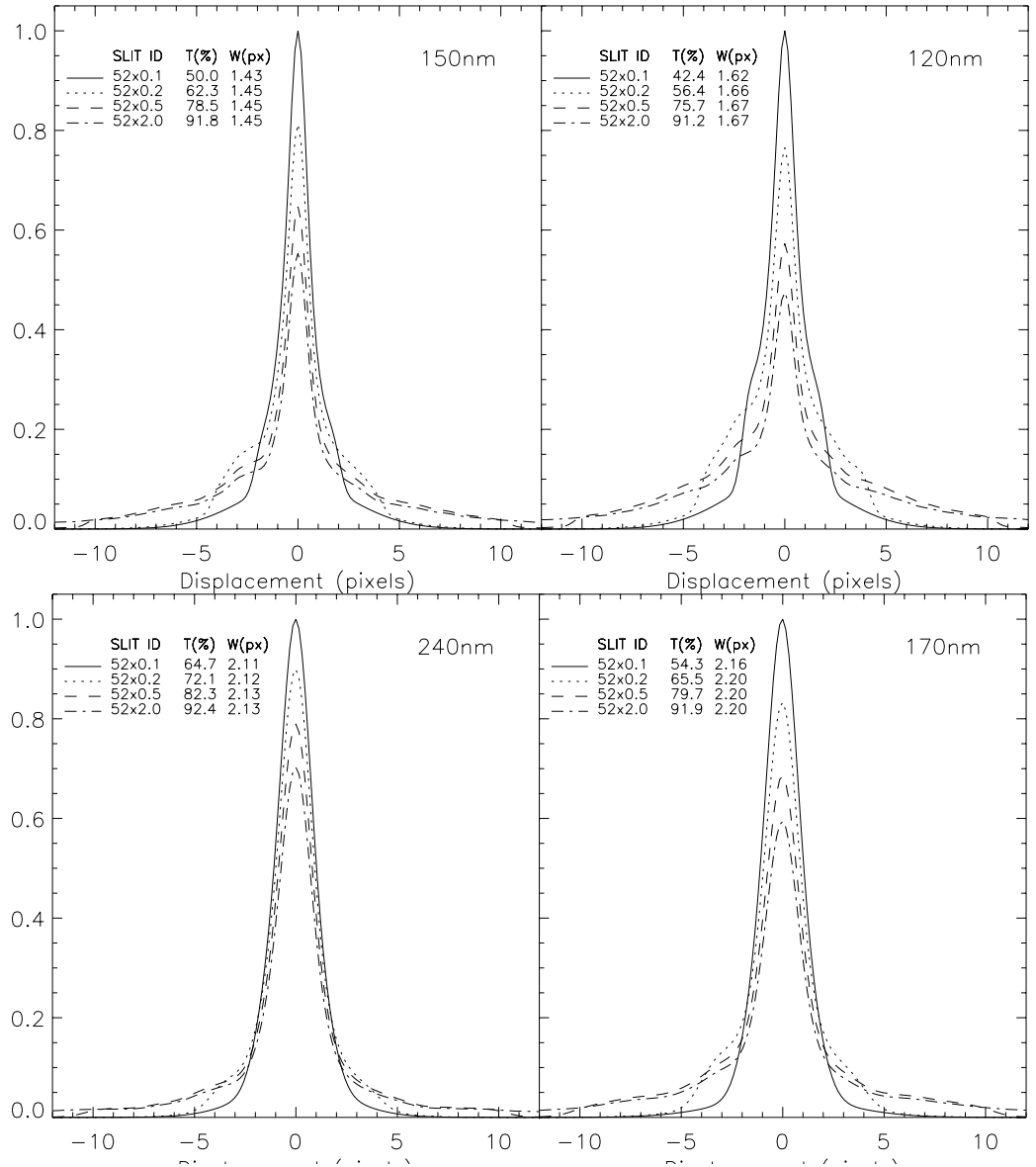

Echelle Line Spread Functions

Table 13.36: Spectral Resolution for Echelle Medium-Resolution Modes (E230M, E140M)

Slit	Spectral Resolution (FWHM in pixels)				
	Point Source				Extended Source
	1200 Å	1500 Å	1700 Å	2400 Å	
0.2X0.2	1.4	1.1	1.1[a], 1.9[b]	1.9	~6
0.2X0.06	1.1	1.1	1.1[a], 1.7[b]	1.7	~2
6X0.2	1.4	1.2	1.2[a], 2[b]	1.9	~6

a. FWHM with FUV-MAMA (E140M).
b. FWHM with NUV-MAMA (E230M).

Figure 13.85: Echelle Line Spread Functions, E140M (top) and E230M (bottom)

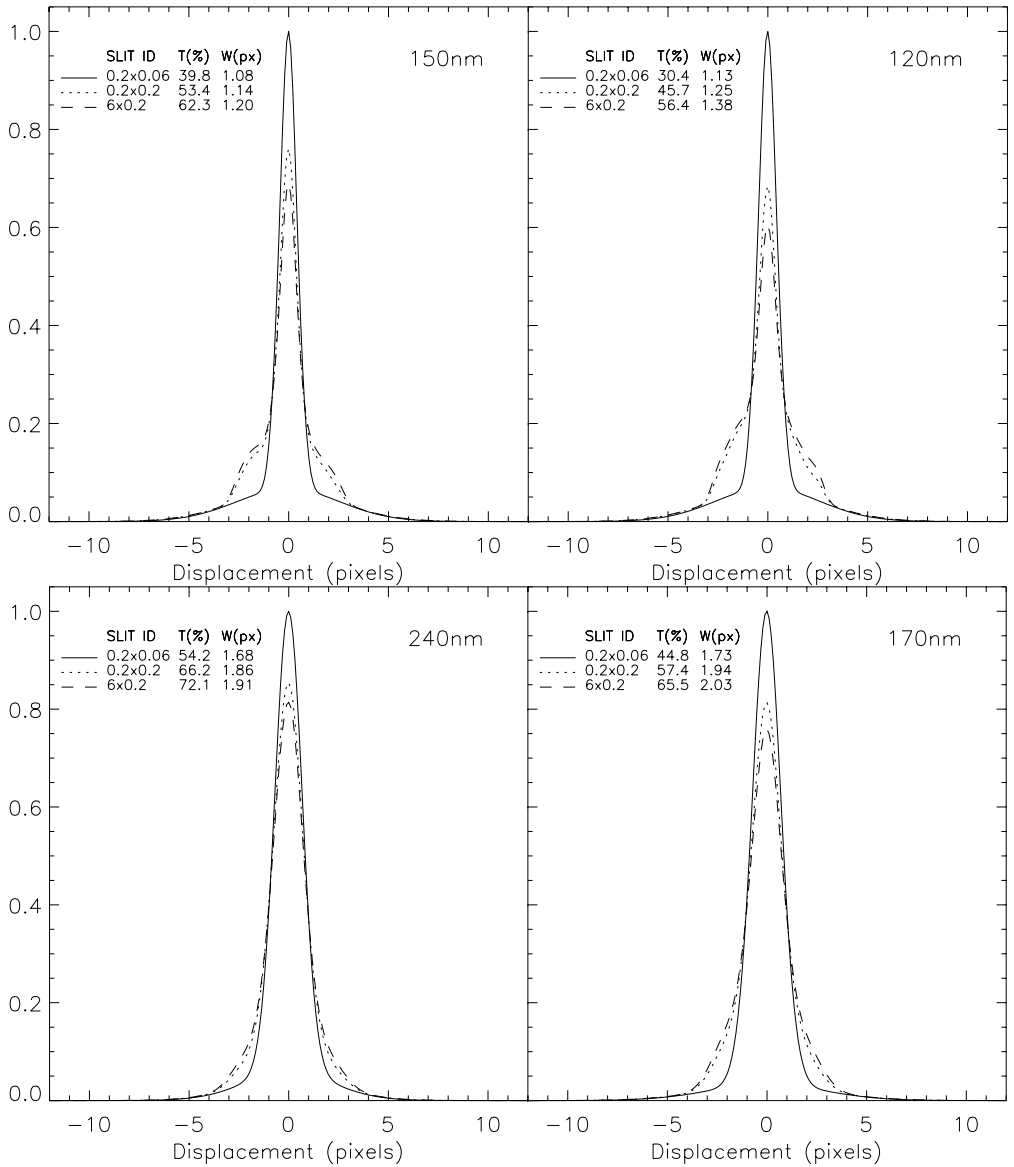

Table 13.37: Spectral Resolution for Echelle High Resolution Modes (E140H, E230H)

Slit	1200	1500	1700	2400	Extended Source
0.2X0.2	1.2	1	1[a], 1.8[b]	1.7	~6
0.2X0.09	1.1	1	1[a], 1.7[b]	1.7	~2
6X0.2	1.3	1.1	1.2[a], 2[b]	1.8	~5

a. FWHM with FUV-MAMA (E140M).
b. FWHM with NUV-MAMA (E230M).

Figure 13.86: Echelle Line Spread Functions, E140H (top) and E230H (bottom)

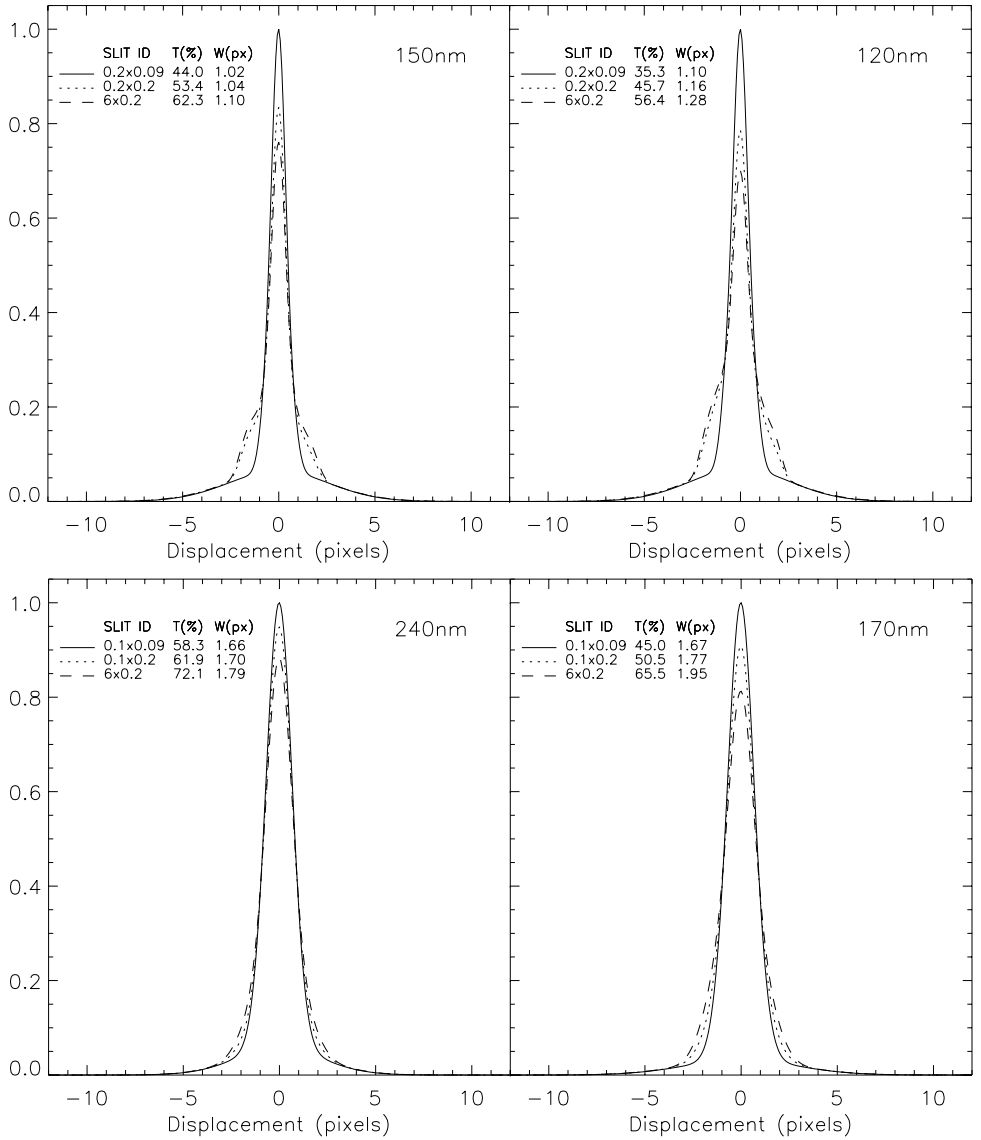

Spectral Purity, Order Confusion, and Peculiarities

If the PSF had an infinitely small FWHM and no extended wings, the spectrum of a point source would produce a spectrum with infinitesimal extension in the spatial direction. Furthermore, the spectral resolution would be essentially the theoretical limit of the spectrograph, independent of the entrance slit. In practice, the Optical Telescope Assembly PSF is wider and more complex, and there is scattered light from both the gratings and the detector itself, leading to decreased spectral resolution and spectral purity.

In Figure 13.87 we have plotted Hβ in the white dwarf Feige 110 observed with the G430L grating and five entrance slits with widths between 2″ and 0.″05. The spectrum observed through the 0.″05 slit and 0.″1 can be considered spectrally pure (remember 0.″1 maps to 2 pixels on the CCD and 0.″05 maps to 2 pixels on the MAMAs). Observations with the 0.″2 slits are still reasonably pure but larger slit widths lead to significant impurity. This becomes evident from the increasing flux in the line core with increasing slit width. The maximum spectral purity is achieved with entrance slits of 0.″2 width or smaller. Similar results can be seen in Figure 13.88 which shows the calcium triplet regions. Observers wishing to study spectral lines of continuum sources should always consider using small entrance slits.

Figure 13.87: Hβ in the White Dwarf Feige 110 Observed with G430L and 5 Entrance Slits

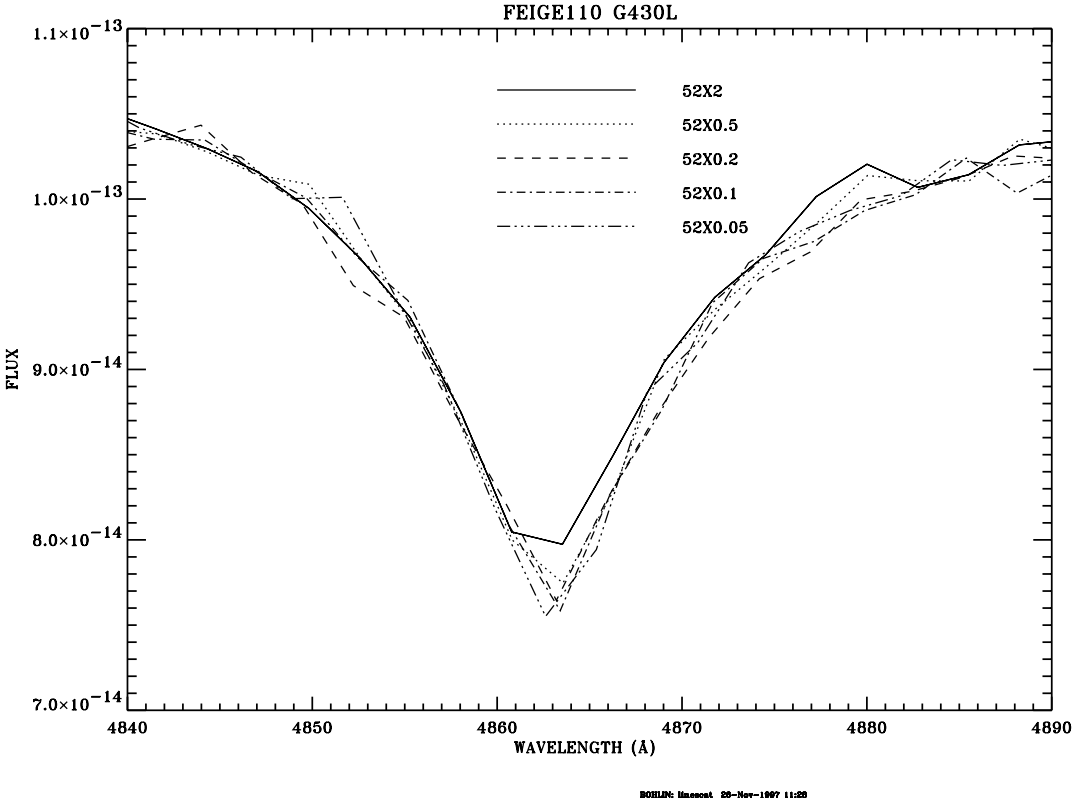

Figure 13.88: Calcium Triplet Observed with G750L and 7 Entrance Slits

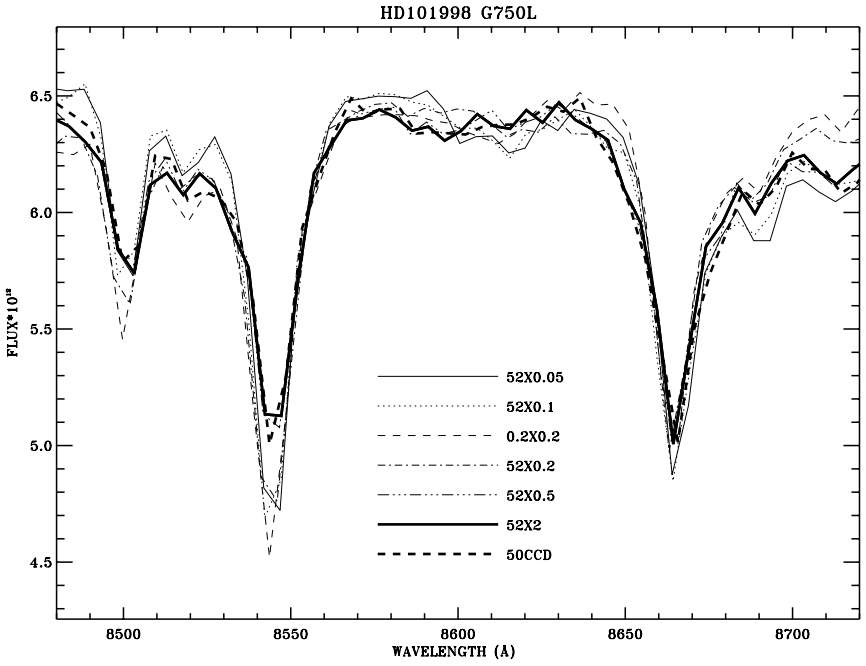

Order Overlap and Scattered Light for Echelle Gratings

As with most other echelle spectrographs, STIS echelle data are affected by spectral order overlap at the shortest wavelengths where adjacent spectral orders are not well separated due to the degraded PSF in the UV. Echelle observations of continuum sources taken slitless or with a 2″ x 2″ entrance slit suffer from severe order overlap. Therefore, an entrance slit of 0.″2 or smaller height should be used.

Figure 13.89 demonstrates the difference in resolution for a narrow absorption line for BD+75˚325 observed in the `0.2X0.2` slit vs a `0.2X0.09` slit. Any difference in the effect of impure light on the depth of the line profiles is less than ~1% of the continuum. An extraction height of 7 pixels is used; and the `0.2X0.09` aperture spectrum is multipled by 1.28 to compensate for the lower transmission. A slight wavelength shift is maintained to improve visibility.

Figure 13.89: Comparison Between 0.2X0.2 (solid line) and 0.2X0.9 (dotted line) Aperture Spectra of BD+75˚325 in the E140H-1416 Mode

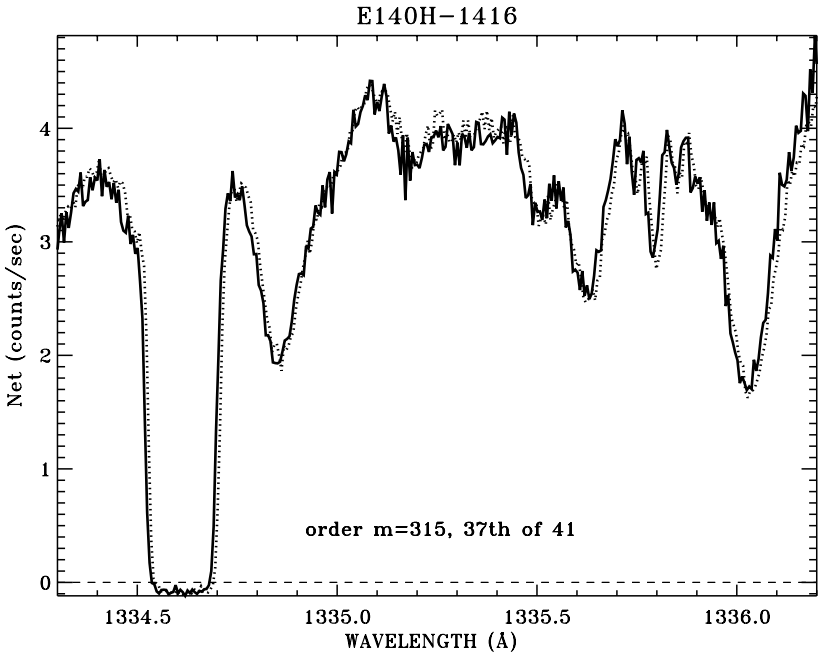

Note the “oversubtraction” of the black line. This is a ramification of oversubtraction of the background; light which is scattered from the echelle, the OTA PSF and the detector into the interorder area is being oversubtracted from the science spectrum in the straightforward background subtraction procedure used. The E230M and E230H gratings are only a little affected by this scatter (7% of the light is scattered at ~ 2000 Å, 4% at 2500 Å). However, the E140M and E140H modes do have appreciable scatter; 33% of the light scattered at 1235 Å for E140M and 15% for E140H; at 1600 Å this drops to ~12% and 8%, respectively. This scattered light component was not taken into account in the global count rate prediction in the Cycle 7 Handbook, but is in this Cycle 8 version (hence observers will note the bright object protection limits are now more conservative for the echelle modes). The STScI provides an exposure time calculator (ETC), which predicts global and net countrates to sufficient accuracy for planning purposes. An estimate of the *net* S/N and the *net + scattered light* in an echelle observation are produced for a specified input spectrum, including an approximation to the scattered component.

Spectroscopic Mode Peculiarities

During SMOV and initial observations, a number of first-order mode spectra have been obtained which show additional features which may affect the scientific goals of the observations. One class of spectroscopic images show diffraction structure of the PSF re-imaged at the various STIS detectors. A second

class, commonly referred to as railroad tracks, display additional "spectra" displaced and parallel to the primary spectrum. Some examples and impacts are presented below.

PSF Reimaging

The STIS corrector mirrors, reimage the OTA PSF at an intermediate focus within STIS at the location of the slit wheel. This intermediate image is reimaged to one of the detectors via the selected mode, either imaging or spectroscopic. Any PSF structure present in the slit plane image will be reimaged at the detectors, however its appearance in a final spectrum or image depends on the selected mode and the slit or aperture used.

In the imaging modes, little PSF diffraction structure is apparent, since the available filters are typically relatively broad band, smoothing out any structure. The spectroscopic modes however, create a series of near monochromatic images at the detector plane and the PSF diffraction structure can be detected with the two dimensional STIS detectors.

Point Source: Figure 13.90 shows the spectrum of a point source target, using G140L and slit `52X0.05`.

Figure 13.90: Spectrum of a Point Source (Stellar) Target

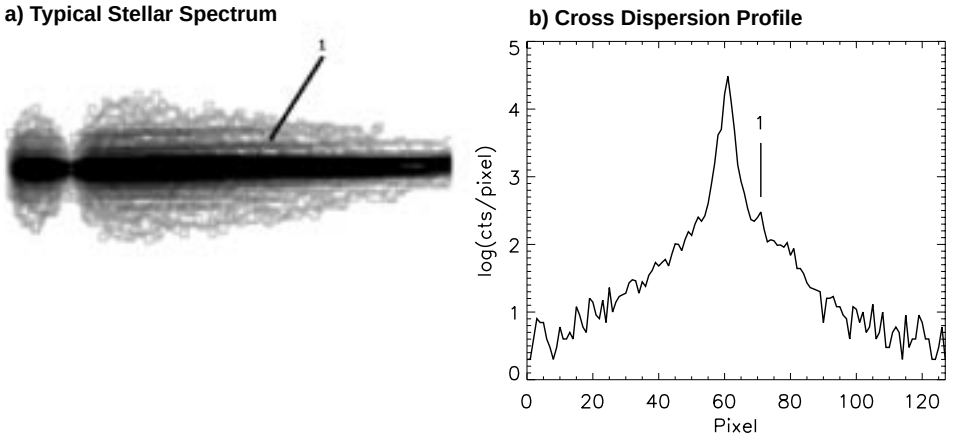

This typical stellar spectrum (1150–1700 Å) shown in panel a, was of a white dwarf for instrument calibration. The Lyman-α absorption feature is apparent near the left end. This image was processed and log stretched to enhance the “fringes” seen above and below the stellar spectrum. These fringes are weak, diverge from the spectrum proportional to wavelength, and are not present in the Lyman-α gap, indicating they are connected with the source at the slit plane and are not the result of STIS internal scatter. Panel b shows a cross dispersion profile of the original image, cut near the center of the spectrum at about 1430 Å. The brightest fringe (labelled “1”) is indicated; the peak of the fringe is roughly 0.005 times the peak of the stellar spectrum.

Figure 13.91 illustrates how such fringes are created at the detector. At each wavelength, the portion of the PSF at the slit plane which passes the slit, is re-imaged onto the detector. The envelope of all such PSF portions forms the

complete image at the detector, as shown. The characteristic fringe separation, proportional to wavelength, is expected as the diffraction structure in the PSF increases with wavelength as shown. In the medium resolution modes, with much less bandpass than the low resolution modes, the tilt of the fringes is much less—they are nearly parallel to the primary spectrum.

Figure 13.91: How Fringes are Created

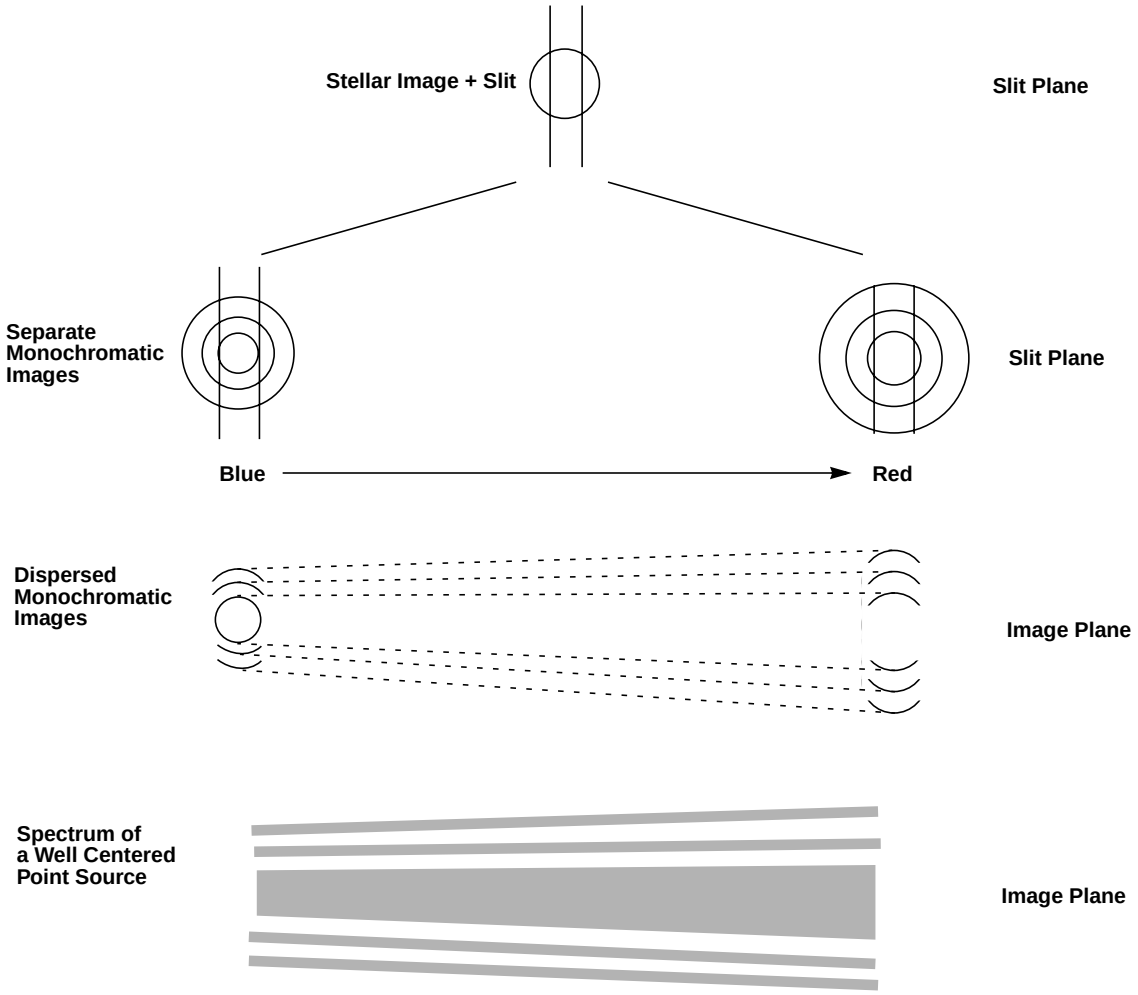

The fringe visibility is decreased with increasing slit width. Figure 13.91 illustrates this—as the slit broadens, more of a curved portion of the diffraction rings is transmitted. The envelope of these more curved sections is broader with lower contrast compared to the sharp segments visible with a narrow slit.

Out of slit point source: Figure 13.92 shows the spectrum (G140L) of a stellar source, in which the target was mis-located and not nominally in the `52X0.05` slit. While the target center was not located in the slit, the extended PSF structure did cover the slit opening and was transmitted and re-imaged at the detector plane. This image has been processed and log stretched to enhance the faint fringe structure which is apparent.

Figure 13.92: Mis-Located Target—Stellar Source

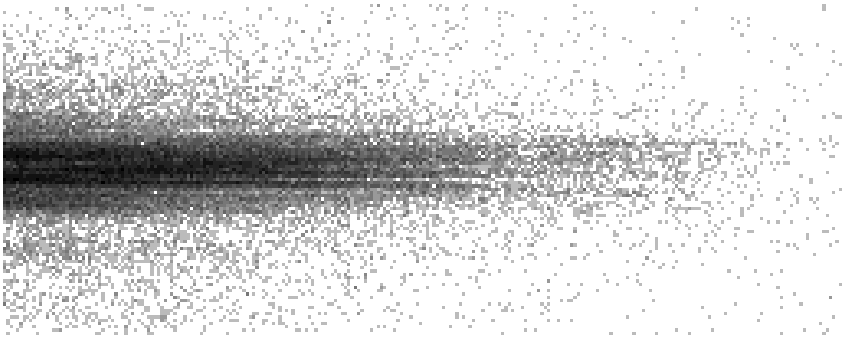

Figure 13.93 shows a similar case in which the spectrum of a galaxy with a very bright core was obtained with the core located roughly 0.1" from the center of the 0.1" wide slit in the visible mode G750L. The images were processed and log stretched to enhance the fringe appearance. Divergent fringes are apparent above and below the spectrum. A principle component of the “spectrum” consists of the upper and lower portions of the offset, first Airy ring, seen clearly separated at the long wavelength end of the spectrum. These two fringes converge at shorter wavelengths forming a single fringe which overlays the much fainter, off-core portion of the galaxy. The evident blueness of the core spectrum in this particular source makes the combined blue fringes much brighter than the combination of the separated red fringes.

Figure 13.93: Mis-Centered Spectrum of Galaxy with Bright Core

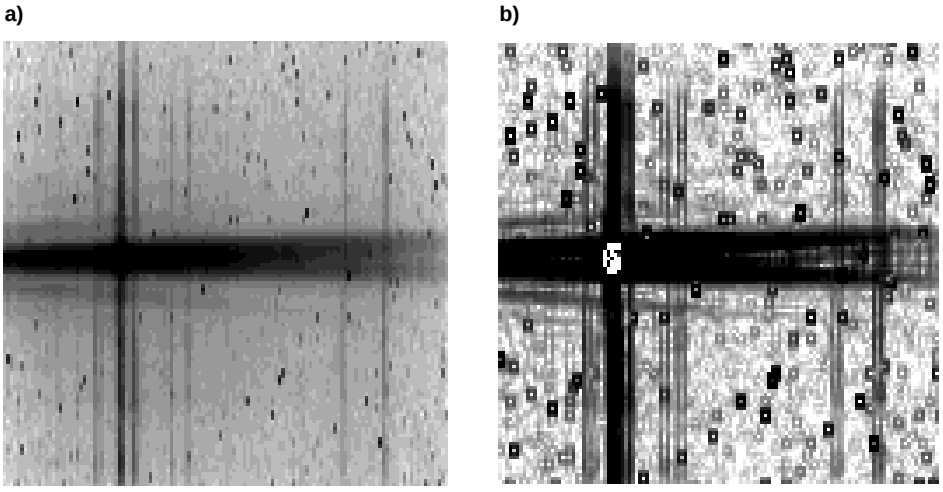

Impact

Diffraction structure in the PSF will set a limit to extracting spectra near a bright source. Blocking the bright source, either by using a coronagraphic aperture or by moving the bright source out of the slit does not remove the inherent, adjacent PSF or diffraction structure. In the case of a faint companion

adjacent to a bright, primary souce, note that the spectra of the primary and companion will be parallel while the PSF fringes will be tilted. This is especially true in the low resolution modes and may allow the unambiguous identification of a faint companion even in the presence of comparably bright PSF structure.

Railroad Tracks

Figure 13.94 (panel a) shows a processed spectrum of a continuum lamp in mode G750M, λ_C = 10,363 and slit `0.1X0.2` obtained during ground testing. Besides the spectrum, two adjacent, parallel, secondary spectra are seen symmetrically displaced about 13 pixels from the lamp spectrum. Panel b shows a cross dispersion profile illustrating the magnitude and shape of the spectra. The secondary spectra have peak intensities about 8% of the primary spectrum but are broader and asymmetric. This was the only example of this peculiar condition noticed during ground testing, however subsequent review showed one additional example also obtained during ground testing. This second case was a similar continuum lamp spectrum using G750M, λ_C = 7795, with the same slit. Secondary spectra were ~8% and 3% (peak intensity) of the primary peak intensity.

Figure 13.94: Railroad Tracks

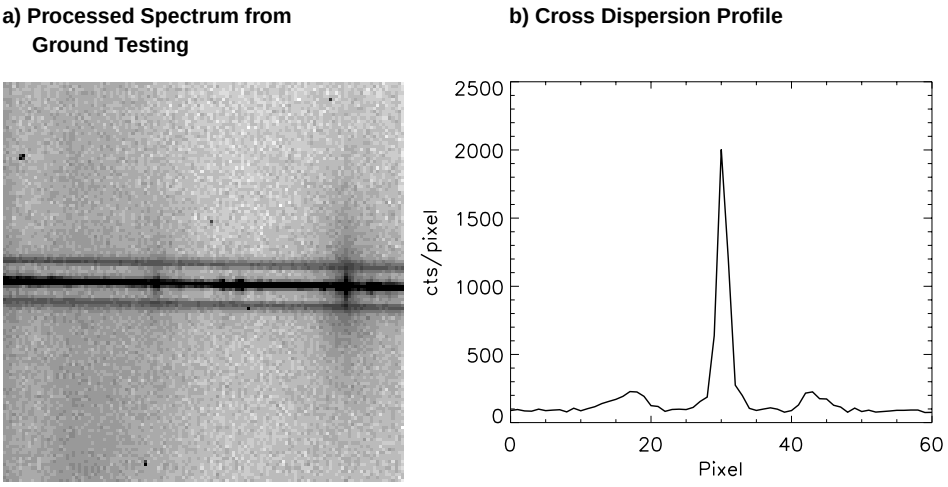

One similar example has been obtained in flight to date, with the UV mode G230LB and the CCD. The target was a very red star. The parallel, secondary spectra are visible at a level of about 8% of peak intensity.

The cause of these secondary spectra in these three observations is not known. The three cases observed have all been with the CCD: no MAMA examples have been obtained. Other observations in these modes under similar conditions have not shown such effects. In all cases, a red source was observed. The broad profile and relatively bright intensity of the secondary spectra suggest a multiple reflection instead of diffraction origin but no way of producing dual, symmetric features has yet been proposed which is consistent with these observations.

MAMA Spectroscopic Bright-Object Limits

As described in "MAMA Bright-Object Limits" on page 115, in Chapter 7, the MAMA's are subject to absolute brightness limits, above which sources cannot be observed or they would potentially damage the detectors. In Table 13.38, below, we present the complete set of absolute bright object point source spectroscopic screening magnitudes and fluxes for the MAMA spectroscopic modes. These screening magnitudes are presented as a *guide*. Whether an individual source can be observed is ultimately determined by whether, in the desired configuration, the spectrum of that source is predicted to exceed the global and local observing count rate limits, as described in Chapter 7. The information presented here should be used in conjunction with the material presented in Chapter 7. Remember, sources cannot be observed in configurations where they exceed the absolute bright object limits. A few important points to note are:

- The screening limits are given either as V magnitude or CGS units as indicated.
- The screening limits in this table have been calculated assuming zero slit losses. To determine if your source will violate the limits in this table, you must first correct the magnitude limit for the aperture throughput for your chosen slit. The maximum magnitude correction achieved without use of a neutral density filter using a supported slit is ~0.75 magnitudes. An exception to this are the values for the local surface brightness limits in row 1 of Table 13.38. They were calculated for a 52X2 slit.
- The screening limits in the tables assume zero extinction. To determine if your source will violate the limits in this table, correct the magnitude limit for the extinction of your source.
- The peak flux from an emission line or from the continuum from your source must be less than flux limit given in row two (for point sources—remember to correct for your aperture throughput) and row one for diffuse sources (remember to correct for the width of your source by scaling by your slit width in arcseconds divided by 2.0).
  - For echelle observations, the global limit of 200,000 counts sec^{-1} over the detector sets the magnitude limits, and but you must also assure that your source does not violate the local limit, e.g., if it had a bright emission line.
  - If you are observing a source which has high equivalent width line emission (i.e., whose flux is dominated by line emission), you must assure that the *line emission* does not exceed the limits. This may be a concern for stars with strong emission lines, such as Wolf Rayet or T-Tauri stars.
- If you plan to place multiple bright stars in the long slit, or observe slitless, you must also assure that the sum from all targets imaged on the detector do not exceed the applicable global limit.

- The limits in this table are the worst case limits for the scanned gratings; use of a less sensitive central wavelength may have a brighter true limit, allowing you to observe your target.

Table 13.38: MAMA Spectroscopic Bright-Object Limits—V Mags and cgs Units

Spectral Type	G140L	G140M	E140M	E140H	G230L	G230M	E230M	E230H
Local limit surface brightness[a]	$9.5x10^{-12}$	$2.0x10^{-10}$	$1.3x10^{-9}$	$3.3x10^{-9}$	$2.9x10^{-12}$	$1.1x10^{-10}$	$3.2x10^{-10}$	$1.9x10^{-9}$
Local limit point source flux[b]	$3.1x10^{-12}$	$7.9x10^{-11}$	$5.2x10^{-10}$	$1.4x10^{-9}$	$5.4x10^{-13}$	$2.6x10^{-11}$	$7.4x10^{-11}$	$4.4x10^{-10}$
O5 V[c]	15.2	13.1	12.0	11.5	14.8	11.2	11.8	10.4
B1 V	14.7	12.2	11.5	10.9	14.3	10.9	11.2	9.9
B3 V	14.2	11.8	10.9	10.3	13.9	10.5	10.8	9.5
B6 V	13.1	10.9	10.1	9.5	13.4	9.9	10.3	8.9
B9 V	11.8	9.6	8.9	8.2	12.7	8.9	9.6	8.1
A1 V	10.3	8.3	7.7	7.1	12.1	8.6	9.2	7.7
A3 V	9.0	6.5	6.2	5.9	11.7	8.2	8.7	7.3
A5 V	7.8	4.9	5.0	4.7	11.3	7.8	8.3	6.9
A9 IV	4.9	2.6	2.3	1.6	10.7	7.3	7.9	6.5
F2 V	3.4	1.0	-0.3	-1.4	10.3	7.0	7.6	6.2
F4 V	2.8	0.1	<-2.0	<-2.0	10.1	6.8	7.4	6.1
F6 V	2.0	-0.9			9.9	6.6	7.2	6.0
F8 V	1.3	-1.7			9.7	6.5	7.0	5.9
G2 V	-0.1	<-2.0			9.2	6.2	6.7	5.7
G5 IV	-1.2				8.9	6.0	6.3	5.5
G7 IV	<-2.0				8.8	5.8	6.2	5.3
K0 IV					8.4	5.5	5.8	4.9
K4 V					7.8	4.9	5.1	4.1
K8 V					7.1	4.6	4.2	3.2
M2 V					6.3	3.9	3.5	2.8
M4 V					6.0	3.5	3.1	2.6
M6 V					5.6	3.2	2.8	2.3
T~50000°K[d]	15.1	13.0	11.9	11.4	14.7	11.1	11.7	10.3
λ^{-1} [e]	11.4	8.6	8.4	7.6	12.3	8.8	8.5	7.7

[a] Peak surface brightness in ergs sec^{-1} cm^{-2} $Å^{-1}$ $arcsec^{-2}$ of the continuum or of an emission line from a diffuse source for a 52X2 slit.
[b] Peak flux in ergs sec^{-1} cm^{-2} $Å^{-1}$ of an emission line from a point source.
[c] Limits are V magnitudes, assuming zero reddening.
[d] Limits for a black body with a temperature of 50,000 degrees K.
[e] Limits for a source with a spectrum F_λ proportional to λ^{-1}.

CHAPTER 14
Imaging Reference Material

In This Chapter...

In this Chapter, we provide imaging reference material, in support of the information presented in Chapter 5.

Introduction

This chapter provides reference material to help you select your filter and detector configuration and determine your observing plan (e.g., total required exposure time, and number of exposures). This chapter is, for the most part, organized by *filter and detector.* For each imaging mode the following are provided:

- A table of integrated system efficiencies and zeropoints for all the modes.
- Plots and tables of throughput and sensitivity as a function of wavelength.
- Where useful, plots of throughput on a logarithmic scale to show out-of band throughput (redleak or blueleak) for the different filters.
- Plots of the time needed to achieve a desired signal-to-noise ratio vs. magnitude for broadband filters and vs. line flux for narrowband filters.
- Plots of the PSF and encircled energies, along with a logarithmic-scale image of the PSF.

In addition, we provide the following sections:

- “MAMA Imaging Bright Object Limits” on page 368 presents screening tables of bright object magnitudes for sources of different spectral type, for use in deciding if a MAMA imaging observation is safe.
- “Image-Mode Geometric Distortion” on page 364 presents information on the geometry of the MAMA and CCD imaging modes.
- “Spatial Dependence of the STIS PSF” on page 365 presents information on the changes of the PSF with position in the STIS field of view.

Using the Information in this Chapter

Sensitivity Units and Conversions

This chapter contains plots of throughputs and tables of sensitivities and throughputs for each grating mode. “Determining Count Rates from Sensitivities” on page 70 explains how to use these sensitivities to calculate expected counts rates from your source.

The first table for each filter provides the following quantities:

Pivot wavelegth

Source-independent measure of the characteristic wavelength of the bandpass, defined such that it is the same if the input spectrum is in units of f_λ or f_ν:

$$\lambda_p = \sqrt{\frac{\int T(\lambda) d\lambda}{\int T(\lambda)((d\lambda)/\lambda)}}$$

For filters with redleaks, the pivot wavelength and FWHM correspond to the "in-band" region, and do not include the redleak.

FWHM

Full-width at half-maximum of the throughput $T(\lambda)$.

AB mag zeropoint

AB magnitude of a source that produces a flux of one count per second.

S^P_{peak}

Peak sensitivity (electrons s^{-1} $Å^{-1}$ per incident erg cm^{-2} s^{-1} $Å^{-1}$).

B_λ

Equivelant bandpass of filter, defined such that $\int S^P_\lambda d\lambda = S^P_{peak} B_\lambda$ (see Chapter 6).

For filters with redleaks this integration includes only the primary bandpass.

Radius for 80% of point source flux

Radius in arcseconds of an aperture that encloses 80% of the flux of a point source.

% flux in central pixel

Percentage of the flux of a point source that falls within the central pixel (this estimate is accurate to about 10%).

The first figure for each imaging mode gives the integrated system throughput. This is the combination of the efficiencies of the detector and of the optical elements in the light path. The throughputs in this handbook are based in part on ground-test data. Preliminary analysis of orbital data indicates that they are correct to within 15% for all modes. The bottom section of the throughput figures includes wavelengths beyond the nominal passband of that mode, showing any red or blue "leak" on a log scale. The throughput is defined as the number of detected counts per second per cm^2 of telescope area relative to the incident flux in photons per cm^2 per second. For the CCD "counts" is the number of electrons detected. For the MAMA, "counts" is the number of valid events processed by the detector electronics after passing through the various pulse-shape and anti-coincidence filters. In both cases the detected counts obey Poisson statistics. The throughput includes all obscuration effects in the optical train (e.g., due to the HST secondary and due to the STIS CCD Lyot stops). The "effective area" of the mode can be computed from the throughput by multiplying by the physical area of the HST primary mirror (45238.93416 cm^2). This is shown on the ordinate label on the right side of each plot.

The table for each mode gives the throughput and the point-source sensitivity as a function of wavelength. Throughput has the meaning described above. The *imaging point-source sensitivity* S^p_λ has units of counts $sec^{-1}Å^{-1}$ per incident erg cm^{-2} s^{-1} $Å^{-1}$ for the MAMAs, and electrons $sec^{-1}Å^{-1}$ per incident erg cm^{-2} s^{-1} $Å^{-1}$ for the CCDs. Counts and electrons refer to the total counts from the point source integrated over the PSF.

The *imaging diffuse source sensitivity,* S^d_λ, has the units:

counts sec^{-1} pix^{-1} per incident dimensional erg cm^{-2} sec^{-1} $Å^{-1}$ $arcsec^{-2}$ for the MAMAs and
electrons sec^{-1} pix^{-1} per incident dimensional erg cm^{-2} sec^{-1} $Å^{-1}$ $arcsec^{-2}$ for the CCDs.

Thus S^p_λ and S^d_λ are related through the relation:

$$S^d_\lambda \cong (S^P_\lambda \times m^2)$$

Where *m* is the plate-scale in arcsec per pixel.

Here, we have assumed that the diffuse source has a uniform brightness over the area of interest.

Signal-To-Noise

For each imaging mode, plots are provided to estimate the signal-to-noise (S/N) for a representative source. The first figure shows S/N for point sources (for two different gains for the CCD). The second figure shows S/N for uniform extended sources of area 1 $arcsec^2$ and 0.2 $arcsec^2$.

The different line styles in the S/N figures delineate regions where different sources of noise dominate. A particular source of noise (readnoise for example) is presumed to dominate if it contributes more than half the total noise in the observations.

To the left of the vertical line in the S/N plots, the count rate from the source exceeds the 100 counts sec^{-1} pix^{-1} local count rate limit. This is computed from the on-orbit measured PSF, which gives 6 to 14% of the flux in the central pixel. The bright-object screening limits in Table 14.33 use the more conservative (for this purpose) estimate of 25% of the flux in the central pixel.

The point-source S/N figures are shown for average sky levels, and for sky levels during orbital night. For the CCD the read noise has been computed assuming a number of readouts `NREAD` = integer (*t* / 1000 s), where *t* is the exposure time, with a minium `NREAD=2`. That is, each exposure has a minimum `CR-SPLIT=2`. Different line styles in the figures are used to indicate which source of noise dominates.

For the CCD, the dominant sources of sky background are zodiacal light and scattered earthshine. The `LOW-SKY` requirement can be used to ensure that these backgrounds are kept as low or lower than the rates assumed for these plots. If

your source falls within the sky-dominated portion of the figures, you may want to consider imposing the LOW-SKY requirement.

For the NUV-MAMA the sky background has about equal contributions from zodiacal light and OII 2470 Å emission on the day side of the orbit. On the night side, the OII 2470 Å emission is greatly reduced and the sky background is dominated by zodiacal light. In both cases the sky background is less than the dark current.

For the FUV-MAMA, the dominant source of background is geocoronal emission lines (see Chapter 6). These vary strongly from the day to night side of the orbit. For broad-band the contribution from the geocoronal lines can be minimized by using the F25QTZ filter, or observing with the DARKTIME special requirement.

In situations requiring more detailed calculations (non-stellar spectra, extended sources, other sky background levels, unknown target V magnitude, etc.), the STIS Exposure-Time Calculator, located at the STIS web page, should be used.

Follow these steps to use the signal-to-noise plots:

1. Determine the AB magnitude of your source at the wavelength of interest. There are several ways to do this.
   - Examine Table 14.1 and find AB_ν for the desired spectral type and filter. Sum the V magnitude of the target and AB_ν derived from the table.
   - Alternatively, compute ABMAG (=V+AB_ν) from the source flux, using the relation $ABMAG = -2.5\log f_\nu - 48.60$, or $ABMAG = -2.5\log f_\lambda - 5\log\lambda - 2.406$.
2. Find the appropriate plot for the filter in question, and locate V+AB_ν on the horizontal axis. Then read off the signal-to-noise ratio for the desired exposure time, or vice-versa.

The “x” characters at the top of each plot indicate the onset of saturation, in the case of the CCD. The “x” shows where the total number of counts exceeds the 16-bit buffer size of 65,535.

We now give a sample S/N calculation using these plots. Consider a V=27 star of spectral class G2V, for which we want to obtain S/N = 20 with F28X50LP observing with the CCD. From Table 14.1 we find a correction $AB_\nu = -0.21$ to go from V magnitude to AB magnitude near the center of the F28X50LP bandpass. We thus have V+AB_ν=26.79. We look at Figure 14.8 on page 323 and find this value on the horizontal axis and read up to find the curve that intersects the desired S/N. We find approximately 10,000 seconds are needed to reach S/N = 20 in conditions of low sky background.

Point Spread Functions

The final figures and table for each imaging mode contain information on the point-spread function. The encircled energy plots and tables are normalized to 1 at a radius of 1 arcsecond. In actuality about 10% of the light from a point source falls beyond this radius; however high S/N observations extending out to large

radius exist for only a few modes from on-orbit data. The intensity vs. radius plots are normalized to a total integrated flux of 1. The PSF image is shown on a logarithmic intensity scale to enhance faint features in the wings of the PSF. Note the stellar like ‘ghost’ at approximately 45 pixels left of the peak pixel in the NUVMAMA+Filter images. The ghost is a few tenths of a percent of the psf peak intensity. See Bowers (1997 HST Calibration Workshop) for a discussion of HST “breathing” effects on the PSF.

Table 14.1: Color Corrections AB_ν to go from Johnson V Magnitude to AB Magnitude

Spectrum	F28x50LP	50CCD	OIII	OII	NUVMAMA	NUV QTZ	NUV CN270	NUV MgII	NUV CN182	NUV CIII	FUVMAMA	FUV QTZ	FUV SRF2	FUV LYA
Sky	-0.31	0.13	0.23	1.79	0.15	3.17	4.96	4.88	1.87	4.33	-2.53	11.83	-0.30	-3.72
Sky (shadow)	-0.18	0.17	0.17	1.36	0.74	4.13	3.61	3.55	2.55	6.01	-2.04	10.74	2.87	-3.32
O5V	0.48	-0.23	-0.13	-0.64	-1.59	-1.50	-1.21	-1.14	-1.69	-1.66	-2.07	-1.9	-1.99	-2.18
B0V	0.47	-0.15	-0.16	-0.59	-1.26	-1.19	-0.96	-0.90	-1.36	-1.30	-1.61	-1.62	-1.68	-1.46
A0V	0.27	0.26	-0.06	0.83	1.79	1.70	1.56	1.54	1.80	1.75	2.81	1.94	2.32	4.62
A5V	0.18	0.27	-0.02	0.97	2.67	2.51	2.20	2.12	2.82	2.61	5.90	4.21	5.31	9.00
F2V	-0.02	0.22	0.07	1.06	3.35	3.18	2.61	2.57	4.11	4.06	8.65	6.83	8.05	12.24
G2V	-0.21	0.16	0.17	1.34	4.45	4.28	3.77	3.54	6.49	6.65	14.77	12.93	14.16	18.56
K0V	-0.31	0.14	0.21	1.85	5.60	5.43	5.13	4.9	7.62	7.22	10.17	9.67	9.97	10.54
M0V	-0.97	-0.30	0.68	3.29	6.93	6.75	6.64	6.41	9.12	8.56	11.67	11.17	11.48	12.04
M6V	-1.78	-1.03	0.74	3.44	7.32	7.14	7.12	6.89	9.59	8.86	12.15	11.65	11.96	12.52
O7I	0.45	-0.04	-0.12	-0.57	-0.50	-0.49	-0.56	-0.59	-0.53	-0.50	-0.52	-0.68	-0.62	-0.34
B0I	0.38	-0.06	-0.10	-0.42	-0.71	-0.70	-0.68	-0.64	-0.72	-0.71	-0.75	-0.77	-0.85	-0.50
F0III	0.05	0.25	0.02	1.08	3.55	3.38	2.89	2.79	4.20	4.04	8.57	6.74	7.97	12.21
G0III	-0.26	0.15	0.18	1.58	5.34	5.16	4.82	4.67	7.34	6.92	9.90	9.39	9.70	10.27
K2III	-0.52	0.03	0.36	2.77	7.39	7.21	7.84	7.12	10.34	8.5	13.42	12.92	13.22	13.79
M0III	-0.98	-0.32	0.61	3.89	7.58	7.41	7.33	7.00	9.23	8.89	11.16	10.66	10.97	11.53
M6III	-2.66	-1.87	1.54	3.16	7.12	6.96	6.63	6.30	8.54	8.14	10.47	9.97	10.27	10.84
Elliptical	-0.61	-0.05	0.36	2.17	5.16	5.05	4.94	4.91	5.57	5.43	6.33	5.99	6.16	6.96
Sa	-0.56	-0.03	0.28	1.79	4.2	4.08	3.73	3.70	4.71	4.67	5.78	5.30	5.55	6.50
Sb	-0.55	-0.03	0.29	1.77	3.65	3.55	3.33	3.30	3.99	3.97	4.73	4.30	4.52	5.43
Sc	0.15	0.16	-1.62	-0.54	1.82	1.71	1.31	1.27	2.26	2.35	2.98	2.48	2.70	3.84
Starburst E(B-V) 0.51-0.60	-0.47	-0.06	-0.41	0.68	1.92	1.84	1.70	1.73	2.02	1.99	2.79	2.37	2.52	3.64
Starburst E(B-V)<0.1	-0.11	0.07	-1.85	0.07	1.04	1.01	0.98	0.94	1.05	1.06	1.42	1.11	1.18	2.17
Sun	-0.19	0.19	0.21	1.40	4.67	4.49	3.95	3.87	6.53	6.57	12.31	11.68	12.67	11.62
Vega	0.29	0.25	-0.06	0.87	1.75	1.65	1.49	1.47	1.80	1.74	2.91	2.07	2.43	4.64

CCD Clear Imaging—50CCD

Description

The `50CCD` mode is currently the most sensitive on HST for broad-band optical imaging. For a fixed exposure time it can detect point sources roughly 0.8 mag fainter than with WFPC2 with the F606W filter.

Recommended Uses

Recommended for deep imaging where detailed color information is not needed.

Special Considerations

Very red sources may show significant wings from detector halo (see “Optical Performance” on page 99).

Pivot λ (Å)	FWHM (Å)	AB mag zeropoint	S_{peak}	B_λ	R_{80} (arcsec)	Flux in central pixel
5851.5	2496.6	26.386	2.30×10^{15}	4898.9	0.16	14%

Figure 14.1: Throughput for 50CCD

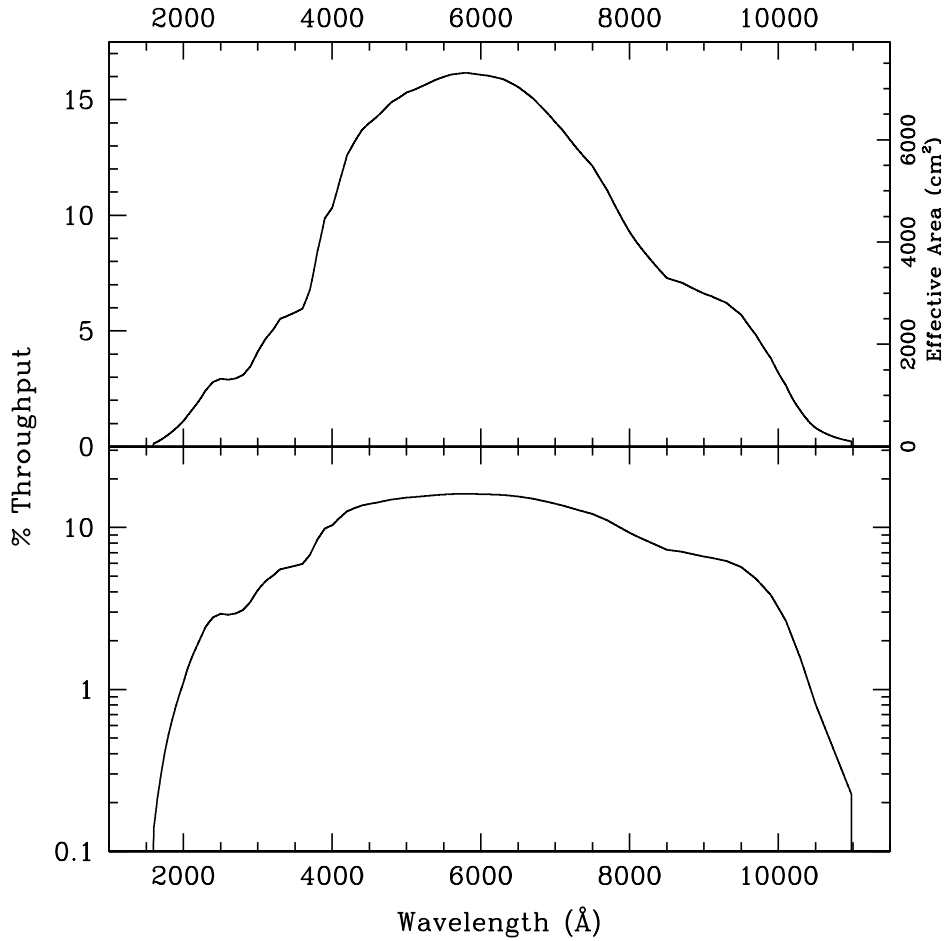

Table 14.2: Throughputs and Sensitivities for 50CCD

λ	Sensitivity	Throughput %
2500.	1.67E14	2.93
3000.	2.81E14	4.11
3500.	4.62E14	5.80
4000.	9.41E14	10.33
4500.	1.43E15	13.99
5000.	1.74E15	15.31
5500.	2.00E15	15.99
6000.	2.20E15	16.07
6500.	2.30E15	15.55
7000.	2.24E15	14.03
7500.	2.07E15	12.13
8000.	1.69E15	9.28
8500.	1.41E15	7.29
9000.	1.36E15	6.61
9500.	1.23E15	5.70
10000.	7.25E14	3.18
10500.	1.94E14	0.81

Figure 14.2: Point Source S/N vs. V+AB$_\nu$ for the 50CCD filter. Top curves are for low sky; bottom curves are for average sky.

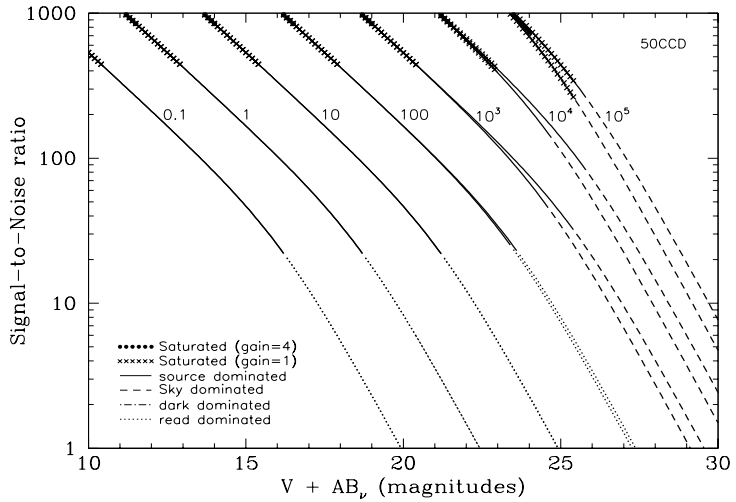

Figure 14.3: Extended Source S/N vs. V+AB$_\nu$ for the 50CCD filter for gain=1. Top curves are for a source area of 0.2 arcsec^2; bottom curves are for 1 arcsec^2 . Average sky assumed.

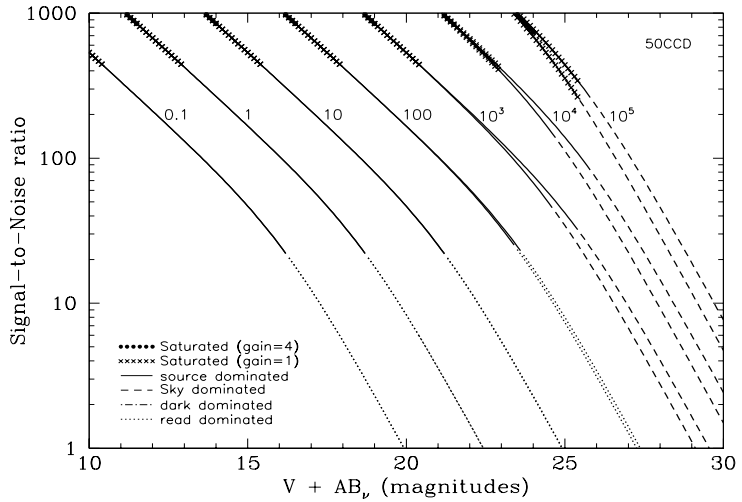

Table 14.3: Radial Profile for 50CCD

Radius		Intensity	Encircled Energy
Pixels	Arcsec		
1	0.050	1.614e-02	0.321
2	0.075	7.765e-03	0.495
2	0.100	4.320e-03	0.621
3	0.150	1.629e-03	0.787
4	0.200	4.904e-04	0.868
5	0.250	1.978e-04	0.902
10	0.500	2.499e-05	0.964
15	0.750	7.654e-06	0.986
20	1.000	2.687e-06	0.996

Figure 14.4: Point Source PSF for 50CCD, 7.″5 square (at pixel 518,517, log scaled, B-V=-0.25).

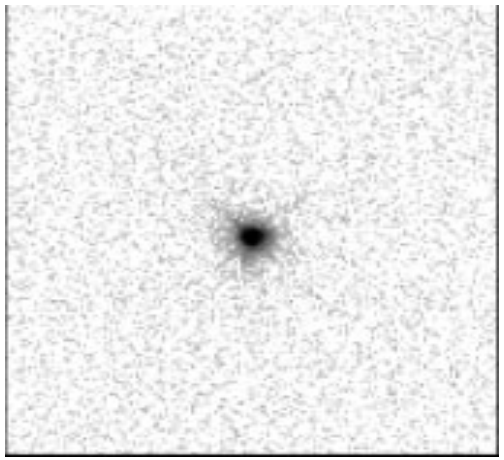

Figure 14.5: Point Source Encircled Energy for 50CCD

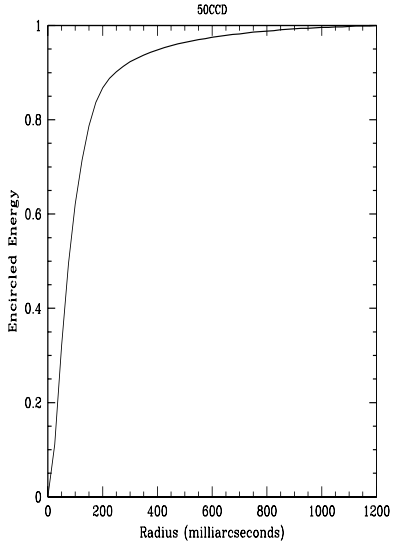

Figure 14.6: Point Source Intensity vs. Radius for 50CCD

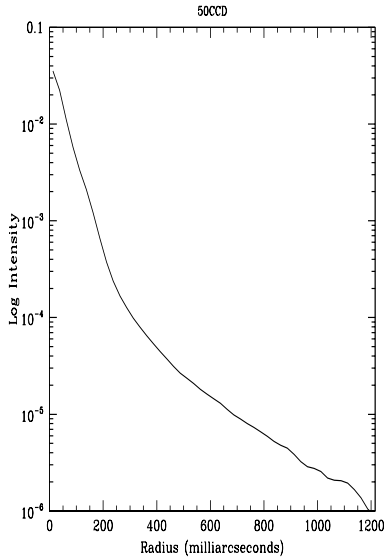

CCD Long-Pass Imaging F28X50LP

Description

The F28X50LP mode is useful for deep imaging longward of 5500 Å. For a fixed exposure time it can detect point sources roughly as faint faint as with WFPC2 with the F606W filter, but with higher spatial resolution. The field of view is 28x50".

Recommended Uses

Recommended for deep high-resolution imaging between 5500 Å and 10,000Å. Default aperture for target acquisitions.

Special Considerations

Very red sources may show significant wings from detector halo (see "Optical Performance" on page 99).

Pivot λ (Å)	FWHM (Å)	AB mag zeropoint	S_{peak}	B_λ	R_{80} (arcsec)	Flux in central pixel
7228.5	1998.1	25.191	1.64e+15	3495.7	0.15	14%

Figure 14.7: Throughput for F28x50LP

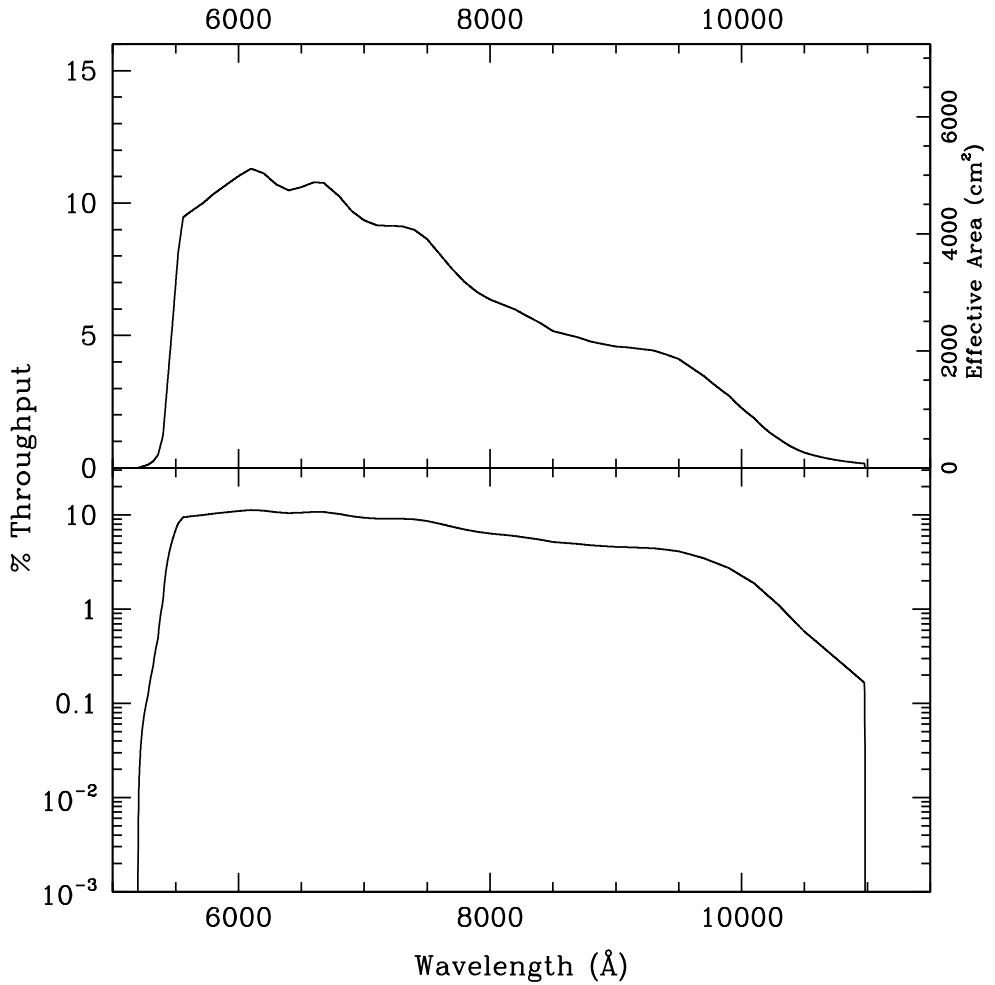

Table 14.4: Throughputs and Sensitivities for F28X50LP

λ	Sensitivity	Throughput %
5400.	1.53E14	1.25
5600.	1.23E15	9.61
5800.	1.37E15	10.34
6000.	1.51E15	11.02
6200.	1.57E15	11.12
6400.	1.53E15	10.48
6600.	1.62E15	10.79
6800.	1.59E15	10.26
7000.	1.49E15	9.35
7200.	1.50E15	9.14
7400.	1.51E15	8.99
7600.	1.40E15	8.08
7800.	1.25E15	7.01
8000.	1.16E15	6.36
8800.	9.57E14	4.77
9200.	9.41E14	4.49
9400.	9.17E14	4.28
9600.	8.29E14	3.79
9800.	6.88E14	3.08
10000.	5.16E14	2.26

Figure 14.8: Point Source S/N vs. V+AB$_\nu$ for the F28X50LP filter. Top curves are for low sky; bottom curves are for average sky.

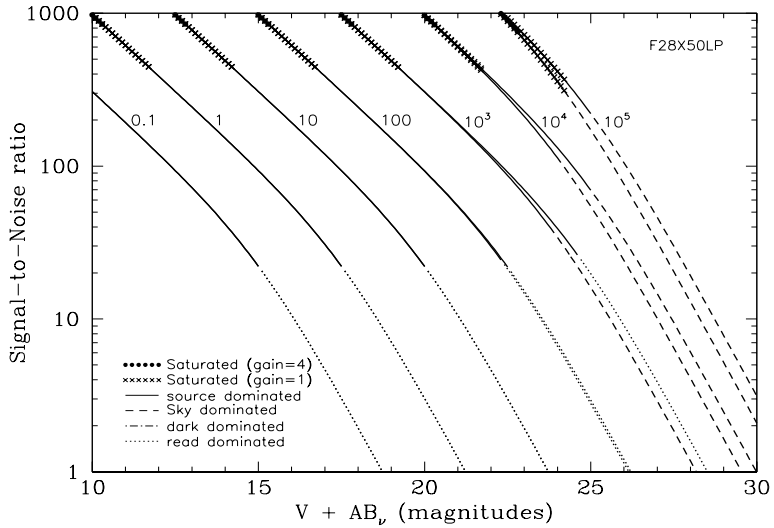

Figure 14.9: Extended Source S/N vs. V+AB$_\nu$ for the F28X50LP filter for gain=1. Top curves are for a source area of 0.2 arcsec^2; bottom curves are for 1 arcsec^2. Average sky assumed.

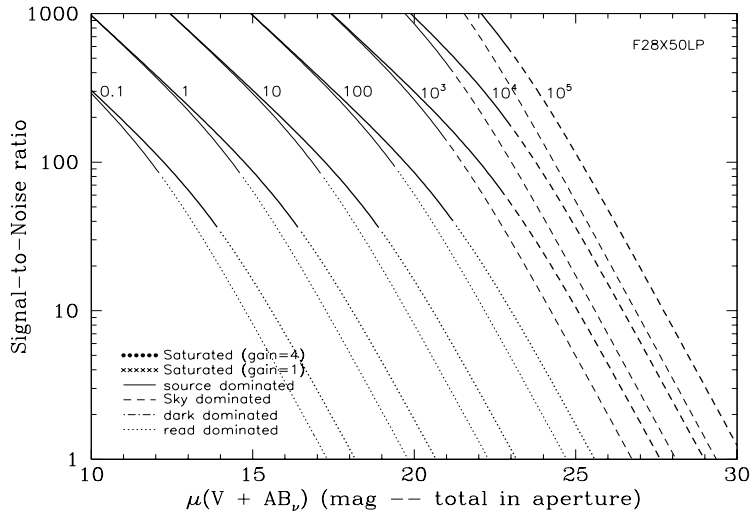

Table 14.5: Radial Profile for F28X50LP

Radius		Intensity	Encircled Energy
Pixels	**Arcsec**		
1	0.050	1.703e-02	0.337
2	0.075	7.468e-03	0.512
2	0.100	4.196e-03	0.632
3	0.150	1.733e-03	0.804
4	0.200	4.246e-04	0.883
5	0.250	1.660e-04	0.911
10	0.500	2.469e-05	0.976
15	0.750	5.360e-06	0.996
19.25	0.963	3.333e-07	1.000

Figure 14.10: Point Source Encircled Energy for F28X50LP

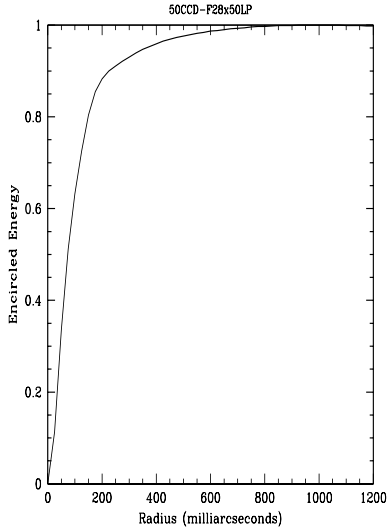

Figure 14.11: Point Source Intensity vs. Radius for F28X50LP

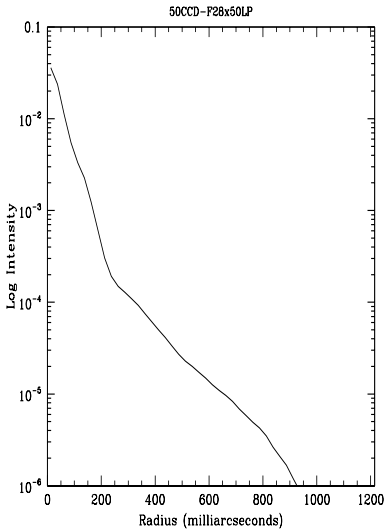

F28X50OIII—CCD

Description

The `F28X50OIII` mode is useful for narrow-band imaging of O III 5007 Å. The narrow bandpass and high spatial resolution provides some advantages over WFPC2 with the F502N filter.

Recommended Uses

Recommended for deep high-resolution O III imaging.

Special Considerations

This filter has a significant red leak longward of 1 micron. Depending on the source spectrum, the contribution from redleak may swamp the contribution from line emission.

Pivot λ (Å)	FWHM (Å)	AB mag zeropoint	S_{peak}	B_λ	R_{80} (arcsec)	Flux in central pixel
5005.8	6.2	18.846	1.26e+15	6.3	0.13	17%

Figure 14.12: Throughput for F28x50OIII

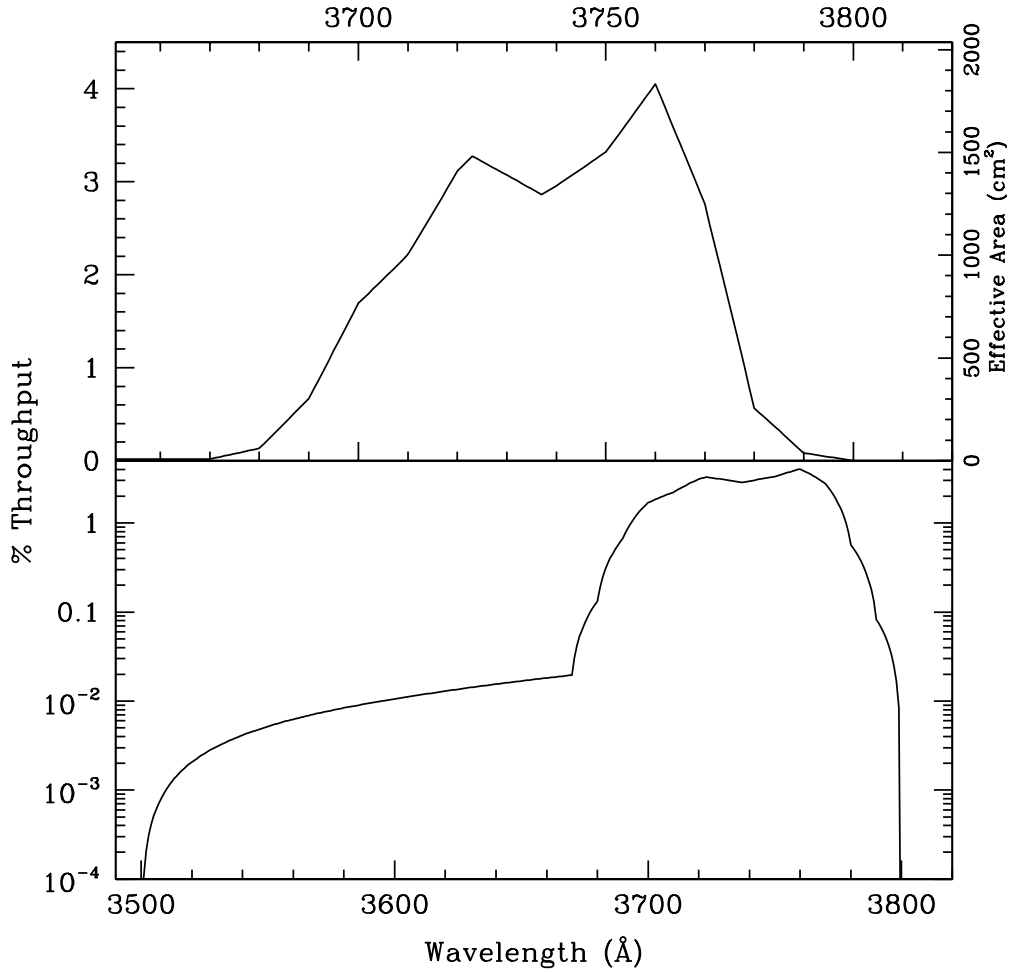

Table 14.6: Throughput and Sensitivity for F28X50OIII

λ	Sensitivity	Throughput %
4999.	5.23E13	0.46
5000.	1.22E14	1.07
5001.	2.09E14	1.84
5002.	4.01E14	3.52
5003.	6.46E14	5.67
5004.	9.25E14	8.12
5005.	1.22E15	10.72
5006.	1.26E15	11.03
5007.	1.12E15	9.80
5008.	8.74E14	7.66
5009.	5.42E14	4.75
5010.	2.97E14	2.60
5011.	1.40E14	1.23
5012.	5.25E13	0.46

Figure 14.13: Point Source S/N vs. V+AB$_v$ for the F28X50OIII filter.Top curves are for low sky; bottom curves are for average sky.

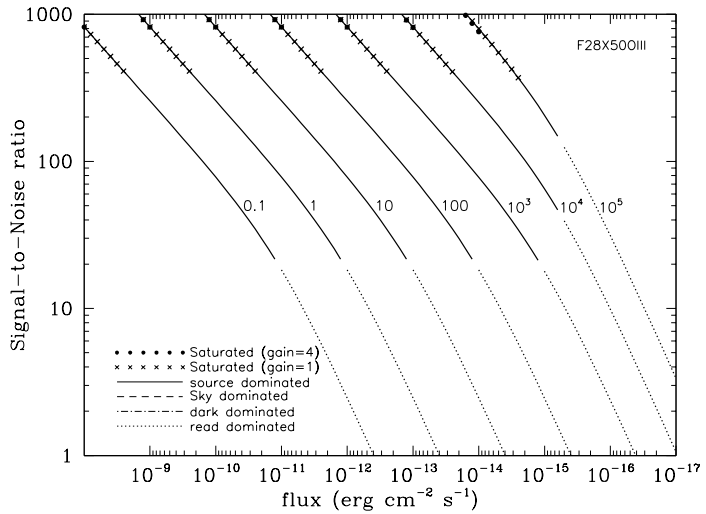

Figure 14.14: Extended Source S/N vs. V+AB$_v$ for the F28X50OIII for gain=1. Top curves are for a source area of 0.2 arcsec^2; bottom curves are for 1 arcsec^2. Average sky assumed.

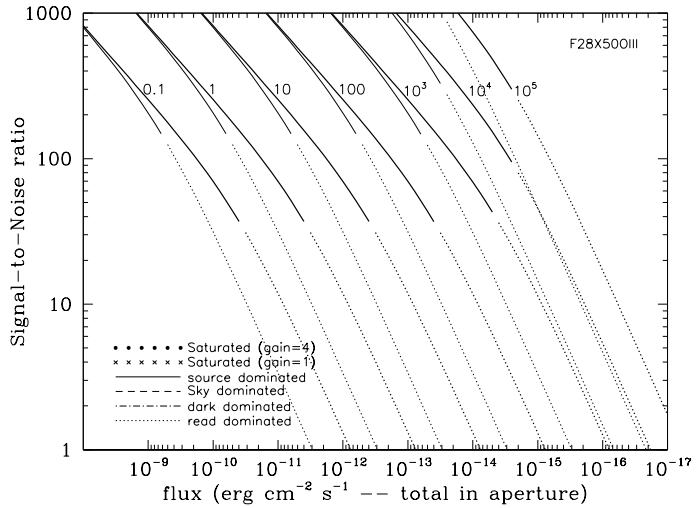

Table 14.7: Radial Profile for F28X50OIII

Radius		Intensity	Encircled Energy
Pixels	Arcsec		
1	0.050	1.750e-02	0.358
2	0.075	9.783e-03	0.574
2	0.100	4.193e-03	0.711
3	0.150	8.194e-04	0.844
4	0.200	3.245e-04	0.884
5	0.250	2.403e-04	0.916
10	0.500	2.049e-05	0.979
15	0.750	4.391e-06	0.995
20	1.000	8.462e-07	1.000

Figure 14.15: Point Source PSF for F28X50OIII, 7.″5 square (pixel 493,542, log scaled, B-V=-0.34)

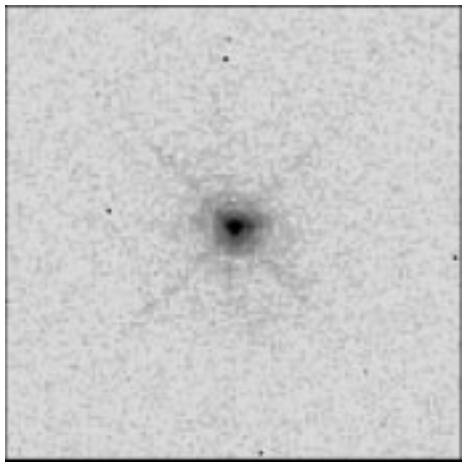

Figure 14.16: Point Source Encircled Energy for F28X50OIII

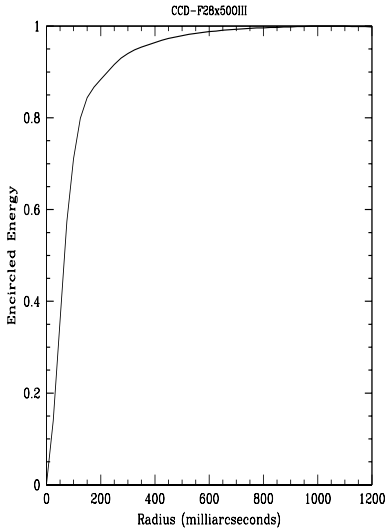

Figure 14.17: Point Source Intensity vs. Radius for F28X50OIII

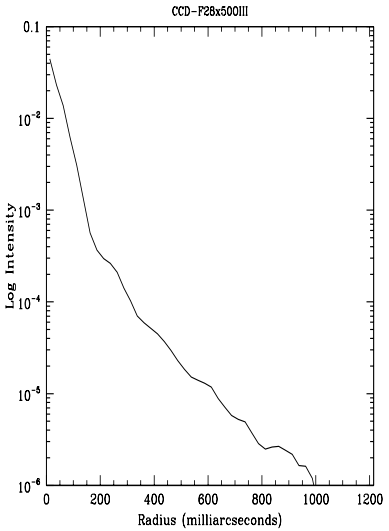

F28X50OII—CCD

Description

The `F28X50OII` mode is useful for narrow-band imaging of OII 3727 Å. The high throughput and high spatial resolution provide a significant advantage over WFPC2 imaging with the F375N filter for some purposes.

Recommended Uses

Recommended for deep high-resolution O II imaging.

Special Considerations

This filter does not have a significant red leak. Flatfield images taken through this filter show scattered light at the top and bottom of the frame. This is not expected to be a problem for astronomical targets.

Pivot λ (Å)	FWHM (Å)	AB mag zeropoint	S_{peak}	B_λ	R_{80} (arcsec)	Flux in central pixel
3737.3	62.9	20.541	3.47e+14	60.9	0.12	17%

Figure 14.18: Throughput for F28x50OII

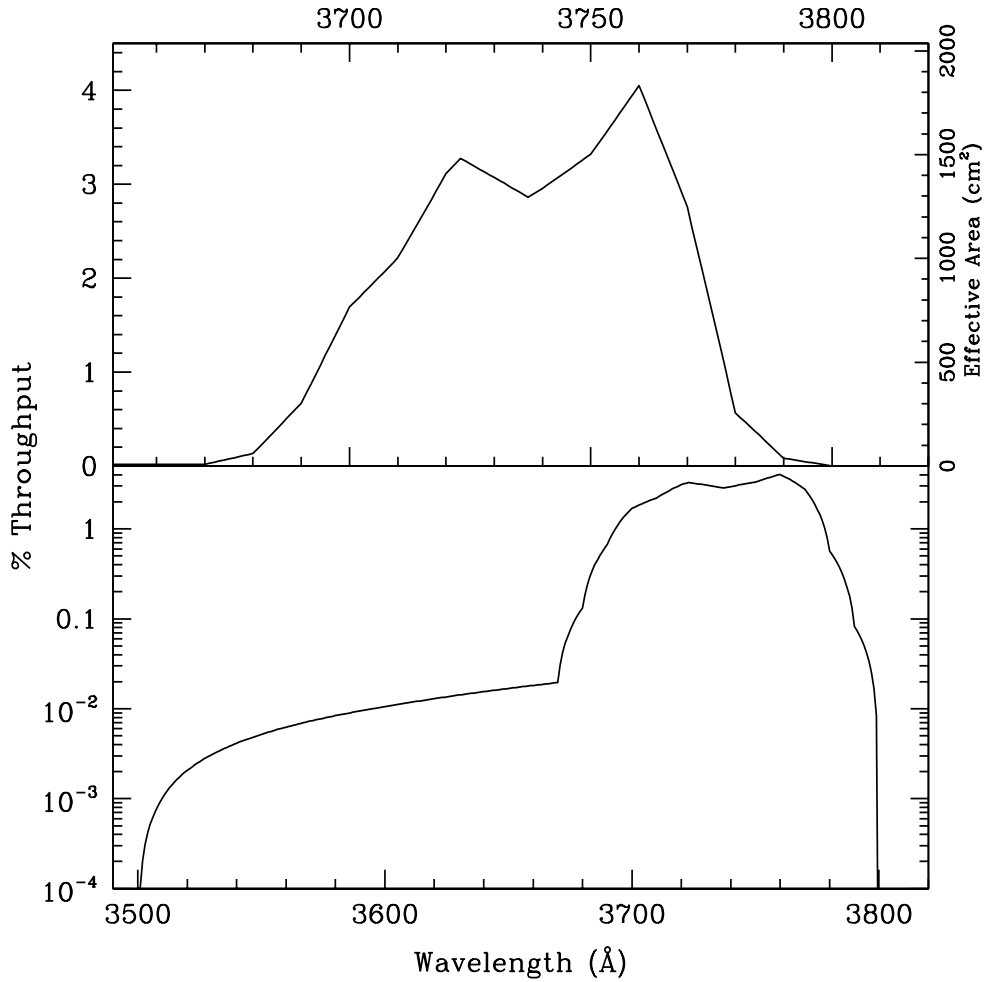

Table 14.8: Throughput and Sensitivity for F28X50OII

λ	Sensitivity	Throughput %
3675.	6.32E12	0.08
3685.	3.35E13	0.40
3695.	9.91E13	1.18
3705.	1.65E14	1.95
3715.	2.25E14	2.66
3725.	2.73E14	3.22
3735.	2.49E14	2.92
3745.	2.68E14	3.14
3755.	3.15E14	3.68
3765.	2.93E14	3.41
3775.	1.44E14	1.67
3785.	2.81E13	0.33

Figure 14.19: Point Source S/N vs. Line Flux for the F28X50OII filter. Top curves are for low sky; bottom curves are for average sky.

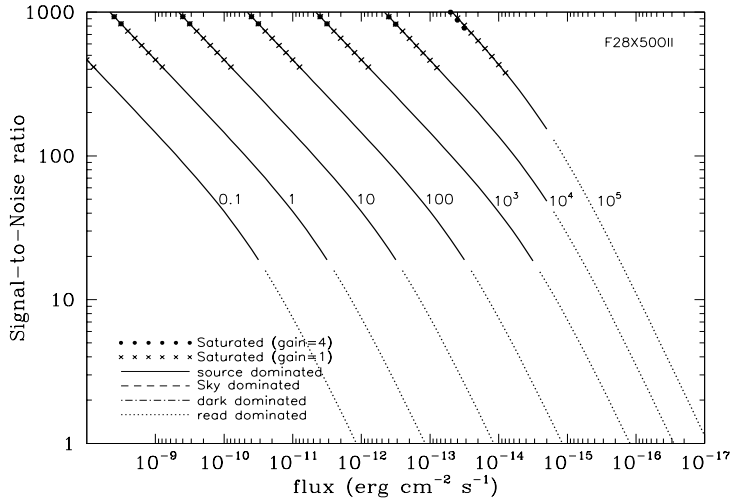

Figure 14.20: Extended Source S/N vs. V+AB_V for the F28X50OII for gain =1.Top curves are for an area of 0.2 arcsec^2; bottom curves are for 1 arcsec^2. Average sky assumed.

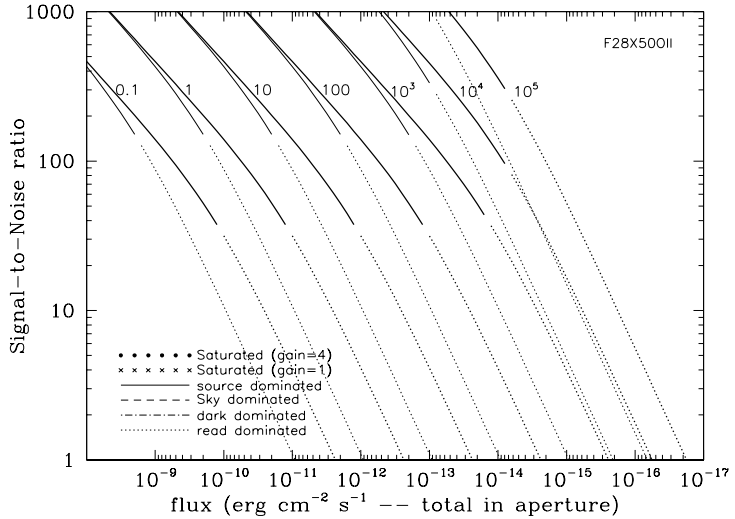

Table 14.9: Radial Profile for F28X50OII

Radius		Intensity	Encircled Energy
Pixels	Arcsec		
1	0.050	1.945e-02	0.405
2	0.075	9.266e-03	0.622
2	0.100	3.589e-03	0.750
3	0.150	7.742e-04	0.849
4	0.200	3.628e-04	0.895
5	0.250	1.826e-04	0.924
10	0.500	1.966e-05	0.982
15	0.750	4.876e-06	0.997
20	1.000	5.800e-07	1.000

Figure 14.21: Point Source Encircled Energy for F28X50OII

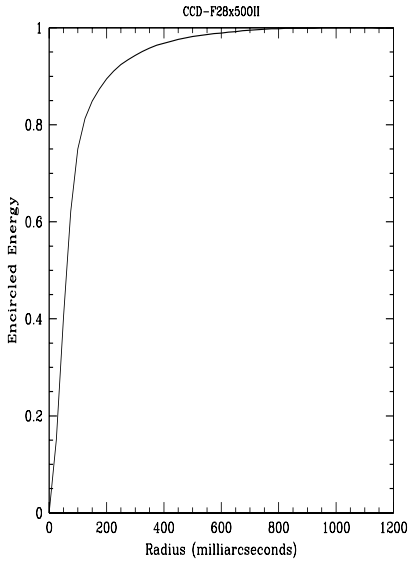

Figure 14.22: Point Source Intensity vs. Radius for F28X50OII

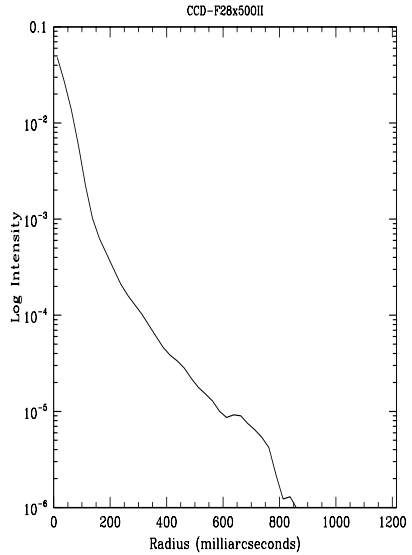

50CORON—Clear CCD

Description

The `50CORON` imaging mode is useful for imaging of faint targets next to bright ones. The STIS CCD optics includde a Lyot stop, which supresses the wings of the PSF. See “CCD Clear Imaging—50CCD” on page 319 for sensitivities, throughputs, and encircled energies. See Chapter 5 for the PSF, and Chapter 12 for a discussion of coronographic imaging.

Recommended Uses

Recommended for broad-band coronographic imaging.

Pivot λ (Å)	FWHM (Å)	AB mag zeropoint	S_{peak}	B_λ	R_{80} (arcsec)	Flux in central pixel
5851.5	2496.6	26.386	2.30×10^{15}	4898.9	0.16	14%

25MAMA—NUV-MAMA, Clear

Description

The 25MAMA mode with the NUV-MAMA provides high-throughput broad-band near-UV imaging with the highest available throughput at ~2500 Å and the highest possible spatial resolution. The field of view is 25 x 25 arcsec.

Recommended Uses

Recommended for broad-band near-UV imaging.

Special Considerations

For long exposures of faint targets, sky background is likely to be a limiting factor. Observers should consider the use of DARKTIME or (preferably) use the F25QTZ filter, which has nearly the same throughput but rejects geocoronal Lyman-α.

NUV-MAMA clear images will be slightly out of focus because the mirror optimally focuses for use of a filter. Whenever possible, use F25SRF2 instead of 25MAMA for NUV-MAMA imaging.

Pivot λ (Å)	FWHM (Å)	AB mag zeropoint	S_{peak}	B_λ	R_{80} (arcsec)	Flux in central pixel
2222.8	931.9	24.187	1.76e+14	1218.7	0.32	8%

Figure 14.23: 25MAMA NUV-MAMA Integrated System Throughput and Redleak

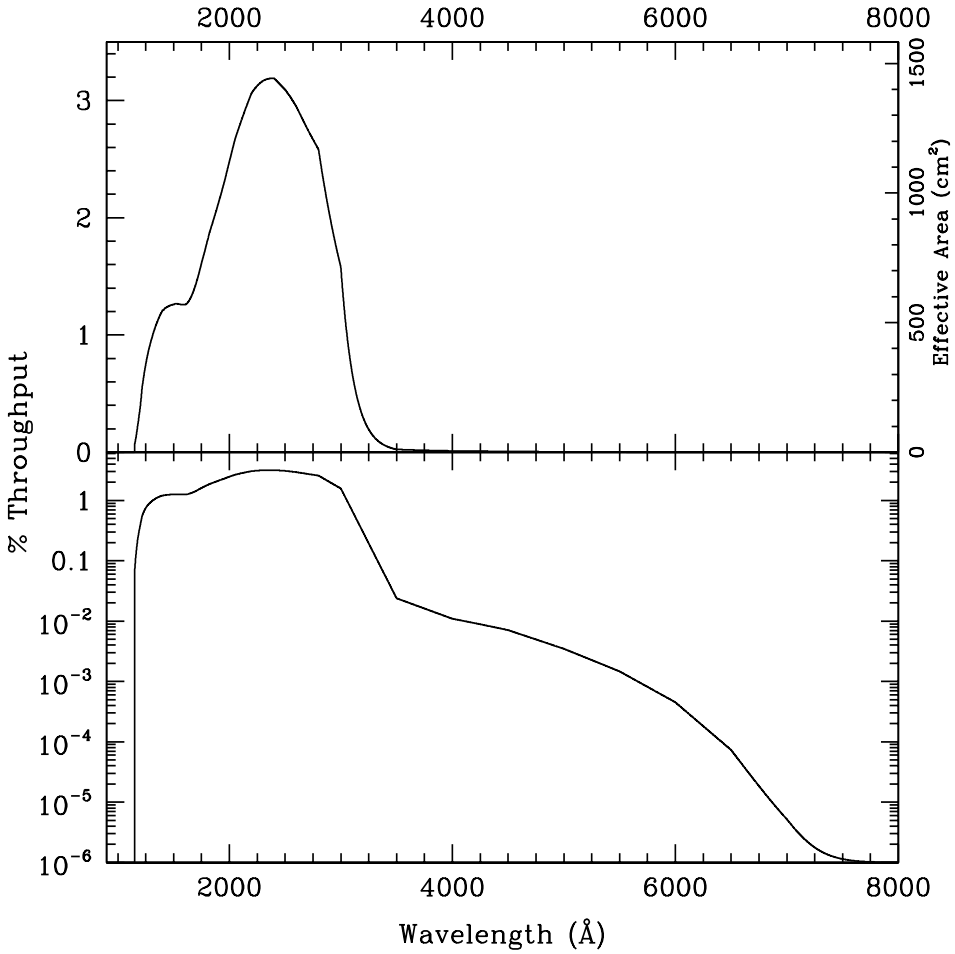

Table 14.10: Throughput and Sensitivity for 25MAMA NUV-MAMA

λ	Sensitivity	Throughput %
1200.	1.04E13	0.38
1300.	2.84E13	0.96
1400.	3.86E13	1.21
1500.	4.30E13	1.26
1600.	4.59E13	1.26
1700.	5.56E13	1.44
1800.	7.35E13	1.79
1900.	9.17E13	2.12
2000.	1.13E14	2.48
2100.	1.34E14	2.81
2200.	1.54E14	3.06
2300.	1.66E14	3.17
2400.	1.74E14	3.19
2500.	1.76E14	3.09
2600.	1.75E14	2.95
2700.	1.70E14	2.76
2800.	1.65E14	2.58
2900.	1.33E14	2.02
3000.	1.08E14	1.58
3100.	4.83E13	0.68

Figure 14.24: Point Source S/N vs. V+AB$_\nu$ for the 25MAMA NUV-MAMA mode. Top curves are for DARKTIME. Bottom curves are for average sky. Top curves are for DARKTIME. Bottom curves are for average sky.

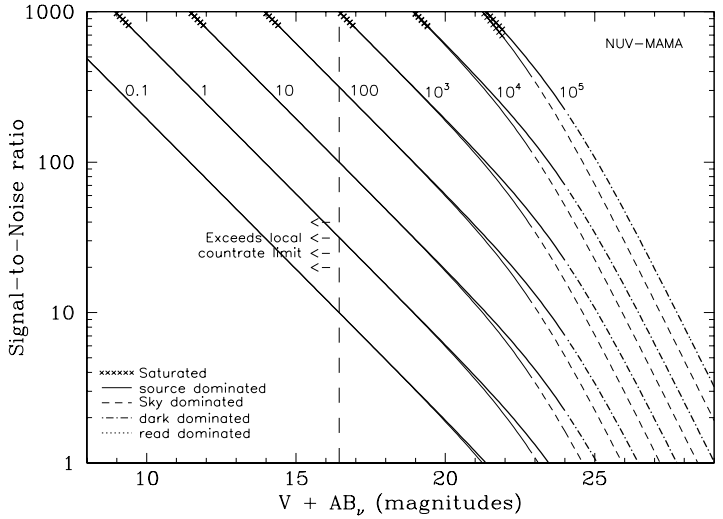

Figure 14.25: Extended Source S/N vs. V+AB$_\nu$ for the 25MAMA NUV-MAMA mode. Top curves are for an area of 0.2 arcsec^2; bottom curves are for 1 arcsec^2. Average sky assumed.

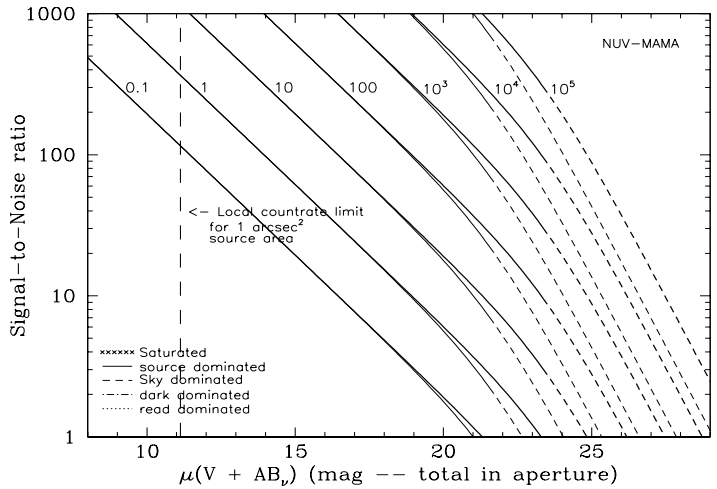

Table 14.11: Radial Profile for 25MAMA

Radius			Encircled energy
Pix	arcsec	intensity	
1	0.024	3.267e-02	0.141
2	0.037	2.107e-02	0.236
2	0.049	1.345e-02	0.331
3	0.073	6.141e-03	0.467
4	0.098	2.981e-03	0.557
5	0.122	1.485e-03	0.614
10	0.245	3.377e-04	0.746
15	0.367	1.676e-04	0.834
20	0.490	9.542e-05	0.900
25	0.613	4.543e-05	0.947
30	0.735	2.065e-05	0.972
40	0.980	5.088e-06	0.994

Figure 14.26: Point Source Encircled Energy for 25MAMA NUV-MAMA

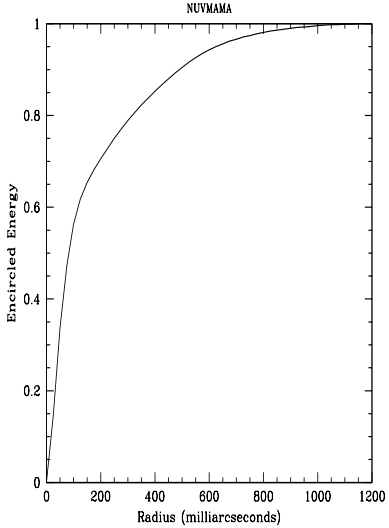

Figure 14.27: Point Source Intensity vs. Radius for 25MAMA NUV-MAMA

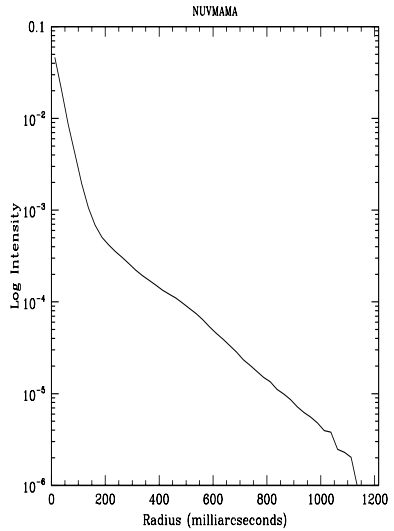

F25QTZ—NUV-MAMA, Longpass

Description

The F25QTZ filter with the NUV-MAMA provides high-throughput broad-band near-UV imaging with better rejection of geocoronal emission than the F25MAMA or F25SRF2 modes, the same field of view, and the same high spatial resolution.

Recommended Uses

Recommended for broad-band near-UV imaging of faint targets.

Special Considerations

Sky background on the day side of the orbit contains a significant contribution from O II airglow emission at 2470 Å. In high-background conditions, the sky background can dominate the detector background. In average day-side observing conditions about half the background will be from the sky and half from detector dark current. Observers can limit the background (with some cost to the total amount of observing time per orbit) by using the DARKTIME special requirement.

Pivot λ (Å)	FWHM (Å)	AB mag zeropoint	S_{peak}	B_λ	R_{80} (arcsec)	Flux in central pixel
2329.7	849.7	23.887	1.57e+14	1142.7	0.32	8%

Figure 14.28: F25QTZ NUV-MAMA Integrated System Throughput and Redleak

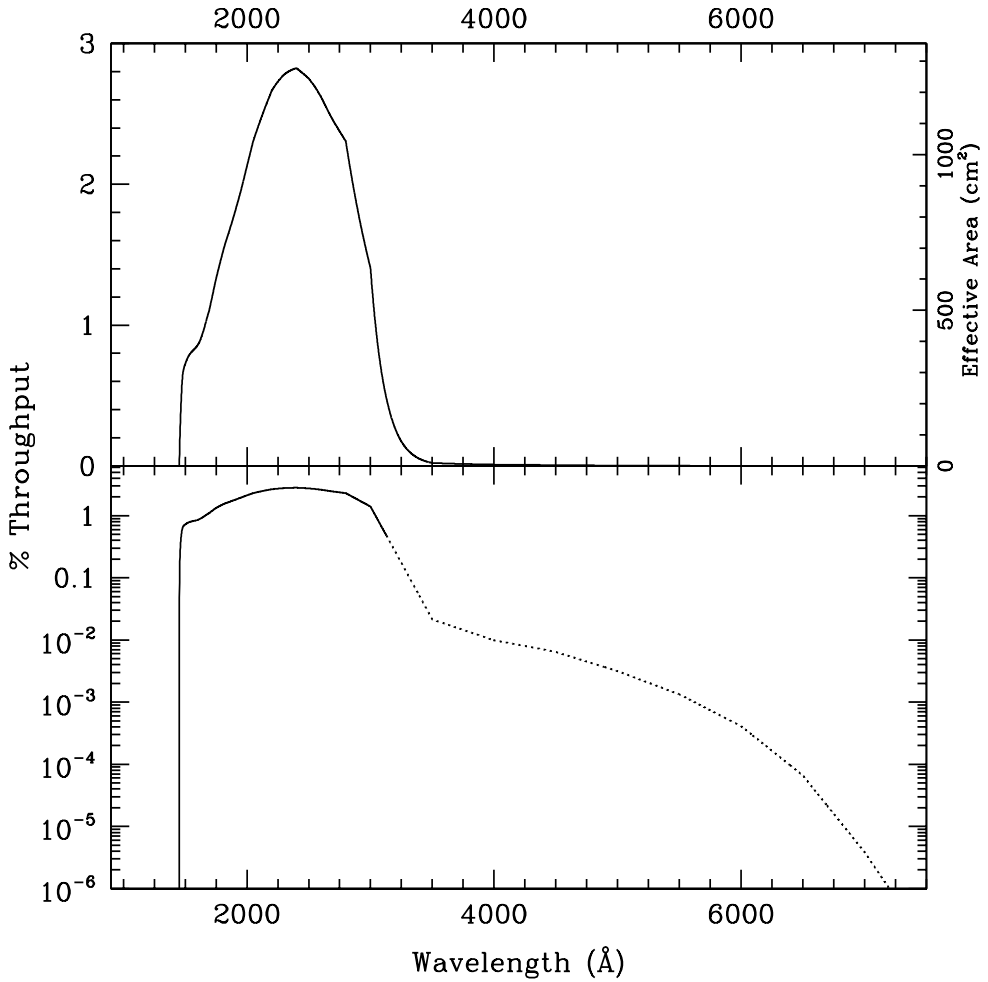

Table 14.12: Throughput and Sensitivity for F25QTZ NUV-MAMA

λ	Sensitivity	Throughput %
1500.	2.47E13	0.72
1600.	3.12E13	0.86
1700.	4.36E13	1.13
1800.	6.16E13	1.50
1900.	7.77E13	1.80
2000.	9.70E13	2.13
2100.	1.16E14	2.43
2200.	1.33E14	2.66
2300.	1.46E14	2.78
2400.	1.54E14	2.82
2500.	1.57E14	2.75
2600.	1.55E14	2.62
2700.	1.51E14	2.45
2800.	1.47E14	2.31
2900.	1.19E14	1.80
3000.	9.60E13	1.40

Figure 14.29: Point Source S/N vs. V+AB$_\nu$ for the F25QTZ NUV-MAMA mode. Top curves are for DARKTIME. Bottom curves are for average sky.

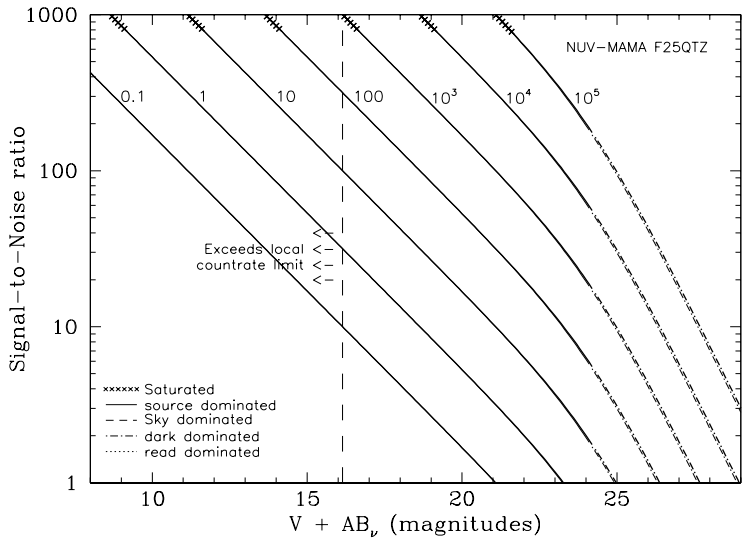

Figure 14.30: Extended Source S/N vs. V+AB$_\nu$ for the F25QTZ NUV-MAMA mode. Top curves are for an area of 0.2 arcsec^2; bottom curves are for 1 arcsec^2. Average sky assumed.

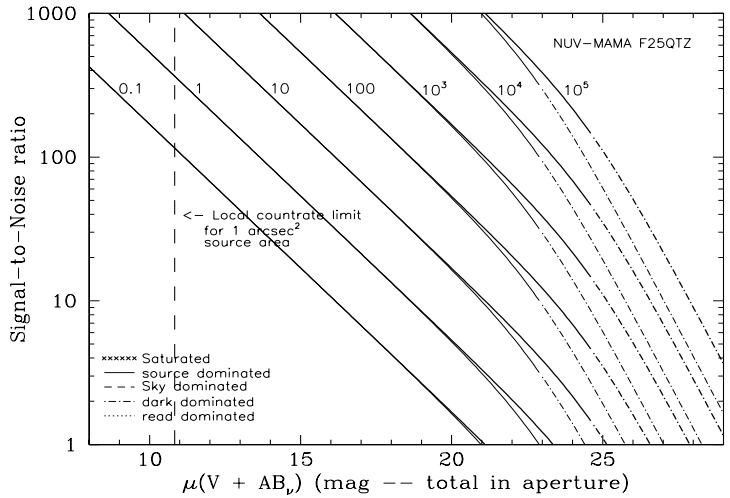

Table 14.13: Radial Profile for F25QTZ

Radius		Intensity	Encircled Energy
Pixel	Arcsec		
1	0.024	6.046e-02	0.210
2	0.037	4.292e-02	0.328
2	0.049	2.825e-02	0.440
3	0.073	1.036e-02	0.591
4	0.098	4.085e-03	0.667
5	0.122	1.839e-03	0.718
10	0.245	2.099e-04	0.820
15	0.367	9.929e-05	0.874
20	0.490	4.775e-05	0.911
25	0.613	2.706e-05	0.934
30	0.735	1.876e-05	0.953
40	0.980	8.441e-06	0.983

Figure 14.31: Point Source PSF for F25QTZNUV-MAMA, 7.″5 square (at pixel 606,649, log scaled). Note PSF ghost ~45 pixels left of peak pixel and a few 10^{-3} of the peak..

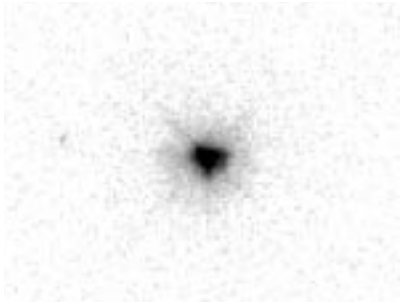

Figure 14.32: Point Source Encircled Energy for F25QTZ NUV-MAMA

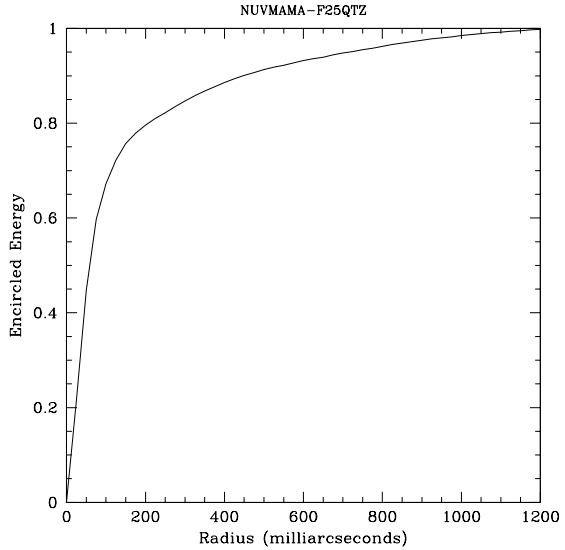

Figure 14.33: Point Source Intensity vs. Radius for F25QTZ NUV-MAMA

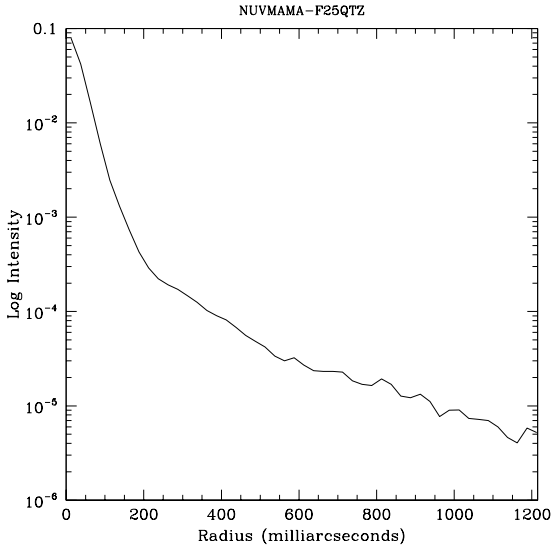

F25SRF2—NUV-MAMA, Longpass

Description

The F25SRF2 filter with the NUV-MAMA provides high-throughput broad-band near-UV imaging with better rejection of geocoronal emission than the F25MAMA but worse than or F25QTZ modes. It provides the same field of view and high spatial resolution.

Recommended Uses

This filter has slightly higher throughput than F25QTZ, but lets in geocoronal OI 1302 Å. In most cases even when this line is bright the sky background will still be lower than the detector background.

Special Considerations

Sky background on the day side of the orbit contains a significant contributions from OII airglow emission at 2470 Å and OI airglow at 1302 Å. In high-background conditions, the sky background can dominate the detector background. In average day-side observing conditions about half the background will be from the sky and half from detector dark current. In average dayside conditions the background through F25SRF2 will be about 10% higher than through F25QTZ. Observers can limit the background (with some cost to the total amount of observing time per orbit) by using the DARKTIME special requirement.

Pivot λ (Å)	FWHM (Å)	AB mag zeropoint	S_{peak}	B_λ	R_{80} (arcsec)	Flux in central pixel
2266.9	924.5	24.015	1.62e+14	1176.6	0.32	8%

Figure 14.34: F25SRF2 NUV-MAMA Integrated System Throughput and Redleak

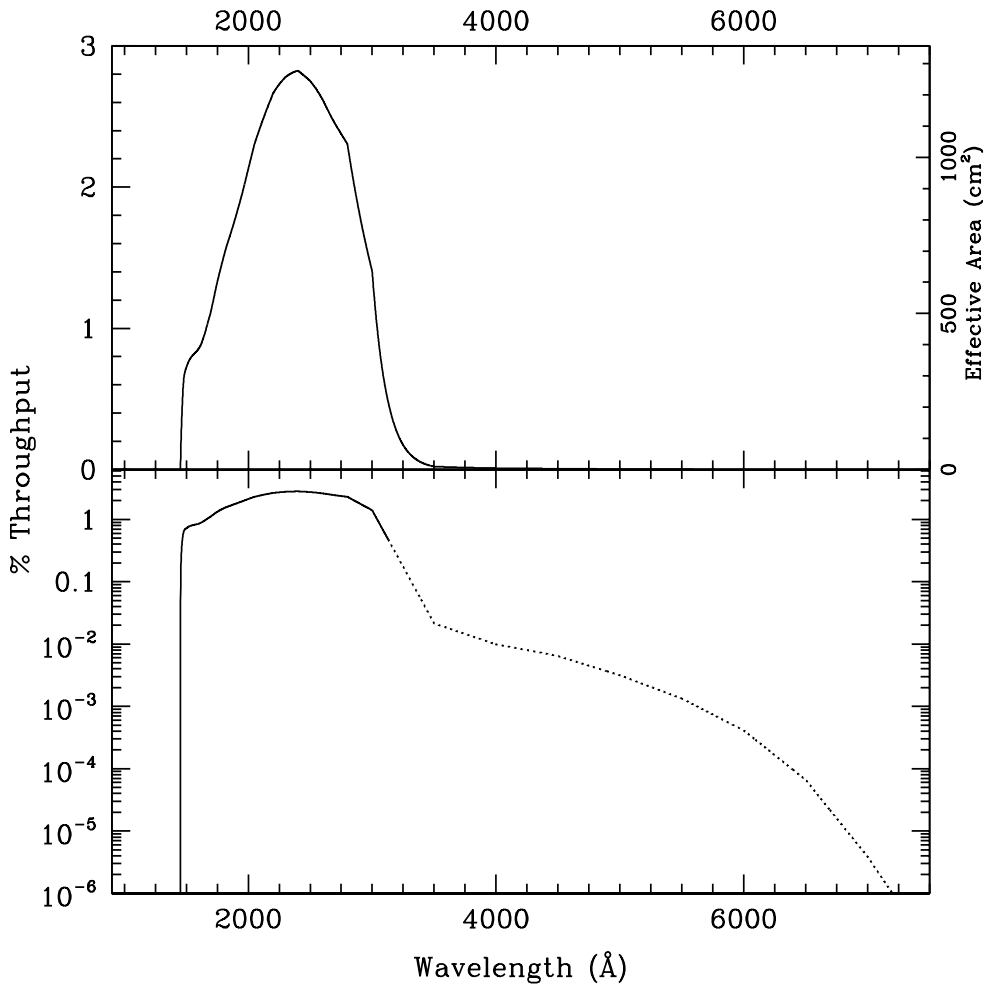

Table 14.14: Throughput and Sensitivity for F25SRF2 NUV-MAMA

λ	Sensitivity	Throughput %
1300.	1.63E13	0.55
1400.	2.96E13	0.93
1500.	3.53E13	1.03
1600.	3.87E13	1.06
1700.	4.69E13	1.21
1800.	6.30E13	1.54
1900.	8.01E13	1.85
2000.	9.96E13	2.19
2100.	1.19E14	2.49
2200.	1.37E14	2.74
2300.	1.50E14	2.87
2400.	1.59E14	2.92
2500.	1.62E14	2.84
2600.	1.61E14	2.72
2700.	1.56E14	2.54
2800.	1.52E14	2.38
2900.	1.23E14	1.86
3000.	1.01E14	1.47
3100.	4.55E13	0.64
3200.	1.76E13	0.24

Figure 14.35: Point Source S/N vs. V+AB_v for the F25SRF2 NUV-MAMA mode. Top curves are for DARKTIME. Bottom curves are for average sky.

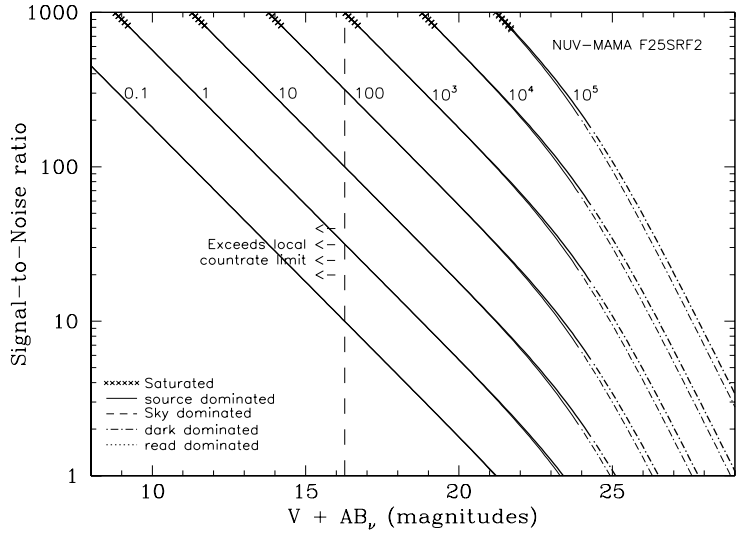

Figure 14.36: Extended Source S/N vs. V+AB_v for the F25SRF2 NUV-MAMA mode. Top curves are for an area of 0.2 arcsec^2; bottom curves are for 1 arcsec^2. Average sky assumed.

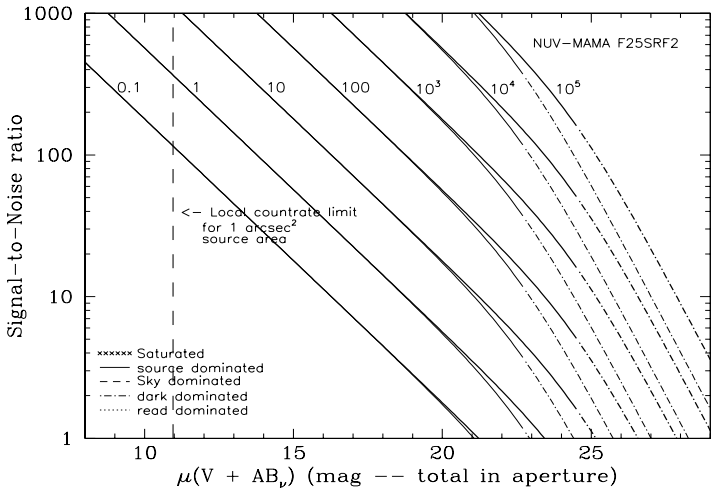

F25MGII—NUV-MAMA

Description

The `F25MGII` filter with the NUV-MAMA provides narrow-band imaging centered on the 2798 Å MgII feature.

Recommended Uses

Narrowband imaging.

Special Considerations

There is a substantial redleak in this filter. Sources with a red underlying continuum may be difficult to observe. Users should be careful to take into account the underlying continuum in estimating whether the observation will fall within the bright-object protection limits.

Pivot λ (Å)	FWHM (Å)	AB mag zeropoint	S_{peak}	B_λ	R_{80} (arcsec)	Flux in central pixel
2809.0	48.1	19.516	8.20e+13	56.6	0.18	14%

Figure 14.37: F25MGII NUV-MAMA Integrated System Throughput and Redleak

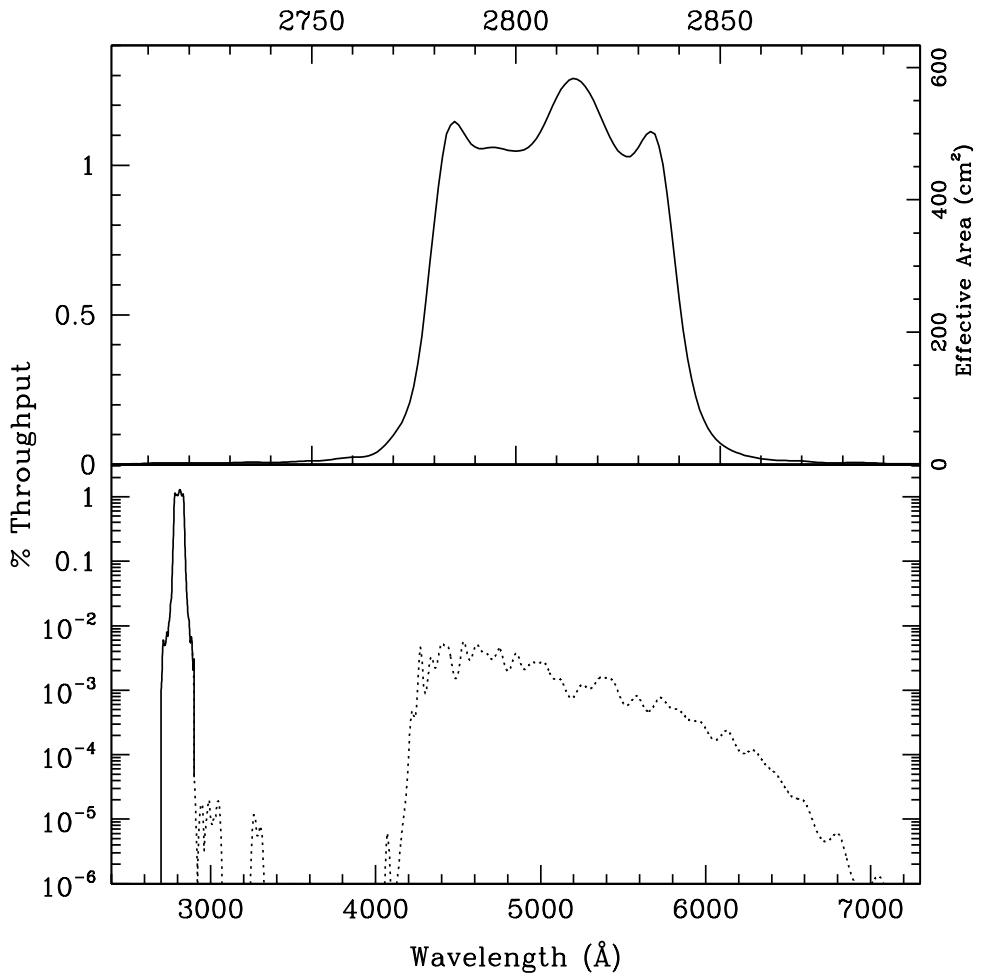

Table 14.15: Throughput and Sensitivity for F25MGII NUV-MAMA

λ	Sensitivity	Throughput %
2765.	2.20E12	0.03
2770.	6.19E12	0.10
2775.	1.66E13	0.26
2780.	5.13E13	0.81
2785.	7.27E13	1.15
2790.	6.74E13	1.06
2795.	6.74E13	1.06
2800.	6.67E13	1.05
2805.	6.95E13	1.09
2810.	7.85E13	1.23
2815.	8.25E13	1.29
2820.	7.62E13	1.19
2825.	6.74E13	1.05
2830.	6.83E13	1.06
2835.	6.87E13	1.06
2840.	3.60E13	0.56
2845.	1.18E13	0.18
2850.	4.62E12	0.07

Figure 14.38: Point Source S/N vs. V+AB_v for the F25MGII NUV-MAMA mode.

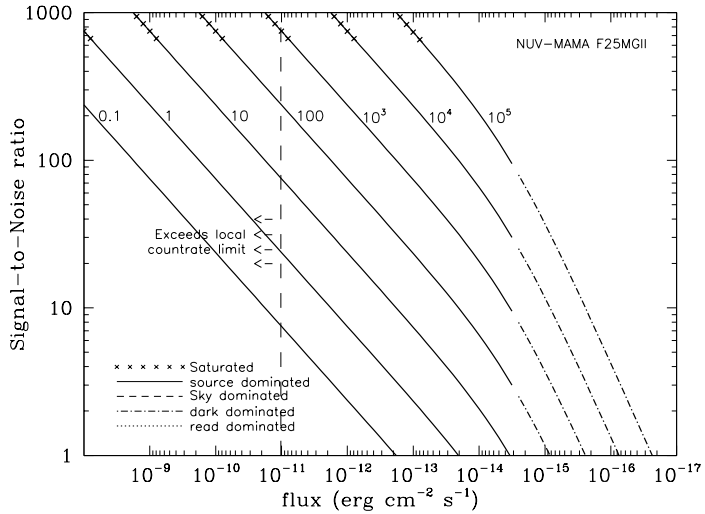

Figure 14.39: Extended Source S/N vs. V+AB_v for the F25MGII NUV-MAMA mode. Top curves are for an area of 0.2 arcsec^2; bottom curves are for 1 arcsec^2. Average sky assumed.

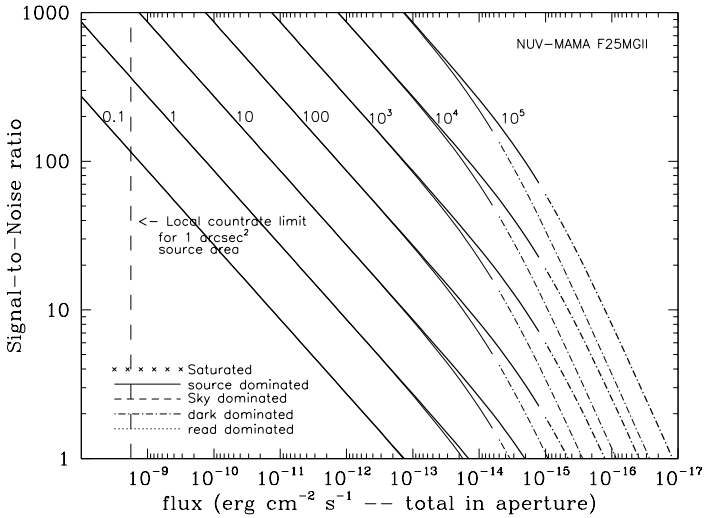

Table 14.16: Radial Profile for F25MGII

Radius		Intensity	Encircled Energy
Pixels	Arcsec		
1	0.024	5.302e-02	0.257
2	0.037	2.834e-02	0.391
2	0.049	1.466e-02	0.510
3	0.073	4.989e-03	0.641
4	0.098	1.739e-03	0.697
5	0.122	1.302e-03	0.738
10	0.245	2.035e-04	0.843
15	0.367	1.119e-04	0.899
20	0.490	3.763e-05	0.932
25	0.613	2.057e-05	0.949
30	0.735	1.692e-05	0.965
40	0.980	6.931e-06	0.988

Figure 14.40: Point Source PSF for F25MGII NUV-MAMA7.″5 square (at pixel 316,658, log scaled, B-V=-0.04). Note psf ghost ~45 pixels left of peak pixel and a few 10-3 of the peak

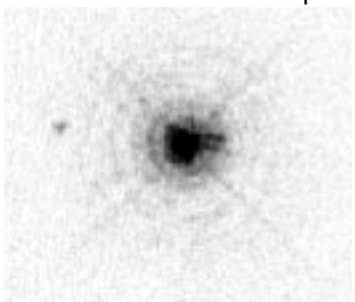

Figure 14.41: Point Source Encircled Energy for F25MGII NUV-MAMA

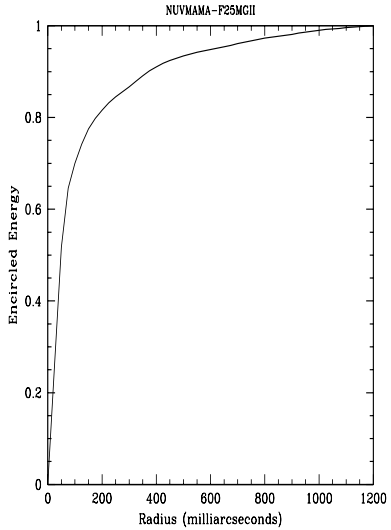

Figure 14.42: Point Source Intensity vs. Radius for F25MGII NUV-MAMA

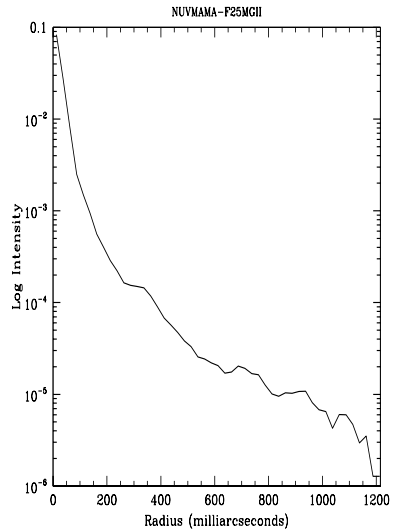

F25CN270—NUV-MAMA

Description

The `F25CN270` filter with the NUV-MAMA provides medium bandwidth imaging near the 2798 Å MgII feature.

Recommended Uses

Continuum filter for MgII imaging.

Special Considerations

There is a substantial redleak in this filter. Sources with a red underlying continuum may be difficult to observe. Users should be careful to take into account the underlying continuum in estimating whether the observation will fall within the bright-object protection limits.

Pivot λ (Å)	FWHM (Å)	AB mag zeropoint	S_{peak}	B_λ	R_{80} (arcsec)	Flux in central pixel
2710.6	160.6	21.450	1.27e+14	202.9	0.17	14%

Figure 14.43: F25CN270 NUV-MAMA Integrated System Throughput and Redleak

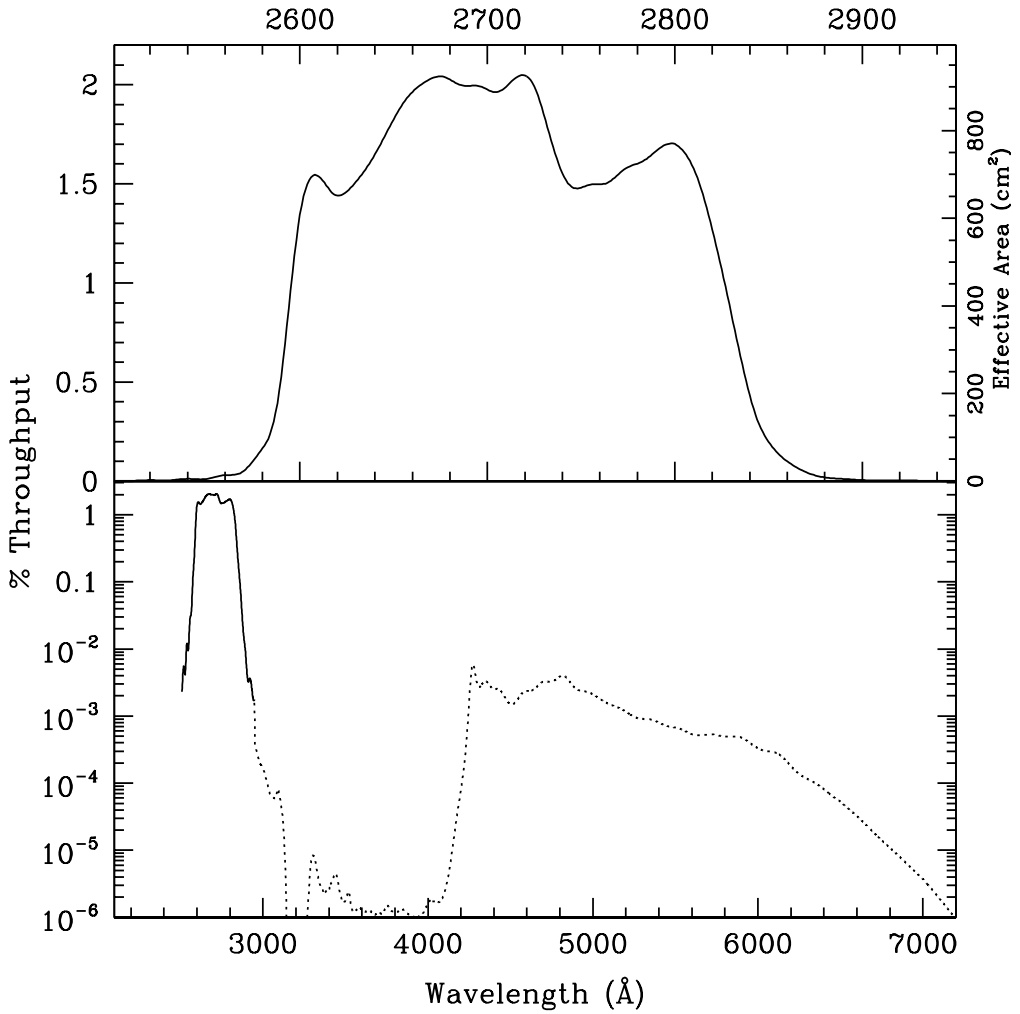

Table 14.17: Throughput and Sensitivity for F25CN270 NUV-MAMA

λ	Sensitivity	Throughput %
2575.	6.01E12	0.10
2600.	7.96E13	1.34
2625.	8.74E13	1.46
2650.	1.10E14	1.83
2675.	1.24E14	2.04
2700.	1.21E14	1.98
2725.	1.24E14	1.99
2750.	9.28E13	1.48
2775.	1.00E14	1.58
2800.	1.09E14	1.70
2825.	6.87E13	1.07
2850.	1.29E13	0.20

Figure 14.44: Point Source S/N vs. V+AB$_\nu$ for the F25CN270 NUV-MAMA mode.

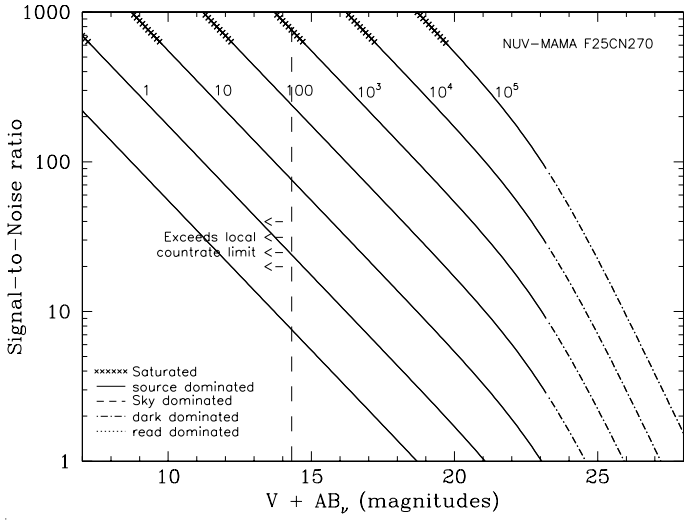

Figure 14.45: Extended Source S/N vs. V+AB$_\nu$ for the F25CN270 NUV-MAMA mode. Top curves are for an area of 0.2 arcsec^2; bottom curves are for 1 arcsec^2. Average sky assumed.

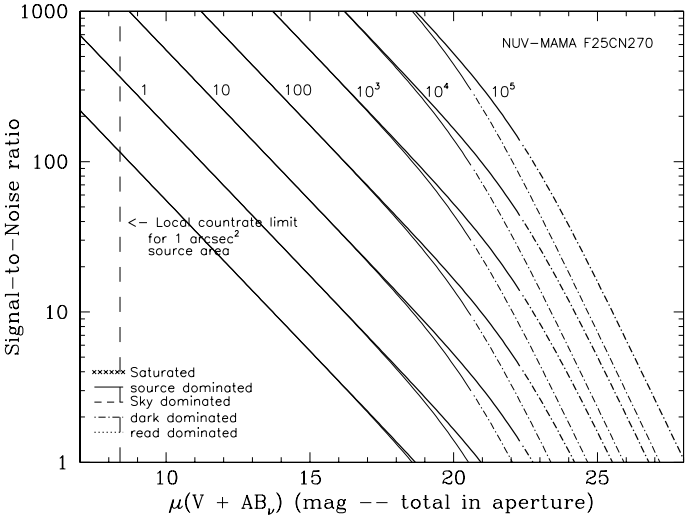

Table 14.18: Radial Profile for F25CN270

Radius			Encircled Energy
Pixels	Arcsec	intensity	
1	0.024	5.158e-02	0.240
2	0.037	2.953e-02	0.378
2	0.049	1.608e-02	0.504
3	0.073	5.260e-03	0.643
4	0.098	2.022e-03	0.708
5	0.122	1.215e-03	0.750
10	0.245	2.048e-04	0.854
15	0.367	9.848e-05	0.908
20	0.490	4.138e-05	0.942
25	0.613	1.817e-05	0.960
30	0.735	1.440e-05	0.974
40	0.980	4.656e-06	0.994

Figure 14.46: Point Source Encircled Energy for F25CN270 NUV-MAMA

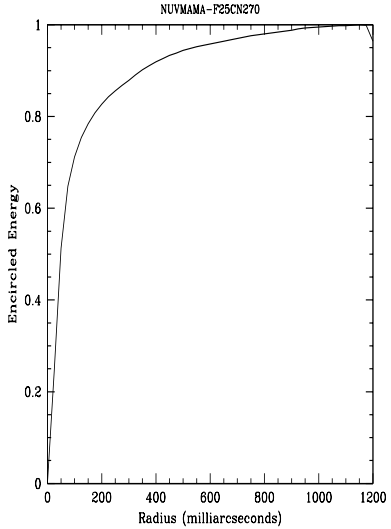

Figure 14.47: Point Source Intensity vs. Radius for F25CN270 NUV-MAMA

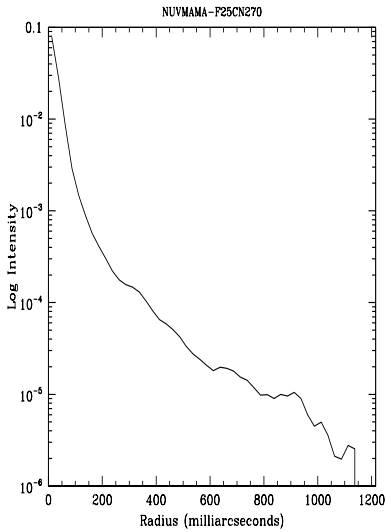

F25CIII—NUV-MAMA

Description

The `F25CIII` filter with the NUV-MAMA provides narrow band imaging of the 1909 Å C III] feature.

Recommended Uses

C III] imaging.

Pivot λ (Å)	FWHM (Å)	AB mag zeropoint	S_{peak}	B_λ	R_{80} (arcsec)	Flux in central pixel
2001.7	417.2	19.640	1.31e+13	201.0	0.23	10%

Figure 14.48: F25CIII NUV-MAMA Integrated System Throughput and Redleak

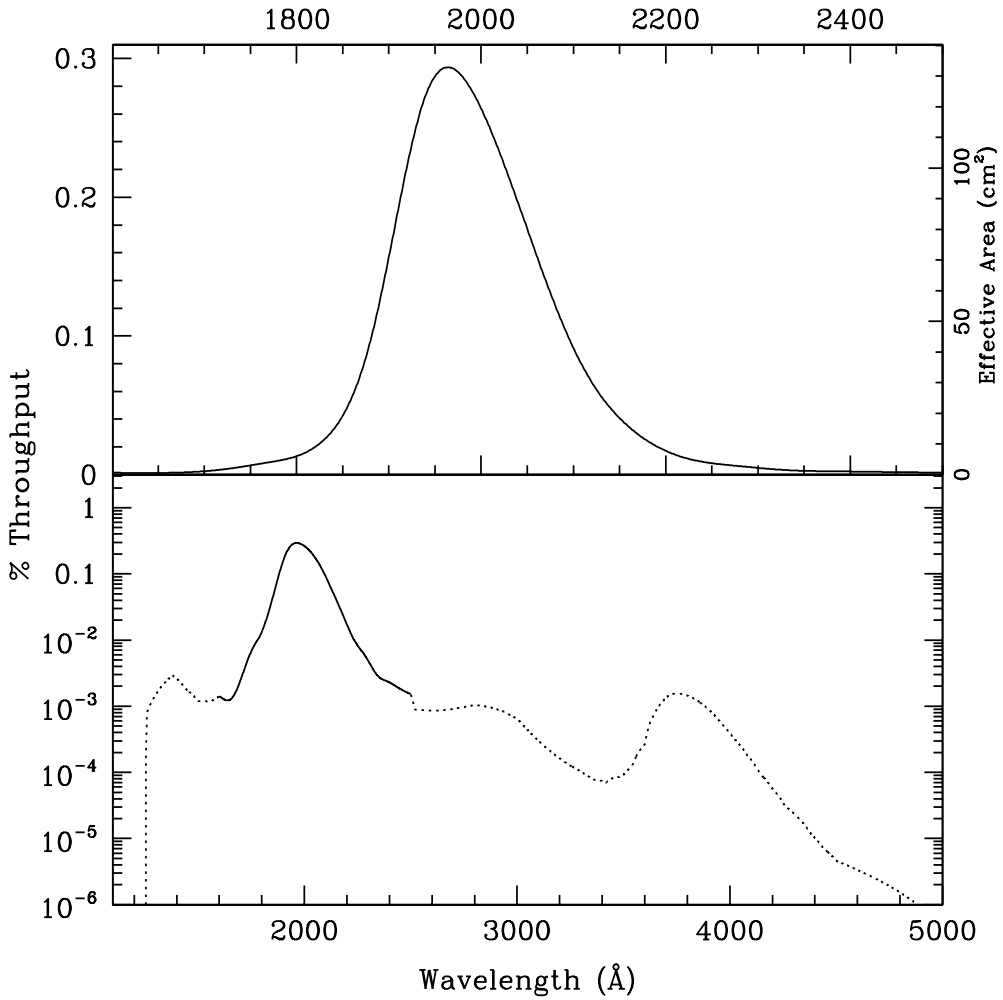

Table 14.19: Throughput and Sensitivity for F25CIII NUV-MAMA

λ	Sensitivity	Throughput %
1750.	2.67E11	0.01
1800.	5.46E11	0.01
1850.	1.79E12	0.04
1900.	6.79E12	0.16
1950.	1.28E13	0.29
2000.	1.20E13	0.26
2050.	8.28E12	0.18
2100.	4.37E12	0.09
2150.	2.00E12	0.04
2200.	8.62E11	0.02
2250.	4.23E11	0.01

Figure 14.49: Point Source S/N vs. V+AB_v for the F25CIII NUV-MAMA mode.

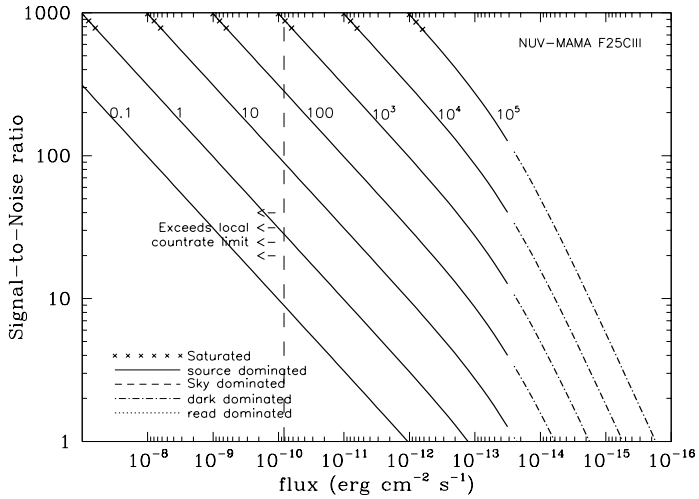

Figure 14.50: Extended Source S/N vs. V+AB_v for the F25CIII NUV-MAMA mode. Top curves are for an area of 0.2 arcsec^2; bottom curves are for 1 arcsec^2. Average sky assumed.

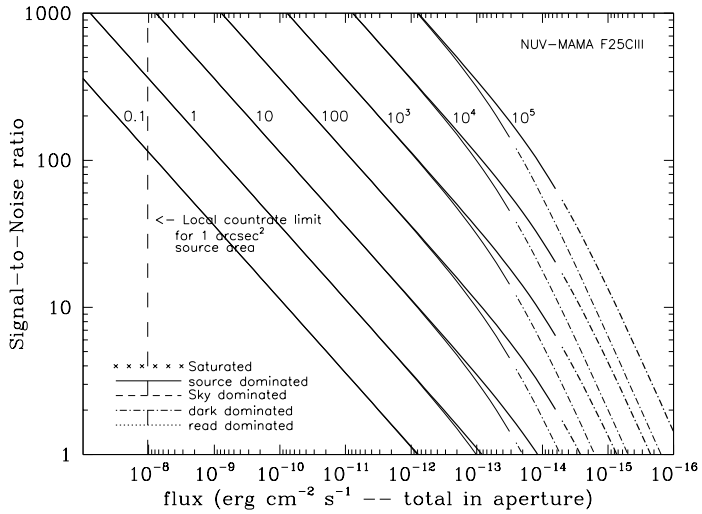

Table 14.20: Radial Profile for F25CIII

Radius			Encircled Energy
Pixels	Arcsec	intensity	
1	0.024	4.859e-02	0.173
2	0.037	3.660e-02	0.284
2	0.049	2.557e-02	0.392
3	0.073	9.899e-03	0.528
4	0.098	3.609e-03	0.598
5	0.122	1.832e-03	0.649
10	0.245	2.759e-04	0.753
15	0.367	1.339e-04	0.822
20	0.490	7.056e-05	0.873
25	0.613	4.358e-05	0.911
30	0.735	3.353e-05	0.944
40	0.980	1.002e-05	0.981

Figure 14.51: Point Source PSF for F25CIII NUV-MAMA, 7.″5 square (at pixel 741,402, log scaled, B-V=-0.04). Note PSF ghost ~45 pixels left of peak pixel and a few 10-3 of the peak

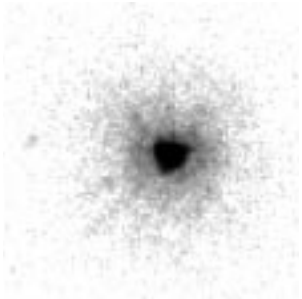

Figure 14.52: Point Source Encircled Energy for F25CIII NUV-MAMA

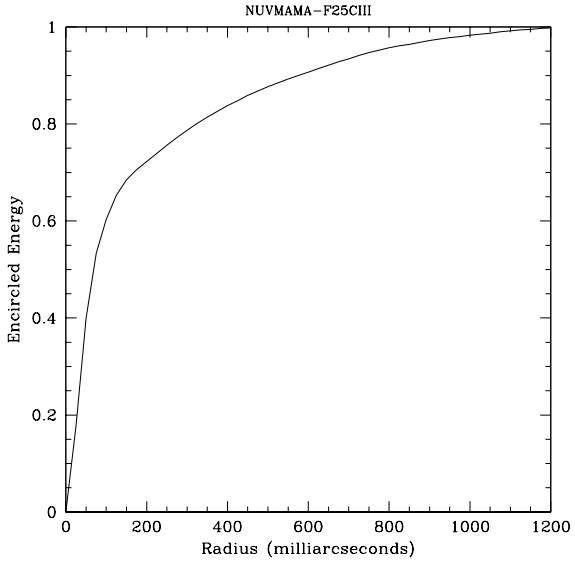

Figure 14.53: Point Source Intensity vs. Radius for F25CIII NUV-MAMA

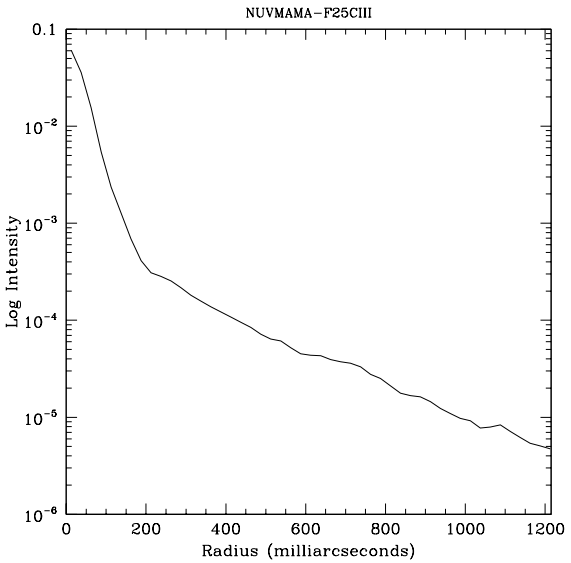

F25CN182—NUV-MAMA

Description

The F25CN182 filter with the NUV-MAMA provides medium bandwidth imaging of the continuum near 1900 Å.

Recommended Uses

Continuum filter for C III].

Pivot λ (Å)	FWHM (Å)	AB mag zeropoint	S_{peak}	B_λ	R_{80} (arcsec)	Flux in central pixel
1982.9	630.0	21.825	3.04e+13	637.3	0.23	10%

Figure 14.54: F25CN182 NUV-MAMA Integrated System Throughput and Redleak

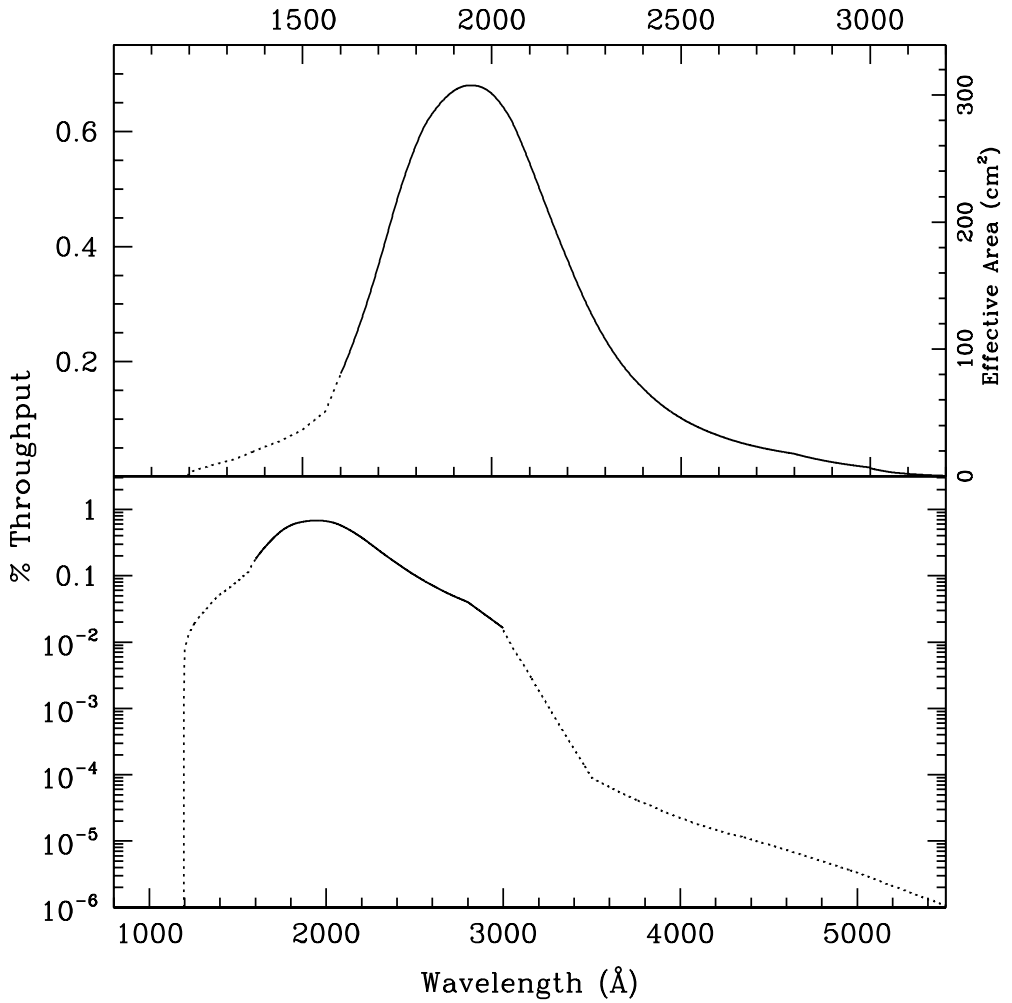

Table 14.21: Throughput and Sensitivity for F25CN182 NUV-MAMA

λ	Sensitivity	Throughput %
1300.	8.04E11	0.03
1400.	1.67E12	0.05
1500.	2.80E12	0.08
1600.	6.48E12	0.18
1700.	1.42E13	0.37
1800.	2.36E13	0.58
1900.	2.90E13	0.67
2000.	3.03E13	0.67
2100.	2.61E13	0.54
2200.	1.89E13	0.38
2300.	1.25E13	0.24
2400.	8.41E12	0.15
2500.	5.82E12	0.10
2600.	4.24E12	0.07
2700.	3.22E12	0.05
2800.	2.55E12	0.04

Figure 14.55: Point Source S/N vs. V+AB$_\nu$ for the F25CN182 NUV-MAMA mode.

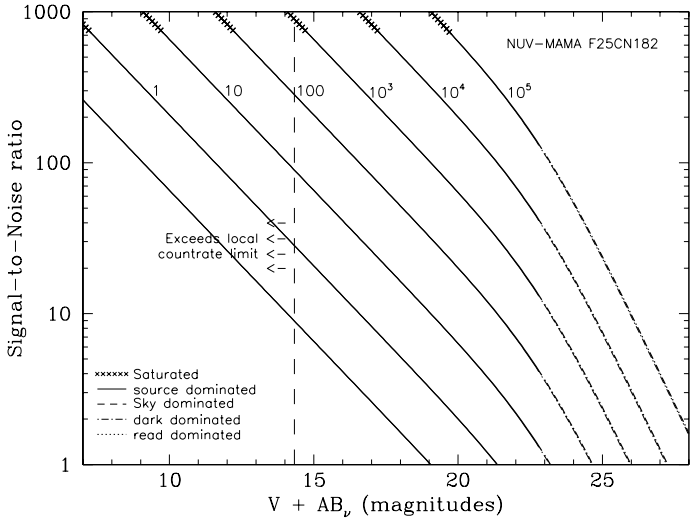

Figure 14.56: Extended Source S/N vs. V+AB$_\nu$ for the F25CN182 NUV-MAMA mode. Top curves are for an area of 0.2 arcsec^2; bottom curves are for 1 arcsec^2. Average sky assumed.

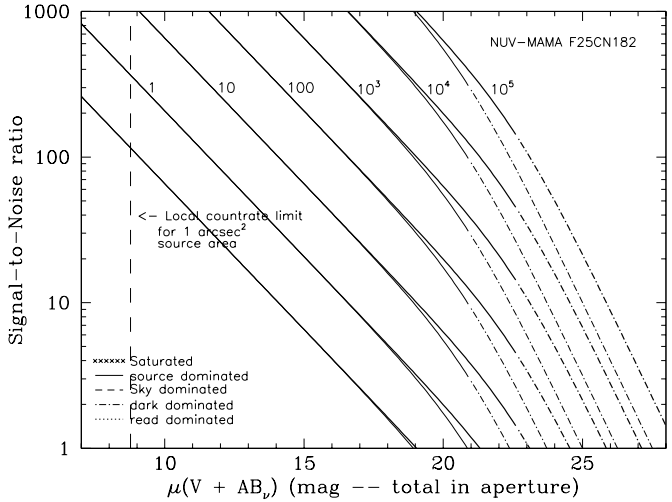

Table 14.22: Radial Profile for F25CN182

Radius		Intensity	Encircled Energy
Pixels	Arcsec		
1	0.024	4.177e-02	0.179
2	0.037	2.686e-02	0.302
2	0.049	1.620e-02	0.422
3	0.073	5.757e-03	0.565
4	0.098	2.720e-03	0.647
5	0.122	1.425e-03	0.700
10	0.245	2.600e-04	0.810
15	0.367	1.234e-04	0.876
20	0.490	6.357e-05	0.925
25	0.613	3.483e-05	0.956
30	0.735	2.099e-05	0.979
40	0.980	2.113e-06	0.999

Figure 14.57: Point Source Encircled Energy for F25CN182 NUV-MAMA

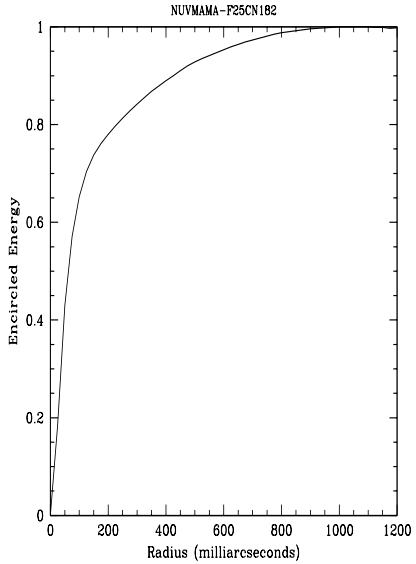

Table 14.23: Point Source Intensity vs. Radius for F25CN182 NUV-MAMA

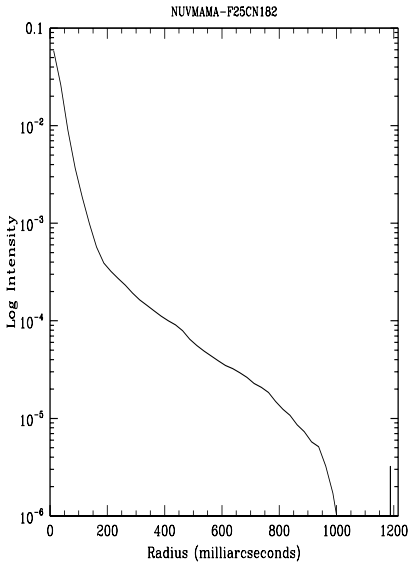

25MAMA—FUV-MAMA Clear

Description

The 25MAMA mode with the FUV-MAMA detector provides high-throughput broad-band far-UV imaging with the highest available throughput at ~1500 Å and the highest possible spatial resolution. The field of view is 25 x 25 arcsec.

Recommended Uses

Recommended for broad-band near-UV imaging of sources where sky background is not a consideration.

Special Considerations

For long exposures of faint targets, sky background is likely to be a limiting factor. Observers should consider the use of DARKTIME or (preferably) use the F25QTZ filter, which has nearly the same throughput but rejects geocoronal Lyman-α and OI 1302 Å airglow.

Pivot λ (Å)	FWHM (Å)	AB mag zeropoint	S_{peak}	B_λ	R_{80} (arcsec)	Flux in central pixel
1374.3	272.1	23.595	1.30e+14	366.9	0.32	8%

Figure 14.58: 25MAMA FUV-MAMA Integrated System Throughput and Redleak

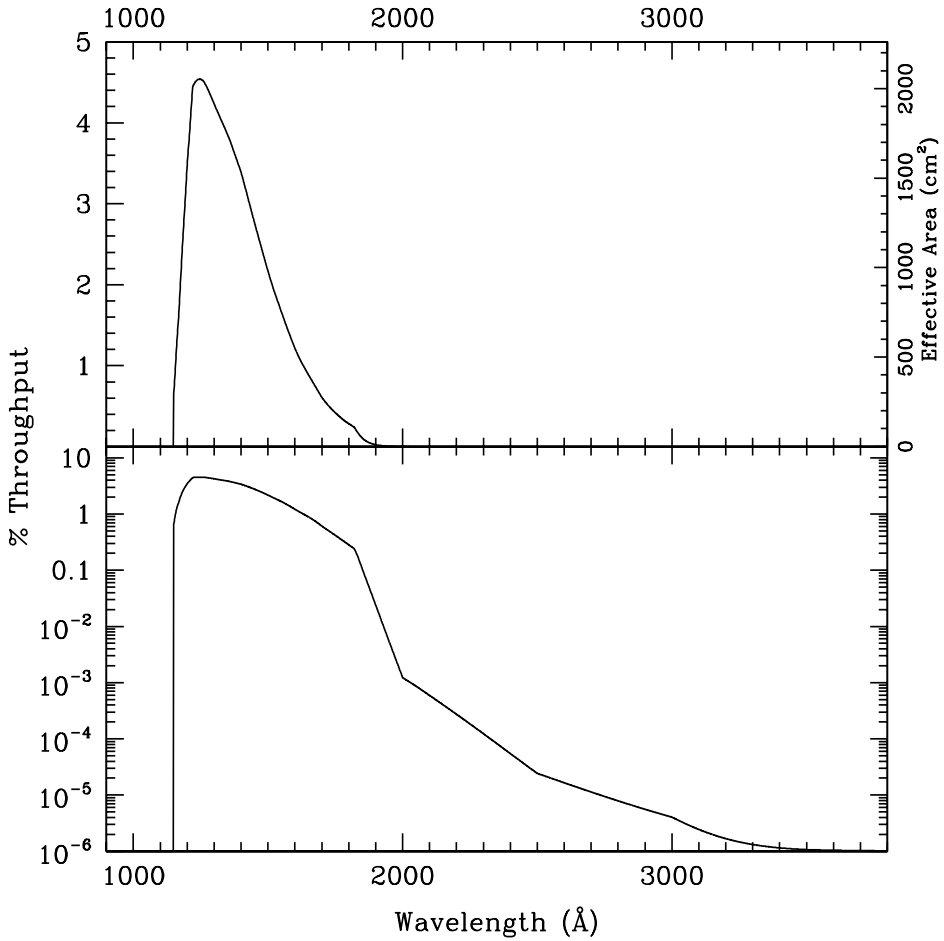

Table 14.24: Throughput and Sensitivity for 25MAMA FUV-MAMA

λ	Sensitivity	Throughput %
1150.	1.72E13	0.66
1175.	5.41E13	2.02
1200.	9.51E13	3.48
1225.	1.25E14	4.48
1250.	1.29E14	4.54
1300.	1.25E14	4.23
1350.	1.18E14	3.85
1375.	1.14E14	3.63
1400.	1.08E14	3.39
1425.	9.99E13	3.08
1450.	9.14E13	2.77
1475.	8.28E13	2.46
1500.	7.41E13	2.17
1550.	5.87E13	1.66
1600.	4.43E13	1.21
1650.	3.34E13	0.89
1700.	2.36E13	0.61
1750.	1.67E13	0.42
1800.	1.16E13	0.28
1850.	4.45E12	0.11
1875.	2.17E12	0.05

Figure 14.59: Point Source S/N vs. V+AB_v for the 25MAMA FUV-MAMA mode.

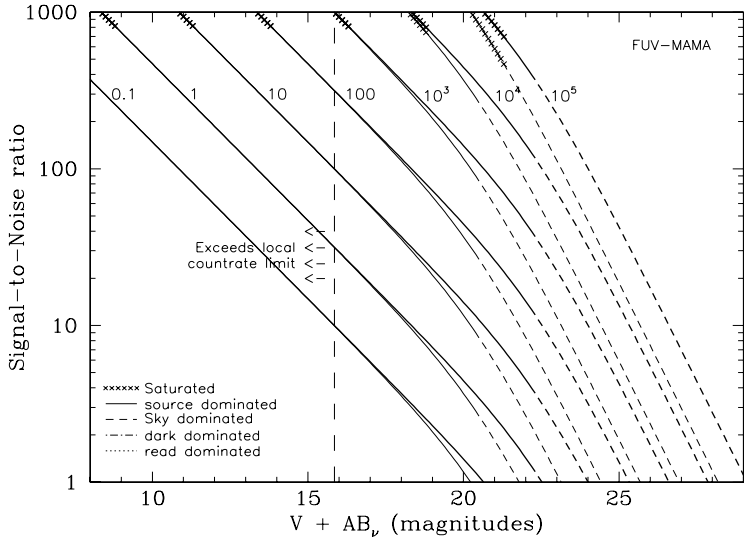

Figure 14.60: Extended Source S/N vs. V+AB_v for the 25MAMA FUV-MAMA mode. Top curves are for an area of 0.2 arcsec^2; bottom curves are for 1 arcsec^2. Average sky assumed.

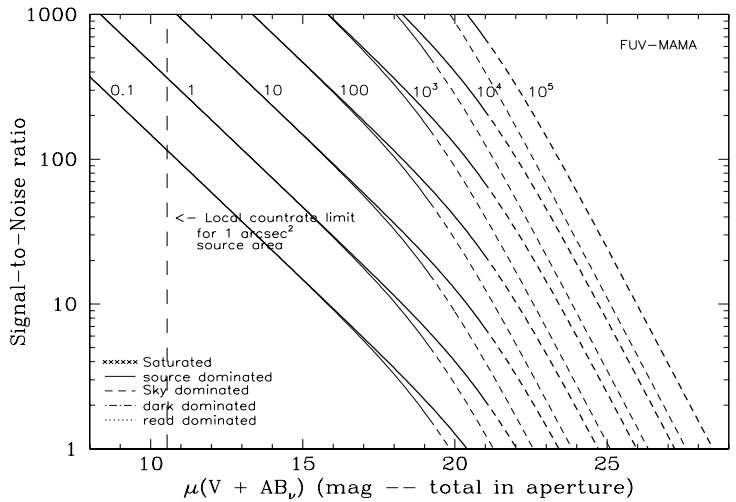

Table 14.25: Radial Profile for 25MAMA

Radius		Intensity	Encircled Energy
Pixels	Arcsec		
1	0.024	3.267e-02	0.141
2	0.037	2.107e-02	0.236
2	0.049	1.345e-02	0.331
3	0.073	6.141e-03	0.467
4	0.098	2.981e-03	0.557
5	0.122	1.485e-03	0.614
10	0.245	3.377e-04	0.746
15	0.367	1.676e-04	0.834
20	0.490	9.542e-05	0.900
25	0.613	4.543e-05	0.947
30	0.735	2.065e-05	0.972
40	0.980	5.088e-06	0.994

Figure 14.61: Point Source Encircled Energy for 25MAMA FUV-MAMA

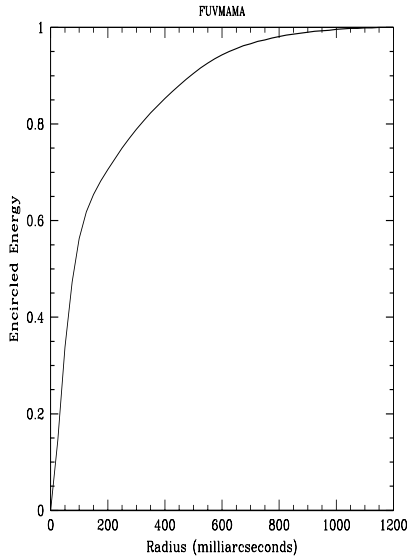

Figure 14.62: Point Source Intensity vs. Radius for 25MAMA FUV-MAMA

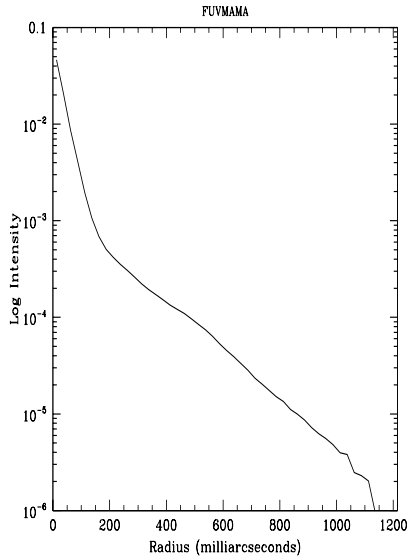

F25QTZ—FUV-MAMA, Longpass

Description

The F25QTZ filter with the FUV-MAMA provides high-throughput broad-band far-UV imaging with better rejection of geocoronal emission than the F25MAMA or F25SRF2 modes and the same field of view and spatial resolution.

Recommended Uses

Recommended filter for broad-band far-UV imaging of faint targets.

Special Considerations

With this filter the background is dominated by detector dark current. The dark current is not constant across the detector and not constant in time. This could limit the sensitivity for very extended faint targets, however, note that the FUV-MAMA dark is extremely low.

Pivot λ (Å)	FWHM (Å)	AB mag zeropoint	S_{peak}	B_λ	R_{80} (arcsec)	Flux in central pixel
1595.1	205.6	21.539	4.29e+13	225.0	0.28	10%

Figure 14.63: F25QTZ FUV-MAMA Integrated System Throughput and Redleak

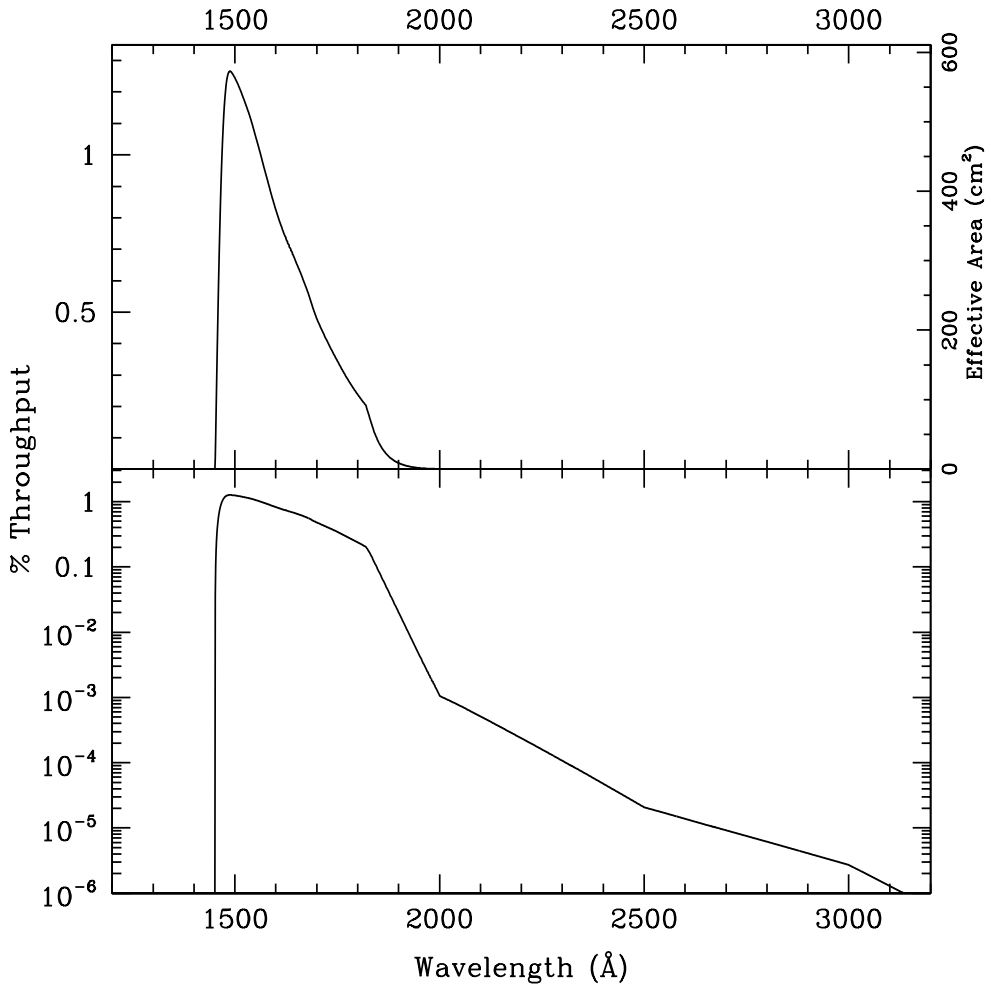

Table 14.26: Throughput and Sensitivity for F25QTZ FUV-MAMA

λ	Sensitivity	Throughput %
1475.	3.93E13	1.17
1500.	4.25E13	1.24
1525.	4.05E13	1.17
1550.	3.75E13	1.06
1575.	3.38E13	0.94
1600.	3.01E13	0.83
1625.	2.72E13	0.73
1650.	2.46E13	0.65
1675.	2.19E13	0.57
1700.	1.85E13	0.48
1725.	1.60E13	0.41
1750.	1.38E13	0.35
1775.	1.16E13	0.29
1800.	9.75E12	0.24
1825.	7.59E12	0.18
1850.	3.75E12	0.09
1875.	1.83E12	0.04
1900.	8.71E11	0.02

Figure 14.64: Point source S/N vs. V+AB$_\nu$ for the F25QTZ FUV-MAMA mode.

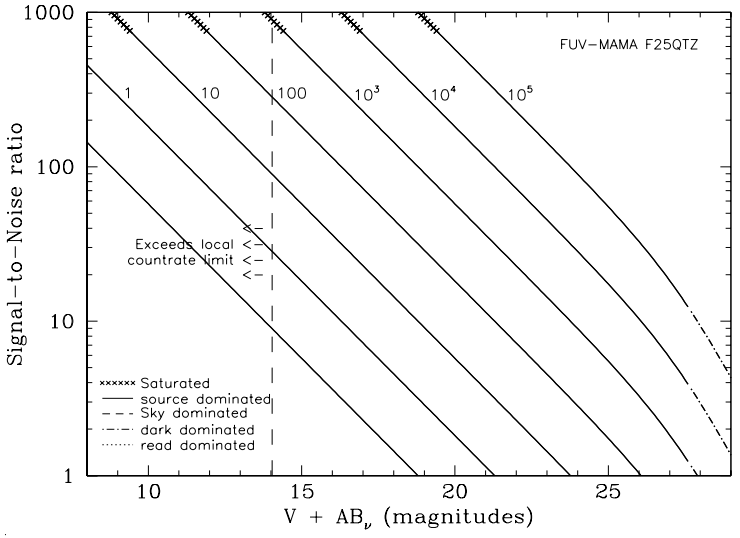

Figure 14.65: Extended source S/N vs. V+AB$_\nu$ for the F25QTZ FUV-MAMA mode. Top curves are for an area of 0.2 arcsec^2; bottom curves are for 1 arcsec^2. Average sky assumed.

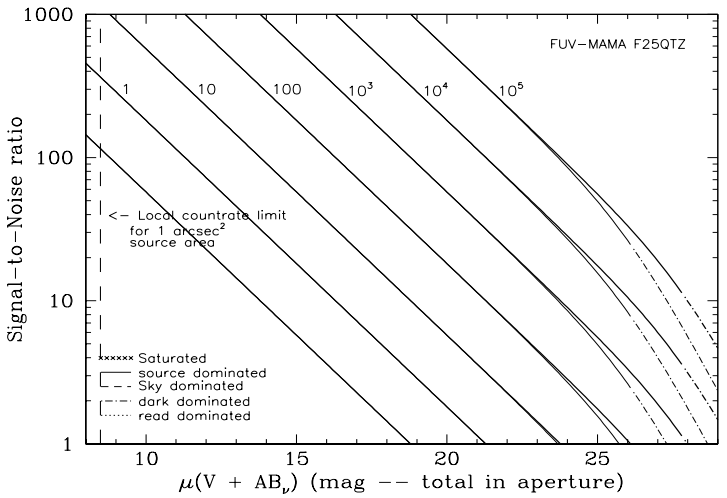

Table 14.27: Radial Profile for F25QTZ

Radius			Encircled energy
Pix	arcsec	intensity	
1	0.024	3.961e-02	0.172
2	0.037	2.515e-02	0.287
2	0.049	1.505e-02	0.398
3	0.073	5.412e-03	0.532
4	0.098	2.570e-03	0.609
5	0.122	1.373e-03	0.659
10	0.245	2.735e-04	0.778
15	0.367	1.447e-04	0.851
20	0.490	7.887e-05	0.909
25	0.613	4.703e-05	0.953
30	0.735	2.117e-05	0.980
40	0.980	1.135e-05	1.000

Figure 14.66: Point Source Encircled Energy for F25QTZ FUV-MAMA

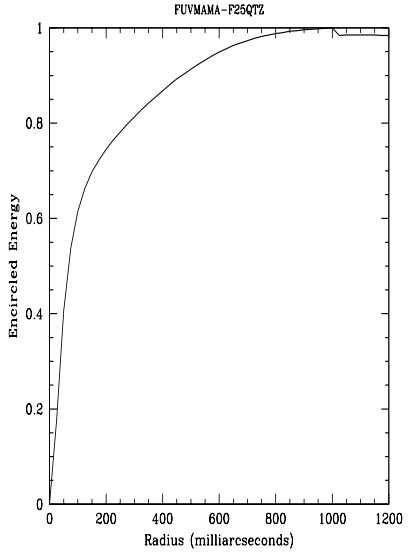

Figure 14.67: Point Source Intensity vs. Radius for F25QTZ FUV-MAMA

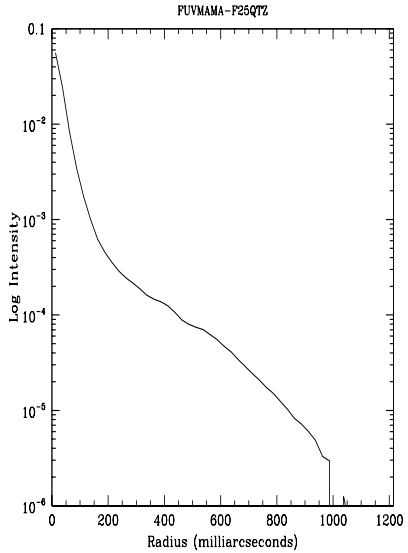

F25SRF2—FUV-MAMA, Longpass

Description

The F25SRF2 filter with the FUV-MAMA provides high-throughput broad-band far-UV imaging with better rejection of geocoronal emission than the F25MAMA but worse than or F25QTZ modes. It provides the same field of view and spatial resolution as these modes.

Recommended Uses

This filter has slightly higher throughput than F25QTZ, but lets in geocoronal OI 1302 Å. For sky-limited imaging F25QTZ is usually a better choice.

Special Considerations

Sky background on the day side of the orbit contains a significant contributions from OI airglow emission at 1356 Å and at 1302 Å. In high-background conditions, the sky background can dominate the detector background. In average day-side observing conditions the sky background through this filter will be about a factor of 100 higher than for F25QTZ. Observers can limit the background (with some cost to the total amount of observing time per orbit) by using the DARKTIME special requirement.

Pivot λ (Å)	FWHM (Å)	AB mag zeropoint	S_{peak}	B_λ	R_{80} (arcsec)	Flux in central pixel
1457.4	243.7	22.825	8.67e+13	303.5	0.30	9%

Figure 14.68: F25SRF2 FUV-MAMA Integrated System Throughput and Redleak

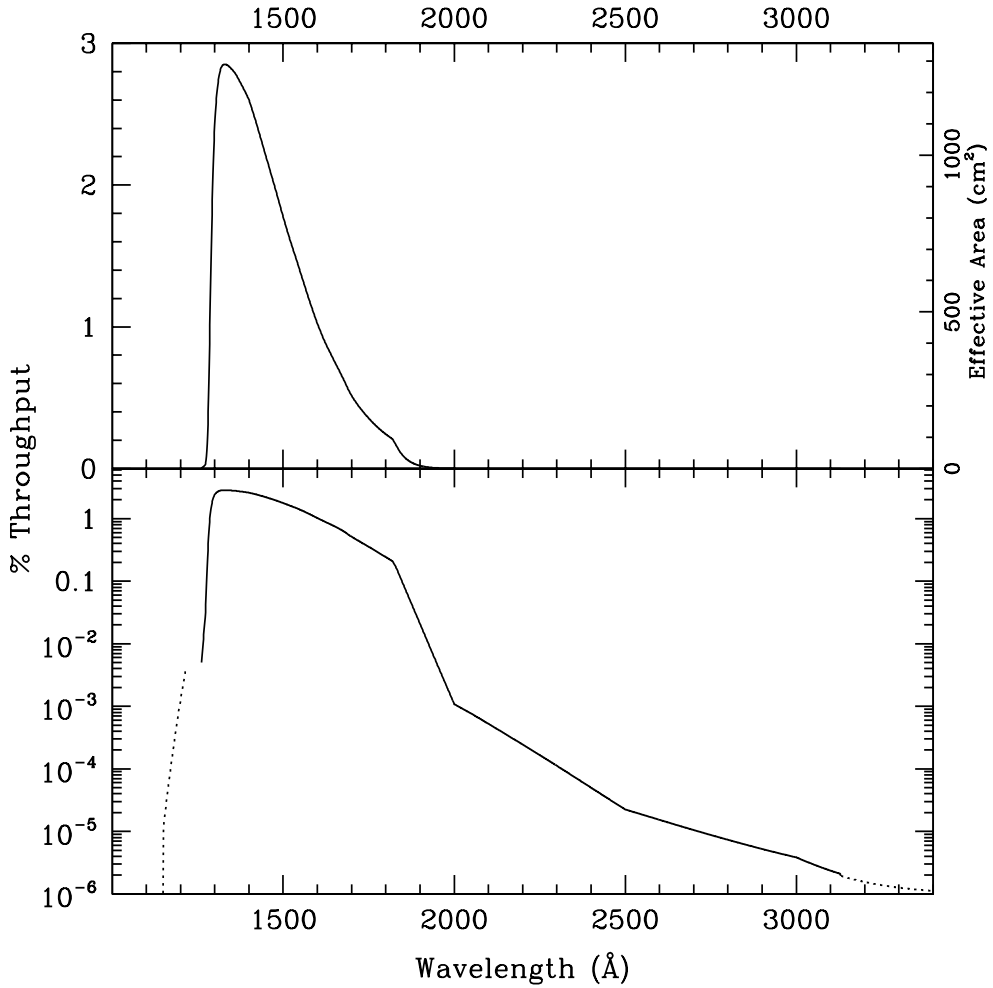

Table 14.28: Throughput and Sensitivity for F25SRF2 FUV-MAMA

λ	Sensitivity	Throughput %
1300.	7.18E13	2.42
1325.	8.60E13	2.85
1350.	8.66E13	2.82
1375.	8.53E13	2.72
1400.	8.30E13	2.60
1425.	7.82E13	2.41
1450.	7.27E13	2.20
1475.	6.69E13	1.99
1500.	6.07E13	1.78
1525.	5.47E13	1.58
1550.	4.90E13	1.39
1575.	4.30E13	1.20
1600.	3.73E13	1.02
1625.	3.25E13	0.88
1650.	2.84E13	0.76
1675.	2.43E13	0.64
1700.	1.99E13	0.51
1725.	1.68E13	0.43
1750.	1.42E13	0.36
1775.	1.19E13	0.29
1800.	9.96E12	0.24

Figure 14.69: Point Source S/N vs. V+AB_ν for the F25SRF2 FUV-MAMA mode.

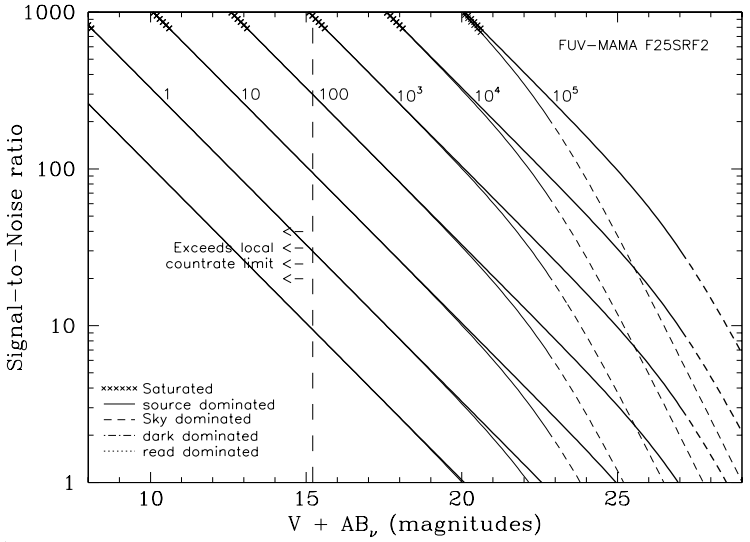

Figure 14.70: Extended Source S/N vs. V+AB_ν for the F25SRF2 FUV-MAMA mode. Top curves are for an area of 0.2 arcsec^2; bottom curves are for 1 arcsec^2. Average sky assumed.

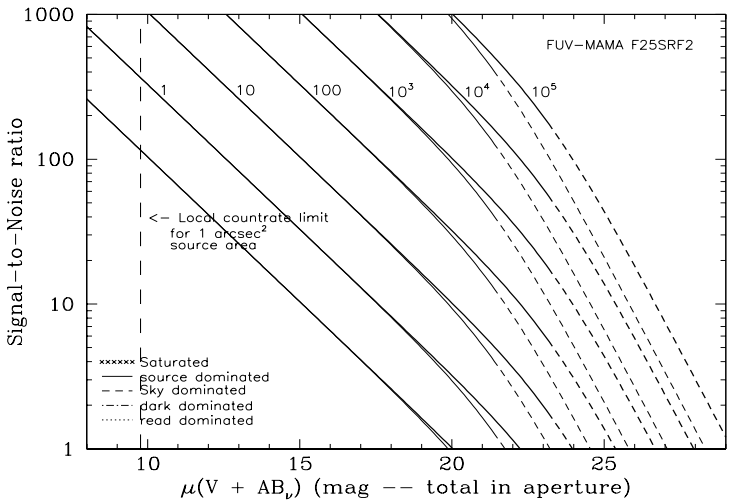

Table 14.29: Radial Profile for F25SRF2

Radius		Intensity	Encircled Energy
Pixels	Arcsec		
1	0.024	3.544e-02	0.154
2	0.037	2.268e-02	0.256
2	0.049	1.408e-02	0.358
3	0.073	5.787e-03	0.493
4	0.098	2.765e-03	0.576
5	0.122	1.514e-03	0.630
10	0.245	3.098e-04	0.762
15	0.367	1.677e-04	0.847
20	0.490	8.854e-05	0.910
25	0.613	4.487e-05	0.954
30	0.735	2.080e-05	0.980
40	0.980	1.510e-06	0.999

Figure 14.71: Point Source Encircled Energy for F25SRF2 FUV-MAMA

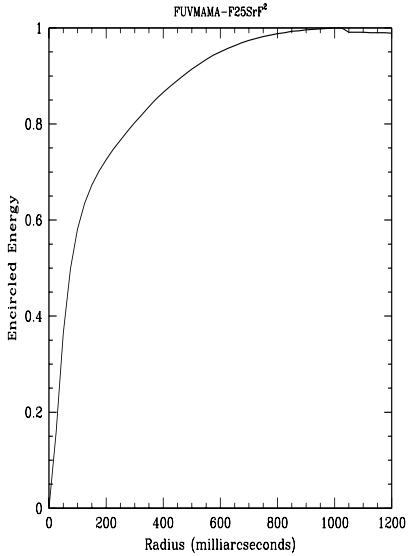

Figure 14.72: Point Source Intensity vs. Radius for F25SRF2 FUV-MAMA

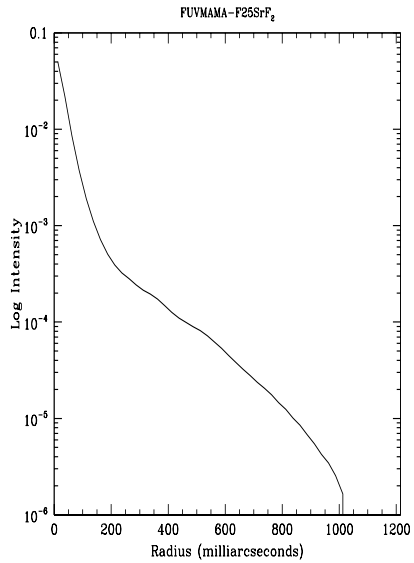

F25LYA—FUV-MAMA, Lyman-α

Description

The F25LYA filter with the FUV-MAMA provides narrowband imaging of the HI 1216 Å Lyman-α line.

Recommended Uses

Lyman α imaging. Differencing two images taken with 25MAMA and F25SRF2 is another option.

Special Considerations

Sensitivity is limited by geocoronal Lyman-α. Observers can limit the background (with some cost to the total amount of observing time per orbit) by using the DARKTIME special requirement.

Pivot λ (Å)	FWHM (Å)	AB mag zeropoint	S_{peak}	B_λ	R_{80} (arcsec)	Flux in central pixel
1243.1	121.9	19.569	9.44e+12	101.1	0.35	6%

Figure 14.73: F25LYA FUV-MAMA Integrated System Throughput and Redleak

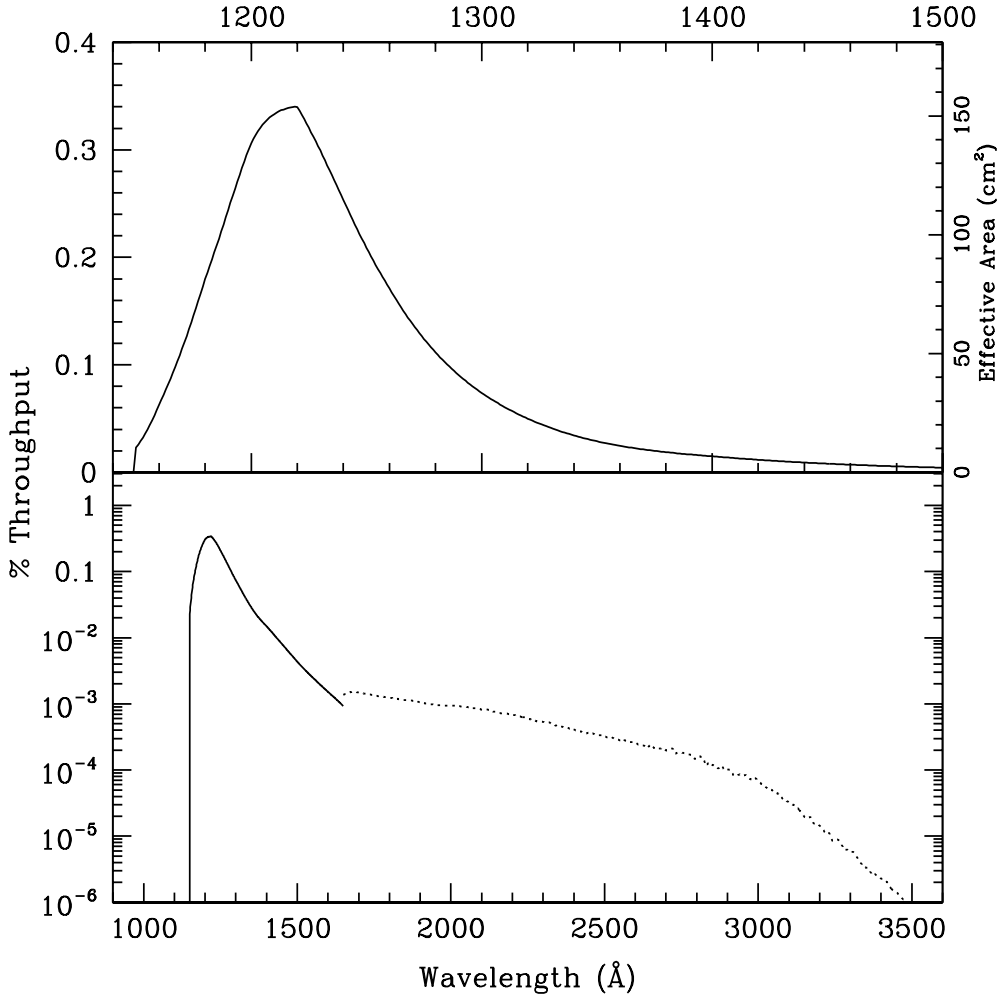

Table 14.30: Throughput and Sensitivity for F25LYA FUV-MAMA

λ	Sensitivity	Throughput %
1150.	6.01E11	0.02
1175.	3.91E12	0.15
1200.	8.37E12	0.31
1225.	8.94E12	0.32
1250.	5.95E12	0.21
1275.	3.60E12	0.12
1300.	2.19E12	0.07
1325.	1.37E12	0.05
1350.	8.90E11	0.03
1375.	6.26E11	0.02

Figure 14.74: Point Source S/N vs. V+AB$_v$ for the F25LYA FUV-MAMA mode.

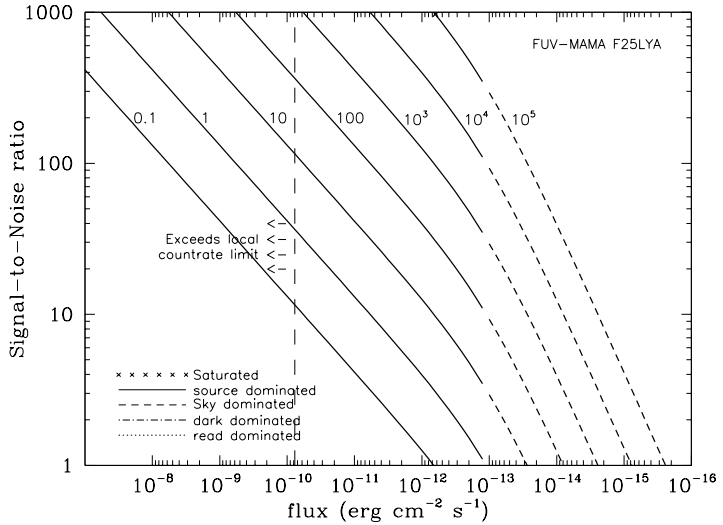

Figure 14.75: Extended Source S/N vs. V+AB$_v$ for the F25LYA FUV-MAMA mode. Top curves are for an area of 0.2 arcsec^2; bottom curves are for 1 arcsec^2. Average sky assumed.

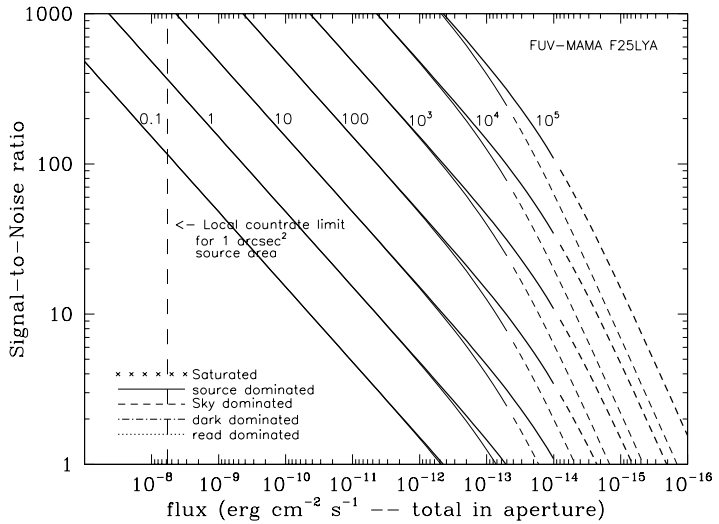

Table 14.31: Radial Profile for F25LYA

Radius			Encircled energy
Pix	arcsec	intensity	
1	0.024	2.440e-02	0.100
2	0.037	1.702e-02	0.174
2	0.049	1.199e-02	0.254
3	0.073	6.423e-03	0.387
4	0.098	3.326e-03	0.485
5	0.122	1.718e-03	0.549
10	0.245	3.888e-04	0.712
15	0.367	2.140e-04	0.816
20	0.490	1.044e-04	0.895
25	0.613	4.910e-05	0.943
30	0.735	1.741e-05	0.968
40	0.980	8.124e-06	0.994

Figure 14.76: Point Source PSF for F25LYA FUV-MAMA, 7.″5 square (at pixel 739, 368, log scaled, B-V=-0.04)

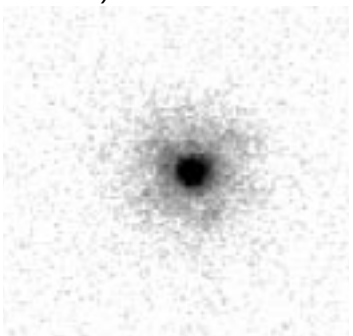

Figure 14.77: Point Source Encircled Energy for F25LYA FUV-MAMA

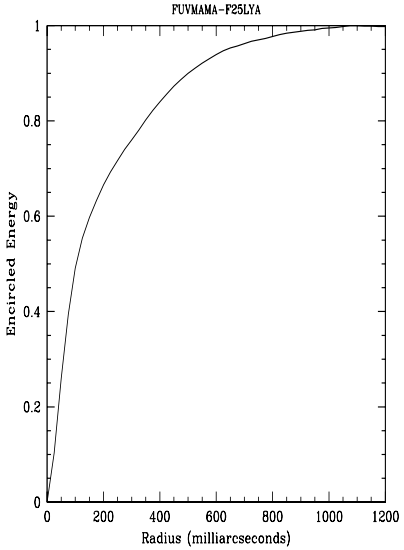

Figure 14.78: Point Source Intensity vs. Radius for F25LYA FUV-MAMA

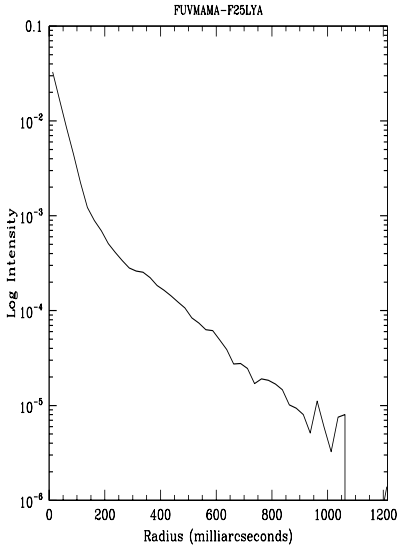

Image-Mode Geometric Distortion

The STIS cameras have significant geometric distortion which not only affects astrometry, but also in principle affects photometry (because the extended sources used to generate flat fields have an induced change in the apparent surface brightness). In the CCD the image distortions are less than one pixel across the whole detector, and can often be ignored. For the MAMA the distortions are larger, approaching 3 pixels at the corners of cameras.

Geometric distortion and plate scales for the STIS imaging modes have been measured on-orbit by observing star fields shifted to different positions in the field, following a procedure similar to that used for WFPC-2 (Holtzman et al., PASP, 107, 156). The analysis for the CCD and the FUV-MAMA are described by Malumuth and Bowers (1997 HST Calibration workshop, page 144). The geometric distortion data data also allowed a determination of the plate scale. For the CCD the scale is $0\farcs05071 \pm 0\farcs00007$. For the FUV-MAMA the scale is $0\farcs02447 \pm 0\farcs00001$ in the *x* (row) direction and $0\farcs02467 \pm 0\farcs00002$ in the *y* (column) direction. Portions of the NUV-MAMA calibration were lost due to an on-board computer problem; the data that were obtained yield a slightly less precise solution. The NUV-MAMA plate scale is $0\farcs02455 \pm 0\farcs00013$ in *x* and $0\farcs02479 \pm 0\farcs000096$ in *y*. The errors quoted are formal random errors derived from the uncertainties in measuring the positions of the sources.

The geometric distortion for the STIS cameras has been characterized in the same way as for WFPC2, with a cubic distortion solution, which relates the true x and y positions of the stars, x_t and y_t, in pixel coordinates from the center of the image, to the observed positions *x* and *y* also in pixels measured from the center of the image:

$$x_t = C_0 + C_1 x + C_2 y + C_3 x^2 + C_4 xy + C_5 y^2 + C_6 x^3 + C_7 yx^2 + C_8 xy^2 + C_9 y^3$$

$$y_t = D_0 + D_1 x + D_2 y + D_3 x^2 + D_4 xy + D_5 y^2 + D_6 x^3 + D_7 yx^2 + D_8 xy^2 + D_9 y^3$$

The coefficients are listed in Table 14.32.

Table 14.32: STIS Imaging Mode Cubic Distortion Coefficients

Coefficients C,D	CCD		FUV-MAMA		NUV-MAMA	
C_0,D_0	0.0	0.0	0.0	0.0	0.0	0.0
C_1,D_1	1.0011324	-5.6351965e-05	0.9990498	-0.0001417	0.9987784	0.0004347
C_2,D_2	-1.2427886e-04	1.0006398	-0.0005722	1.0005972	-0.0010297	1.0021945
C_3,D_3	-3.9052366e-07	1.4414957e-07	2.1279013e-07	6.5272699e-07	4.3208795e-06	-2.7073310e-07
C_4,D_4	-2.3388352e-07	2.1911561e-06	6.1468474e-06	4.7377267e-07	4.7693180e-06	3.9164061e-06
C_5,D_5	-2.7747067e-06	-1.5699432e-07	2.3167273e-06	-2.6421370e-06	2.7909658e-06	-2.1755042e-06
C_6,D_6	-5.8339901e-09	2.2058683e-10	4.6704462e-09	5.5607193e-10	4.4155962e-09	-3.7271427e-09
C_7,D_7	1.4677396e-09	-3.0218644e-09	1.2221236e-09	-8.2054558e-10	-3.5393975e-10	-8.4647093e-09
C_8,D_8	-3.4363894e-09	8.2253175e-10	-4.5285643e-09	7.4727479e-10	-3.2033493e-09	1.2216235e-09
C_9,D_9	6.8542388e-10	-3.1486902e-09	1.5149124e-09	-1.5672843e-09	3.9776611e-11	-2.8687795e-10

Spatial Dependence of the STIS PSF

The STIS PSF varies across the field of view. Observations of Omega Cen and NGC6681 have been used to study the PSF variations, and confirm that they show the behavior expected from the optics. One way of characterizing the spatial variation is to measure the flux in a fixed aperture. Figure 14.79 through Figure 14.82 show the fraction of the flux enclosed within a 0.05 arcsec radius aperture. This parameter is relatively constant for the CCD, but is more pronounced for the MAMA detectors. For example, the 0.05” encircled energy varies from 47% to 31% across the NUV-MAMA with the `F25CN182` filter.

See Bowers (1997 HST Calibration Workshop) for a discussion of HST “breathing” effects on the PSF.

Figure 14.79: Fraction of the total flux of a point source that passes through an aperture of 0.05” radius for the CCD and a clear aperture (50CCD). The data were obtained from observations of the Omega Cen star cluster. Crosses represent stars that have little or no contamination from other sources, while trianges are sources that were marginally contaminated in the region outside the PSF core. No objects were used that had contamination within 0.15” of the center.

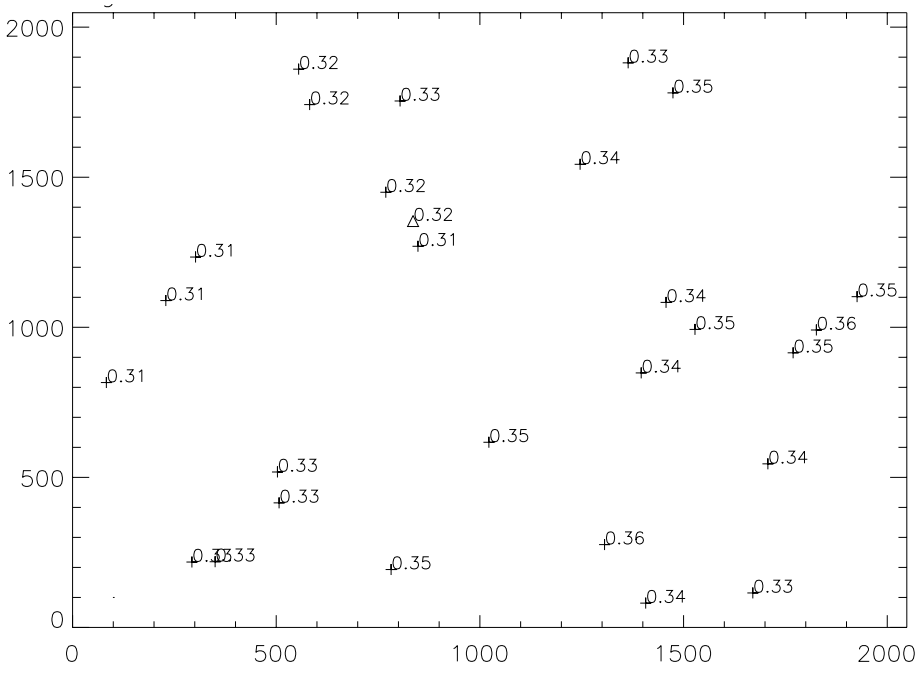

Figure 14.80: Fraction of the total flux of a point source that passes through an aperture of 0.05” radius for the NUV-MAMA with the F25CN270. The data were obtained from observations of the star cluster NGC 6881. Crosses represent stars that have little or no contamination from other sources, while trianges are sources that were marginally contaminated in the region outside the PSF core. No objects were used that had contamination within 0.15” of the center

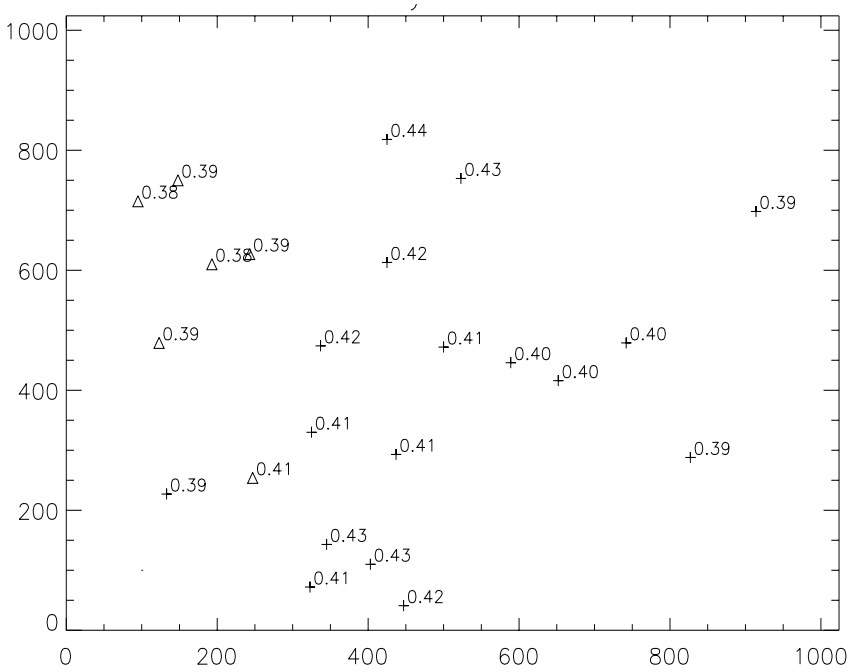

Figure 14.81: Fraction of the total flux of a point source that passes through an aperture of 0.05” radius for the NUV-MAMA with the F25CN270 filter. The data were obtained from observations of the star cluster NGC 6881. Crosses represent stars that have little or no contamination from other sources, while triangles are sources that were marginally contaminated in the region outside the PSF core. No objects were used that had contamination within 0.15” of the center.

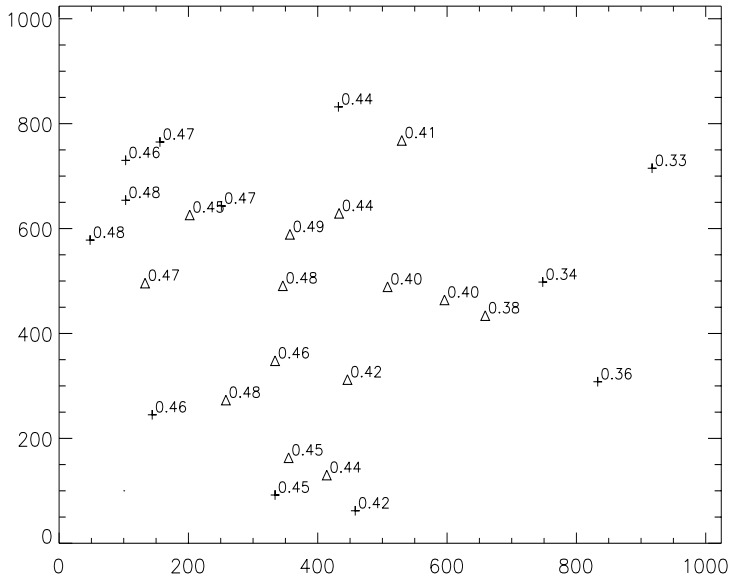

Figure 14.82: Fraction of the total flux of a point source that passes through an aperture of 0.05” radius for the FUV-MAMA with the F25QTZ filter. The data were obtained from observations of the star cluster NGC 6881. Crosses represent stars that have little or no contamination from other sources, while triangles are sources that were marginally contaminated in the region outside the PSF core. No objects were used that had contamination within 0.15” of the center

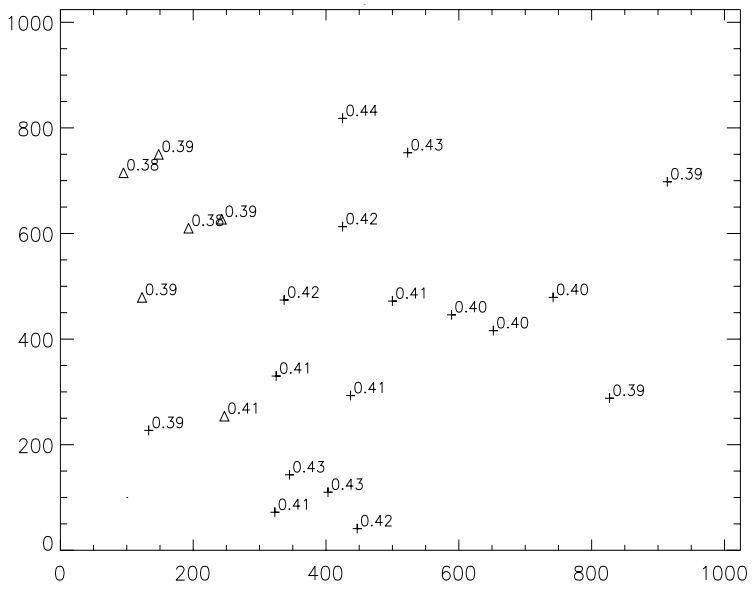

MAMA Imaging Bright Object Limits

As described in “MAMA Bright-Object Limits” on page 115 in Chapter 7. the MAMA’s are subject to absolute brightness limits, above which sources cannot be observed or they would potentially damage the detectors. In Table 14.33, below, we present the complete set of bright object point source and integrated magnitude screening limits for the MAMA imaging modes. These screening magnitudes are presented as a *guide*. Whether or not an individual source can be observed is determined by whether the desired configuration and the spectrum of that source is predicted to exceed the global and local absolute observing count rate limits, as described in Chapter 7. Remember, sources cannot be observed in configurations where they exceed the absolute bright object limits. The information presented here should be used in conjunction with the material presented in Chapter 7.

A few important points to note.

- Limits are given as V magnitudes or in CGS units as indicated.
- The limits were derived assuming zero slit loss.
- The imaging table includes a single point source limit. No single source in the field of view can exceed this limit.
- The limits in the tables assume zero extinction. If your source, when corrected for Galactic extinction, does not exceed the absolute limits, then you will be allowed to observe your source.
- The imaging table also includes an integrated magnitude limit. Remember that the global limit of 200,000 counts sec^{-1} applies to all sources imaged onto the MAMA detector. The integrated magnitude limit gives the total magnitude from all stars (or galaxies, or diffuse objects) of spectral type O which can appear in the MAMA field of view. Initial screening of all MAMA imaging observations will be done assuming all stars are O stars, however, ultimately for the final decision, the colors of the stars are taken into account whenever such information is available (see Chapter 7).

Table 14.33: MAMA Imaging Bright-Object Limits (V magnitudes and CGS units as indicated)

Spectral Type	FUV-MAMA				NUV-MAMA						
	25MAMA (clear)	**F25SRF2 (longpass)**	**F25QTZ (longpass)**	**F25LYA (Lyα)**	**25MAMA (clear)**	**F25SRF2 longpass**	**F25QTZ longpass**	**F25CIII (CIII)**	**F25CN182 (182 cont)**	**F25CN270 (270 cont)**	**F25MGII (MgII)**
Surface Brightness[a]	$1.4x10^{-12}$	$3.1x10^{-12}$	$6.0x10^{-12}$	$5.6x10^{-11}$	$3.1x10^{-13}$	$3.9x10^{-13}$	$3.7x10^{-13}$	$2.1x10^{-11}$	$3.1x10^{-12}$	$2.8x10^{-12}$	$1.1x10^{-11}$
Point Source Flux[b]	$3.3x10^{-15}$	$7.3x10^{-15}$	$1.4x10^{-14}$	$1.4x10^{-13}$	$7.5x10^{-16}$	$9.3x10^{-16}$	$8.8x10^{-16}$	$5.1x10^{-14}$	$7.5x10^{-15}$	$6.7x10^{-15}$	$2.7x10^{-14}$
O5 V[c]	20.2	19.3	18.1	16.5	20.2	19.9	19.9	16.0	18.2	17.1	15.4
B1 V	19.9	18.8	17.8	15.7	19.8	19.5	19.5	15.5	17.8	16.7	15.0
B3 V	19.5	18.4	17.3	15.0	19.4	19.2	19.1	15.2	17.3	16.5	14.7
B6 V	18.4	17.5	16.6	13.8	18.8	18.5	18.5	14.6	16.7	15.9	14.2
B9 V	17.2	16.3	15.5	12.3	17.9	17.6	17.6	13.5	15.7	15.2	13.6
A1 V	16.0	15.6	14.7	10.8	17.3	17.2	17.2	13.0	15.2	14.8	13.2
A3 V	14.8	14.2	13.8	8.5	16.9	16.7	16.6	12.6	14.6	14.4	12.8
A5 V	13.6	13.2	13.0	6.7	16.6	16.3	16.3	12.1	14.2	14.2	12.7
A9 IV	11.4	10.8	11.1	3.8	15.8	15.8	15.8	11.3	13.3	13.6	12.3
F2 V	10.1	9.8	9.8	2.5	15.4	15.2	15.2	10.5	12.8	13.3	11.8
F4 V	9.3	9.1	9.0	1.7	15.2	15.0	15.0	10.2	12.2	13.1	11.7
F6 V	8.8	8.3	8.7	0.9	15.0	14.8	14.8	9.7	11.8	12.9	11.5
F8 V	7.9	7.8	7.8	0.2	14.8	14.7	14.6	9.2	11.5	12.7	11.4
G2 V	6.5	6.8	6.6	-1.2	14.6	14.3	14.3	8.5	10.8	12.5	11.1
G5 IV	5.4	5.2	5.3	<-2.0	14.3	14.0	14.0	7.8	10.1	12.2	10.8
G7 IV	4.7	4.2	4.4		14.1	13.9	13.9	7.6	9.8	11.9	10.7
K0 IV	3.8	2.2	2.2		13.8	13.4	13.3	7.0	9.4	11.6	10.5
K4 V	-0.9	-1.9	-1.8		13.2	12.8	12.8	6.6	8.6	11.2	10.3
K8 V	<-2.0	<-2.0	<-2.0		12.7	12.2	12.2	6.1	7.8	10.8	10.2
M2 V					11.9	11.7	11.7	5.7	7.3	10.3	10.0
M4 V					11.5	11.5	11.5	5.6	7.0	10.0	9.9
M6 V					10.8	11.0	11.0	5.4	6.7	9.8	9.8
T~50000°K[d]	20.1	19.2	18.0	16.3	20.1	19.8	19.8	16.0	18.2	17.1	15.3
λ^{-1} [e]	16.5	15.8	14.9	12.7	18.0	17.6	17.6	13.3	15.3	15.1	13.5
Integrated Magnitude[f]	13.4	13.3	11.4	9.6	13.5	13.2	13.2	9.2	11.4	10.4	8.7

a. Peak allowed diffuse source surface brightness in ergs sec^{-1} cm^{-2} $Å^{-1}$ $arcsec^{-2}$.
b. Peak allowed point source flux in ergs sec^{-1} cm^{-2} $Å^{-1}$.
c. Limits given are V magnitudes, for unreddened stars.
d. Limits calculated for a black body at 50,000 degrees K.
e. Limits calculated for a source with spectrum F_λ proportional to λ^{-1}.
f. Maximum integrated magnitude of all stars in field, assuming all are O stars.

PART 4

Calibration

The chapters in this part describe the calibration of STIS. These chapters include an overview of the calibration pipeline process, expected accuracies for data taken in Cycle 7, and plans for calibrating and verifying the instrument's performance.

CHAPTER 15
Overview of Pipeline Calibration

In This Chapter...

In this chapter we summarize briefly the basic reductions and calibrations that are performed in the STScI STIS pipeline. This information is intended to provide enough background to develop robust observing proposals. The STIS chapters in the *HST Data Handbook* provide the detailed information needed for analyzing your data.

Pipeline Processing Overview

Science data taken by STIS are received from the Space Telescope Data Capture Facility and sent to the STScI pipeline, where the data are unpacked, keywords extracted from the telemetry stream, and the science data reformatted and repackaged into raw (uncalibrated) FITS[1] files by the generic conversion process. All STIS data products are FITS files. The vast majority of the STIS data products are two-dimensional images that are stored in FITS image extension files as triplets of science, error, and data quality arrays. Fits image extensions offer great flexibility in data storage and allow us to package related science data that are processed through calibration as a single unit together into one file. The uncalibrated FITS files are passed through **calstis**, the software code that calibrates the data, producing *calibrated* FITS files. For more details on STIS data structure and the naming conventions for the uncalibrated and calibrated data products, see chapter 20 of the *HST Data Handbook.*

Calstis performs the following basic science data calibrations:

1. Flexible Image Transport System.

- Basic, two-dimensional image reduction producing a flat fielded output image (*rootname*_flt.fits), which, depending on whether the data is from the MAMA or the CCD and whether it is imaging or spectroscopic data, includes the following: data quality initialization, dark subtraction, bias subtraction, non-linearity flagging, flat fielding, and photometric calibration.
- Two-dimensional spectral extraction producing a flux calibrated, rectified spectroscopic image (*rootname*_x2d.fits) with distance along the slit running linearly along the Y axis and wavelength running linearly along the X axis, for spectroscopic first-order mode data.
- One-dimensional spectral extraction producing a one-dimensional spectrum of flux versus wavelength (*rootname*_x1d.fits), uninterpolated in wavelength space, but integrated across an extraction aperture in the spatial direction, for first-order and echelle spectroscopic data.

In addition, **calstis** performs two types of contemporaneous calibrations:

- For CCD exposures which have been CR-SPLIT, **calstis** combines the exposures, producing a cosmic-ray rejected image (*rootname*_crj.fits) which is then passed through subsequent calibration (e.g., spectral extraction).
- For spectroscopic exposures, **calstis** processes the associated wavecal exposure (see “Routine Wavecals” on page 24) to determine the zero point offset of the wavelength and spatial scales in the science image, thereby correcting for thermal drifts and the lack of repeatability of the mode select mechanism. Whereas the uncalibrated science data are stored in the *rootname*_raw.fits file, the accompanying wavecal observations are stored in the file *rootname*_wav.fits.[2]

Figure 15.1 through Figure 15.3 show example output from the **calstis** pipelines. **calstis** program propagates statistical errors and tracks data quality flags through the calibration process. **calstis** is available to users in STSDAS, so they can recalibrate their data as needed.[3] Recalibration may be performed in its entirety in a manner identical to the pipeline calibration by using **calstis**, or modular components of **calstis**, such as basic two-dimensional image reduction (**basic2d**), two-dimensional spectral extraction (**x2d**), one-dimensional spectral extraction (**x1d**), or cosmic ray rejection (**ocrreject**). The calibration steps that **calstis** performs on a given set of science observations depends on the nature of those observations.[4]

Data taken in TIME-TAG mode are corrected for the Doppler shift from the spacecraft motion and output as an uncalibrated event stream by the pipeline in a

---

2. Unassociated wavecal observations are stored in *rootname*_raw.fits.

3. The **calstis** software is written in C and uses open IRAF in conjunction with a specially written I/O interface to the FITS data file.

4. Available mode data are not calibrated in the pipeline: the observer receives only the raw data files.

FITS binary table (*rootname*_`tag.fits`). The time-tag data stream is also integrated in time to produce an uncalibrated `ACCUM` mode image (*rootname*_`raw.fits`) which is then passed through standard calibration. The **odelaytime** task in STSDAS can be used off-line to correct the `TIME-TAG` times, which are spacecraft times, to heliocentric.

More detailed descriptions of the **calstis** software and its modular components are available in the *HST Data Handbook* chapter 21, and in a series of Instrument Science Reports (ISRs) accessible via the STIS WWW pages at:

`http://www.stsci.edu/instruments/stis`

New releases of **calstis** are accompanied by updates under "Calibration/Pipeline Software History" on the web pages.

Figure 15.1: Two-Dimensional Rectification

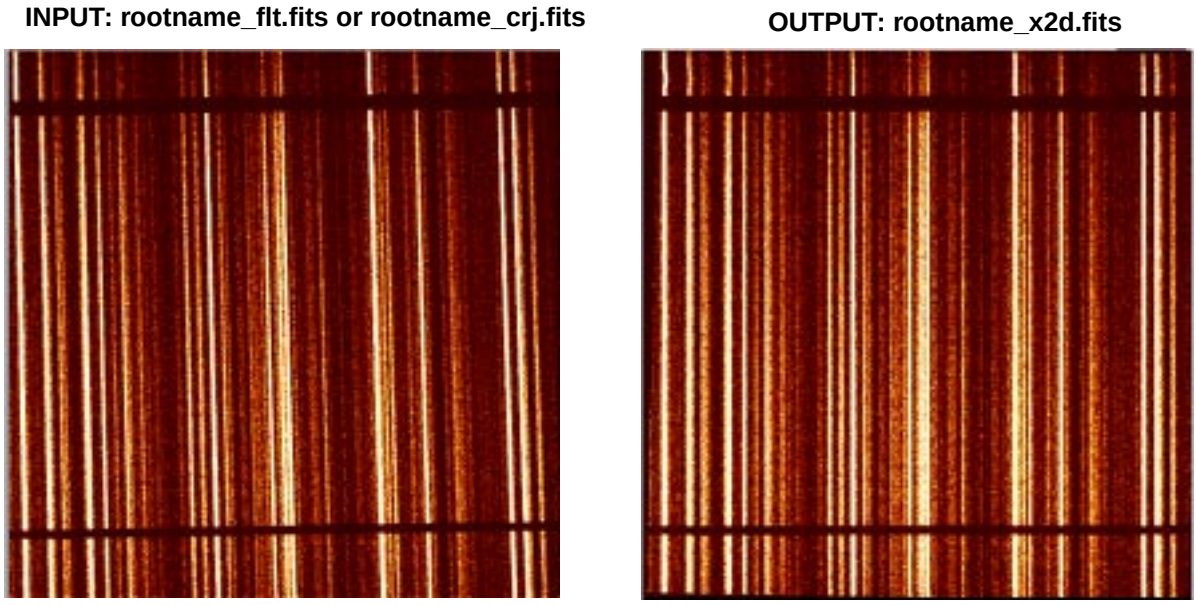

Figure 15.2: Cosmic Ray Rejection

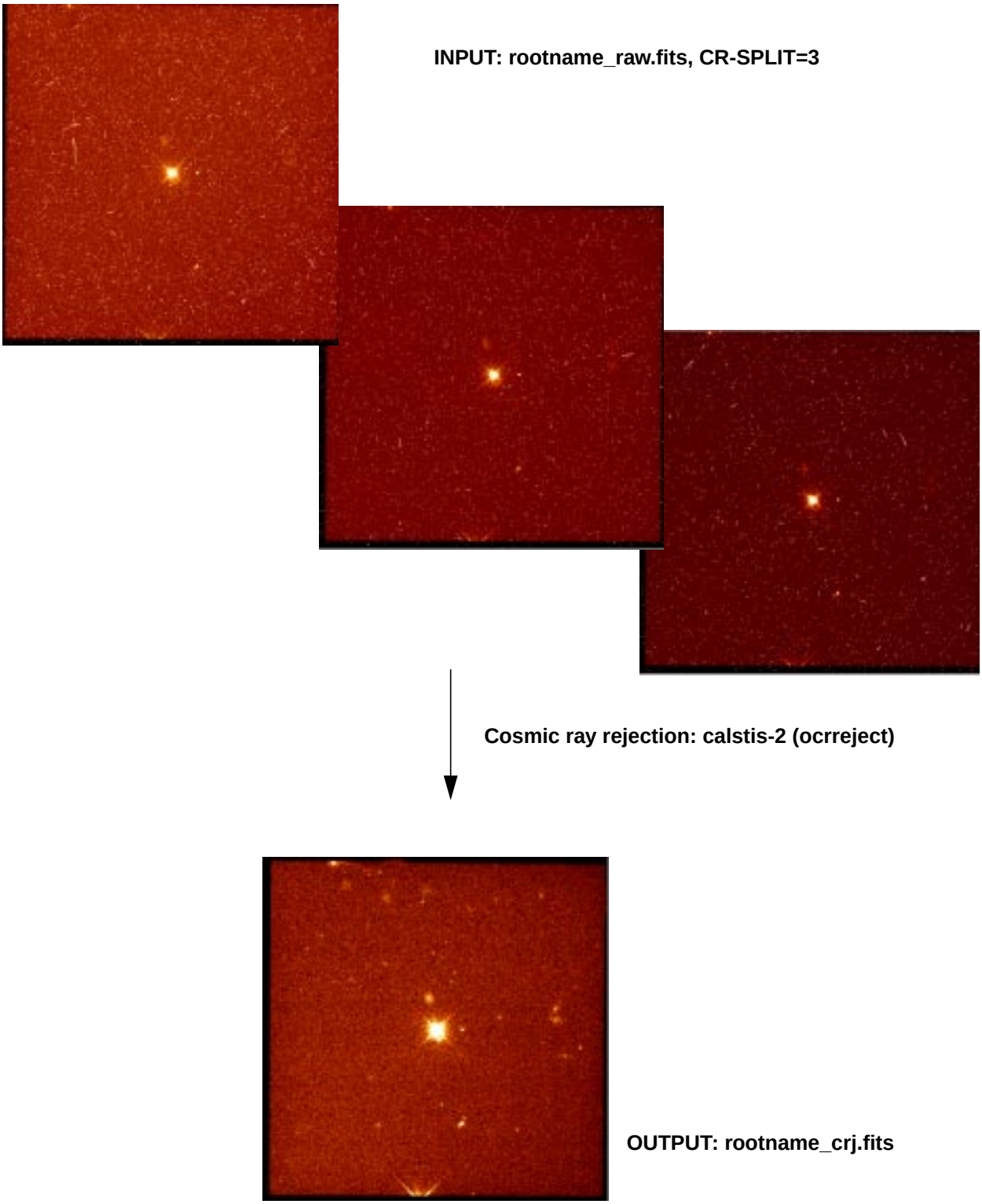

Figure 15.3: One-Dimensional Spectral Extraction

INPUT: rootname_raw.fits, NUV-MAMA, E230H, cenwave=2762

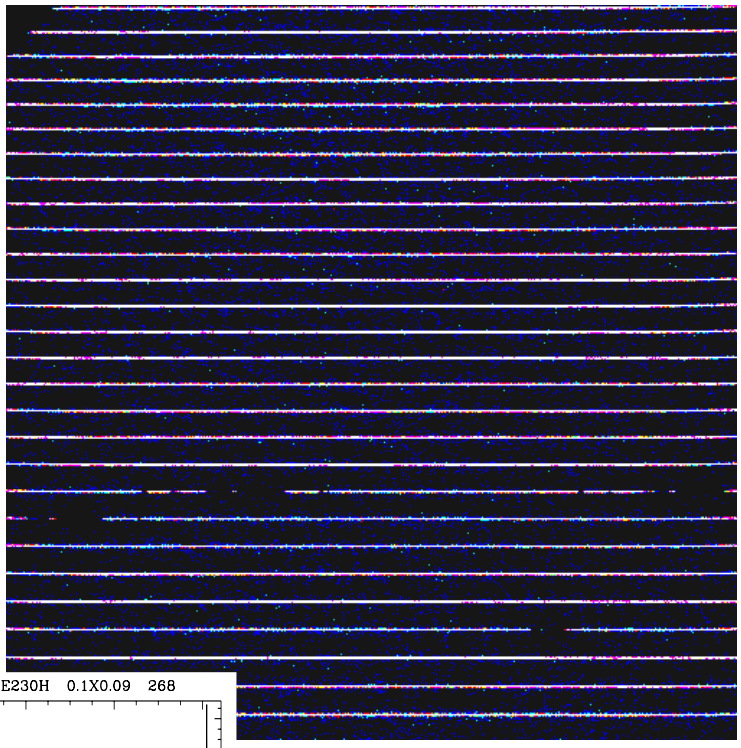

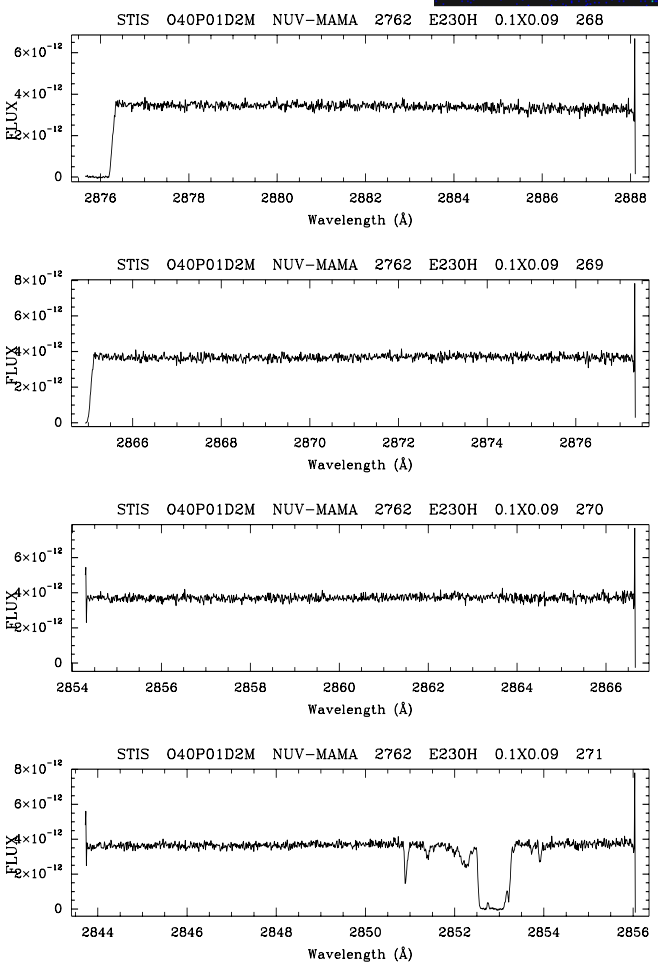

OUTPUT: rootname_x1d.fits, plotted by echplot (only a few spectral orders are plotted)

CHAPTER 16
Accuracies

In This Chapter...

In this chapter we describe the accuracies we hope to achieve during Cycle 8 for STIS photometric, spectral, and astrometric calibration.

Summary of Accuracies

In Tables 16.1 through 16.5, the accuracies are listed for each of STIS's basic observation modes: CCD spectroscopy, MAMA spectroscopy, CCD imaging, MAMA imaging and target acquisitions. All accuracies quoted are 2σ limits. The accuracies reflect our current understanding of STIS as of May 1998 and are those we expect the pipeline calibration or recalibration of archive data to achieve during Cycle 8.

We maintain on the STIS web pages (under "Calibration") both a table of our ultimate expected accuracies and a table of the accuracies delivered by pipeline data at any one time. The latter is frequently updated as we continue to work through the on-orbit calibration of STIS providing updated calibration reference files to the pipeline and the archive for STIS's many modes and capabilities. (See also the STIS section of the *HST Data Handbook*.)

We remind you that calibration data is immediately non-proprietary and should you have need for extreme accuracy or urgent results, you may wish to consider direct analysis of the calibration data for your particular observing mode (see also Chapter 17 for a description of our on-orbit calibration program).

Table 16.1: CCD Spectroscopic Accuracies

Attribute	Accuracy[a]	Limiting Factors
Relative wavelengths—within an exposure	0.1–0.3 pixels	• Stability of optical distortion • Accuracy of dispersion solutions
Absolute wavelengths—across exposures	0.2–0.5 pixels[b]	• Thermal stability • Derivation of wavecal zero point • Accuracy of dispersion solutions
Absolute photometry[b,c,d]		Instrument stability and photometric calibration
L modes	3%	
M modes	5%	
Relative photometry[b,c] (within an exposure):		Instrument stability and photometric calibration
L modes	2%	
M modes	2%	

a. All accuracies refer to prime wavelength settings and directly calibrated special secondary settings. Intermediate settings have roughly a factor of two less accuracy.
b. Assumes star is well-centered in slit. See the *HST Data Handbook* for a more complete description of the impact of centering on accuracies.
c. Assumes use of a wide photometric slit. See the *HST Data Handbook* for a fuller description of the impact of slit width on photometric accuracy.
d. Photometric accuracies referenced are for continuum sources, equivalent width and line profile measures are subject to other uncertainties (such as spectral purity and background subtraction).

Table 16.2: MAMA Spectroscopic Accuracies

Attribute	Accuracy[a]	Limiting Factor
Relative wavelengths—within an exposure	0.25–0.5 pixels	• Stability of small scale geometric detector + • Optical distortion • Accuracy of dispersion solution
Absolute wavelengths[a]	0.5–1.0 pixel	• Thermal stability • Derivation of wavecal zero point • Accuracy of dispersion solutions
Absolute photometry[a,b,c]:		Instrument stability and calibration
L modes	4%	
M modes	5%	
Echelle modes	10%	
Relative photometry (within an exposure, typical low dispersion):[b,c]		Instrument stability/flat fields
L modes	2%	
M modes	2%	
Echelle modes	5%	Ripple correction accuracy, scattered light subtraction

a. All accuracies refer to prime wavelength settings and directly calibrated special secondary settings. Intermediate settings have roughly a factor of two less accuracy.
b. Assumes star is well-centered in slit. See the *HST Data Handbook* for a more complete description of the impact of centering on accuracies.
c. Assumes use of a wide photometric slit. See the *HST Data Handbook* for a fuller description of the impact of slit width on photometric accuracy.

Table 16.3: CCD Imaging Accuracies

Attribute	Accuracy	Limiting Factor
Relative astrometry—within an image	0.1 pixels	Stability of optical distortion
Absolute photometry	5%	Instrument stability
Relative photometry within an image	5%	External illumination pattern

Table 16.4: MAMA Imaging Accuracies

Attribute	Accuracy	Limiting Factor
Relative astrometry—within an image	0.25 pixels	Small scale distortion stability
Absolute photometry	5%	Instrument stability and calibration
Relative photometry within an image	5%	Flat fields/external illumination

Table 16.5: Target Acquisition Accuracies

Attribute	Accuracy	Limiting Factor
Guide star acquisition	1–2″	Catalog uncertainties
Following target acquisition exposure: Point sources Diffuse sources	 0.″01 0.01–.1″	Centering accuracy plus plate scale accuracy to convert pixels to arcsecond See Chapter 8
Following peakup acquisition exposure	5% of the slit width	Number of steps in scan + PSF

Flats

We intend to update all library flats to a signal-to-noise of 100:1 per pixel.[1] The CCD flats have shown no sign of significant temporal variation. The MAMA flats have shown some evidence for variation at the 1–2% per resolution element level over roughly year timescales. Due to the limited long life times, we expect to take MAMA flats once per year per detector. As our knowledge grows, we will provide updates on the web pages.

1. A “pixel” for the MAMA refers to 1024 x 1024 native format pixels.

CHAPTER 17
Calibration Status and Plans

In This Chapter...

Introduction

In this chapter we describe the current status of STIS calibration and outline tentative plans for future calibration in Cycle 8. At the time this Handbook is being written, Cycle 7 calibration is about half complete (in terms of observations, not analysis). Detailed planning for Cycle 8 calibration has not yet begun. Below we give a brief guide to the calibrations obtained during ground testing, Servicing Mission Orbital Verification (SMOV) and Cycle 7. We also describe the philosophy we expect to employ in Cycle 8. Further information on calibration, including detailed descriptions of the proposals, can be found on the STIS web pages. When you have questions about updates to the calibration accuracy, you should always check the STIS web page. For further help on calibration issues consult your Contact Scientist, or send email to `help@stsci.edu`. Suggestions for additional calibrations, or different ways of characterizing calibration issues are always welcome.

Ground Testing and Calibration

The STIS Investigation Definition Team (Principal Investigator, Bruce Woodgate, GSFC) was responsible for the ground testing and ground calibration of STIS. Most of the ground-test data were obtained during late 1996, during thermal vacuum testing at Ball Aeorspace in Colorado, and during subsequent testing in a dry-nitrogen environment at GSFC. These tests characterized the basic

properties of the optics, the detectors, and the mechanisms. Certain measurements (e.g., measurements of the quantum efficiency of the STIS detectors vs. wavelength) cannot be repeated in orbit. However, most of the ground tests are superseded by on-orbit tests. Ground test data are stored at STScI, but are not incorporated into the HST Archive.

SMOV Testing and Calibration

The primary goal of the Second Servicing Mission's Orbital Verification (SMOV) was the timely commissioning of the HST observatory for normal science operations. For STIS, this included testing the focus (internal and external), verifying the target acquisition procedures, monitoring instrument stability (both in terms of image motions and in terms of sensitivity), and measuring selected sensitivities: plate scales, slight throughputs, line spread functions, etc. SMOV observations were complete by the summer of 1997, and most of the results of the calibrations were presented in the 1997 *HST Calibration Workshop*, and a high level summary was provided in the Kimble et al. (1998, *ApJ*, 492, L83) paper on STIS on-orbit performance. For a recent update including early Cycle 7 calibration, see also (Baum et al., 1998, SPIE in press). Brief descriptions of the SMOV proposals are given in Table 17.1. Data from calibration proposals are non-proprietary, and can be accessed through StarView using the proposal IDs listed in the table.

Table 17.1: STIS SMOV Proposals

ID	Title
7058	STIS memory load and dump
7059	Science Data Buffer check with Self-Test
7061	CCD Functional
7062	CCD Temperature Set Point Determination
7063	STIS SMOV Contamination monitor
7064	STIS SMOV Contamination monitor
7065	STIS to FGS alignment
7066	STIS Acquisition Aperture and Slit Location
7067	STIS CCD Point Source Acquisition
7068	STIS CCD Diffuse Source Acquisition
7070	STIS CCD Coronagraphic Acquisition
7071	CCD Target Centering
7073	CCD Peakdowns for Coronagraphic Acquisition
7075	STIS Corrector Alignment, Coarse
7076	STIS Corrector Alignment, Fine
7077	Spectroscopic Mode Image Quality
7078	Spectroscopic Mode Image Quality

Table 17.1: STIS SMOV Proposals (Continued)

ID	Title
7079	Camera Mode Image Quality
7080	Camera Mode Image Quality
7081	Repeatability of Image Positions for STIS Modes
7082	Repeatability of Image Positions for STIS Modes
7083	Verification of Optical Format of STIS Modes
7084	Verification of Optical Format of STIS Modes
7085	STIS Slit to Detector Internal Stability
7086	STIS Slit to Detector Internal Stability
7087	OTA-STIS Pointing and Throughput Stability
7088	Occulting Bar Scattered Light
7089	Occulting Bar Scattered Light
7090	PSF measurement in Bands 1 & 2
7091	STIS Pixel-To-Pixel Response Stability
7092	CCD Dark Rate and Read Noise
7093	Dark measurement for MAMA Band 1, and Band2
7094	STIS Sensitivity on axis
7095	STIS Sensitivity (vignetting)
7096	STIS Sensitivity on axis
7097	STIS Sensitivity (vignetting)
7098	Band I and Band II Flat Field uniformity
7099	CCD Flat-Field Stability
7100	SMOV Slit Transmission
7101	SMOV Slit Transmission
7103	STIS Mechanism mini-functional
7104	STIS Onboard Doppler Processing Checkout
7105	MAMA turnon
7106	STIS MAMA Fold Distribution
7107	STIS CCD Hot Pixel Annealing
7108	STIS MAMA Time Tag Mode
7131	STIS image mode geometric distortion
7132	STIS image mode geometric distortion
7133	STIS to FGS alignment
7142	CCD Flatfield monitoring
7143	CCD Internal Image stability with LVPS cycling
7144	STIS Thermal Stability with LVPS cycling
7147	STIS Fine Corrector Alignment with CCD
7148	STIS CCD Target Acquisition Workout
7151	STIS CCD V2V3 Aperture Verification

Table 17.1: STIS SMOV Proposals (Continued)

ID	Title
7159	NUVMAMA Dark Current vs. time from SAA
7160	CCD reconfiguration effects

Cycle-7 Calibration

The STIS Cycle 7 calibration plan includes additional charcterization of STIS performance, along with periodic monitoring of sensitivity, flats, dark current, gain, etc. Because it is not feasible to calibrate the instrument in all possible observing modes, the calibration emphasizes measurements in all the *supported* modes. Observers wishing to use non-standard configurations should be aware that the calibration is likely to be less accurate, and should plan to take their own calibrations as part of their approved proposals if additional accuracy is required. Calibrations are not supplied for available modes.

Table 17.2 lists the Cycle 7 calibrations and gives some pointers to further documentation. The history comments of the reference files provide some details of the analysis, as do the ISRs and Calibration Workshop papers. Details of the planned observations can be found from the Phase II proposals, which are on the STScI WWW site under “Resources for Observers,” then under “Program Status and Visit/Scheduling Unit level Information.”

Calibration Priorities

The task of calibrating STIS has involved a number of important tradeoffs. HST calibration observations have been planned to use a limited number of orbits (no more than about 10% of the total science time allocated in Cycle 7), and to stretch out through the Cycle so that the observing schedule is not too heavily front-loaded with calibrations. The allocation of spacecraft and staff resources to the calibration effort for STIS has followed roughly the following set of priorities:

1. *Monitor the health and safety of STIS*. Carry out the necessary periodic monitoring of STIS to ensure that is operating correctly. Revise operations as necessary to ensure that it will maintain its scientific performance over its (anticipated 13 year) lifetime.
2. *Update and Maintain Pipeline Reference files*. This includes such things as darks, biases, flats, and sensitivities. Information on newly released files is announced via the Space Telescope Analysis Newsletters, and posted to the STIS WWW pages. As new reference files are incorporated into the pipeline, the “recommended reference files” are updated for each dataset in the HST Archive.
3. *Basic sensitivity calibration of spectroscopic modes*. The majority of STIS science observations use the spectroscopic modes. Sensitivity calibration is

important for instrument safety, science optimization, and data analysis. The sensitivity calibration includes basic measurements of on-orbit throughput, and monitoring of time variations either due to contamination or due to gain variations in the detectors.

4. C*haracterization of optical performance.* This includes point-spread functions, line-spread functions, aperture throughputs, enclosed energy for different spectral extraction heights, and imaging and spectroscopic geometric distortion calibrations. Detailed characterization of scattering (e.g., in wavelength in the gratings, or in the far-wings of the imaging PSF) is included, but is orbit-intensive and therefore will be carried out over a longer timescale.

5. *Characterization of detector and observational specific peculiarities.* This includes detector nonlinearities, charge transfer effects, fringing, long-wavelength scattering within the CCD, grating scatter and extended PSF wings, etc.

6. *Calibration and testing of future observing mode strategies.* This includes tests of the cross-dispersed gratings, tests with the FUV-MAMA repeller wire off, or tests of strategies to reduce the NUV-MAMA dark current, and will be performed only on a best-effort basis depending on resources.

Within each of these priority groups, calibration priority is in the following order by observing mode:

1. First order prime L grating modes (G140L, G230L, G430L, G750L).
2. Echelle spectroscopy.
3. First order M mode gratings.
4. CCD imaging (broad band first, then narrow band).
5. MAMA imaging (broad band first, then narrow band).
6. G230LB and G230MB backup modes, including analysis of red scattering.

In addition, on-axis calibrations have higher priority than off-axis calibrations. That is, we seek first to establish the calibrations at the field/slit center and therafter, to expand the calibration to two dimensions.

Calibration Schedule

The overall schedule for STIS calibration was defined in Summer 1997 using the set of priorities outlined above. Major milestones were defined and are shown below with planned completion dates. At the time of writing we are more-or-less on schedule, slightly ahead in some areas, behind slightly in others. The basic sensitivity calibration for all STIS modes is completed as of the writing of this Handbook. The CCD and MAMA flats have yet to be updated. These calibrations, of course, represent a first iteration, which we expect to improve with time as

more data and experience with STIS are gathered. Refer to the “Calibration” area of the STIS WWW page for the latest information.

November 1997	SMOV closed out.
	Darks, biases, CCD flats delivered to pipeline.
December 1997	Routine health and safety monitoring procedures in place.
January 1998	Sensitivities for all modes to 20% accuracy.
	L mode characterization: sensitivity, LSF, cross-dispersion profiles, and flat fields.
April 1998	Echelle modes charaterized: sensitivity, LSF, cross-dispersion profiles and flat fields.
April 1998	Calibration updates included in Cycle 8 handbook
May 1998	Coronography characterized
August 1998	M mod characterization: sensitivity, LSF, cross-dispersion profiles and flat fields.
	CCD imaging photometry, PSFs, flats characterized.
September 1998	MAMA imaging photometry, PSFs, flats characterized.

Table 17.2: STIS Cycle 7 Calibration Programs

ID	Title	Observations	Analysis Documentation, Reference Files
	CCD Monitoring and Detector Calibration		
7601	CCD Darks and Biases Monitor	Complete	DRK, BIA, and BPX reference files.; STSDAS cl script for creating daily darks available on STIS WWW page, under “tools.:
7926	CCD Dark and Bias Monitor, 7601 Cont	7x/week	
7948	CCD Dark and Bias Monitor, June-Dec 98	14x/week	
7949	CCD Dark and Bias Monitor, Jan99-Jun99	14x/week	
7602	Missing CCD Flats	Complete	PFL reference files
7634	CCD Flat Fielding Monitor	Monthly	PFL reference files
7635	Hot Pixel Annealing	Monthly	ISR98-06; Beck et al. 1997 Calibration workshop.
7636	CCD Spectroscopic Internal Flats	Complete	PFL reference files
7928	CCD Spectroscopic Flatfielding, 7636 Cont.	Monthly	PFL reference files
7637	CCD Residual Images Following overillumination	Complete	
7659	Daily Darks for Acquisition Hot Px List Update	Complete	BPX reference files; STSDAS cl script for creating daily darks available on STIS WWW page, under “tools.
7802	Daily Darks Part II, 7659 Cont.	Complete	
7803	Daily Darks Part III	Daily	
7711	CCD Fringe Flats	Complete	ISR97-15, 97-16
7783	CCD External Flats, Sky Parallels	Frequent	
7930	CCD Biases for 1x2 Binning	Semi-annual	BIA reference files

Table 17.2: STIS Cycle 7 Calibration Programs (Continued)

ID	Title	Observations	Analysis Documentation, Reference Files
7944	CCD Performance Monitor Cont. & Sparse Field CTE	Semi-annual	CCD Performance is described in ISR97-10; and Kimble et al. (1998, ApJ, 492, L83)
	MAMA Monitoring and Detector Calibration		
7604	MAMA Dark Monitor	5x/week	DRK reference files
7950	MAMA Dark Monitor, 7604 Cont, start~9Nov98	2x/week	
7643	MAMA Fold Distribution	Semi-annual	ISR98-02
7644	NUV-MAMA Monitoring Flats	Complete	ISR98-15
7645	MAMA FUV-MAMA Flats	Semi-annual	
7647	MAMA NUV-MAMA Flats	Semi-annual	
7728	FUV-MAMA Monitoring Flats	Complete	
7670	MAMA Ramp-up Check	Middle 1998	
7937	MAMA Off-axis Sensitivity (Vignetting)	Middle 1998	LFL reference files
	Spectroscopic Wavelength and Geometric Distortion		
7648	Missed Dispersion Solutions, CCD	Complete	DSP reference files
7649	Missed Dispersion Solutions, MAMA	Complete	
7650	Dispersion Solution Check, CCD	Yearly	
7651	Dispersion Solution Check, MAMA	Yearly	
7652	LSF Measure, CCD	~Complete	ISR98-04
7653	LSF Measure, MAMA	January 1999	
7654	Slitless Spectroscopy,CCD	Middle 1998	
7665	Geometric Distortion, CCD	Complete	SDC reference files
7667	Geometric Distortion, MAMA	Complete	
7668	Missing Incidence Angle Correction, CCD	Complete	IAC reference files
7669	Missing Incidence Angle Correction, MAMA	Middle 1998	
7935	Cross Disperser Mode Testorrection, MAMA	Early 1998	
7936	External to Internal Wavelength Correction	Early 1998	
	Spectroscopic Photometry		
7656	Spectroscopic and Imaging Sensitivity, CCD	Yearly	PHT reference files; ISR97-14
7657	Spectroscopic and Imaging Sensitivity, MAMA	Yearly	
7672	Contamination/Sensitivity Monitor, CCD	~Quarterly	
7673	Contamination/Sensitivity Monitor, MAMA	~Quarterly	
7674	IR Standards	Complete	
7723	Grating scatter	Complete	
7805	Contamination: Tie SMOV Stars to Cycle-7 Star	Complete	PHT reference files; ISR97-14
7809	Prism Sens./Faint Calib. Standard Extension	Yearly	
7810	Sensitivity Cal. :Secondary Wavel., CCD & MAMA	Yearly	

Table 17.2: STIS Cycle 7 Calibration Programs (Continued)

ID	Title	Observations	Analysis Documentation, Reference Files
7917	Affect of MAMA Charge Offsetting on Sensitivity and Dispersion solutions	Complete	
7931	Scattered light in Echelle Modes, MAMA	Early 1999	
7932	Spectral Purity & Slit Throughputs, First Order Modes	Early 1999	
7943	Transmission of Filtered Echelle Slits, MAMA	April 1998	PHT reference files.
	Imaging Photometry and Geometry		
7639	CCD Contamination/Sensitivity over Full Field	~Quarterly	
7641	CCD External Flats, Stellar	Complete	Ferguson 1997 Calibration Workshop
7642	CCD Red Light PSF halo	Complete	
7661	STIS MAMA Filter Red Leak Measurement	Yearly	
7666	CCD Linearity and Shutter Stability Test	Complete	
7720	MAMA Full Field Sensitivity	Semi-annual	
7774	Deep MAMA PSF measurement	Complete	
7788	MAMA Image Location and Geometric Distortion	Complete	Malumuth & Bowers 1997 Calibration Workshop; Cycle-8 Handbook, Chapter 14
	Operations and Engineering		
7605	Target acquisition workout	Complete	ISR 97-12; Kraemer et al. 1997 Calibration workshop; Cycle-8 handbook Chapter 8.
7646	CCD Scattered Light from Earth Limb...	Complete	ISR 98-??
7660	STIS to FGS Alignment - Cycle 7 Check (CCD)	Complete	
7719	FUV, MAMA Anomalous Recovery Procedure	Middle 1998	ISR 98-03
7721	Slit Throughputs, MAMA	Complete	APT reference files
7722	Lamp Flux Measurement	Complete	ETC updates, auto-wavecal tables
7725	NUV, MAMA Anomalous Recovery Procedure	Middle 1998	ISR 98-03
7905	CCD Acquisition Checkout for Flight Software Hot Pixel Fix	Complete	
7934	Repeller Wire Off Test	Early 1999	
7942	MSM Update, Test	Middle 1998	
7951	CCD G750L w/bar Anomalous ‘scatter’	Late 1998	
7953	Slit Wheel Repeatability	Late 1998	
7965	MAMA Fold Analysis for Cycle 7	Middle 1998	ISR 98-02

Cycle-8 Calibration

The Cycle 8 calibration plan will be modeled closely on the Cycle 7 calibration plan. Once again *supported* modes will be monitored for such things as sensitivity changes, flatfield evolution, and dispersion solutions. No additional calibrations will be taken for *available-but-unsupported* configurations. Observers wishing to use non-standard configurations should assess their calibration needs and include time in the proposal for any additional calibrations that are needed.

Observers with specific requirements for the supported modes, beyond those described above for Cycle 7 are encouraged to contact us with suggestions. The best way to do this is by sending a message to `help@stsci.edu` with a fairly detailed discussion of the calibration (including why it is needed, what kind of science it will support, and some suggestions for targets and observing strategies). Such suggestions will of course have to be weighed against other demands on the telescope, but we welcome your input.

If your program requires unique calibrations beyond those that are planned (use the Cycle 7 Calibration Program as a guide) and of direct benefit to other users of STIS, then you should apply directly for this calibration in your Phase I proposal.

Glossary

The following terms and acronyms are used in this Handbook.

A-D: Analog to digital.

ABMAG: –2.5 log (F_ν) – 4860 where F_ν is the flux from the source in erg cm^{-2} sec Hz.

CCD: Charge-coupled device. Solid-state, light detecting device.

CDBS: Calibration Data Base. System for maintaining reference files and tables used to calibrate HST observational datasets.

CEI: Contract End Item

CIM: Calibration insert mechanism.

COSTAR: Corrective Optics Space Telescope Axial Replacement.

CP: Call for Proposals.

CR: Cosmic ray.

CVZ: Continuous viewing zone.

DQ: Data quality.

DQE: Detector quantum efficiency.

DN: Data number.

FAQ: Frequently asked questions.

FGS: Fine Guidance Sensors.

FITS: Flexible Image Transport System. A generic IEEE- and NASA-defined standard used for storing image data.

FOC: Faint Object Camera.

FOS: Faint Object Spectrograph.

FOV: Field of view.

FSW: Flight software.

FTP: File Transfer Protocol. Basic tool used to retrieve files from a remote system. Ask your system manager for information about using FTP.

FUV: Far ultraviolet.

FWHM: Full width at half maximum.

GEIS: Generic Edited Information Set. The multigroup format used by STSDAS for storing some HST image data.

GHRS: Goddard High-Resolution Spectrograph.

GO: General Observer.

GTO: Guaranteed Time Observer.

HITM: Hole in the Mirror.

HSP: High-Speed Photometer.

HST: Hubble Space Telescope.

ICD: Interface control document. Defines data structures used between software or systems to ensure compatibility.

IDT: Investigation Development Team.

IM: Insert Mechanism.

IR: Infrared.

IRAF: Image Reduction and Analysis System. The system on which STSDAS is built.

IUE: International Ultraviolet Explorer.

K: Degree Kelvin.

LMC: Large Magellanic Cloud.

LSF: Line spread function.

MAMA: Multi-Anode Microchannel Array.

MCP: Microchannel Plate.

MSM: Mode Selection Mechanism.

ND: Neutral density.

NICMOS: Near-Infrared Camera and Multi-Object Spectrograph.

NUV: Near ultraviolet.

OSS: Observation Support System.

PI: Principal investigator.

PSF: Point spread function.

QE: Quantum efficiency.

QEH: Quantum efficiency hysteresis.

QPOE: Quick Position-Oriented Event (IRAF data format for x-ray data).

QSO: Quasi-stellar object.

RA: Right ascension.

rms: Root mean square.

SIM: Space Interferometry Mission.

SITe: Scientific Image Technologies.

SMOV: Servicing Mission Orbital Verification.

S/N: Signal-to-noise ratio.

ST-ECF: Space Telescope European Coordinating Facility.

STIS: Space Telescope Imaging Spectrograph.

STMAG: –2.5 log (F_λ) –21.10 where F_λ is the flux from the source in erg cm^{-2} sec Å.

STScI: Space Telescope Science Institute.

STSDAS: Space Telescope Science Data Analysis System. The complete suite of data analysis and calibration routines used to process HST data.

SV: Science verification. Process of taking observations that can be used for HST instrument calibration.

TAC: Telescope Allocation Committee.

URL: Uniform resource locator. Address for WWW.

UV: Ultraviolet.

WF/PC: Wide Field/Planetary Camera.

WFPC2: Wide Field Planetary Camera-2. Replacement for WF/PC installed during first servicing mission of December 1993.

WWW: World Wide Web. Hypertext-oriented method for finding and retrieving information over the Internet.

Index

C

D

E

F

G

H

I

J

L

M

N

O

P

Q

R

S

T

U

V

W